

Cardiac MRI in arrhythmogenic right ventricular cardiomyopathy

Implementation of novel techniques



Mimount Bourfiss

Cardiac MRI in arrhythmogenic right ventricular cardiomyopathy

Implementation of novel techniques

Mimount Bourfiss

Cardiac MRI in arrhythmogenic right ventricular cardiomyopathy

-Implementation of novel techniques -

Mimount Bourfiss

Cardiac MRI in arrhythmogenic right ventricular cardiomyopathy

-Implementation of novel techniques-

Cardiale MRI in aritmogene rechter ventrikel cardiomyopathie

-Implementatie van nieuwe technieken-

(met een samenvatting in het Nederlands)

Proefschrift

Ter verkrijging van de graad van doctor aan de
Universiteit Utrecht

Op gezag van de

Rector magnificus, prof. Dr. H.R.B.M. Kummeling

Ingevolge het besluit van het college voor promoties

In het openbaar te verdedigen op

donderdag 8 juni 2023 des middags te 4.15 uur

door

Mimount Bourfiss

Geboren op 6 september 1992

te Zeist

Cardiac Magnetic Resonance imaging in arrhythmogenic right ventricular cardiomyopathy.

Implementation of novel techniques.

Academic thesis, Utrecht University, the Netherlands

Cover design: Atelier ink Amsterdam | www.ink-amsterdam.nl

Lay-out: Ilse Modder | www.ilsemodder.nl

Printing: Gildeprint Enschede | www.gildeprint.nl

ISBN: 978-90-393-7549-5

Financial support by the Dutch Heart Foundation for the publication of this thesis is gratefully acknowledged.

Copyright ©2023, Mimount Bourfiss

All rights reserved. No part of this thesis may be reproduced, stored in an archival system or transmitted in any form or by any means without prior permission of the copyright owner.

Promotoren

Prof. Dr. B.K. Velthuis

Prof. Dr. F.W. Asselbergs

Copromotor

Dr. A.S.J.M. te Riele

Beoordelingscommissie

Prof. dr. P.A.F.M. Doevendans

Prof. dr. R. Nijveldt

Prof. dr. E. van Rooij

Prof. dr. H.S. Tandri

Prof. dr. J.P. van Tintelen

Voor mijn ouders

Patience is not sitting and waiting, it is foreseeing- S. Tabrizi

CONTENTS

Chapter 1	General introduction and thesis outline	13	PART III	Atrial involvement in ARVC	169
Chapter 2	Current challenges in the diagnosis of arrhythmogenic cardiomyopathies <i>Current concepts in arrhythmogenic cardiomyopathy. Minneapolis: Cardiotext Publishing; 2021. 73-85</i>	25	Chapter 9	Influence of genotype on structural atrial abnormalities and atrial fibrillation or flutter in arrhythmogenic right ventricular dysplasia/cardiomyopathy <i>J Cardiovasc Electrophysiol. 2016 Dec;27(12):1420-1428</i>	171
Part I	Feasibility and reproducibility of novel CMR techniques in ARVC	41	Chapter 10	Atrial dysfunction in arrhythmogenic right ventricular cardiomyopathy <i>Circ Cardiovasc Imaging. 2018 Sep;11(9):e007344</i>	193
Chapter 3	Feature tracking CMR reveals abnormal strain in preclinical arrhythmogenic right ventricular dysplasia/ cardiomyopathy: a multisoftware feasibility and clinical implementation study <i>J Cardiovasc Magn Reson. 2017 Sep 1;19(1):66</i>	43	PART IV	Combining CMR and genetics to unravel genotype phenotype correlations	211
Chapter 4	Feature tracking CMR of the right ventricle: effect of field strength, resolution and imaging sequence <i>Eur J Radiol. 2021 May;138:109671</i>	69	Chapter 11	Prevalence and disease expression of pathogenic and likely pathogenic variants associated with inherited cardiomyopathies in the general population <i>Circ Genom Precis Med. 2022 Dec; 15(6): e003704</i>	213
Chapter 5	A head-to-head comparison of speckle tracking echocardiography and feature tracking CMR imaging in right ventricular deformation <i>Circ Cardiovasc Imaging. 2018 Sep;11(9):e007344</i>	75	Chapter 12	A drug target analysis prioritizing circulating plasma proteins involved with ventricular function and structure <i>Submitted</i>	261
PART II	Clinical value of novel CMR techniques in ARVC	99	Chapter 13	General discussion and future perspectives	309
Chapter 6	Prognostic value of strain by feature-tracking CMR in arrhythmogenic right ventricular cardiomyopathy <i>Eur Heart J Cardiovasc Imaging. 2022 Feb 13;jeac030</i>	101	Appendix	Nederlandstalige samenvatting	324
Chapter 7	Diagnostic value of native T1 mapping in arrhythmogenic right ventricular cardiomyopathy <i>J Am Coll Cardiol Img. 2019 Aug;12(8 Pt 1):1580-1582</i>	121		List of publications	333
Chapter 8	Towards automatic classification of CMR task force criteria for diagnosis of arrhythmogenic right ventricular cardiomyopathy <i>Clin Res Cardiol. 2022 Sep;doi:10.1007/s00392-022-02088-x</i>	139		Acknowledgements/Dankwoord	337
				Curriculum vitae	344

CHAPTER

General Introduction and
Thesis Outline

1

GENERAL INTRODUCTION

Every day the lives of twenty-eight European families are turned up-side down due to the sudden cardiac death of a relative¹. In many of these cases, this was the first disease presentation. Sudden cardiac arrest is not only a tragedy for the individual and their family, but also a large public health problem since the overall chances to survive a sudden cardiac arrest is low at approximately 10%². Furthermore, surviving a sudden cardiac arrest is associated with significant morbidity. Therefore, early diagnosis and adequate risk stratification of persons at risk of sudden cardiac death are the cornerstone in preventing these tragic outcomes. Unraveling the underlying, especially inheritable, cause of a sudden cardiac death or sudden cardiac arrest is important for further risk stratification of the individual patient and for early diagnosis and risk stratification of family members, especially since inherited conditions occur in up to 50% of families of young victims of sudden cardiac death³.

Sudden cardiac death due to ventricular arrhythmias is frequently observed in families with inherited cardiomyopathies. Inherited cardiomyopathies are classified based on morphological and functional features and include dilated cardiomyopathy (DCM), hypertrophic cardiomyopathy (HCM) and arrhythmogenic right ventricular cardiomyopathy (ARVC). While DCM and HCM are characterized by structural abnormalities with dilatation and hypertrophy of the left ventricle (LV) respectively, ARVC is characterized by ventricular arrhythmias prior to visible structural abnormalities. Accurate recognition of this disease is vital since the implantation of an implantable cardioverter defibrillator (ICD) can be life-saving.

Arrhythmogenic Right Ventricular Cardiomyopathy

ARVC has an estimated prevalence of 1:5000⁴. Disease presentation is usually in the second to fifth decade of life. Interestingly, the first disease presentation can be life-threatening ventricular arrhythmias leading to sudden cardiac arrest or death, especially in the young and in athletes⁴. ARVC is predominantly a right ventricular (RV) disease, but LV involvement is common. This heritable heart disease is mainly caused by a pathogenic variant in one of the components of the intercalated disk, especially the desmosomes such as Plakophilin-2, Desmoglein-2 and Desmoplakin. The intercalated disc forms not only a mechanical connection of cardiomyocytes through the desmosomes and adherence junctions, but also an electrical connection through gap junctions to ensure the propagation of electrical signals. Interestingly, these different components of the intercalated disc (desmosomes, gap junctions, sodium channels) form an interaction⁵. Therefore, pathogenic variants in one of these components could interrupt myocardial cell signaling and adhesion. This can be exaggerated under conditions of increased mechanical stress and stretch, such as strenuous exercise, leading to detachment of myocytes and alteration of intracellular signal transduction causing fibrofatty replacement of the myocardium. Surviving myocardial fibers within the fibro-fatty tissue form zones of slow conduction that provide a medium for re-

entry ventricular arrhythmias. These pathological changes can lead to scar related macro-reentry ventricular tachycardia⁵.

The first case series to describe ARVC, published by Marcus *et al.* identified RV dilatation in patients using 2-Dimensional echocardiography⁶. However, we now know that the natural history of classical right-sided ARVC can roughly be divided into four stages. In the concealed phase, no or minimal structural abnormalities can be detected using conventional techniques, although the patient is already at risk of sudden cardiac arrest. In the second phase, ventricular arrhythmias, mostly arising from the RV outflow tract, and structural and functional changes can be measured in especially the RV using different imaging techniques like echocardiography or cardiac magnetic resonance imaging. In the third phase, RV heart failure is seen, usually with preserved LV function. In the last phase, overt LV involvement is seen⁷. Current concepts of ARVC, include a biventricular or predominantly left-sided ARVC, where LV involvement is already seen in earlier stages⁸.

ARVC is diagnosed according to the revised 2010 Task Force Criteria (TFC)⁹. The TFC are a set of consensus-based diagnostic criteria including major and minor criteria in six different categories. Apart from electrocardiographic, arrhythmic, histological and genetic features, an important role is assigned to the assessment and scoring of ventricular dysfunction and structural alterations using catheter angiography, echocardiography or cardiac magnetic resonance imaging (CMR). Qualitatively assessed RV wall motion abnormalities (akinesia, dyskinesia or dyssynchronous contraction) are a prerequisite in the imaging criteria. Furthermore, the level of quantified RV dilatation or RV dysfunction determines whether or not a minor or major ARVC criterion is met.

Cardiac Magnetic Resonance imaging

CMR is the modality of choice for assessment of cardiac function and dimensions in ARVC¹⁰ because of its high spatial resolution¹¹, allowing accurate and reproducible evaluation of the RV. This is necessary since in healthy individuals without ARVC, the mean RV free-wall thickness is already only 2.7±0.4 mm¹², while in ARVC the RV wall is even thinner due to pathological wall thinning. Furthermore, the asymmetric geometry and the position of the RV in the chest can hamper visualization of the entire RV by 2-D echocardiography¹³. In addition to the structural and functional CMR parameters as mentioned in the TFC, CMR is able to provide tissue characterization using late gadolinium enhancement (LGE). This enables the identification of myocardial fibrosis, as one of the key features in ARVC. However, it has been shown that the diagnostic yield of LGE in patients suspected of ARVC is low¹⁴. LGE can be a sign of focal myocardial fibrosis, leaving subtle or diffuse fibrotic changes undetected.

The performance of the TFC criteria, including the CMR criteria of the TFC were validated in a recent study¹⁵. CMRs were re-evaluated by two blinded expert radiologists and the

final diagnosis was determined by an expert panel. Interestingly, the clinically observed TFC was false negative in 11% and false positive in 14% of patients¹⁵. A previous study also showed that misdiagnosis in ARVC is commonly based on CMR misinterpretation: only 27% of people referred to a tertiary center with a suspected ARVC diagnosis finally meet diagnostic criteria for ARVC¹⁶. An important problem is the qualitative assessment of RV wall motion abnormalities which hampers inter-observer reproducibility since the definition of normal versus subtle variants of abnormal RV contraction is open to different interpretations. Furthermore, the quantitative assessment of RV ejection fraction and volumes are also affected by considerable inter-reader variation¹⁷. Therefore, this thesis focusses on implementation of novel quantitative CMR techniques overcoming these issues.

THESIS OUTLINE

CMR is the reference standard for the assessment of cardiac anatomy and function. Over the years various new CMR techniques have emerged, offering the opportunity to cope with previously mentioned issues in current qualitative and quantitative CMR assessment: feature tracking CMR (FT-CMR) has been developed for the evaluation of regional myocardial function; T1 mapping for the evaluation of tissue characterization; and machine learning for the automatic evaluation of CMR imaging. This thesis primarily focuses on the improvement of early diagnosis and risk stratification of ARVC patients and their relatives using these advanced CMR techniques. Not only did I focus on the RV and the LV, but also explored the involvement of the atria in ARVC. In the quest to diagnose patients at risk of sudden cardiac arrest at an early stage, genetic testing has become an important part of routine clinical care in the diagnosis of ARVC. The American College of Medical Genetics and Genomics has even recommended the reporting of incidental or secondary findings related to ARVC from clinical genomic sequencing. Interestingly, only little is known about disease expression and functional and structural cardiac involvement in asymptomatic ARVC genetic variant carriers from the general population. Beside these rare genetic variants, it is also unknown which common genetic variants affect cardiac function and dimension as measured on CMR.

In this line, I focused on four main research questions.

1. What is the reproducibility, variability and applicability of FT-CMR in the clinical setting?
2. What is the clinical value of FT-CMR, T1 mapping and machine learning in ARVC?
3. Is atrial involvement present in ARVC?
4. What is the contribution of rare and common variants on right and left ventricular function in individuals from the general population?

Chapter 2 is an overview and in depth description of the ARVC phenotype. **Chapters 3-12** are divided into four parts, each focusing on one of the four different research questions.

In these thesis I have mainly utilized data from the Netherlands ARVC Registry collected in the research electronic data capture (REDCap) platform. The design and implementation of this multicenter, longitudinal, observational cohort study has been published previously¹⁸. Furthermore, I have been privileged to use patient data from the Johns Hopkins ARVD/C registry. For the assessment of variations in the general population I have leveraged CMR, genetic and phenotypic data from the UK Biobank. The design and implementation of this database have also been published previously¹⁹.

Part 1. Feasibility of novel CMR techniques in ARVC

FT-CMR is an increasingly popular approach for the quantification and non-invasive evaluation of regional myocardial function. It employs a frame-to-frame recognition of a preset feature during the cardiac cycle, which enables the calculation of myocardial displacement during systole²⁰ and therefore allows for the evaluation of regional myocardial function. FT-CMR can be applied to routine cine CMR acquisitions without extending the image protocol or duration of the CMR examination. Recently, it was shown that quantitative strain analysis had higher sensitivity and accuracy than qualitative wall motion assessment done by visual inspection by two experts at tertiary centers²¹. However, before clinical implementation of a novel technique is possible, validation and assessment of feasibility has to be studied. The research question that governed this first part was:

“What is the reproducibility, variability and applicability of FT-CMR in the clinical setting?”

First, various commercially available software methods have been developed to analyze myocardial strain. However, little is known about the agreement between these methods. In **chapter 3** we assessed the inter-software agreement of RV global and regional strain using FT-CMR by providing a head-to-head comparison of four commercially available software methods. Furthermore, we assessed inter- and intra-observer reproducibility per software method. From our multicenter experience we know that different CMR sequence parameters and field strengths are used within and among centers. The impact of these parameters on RV strain values is still unknown. In **chapter 4**, we assessed the effect of field strength, imaging resolution and imaging sequence on the FT-CMR vales of the RV. Limited knowledge exists on different intra-modality factors that may influence RV strain values and inter-modality differences. Echocardiography is often used in patients with possible ARVC or other cardiomyopathies and deformation imaging using speckle tracking is increasingly being used as a different measure for strain analysis. Unfortunately, the interchangeability of RV strain values measured by FT-CMR versus speckle tracking echocardiography is

unknown. In **chapter 5** we performed a head-to-head comparison of speckle tracking echocardiography and FT-CMR in RV deformation.

Part 2. Clinical value of novel CMR techniques in ARVC

Next, we set out to assess the clinical value of novel CMR techniques in ARVC. Beside FT-CMR, we also assessed T1 mapping. T1 mapping allows for the non-invasive quantitative assessment of myocardial fibrosis using a pixel-wise measurement of absolute T1 relaxation times in milliseconds²². These T1 relaxation times vary depending on the cardiac microstructure and the presence of for example fat, fibrosis, oedema and amyloid deposition. Compared to the current standard for non-invasive detection of myocardial fibrosis (LGE CMR), T1 mapping is not limited by use of gadolinium and does not require ‘nulling’ of the background myocardium. This enables detection of either diffuse or subtle focal changes in the cardiac microstructure. Furthermore, machine learning is rapidly gaining ground in the clinical arena and is likely to change clinical practice in the coming years²³. CMR segmentation to measure functional and structural parameters is a laborious task, taking about 25 minutes to segment both ventricles in end-diastole (ED) and end-systole (ES) accurately, of which RV segmentation takes two-thirds of this segmentation time. Moreover, manual segmentation is prone to intra- and inter-observer variability. The use of automatic methods for the segmentation of the ventricles may overcome these challenges. Over the last few years many state-of-the-art deep learning segmentation approaches for short-axis CMR have been developed. For automatic LV segmentation such methods can achieve performance level of human experts. However most previous methods have been evaluated on CMR datasets with limited pathology especially related to the RV.

The research question answered in this part is as follows:

“What is the clinical value of FT-CMR, T1 mapping and machine learning in ARVC?”

In **chapter 3** we performed a software comparison and assessed the diagnostic value of FT-CMR in affected ARVC patients and unaffected at-risk family members. **Chapter 6** elaborates on these findings and assesses the prognostic value of FT-CMR in affected ARVC patients. We also assessed the diagnostic value of native T1 mapping in **chapter 7**. Finally, in **chapter 8** we improved and assessed the performance of a machine learning method for the automatic segmentation of RV and LV CMR measurements. This chapter also compares the CMR TFC classification by manual CMR measures to CMR TFC classification using our machine learning method.

Part 3. Atrial involvement in ARVC

As previously mentioned, ARVC is predominantly a disease of the cardiac desmosomes. Desmosomes are not only present in the RV and LV, but also in the atrial wall, however only little is known about the structural and functional involvement of the atria in ARVC. Previous studies already showed atrial arrhythmias (atrial fibrillation and atrial flutter) in a considerable number of ARVC patients, but these studies lacked information on atrial structure and function, which may precede the occurrence of atrial arrhythmias^{24,25}. Also, the influence of genotype on these atrial arrhythmias and structural atrial abnormalities is largely unknown. Determination of the atrial involvement in ARVC could give important understanding of the disease and the natural progression and may contribute to prevention of embolic cerebrovascular accidents due to atrial fibrillation. Furthermore, an increased risk of atrial arrhythmias would dictate proper implantable device programming and selection. As the gold standard for the structural and functional analysis of ARVC, CMR renders itself useful for the assessment of the atria. Previous studies have shown the feasibility and reproducibility of FT-CMR to analyze atrial function^{26,27}. However, this has not been applied on ARVC patients yet.

In this part, we focused on the following research question:

“Is atrial involvement present in ARVC?”

In **chapter 9** we aimed to describe the extent and clinical significance of structural atrial involvement and atrial arrhythmias in ARVC. Furthermore we examined the influence of genotype on atrial arrhythmias and structural atrial abnormalities. **Chapter 10** builds on the evidence from the prior chapter and aimed to detect predictors of atrial arrhythmias in ARVC patients using FT-CMR.

Part 4. Combining CMR and genetics to unravel genotype phenotype correlations

In the previous chapters of this thesis we focused on the “hospital population”, subjects with overt disease or their preclinical family members who carry a known pathogenic variant. However, data from the general population (including individuals who had no reason to seek medical care) are a tremendous gold mine of information regarding signs of disease in asymptomatic pathogenic variant carriers from the pre-hospital population. This could give more insight into disease penetrance in pathogenic variant carriers. Over the years, large population-scale biobanks with complete genome-sequencing and phenotype data have been established to study genomics at a population-level, such as the UK Biobank. The UK Biobank contains genotype data, physical measurements, CMR imaging, medical record and questionnaire-based health data of up to 500,000 individuals²⁸.

The final research question of this thesis is as follows:

“What is the contribution of rare and common variants on right and left ventricular function in individuals from the general population?”

For **chapter 11** we leveraged whole exome sequencing (WES) and CMR data from the UK Biobank to identify the presence of CMR abnormalities in undiagnosed pathogenic variant carriers associated with inherited cardiomyopathies from the general population. This chapter also provides the prevalence and disease penetrance of individuals with a pathogenic variant associated with the inherited cardiomyopathies in the general population. Furthermore, we aimed to assess which common variants contribute to LV and RV function and structure (as measured with CMR). Therefore, in **chapter 12** we performed a genome-wide association study (GWAS) in up to 36,548 participants from the UK Biobank to identify genomic variants associated with RV and LV function and structure measured with CMR. Since genetic testing has become a routine clinical care in the diagnosis of inherited cardiomyopathies of patients and family members and thanks to the developments in diagnostic tools, patients and family members are detected at an earlier stage of disease. Early detection of disease, especially in preclinical asymptomatic subjects, provides the opportunity to intervene with prevention strategies or treatments to reduce overall disease morbidity and mortality. However, no treatment exists yet (besides the implantation of an ICD to prevent sudden cardiac death and conventional heart failure treatment). Since genetic variants are randomly allocated at conception, genetic studies in human populations can mirror the design of a randomized controlled trial, also known as mendelian randomization. In chapter 12 a combination of genetic variants identified from our GWAS, protein quantitative trait loci analysis (used to identify genetic variants associated with circulating protein levels) and mendelian randomization were employed to identify potential drug targets for LV and RV dysfunction.

REFERENCES

- Jean-Philippe E, Lerner I, Valentin E, Folke F, Böttiger B, Gislason G, et al. Incidence of Sudden Cardiac Death in the European Union. *J Am Coll Cardiol* 2022;79:1818-1827.
- Al-Khatib SM, Stevenson WG, Ackerman MJ, Bryant WJ, Callans DJ, Curtis AB, et al. 2017 AHA/ACC/HRS Guideline for management of patients with ventricular arrhythmias and the prevention of sudden cardiac death: a report of the American College of Cardiology/American Heart Association Task Force on Clinical Practice Guidelines. *J Am Coll Cardiol* 2018;72:e91–e220. doi:10.1016/j.jacc.2017.10.054.
- Behr ER, Dalageorgou C, Christiansen M, Syrris P, Hughes S, Tome Esteban MT, et al. Sudden arrhythmic death syndrome: familial evaluation identifies inheritable heart disease in the majority of families. *Eur Heart J* 2008;29:1670–1680. doi:10.1093/eurheartj/ehn219.
- Corrado D, Link MS, Calkins H. Arrhythmogenic Right Ventricular Cardiomyopathy. *N Engl J Med* 2017;376:61–72. doi:10.1056/NEJMr1509267.
- van Opbergen CJM, Delmar M, van Veen TAB. Potential new mechanisms of pro-arrhythmia in arrhythmogenic cardiomyopathy: focus on calcium sensitive pathways. *Netherlands Hear J* 2017;25:157–169. doi:10.1007/s12471-017-0946-7.
- Marcus FI, Fontaine GH, Guiraudon G, Frank R, Laurenceau JL, Malergue C, et al. Right ventricular dysplasia: a report of 24 adult cases. *Circulation* 1982;65:384–398.
- Asimaki A, Kleber AG, Saffitz JE. Pathogenesis of Arrhythmogenic Cardiomyopathy. *Can J Cardiol* 2015;31:1313–1324. doi:10.1016/j.cjca.2015.04.012.
- Corrado D, Basso C. Arrhythmogenic left ventricular cardiomyopathy. *Heart* 2022;108:733–743.
- Marcus FI, McKenna WJ, Sherrill D, Basso C, Baucé B, Bluemke DA, et al. Diagnosis of arrhythmogenic right ventricular cardiomyopathy/dysplasia: proposed modification of the task force criteria. *Circulation* 2010;121:1533–1541. doi:10.1161/CIRCULATIONAHA.108.840827.
- Te Riele ASJM, Tandri H, Sanborn DM, Bluemke DA. Noninvasive multimodality imaging in ARVD/C. *JACC Cardiovasc Imaging* 2015;8:597–611. doi:10.1016/j.jcmg.2015.02.007.
- Borgquist R, Haugaa KH, Gilljam T, Bundgaard H, Hansen J, Eschen O, et al. The diagnostic performance of imaging methods in ARVC using the 2010 task force criteria. *Eur Heart J Cardiovasc Imaging* 2014;15. doi:10.1093/ehjci/jeu109.
- Bluemke DA, Krupinski EA, Ovit T, Gear K, Unger E, Axel L, et al. MR Imaging of arrhythmogenic right ventricular cardiomyopathy: morphologic findings and interobserver reliability. *Cardiology* 2003;99:153–162. doi:10.1159/000070672.
- von Knobelsdorff-Brenkenhoff F, Pilz G, Schulz-Menger J. Representation of cardiovascular magnetic resonance in the AHA / ACC guidelines. *J Cardiovasc Magn Reson* 2017;19:70. doi:10.1186/s12968-017-0385-z.
- van Hoorn F, Paproski J, Spears D, Nguyen ET, Wald RM, Ley S, et al. Low diagnostic yield of Late Gadolinium Enhancement (LGE) in screening patients with suspected Arrhythmogenic Right Ventricular Cardiomyopathy (ARVC) by Cardiovascular Magnetic Resonance (CMR). *J Cardiovasc Magn Reson* 2012;14:141. doi:10.1186/1532-429X-14-S1-P141.
- Bosman LP, Cadrin-Tourigny J, Bourfiss M, Aliyari Ghasabeh M, Sharma A, Tichnell C, et al. Diagnosing arrhythmogenic right ventricular cardiomyopathy by 2010 Task Force Criteria: clinical performance and simplified practical implementation. *Eur Eur Pacing, Arrhythmias, Card Electrophysiol J Work Groups Card Pacing, Arrhythmias, Card Cell Electrophysiol Eur Soc Cardiol* 2020;22:787–796. doi:10.1093/europace/ euaa039.
- Bomma C, Rutberg J, Tandri H, Nasir K, Roguin A, Tichnell C, et al. Misdiagnosis of arrhythmogenic right ventricular dysplasia/cardiomyopathy. *J Cardiovasc Electrophysiol* 2004;15:300–306. doi:10.1046/j.1540-8167.2004.03429.x.
- Grothues F, Moon JC, Bellenger NG, Smith GS, Klein HU, Pennell DJ. Interstudy reproducibility of right ventricular volumes, function, and mass with cardiovascular magnetic resonance. *Am Heart J* 2004;147:218–223. doi:10.1016/j.ahj.2003.10.005.
- Bosman LP, Verstraelen TE, van Lint FHM, Cox MGPJ, Groeneweg JA, Mast TP, et al. The Netherlands Arrhythmogenic Cardiomyopathy Registry: design and status update. *Netherlands Hear J* 2019;27:480–486. doi:10.1007/s12471-019-1270-1.
- Petersen SE, Matthews PM, Bamberg F, Bluemke DA, Francis JM, Friedrich MG, et al. Imaging in population science: cardiovascular magnetic resonance in 100,000 participants of UK Biobank - rationale, challenges and approaches. *J Cardiovasc Magn Reson* 2013;15:46. doi:10.1186/1532-429X-15-46.
- Pedrizzetti G, Claus P, Kilner PJ, Nagel E. Principles of cardiovascular magnetic resonance feature tracking and echocardiographic speckle tracking for informed clinical use. *J Cardiovasc Magn Reson* 2016;18:51. doi:10.1186/

- s12968-016-0269-7.
21. Vigneault DM, te Riele ASJM, James CA, Zimmerman SL, Selwaness M, Murray B, et al. Right ventricular strain by MR quantitatively identifies regional dysfunction in patients with arrhythmogenic right ventricular cardiomyopathy. *J Magn Reson Imaging* 2016;43:1132–1139. doi:10.1002/jmri.25068.
 22. Moon JC, Messroghli DR, Kellman P, Piechnik SK, Robson MD, Ugander M, et al. Myocardial T1 mapping and extracellular volume quantification: a Society for Cardiovascular Magnetic Resonance (SCMR) and CMR Working Group of the European Society of Cardiology consensus statement. *J Cardiovasc Magn Reson* 2013;15:92. doi:10.1186/1532-429X-15-92.
 23. Leiner T, Rueckert D, Suinesiaputra A, Baeßler B, Nezafat R, I'gum I, et al. Machine learning in cardiovascular magnetic resonance: basic concepts and applications. *J Cardiovasc Magn Reson* 2019;21:61. doi:10.1186/s12968-019-0575-y.
 24. Camm CF, James CA, Tichnell C, Murray B, Bhonsale A, te Riele ASJM, et al. Prevalence of atrial arrhythmias in arrhythmogenic right ventricular dysplasia/cardiomyopathy. *Heart Rhythm* 2013;10:1661–1668. doi:10.1016/j.hrthm.2013.08.032.
 25. Platonov PG, Christensen AH, Holmqvist F, Carlson J, Haunsø S, Svendsen JH. Abnormal atrial activation is common in patients with arrhythmogenic right ventricular cardiomyopathy. *J Electrocardiol* 2011;44:237-241. doi:10.1016/j.jelectrocard.2010.08.008.
 26. Zareian M, Ciuffo L, Habibi M, Opdahl A, Chamera EH, Wu CO, et al. Left atrial structure and functional quantitation using cardiovascular magnetic resonance and multimodality tissue tracking: validation and reproducibility assessment. *J Cardiovasc Magn Reson* 2015;17:52. doi:10.1186/s12968-015-0152-y.
 27. Kowallick JT, Kutty S, Edelmann F, Chiribiri A, Villa A, Steinmetz M, et al. Quantification of left atrial strain and strain rate using Cardiovascular Magnetic Resonance myocardial feature tracking: a feasibility study. *J Cardiovasc Magn Reson Off J Soc Cardiovasc Magn Reson* 2014;16:60. doi:10.1186/s12968-014-0060-6.
 28. Bycroft C, Freeman C, Petkova D, Band G, Elliott LT, Sharp K, et al. The UK Biobank resource with deep phenotyping and genomic data. *Nature* 2018;562:203–209. doi:10.1038/s41586-018-0579-z.

CHAPTER

2

Current challenges in the diagnosis of arrhythmogenic cardiomyopathies

Mimount Bourfiss, MD;
Richard N. Hauer, MD, PhD

*In C. Brunckhorst, A.M. Saguner, F. Duru, editors. **Current concepts
in arrhythmogenic cardiomyopathy.** Minneapolis: Cardiotext
Publishing; 2021. 73-85*

INTRODUCTION

Arrhythmogenic cardiomyopathies (ACMs) are a group of heart muscle diseases, usually hereditary, characterized histologically by ventricular fibrofatty alteration spreading from the subepicardium toward the subendocardium and clinically by ventricular arrhythmias (VAs) that usually start early in the disease process.¹⁻⁴ Although structural myocardial changes may occur in the early stage, hemodynamic dysfunction is usually an end-stage phenomenon. These characteristics distinguish ACM from dilated cardiomyopathy (DCM) with a different histology, early occurrence of heart failure, and usually ventricular and atrial arrhythmias at later stages. Arrhythmogenic right ventricular dysplasia/cardiomyopathy (ARVD/C) or classical ARVC is the large subcategory of ACM with predominantly right ventricular (RV) involvement, described in the early 1980s by Fontaine and Marcus.¹ However, even in these early years, additional left ventricular (LV) involvement was observed in the end stage of disease. In more recent years, evidence of LV involvement in earlier disease stages at the molecular level has also been identified with immunofluorescence techniques.⁵ Finally, balanced biventricular and predominant LV disease with similar histologic findings and early VA were discovered.⁶ Recently, these observations supported the use of ACM as preferred nomenclature in an increasing number of publications. According to the most widely used definition of ACM, conditions without the typical fibrofatty alteration pattern are not included in this chapter on diagnosis. An alternative definition with a much wider disease spectrum and including also very different histologic patterns such as amyloidosis and Chagas disease has been proposed in a recent Heart Rhythm Society document.⁷ However, that definition is not universally accepted and hence not chosen in this report. The gold standard for ACM diagnosis is the fibrofatty alteration starting subepicardially and moving to the subendocardium.⁴ This means that early in the disease process myocardial cell death and fibrofatty replacement are confined to subepicardial layers. Since fat is a physiologic phenomenon in the subepicardial area and more outspread in the so called cor adiposum, differentiation from ACM may be difficult.⁸ An incremental amount of fibrotic tissue and, if present, cell death are obligatory features for ACM diagnosis.^{3,8} In more advanced stages, the typical histologic changes are frequently transmural in the thin-walled RV. Transmurality is rare in the LV. However, acquisition of appropriate histologic material by endomyocardial biopsy is hampered by the segmental nature of affected areas, usually absent involvement of interventricular septum and predominant subepicardial lesions early in the disease. Obviously, acquisition is easier during cardiac surgery, but only applicable at the end stage. These histologic limitations prompted the development of international consensus-based Task Force Criteria (TFC) for ARVC diagnosis in 1994, and revisions in 2010 (2010 TFC), as the surrogate gold standard.^{9,10} These diagnostic TFC consist of a set of clinically available major and minor criteria in 6 categories (dysfunction and structural, histopathological, repolarization abnormalities, depolarization abnormalities, arrhythmias, and family history). At least 2 major, 1 major + 2 minor, or 4 minor TFC are required for

fulfillment of ARVC diagnosis. In addition, ACM-mimicking disorders should be excluded. The 2010 TFC and methods for acquisition are illustrated in **Table 7.1**.¹⁰ The 2010 TFC are a major improvement for classical ARVC diagnosis since they allow unequivocal diagnosis, facilitate comparison of studies, and are universally accepted. However, the 2010 TFC also have limitations. With focus on the RV, 2010 TFC are less appropriate for LV involvement and inadequate for predominant LV disease. In addition, the focus in the RV is on the RV outflow tract (RVOT), which is open to criticism. Finally, weighing of electrocardiographic and genetic criteria should be reconsidered.

Table 7.1 Revised Task Force Criteria (2010)

Global and/or regional dysfunction and structural alterations (echo, MRI, cine-angio)
Tissue characterizations (histology from biopsy or autopsy)
Repolarization abnormalities (ECG)
Depolarization/conduction abnormalities (ECG, SAECG)
Arrhythmias (ECG, holter, exercise test)
Family history (ARVD/C in first-degree relative, pathogenic mutation)

ARVD/C diagnosis required: 2 major criteria, 1 major + 2 minor or 4 minor criteria, in the absence of other cause.

DIAGNOSIS IN BIVENTRICULAR AND PREDOMINANT LV DISEASE

Clinically relevant LV disease is unusual in classical ARVC, with the exception of the end stage (see **Figure 7.1**), which exhibits similar fibrofatty alteration in the RV and LV (**Figure 7.2**). RV predominance is very typical for ACM-associated desmosomal PKP2 mutation carriers.¹¹⁻¹⁴ In many cohorts, PKP2 is by far the most frequent molecular genetic abnormality in classical ARVC. Although ACM is frequently described as a disease of the desmosome, different desmosomal mutations may be associated with different disease patterns. The desmosomal DSP is associated with biventricular or even predominant LV disease (**Figure 7.3**), similar to the non-desmosomal PLN mutation.^{13,15-19} Nevertheless, all these different disease entities show very similar fibrofatty alteration patterns, justifying ACM as unifying preferred terminology.⁴ In the 2010 TFC, only inverted T waves in the left precordial leads V4–V6 reflect LV involvement and only as a minor criterion.¹⁰

In ACM with LV disease, the majority of electrocardiographic and imaging 2010 TFC may be absent, hampering diagnostic fulfillment. In addition, ACM patients with LV disease may not show ventricular tachycardia (VT) with left bundle branch block (LBBB) morphology. Different from classical ARVC, they may show VT with right bundle branch block (RBBB) morphology, reflecting the LV origin of the arrhythmia. However, RBBB-VT is not part of the 2010 TFC. Since ventricular mass is predominantly related to LV mass, and myocardial

mass is related to QRS amplitude, low voltages in the electrocardiogram (ECG) during sinus rhythm are expected in late stages of LV disease.²⁰ Similarly, this larger LV mass precludes akinesia, dyskinesia, dilatation, and lowering of the ejection fraction in the earlier stages of LV disease with usually nontransmural lesions.²¹ Thus, structural and hemodynamic dysfunction equivalents of ACM starting in the RV are not likely seen in the LV, at least in the earlier stages. This means that the role of echocardiography and conventional cardiac magnetic resonance (CMR) is limited. Fortunately, the newer late gadolinium enhancement (LGE) technique during CMR, not used in the 2010 TFC scoring, is able to visualize smaller, non-transmural lesions reflecting fibrofatty areas.²¹ Thus, awareness of ACM as not only an RV disease but frequently also an LV disease and existence of even predominant LV sub-categories prompt consideration of the following additional parameters for diagnostic evaluation:

- LGE-CMR to demonstrate LV lesions
- VT with RBBB morphology
- Low-voltage ECG (< 0.5 mV in standard leads during sinus rhythm)

Adding these parameters to the 2010 TFC will avoid ACM underdiagnosis. However, it should be realized that these parameters need confirmation and that their weight in relation to existing TFC is still unknown.

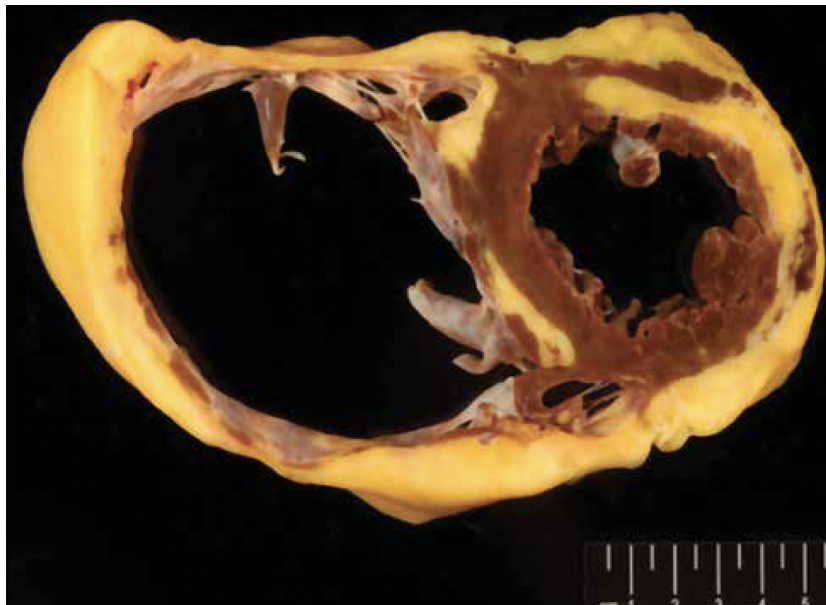


Figure 7.1 Slice of the explanted heart from a 56-year-old woman with end-stage ACM and the pathogenic missense mutation PKP2 c.2386T>C. The RV is severely dilated, and the free wall is nearly completely transmurally replaced by fibrofatty tissue. In addition, there is extensive fibrofatty alteration in the LV and septum. The LV shows the typical predominant subepicardial involvement.

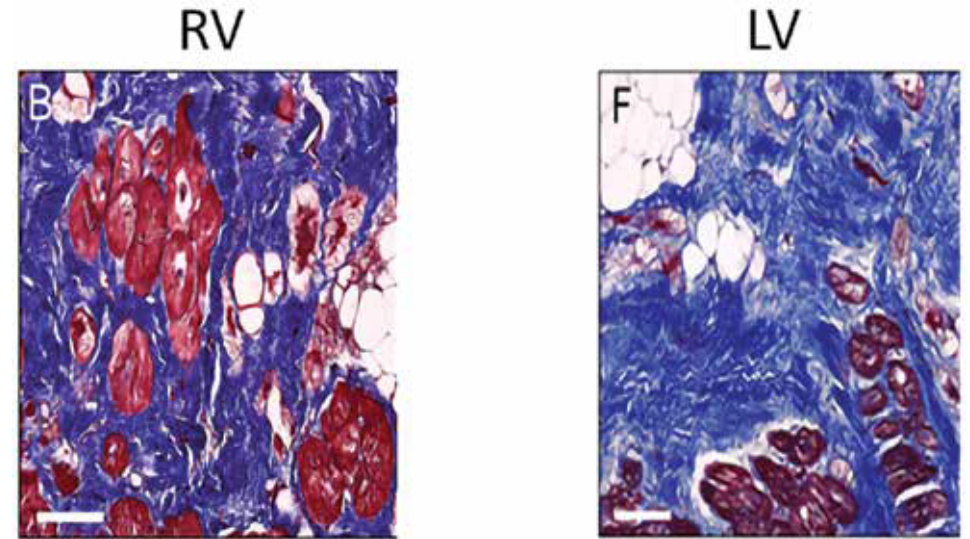


Figure 7.2 Histology from the heart in Figure 7.1 of the RV (left panel) and LV (right panel) shows similar fibrofatty alterations (modified AZAN staining). Surviving myocardial bundles are shown (red) embedded in fibrous tissue (blue) and fields of fat cells (white).

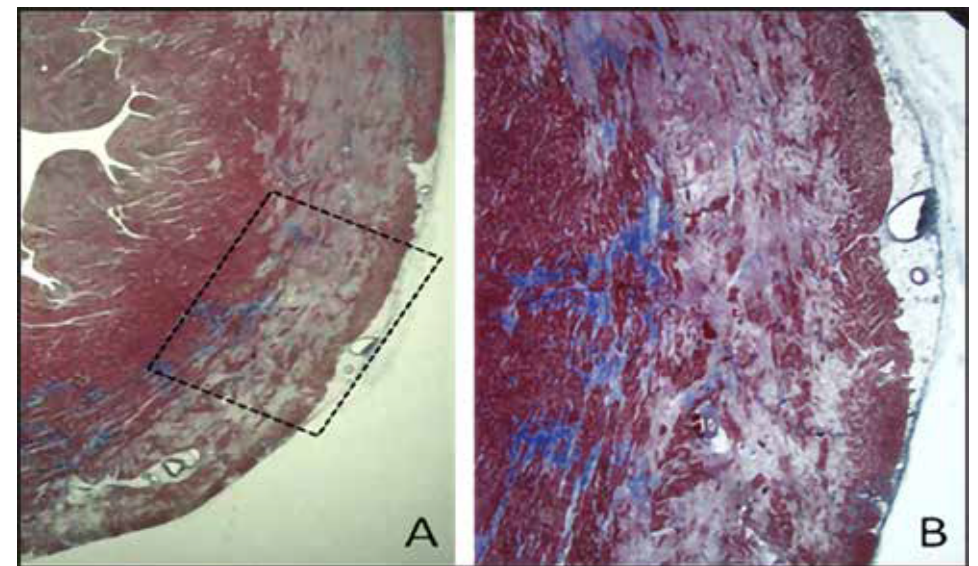


Figure 7.3 LV histology at two different magnifications from a 15-year-old sudden cardiac death victim with a pathogenic DSP mutation. In Panel A, the typical subepicardial involvement is visible. In Panel B, with more magnification, fibrofatty alterations are seen. The RV did not show obvious abnormality. Eight months before death, none of the 2010 TFC have been identified. (Figure reproduced with permission from Oxford University Press. Zorzi et al., *Europace*. 2016;18(7):953–954.16)

ELECTROCARDIOGRAPHIC CHALLENGES IN ACM DIAGNOSIS

In the 2010 TFC, the epsilon wave is a major criterion, since this finding is associated with advanced ACM. Comparing different studies, the incidence of epsilon waves varies between 2% in family members of ACM patients and 15% in index patients in the largest ACM study consisting of more than 1000 ACM patients and their family members, and much higher percentages in some other studies.¹⁴ These differences may be due to differences in disease severity, but may also relate to the use of different definitions of the epsilon wave. Lower percentages are obtained by using the original definition by Fontaine *et al.* as low-amplitude signals after and clearly separated from the QRS complex in leads V1–V3.^{22,23} Separation suggests the presence of an isoelectric line between the epsilon wave and the preceding QRS complex. However, identification of this isoelectric line depends on recording speed, filter setting, magnification, and sampling frequency. **Figure 7.4** shows an example of an ECG recorded from a patient with advanced ACM, negative T waves in V1–V5 (major repolarization criterion), prolonged terminal activation duration (TAD, 110 ms), and the suggestion of an epsilon wave (major depolarization criterion).²³ With 2 major criteria, this ECG already fulfills 2010 TFC for ACM diagnosis. However, separation from the QRS complex may be questioned, since very tiny signals are visible. Those who do not include the separation are faced with defining the end of the QRS complex and the onset of the epsilon wave. In a multicenter study by Platonov *et al.*, epsilon wave identification showed high interobserver variability.²⁴ In addition, all patients with interpretation of an epsilon wave had prolonged TAD (minor depolarization criterion) and showed ACM fulfillment independent of the epsilon wave.

Inverted T waves in the right precordial leads is much more common in athletes than in nonathletes in an apparently normal population.²⁵ Particularly with negative T waves in V1–V3 and beyond (major TFC criterion) and dilated RV, which can be found in normal athletes, differentiation with ACM may be difficult. Absence of abnormal depolarization and akinesia/dyskinesia support absence of ACM. In a recent study comparing 100 healthy athletes with 100 ACM patients, no premature ventricular complexes (PVCs) in the athletes and at least 1 PVC in 18 ACM patients ($P < 0.001$) were recorded during 10-second ECG recording. In addition, QRS voltages were significantly higher in the athletes.²⁶

Both the depolarization criteria—epsilon wave and prolonged TAD (≥ 55 ms)—and the repolarization criteria of inverted T wave in V1–V2 and V1–V3 and beyond focus on right precordial leads. That focus may be questioned. The right precordial leads reflect primarily electrical phenomena from the RVOT. However, the frequently recorded VT with LBBB morphology with superior axis (major arrhythmia TFC) is not originating from the RVOT.¹⁰ The RVOT belongs to the “triangle of dysplasia” consisting of the 3 RV sites—the RVOT

and subtricuspid and apical areas—most often affected in classical ARVC according to the original description of the disease in 1982.¹ This observation was primarily obtained from studying patients in advanced disease stages. A recent CMR study by te Riele *et al.* could confirm this observation if ≥ 3 RV regions were affected.²¹ However, with only 1 or 2 affected regions, it was exclusively localized in the subtricuspid (or peritricuspid) area. This finding suggests disease onset close to the tricuspid valve and not in the RVOT or RV apex (**Figure 7.5**). This finding is clinically relevant since it prompts us to identify subtricuspid disease markers for early disease detection. Under physiologic conditions, the RVOT is usually the latest activated area. Thus, additional pathological activation delay is relatively easily detectable in the RVOT and thus in right precordial leads by TAD prolongation.²³ Physiologically, subtricuspid activation is usually earlier, indicating that local additional delay may remain buried within the QRS complex. Nevertheless, extreme delay may become visible as late activation mimicking precordial TAD but now recorded from the inferior leads (see **Figure 7.4**, **Figure 7.6**, and **Figure 7.7**).

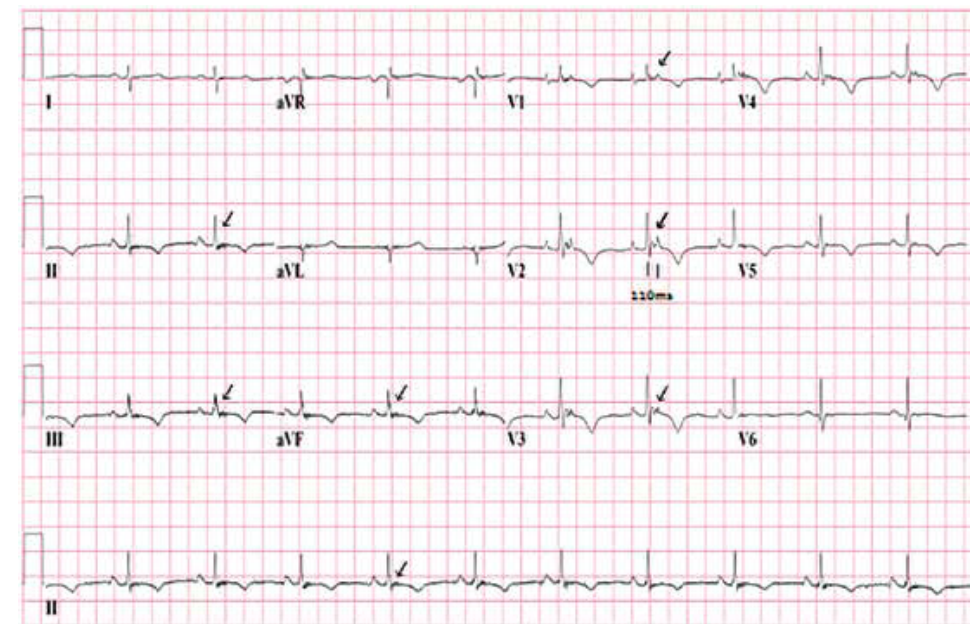


Figure 7.4 ECG during sinus rhythm from a patient with advanced ACM. Terminal activation duration is severely prolonged at 110 ms (minor criterion). The latest depolarization deflection indicated by arrows in V1–V3 may be interpreted as epsilon waves. However, tiny deflections are visible between this deflection and the preceding QRS complex. T-wave inversion in V1–V5 (major criterion). In addition, multiple late signals are present in inferior leads. (Reproduced with permission from Cardiotext Publishing, LLC.)

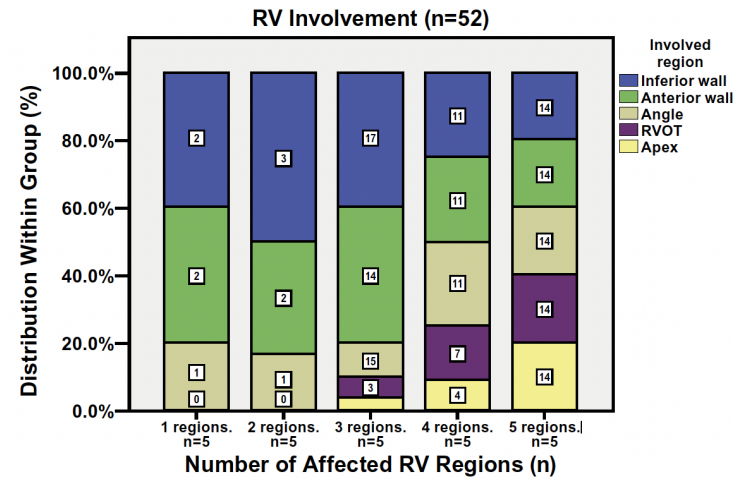


Figure 7.5 Number of affected RV regions in 52 ACM patients related to distribution of specific regions in percentages. If only 1 or 2 regions are affected, RV apex and RVOT are not involved. (Figure reproduced with permission from Wiley. Te Riele et al., *J Cardiovasc Electrophysiol.* 2013;24:1311–1320.21)

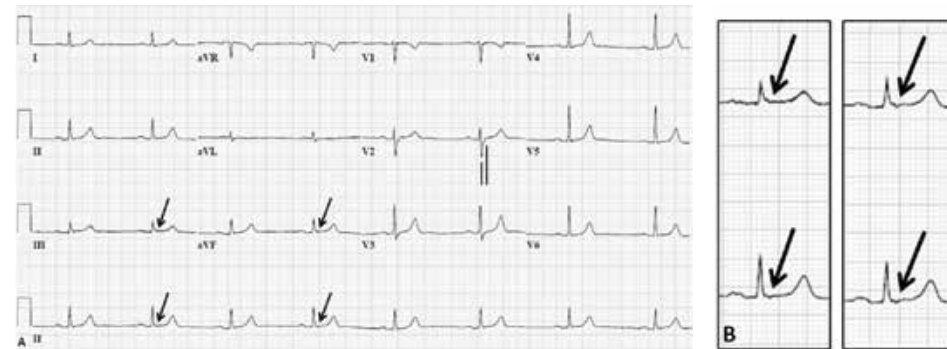


Figure 7.6 Apparently normal ECG during sinus rhythm, although terminal activation duration is marginally prolonged at 60 ms. However, very low amplitude but reproducible late depolarization signals are recorded in the inferior leads, enlarged in the right panel. (Reproduced with permission from Cardiotext Publishing, LLC.)

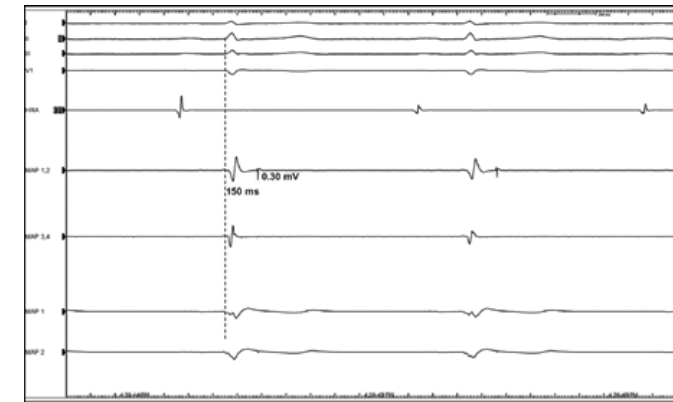


Figure 7.7 Electrophysiologic study during sinus rhythm in the patient from Figure 7.6. From above, ECG leads I, II, III, and V1, bipolar recordings from the high right atrium, subtricuspid area (MAP 1,2 and MAP 3,4), and corresponding unipolar recordings MAP1 and MAP 2, from tip and second electrode. The vertical line indicates the onset of the QRS complex. In MAP1,2 a late 0.30 mV high dV/dt signal is recorded at 150 ms after QRS onset. The unipolar recording shows that this signal is derived from close to the position of electrode MAP2 in the subtricuspid area. Earlier, higher-amplitude but lower dV/dt signals are from remote regions. (Reproduced with permission from Cardiotext Publishing, LLC.)

Recordings in **Figure 7.4** are from a severely affected patient with 2 major electrocardiographic TFC from right precordial leads. In addition, late depolarization with multiple deflections and inverted T waves are recorded from the inferior leads. **Figure 7.6** shows an apparently normal ECG in a patient with a pathogenic PKP2 mutation. However, TAD is marginally at 60 ms prolonged, and with close observation, reproducibly isolated, late, low-amplitude signals are visible derived from the inferior leads. Remarkably, no inverted T waves are seen in this recording. An electrophysiologic study proved late depolarization as cause of these signals (**Figure 7.7**).²⁷ CMR showed a subtricuspid aneurysm in the absence of other pathologic markers (**Figure 7.8**).²⁷ Since in less advanced ACM stages, ECG signs of subtricuspid involvement remain invisible, other diagnostic techniques such as LGE-CMR, feature tracking CMR, and echocardiographic deformation imaging are promising for early ACM diagnosis.^{28–30} The last 2 techniques are based on delayed contraction, at least partly due to late electrical activation. **Figure 7.9** shows a normal 12-lead ECG without any sign of depolarization or repolarization abnormality. However, echocardiographic deformation imaging shows exclusively late contraction in the subtricuspid area (**Figure 7.10**).²⁸ Similar results are obtainable with feature tracking CMR.³⁰ More focus on the early affected subtricuspid area is clinically relevant since Sudden Cardiac Death (SCD) is frequently the first ACM manifestation, particularly in young individuals as shown in several studies.^{13,31–33} One of these studies compared first presentation with ACM in 427 adults >18 years of age versus 75 pediatric patients < 18 years.³² Combined SCD and resuscitated cardiac arrest in the adult and pediatric population occurred in 9% and 26%, respectively (**Figure 7.11**). In another study with 66 cardiac arrest cases in ACM, more than half of the victims appeared

to be asymptomatic before this event.³³ In young individuals still in the early preclinical or concealed stages of ACM, fulfillment of diagnostic criteria may be absent. Ventricular fibrillation (VF) may be labeled as idiopathic VF and an implantable cardioverter-defibrillator (ICD) is implanted to prevent sudden death.³⁴ Beside ICD interrogation, regular cardiologic evaluation with at least family history, 12-lead ECG, and echocardiography is needed, and in some cases also additional DNA analysis.

Using this continuous evaluation ACM diagnostic fulfillment may occur many years after first presentation.³⁴ Definite diagnosis is important for cascade screening of family members as a first step in risk stratification. Use of alternative diagnostic ECG methods such as signal averaged ECG (SAECG, included in 2010 TFC) and QRS fractionation (fQRS) are hampered by several limitations.^{35–38} Both methods are not universally used, and the use of SAECG for ACM diagnosis is decreasing. Moreover, late potentials recorded by SAECG are equivalents of easily obtained prolonged TAD in V1–V3 and late depolarization signals derived from other leads in the routine 12-lead ECG. Qualitative fQRS is prone to subjectivity and poor reproducibility between studies.^{36–38} Quantitative methods for ACM diagnosis are not available yet.

Thus, contribution of the routine 12-lead ECG to ACM diagnosis is hampered by:

- Inaccuracy and nonreproducibility of epsilon wave recording.
- Although very appropriate in overt classic ARVC stages, less usefulness of precordial depolarization/repolarization abnormality detection in the early disease stage, because of evidence of early exclusive subtricuspid involvement.
- Absence of ECG detectability of subtricuspid involvement except in advanced stages, necessitating the use of new imaging techniques.
- ACM overdiagnosis by precordial T-wave inversion creating ACM phenocopies in athletes.

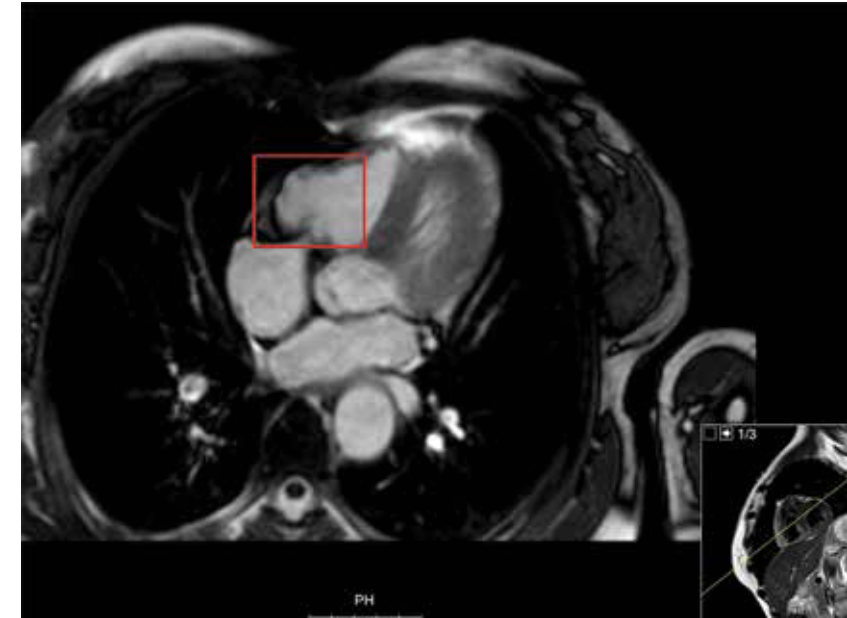


Figure 7.8 CMR image from the patient in Figures 7.6 and 7.7, showing a subtricuspid aneurysm. (Reproduced with permission from Cardiotext Publishing, LLC.)

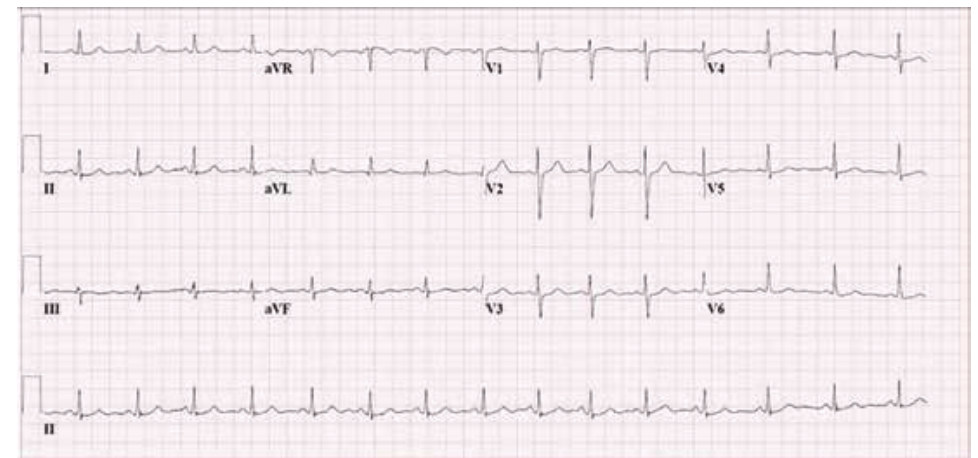


Figure 7.9 ECG from an asymptomatic pathogenic PKP2 (c.397C>T) carrier. The ECG is normal and without depolarization or repolarization abnormalities. (Reproduced with permission from Wiley.)

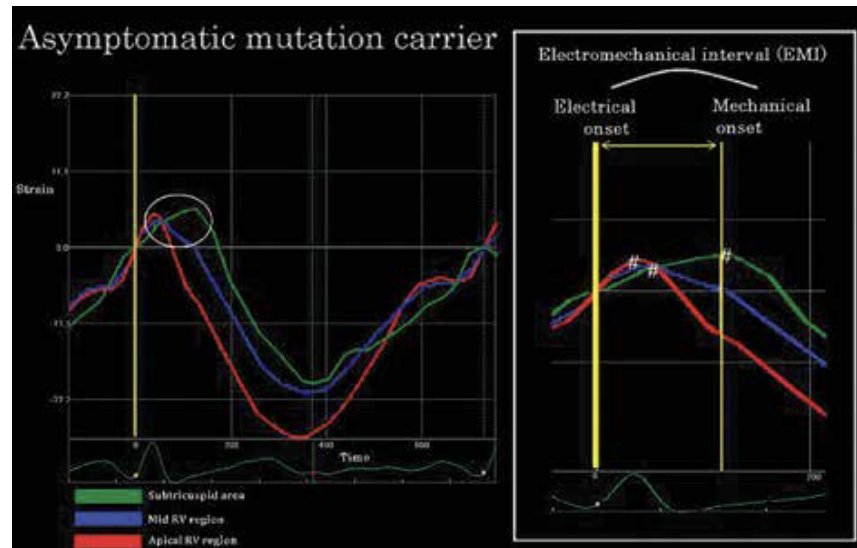


Figure 7.10 RV deformation imaging in the asymptomatic patient from Figure 7.9, magnified at the right side. Apical and midventricular curves are normal, whereas the subtricuspid area shows marked delayed contraction, at least partly due to local delayed electrical activation, not visible with the ECG. (Reproduced with permission from Wiley.)

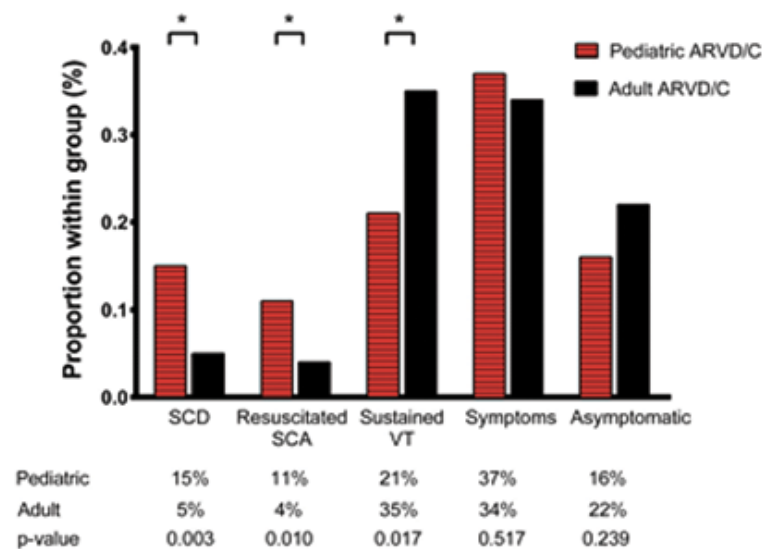


Figure 7.11 First presentation in ACM in adult (age ≥ 18 years, $n = 475$) versus pediatric (age < 18 years, $n = 75$) patients. SCD and resuscitated cardiac arrest are the first ACM manifestations in 9% of adult population and in the 26% of children. (Figure reproduced with permission from Elsevier. Te Riele et al., *JACC Clin Electrophysiol.* 2015;1:551–560.32)

GENETIC CHALLENGES IN ACM DIAGNOSIS

The current 2010 TFC consist of 3 major and 3 minor genetic criteria.¹⁰ Further weighting within the major and minor criteria is not available yet. A pathogenic or likely pathogenic mutation is counted as major criterion. However, the high genetic noise due to frequent disease associated genetic variants in the normal population and other cardiomyopathies are associated with the risk of misdiagnosis, particularly if the phenotype scoring reveals only 1 major or 2 minor criteria.^{35,39} In addition, increasing genetic knowledge may devalue a likely pathogenic variant to a variant of unknown significance. This means that results of molecular-genetic analysis should be interpreted by experts in the field. Since identification of a disease causing mutation in the proband allows cascade screening in the family as a first step in their risk stratification, molecular-genetic analysis remains pivotal.^{13,14}

CONCLUSION

Appropriate weighting of the contribution of each individual criterion of the 2010 TFC is still missing. Diagnostic challenges in ACM are in under- and overdiagnosis. Underdiagnosis is related to (1) ignorance of LV and RV subtricuspid involvement and (2) paucity of criteria in early disease stage and young individuals. Inclusion of LGE-CMR and new imaging techniques such as echocardiographic deformation imaging and feature tracking CMR may contribute to improve the current TFC. Overdiagnosis relates to (1) inappropriate use of ECG and imaging criteria, (2) uncertainty about pathogenicity of gene variants, and (3) ACM phenocopies. Devaluation of major criterion status of epsilon wave and likely pathogenicity may contribute to decrease of overdiagnosis.

REFERENCES

- Marcus FI, Fontaine GH, Guiraudon G, et al. Right ventricular dysplasia: A report of 24 adult cases. *Circulation*. 1982;65(2):384–398.
- Corrado D, Basso C, Thiene G, et al. Spectrum of clinicopathologic manifestations of arrhythmogenic right ventricular cardiomyopathy/dysplasia: A multicenter study. *J Am Coll Cardiol*. 1997;30:1512–1520.
- Basso C, Thiene G, Corrado D, et al. Arrhythmogenic right ventricular cardiomyopathy: Dysplasia, dystrophy, or myocarditis? *Circulation*. 1996;94:983–991.
- Sepehrkhouy S, Gho J, van Es R, et al. Distinct fibrosis pattern in desmosomal and phospholamban mutation carriers in hereditary cardiomyopathies. *Heart Rhythm*. 2017;14:1024–1032.
- Asimaki A, Tandri H, Huang H, et al. A new diagnostic test for arrhythmogenic right ventricular cardiomyopathy. *N Engl J Med*. 2009;360:1075–1064.
- Sen-Chowdry S, Syrris P, Prasad SK, et al. Left-dominant arrhythmogenic cardiomyopathy: An under-recognized clinical entity. *J Am Coll Cardiol*. 2008;52:2175–2187.
- Towbin JA, McKenna WJ, Abrams DJ, et al. 2019 HRS expert consensus statement on evaluation, risk stratification, and management of arrhythmogenic cardiomyopathy. *Heart Rhythm*. 2019;16(11):e301–e372.
- Basso C, Thiene G. Adipositas cordis, fatty infiltration of the right ventricle, and arrhythmogenic right ventricular cardiomyopathy. Just a matter of fat? *Cardiovasc Pathol*. 2005.
- McKenna WJ, Thiene G, Nava A, et al. Diagnosis of arrhythmogenic right ventricular dysplasia/cardiomyopathy. Task Force of the Working Group Myocardial and Pericardial Disease of the European Society of Cardiology and of the Scientific Council on Cardiomyopathies of the International Society and Federation of Cardiology. *Br Heart J*. 1994;71:215–218.
- Marcus FI, McKenna WJ, Sherrill D, et al. Diagnosis of arrhythmogenic right ventricular cardiomyopathy/dysplasia: Proposed modification of the task force criteria. *Eur Heart J*. 2010;31:806–814.
- Van Tintelen JP, Entius MM, Bhuiyan ZA, et al. Plakophilin-2 mutations are the major determinant of familial arrhythmogenic right ventricular dysplasia/cardiomyopathy. *Circulation*. 2006;113:1650–1658.
- Cox MG, van der Zwaag PA, van der Werf C, et al. Arrhythmogenic right ventricular dysplasia/cardiomyopathy: Pathogenic desmosome mutations in index-patients predict outcome of family screening: Dutch arrhythmogenic right ventricular dysplasia/cardiomyopathy genotype-phenotype follow-up study. *Circulation*. 2011;123:2690–2700.
- Bhonsale A, Groeneweg JA, James CA, et al. Impact of genotype on clinical course in arrhythmogenic right ventricular dysplasia/cardiomyopathy-associated mutation carriers. *Eur Heart J*. 2015;36:847–855.
- Groeneweg JA, Bhonsale A, James CA, et al. Clinical presentation, long-term follow-up, and outcomes of 1001 arrhythmogenic right ventricular dysplasia/cardiomyopathy patients and family members. *Circ Cardiovasc Genet*. 2015;8:437–446.
- Norman M, Simpson M, Mogensen J, et al. Novel mutation in desmoplakin causes arrhythmogenic left ventricular cardiomyopathy. *Circulation*. 2005;112:636–642.
- Zorzi A, Rigato I, Pilichou K, et al. Phenotypic expression is a prerequisite for malignant arrhythmic events and sudden cardiac death in arrhythmogenic right ventricular cardiomyopathy. *Europace*. 2016;18(7):953–954.
- Van der Zwaag PA, van Rijsingen IA, Asimaki A, et al. Phospholamban R14del mutation in patients diagnosed with dilated cardiomyopathy or arrhythmogenic right ventricular cardiomyopathy: Evidence supporting the concept of arrhythmogenic cardiomyopathy. *Eur J Heart Fail*. 2012;14:1199–1207.
- Groeneweg JA, van der Zwaag PA, Jongbloed JD, et al. Left-dominant arrhythmogenic cardiomyopathy in a large family: Associated desmosomal or nondesmosomal genotype? *Heart Rhythm*. 2013;10:548–559.
- Groeneweg JA, van der Zwaag PA, Olde Nordkamp LR, et al. Arrhythmogenic right ventricular dysplasia/cardiomyopathy according to revised 2010 Task Force Criteria with inclusion of non-desmosomal phospholamban mutation carriers. *Am J Cardiol*. 2013;112:1197–206.
- di Gioia CR, Giordano C, Cerbelli B, et al. Nonischemic left ventricular scar and cardiac sudden death in the young. *Hum Pathol*. 2016;58:78–89.
- te Riele AS, James CA, Philips B, et al. Mutation-positive arrhythmogenic right ventricular dysplasia/cardiomyopathy: The triangle of dysplasia displaced. *J Cardiovasc Electro-physiol*. 2013;24:1311–1320.
- Fontaine G, Umemura J, Di Donna P, et al. Duration of QRS complexes in arrhythmogenic right ventricular dysplasia-cardiomyopathy: A new non-invasive diagnostic marker. *Ann Cardiol Angeiol (Paris)*. 1993;42:399–405.
- Cox MGPJ, Nelen MR, Wilde AAM, et al. Activation delay and VT parameters in arrhythmogenic right ventricular dysplasia/cardiomyopathy toward improvement of diagnostic ECG criteria. *J Cardiovasc Electro-physiol*. 2008;19:775–781.
- Platonov PG, Calkins H, Hauer RN, et al. High interobserver variability in the assessment of epsilon waves: Implications for diagnosis of arrhythmogenic right ventricular cardiomyopathy/dysplasia. *Heart Rhythm*. 2016;13:208–216.
- Zaidi A, Sheikh N, Jongman JK, et al. Clinical differentiation between physiological remodeling and arrhythmogenic right ventricular cardiomyopathy in athletes with marked electrocardiographic repolarization anomalies. *J Am Coll Cardiol*. 2015;65:2702–2711.
- Brosnan MJ, te Riele ASJM, Bosman LP, et al. Electrocardiographic features differentiating arrhythmogenic right ventricular cardiomyopathy from an athlete's heart. *JACC Clin Electrophysiol*. 2018;4(12):1626–1628.
- ECG masters' collection, eds. Shenassa M, Josephson ME, Estes NA, Amsterdam EA, Scheinman M. 2017:461–463.
- Mast TP, Teske AJ, te Riele ASJM, et al. Prolonged electromechanical interval unmasks arrhythmogenic right ventricular dysplasia/cardiomyopathy in the subclinical stage. *J Cardiovasc Electro-physiol*. 2016;27(3):303.
- Mast TP, James CA, Calkins H, et al. Evaluation of structural progression in arrhythmogenic right ventricular dysplasia/cardiomyopathy. *JAMA Cardiol*. 2017;2:293–302.
- Bourfiss M, Vigneault DM, Aliyari Ghasebeh, et al. Feature tracking CMR reveals abnormal strain in preclinical arrhythmogenic right ventricular dysplasia/cardiomyopathy: a multisite feasibility and clinical implementation study. *J Cardiovasc Magn Reson*. 2017;19(1):66. <https://doi.org/10.1186/s12968-017-0380-4>.
- Quarta G, Muir A, Pantazis A, et al. Familial evaluation in arrhythmogenic right ventricular cardiomyopathy: Impact of genetics and revised task force criteria. *Circulation*. 2011;123:2701–2709.
- te Riele A, James CA, Sawant AC, et al. Arrhythmogenic right ventricular dysplasia/cardiomyopathy in the pediatric population: Clinical characterization and comparison with adult-onset disease. *JACC Clin Electrophysiol*. 2015;1:551–560.
- Gupta R, Tichnell C, Murray B, et al. Comparison of features of fatal versus nonfatal cardiac arrest in patients with arrhythmogenic right ventricular dysplasia/cardiomyopathy. *Am J Cardiol*. 2017 Jul 1;120(1):111–117.
- Blom LJ, te Riele ASJM, Vink A, et al. Late evolution of arrhythmogenic cardiomyopathy in patients with initial presentation as idiopathic ventricular fibrillation. *Heart Rhythm Case Rep*. 2019;5(1):25–30.

PART I

Feasibility and reproducibility of novel CMR techniques in ARVC



CHAPTER

3

Feature tracking CMR reveals abnormal strain in preclinical arrhythmogenic right ventricular dysplasia/ cardiomyopathy: a multisoftware feasibility and clinical implementation study

Mimount Bourfiss, BS;
Davis M. Vigneault, BS;
Mounes Aliyari Ghasebeh, MD;
Brittney Murray, MS;
Cindy A. James, PhD;
Crystal Tichnell, MGC;
Firdaus A. Mohamed Hoesein, MD, PhD;
Stefan L. Zimmerman, MD;
Ihab R. Kamel, MD, PhD;
Hugh Calkins, MD;
Harikrishna Tandri, MD;
Birgitta K. Velthuis, MD, PhD;
David A. Bluemke, MD, PhD;
Anneline S.J.M. te Riele, MD, PhD.

ABSTRACT

Background: Regional right ventricular (RV) dysfunction is the hallmark of Arrhythmogenic Right Ventricular Dysplasia/Cardiomyopathy (ARVD/C), but is currently only qualitatively evaluated in the clinical setting. Feature Tracking Cardiac Magnetic Resonance (FT-CMR) is a novel quantitative method that uses cine CMR to calculate strain values. However, most prior FT-CMR studies in ARVD/C have focused on global RV strain using different software methods, complicating implementation of FT-CMR in clinical practice. We aimed to assess the clinical value of global and regional strain using FT-CMR in ARVD/C and to determine differences between commercially available FT-CMR software packages.

Methods: We analyzed cine CMR images of 110 subjects (39 overt ARVD/C [mutation+/phenotype+], 40 preclinical ARVD/C [mutation+/phenotype-] and 31 control) for global and regional (subtricuspid, anterior, apical) RV strain in the horizontal longitudinal axis using four FT-CMR software methods (Multimodality Tissue Tracking, TomTec, Medis and Circle Cardiovascular Imaging). Intersoftware agreement was assessed using Bland Altman plots.

Results: For global strain, all methods showed reduced strain in overt ARVD/C patients compared to control subjects ($p < 0.041$), whereas none distinguished preclinical from control subjects ($p > 0.275$). For regional strain, overt ARVD/C patients showed reduced strain compared to control subjects in all segments which reached statistical significance in the subtricuspid region for all software methods ($p < 0.037$), in the anterior wall for two methods ($p < 0.005$) and in the apex for one method ($p = 0.012$). Preclinical subjects showed abnormal subtricuspid strain compared to control subjects using one of the software methods ($p = 0.009$). Agreement between software methods for absolute strain values was low (Intraclass Correlation Coefficient=0.373).

Conclusions: Despite large intersoftware variability of FT-CMR derived strain values, all four software methods distinguished overt ARVD/C patients from control subjects by both global and subtricuspid strain values. In the subtricuspid region, one software package distinguished preclinical from control subjects, suggesting the potential to identify early ARVD/C prior to overt disease expression.

Keywords: Feature Tracking Cardiac Magnetic Resonance Imaging, regional myocardial strain, global myocardial strain, software comparison study, Arrhythmogenic Right Ventricular Dysplasia/Cardiomyopathy.

BACKGROUND

Feature Tracking Cardiac Magnetic Resonance (FT-CMR) is a rapidly emerging approach for the quantitative and noninvasive evaluation of regional myocardial function. It employs a frame-to-frame recognition of a preset feature during the cardiac cycle, which allows for the calculation of myocardial displacement during systole expressed in strain values^{1,2}. Compared to other strain analysis techniques, e.g. CMR tissue tagging and echocardiographic speckle tracking, FT-CMR has shorter post-processing times, may be less operator dependent, and can be applied to routine cine CMR images³. In addition, FT-CMR has major advances over other deformation techniques in the evaluation of the right ventricle (RV), since it allows for reliable tracking of the highly trabeculated and thin walled RV and is not hampered by the anatomic localization of the RV behind the sternum^{4,5}. As such, FT-CMR may play an important role in the evaluation of diseases affecting the RV.

Arrhythmogenic right ventricular dysplasia/cardiomyopathy (ARVD/C) is an inherited cardiomyopathy that primarily affects RV morphology and function⁶. Since one of the most feared disease presentations (especially in the young and in athletes) is sudden cardiac death, early diagnosis is of utmost importance^{7,8}. One of the hallmarks of ARVD/C is regional dysfunction of the RV wall⁹. However, most prior studies have focused on evaluation of global RV strain in clinically overt ARVD/C patients¹⁰⁻¹². We hypothesize that FT-CMR may be useful for early disease detection in ARVD/C by identifying regional myocardial dysfunction prior to overt disease development.

FT-CMR of the RV is relatively new, and early results have shown the feasibility of the method in ARVD/C¹²⁻¹⁴. For clinical implementation, it is important that FT-CMR is reproducible and that different software methods provide comparable strain values. We therefore aimed to 1) assess intersoftware agreement of RV global and regional longitudinal strain using FT-CMR; and 2) compare global and regional strain in definite ARVD/C patients, preclinical ARVD/C subjects and control subjects to analyze the value of regional strain as an early diagnostic parameter. To accomplish this, we used a unique cohort of well-phenotyped ARVD/C subjects that includes both affected patients and at-risk mutation carriers.

MATERIALS AND METHODS

Study Population

We included 110 subjects who were evaluated for ARVD/C at the Johns Hopkins Hospital and were included in the Johns Hopkins ARVD/C registry (*ARVD.com*). Cases included 79 ARVD/C-associated desmosomal mutation carriers who were divided in two groups: 1) overt ARVD/C (those fulfilling 2010 diagnostic Task Force Criteria [TFC] for ARVD/C, n=39);

and 2) preclinical ARVD/C (those not fulfilling 2010 diagnostic TFC for ARVD/C, $n=40$)¹⁵. All overt patients were diagnosed with ARVD/C independent of CMR, so that the diagnostic TFC provide an independent standard of reference. As a control group, we included 31 individuals who were mutation-negative family members of mutation-positive ARVD/C patients ($n=9$), or subjects without ARVD/C upon comprehensive clinical evaluation ($n=22$). All subjects were also included in a prior study from our group¹³. Patients provided written informed consent, and the study protocol was approved by the Johns Hopkins School of Medicine Institutional Review Board.

CMR Acquisition

All CMR images were acquired on a 1.5 Tesla scanner (Avanto, Siemens Medical Imaging, Erlangen, Germany) using a balanced, steady state free precession sequence (repetition time/echo time/flip angle -2.4/1.2/50-75 degrees, matrix 256-192, field of view 30-36cm, temporal resolution ≤ 40 msec, slice thickness 6-8mm).

FT-CMR software methods

Peak longitudinal strain measurements were performed using four different commercially available FT-CMR software methods: 1) Medis Qstrain Software (Medis Medical Imaging Systems, version 2.1.12.2. Leiden, the Netherlands); 2) TomTec (TomTec Imaging Systems, version 2D CPA MR 1.2. Unterschleissheim, Germany); 3) Multimodality Tissue Tracking (MTT) (Toshiba Medical Systems Corporation, version 6.0.4725. Tokyo, Japan); and 4) Circle Cardiovascular Imaging (CVI42, version 5.6.2. Calgary, Canada). The most recent software versions available at time of measurement were used.

Quantitative analysis

Myocardial strain analysis using FT-CMR

Since previous studies have shown that wall motion abnormalities in ARVD/C are most reliably measured in the horizontal long axis (HLA, i.e. four chamber view), we used this view to determine peak longitudinal strain as a primary variable of interest^{3,13,14}. To ensure comparability between measurements, the most central slice in which the valve plane was visible was chosen for analysis. RV free wall endocardial contours were manually drawn during end-diastole and/or end-systole (as required by the individual software method) with subsequent automatic tracking during the cardiac cycle. As an example, a cine CMR movie file of the RV free wall endocardial tracking is available as **Additional File 1**. Endocardial tracking was visually evaluated and manually corrected if possible to ensure accurate tracking. Subsequently, the endocardial border was automatically segmented into three regions of equal size that were denoted subtricuspid, anterior, and apical wall (see **Figure 1**), as previously described¹³. Global strain was defined as the average peak strain value across all segments.

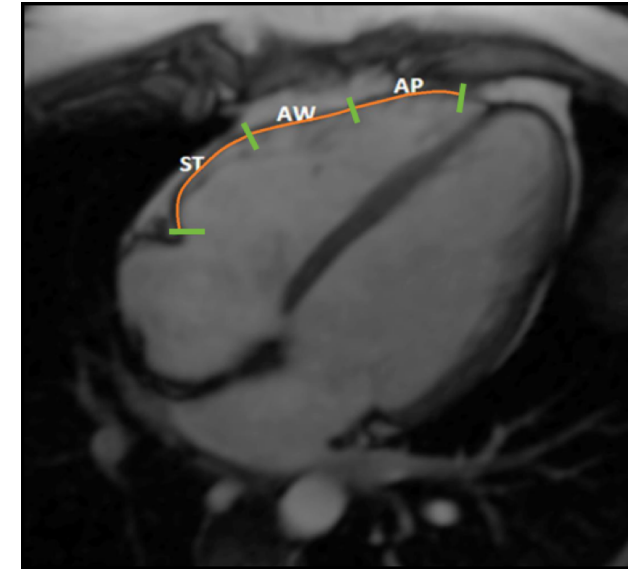


Figure 1: representative right ventricular segmentation used in Feature Tracking Cardiac Magnetic Resonance Imaging. Abbreviations: ST= subtricuspid region; AW= anterior wall region; AP= apical region

Global RV size and ejection fraction

RV and left ventricular (LV) dimensions and function were measured with CVI42 (Circle Cardiovascular Imaging; Client Version 248, Server Version 258). Ventricular end-diastolic (EDV) and end-systolic volumes (ESV) were corrected for body surface area (BSA) according to the DuBois formula¹⁶.

Qualitative analysis

Feasibility

FT-CMR tracking quality of the endocardial border was visually assessed in each software method by one observer who was blinded for study group and demographic data. Segments in which FT tracking was obviously beyond the contours of the RV were excluded. To ensure consistency in the exclusion of segments, a second observer independently assessed a randomly selected subset of 40 patients.

Reproducibility

Intra-observer variability was evaluated by re-measuring RV peak strain in 40 randomly selected subjects by the first observer. For inter-observer variability, the same 40 subjects were measured by a second observer, independent from the first observer. Intra- and inter-observer variability was assessed for every software method separately. Observers were blinded for clinical and demographic data at the time of CMR measurements.

Statistical analysis

Continuous and categorical variables are presented as mean (\pm standard deviation) and *n* (%), respectively. For continuous comparisons of two groups, two-tailed Student's t-test was used (paired and unpaired as appropriate). For continuous comparisons of three or more groups, one-way ANOVA or Kruskal Wallis was used. Categorical data were compared using the chi-square test. A p-value of <0.05 was considered significant. Intra- and inter-observer reproducibility of strain measurements was evaluated visually by Bland-Altman analysis (MedCalc Software, version 16.8.4, Mariakerke, Belgium). Correlation was assessed by Intraclass Correlation Coefficient (ICC). For ICC, a value ≥ 0.75 was considered excellent, <0.75 and ≥ 0.40 moderate, and <0.40 poor. Diagnostic accuracy was evaluated using the area under the Receiver Operating Characteristic (ROC) curve. For the area under the curve (AUC), a value of 0.90-1.0 was considered excellent, 0.80-0.90 good, 0.70-0.80 moderate and <0.60 poor. Statistical analyses were performed using IBM SPSS statistics (IBM, version 21, Chicago, IL, USA).

RESULTS

Baseline Characteristics

We evaluated CMR images of 110 subjects including 39 (36%) overt ARVD/C patients (mutation+, phenotype+), 40 (36%) preclinical ARVD/C subjects (mutation+, phenotype-) and 31 (28%) healthy control subjects. Baseline characteristics of the study population are shown in **Table 1**. Overall, 56 (51%) subjects were male with a mean age of 33.3 ± 15.8 years. There were no significant differences between overt ARVD/C patients, preclinical ARVD/C patients, and control subjects in age ($p=0.341$) and sex ($p=0.639$). As expected, overt ARVD/C patients had higher RV EDV/BSA (88.3 ± 25.6 mL/m²) compared to preclinical (68.4 ± 14.4 mL/m²) and control subjects (69.7 ± 12.9 mL/m²) ($p < 0.001$ for trend). In addition, RV function was decreased in overt ($48.3 \pm 11.7\%$) compared to preclinical ($54.9 \pm 9.6\%$) and control subjects ($56.9 \pm 9.7\%$) ($p=0.005$ for trend). LV volume and function did not differ between the groups (**Table 1**).

Table 1: Baseline characteristics of the study population

	OVERT ARVD/C (N=39)	PRECLINICAL ARVD/C (N=40)	CONTROLS (N=31)
FEMALE (%)	22 (56)	18 (45)	14 (45)
AGE (YRS)	32.3 ± 13.5	31.3 ± 18.1	37.2 ± 14.9
GLOBAL CMR PARAMETERS			
RV EDV/BSA (ML/M ²)	$88.3 \pm 25.6^*$	68.4 ± 14.4	69.7 ± 12.9
RV ESV/BSA (ML/M ²)	$47.4 \pm 24.9^*$	31.1 ± 9.8	30.0 ± 8.6
RV EF (%)	$48.3 \pm 11.7^*$	54.9 ± 9.6	56.9 ± 9.7
LV EDV/BSA (ML/M ²)	77.4 ± 12.1	69.1 ± 12.9	73.5 ± 9.6
LV ESV/BSA (ML/M ²)	30.6 ± 9.5	25.2 ± 7.0	30.9 ± 15.1
LV EF (%)	62.7 ± 6.3	63.2 ± 11.7	58.9 ± 13.3

Table 1: Continued.

	OVERT ARVD/C (N=39)	PRECLINICAL ARVD/C (N=40)	CONTROLS (N=31)
CLINICAL PHENOTYPE			
REPOLARIZATION CRITERIA			-
MAJOR	36 (93)	1 (3)	
MINOR	22 (54)	19 (48)	
DEPOLARIZATION CRITERIA			-
MAJOR	3 (8)	0 (0)	
MINOR	19 (49)	18 (45)	
ARRHYTHMIA CRITERIA			-
MAJOR	7 (18)	0 (0)	
MINOR	26 (67)	4 (10)	
STRUCTURAL CRITERIA			-
MAJOR	16 (41)	0 (0)	
MINOR	7 (18)	0 (0)	
TFC FULFILLMENT: NUMBER OF CRITERIA (MEDIAN)	6 (IQR 5-7)	2 (IQR 2-3)	-

*= Statistical significant difference compared to control subjects.

Abbreviations: ARVD/C = Arrhythmogenic Right Ventricular Dysplasia/Cardiomyopathy; BSA= Body Surface Area; EDV= End-Diastolic Volume; EF= Ejection Fraction; ESV= End-Systolic Volume; TFC= Task Force Criteria; N= number of subjects.

Feasibility Comparison among Software Methods

We first performed a quality assessment to determine feasibility of strain measurements for every FT-CMR software method separately. Tracking quality was visually assessed for every study subject and dichotomized into adequate and inadequate tracking. **Figure 2** shows the percentage of cases with adequate tracking quality stratified by segment and by software method. Zero subjects from Medis, 4 from TomTec, 7 from MTT and 9 from Circle were excluded in cases where the software would not read the image data. Of the remaining cases, tracking quality was highest in Medis (93% [308/330 segments of 95/110 subjects]), followed by Circle (89% [271/303 segments of 79/101 subjects]), TomTec (87% [277/318 segments of 80/106 subjects]) and MTT (84% [259/309 segments of 78/103 subjects included]). Furthermore, the tracking quality in the apical region (95%, 92%, 87%, and 87% for Medis, TomTec, MTT, and Circle respectively), anterior wall region (94%, 92%, 85%, and 91% for Medis, TomTec, MTT, and Circle respectively) and the subtricuspid region (92%, 78%, 79%, and 90% for Medis, TomTec, MTT, and Circle respectively) (**Figure 2**) differed per software method. When stratifying by diagnostic group, the highest tracking quality was observed in preclinical ARVD/C (92% [429/468 segments]) and control subjects (91% [328/360 segments]), followed by overt ARVD/C patients (83% [365/438 segments]). Twenty percent of cases with low tracking quality showed overlap with at least one other software method. The minor overlap in cases of low tracking quality among software methods suggests that tracking quality is software-specific and not image quality- or patient-specific.

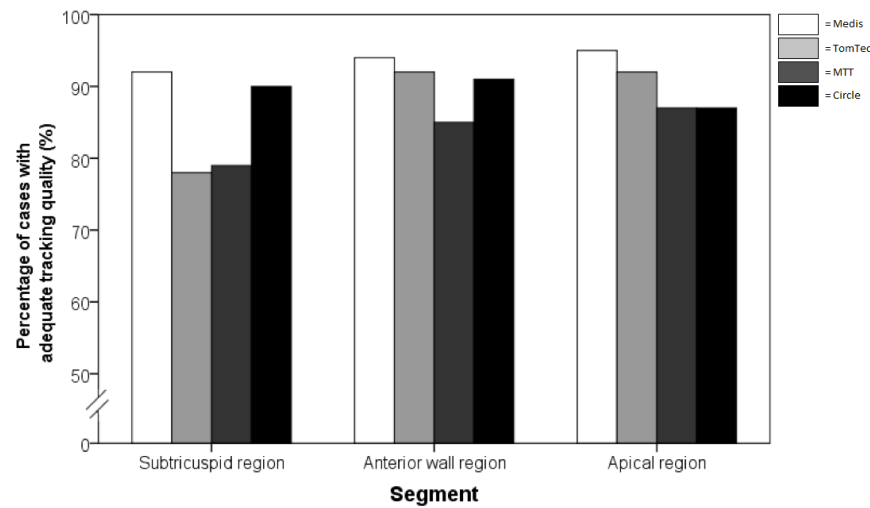


Figure 2: percentage of cases with adequate tracking quality of the endocardial border stratified per segment and software method.

FT-CMR Intersoftware Comparison of Global and Regional Longitudinal Strain

For the second part of our analyses, we excluded subjects with low tracking quality, since disturbed tracking will result in outliers that are not representative for actual wall motion of the included subjects. Analyses including all subjects regardless of tracking quality can be found in **Additional Files 2, 3, 4, and 5**.

Global strain

Table 2 shows global (average) peak strain for the four software methods stratified by ARVD/C diagnosis. While the magnitude of strain values was smaller (i.e. closer to zero) with TomTec than with the other three methods ($p < 0.001$ in the overall study population), all four methods showed a relative group difference with a trend towards lower strain values in overt ARVD/C patients compared to preclinical and control subjects. As shown in **Figure 3**, Bland-Altman analyses with 95% limits of agreement shows a wide limit of agreement of $>20\%$ between the various software methods. This is also expressed by the ICC of 0.442 for absolute global strain values between the four software methods. In contrast, the distributions (standard deviations) of the average peak strain values were comparable between the different software methods, indicating that the spread of measurement is similar among software methods (**Figure 4**).

Table 2: Right ventricular global (average) strain values stratified by diagnostic group¹

	OVERT ARVD/C (N=39)	PRECLINICAL ARVD/C (N=40)	CONTROLS (N=31)	P-VALUE [#]
MEDIS	$-17.6 \pm 6.3^{*\wedge}$	-21.8 ± 4.6	-21.4 ± 5.5	0.001
TOMTEC	$-14.3 \pm 7.1^{*\wedge}$	-17.7 ± 6.6	-17.8 ± 5.6	0.057
MTT	$-19.3 \pm 6.2^{*\wedge}$	-26.2 ± 5.0	-27.7 ± 5.5	<0.001
CIRCLE	$-21.3 \pm 5.3^*$	-22.9 ± 3.7	-23.7 ± 2.3	0.065

*= Statistical significant difference compared to control subjects; \wedge = Statistical significant difference compared to preclinical subjects; $\#$ =Trend between overt ARVD/C patients, preclinical ARVD/C and control subjects (OneWay ANOVA). Abbreviations: ARVD/C= Arrhythmogenic Right Ventricular Dysplasia/ Cardiomyopathy; MTT= Multimodality Tissue Tracking; N= number of subjects.

Segments included based on adequate tracking quality: 365/438, 429/468, and 328/360 segments in overt ARVD/C, preclinical ARVD/C and control subjects respectively.

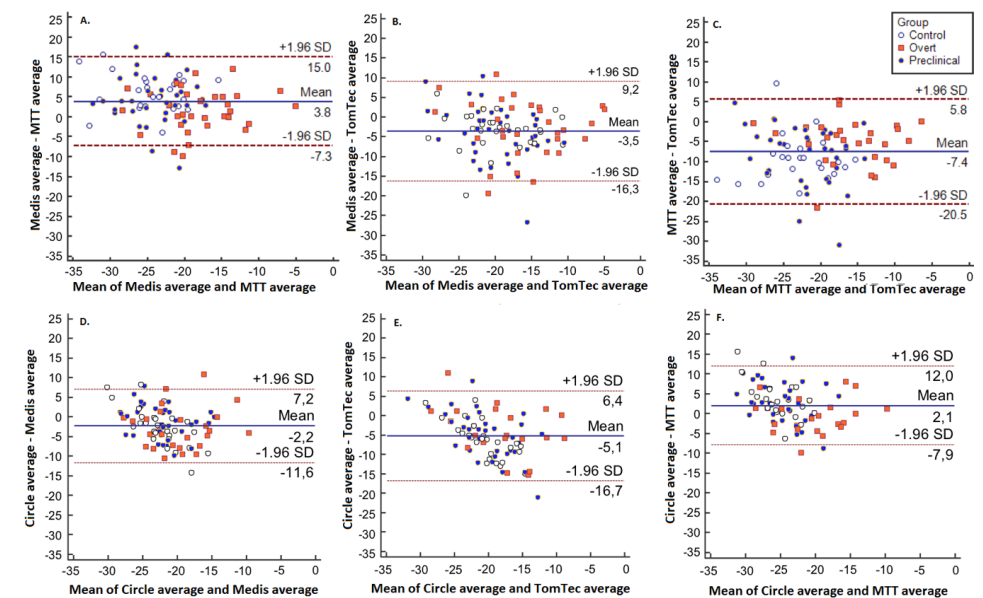


Figure 3: Bland-Altman plots per intersoftware variability of average right ventricular strain values. Intersoftware variability of strain values in A) Medis vs. MTT; B) Medis vs. TomTec; C) MTT vs. TomTec; D) Circle vs. Medis; E) Circle vs. TomTec; F) Circle vs. MTT.

Regional strain

Table 3 shows regional (segmental) peak strain for the four software methods stratified by ARVD/C diagnosis. Again, the magnitude of the strain values in the anterior wall and the apical region was smaller (i.e. closer to zero) with TomTec compared to the other three methods ($p < 0.001$ in the overall study population). All four software methods showed a relative group difference with a trend towards lower strain in overt ARVD/C patients compared to preclinical and control subjects. As shown in **Figure 5**, Bland-Altman analyses with 95% limits of agreement showed that there is moderate agreement between the

software methods with wide limits of agreement for absolute subtricuspid strain values. This is also expressed by the ICC of 0.373 for absolute subtricuspid strain values between the four software methods. The distribution (standard deviation) of the segmental strain, especially in the subtricuspid region, was wider in TomTec than in other methods indicating a wider spread of measurements (**Figure 6**). On the contrary, Circle showed a consistently lower distribution of the segmental strain and therefore a smaller spread of measurements. **Reproducibility.** As shown in **Table 4**, software methods showed moderate to excellent inter- and intra-observer reproducibility for the regional strain values, with inter-observer reproducibility ranging from 0.519 to 0.896 in the subtricuspid region, 0.677 to 0.864 in the anterior wall, and 0.472 to 0.861 in the apical wall. For all regions, the highest intra-observer reproducibility was seen in Circle (ICC ranging from 0.944 to 0.980), followed by Medis (ICC ranging from 0.909 to 0.954), TomTec (ICC ranging from 0.699 to 0.864), and MTT (ICC ranging from 0.696 to 0.806).

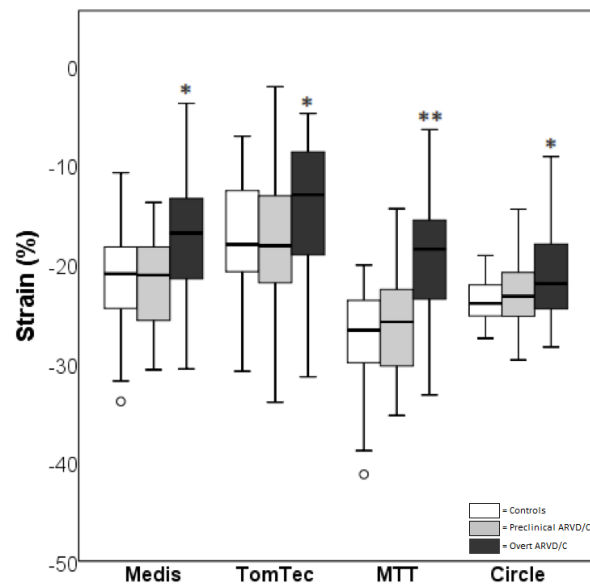


Figure 4: Global (average) strain by group per software package.

Statistical significant difference compared to control subjects is expressed in *= $p < 0.05$ and **= $p < 0.01$. Abbreviations: MTT= Multimodality Tissue Tracking.

Table 3: Right ventricular regional (segmental) strain values stratified by diagnostic group¹

	OVERT ARVD/C (N=39)	PRECLINICAL ARVD/C (N=40)	CONTROLS (N=31)	P-VALUE [*]
SUBTRICUSPID REGION				
MEDIS	-28.4 ± 14.8*	-31.6 ± 10.4*	-38.1 ± 8.1	0.007
TOMTEC	-24.7 ± 18.3*	-32.4 ± 12.6	-34.3 ± 11.4	0.045
MTT	-24.4 ± 10.8 [^]	-33.4 ± 10.9	-36.9 ± 10.5	<0.001
CIRCLE	-23.0 ± 8.4*	-26.2 ± 6.3	-27.0 ± 5.0	0.067
ANTERIOR WALL REGION				
MEDIS	-20.6 ± 10.5 [^]	-28.6 ± 10.3	-29.0 ± 11.1	0.001
TOMTEC	-17.5 ± 11.9	-19.7 ± 11.1	-22.6 ± 12.5	0.248
MTT	-17.7 ± 6.4 [^]	-23.0 ± 6.1	-22.8 ± 6.3	0.001
CIRCLE	-22.8 ± 6.2	-24.2 ± 5.0	-25.3 ± 3.4	0.168
APICAL REGION				
MEDIS	-22.8 ± 10.0 [^]	-27.8 ± 8.7	-25.1 ± 9.6	0.072
TOMTEC	-12.7 ± 10.7	-14.7 ± 10.4	-13.1 ± 8.6	0.674
MTT	-18.6 ± 8.8 [^]	-23.3 ± 7.8	-25.5 ± 9.6	0.019
CIRCLE	-18.3 ± 5.4	-19.9 ± 5.1	-19.5 ± 5.6	0.521

*= Statistical significant difference compared to control subjects; ^= Statistical significant difference compared to preclinical subjects; #= Trend between overt ARVD/C patients, preclinical ARVD/C and control subjects (OneWay ANOVA). Abbreviations: ARVD/C= Arrhythmogenic Right Ventricular Dysplasia/ Cardiomyopathy; MTT= Multimodality Tissue Tracking; N= number of subjects.

¹Segments included based on adequate tracking quality: 365/438, 429/468, and 328/360 segments in overt ARVD/C, preclinical ARVD/C and control subjects respectively.

Table 4: Intra- and inter-observer reproducibility of regional (segmental) strain per software method

method	INTRA-OBSERVER ICC	INTER-OBSERVER ICC
SUBTRICUSPID REGION		
MEDIS	0.928	0.896
TOMTEC	0.816	0.538
MTT	0.696	0.519
CIRCLE	0.980	0.719
ANTERIOR WALL REGION		
MEDIS	0.954	0.792
TOMTEC	0.699	0.864
MTT	0.806	0.677
CIRCLE	0.969	0.783
APICAL REGION		
MEDIS	0.909	0.807
TOMTEC	0.790	0.861
MTT	0.787	0.472
CIRCLE	0.944	0.577

An ICC ≥ 0.75 was considered excellent, an ICC between <0.75 and ≥ 0.40 moderate, and an ICC <0.40 poor. Abbreviations: MTT= Multimodality Tissue Tracking; ICC= Intraclass Correlation Coefficient

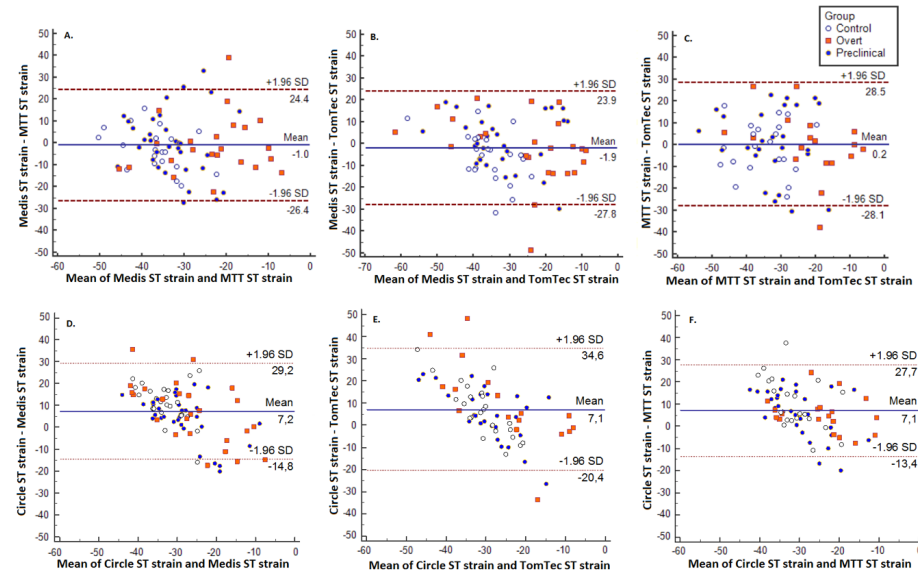


Figure 5: Bland-Altman plots per intersoftware variability of right ventricular subtricuspid strain values. Intersoftware variability of strain values in the subtricuspid region in A) Medis vs. MTT; B) Medis vs. TomTec; C) MTT vs. TomTec; D) Circle vs. Medis; E) Circle vs. TomTec; F) Circle vs. MTT. ST= subtricuspid region.

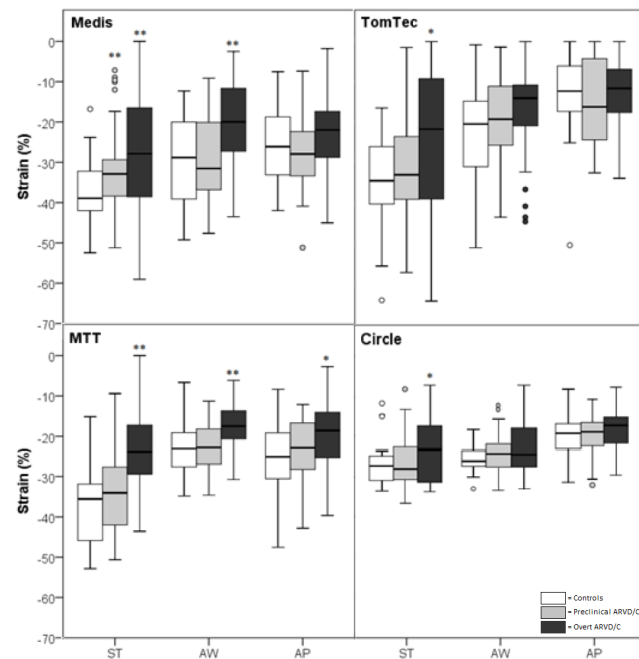


Figure 6: Regional strain by subgroup per software package. Statistical significant difference compared to control subjects is expressed in * $p < 0.05$ and ** $p < 0.01$. Abbreviations: ST= subtricuspid region; AW= anterior wall region; AP= apical region; MTT= Multimodality Tissue Tracking.

Clinical Implementation of FT-CMR for Early ARVD/C Disease Detection

With regards to global (average) strain (**Figure 4**), overt patients had reduced strain compared to control subjects, which reached significance in all software methods ($p < 0.041$). In contrast, global strain was similar in preclinical and control subjects for all software methods ($p > 0.275$), suggesting that global strain is insensitive for early disease detection. With regards to regional (segmental) strain (**Figure 6**), overt patients had reduced strain compared to control subjects, reaching statistical significance in the subtricuspid region for Medis, TomTec, MTT and Circle ($p < 0.037$), in the anterior wall for Medis and MTT ($p < 0.005$) and in the apex for MTT only ($p = 0.012$). While comparable regional strain values were observed for the anterior wall and apex, preclinical patients were separated from controls in the subtricuspid region by Medis software ($p = 0.009$). This is also illustrated by a moderate discriminative accuracy of subtricuspid strain to distinguish preclinical from control subjects using Medis (AUC=0.70), and a poor discriminative accuracy for the same comparison in the other three software methods (AUC 0.53-0.58). Furthermore, the discriminative accuracy of FT-CMR in overt ARVD/C patients and control subjects was moderate to good in the subtricuspid region (AUC 0.64-0.80) and poor to moderate in both the anterior wall (AUC 0.61-0.74) and the apical wall region (AUC 0.47-68). AUC for global and regional longitudinal strain values in ARVD/C vs. control and preclinical vs. control can be found in Additional File 6.

DISCUSSION

Over the years, we have come to appreciate that ARVD/C starts as a regional rather than a global disease^{9,17}. This is reflected in the 2010 diagnostic TFC, which require the presence of regional RV wall motion abnormalities for fulfillment of diagnostic criteria¹⁵. Up to now, these wall motion abnormalities are assessed qualitatively and are thereby 'in the eye of the beholder'¹⁸. FT-CMR is a novel technique that may be useful for quantitative evaluation of regional RV strain. A challenge for clinical implementation is the absence of an independent standard of reference for RV strain values. The study of ARVD/C patients with FT techniques is advantageous in this regard, in that multiple independent criteria are used for diagnosis of the disease, including genetic testing, electrical abnormalities and family history. Our study aimed to assess intersoftware agreement of RV global and regional strain using FT-CMR. Our results show that significant variability exists between FT software methods, including 1) sporadic failure of RV wall tracking and 2) significant differences in absolute RV strain values. However, despite software variability, all four software methods were able to identify overt ARVD/C patients from control subjects on a group perspective using global strain. This may suggest some robustness of the FT-CMR approach. In addition, regional strain was reduced in overt ARVD/C patients compared to control subjects in all segments, which was most apparent in the subtricuspid region. Preclinical patients were

also distinguished from control subjects by decreased subtricuspid strain using one software method. These results suggest a role for FT-CMR in ARVD/C evaluation, pending further technological refinements.

Overview of Strain Measurements of the Right Ventricle

Starting with the application of crystal sonomicrometry in dogs in the 1970s, the last decades have witnessed a surge in imaging techniques that can visualize local myocardial wall motion (deformation)¹⁹. Tissue tagging, a CMR technique that prescribes multiple grids on the myocardial tissue to track deformation throughout the cardiac cycle, is typically regarded as the gold standard for LV deformation²⁰. Echocardiographic deformation imaging using either speckle tracking or tissue Doppler imaging has also gained popularity for those patients unfit to undergo CMR examinations^{2,21}. Of note, these techniques are technically demanding, time consuming, and have primarily been validated for use in the LV, but render themselves less suitable for the thin-walled and highly trabeculated RV²². In the context of these shortcomings, FT-CMR has been developed as an alternative for the assessment of both LV and RV strain. After the first publication on FT-CMR by Maret *et al.*²³, several research groups have confirmed its diagnostic value for LV evaluation^{5,24-27}. FT-CMR also gained popularity for assessment of the RV: it has been shown to be of clinical value in (repaired) tetralogy of Fallot^{3,28} and pulmonary hypertension^{29,30}. In addition, we and others have used FT-CMR in an ARVD/C population¹²⁻¹⁴. **Additional File 7** provides an overview of global and regional strain values obtained in these prior ARVD/C populations. Heermann *et al.* showed that global RV strain values were significantly reduced in overt ARVD/C patients (n=20) compared to healthy volunteers (n=10) and family members (n=22)¹⁴. Vigneault *et al.* (whose study population was identical to the present study) confirmed these findings and determined the horizontal longitudinal axis as the most reliable view to perform strain measurements¹³. Subsequently, Prati *et al.* showed that reduced global RV strain is present when global RV function is still preserved. While these results are promising, routine use of FT-CMR in clinical practice remains premature: FT-CMR needs to be standardized between software methods and RV wall tracking requires to be more reliably tracked¹². Our study provides data addressing both these concerns.

Feasibility of FT-CMR using Different Software Methods

Our study provides a head-to-head comparison of four commercially available software methods for FT-CMR measurements of the RV. We show that feasibility of RV strain by FT-CMR is not uniform across software methods, and that absolute strain values correlate poorly with large limits of agreement. It therefore remains impossible to translate strain values obtained in one software method to another, at least on a patient-by-patient level. These findings are in line with previous studies using speckle tracking echocardiography, which showed poor correlation across software methods in healthy controls^{31,32}. Nagata *et al.* even showed significant variability of measurements using different versions of the same

speckle tracking software³¹. The optimal performance of feature tracking relies on both algorithm-dependent and algorithm-independent properties¹. As for algorithm-dependent properties, accuracy of feature tracking is determined by the interrogation window that determines the frame-to-frame tracking of the feature, the specific features which are extracted and the influence of other motions such as blood flow near the endocardial border^{1,33,34}. As for algorithm-independent properties, image quality and spatial/temporal resolution are essential determinants of accurate strain measurement^{1,35}. Our study is unique in the sense that it used the same CMR scans to test four software methods, so that the observed differences are due to an algorithm-dependent difference. Indeed, the subset of scans excluded based on low tracking quality (i.e. feasibility) was different for every software method, suggesting that tracking quality is algorithm-dependent. While it is expected that MTT, TomTec, Medis and Circle use different strain calculation algorithms, the low agreement between these methods is remarkable since tracking quality was determined to be adequate by two independent observers and patient-specific factors were constant by study design. Because no gold standard for RV strain exists, a normative comparison of the quality of these algorithms remains challenging³⁶. Further refinements of the technique are necessary to increase comparability among software methods.

Inter- and Intra-observer Reproducibility

All software methods showed a moderate to excellent inter- and intra-observer reproducibility, with higher intra-observer (ICC 0.69-0.98) compared to inter-observer (ICC 0.47-0.90) reproducibility. In general, Medis and Circle had higher inter- and intra-observer reproducibility than TomTec and MTT. Indeed, Medis and Circle showed higher tracking quality than the other two packages. Both TomTec and MTT required more manual adjustments of the endocardial contour. These manual adjustments may have influenced reproducibility, especially for inter-observer reproducibility. A difference between inter- and intra-observer reproducibility was also observed in previous studies^{3,12,30,37}. These studies all focused on the reproducibility of global strain, and all used the TomTec software method^{3,12,30,37,38}. The inter-observer (ICC 0.61-0.75 and coefficient of variation (CV) 8.3-9.9%) and intra-observer (ICC 0.96-0.99 and CV 8.6-28.7%) reproducibility of these studies varied from moderate to excellent, which is comparable to our results^{30,35,37,38}. To the best of our knowledge, no previous studies investigated inter- and intra-observer reproducibility for RV regional strain. While the similarity between our results and prior observations is reassuring, it is important to note that especially inter-observer variability remains relatively poor for some of the software packages. Future refinement of the software algorithms will be necessary to further reduce variability between readers.

Clinical Value of Global Strain in ARVD/C Evaluation

Despite the abovementioned intersoftware variability, our study shows that global strain is significantly reduced in overt ARVD/C patients compared to controls for all four software

methods. This suggests that FT-CMR has the potential to differentiate healthy from diseased subjects, at least in group analysis. However, for an individual study subject, identification of global and regional strain abnormalities is variable, depends on image quality and varies between different software packages. Also, a wide limit of agreement between the various software methods exists, limiting the ability to draw conclusions at an individual patient level. One could argue that differences in software variability are less visible for global strain measurements, since it provides a mean of all RV segments thereby averaging out measurement errors in a “trend towards the mean”. While these results are reassuring, the finding of lower global strain in overt ARVD/C patients may not be surprising, since global structural abnormalities are thought to occur late in the disease course of ARVD/C and are therefore expected to be abnormal at time of overt disease¹⁷. Indeed, RV ejection fraction by itself may be easier to implement and interpret compared to FT-CMR. Nevertheless, given the high degree of difficulty for interpretation of the RV, CMR physicians may be reassured by the finding of abnormal global RV strain in overt ARVD/C.

Clinical Value of Regional Strain in ARVD/C Evaluation: Role for Early Disease Detection?

Several studies have indicated that regional abnormalities occur prior to the onset of global changes in ARVD/C^{17,39}. As such, regional strain would be of particular interest as a tool for (early) diagnosis of this disease. Indeed, the results of our study show that regional strain is reduced in ARVD/C patients compared to controls, which is most consistent for the subtricuspid region. This is intriguing since abnormal subtricuspid strain has previously been shown (in a multivariable analysis controlling for gender, RV EF and RV EDV) to be an independent predictor for ARVD/C diagnosis, suggesting added value beyond RV size and function¹³. Furthermore, these results are also interesting in the context of our understanding of ARVD/C as a regional disease. In 1982, Marcus *et al.* described the “Triangle of Dysplasia” involving dyskinesia/aneurysms in the RV inferior wall (inflow tract), RV outflow tract, and RV apex in ARVD/C patients with a severe clinical phenotype⁴⁰. More recently, we have come to appreciate that (mutation-positive) ARVD/C preferentially affects the subtricuspid region^{9, 41-43}, and spreads to the RV outflow tract and apex in later stages of disease⁹. Of note, subtricuspid strain was reduced in preclinical patients compared to control subjects for Medis software, suggesting a role for subtricuspid strain in early ARVD/C diagnosis. However, one should keep in mind that these results were obtained for one software method only, and should be validated in an external patient sample. It would be interesting for future studies to evaluate disease development over time in preclinical subjects with reduced subtricuspid strain and to investigate the value of FT-CMR in discriminating subjects with favorable and adverse clinical outcome.

Limitations and Perspective on Clinical FT-CMR Implementation

Our results highlight the potentially interesting role of FT-CMR for ARVD/C evaluation, but also indicate the need for further refinements in this technique. While the moderate to

excellent reproducibility of FT-CMR renders this technique suitable for follow-up of ARVD/C patients, determination of the spectrum of normal RV strain values and thresholds for disease will help in standardization of FT-CMR. Evaluation of intersoftware variability of LV strain would be interesting but was beyond the scope of this study. Similar to the 2D speckle tracking-derived bull’s eye plots for LV longitudinal strain in cardiomyopathy patients, future FT-CMR studies on RV strain should consider incorporating a mapping for RV strain⁴⁴. This may improve our understanding of RV strain distribution in health and disease. A limitation of this study is that we did not include a reference standard for RV strain. However, no validated reference standard for RV strain currently exists. Future studies should compare FT-CMR to other (CMR-based) deformation techniques to further optimize the FT technique. In addition, studies specifically investigating algorithm-independent properties such as the influence of spatial or temporal resolution will be helpful for further technical refinements of FT-CMR. Until that time, routine use of FT-CMR in ARVD/C evaluation should take place at an experienced center with experienced CMR readers.

CONCLUSIONS

In this cohort of well-phenotyped ARVD/C patients and healthy controls, we performed FT-CMR to measure RV strain using four commercially available software methods. We demonstrate that intersoftware variability exists for both feasibility and absolute strain values. Regardless, all software methods are able to differentiate affected ARVD/C patients from controls by global strain, suggesting robustness of FT-CMR measures. In addition, we reveal that the subtricuspid region is an indicator region of ARVD/C, in which abnormal strain is visible both in overt patients and those prior to disease expression. These results highlight the potential of FT-CMR as an early diagnostic test in ARVD/C.

List of abbreviations

ARVD/C= Arrhythmogenic Right Ventricular Dysplasia/Cardiomyopathy
 BSA= Body Surface Area
 CMR= Cardiac Magnetic Resonance imaging
 EDV= End Diastolic Volume
 ESV= End Systolic Volume
 FT-CMR= Feature Tracking Cardiac Magnetic Resonance
 HLA= Horizontal Longitudinal Strain
 ICC= Intraclass Correlation Coefficient
 LV= Left Ventricle
 MTT= Multimodality Tissue Tracking
 RV= Right Ventricle
 TFC= Task Force Criteria

Declarations

Ethics approval and consent to participate. Patients provided written informed consent, and the study protocol was approved by the Johns Hopkins School of Medicine Institutional Review Board.

Consent for publication. Not applicable

Availability of data and material. All data generated or analyzed during this study are included in this published article [and its additional information files].

Competing interests. None.

Funding. ASJMR is supported by the Dutch Heart Foundation (2015T058) and the UMC Utrecht (Fellowship Clinical Research Talent). DMV is supported by the NIH-Oxford Scholars program and the NIH Intramural Research Program. The Johns Hopkins ARVD/C Program is supported by the Dr. Francis P. Chiaramonte Private Foundation, the St. Jude Medical Foundation, the Leyla Erkan Family Fund for ARVD research, the Dr. Satish, Rupal, and Robin Shah ARVD Fund at Johns Hopkins, the Bogle Foundation, the Healing Hearts Foundation, the Campanella family, the Patrick J. Harrison Family, the Peter French Memorial Foundation, and the Wilmerding Endowments.

Authors' contributions. MB made major contributions to the acquisition, analysis and interpretation of data. MB has also been a major contributor in writing the manuscript. DMV made substantial contributions to the acquisition, analysis and interpretation of data. DMV, BM, CAJ, CT, SLZ, IRK, HC, HT, and BKV have been involved in revising the manuscript critically for important intellectual content. MAG and FMH made substantial contributions to the acquisition of data and have been involved in revising the manuscript critically for important intellectual content. DAB made substantial contributions to conception and design of the study and interpretation of data and has been involved in critically revising the manuscript for important intellectual content. ASJMR made substantial contributions to the conception and design of the study and the interpretation of data, and was a major contributor in writing the manuscript. All authors read and approved the final manuscript.

Acknowledgements. The authors are grateful to the ARVD/C patients and families who made this work possible.

REFERENCES

- Pedrizetti G, Claus P, Kilner PJ, Nagel E. Principles of cardiovascular magnetic resonance feature tracking and echocardiographic speckle tracking for informed clinical use. *J Cardiovasc Magn Reson.* 2016;18(1):51
- Claus P, Omar AM, Pedrizetti G, Sengupta PP, Nagel E. Tissue Tracking Technology for Assessing Cardiac Mechanics: Principles, Normal Values, and Clinical Applications. *JACC Cardiovasc Imaging.* 2015;8(12):1444-1460.
- Kempny A, Fernandez-Jimenez R, Orwat S, Schuler P, Bunck AC, Maintz D, et al. Quantification of biventricular myocardial function using cardiac magnetic resonance feature tracking, endocardial border delineation and echocardiographic speckle tracking in patients with repaired tetralogy of Fallot and healthy controls. *J Cardiovasc Magn Reson.* 2012;14:32.
- Shehata ML, Cheng S, Osman NF, Bluemke DA, Lima JA. Myocardial tissue tagging with cardiovascular magnetic resonance. *J Cardiovasc Magn Reson.* 2009;11:55.
- Augustine D, Lewandowski AJ, Lazdam M, Rai A, Francis J, Myerson S, et al. Global and regional left ventricular myocardial deformation measures by magnetic resonance feature tracking in healthy volunteers: comparison with tagging and relevance of gender. *J Cardiovasc Magn Reson.* 2013;15(1):8.
- Te Riele AS, Tandri H, Bluemke DA. Arrhythmogenic right ventricular cardiomyopathy (ARVC): cardiovascular magnetic resonance update. *J Cardiovasc Magn Reson.* 2014;16(1):50.
- Dalal D, Nasir K, Bomma C, Prakasa K, Tandri H, Piccini J, et al. Arrhythmogenic right ventricular dysplasia: a United States experience. *Circulation.* 2005;112(25):3823-3832.
- van der Werf C, Hofman N, Tan HL, van Dessel PF, Alders M, van der Wal AC, et al. Diagnostic yield in sudden unexplained death and aborted cardiac arrest in the young: the experience of a tertiary referral center in The Netherlands. *Heart Rhythm.* 2010;7(10):1383-1389.
- Te Riele AS, James CA, Phillips B, Rastegar N, Bhonsale A, Groeneweg JA, et al. Mutation-positive arrhythmogenic right ventricular dysplasia/cardiomyopathy: the triangle of dysplasia displaced. *J Cardiovasc Electrophysiol.* 2013;24(12):1311-20.
- Aneq MA, Engvall J, Brudin L, Nylander E. Evaluation of right and left ventricular function using speckle tracking echocardiography in patients with arrhythmogenic right ventricular cardiomyopathy and their first degree relatives. *Cardiovasc Ultrasound.* 2012;10:37.
- Prakasa KR, Wang J, Tandri H, Dalal D, Bomma C, Chojnowski R, et al. Utility of tissue Doppler and strain echocardiography in arrhythmogenic right ventricular dysplasia/cardiomyopathy. *Am J Cardiol.* 2007;100(3):507-512.
- Prati G, Vitrella G, Allocca G, Muser D, Buttignoni SC, Piccoli G, et al. Right Ventricular Strain and Dyssynchrony Assessment in Arrhythmogenic Right Ventricular Cardiomyopathy: Cardiac Magnetic Resonance Feature-Tracking Study. *Circ Cardiovasc Imaging.* 2015;8(11):e003647
- Vigneault DM, te Riele AS, James CA, Zimmerman SL, Selwaness M, Murray B, et al. Right ventricular strain by MR quantitatively identifies regional dysfunction in patients with arrhythmogenic right ventricular cardiomyopathy. *J Magn Reson Imaging.* 2016;43(5):1132-1139.
- Heermann P, Hedderich DM, Paul M, Schulke C, Kroeger JR, Baessler B, et al. Biventricular myocardial strain analysis in patients with arrhythmogenic right ventricular cardiomyopathy (ARVC) using cardiovascular magnetic resonance feature tracking. *J Cardiovasc Magn Reson.* 2014;16:75.
- Marcus FI, McKenna WJ, Sherrill D, Basso C, Bauce B, Bluemke DA, et al. Diagnosis of arrhythmogenic right ventricular cardiomyopathy/dysplasia: proposed modification of the task force criteria. *Circulation.* 2010;121(13):1533-1541.
- Du Bois EF: a formula to estimate the approximate surface area if height and weight be known. *Nutrition.* 1989;5:303-11
- Te Riele AS, Tandri H, Sanborn DM, Bluemke DA. Noninvasive Multimodality Imaging in ARVD/C. *JACC Cardiovasc Imaging.* 2015;8(5):597-611.
- Bluemke DA. ARVC: Imaging diagnosis is still in the eye of the beholder. *JACC Cardiovasc Imaging.* 2011;4(3):288-91.
- Carlsson E, Milne EN. Permanent implantation of endocardial tantalum screws: a new technique for functional studies of the heart in the experimental animal. *J Can Assoc Radiol.* 1967;18(2):304-309.
- Wu L, Germans T, Guclu A, Heymans MW, Allaart CP, van Rossum AC. Feature tracking compared with tissue tagging measurements of segmental strain by cardiovascular magnetic resonance. *J Cardiovasc Magn Reson.* 2014;16:10.
- Abraham TP, Dimaano VL, Liang HY. Role of tissue Doppler and strain echocardiography in current clinical practice. *Circulation.* 2007;116(22):2597-2609.
- Mertens LL, Friedberg MK. Imaging the right ventricle—current state of the art. *Nature reviews Cardiology.* 2010;7(10):551-63
- Maret E, Todt T, Brudin L, Nylander E, Swahn E, Ohlsson JL, et al. Functional measurements based on feature tracking of cine magnetic resonance images identify left ventricular segments with myocardial scar. *Cardiovasc*

- Ultrasound. 2009;7:53.
24. Schneeweis C, Qiu J, Schnackenburg B, Berger A, Kelle S, Fleck E, *et al.* Value of additional strain analysis with feature tracking in dobutamine stress cardiovascular magnetic resonance for detecting coronary artery disease. *J Cardiovasc Magn Reson.* 2014;16:72.
 25. Schuster A, Hor KN, Kowallick JT, Beerbaum P, Kutty S. Cardiovascular Magnetic Resonance Myocardial Feature Tracking: Concepts and Clinical Applications. *Circulation Cardiovasc Imaging.* 2016;9(4).
 26. Buss SJ, Breuninger K, Lehrke S, Voss A, Galuschky C, Lossnitzer D, *et al.* Assessment of myocardial deformation with cardiac magnetic resonance strain imaging improves risk stratification in patients with dilated cardiomyopathy. *Eur Heart J Cardiovasc Imaging.* 2015;16(3):307-315.
 27. Onishi T, Saha SK, Ludwig DR, Onishi T, Marek JJ, Cavalcante JL, *et al.* Feature tracking measurement of dyssynchrony from cardiovascular magnetic resonance cine acquisitions: comparison with echocardiographic speckle tracking. *J Cardiovasc Magn Reson.* 2013;15:95.
 28. Jing L, Haggerty CM, Suever JD, Alhadad S, Prakash A, Cecchin F, *et al.* Patients with repaired tetralogy of Fallot suffer from intra- and inter-ventricular cardiac dyssynchrony: a cardiac magnetic resonance study. *Eur Heart J Cardiovasc Imaging.* 2014;15(12):1333-1343.
 29. Ohyama Y, Ambale-Venkatesh B, Chamera E, Shehata ML, Corona-Villalobos CP, Zimmerman SL, *et al.* Comparison of strain measurement from multimodality tissue tracking with strain-encoding MRI and harmonic phase MRI in pulmonary hypertension. *Int J Cardiol.* 2015;182:342-348.
 30. De Siqueira MEM, Pozo E, Fernandes VR, Sengupta PP, Modesto K, Gupta SS, *et al.* Characterization and clinical significance of right ventricular mechanics in pulmonary hypertension evaluated with cardiovascular magnetic resonance feature tracking. *J Cardiovasc Magn Reson.* 2016;18(1):39.
 31. Nagata Y, Takeuchi M, Mizukoshi K, Wu VC, Lin FC, Negishi K, *et al.* Intervendor variability of two-dimensional strain using vendor-specific and vendor-independent software. *J Am Soc Echocardiogr.* 2015;28(6):630-641.
 32. Farsalinos KE, Daraban AM, Unlu S, Thomas JD, Badano LP, Voigt JU. Head-to-Head Comparison of Global Longitudinal Strain Measurements among Nine Different Vendors: The EACVI/ASE Inter-Vendor Comparison Study. *J Am Soc Echocardiogr.* 2015;28(10):1171-1181.
 33. Barron JL, Fleet DJ, Beauchemin SS. Performance of optical flow techniques. *Int J Comput Vis.* 1994;12(1):43-77.
 34. Miozzi M, Jacob B, Olivieri A. Performances of feature tracking in turbulent boundary layer investigation. *Exp Fluids.* 2008;45(4):765.
 35. Schuster A, Morton G, Hussain ST, Jogiya R, Kutty S, Asrress KN, *et al.* The intra-observer reproducibility of cardiovascular magnetic resonance myocardial feature tracking strain assessment is independent of field strength. *Eur J Radiol.* 2013;82(2):296-301.
 36. Tandri H, Castillo E, Ferrari VA, *et al.* Magnetic resonance imaging of arrhythmogenic right ventricular dysplasia. Sensitivity, specificity, and observer variability of fat detection versus functional analysis of the right ventricle. *J Am Coll Cardiol.* 2006;48:2277-84.
 37. Schmidt B, Dick A, Treutlein M, Schiller P, Bunck AC *et al.* Intra- and inter-observer reproducibility of global and regional magnetic resonance feature tracking derived strain parameters of the left and right ventricle. *European Journal of Radiology.* 2017;89:97-105
 38. Orwat S, Kempny A, Diller GP, Bauerschmitz P, Bunck AC *et al.* Cardiac magnetic resonance feature tracking: a novel method of assessing myocardial strain. Comparison with echocardiographic speckle tracking in healthy volunteers and in patients with left ventricular hypertrophy. *Kardiol Pol.* 2014;72(4):363-371.
 39. Bomma C, Dalal D, Tandri H, Prakasa K, Nasir K, Roguin A, *et al.* Regional differences in systolic and diastolic function in arrhythmogenic right ventricular dysplasia/cardiomyopathy using magnetic resonance imaging. *Am J Cardiol.* 2005;95(12):1507-11.
 40. Marcus FI, Fontaine GH, Guiraudon G, Frank R, Laurenceau JL, Malergue C, *et al.* Right ventricular dysplasia: a report of 24 adult cases. *Circulation.* 1982;65(2):384-398.
 41. Marchlinski FE, Zado E, Dixit S, Gerstenfeld E, Callans DJ, Hsia H, *et al.* Electroanatomic substrate and outcome of catheter ablation therapy for ventricular tachycardia in setting of right ventricular cardiomyopathy. *Circulation.* 2004;110(16):2293-2298.
 42. Bomma C, Dalal D, Tandri H, Prakasa K, Nasir K, Roguin A, *et al.* Evolving role of multidetector computed tomography in evaluation of arrhythmogenic right ventricular dysplasia/cardiomyopathy. *Am J Cardiol.* 2007;100(1):99-105.
 43. Marra MP, Leoni L, Bauce B, Corbetti F, Zorzi A, Migliore F, *et al.* Imaging study of ventricular scar in arrhythmogenic right ventricular cardiomyopathy: comparison of 3D standard electroanatomical voltage mapping and contrast-enhanced cardiac magnetic resonance. *Circ Arrhythm Electrophysiol.* 2012;5(1):91-100.
 44. Liu D, Hu K, Nordbeck P, Ertl G, Störk S and Weidemann F. Longitudinal strain bull's eye plot patterns in patients with cardiomyopathy and concentric left ventricular hypertrophy. *European journal of medical research.* 2016; 21(1):21.

ADDITIONAL FILES

Unable to insert .mov in a Word document. Please see:

<https://jcmr-online.biomedcentral.com/articles/10.1186/s12968-017-0380-4>

Additional File 1: Movie Clip; Example of RV free wall endocardial tracking (Circle Cardiovascular Imaging)(.mov)

Additional File 2: Table 1; RV average strain values stratified by diagnostic group, without exclusions based on tracking quality

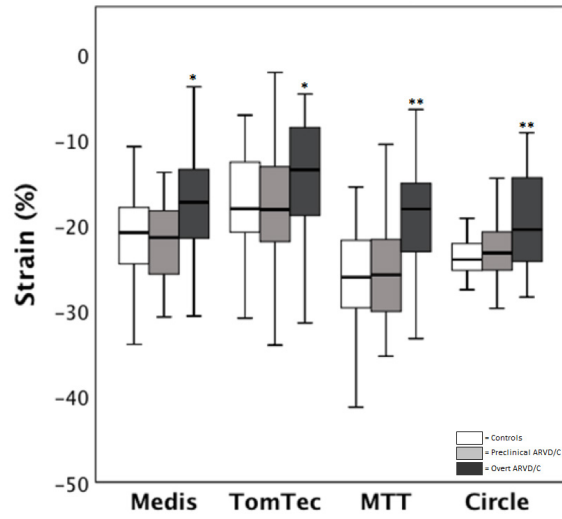
	OVERT ARVD/C (N=39)	PRECLINICAL ARVD/C (N=40)	CONTROLS (N=31)	P-VALUE#
MEDIS	-17.6 ± 6.1 [^]	-21.9 ± 4.6	-21.1 ± 5.6	0.002
TOMTEC	-14.2 ± 7.0 [^]	-17.7 ± 6.6	-17.8 ± 5.6	0.043
MTT	-18.7 ± 6.2 [^]	-25.4 ± 5.7	-25.8 ± 7.2	<0.001
CIRCLE	-19.4 ± 5.9 [^]	-22.6 ± 3.9	-23.7 ± 2.3	<0.001

*= Statistical significant difference compared to control subjects; [^]= Statistical significant difference compared to preclinical subjects; #=Trend between overt ARVD/C patients, preclinical ARVD/C and control subjects (OneWay ANOVA). Abbreviations: MTT= Multimodality Tissue Tracking.

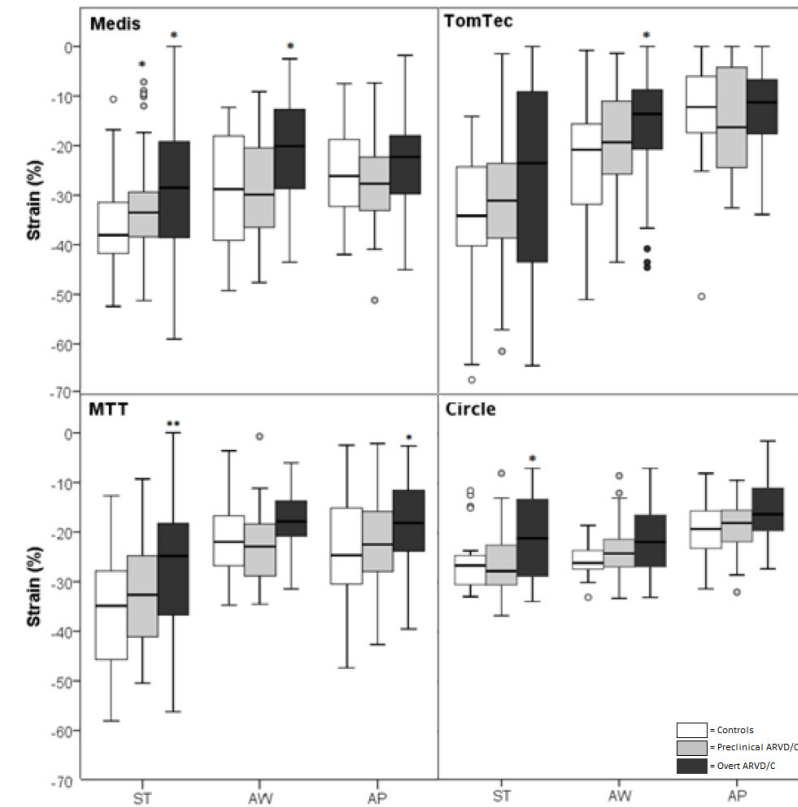
Additional File 3: Table 2; RV segmental strain values stratified by diagnostic group, without exclusions based on tracking quality

	OVERT ARVD/C (N=39)	PRECLINICAL ARVD/C (N=40)	CONTROLS (N=31)	P-VALUE#
SUBTRICUSPID REGION				
MEDIS	-29.3 ± 14.4*	-31.6 ± 10.3*	-36.6 ± 9.5	0.038
TOMTEC	-27.7 ± 18.8	-31.8 ± 14.3	-34.1 ± 13.5	0.247
MTT	-25.5 ± 12.9 [^]	-32.8 ± 10.5	-36.0 ± 11.7	0.001
CIRCLE	-20.5 ± 8.6 [^]	-25.8 ± 6.7	-25.3 ± 6.2	0.005
ANTERIOR WALL REGION				
MEDIS	-21.4 ± 10.8 [^]	-28.4 ± 10.0	-28.51 ± 11.2	0.005
TOMTEC	-16.1 ± 11.9*	-19.73 ± 11.1	-23.3 ± 12.8	0.051
MTT	-18.2 ± 6.6 [^]	-23.3 ± 7.3	-20.9 ± 7.8	0.010
CIRCLE	-21.4 ± 6.7*	-23.6 ± 5.5	-25.3 ± 3.4	0.019
APICAL REGION				
MEDIS	-23.1 ± 10.0 [^]	-27.5 ± 8.7	-25.1 ± 9.3	0.114
TOMTEC	-12.5 ± 8.6	-14.7 ± 10.4	-12.6 ± 10.2	0.540
MTT	-18.3 ± 9.1 [^]	-22.4 ± 8.3	-23.7 ± 11.2	0.053
CIRCLE	-16.5 ± 6.4*	-18.4 ± 5.1	-20.5 ± 6.7	0.035

*= Statistical significant difference compared to control subjects; [^]= Statistical significant difference compared to preclinical subjects; #= Trend between overt ARVD/C patients, preclinical ARVD/C and control subjects (OneWay ANOVA). Abbreviations: ARVD/C= Arrhythmogenic Right Ventricular Dysplasia/ Cardiomyopathy; MTT= Multimodality Tissue Tracking.



Additional File 4: Figure 1; Global (average) strain by group per software package without exclusions based on tracking quality
 Statistical significant difference compared to control subjects expressed in $*=p<0.05$ and $**=p<0.01$.
 Abbreviations: MTT= Multimodality Tissue Tracking.



Additional File 5: Figure 2; Regional strain by subgroup per software package without exclusions based on tracking quality
 Statistical significant difference compared to control subjects expressed in $*=p<0.05$ and $**=p<0.01$.
 Abbreviations: ST= subtricuspid region; AW= anterior wall region; AP= apical region; MTT= Multimodality Tissue Tracking.

Additional File 6: Table 3; AUC for global and regional longitudinal strain values in overt ARVD/C vs. control and preclinical vs. control

	OVERT ARVD/C VS. CONTROL				PRECLINICAL VS. CONTROL			
	Medis	TomTec	MTT	Circle	Medis	TomTec	MTT	Circle
GLOBAL STRAIN	0.67	0.67	0.86	0.63	0.48	0.50	0.56	0.57
REGIONAL STRAIN								
Subtricuspid	0.72	0.70	0.80	0.64	0.70	0.53	0.58	0.53
Anterior wall	0.71	0.64	0.74	0.61	0.50	0.56	0.51	0.57
Apex	0.57	0.47	0.68	0.58	0.43	0.42	0.56	0.49

Abbreviations: AUC= Area under the (ROC) curve; ARVD/C= Arrhythmogenic Right Ventricular Dysplasia/ Cardiomyopathy; MTT= Multimodality Tissue Tracking.

Additional File 7: Table 4; Global and regional longitudinal strain values in previous studies in overt ARVD/C and preclinical subjects

ARTICLE (SOFTWARE)	GLOBAL	SUBTRICUSPID REGION	ANTERIOR WALL REGION	APICAL REGION
OVERT ARVD/C PATIENTS				
VIGNEAULT ET AL. (MTT)	-19.3±6.2	-24.4±10.8	-17.7±6.4	-18.6±8.8
HEERMANN ET AL. (TomTec)	-12.7±7.3	-	-	-
PRATI ET AL. (TomTec)	-17±5	-22±11	-15±8	-14±8
PRECLINICAL ARVD/C SUBJECTS				
VIGNEAULT ET AL. (MTT)	-26.2±5.0	-33.4±10.9	-23.0±6.1	-23.3±7.8
HEERMANN ET AL. (TomTec)	-20.4±4.8	-	-	-

Abbreviations: ARVD/C= Arrhythmogenic Right Ventricular Dysplasia/ Cardiomyopathy; MTT= Multimodality Tissue Tracking.

CHAPTER

4

Feature-tracking cardiac magnetic resonance of the right ventricle: effect of field strength, resolution and imaging sequence

Mimount Bourfiss, MD*;
Bart R. Steensma, PhD*;
Anneline S.J.M. te Riele, MD, PhD;
Tim Leiner, MD, PhD;
Birgitta K. Velthuis, MD, PhD;
Alexander J.E. Raaijmakers, PhD

*Shared first authorship

Feature-tracking cardiac magnetic resonance imaging (FT-CMR) is increasingly used to assess right ventricular (RV) mechanics by quantifying strain¹. While varying sequence parameters and field strengths are used in clinical practice, little is known about the impact of these CMR parameters on RV strain values. In this study we analyzed the impact of field strength, spatial resolution and imaging sequence on the quantification of RV wall motion using FT-CMR.

Cine CMR images on 1.5 Tesla (T), 3T and 7T were acquired in 10 healthy volunteers (mean age 28±4 years and 60% male). We used two acquisition methods: balanced Steady State Free Precession (bSSFP) on 1.5 T and 3T (not possible on 7T) and Fast Low Angle Shot (FLASH) on 3T and 7T. These different acquisitions/field strengths were acquired with three different progressively increasing spatial resolutions (2.0x2.0x10.0mm³, 1.7x1.7x8.0mm³, 1.3x1.3x8.0mm³). All scans (Ingenia [1.5T and 3T]/Achieva[7T] Philips Healthcare, the Netherlands) had a temporal resolution of 30ms. FT-CMR (Medis Medical Imaging Systems, version 3.1.16.8, the Netherlands) was performed on RV 4-chamber axis to calculate global-longitudinal (GLS) and regional longitudinal strain (RLS) as strain is most reproducible in this axis¹. RV endocardial contours were manually drawn during end-diastole and end-systole (**Figure 1A**). Correlations were calculated using Pearson's correlation coefficient (*r*). Reproducibility was calculated using the intraclass correlation coefficient (ICC). Agreement was visually evaluated by Bland Altman analysis. Only one variable was altered for every comparison. Statistical analyses were performed using IBM SPSS statistics (version 25, USA)

Comparison of field strengths. 1.5T and 3T bSSFP images (1.3x1.3x8.0mm³) showed a good correlation for RV GLS (-24±4% and -24±4%, respectively; *r*=0.92 [*p*=0.001]), but a poor correlation for RV RLS (*r* ≤0.45 [*p*≥0.22]). This is also shown in the Bland Altman plots in **Figure 1B** in which relatively small limits of agreement (LoA) are seen for GLS (**panel I**) and wide LoA in the subtricuspid region (**panel II**). In contrast, 3T and 7T FLASH images (1.3x1.3x8.0mm³), showed poor correlation for both GLS and RLS (*r* ≤0.23 [*p*≥0.16]).

Comparison of spatial resolution. A good correlation was seen for GLS at a spatial resolution of 1.7x1.7x8.0mm³ and 2.0x2.0x10.0mm³ compared to 1.3x1.3x8.0mm³ (*r*=0.72 [*p*<0.02] and *r*=0.90 [*p*<0.01], respectively for 1.5T and *r*=0.75 [*p*=0.02] and *r*=0.90 [*p*<0.02], respectively for 3T). **Figure 1B (panel III and IV)** shows a moderate to good agreement between 1.3x1.3x8.0mm³ and 1.7x1.7x8.0mm³ on both 1.5T as well as 3T. For RLS, the correlation differed strongly per region (*r* 0.15-0.93, *p*≤0.85).

Comparison of imaging sequence. On 3T (1.3x1.3x8.0mm³), a poor correlation of both GLS and RLS RV strain values was observed between bSSFP and FLASH (*r* 0.15-0.60, *p*≥0.11). Also, there was poor agreement in the Bland Altman analysis in **Figure 1B (panel V)**, with wide LoA.

The intra-observer reproducibility of RV GLS on 1.5T and 3T was good (ICC 0.79-0.84) for 1.3x1.3x8.0mm³, 1.7x1.7x8.0mm³ and 2.0x2.0x10.0mm³. For 7T the intra-observer reproducibility was moderate (ICC 0.74).

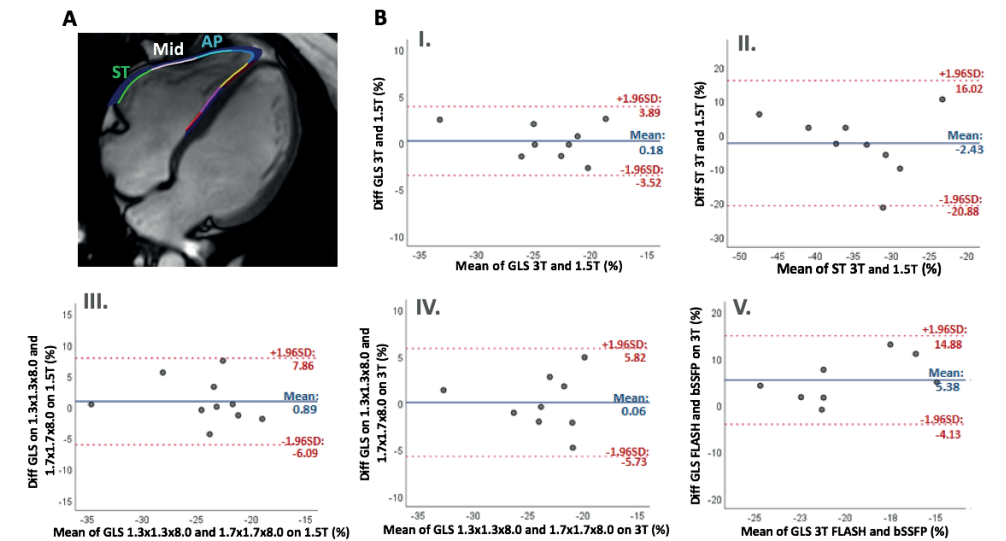


Figure 1: A) FT-CMR segmentation; **B)** Comparisons between I. Field strength 1.5T vs. 3T of GLS and; II. ST; III. Spatial resolution 1.3x1.3x8mm³ vs. 1.7x1.7x8mm³ on 1.5T and; IV. on 3T; V. Imaging sequence bSSFP vs. FLASH. GLS= global longitudinal strain; ST= subtricuspid region; Mid=midventricular region; AP= apical region

In this study we analyzed the influence of field strength, spatial resolution and imaging sequence on the quantification of RV wall motion using FT-CMR. For RV GLS, the inter-field strength (1.5T and 3T) and the inter-resolution agreement was good for the bSSFP sequence. A previous study reported a fair inter-field strength correlation between 1.5T and 3T for left ventricular GLS². The poor correlation of 7T FLASH and 3T FLASH, may be due to greater artefacts on 7T or the used FLASH imaging sequence. Since there is no accepted reference standard for RV strain, a normative comparison of the strain values using different CMR parameters remains challenging. Although 7T CMR is not yet used in clinical practice, it has great potential to detect subtle wall abnormalities due to higher signal-to-noise ratio which enables higher spatial resolutions³. This is especially interesting for the RV where the complex anatomy and contraction pattern hampers detection of subtle regional changes. For most RV regions, a poor correlation exists when comparing images obtained at different field strengths and with different CMR parameters, indicating that RLS cannot be used interchangeably and field-strength specific reference values are necessary. This

is clinically relevant since various diseases, for example Arrhythmogenic Right Ventricular Cardiomyopathy, show affected RLS (i.e. subtricuspid region) in a preclinical stage making RLS especially interesting for early diagnosis¹.

In conclusion, for 1.5T and 3T with bSSFP and varying resolutions a good correlation is seen for GLS, whereas a moderate to poor correlation is seen for RLS. For 7T and comparison of bSSFP with FLASH both GLS and RLS show a poor correlation.

REFERENCES

1. Vigneault DM, te Riele ASJM, James CA, et al. Right ventricular strain by MR quantitatively identifies regional dysfunction in patients with arrhythmogenic right ventricular cardiomyopathy. *J Magn Reson imaging*. 2016;43(5):1132-1139. doi:10.1002/jmri.25068
2. Schuster A, Morton G, Hussain ST, et al. The intra-observer reproducibility of cardiovascular magnetic resonance myocardial feature tracking strain assessment is independent of field strength. *Eur J Radiol*. 2013;82(2):296-301. doi:10.1016/j.ejrad.2012.11.012
3. Steensma BR, Voogt IJ, Leiner T, et al. An 8-channel Tx/Rx dipole array combined with 16 Rx loops for high-resolution functional cardiac imaging at 7 T. *MAGMA*. 2018;31(1):7-18. doi:10.1007/s10334-017-0665-5

CHAPTER

5

A head-to-head comparison of speckle tracking echocardiography and feature tracking cardiovascular magnetic resonance imaging in right ventricular deformation

Mimount Bourfiss, MD*;

Karim Taha, MD*;

Anneline S.J.M. te Riele, MD, PhD;

Maarten-Jan M. Cramer, MD, PhD;

Jeroen F. van der Heijden, MD, PhD;

Folkert W. Asselbergs, MD, PhD;

Birgitta K. Velthuis, MD, PhD[§];

Arco J. Teske, MD, PhD[§]

* Shared first authorship

§ Shared last authorship

ABSTRACT

Aims: Speckle tracking echocardiography (STE) and feature tracking cardiovascular magnetic resonance imaging (FT-CMR) are advanced imaging techniques which are both used for quantification of global and regional myocardial strain. Direct comparisons of STE and FT-CMR regarding right ventricular (RV) strain analysis are limited. We aimed to study clinical performance, correlation and agreement of RV strain by these techniques, using arrhythmogenic right ventricular cardiomyopathy (ARVC) as a model for RV disease.

Methods and results: We enrolled 110 subjects, including 34 patients with definite ARVC, 30 preclinical relatives of ARVC patients and 46 healthy control subjects. Global and regional RV longitudinal peak strain (PS) were measured by STE and FT-CMR. Both modalities showed reduced strain values in ARVC patients compared to ARVC relatives (STE global PS: $p < 0.001$; FT-CMR global PS: $p < 0.001$) and reduced strain values in ARVC relatives compared to healthy control subjects (STE global PS: $p = 0.042$; FT-CMR global PS: $p = 0.084$). There was a moderate, albeit significant correlation between RV strain values obtained by STE and FT-CMR (global PS $r = 0.578$ [95% CI 0.427-0.697], $p < 0.001$). Agreement between the techniques was weak (limits of agreement for global PS: $\pm 11.8\%$). Correlation and agreement both deteriorated when regional strain was studied.

Conclusion: RV STE and FT-CMR show a similar trend within the spectrum of ARVC and have significant correlation, but inter-modality agreement is weak. STE and FT-CMR may therefore both individually have added value for assessment of RV function, but RV PS values obtained by these techniques currently cannot be used interchangeably in clinical practice.

INTRODUCTION

Speckle tracking echocardiography (STE) and feature tracking cardiovascular magnetic resonance imaging (FT-CMR) are advanced tools within the field of cardiac imaging, which both enable quantification of myocardial deformation.¹ Although these two techniques are used within different imaging platforms (i.e. echocardiography and CMR), both techniques use dedicated post-processing algorithms to identify markers in the myocardium and follow these markers throughout the cardiac cycle to track myocardial motion. The most fundamental parameter that is derived by these techniques is myocardial strain, which represents the amount of myocardial shortening during the cardiac cycle.

STE and FT-CMR are currently both applied to quantify right ventricular (RV) function in several diseases.²⁻¹³ One of particular interest is arrhythmogenic right ventricular cardiomyopathy (ARVC). ARVC is an inheritable cardiomyopathy that is characterized by fibro-fatty replacement of the myocardium, typically of the RV.¹⁴ Since the presence of structural heart disease identifies individuals who are at higher risk of life-threatening arrhythmias, echocardiography and CMR are sequentially performed in ARVC patients and their at-risk relatives.¹⁵ STE and FT-CMR both enable detection of impaired RV strain in early stages of disease, which largely goes unnoticed by conventional imaging measurements.²⁻⁸ These subclinical abnormalities have recently been associated with development of clinical disease progression, and therefore RV strain analysis may improve screening protocols in relatives of ARVC patients.⁵

Since STE and FT-CMR are both applied in similar patients for measurement of RV strain, insight into the interchangeability of these measurements is of clinical relevance. STE and FT-CMR have been extensively compared in previous studies, but these studies mainly focused on left ventricular (LV) strain measurements.¹⁶⁻¹⁸ In the present study we aimed (1) to compare RV strain analysis by STE and FT-CMR with regard to clinical performance in ARVC, and (2) to study correlation and agreement between these techniques.

METHODS

Study population

Subjects that were eligible for this study were patients with definite ARVC according to the 2010 Task Force Criteria (TFC) and relatives of ARVC patients (not fulfilling definite ARVC diagnosis) who were evaluated at the University Medical Center Utrecht between 2004 and 2018.^{19,20} In this period, 297 unique subjects underwent echocardiography and 242 underwent CMR as part of routine clinical care. Relatives who underwent genetic testing but who were not found to carry the index mutation were excluded. Subjects who underwent

both echocardiography and 1.5 Tesla CMR within one month were included in the final study population, provided that the images were appropriate for RV strain analysis by both STE and by FT-CMR. A group of healthy non-athlete subjects who underwent echocardiography and 1.5 Tesla CMR within one day for a previous study served as control group.²¹ The control group was age- and gender matched with ARVC relatives. This study was approved by the local institutional ethics committee and was performed according to the principles of the Declaration of Helsinki and the European General Data Protection Regulation.

Echocardiography and STE

All echocardiograms were obtained with Vivid 7 or Vivid E9 (GE Healthcare, Horten, Norway) according to a standardized protocol.²² RV outflow-tract (RVOT) dimensions were measured in the parasternal long-axis view and parasternal short-axis view (PLAX/PSAX), and fractional area change (FAC) was measured in the apical 4-chamber view.¹⁹ Longitudinal strain analysis was performed offline with GE EchoPac version 202.39 (GE Healthcare, Horten, Norway) by two experienced observers who were blinded for clinical data and FT-CMR results. Inter- and intra-observer agreement was recently shown to be excellent: reported kappa values were respectively 0.94 and 0.93.^{5,6} The analyses were performed according to a previously published protocol.²² In brief, a narrow-angle RV-focused recording from the apical 4-chamber view was used.²³ Frame rates between 55 and 110 frames/second were accepted for deformation imaging. Onset of systole was set at the beginning of the QRS-complex on the electrocardiogram (ECG). The endocardial border of the RV lateral wall was manually traced. The apical cap was not included in the region of interest. When necessary, the region of interest thickness was adjusted manually to include the RV myocardium or to exclude the pericardium. The region of interest was automatically divided into a basal, mid and apical segment. A representative example is shown in **Figure 1**.

CMR and FT-CMR

All CMR images were acquired using a 1.5 Tesla scanner (Philips Medical Systems, Best, the Netherlands). RV dimensions and ejection fraction (RVEF) were measured on short axis (repetition time/echo time/flip angle 2.9/1.4/60 degrees, matrix 192-256, field of view 320mm, temporal resolution ≤ 50 msec, slice thickness 8mm). Ventricular end-diastolic (EDV) and end-systolic volumes (ESV) were measured and corrected for body surface area. Longitudinal strain analysis was performed in the horizontal long axis using Medis Qstrain Software (Medis Medical Imaging Systems, version 3.1, Leiden, the Netherlands) by one experienced observer blinded for clinical data and STE results. Endocardial contours of the RV (from lateral to septal) were manually drawn during end-diastole and end-systole with subsequent automatic tracking during the cardiac cycle. Onset of systole was determined on the basis of ventricular volumes. The endocardial border was automatically segmented into seven regions of equal size; three segments in the lateral free wall (basal, mid, apical), apical cap and three segments in the septal wall (basal, mid, apical). A representative example is presented in **Figure 1**.

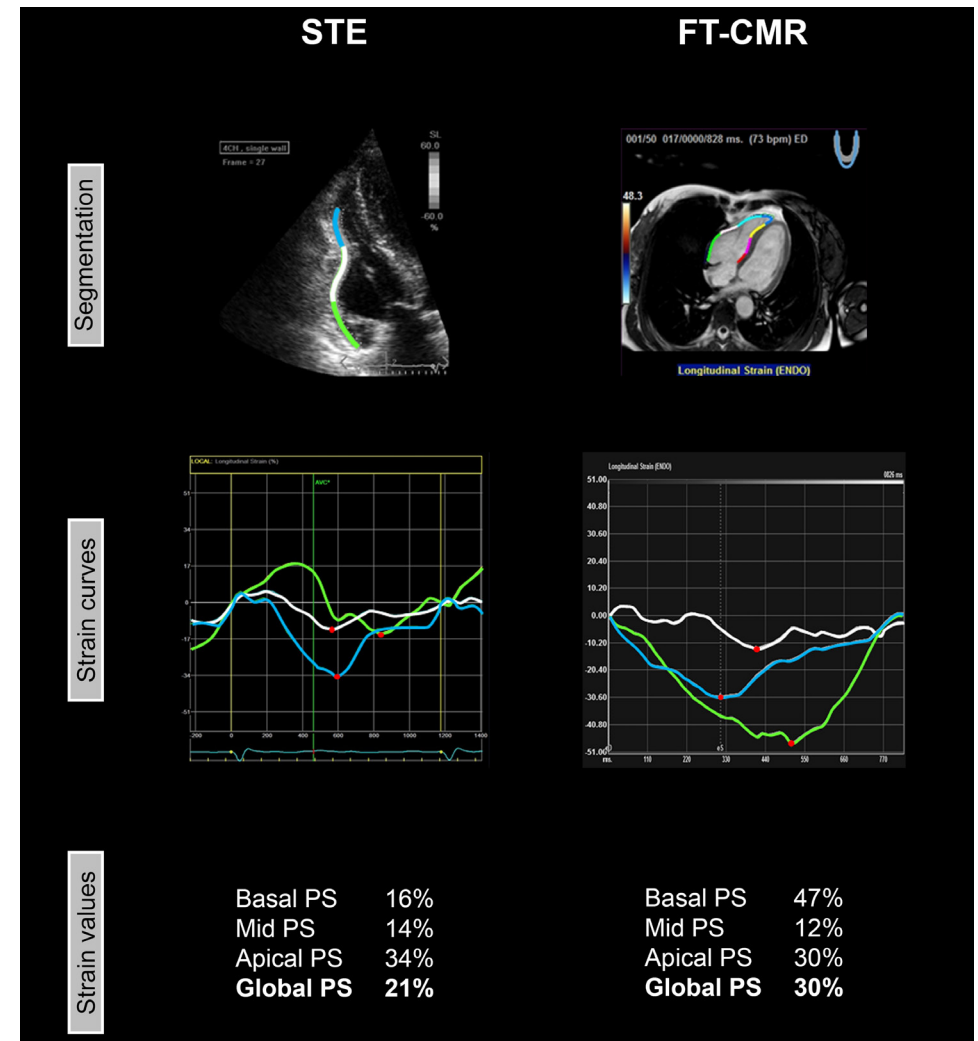


Figure 1: Representative example of RV analysis by STE and FT-CMR in one patient

The RV lateral wall was analysed with STE (left) and FT-CMR (right). In both techniques, the RV lateral wall was automatically divided in three segments (basal/green, mid/white, apical/blue). From these three segments, PS was derived, which is defined as the maximum amount of myocardial shortening (red dots). Global PS is defined as the average PS from the three RV segments. Abbreviations: FT-CMR=feature tracking cardiovascular magnetic resonance imaging; PS=peak strain; STE=speckle tracking echocardiography.

Strain parameters

All strain values in this study are reported as absolute values. With STE and FT-CMR, regional peak strain (PS) was derived from the basal, mid and apical region of the RV lateral wall (**Figure 1**). The apical cap was not included in the analysis according to current recommendations.²³ The interventricular septum was not taken into account, because it is

also considered to be part of the left ventricle.²³ PS was defined as the maximum amount of myocardial shortening during the cardiac cycle, expressed in percent. Global PS was defined as the average PS of the three segments of the RV lateral wall. Global PS was only calculated when all three RV lateral wall segments were eligible for analysis by both modalities.

Vendor-independent analysis

The aforementioned analyses were performed with different software packages for STE and FT-CMR. To study the effect of software-dependence, we additionally measured global and regional PS in the RV free wall with a vendor-independent software package that can process both echocardiographic and CMR data for STE and FT-CMR analysis (TomTec Image Arena version 4.6, Unterschleissheim, Germany). This software package automatically determines onset of systole on the basis of ventricular volumes (i.e. frame/phase with largest RV area on echocardiography or CMR). The vendor-independent analysis was performed in a random selection of 30 subjects (10 ARVC patients, 10 ARVC relatives, 10 controls).

Statistical method

Data are expressed as mean \pm standard deviation (SD) or as median [IQR]. Normal distribution was tested using the Shapiro-Wilk test. Significance of differences between three groups was calculated using a one-way analysis of variance (ANOVA) or a Kruskal-Wallis test. Significance of differences between two groups was calculated using an independent students t-test or Mann-Whitney U test. Binary data were compared using a Fischer's exact test. Bonferroni correction was applied in case of multiple testing (i.e. multiplication of obtained p-value by the number of tests). Direct comparison of strain values by STE and FT-CMR was performed by a paired t-test or a Wilcoxon signed rank test. For assessment of correlation, Pearson's r test was used. In case of non-linearity, Spearman's rank test was performed. Agreement between the two modalities was assessed by Bland-Altman analysis. The bias was calculated as the mean measurement difference between the two techniques (FT-CMR – STE), whereas 95% limits of agreement were calculated as twice the SD of the measurement difference. P-values of <0.05 were considered to indicate statistical significance. P-values between 0.05 and 0.1 were considered to be borderline significant. All statistical analyses were performed using SPSS Statistics for Windows version 23.0, IBM, Armonk, New York.

RESULTS

Baseline characteristics

The study population consisted of 110 subjects, including 34 ARVC patients (31%), 30 ARVC relatives (27%) and 46 healthy control subjects (42%). Baseline characteristics are shown in **Table 1**. By design, ARVC relatives and control subjects were age- and gender matched.

ARVC patients were older than the other groups ($p<0.001$). Gender was equally distributed between ARVC patients and the other groups ($p=0.834$). The number of subjects carrying a pathogenic mutation was equal in ARVC patients and ARVC relatives ($n=27$ [79%] vs. $n=24$ [80%], $p=1.000$). ARVC relatives without a proven mutation were either relatives who did not undergo genetic testing ($n=4$) or relatives of mutation-negative index patients ($n=2$).

Table 1: Baseline characteristics

	ARVC patients (n=34)	ARVC relatives (n=30)	Control subjects (n=46)	p-value
Age (years)	43.4 \pm 17.9**	32.6 \pm 16.8	27.3 \pm 5.4	<0.001
Males	18 (53)	14 (47)	21 (46)	0.834
Pathogenic mutation	27 (79)	24 (80)	-	1.000
Desmosomal	23 (68)	16 (53)	-	0.307
Non-desmosomal	4 (12)	8 (27)	-	0.199
2010 TFC	6 [4]*	2 [1]	-	<0.001
Structural TFC	25 (74)*	2 (7)	-	<0.001
Depolarization TFC	20 (59)*	5 (17)	-	0.001
Repolarization TFC	20 (59)*	3 (10)	-	<0.001
Arrhythmia TFC	30 (88)*	5 (17)	-	<0.001
Family history TFC	29 (85)*	30 (100)	-	0.253
Echocardiography				
RVOT-PLAX (mm)	35.4 [9.0]**	27.8 [9.0]	26.1 [5.6]	<0.001
RVOT-PSAX (mm)	36.5 [6.9]**	29.4 [5.4]	28.8 [4.0]	<0.001
FAC (%)	37.5 \pm 11.0**	47.7 \pm 7.0	45.2 \pm 4.2	<0.001
CMR				
RV-EDV (ml/m²)	116.3 [59.4]**	90.4 [23.6]*	99.8 [27.1]	<0.001
RV-ESV (ml/m²)	63.2 [56.4]**	39.9 [16.5]*	47.3 [17.1]	<0.001
RVEF (%)	42.2 \pm 12.6**	55.7 \pm 6.8	53.3 \pm 5.2	<0.001

Values are presented as mean \pm SD, median [IQR] or n (%). An asterisk (*) indicates a statistical significant difference ($p<0.05$) compared to the adjacent group at the right and a double asterisk (**) indicates a statistical significant difference compared to the two adjacent groups at the right. Statistical tests between subgroups are performed with a Bonferroni correction for multiple testing. Abbreviations: ARVC=arrhythmogenic right ventricular cardiomyopathy; EDV=end diastolic volume; ESV= end-systolic volume; FAC=fractional area change; PLAX=parasternal long-axis view; PSAX=parasternal short-axis view; RV=right ventricular; RVEF=right ventricular ejection fraction; RVOT= right ventricular outflow tract; TFC= task force criteria.

By design, all control subjects had echocardiography and CMR within one day. The timeframe between echocardiography and CMR was equal in ARVC patients and relatives (4 \pm 8 days vs. 3 \pm 6 days, $p=0.115$).

By conventional measurements, echocardiography and CMR both showed increased RV size ($p<0.001$) and decreased RV function ($p<0.001$) in ARVC patients compared to ARVC relatives and control subjects (**Table 1**). RV size and RV function were within normal range by conventional measurements in ARVC relatives when compared to control subjects.²⁴ More conventional measurements are shown in **supplementary table 1**.

Strain analysis

With STE, 315 segments (95%) were eligible for strain analysis; the basal segment was excluded in one subject, the mid segment was excluded in three subjects and the apical segment was excluded in 11 subjects. With FT-CMR, 328 segments (99%) were eligible for strain analysis; the mid segment was excluded in one subject and the apical segment was excluded in another. Overall, higher PS values were seen with FT-CMR compared to STE (**Table 2**). Furthermore, a wider range of PS values was seen with FT-CMR compared to STE (**supplementary figures 1-4**).

With STE, mean PS in the apical segment was higher than in the basal segment (27.5±5.5% vs. 20.8±6.1%, $p<0.001$). With FT-CMR this gradient was reversed; mean PS in the basal segment was higher than in the apical segment (38.0±9.1% vs. 32.6±11.8%, $p<0.001$). While with STE the lowest PS values were found in the basal segment, FT-CMR showed the lowest PS values in the mid segment.

Table 2: Mean strain values, agreement and correlation

	Global PS (n=96)	Basal PS (n=109)	Mid PS (n=106)	Apical PS (n=98)
STE PS (%)	24.3±5.2	20.8±6.1	24.7±5.8	27.5±5.5
FT-CMR PS (%)	33.2±7.1	38.0±9.1	29.0±11.3	32.6±11.8
Rho [95% CI]	0.578 [0.427-0.697]*	0.490 [0.333-0.620]*	0.399 [0.159-0.497]*	0.261 [0.066-0.436]*
Bias (%)	8.8	17.5	4.2	4.8
Limits of agreement (%)	±11.8	±16.2	±21.6	±23.4

Strain measurements are presented as absolute values (mean ± SD). An asterisk (*) indicates a significant correlation ($p<0.05$). Abbreviations: FT-CMR=feature tracking cardiovascular magnetic resonance imaging; PS=peak strain; STE=speckle tracking echocardiography.

Clinical performance

Global strain

STE and FT-CMR both showed significantly lower global PS values in ARVC patients compared to ARVC relatives (**Table 3, Figure 2**): global PS with STE was 19.7±5.7% in ARVC patients and 25.1±3.4% in ARVC relatives ($p<0.001$), global PS with FT-CMR was 27.9±6.7% in ARVC patients and 33.6±5.2% in ARVC relatives ($p<0.001$). When comparing ARVC relatives with control subjects, STE and FT-CMR both showed reduced global PS in ARVC relatives, which was statistically significant with STE and borderline statistically significant with FT-CMR (**Table 3, Figure 2**): global PS in control subjects was 27.1±3.5% ($p=0.042$) with STE and 36.4±6.0% with FT-CMR ($p=0.084$).

Table 3: Comparison of measurements in different clinical stages

	STE				FT-CMR			
	ARVC patients (n=34)	ARVC relatives (n=30)	Control subjects (n=46)	p-value relatives- controls	ARVC patients (n=34)	ARVC relatives (n=30)	Control subjects (n=46)	p-value relatives- controls
Global PS (%)	19.7±5.7	25.1±3.4	27.1±3.5	0.042	27.9±6.7	33.6±5.2	36.4±6.0	<0.001
Basal PS (%)	15.0±6.5	22.0±3.7	24.0±3.8	0.078	32.3±9.4	37.7±8.3	41.8±7.6	0.030
Mid PS (%)	19.7±6.0	25.2±3.5	27.7±4.3	0.040	22.2±10.9	28.5±9.5	33.7±10.4	0.034
Apical PS (%)	24.2±6.8	27.3±4.0	29.6±4.0	0.110	29.3±12.7	34.8±9.3	33.7±12.5	0.114

Strain measurements are presented as absolute values (mean ± SD). Abbreviations: ARVC=arrhythmogenic right ventricular cardiomyopathy; FT-CMR=feature tracking cardiovascular magnetic resonance imaging; PS=peak strain; STE=speckle tracking echocardiography.

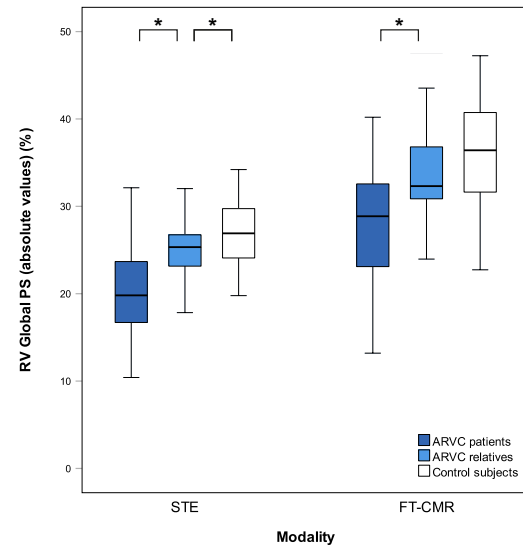


Figure 2: Global RV PS in different clinical stages by STE and FT-CMR

With STE (left) and FT-CMR (right), similar differences of RV strain values are seen between ARVC patients, ARVC relatives and healthy controls. An asterisk (*) indicates a statistically significant difference ($p < 0.05$). Abbreviations: ARVC=arrhythmogenic right ventricular cardiomyopathy; PS=peak strain; RV=right ventricle/ventricular.

Regional strain

STE showed lower strain values in ARVC patients compared to ARVC relatives in the basal segment ($p < 0.001$), in the mid segment ($p < 0.001$) and in the apical segment ($p = 0.052$) (**Table 3**). FT-CMR also showed lower strain values in ARVC patients compared to ARVC relatives in the basal segment ($p = 0.030$) and in the mid segment ($p = 0.034$) (**Table 3**). When comparing ARVC relatives with control subjects, STE showed lower strain values in ARVC relatives in the basal segment ($p = 0.078$) and in the mid segment ($p = 0.040$). This was also seen with FT-CMR in the basal segment ($p = 0.070$) and in the mid segment ($p = 0.070$).

Correlation and agreement

Global strain

Correlation between STE and FT-CMR for global PS was moderate ($r = 0.578$ [0.427-0.697], $p < 0.001$). Bland-Altman plots for global PS are displayed in **Figure 3**. For global PS, bias between STE and FT-CMR was 8.8% and limits of agreement were $\pm 11.8\%$. Limits of agreement for global PS were comparable for ARVC patients, ARVC relatives and control subjects (respectively ± 13.0 , ± 10.6 and ± 11.6 , **supplementary figure 5**).

A subgroup analysis was performed for subjects who had echocardiography and CMR on the same day ($n = 81$). Correlation and agreement did not improve in this subgroup

(**supplementary table 2**), nor did correlation and agreement improve when STE and FT-CMR were performed with a similar software package (**supplementary figure 9, supplementary table 3**).

Regional strain

Correlation was weaker for regional PS than for global PS (**Table 2**). Bland-Altman plots for regional PS in the basal, mid and apical segments are displayed in **Figure 3**. Limits of agreement were wider for regional PS than for global PS (basal segment $\pm 16.2\%$; mid segment $\pm 21.6\%$; apical segment $\pm 23.4\%$). Limits of agreement for regional PS were comparable for ARVC patients, ARVC relatives and control subjects (**supplementary figures 6-8**). Consistently higher PS values were measured with FT-CMR in the basal segment compared to STE (lower limit of agreement: 1.3% upper limit of agreement: 33.7%).

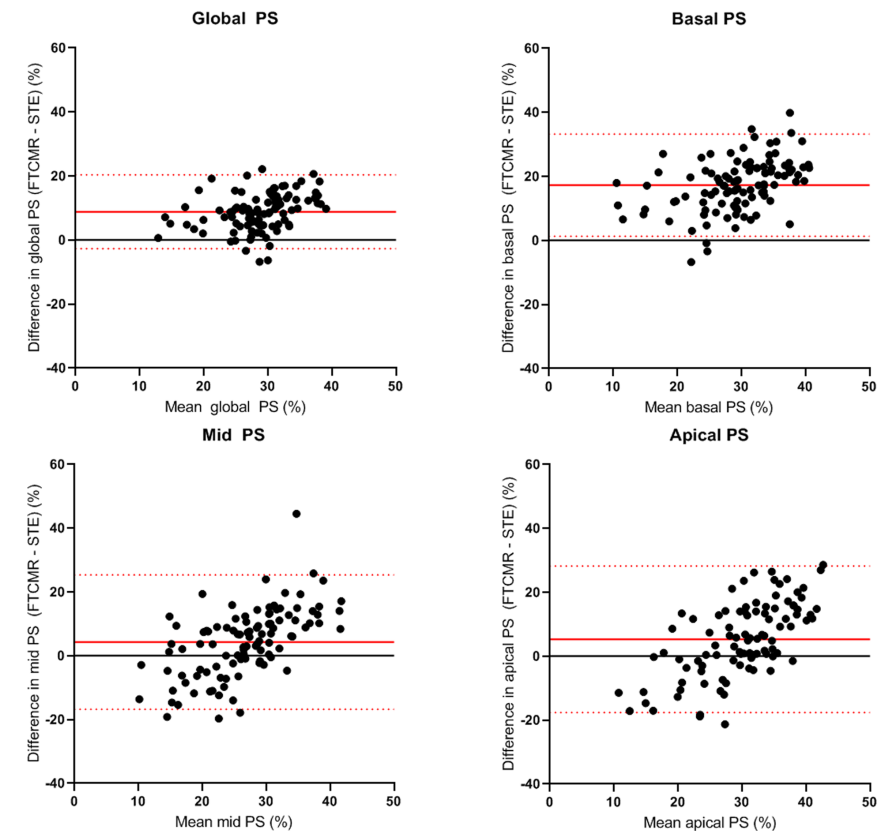


Figure 3: Bland-Altman plots for global and segmental RV PS

Bland-Altman plots show weak agreement between STE and FT-CMR. Agreement is best for global RV PS (upper left plot) and becomes worse when performing regional analysis. Abbreviations: FT-CMR=feature tracking cardiovascular magnetic resonance imaging; PS=peak strain; STE=speckle tracking echocardiography.

DISCUSSION

The present study is among the first to compare RV strain values derived by STE and FT-CMR. We found that STE and FT-CMR show a comparable trend of RV strain values among ARVC patients and relatives. This led to a significant correlation between the modalities, but suboptimal agreement. Based on our findings, we can neither recommend using STE and FT-CMR interchangeably, nor can we provide a correction factor to correct the bias between the two different techniques.

Clinical utility in ARVC

STE and FT-CMR are both increasingly applied to quantify global and regional RV deformation in ARVC.²⁻⁹ In our study, both techniques independently showed comparable differences between subgroups in ARVC. Both techniques showed significant differences between ARVC patients and relatives of ARVC patients (who do not fulfil ARVC diagnosis) with both global and regional RV strain. Interestingly, both techniques also found lower strain values in at-risk relatives than in healthy control subjects. These abnormalities were not picked up by conventional imaging measurements, which supports the hypothesis that conventional imaging modalities lack sensitivity to detect early structural signs of ARVC. The differences between ARVC relatives and healthy control subjects were found to be statistically significant with STE and borderline statistically significant with FT-CMR, which might suggest that STE is more sensitive for a subtle decrease of RV PS values than FT-CMR.

Correlation and agreement

Previous studies comparing RV STE and RV FT-CMR showed a moderate correlation between these techniques (respectively $r=0.45$ and $r=0.56$).^{10,11} Previous studies investigating agreement between RV STE and RV FT-CMR are scarce and of small sample size. Kempny *et al.* performed RV strain analysis by STE and FT-CMR in a cohort of 28 adult patients with repaired tetralogy of Fallot (TOF) and 25 healthy controls, and reported limits of agreement of $\pm 8.3\%$ for RV global longitudinal peak strain.¹² Furthermore, Padiyath *et al.* compared STE and FT-CMR in 20 patients with TOF and 20 control subjects, and reported comparable limits of agreement for RV global longitudinal peak strain of ± 8.5 .¹³ The wide limits of agreement in both aforementioned studies already suggested that strain values derived by STE and FT-CMR cannot be used interchangeably in clinical practice. However, since these studies were both performed in patients with congenital heart disease and subsequent RV remodelling (i.e. RV hypertrophy), these results cannot be compared to the results of the present study.

In accordance with the previous studies, we found a moderate but significant correlation between STE and FT-CMR. We found inter-modality agreement between STE and FT-CMR for RV strain analysis to be poor. FT-CMR tended to show higher RV strain

values (particularly in the basal segment). The magnitude of the global and regional RV strain values that were found with FT-CMR were not reported before by the reference standard sonomicrometry.^{25,26} Remarkably, we observed reversed gradients of peak strain from the basal to the apical segment of the RV free wall in the two techniques (which is in accordance with previous studies).^{4,21} Our results confirm that global and regional RV strain measurements by STE and FT-CMR currently cannot be used interchangeably on an individual level.

The following factors may have contributed to the observed inter-modality differences:

- STE and FT-CMR are based on similar physical principles, but the techniques use different markers to quantify myocardial motion. In STE, “speckles” are followed throughout the cardiac cycle, which are distinct acoustic backscatters that result from interference of ultrasound waves with the myocardium. CMR images do not have such scatters, and instead FT-CMR algorithms use “features” which are anatomic elements that are identified along the cavity-myocardial interface. It remains unknown whether the motion of speckles and features are equally representative for RV myocardial deformation.
- The difficulty to match myocardial segments between echocardiography and CMR due to different scanning angles is a known source of inter-modality variation. This is particularly true for the RV because of its complex geometry and anatomical position in the chest. In this study, we aimed to analyse the RV lateral wall with both techniques, but slight differences in slice position between the two modalities are inevitable and cannot be excluded.
- Echocardiography and CMR are known to differ in spatial and temporal resolution. While the signal-to-noise ratio is relatively high in CMR, echocardiography may be limited by suboptimal acoustic windows and thus suboptimal endocardial delineation, particularly when imaging the RV. This is illustrated by a higher number of excluded segments in echocardiography than in CMR in the present study. On the other hand, the temporal resolution is higher in echocardiography, which is considered to be beneficial for deformation imaging.¹ This may be a more important factor in the quantification of RV deformation values due to the higher velocities of the RV free wall compared to the LV myocardial velocities (in particular the RV basal segment).²⁷ Whether this impacts the feature tracking algorithm is unknown.
- The reference method for defining onset of systole was different between STE and FT-CMR in this study. While the timing of these events was ECG-gated with STE, FT-CMR algorithms use ventricular volumes to determine the timing. These differences in timing may have also contributed to the differences in strain values, although the absolute effect of this difference will not explain the mean bias observed in our study.

Future directions

Future studies should be of a longitudinal design to compare the added prognostic values of both techniques. In our study we only investigated RV PS, because other RV measurements derived by STE (e.g. systolic PS, post-systolic shortening, electromechanical interval, mechanical dispersion) have not been applied in FT-CMR yet.^{3,5-7,28} Future studies comparing other RV parameters between STE and FT-CMR may lead to an improvement of agreement and correlation between these techniques. Furthermore, we did not include septal segments in our study because these segments are also part of the left ventricle. Future studies including these segments would be of interest.

Limitations

The relatively small number of patients that is included in this study might be a potential limitation. However, regarding the magnitude of the differences that were observed between the techniques, we assume that a larger study population will not improve inter-modality agreement to such an extent that the measurements can be used interchangeably.

We included patients only when at least one of the segments of the RV was eligible for strain analysis by both echocardiography and CMR. Therefore, the feasibility of these techniques may be overestimated in this study.

Not all the echocardiograms and CMRs in this study were performed on the same day. Since strain values may be affected by physiological differences (such as heart-rate and loading conditions), this one-month timeframe may have also induced some differences between the modalities. Nevertheless, more than half of our population had both examinations within one day. Additionally, a subgroup analysis within this group showed no improvement of correlation and agreement.

Different software packages were used for STE and FT-CMR in this study. To exclude major differences induced by software-variability, we conducted an additional analysis with a similar software package for both techniques that showed no improvement in agreement and correlation. This, in combination with our extensive experience with these particular software packages and the resemblance of regular clinical practice makes the use of different software packages in this study reasonable.

CONCLUSION

STE and FT-CMR both show a similar trend within the spectrum of ARVC and have a significant correlation regarding RV strain measurements. Inter-modality agreement is however suboptimal, in particular for regional assessment. STE and FT-CMR may therefore both individually have added value for assessment of RV function, but the strain values obtained by these techniques cannot be used interchangeably in clinical practice. Future studies should aim to compare the prognostic values of both techniques.

Acknowledgements

This work is supported by the Dutch Heart Foundation (grant number CVON2015-12 eDETECT). M. Bourfiss is supported by the Alexandre Suerman Stipend of the UMC Utrecht (2017). A.S.J.M. te Riele is supported by the Dutch Heart Foundation (grant number 2015T058). F.W. Asselbergs is supported by UCL Hospitals NIHR Biomedical Research Centre.

REFERENCES

1. Amzulescu MS, Craene M De, Langet H, Pasquet A, Vancraeynest D, Pouleur AC, et al. Myocardial strain imaging: review of general principles, validation, and sources of discrepancies. *Eur Heart J Cardiovasc Imaging* 2019;**20**:605–619.
2. Haugaa KH, Basso C, Badano LP, Bucciarelli-Ducci C, Cardim N, Gaemperli O, et al. Comprehensive multi-modality imaging approach in arrhythmogenic cardiomyopathy—an expert consensus document of the European Association of Cardiovascular Imaging. *Eur Heart J Cardiovasc Imaging* 2017;**18**:237–253.
3. Taha K, Mast TP, Cramer MJ, Heijden JF van der, Asselbergs FW, Doevendans PA, et al. Evaluation of Disease Progression in Arrhythmogenic Cardiomyopathy: The Change of Echocardiographic Deformation Characteristics Over Time. *JACC Cardiovasc Imaging* 2020;**13**:631–634.
4. Bourfiss M, Vigneault DM, Aliyari Ghasebeh M, Murray B, James CA, Tichnell C, et al. Feature tracking CMR reveals abnormal strain in preclinical arrhythmogenic right ventricular dysplasia/ cardiomyopathy: a multisoftware feasibility and clinical implementation study. *J Cardiovasc Magn Reson* England; 2017;**19**:66.
5. Mast TP, Taha K, Cramer MJ, Lumens J, Heijden JF van der, Bouma BJ, et al. The Prognostic Value of Right Ventricular Deformation Imaging in Early Arrhythmogenic Right Ventricular Cardiomyopathy. *JACC Cardiovasc Imaging* 2019;**12**:446–455.
6. Mast TP, Teske AJ, Walmsley J, Heijden JF van der, Es R van, Prinzen FW, et al. Right Ventricular Imaging and Computer Simulation for Electromechanical Substrate Characterization in Arrhythmogenic Right Ventricular Cardiomyopathy. *J Am Coll Cardiol* 2016;**68**:2185–2197.
7. Mast TP, Teske AJ, Riele AS te, Groeneweg JA, Heijden JF van der, Velthuis BK, et al. Prolonged Electromechanical Interval Unmasks Arrhythmogenic Right Ventricular Dysplasia/Cardiomyopathy in the Subclinical Stage. *J Cardiovasc Electrophysiol* 2016;**27**:303–314.
8. Heermann P, Hedderich DM, Paul M, Schülke C, Kroeger JR, Baeßler B, et al. Biventricular myocardial strain analysis in patients with arrhythmogenic right ventricular cardiomyopathy (ARVC) using cardiovascular magnetic resonance feature tracking. *J Cardiovasc Magn Reson* 2014;**16**:75.
9. Vigneault DM, Riele ASJM te, James CA, Zimmerman SL, Selwaness M, Murray B, et al. Right ventricular strain by MR quantitatively identifies regional dysfunction in patients with arrhythmogenic right ventricular cardiomyopathy. *J Magn Reson Imaging* 2016;**43**:1132–1139.
10. Houard L, Benaets M-B, Meester de Ravenstein C de, Rousseau MF, Ahn SA, Amzulescu M-S, et al. Additional Prognostic Value of 2D Right Ventricular Speckle-Tracking Strain for Prediction of Survival in Heart Failure and Reduced Ejection Fraction. *JACC Cardiovasc Imaging* 2019;**12**:2373–2385.
11. Tong X, Poon J, Li A, Kit C, Yamada A, Shiino K, et al. Validation of cardiac magnetic resonance tissue tracking in the rapid assessment of RV function: a comparative study to echocardiography. *Clin Radiol* 2018;**73**:324.e9–324.e18.
12. Kempny A, Fernandez-Jimenez R, Orwat S, Schuler P, Bunck AC, Maintz D, et al. Quantification of biventricular myocardial function using cardiac magnetic resonance feature tracking, endocardial border delineation and echocardiographic speckle tracking in patients with repaired tetralogy of Fallot and healthy controls. *J Cardiovasc Magn Reson*; 2012;**14**:32.
13. Padiyath A, Gribben P, Abraham JR, Li L, Rangamani S, Schuster A, et al. Echocardiography and cardiac magnetic resonance-based feature tracking in the assessment of myocardial mechanics in tetralogy of fallot: An intermodality comparison. *Echocardiography* 2013;**30**:203–210.
14. Corrado D, Link MS, Calkins H. Arrhythmogenic Right Ventricular Cardiomyopathy. *N Engl J Med* 2017;**376**:61–72.
15. Corrado D, Wichter T, Link MS, Hauer RNW, Marchlinski FE, Anastakis A, et al. Treatment of Arrhythmogenic Right Ventricular Cardiomyopathy/Dysplasia: An International Task Force Consensus Statement. *Circulation* 2015;**132**:441–453.
16. Obokata M, Nagata Y, Wu VC-C, Kado Y, Kurabayashi M, Otsuji Y, et al. Direct comparison of cardiac magnetic resonance feature tracking and 2D/3D echocardiography speckle tracking for evaluation of global left ventricular strain. *Eur Heart J Cardiovasc Imaging* 2016;**17**:525–532.
17. Aurich M, Keller M, Greiner S, Steen H, Aus dem Siepen F, Riffel J, et al. Left ventricular mechanics assessed by two-dimensional echocardiography and cardiac magnetic resonance imaging: comparison of high-resolution speckle tracking and feature tracking. *Eur Heart J Cardiovasc Imaging* 2016;**17**:1370–1378.
18. Everdingen WM van, Zweerink A, Nijveldt R, Salden OAE, Meine M, Maass AH, et al. Comparison of strain imaging techniques in CRT candidates: CMR tagging, CMR feature tracking and speckle tracking echocardiography. *Int J Cardiovasc Imaging* 2018;**34**:443–456.
19. Marcus FI, McKenna WJ, Sherrill D, Basso C, Bauce B, Bluemke DA, et al. Diagnosis of arrhythmogenic right ventricular cardiomyopathy/dysplasia: proposed modification of the task force criteria. *Circulation* 2010;**121**:1533–1541.
20. Bosman LP, Verstraelen TE, Lint FHM van, Cox MGPJ, Groeneweg JA, Mast TP, et al. The Netherlands Arrhythmogenic Cardiomyopathy Registry: design and status update. *Neth Heart J* 2019;**27**:480–486.
21. Teske AJ, Prakken NH, Boeck BW De, Velthuis BK, Martens EP, Doevendans PA, et al. Echocardiographic tissue deformation imaging of right ventricular systolic function in endurance athletes. *Eur Heart J* 2009;**30**:969–977.
22. Teske AJ, Boeck BWL De, Melman PG, Sieswerda GT, Doevendans PA, Cramer MJM. Echocardiographic quantification of myocardial function using tissue deformation imaging, a guide to image acquisition and analysis using tissue Doppler and speckle tracking. *Cardiovasc Ultrasound* 2007;**5**:27.
23. Badano LP, Kolias TJ, Muraru D, Abraham TP, Aurigemma G, Edvardsen T, et al. Standardization of left atrial, right ventricular, and right atrial deformation imaging using two-dimensional speckle tracking echocardiography: a consensus document of the EACVI/ASE/Industry Task Force to standardize deformation imaging. *Eur Heart J Cardiovasc Imaging* 2018;**19**:591–600.
24. Kawel-Boehm N, Maceira A, Valsangiacomo-Buechel ER, Vogel-Claussen J, Turkbey EB, Williams R, et al. Normal values for cardiovascular magnetic resonance in adults and children. *J Cardiovasc Magn Reson* 2015;**17**:29.
25. Atsumi A, Seo Y, Ishizu T, Nakamura A, Enomoto Y, Harimura Y, et al. Right Ventricular Deformation Analyses Using a Three-Dimensional Speckle-Tracking Echocardiographic System Specialized for the Right Ventricle. *J Am Soc Echocardiogr* 2016;**29**:402–411.e2.
26. Chen R, Zhu M, Amacher K, Wu X, Sahn DJ, Ashraf M. Non-invasive Evaluation of Right Ventricular Function with Real-Time 3-D Echocardiography. *Ultrasound Med Biol* 2017;**43**:2247–2255.
27. Caballero L, Kou S, Dulgheru R, Gonjilashvili N, Athanassopoulos GD, Barone D, et al. Echocardiographic reference ranges for normal cardiac Doppler data: results from the NORRE Study. *Eur Heart J Cardiovasc Imaging*. 2015;**16**:1031–41.
28. Sarvari SI, Haugaa KH, Anfinsen O-G, Leren TP, Smiseth OA, Kongsgaard E, et al. Right ventricular mechanical dispersion is related to malignant arrhythmias: a study of patients with arrhythmogenic right ventricular cardiomyopathy and subclinical right ventricular dysfunction. *Eur Heart J* 2011;**32**:1089–1096.

SUPPLEMENTARY DATA

Supplementary table 1: Additional conventional measurements

	ARVC patients (n=34)	ARVC relatives (n=30)	Control subjects (n=46)	p-value
Echocardiography				
TAPSE (mm)	19.4 ± 4.3**	22.6 ± 2.2	24.0 ± 2.7	<0.001
RV S' velocity (cm/s)	10.9 ± 2.4**	13.2 ± 2.4	12.9 ± 1.7	<0.001
CMR				
LV-EDV (ml/m ²)	91.9 ± 12.4	88.4 ± 17.1	95.1 ± 14.0	0.149
LV-ESV (ml/m ²)	41.0 ± 9.3	37.4 ± 9.4	39.1 ± 9.5	0.348
LVEF (%)	55.8 ± 6.3 [†]	58.0 ± 4.7	59.1 ± 6.3	0.049
LV LGE	12 (35)*	2 (7)	n/a	0.007
RV LGE	10 (29)*	0 (0)	n/a	0.001

Values are presented as mean ± SD, median [IQR] or n (%). An asterisk (*) indicates a statistical significant difference (p<0.05) compared to the adjacent group at the right and a double asterisk (**) indicates a statistical significant difference compared to the two adjacent groups at the right. An obelisk (†) indicates a statistical significant difference between ARVC patients and control subjects. Statistical tests between subgroups are performed with a Bonferroni correction for multiple testing. Abbreviations: ARVC = arrhythmogenic right ventricular cardiomyopathy; EDV = end-diastolic volume; ESV = end-systolic volume; LGE = late gadolinium enhancement; LV = left ventricle/ventricular; LVEF = left ventricular ejection fraction; n/a = not available; RV = right ventricle/ventricular; TAPSE = tricuspid annular plane systolic excursion.

Supplementary table 2: Correlation and agreement in subjects with echo and CMR within one day (n=81)

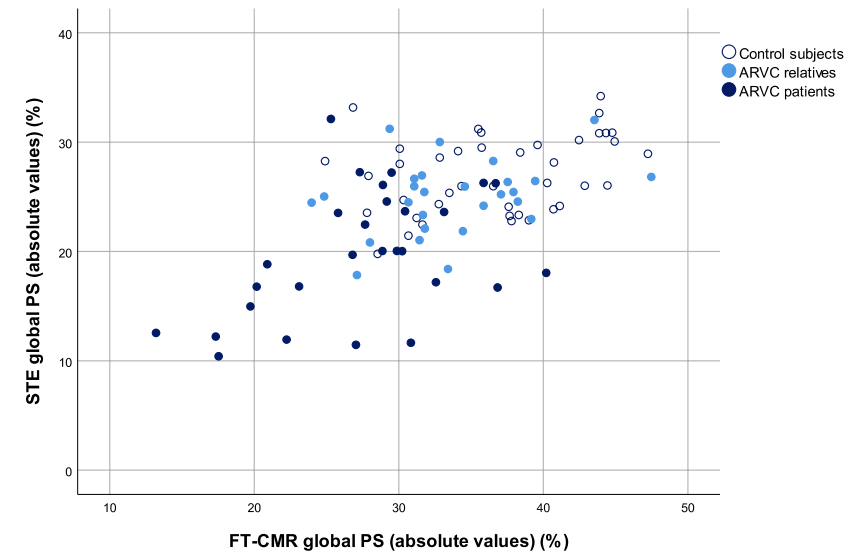
	Global PS	Basal PS	Mid PS	Apical PS
rho	0.497*	0.221*	0.158	0.156
Bias (%)	9.1	17.7	4.1	5.0
Limits of agreement (%)	±12.6	±16.6	±20.4	±25.0

An asterisk (*) indicates a significant (p<0.05) correlation. PS = peak strain.

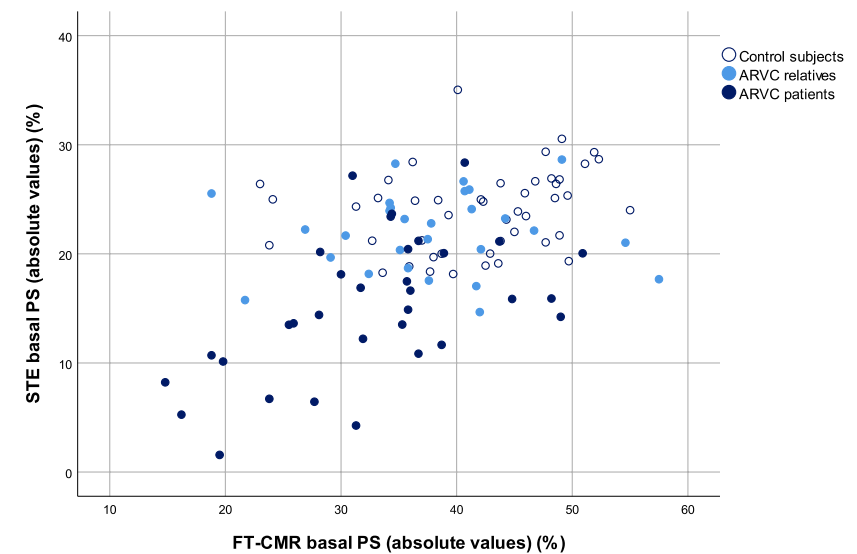
Supplementary table 3: Strain values, correlation and agreement when STE and FT-CMR are performed with a vendor-independent software package (n=30)

	Global PS	Basal PS	Mid PS	Apical PS
STE (%)	22.6 ± 6.0	22.7 ± 8.6	19.4 ± 8.6	25.8 ± 9.5
FT-CMR (%)	28.8 ± 7.8	30.7 ± 14.7	29.7 ± 12.7	28.2 ± 10.4
rho	0.048	0.134	-0.416*	-0.5
Bias (%)	6.2	8.2	10.3	2.1
Limits of agreement (%)	±19.0	±32.1	±36.6	±14.6

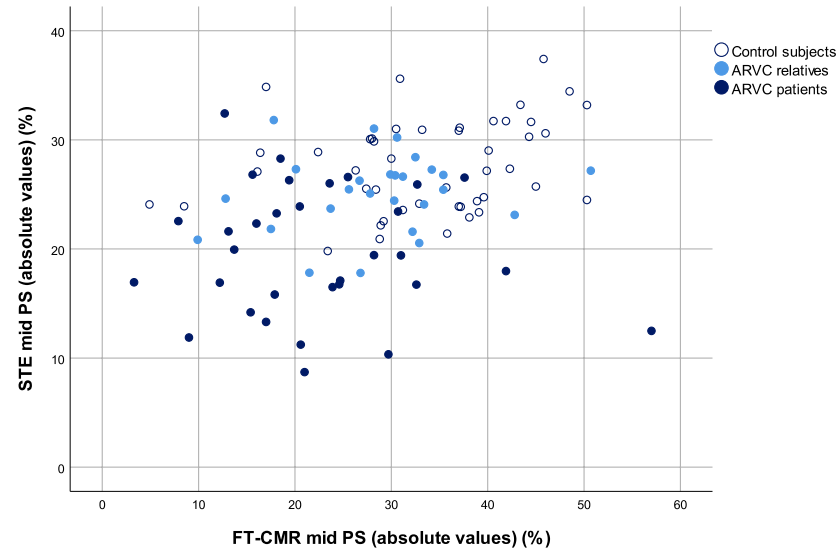
Strain values are presented as absolute values (mean ± SD). An asterisk (*) indicates a significant (p<0.05) correlation. FT-CMR = feature tracking cardiovascular magnetic resonance imaging; PS = peak strain; STE = speckle tracking echocardiography.



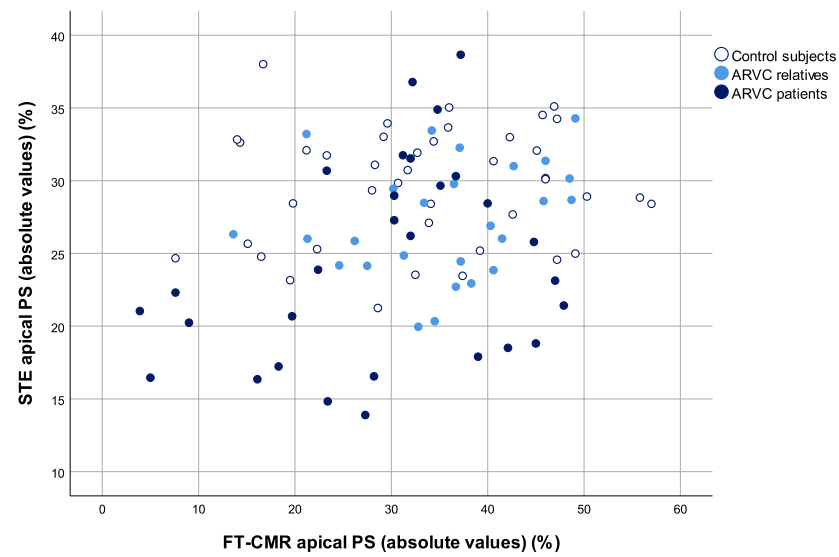
Supplementary figure 1: scatterplot of global PS values



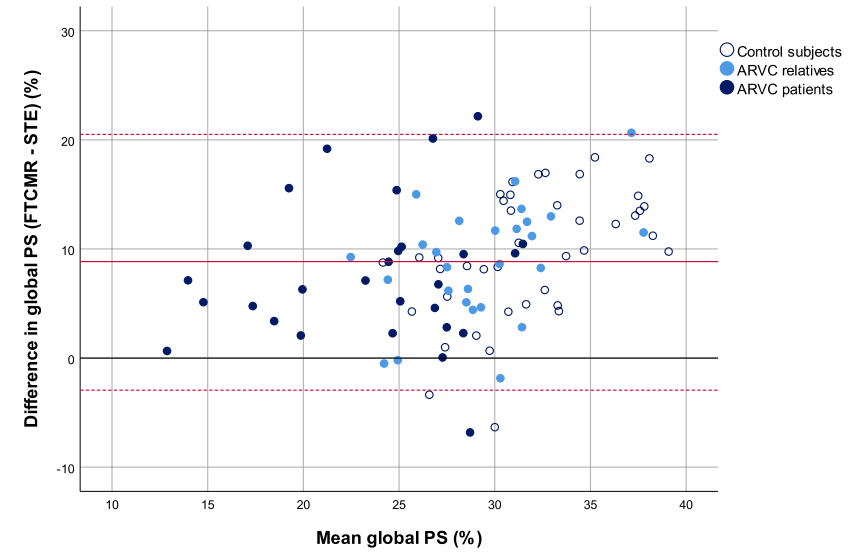
Supplementary figure 2: scatterplot of basal PS values



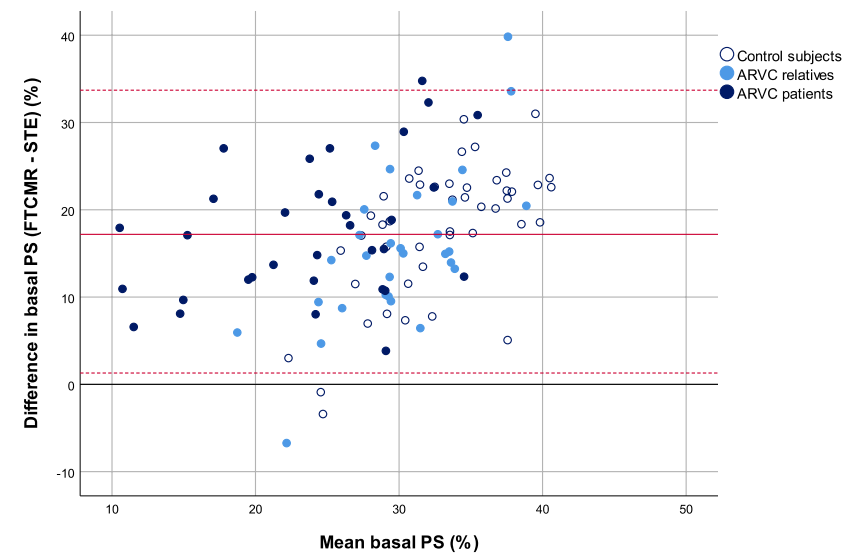
Supplementary figure 3: scatterplot of mid PS values



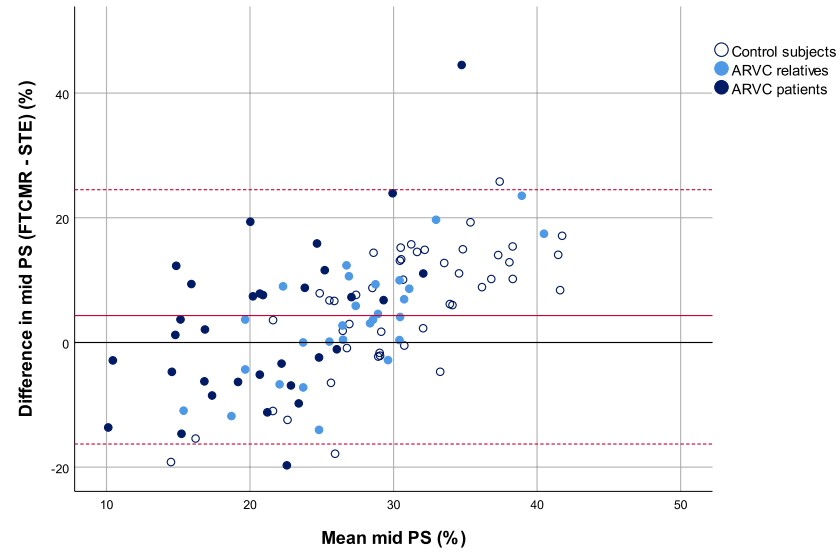
Supplementary figure 4: scatterplot of apical PS values



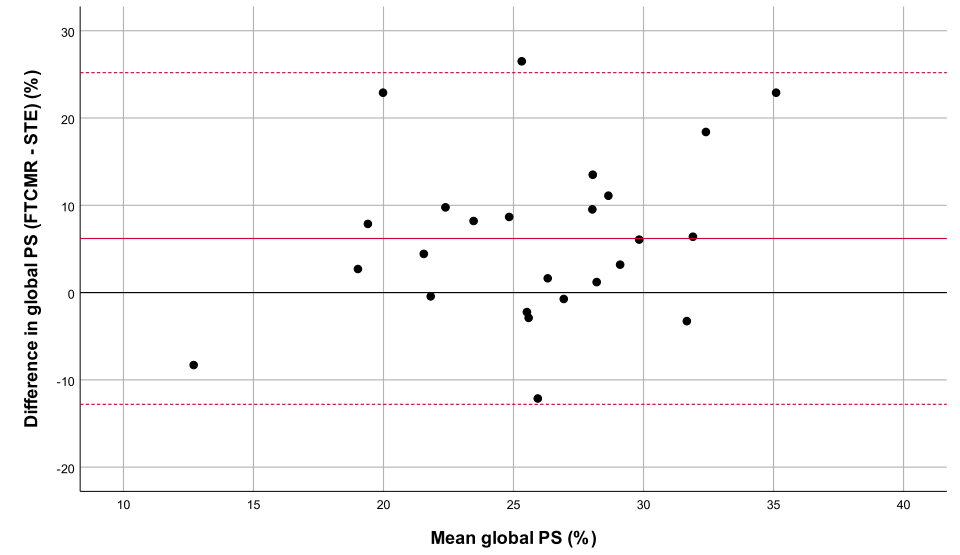
Supplementary figure 5: Bland-Altman plot for the different subgroups (global PS)



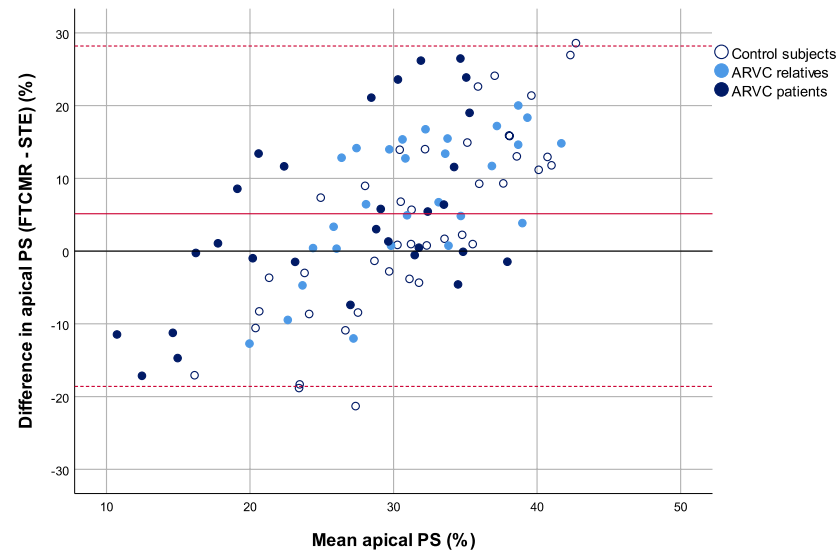
Supplementary figure 6: Bland-Altman plot for the different subgroups (basal PS)



Supplementary figure 7: Bland-Altman plot for the different subgroups (mid PS)



Supplementary figure 9: Bland-Altman plot for global PS when STE and FT-CMR are performed with a similar vendor-independent software package (n=30)



Supplementary figure 8: Bland-Altman plot for the different subgroups (apical PS)

PART II

Clinical value of novel CMR techniques in ARVC



CHAPTER

6

Prognostic value of strain by feature-tracking cardiac magnetic resonance in arrhythmogenic right ventricular cardiomyopathy

Mimount Bourfiss, MD;
Niek H.J. Prakken, MD, PhD;
Cindy A. James, ScM, PhD, CGC;
R.Nils Planken, MD, PhD;
S. Matthijs. Boekholdt, MD, PhD;
Dino Ahmetagic, Bsc;
Maarten P. van den Berg, MD, PhD;
Crystal Tichnell, MGC, RN;
Jeroen F. van der Heijden, MD, PhD;
Peter Loh, MD, PhD;
Brittney Murray, MS, CGC;
Harikrishna Tandri, MD;
Ihab Kamel, MD, PhD;
Hugh Calkins, MD;
Folkert W. Asselbergs, MD, PhD;
Stefan L. Zimmerman, MD, PhD;
Birgitta K. Velthuis, MD, PhD;
Anneline S.J.M. te Riele, MD, PhD

European Heart Journal-Cardiovascular imaging. 2022.

doi.org/10.1093/ehjci/jeac030

ABSTRACT

Aims: Arrhythmogenic right ventricular cardiomyopathy (ARVC) is characterized by ventricular dysfunction and ventricular arrhythmias (VA). Adequate arrhythmic risk assessment is important to prevent sudden cardiac death. We aimed to study the incremental value of strain by feature-tracking cardiac magnetic resonance imaging (FT-CMR) in predicting sustained VA in ARVC patients.

Methods and results: CMR images of 132 ARVC patients (43% male, 40.6±16.0 years) without prior VA were analyzed for global and regional right and left ventricular (RV, LV) strain. Primary outcome was sustained VA during follow-up. We performed multivariable regression assessing strain, in combination with 1) RV ejection fraction (EF); 2) LVEF and; 3) the ARVC risk calculator. False discovery rate adjusted p-values were given to correct for multiple comparisons and c-statistics were calculated for each model. During 4.3 [2.0-7.9] years of follow-up, 19% of patients experienced sustained VA. Compared to patients without VA, those with VA had significantly reduced RV longitudinal ($p \leq 0.03$) and LV circumferential ($p \leq 0.04$) strain. In addition, patients with VA had significantly reduced biventricular EF ($p \leq 0.02$). After correcting for RVEF, LVEF and the ARVC risk calculator separately in multivariable analysis, both RV and LV strain lost their significance (HR 1.03-1.18, $p > 0.05$). Likewise, while strain improved the c-statistic in combination with RVEF, LVEF, and the ARVC risk calculator separately, this did not reach significance ($p \geq 0.18$).

Conclusion: Both RV longitudinal and LV circumferential strain are reduced in ARVC patients with sustained VA during follow-up. However, strain does not have incremental value over RVEF, LVEF, and the ARVC VA risk calculator.

Keywords: Arrhythmogenic right ventricular cardiomyopathy, cardiac magnetic resonance imaging, feature tracking, strain, arrhythmias

INTRODUCTION

Arrhythmogenic right ventricular cardiomyopathy (ARVC) is an inherited heart disease that is characterized by ventricular dysfunction and life-threatening ventricular arrhythmias (VA)¹. Right ventricular (RV) abnormalities predominate in ARVC, but left ventricular (LV) involvement is increasingly recognized². Although early detection of ARVC has improved over the years, risk stratification remains challenging. Adequate assessment of arrhythmic risk is important, since arrhythmias may occur early in the disease course and timely implantable cardioverter-defibrillator (ICD) implantation can be life-saving³.

Cardiac magnetic resonance (CMR) imaging is the non-invasive gold standard for the evaluation of cardiac function in ARVC given its excellent potential to accurately and reproducibly quantify global RV volumes and ejection fraction (EF). In addition, newer techniques such as myocardial strain provide a more sensitive, quantitative evaluation of myocardial function that can detect functional changes before a relevant decrease in EF occurs⁴. Myocardial strain can be measured using feature-tracking CMR (FT-CMR), which quantitatively tracks myocardial features throughout the cardiac cycle on standard cine imaging. This allows quantitative regional myocardial strain assessment, which has been shown to increase diagnostic value for ARVC disease detection in a previous study⁵. As lower RVEF is associated with higher arrhythmic risk in ARVC⁶, and strain parameters are more sensitive than RVEF in assessing regional myocardial function⁴, we hypothesized that RV strain also has incremental prognostic value over conventional arrhythmic risk markers in ARVC⁶. However, the value of FT-CMR derived strain in ARVC risk stratification remains unknown.

The purpose of this study was to 1) assess whether FT-CMR of the RV and LV is able to predict future sustained VA; and 2) evaluate the incremental value of FT-CMR over traditional arrhythmic risk factors in a multicenter cohort of ARVC patients without prior sustained VA (i.e. primary prevention patients).

METHODS

Study population

We included definite ARVC patients without prior sustained VA (i.e. primary prevention patients) from the Netherlands (www.acmregistry.nl) and Johns Hopkins (www.arvd.com) ARVC registries who underwent CMR as part of their clinical work-up. ARVC diagnosis was defined according to the 2010 revised task force criteria (TFC) in which ≥ 4 TFC points are required for ARVC diagnosis⁷. A total of 158 patients met the inclusion criteria, of whom 26 patients were excluded due to CMR images unsuitable for FT-CMR analysis (e.g. artefacts/incomplete images), leading to a total cohort of 132 patients. A total of 108 patients were

included in prior studies involving CMR analysis in ARVC⁹⁻¹⁰. The study conforms to the Helsinki declaration and was approved by local ethics and/or institutional review boards.

CMR acquisition

The CMR study closest to date of diagnosis was used for analyses. CMR images were acquired on a 1.5 Tesla scanner (Avanto, Siemens Medical Imaging, Germany [Amsterdam UMC, UMC Groningen and Johns Hopkins Hospital] or Achieva Philips Medical Systems, the Netherlands [UMC Utrecht]). Short-axis and longitudinal-axis (4-chamber, 2-chamber and 3-chamber views of both ventricles) cine images were acquired using a balanced steady-state free precession sequence (field of view 350mm, matrix size 256x256, slice thickness 8mm [1.3x1.3x8mm³], temporal resolution 40-50ms). Segmented phase-sensitive inversion recovery sequence was used for myocardial fibrosis evaluation using late gadolinium enhancement (LGE).

CMR analysis

Traditional measurements

Locally available software was used for semi-automatic analysis of biventricular EF, end diastolic volume (EDV) and end systolic volume (ESV) (Extended MR-WorkSpace, Philips Medical Systems; QMass Medis Medical Imaging Systems or Circle CVI). Dimensions were indexed (i) to body surface area using the DuBois formula¹¹. The presence of RV and LV LGE was visually evaluated by an experienced cardiovascular radiologist.

Strain analysis

Global and regional biventricular longitudinal strain and LV circumferential strain were measured using Medis QStrain Software (Medis Medical Imaging Systems, version 3.116.8, the Netherlands) by an experienced observer blinded to the arrhythmic outcome (MB). Inter- and intra-observer variability of this observer are previously published⁸. Endocardial and epicardial contours (for LV short-axis) were manually drawn during end-diastole and end-systole with subsequent automatic tracking during the cardiac cycle. This resulted in the measurement of “strain” as a marker of tissue shortening during systole with more negative strain values indicating better contraction.

For the RV, peak longitudinal strain was measured in the most central slice in 4-chamber view, since strain values are most reliable in this view^{5,12}. For regional analysis, segments were divided into basal, mid and apical wall¹³.

For the LV, peak longitudinal strain was measured in 4-chamber, 2-chamber and 3-chamber views to form the 16 segment American Heart Association (AHA) model¹⁴. To measure LV circumferential strain, the basal, mid and apical slices of the short-axis were measured to form the AHA model. Segmentation examples are included in **Supplementary Figure 1**.

Study outcomes

The primary outcome of this study was the occurrence of sustained VA following CMR. As in previous studies⁹, sustained VA was defined as sustained ventricular tachycardia lasting ≥ 30 seconds at ≥ 100 bpm or with hemodynamic compromise, ventricular fibrillation/flutter, sudden cardiac arrest and/or appropriate ICD intervention.

Statistical analysis

Statistical analyses were performed using IBM SPSS Statistics (version 25, USA) and STATA (version 11, StatCorp, USA). Continuous variables are presented as mean (\pm standard deviation) or median (interquartile range), and compared using independent sample t-test or Mann-Whitney U-test. Categorical variables are presented as frequencies (%), and compared using chi-square test or Fisher's exact test. Statistical significance was determined at $p \leq 0.05$. The Kaplan-Meier method was used to estimate the cumulative proportion of patients with VA as a function over time, and groups were compared using log-rank statistic. Follow-up was calculated from the date of CMR to the date of first sustained VA or censoring, which was defined as the latest follow-up visit at which the endpoint could be ascertained. The receiver operating characteristic (ROC) curve was used to determine optimal strain cut-off values for predicting the outcome.

Multivariable analysis

Multivariable Cox regression was performed to assess the association between strain and the primary outcome. To ensure that our results were not affected by overfitting, we added each strain variable to three separate models as follows: i) Model 1: adjusted for RVEF; ii) Model 2: adjusted for LVEF; iii) Model 3: adjusted for the 5-year risk estimate of VA computed using the “ARVC VA risk calculator” (www.arvcrisk.com)⁹. This latter risk prediction model includes male sex, age, recent cardiac syncope, prior non-sustained ventricular tachycardia, 24-hour premature ventricular contraction count, number of leads with T-wave inversion anterior/inferior and RVEF. False Discovery Rate (FDR) corrected p-values were calculated to correct for multiple testing. The prognostic performance of adding strain (strain parameters with the highest hazard ratio [HR] in univariable analysis) to RVEF, LVEF or the ARVC VA risk calculator was assessed by Harrell's concordance (c)-statistic and compared using the DeLong *et al.* method.¹⁵

RESULTS

Study population

CMR images of 132 definite ARVC patients without prior sustained VA were included. Baseline characteristics of the study population are shown in **Table 1**. The mean age at CMR was 40.6 ± 16.0 years and 57 (43%) subjects were male. The median TFC score was 5

[4-6] with 78 (60%) having minor or major structural TFC. A total of 107 (81%) subjects carried a pathogenic mutation, mostly in plakophilin-2 (n=84, 64%), followed by phospholamban (n=13, 10%) and desmoglein-2 (n=5, 4%). None of the patients had an ICD at time of CMR, while n=68 (52%) patients received an ICD for primary prevention after CMR.

Arrhythmic outcome

During a median follow-up of 4.3 [2.0-7.9] years, 25 subjects (19%) developed sustained VA (22 [88%] appropriate ICD interventions and 3 [12%] spontaneous sustained ventricular tachycardia). **Table 1** shows their clinical characteristics. Compared to those without sustained VA, patients experiencing arrhythmic events were more often male (68% vs. 37%, $p<0.01$), proband (60% vs. 29%, $p<0.01$) and had a significantly higher total TFC score (6 [5-7] vs. 5 [4-5] $p<0.01$). No difference in age (39.9±15.7 vs. 40.8±16.1 years, $p=0.80$), genetic background (80% vs. 81% with a pathogenic variant, $p=0.88$) and follow-up duration (3.4 [1.5-8.3] vs. 4.5 [2.1-7.8] years, $p=0.99$) was observed between the groups.

Table 1: Baseline characteristics of the study population

	Overall (n=132)	No sustained VA in follow-up (n=107)	Sustained VA in follow-up (n=25)	p-value
Demographics				
Age at CMR (years)	40.6±16.0	40.8±16.1	39.9±15.7	0.80
Male (%)	57 (43)	40 (37)	17 (68)	<0.01
Follow-up (years)	4.3 [2.0-7.9]	4.5 [2.1-7.8]	3.4 [1.5-8.3]	0.99
Proband (%)	44 (33)	29 (27)	15 (60)	<0.01
Genetic status				
Pathogenic variant	107 (81)	87 (81)	20 (80)	0.88
PKP2 (%)	84 (64)	67 (63)	17 (68)	
DSP (%)	2 (2)	2 (2)	0	
DSG2 (%)	5 (4)	5 (5)	0	
PLN (%)	13 (10)	11 (10)	2 (8)	
Other (%)	3 (2)	2 (2)	1 (4)	
Clinical phenotype				
Total TFC score	5 [4-6]	5 [4-5]	6 [5-7]	<0.01
Repolarization criteria				
Minor	31 (24)	24 (22)	7 (28)	
Major	51 (39)	37 (35)	14 (56)	
Depolarization criteria				
Minor	68 (52)	55 (51)	13 (52)	
Major	6 (5)	4 (4)	2 (8)	
Arrhythmia criteria				
Minor	78 (59)	61 (57)	17 (68)	
Major	13 (10)	8 (8)	5 (20)	
Structural criteria				
Minor	21 (16)	18 (17)	3 (12)	
Major	58 (44)	42 (39)	16 (64)	

Table 1: Continued

	Overall (n=132)	No sustained VA in follow-up (n=107)	Sustained VA in follow-up (n=25)	p-value
Family/genetic criteria				
Minor	4 (3)	3 (3)	1 (4)	
Major	103 (78)	85 (79)	18 (72)	
ARVC VA risk calculator, 5-year risk (%)	21.4±18.9	17.3±14.5	38.9±24.8	<0.01
CMR traditional parameters				
RVEF (%)	47±9	48±9	40±10	<0.01
RVEDVi (ml/m ²)	102±30	100±29	111±32	0.15
LVEF (%)	56±8	57±7	51±11	0.02
LVEDVi (ml/m ²)	92±20	92±21	89±17	0.55
LGE total (%)	40 (30)	27 (25)	13 (52)	0.02
LGE RV (%)	24 (18)	14 (13)	11 (44)	<0.01
LGE LV (%)	20 (15)	15 (14)	5 (20)	0.57

Abbreviations: CMR= cardiac magnetic resonance; DSG2= desmoglein-2; DSP= desmoplakin; EDVi= BSA indexed end-diastolic volume; EF= ejection fraction; LGE= late gadolinium enhancement; LV= left ventricle; N= number of subjects; PKP2= plakophilin-2; PLN= phospholamban; RV= right ventricle; TFC= Task Force Criteria; VA= ventricular arrhythmia.

Traditional CMR parameters

As for traditional CMR parameters, ARVC patients with sustained VA had significantly reduced RVEF (40±10% vs. 48±9%, $p<0.01$) and LVEF (51±11% vs. 57±7%, $p=0.02$) compared to those without sustained VA. LGE was more often present in patients with sustained VA (52% vs. 25%, $p=0.02$), especially in the RV (44% vs. 13%, $p<0.01$). In contrast, both RVEDVi (111±32 ml/m² vs. 100±29 ml/m²) and LVEDVi (89±17 ml/m² vs. 92±21 ml/m²) did not significantly differ between the two groups ($p\geq0.15$). In addition, no significant difference existed in structural TFC between patients with (76% had minor or major criteria) and without (56% had minor or major criteria) sustained VA ($p=0.08$).

FT-CMR as a predictive biomarker for sustained VA

RV and LV strain

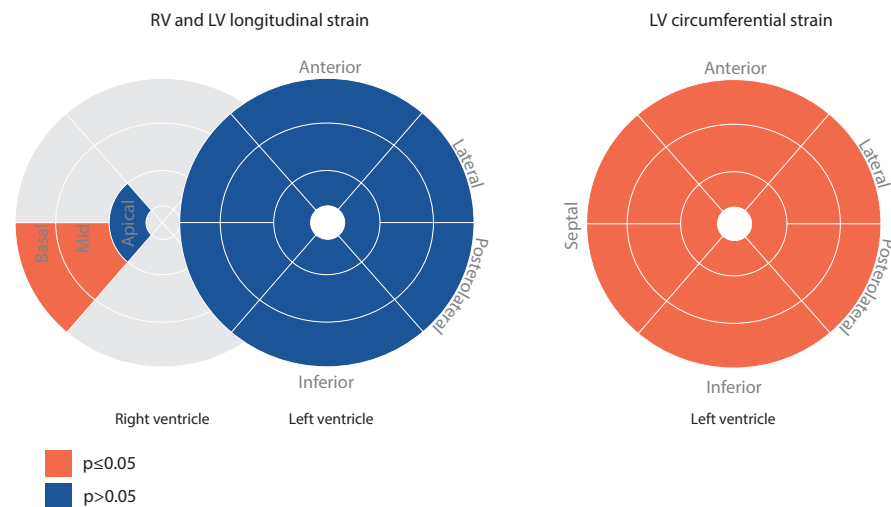
Global and regional strain values stratified by the occurrence of sustained VA are shown in **Table 2** (global and regional strain) and **Figure 1** (regional strain).

For RV strain, global longitudinal strain was significantly reduced (i.e. less negative) in patients with versus without sustained VA (-18.5±5.9% vs. -22.5±8.4%, $p=0.03$). For regional RV longitudinal strain, both basal (-26.9±12.8% vs. -34.4 ±10.9%, $p<0.01$) and mid wall (-19.7±12.2% vs. -25.7±11.0%, $p=0.02$) strain were reduced in patients with sustained VA. Apical strain did not significantly differ between the two groups (-27.8±14.5% vs. -32.5±11.9%, $p=0.09$).

Table 2: RV and LV global and regional strain values stratified by patients with versus without VA

	No sustained VA in follow-up (n=107)	Sustained VA in follow-up (n=25)	p-value
Right ventricular strain			
<i>Global strain</i>			
GLS	-22.5±8.4	-18.5±5.9	0.03
<i>Regional longitudinal strain</i>			
basal	-34.4 ±10.9	-26.9±12.8	<0.01
mid	-25.7±11.0	-19.7±12.2	0.02
apical	-32.5±11.9	-27.8±14.5	0.09
Left ventricular strain			
<i>Global strain</i>			
GCS	-18.8±4.1	-15.3±4.4	<0.01
GLS	-21.7±5.1	-19.2±5.3	0.06
<i>Regional circumferential strain</i>			
anterior	-18.7±6.2	-15.3±5.8	0.03
anterolateral	-22.2±6.9	-17.5±6.2	<0.01
posterolateral	-23.7±6.2	-18.9±5.7	<0.01
inferior	-19.6±6.7	-16.0±7.5	0.04
septal	-20.2±4.5	-16.7±4.8	<0.01
<i>Regional longitudinal strain</i>			
anterior	-20.0±7.3	-19.6±6.6	0.86
anterolateral	-24.4±6.1	-23.0±7.0	0.40
posterolateral	-23.3±10.8	-24.4±9.1	0.77
inferior	-23.5±7.2	-20.3±6.0	0.08
septal	-21.7±5.5	-19.4±4.1	0.24

Abbreviations: GCS= global circumferential strain; GLS= global longitudinal strain; VA= ventricular arrhythmia.

**Figure 1: RV and LV regional strain in the study population**

Schematic overview of longitudinal (left) and circumferential (right) regional strain differences between patients with and without VA during follow-up. Orange; significant differences between those with and without VA. Blue; non-significant differences. Abbreviations as in text.

For LV strain, both global and regional LV longitudinal strain were comparable in patients with and without sustained VA ($p \geq 0.06$). In contrast, global circumferential strain (GCS) was significantly reduced in patients with versus those without sustained VA ($-15.3 \pm 4.4\%$ vs. $-18.8 \pm 4.1\%$, $p < 0.01$), which was also observed in the regional circumferential strain values ($p \leq 0.04$).

Predicting sustained VA using FT-CMR

Determination of cut-off values for abnormal strain using ROC analysis is displayed in **Supplementary Table 1**. We only evaluated cut-off values for RV longitudinal and LV circumferential strain, since these parameters were significant in univariate analysis (in contrast to LV longitudinal strain). The resulting cut-offs were used for the Kaplan Meier survival curves shown in **Figure 2**. For RV strain, survival without sustained VA was significantly lower in patients with reduced global longitudinal ($p < 0.01$) and regional basal ($p = 0.05$) and mid longitudinal strain ($p < 0.01$).

For LV strain, survival without sustained VA was significantly lower in patients with reduced global circumferential ($p = 0.03$) and regional posterolateral ($p = 0.01$) and septal ($p < 0.01$) circumferential strain. No statistical significance was reached for anterior and anterolateral ($p \leq 0.11$) strain.

Clinical value of FT-CMR

To assess the incremental prognostic value of FT-CMR over traditional clinical parameters, we performed multivariable Cox regression analyses for each strain parameter in combination with 1) RVEF; 2) LVEF and; 3) the ARVC VA risk calculator.

Table 3 summarizes the univariable and multivariable regression analyses. RV and LV global and regional strain did not remain significant predictors after correcting for RVEF (HR 1.02-1.17, $p > 0.05$), LVEF (HR 1.06-1.18, $p > 0.10$) or the ARVC VA risk calculator (HR 1.05-1.18, $p > 0.11$). All p-values are corrected for Type I error using FDR. When only including patients with preserved RVEF and LVEF in our analysis (**Supplementary Table 2**), none of the RV and LV strain values were independently associated with VA when included in a model with the ARVC VA risk calculator (HR 0.92-1.17 [0.80-1.52, $p > 0.29$], although analyses were underpowered with a total of 8 events.

Figure 3 illustrates the change in c-statistic when comparing the models separately and after adding LV global and septal circumferential strain (strain parameters with highest HR on univariable analysis). The predictive value of RVEF (0.72 [0.60-0.85] vs. 0.79 [0.68-0.89]), LVEF (0.66 [0.51-0.81] vs. 0.72 [0.59-0.85]) and the ARVC VA risk calculator (0.76 [0.63-0.90] vs. 0.82 [0.72-0.92]) improved after adding LV strain (global strain and septal circumferential strain) to the model, however this did not reach statistical significance ($p > 0.18$).

Table 3: Univariable and multivariable Cox proportional hazards model for sustained VA prediction

	Univariable model		Multivariable model 1 RVEF		Multivariable model 2 LVEF		Multivariable model 3 ARVC VA risk calculator	
	HR (95% CI)	p-value	HR (95% CI)	p-value	HR (95% CI)	p-value	HR (95% CI)	p-value
Right ventricular strain								
GLS	1.05 (1.00-1.11)	0.053	-	-	-	-	-	-
basal region	1.06 (1.02-1.11)	0.015	1.03 (0.98-1.08)	0.238	1.06 (1.01-1.10)	0.099	1.05 (1.00-1.10)	0.107
mid region	1.05 (1.01-1.10)	0.037	1.02 (0.98-1.07)	0.312	1.04 (1.00-1.09)	0.099	1.03 (0.98-1.08)	0.240
apical region	1.03 (1.00-1.07)	0.097	-	-	-	-	-	-
Left ventricular strain								
GCS	1.22 (1.07-1.39)	0.015	1.17 (1.02-1.35)	0.054	1.18 (0.99-1.42)	0.099	1.18 (1.02-1.35)	0.107
anterior region	1.12 (1.01-1.24)	0.047	1.10 (0.99-1.23)	0.105	1.08 (0.97-1.21)	0.152	1.10 (0.98-1.23)	0.177
anterolateral region	1.12 (1.03-1.23)	0.015	1.10 (1.00-1.20)	0.081	1.09 (0.99-1.20)	0.116	1.09 (1.00-1.19)	0.118
posterolateral region	1.15 (1.04-1.26)	0.020	1.12 (1.02-1.24)	0.054	1.11 (1.00-1.23)	0.099	1.10 (1.00-1.22)	0.110
inferior region	1.09 (1.00-1.19)	0.053	-	-	-	-	-	-
septal region	1.18 (1.07-1.31)	0.015	1.16 (1.02-1.32)	0.054	1.15 (0.99-1.32)	0.099	1.17 (1.02-1.33)	0.107

Abbreviations: GCS= global circumferential strain; GLS= global longitudinal strain; LVEF= left ventricular ejection fraction; RVEF= right ventricular ejection fraction. False discovery rate corrected p-values are given in this table.

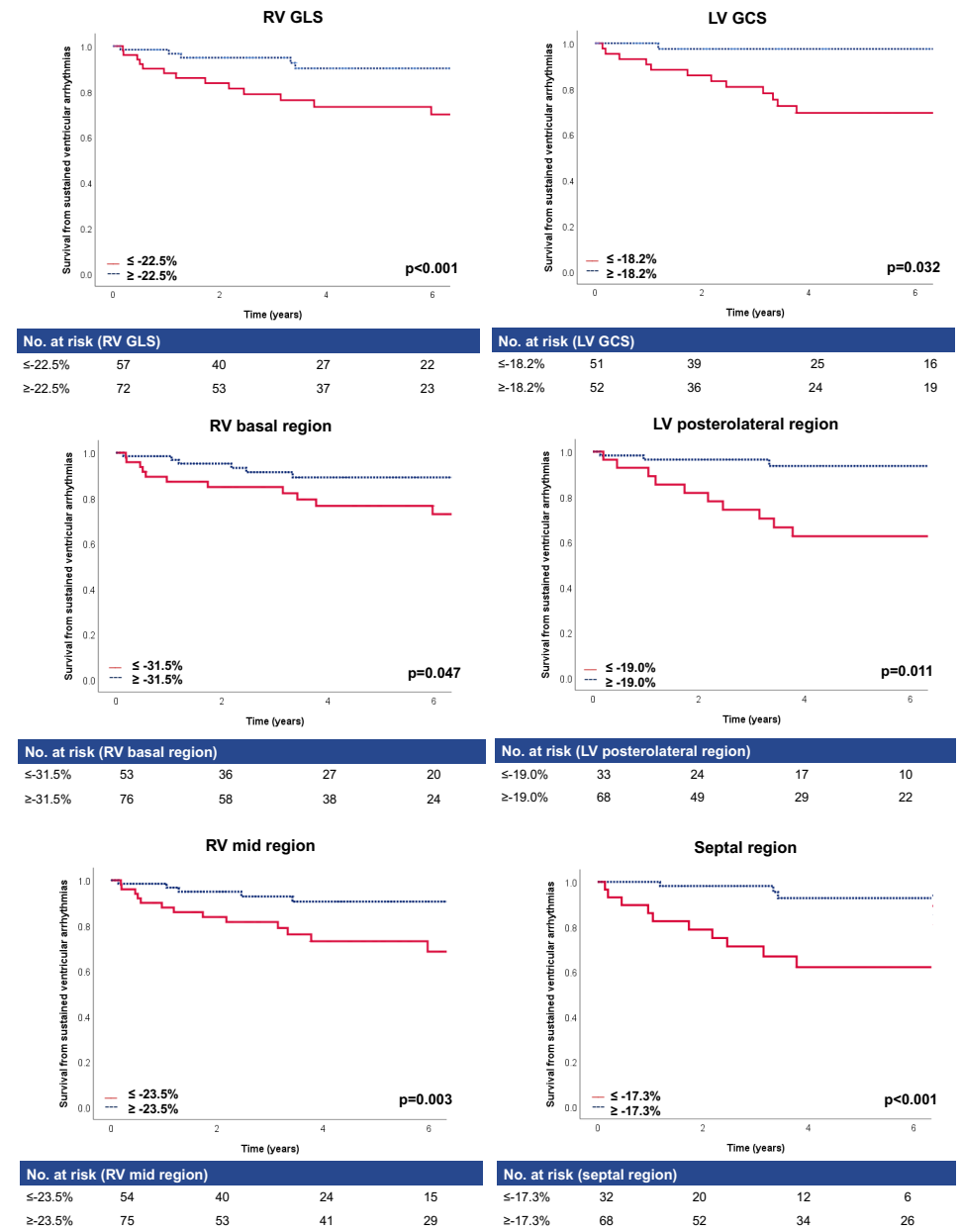


Figure 2: Kaplan Meier survival analysis suggests abnormal RV and LV strain in patients with VA in follow-up.

Kaplan Meier analysis of RV and LV global and regional strain. Cut-offs for abnormal strain (red) and normal strain (blue) are calculated using ROC analysis. P-values were calculated using log-rank test. Abbreviations: GCS= global circumferential strain; GLS= global longitudinal strain, further abbreviations as in text.

LGE was more often present in patients with VA compared to those without arrhythmic events (52% vs. 25%, $p=0.02$). However, LGE did not significantly add to the predictive value of strain (0.73 [0.60-0.85] without vs. 0.77 with LGE [0.64-0.91]) and the ARVC VA risk calculator (0.79 [0.69-0.90] without vs. 0.80 with LGE [0.70-0.91]) ($p \geq 0.40$) (Supplementary Figure 2).

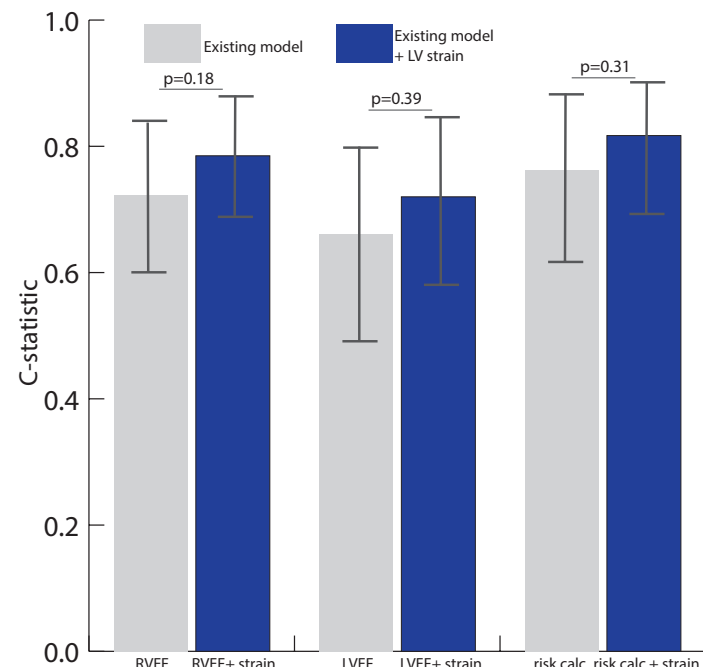


Figure 3: Incremental value of LV strain over conventional arrhythmic risk markers in ARVC

Bar chart with c-statistic per model. Grey bars; model 1 RVEF, model 2 LVEF and model 3 “ARVC VA risk calculator”. Blue bars; addition of LV global and septal strain to these models. Addition of LV strain to the existing models is compared using the DeLong method.(15). Abbreviations as in text.

DISCUSSION

Main findings

This study aimed to assess FT-CMR as a predictor of future sustained VA and to evaluate its incremental value over traditional risk markers in ARVC patients. We showed that both RV as well as LV strain are reduced in patients developing sustained VA during follow-up. Furthermore, survival without VA was significantly lower in patients with reduced RV and LV global and regional strain (basal and mid strain for the RV and posterolateral and septal strain for the LV). However, after correcting for RVEF, LVEF and the ARVC VA risk calculator

and adjusting for multiple testing, RV and LV strain did not remain a significant predictor of sustained VA.

Role of myocardial strain in ARVC

Technical groundwork

Over the years, the advent of FT-CMR in the field of deformation imaging has led to numerous studies confirming its feasibility and validating its use for biventricular regional strain assessment. Importantly, FT-CMR has shown to be a robust technique, with good inter- and intra-observer reproducibility for RV and LV strain, rendering this technique suitable for follow-up of patients^{13,16}. FT-CMR has been compared to several other modalities, including the gold standard for non-invasive strain assessment, myocardial tissue tagging¹⁷. Clinical implementation of tissue tagging is limited due to prolonged imaging and post-processing times¹⁸. In comparison, FT-CMR is less time consuming, as it uses the available cine images and has a more user-friendly post-processing method, especially for the RV. FT-CMR has also been compared to speckle tracking echocardiography which is a valuable comparison as CMR and echocardiography are both used for diagnosis and follow-up of ARVC patients and at-risk relatives. Studies have shown that trends between healthy and diseased were uniform among the modalities, however absolute strain values were not comparable^{19,20}. This emphasizes that FT-CMR and speckle tracking echocardiography cannot be used interchangeably during follow-up of patients. Regardless, we strongly believe that CMR and echocardiography have complimentary roles in ARVC evaluation: the high spatial resolution and multiplane tissue characterization of CMR make this technique extremely useful as a screening tool and to rule out differentials, while echocardiography is cheap and widely available, even in those with an ICD, making it a valuable tool for longitudinal follow-up.

Diagnostic value of strain parameters in ARVC

The importance of regional wall motion abnormalities in ARVC evaluation is emphasized in the diagnostic TFC, in which it is a prerequisite for fulfillment of CMR criteria⁷. Visual evaluation of wall motion abnormalities is, however, subjective, and previous studies have shown the incremental diagnostic value of objective and quantitative wall motion analysis using FT-CMR or speckle tracking echocardiography^{5,21}. For example, Vigneault *et al.* showed a higher sensitivity and specificity for FT-CMR compared to visual assessment in 110 individuals evaluated for ARVC⁵. Similar results were obtained for speckle tracking echocardiography, which is now recommended by the European Association of Cardiovascular Imaging for the assessment of early ARVC²¹. Although LV wall motion abnormalities are not part of the diagnostic TFC for ARVC, a study by Jain *et al.* suggested a promising diagnostic role using CMR tissue tagging: the authors showed reduced LV regional circumferential strain in definite ARVC patients and patients at-risk of developing ARVC compared to controls²².

Prognostic value of strain parameters in ARVC

Our study shows that reduced RV and LV strain are associated with sustained VA during follow-up in ARVC. This is not surprising, as RVEF is a known predictor of sustained VA in ARVC, and abnormal strain is thought to precede global EF changes. Similar results were previously obtained using speckle tracking echocardiography²³: Lie *et al.* found significant echocardiographic RV and LV strain abnormalities (expressed as mechanical dispersion) in ARVC patients with VA in follow-up²³.

In contrast, we found no incremental prognostic value of RV and LV strain after correcting for RVEF and LVEF using FDR adjusted p-values for multiple testing. Of note, advanced structural disease already existed in the majority of patients developing VA: we found significantly lower RVEF and LVEF in patients developing VA during follow-up of whom 76% already had minor or major structural TFC. Indeed, this translated to a high expected 5-year VA risk of 38.9% using the ARVC VA risk calculator. While one may consider it disappointing that strain does not further risk stratify beyond conventional measures, it is not entirely unexpected since 1) strain essentially assesses the same parameter as is included in the conventional measures, namely ventricular systolic function; and 2) arrhythmic risk in our cohort was already very high. In total, 19% of our study population experienced a VA over 4.2 years of follow-up. While one might suggest that this high event rate warrants ICD implantation in all subjects with definite ARVC, device implantation carries considerable risk in these young and active patients who need to live for decades with a device that is not complication free. As such, better risk stratification tools are required to distinguish patients who are most likely to benefit from their device. While there is proven value of adding strain to established CMR parameters for diagnostic purposes⁵, no incremental value is observed in adding strain values for prognostic purposes in ARVC patients. Future studies should focus on the additional prognostic value of strain in subjects at risk of developing ARVC (i.e. family members) without disease expression.

Limitations

We only included primary prevention patients with definite ARVC, and caution should be exercised when extrapolating our results to secondary prevention patients (i.e. those with previous sustained VA) or at-risk relatives who do not fulfill the TFC. While this is the largest study to date evaluating the prognostic value of FT-CMR in ARVC, the number of VAs during follow-up was relatively small, limiting our statistical power to perform multivariable analyses. We handled this by separately adding strain to three different models (i.e. RVEF, LVEF and the ARVC VA risk calculator), maximizing our ability to “correct” for multiple risk factors. To date, no standardized normal values for FT-CMR derived RV and LV global and regional strain exist, which is partly due to wide inter-software variability¹³. Until standardized reference values are available, center-specific references should be used. Future studies should look into the role of LGE taking into account scar quantification and localization.

Furthermore, the prognostic value of strain using other imaging modalities, such as speckle tracking echocardiography, should be determined.

To conclude, FT-CMR is a novel technique that quantitatively and objectively measures biventricular wall motion as strain. In the largest cohort to date of primary prevention ARVC patients evaluated by CMR, we showed that FT-CMR is able to predict sustained VA. However, after adjusting for RVEF, LVEF and the ARVC VA risk calculator no additional value of RV and LV strain assessment in the prediction of sustained VA was observed. Although strain by FT-CMR has proven its diagnostic value in ARVC, no incremental prognostic value in predicting sustained VA is found.

Acknowledgements

We thank the ARVC patients and families who have made this work possible.

REFERENCES

1. Gandjbakhch E, Redheuil A, Pousset F, Charron P, Frank R. Clinical Diagnosis, Imaging, and Genetics of Arrhythmogenic Right Ventricular Cardiomyopathy/Dysplasia: JACC State-of-the-Art Review. *J Am Coll Cardiol*. 2018;72(7):784-804. doi:10.1016/j.jacc.2018.05.065
2. Calkins H, Corrado D, Marcus F. Risk Stratification in Arrhythmogenic Right Ventricular Cardiomyopathy. *Circulation*. 2017;136(21):2068-2082. doi:10.1161/CIRCULATIONAHA.117.030792
3. Corrado D, Wichter T, Link MS, et al. Treatment of Arrhythmogenic Right Ventricular Cardiomyopathy/Dysplasia: An International Task Force Consensus Statement. *Circulation*. 2015;132(5):441-453. doi:10.1161/CIRCULATIONAHA.115.017944
4. Kalam K, Otahal P, Marwick TH. Prognostic implications of global LV dysfunction: a systematic review and meta-analysis of global longitudinal strain and ejection fraction. *Heart*. 2014;100(21):1673-1680. doi:10.1136/heartjnl-2014-305538
5. Vigneault DM, te Riele ASJM, James CA, et al. Right ventricular strain by MR quantitatively identifies regional dysfunction in patients with arrhythmogenic right ventricular cardiomyopathy. *J Magn Reson imaging*. 2016;43(5):1132-1139. doi:10.1002/jmri.25068
6. Canpolat U, Kabakci G, Aytemir K, et al. Fragmented QRS complex predicts the arrhythmic events in patients with arrhythmogenic right ventricular cardiomyopathy/dysplasia. *J Cardiovasc Electrophysiol*. 2013;24(11):1260-1266. doi:10.1111/jce.12202
7. Marcus FI, McKenna WJ, Sherrill D, et al. Diagnosis of arrhythmogenic right ventricular cardiomyopathy/dysplasia: proposed modification of the task force criteria. *Circulation*. 2010;121(13):1533-1541. doi:10.1161/CIRCULATIONAHA.108.840827
8. Bourfiss M, Vigneault DM, Aliyari Ghasebeh M, et al. Feature tracking CMR reveals abnormal strain in preclinical arrhythmogenic right ventricular dysplasia/ cardiomyopathy: a multisoftware feasibility and clinical implementation study. *J Cardiovasc Magn Reson*. 2017;19(1):66. doi:10.1186/s12968-017-0380-4
9. Cadrin-Tourigny J, Bosman LP, Nozza A, et al. A new prediction model for ventricular arrhythmias in arrhythmogenic right ventricular cardiomyopathy. *Eur Heart J*. 2019;40(23). doi:10.1093/eurheartj/ehz103
10. te Riele ASJM, Bhonsale A, James CA, et al. Incremental value of cardiac magnetic resonance imaging in arrhythmic risk stratification of arrhythmogenic right ventricular dysplasia/cardiomyopathy-associated desmosomal mutation carriers. *J Am Coll Cardiol*. 2013;62(19):1761-1769. doi:10.1016/j.jacc.2012.11.087
11. Du Bois D, Du Bois EF. A formula to estimate the approximate surface area if height and weight be known. 1916. *Nutrition*. 1989;5(5):303.
12. Kempny A, Fernandez-Jimenez R, Orwat S, et al. Quantification of biventricular myocardial function using cardiac magnetic resonance feature tracking, endocardial border delineation and echocardiographic speckle tracking in patients with repaired tetralogy of Fallot and healthy controls. *J Cardiovasc Magn Reson*. 2012;14:32. doi:10.1186/1532-429X-14-32
13. Bourfiss M, Vigneault DM, Aliyari Ghasebeh M, et al. Feature tracking CMR reveals abnormal strain in preclinical arrhythmogenic right ventricular dysplasia/ cardiomyopathy: A multisoftware feasibility and clinical implementation study. *J Cardiovasc Magn Reson*. 2017;19(1). doi:10.1186/s12968-017-0380-4
14. Cerqueira MD, Weissman NJ, Dilsizian V, et al. Standardized myocardial segmentation and nomenclature for tomographic imaging of the heart. A statement for healthcare professionals from the Cardiac Imaging Committee of the Council on Clinical Cardiology of the American Heart Association. *Int J Cardiovasc Imaging*. 2002;18(1):539-542.
15. DeLong ER, DeLong DM, Clarke-Pearson DL. Comparing the areas under two or more correlated receiver operating characteristic curves: a nonparametric approach. *Biometrics*. 1988;44(3):837-845.
16. Schmidt B, Dick A, Treutlein M, et al. Intra- and inter-observer reproducibility of global and regional magnetic resonance feature tracking derived strain parameters of the left and right ventricle. *Eur J Radiol*. 2017;89:97-105. doi:10.1016/j.ejrad.2017.01.025
17. Hor KN, Gottliebson WM, Carson C, et al. Comparison of magnetic resonance feature tracking for strain calculation with harmonic phase imaging analysis. *JACC Cardiovasc Imaging*. 2010;3(2):144-151. doi:10.1016/j.jcmg.2009.11.006
18. Bucius P, Erley J, Tanacli R, et al. Comparison of feature tracking, fast-SENC, and myocardial tagging for global and segmental left ventricular strain. *ESC Hear Fail*. 2020;7(2):523-532. doi:10.1002/ehf2.12576
19. Taha K, Bourfiss M, Te Riele ASJM, et al. A head-to-head comparison of speckle tracking echocardiography and feature tracking cardiovascular magnetic resonance imaging in right ventricular deformation. *Eur Heart J Cardiovasc Imaging*. May 2020. doi:10.1093/ehjci/jeaa088
20. Obokata M, Nagata Y, Wu VC-C, et al. Direct comparison of cardiac magnetic resonance feature tracking and 2D/3D echocardiography speckle tracking for evaluation of global left ventricular strain. *Eur Heart J Cardiovasc Imaging*. 2016;17(5):525-532. doi:10.1093/ehjci/jev227
21. Haugaa KH, Basso C, Badano LP, et al. Comprehensive multi-modality imaging approach in arrhythmogenic cardiomyopathy-an expert consensus document of the European Association of Cardiovascular Imaging. *Eur Heart J Cardiovasc Imaging*. 2017;18(3):237-253. doi:10.1093/ehjci/jev229
22. Jain A, Shehata ML, Stuber M, et al. Prevalence of left ventricular regional dysfunction in arrhythmogenic right ventricular dysplasia: a tagged MRI study. *Circ Cardiovasc Imaging*. 2010;3(3):290-297. doi:10.1161/CIRCIMAGING.109.911313
23. Lie ØH, Rootwelt-Norberg C, Dejgaard LA, et al. Prediction of Life-Threatening Ventricular Arrhythmia in Patients With Arrhythmogenic Cardiomyopathy: A Primary Prevention Cohort Study. *JACC Cardiovasc Imaging*. 2018;11(10):1377-1386. doi:10.1016/j.jcmg.2018.05.017

Supplementary Table 1: Cut-off values for strain determined using ROC curve analysis

	Cut-off normal strain (%)	Sensitivity (%)	Specificity (%)
Right ventricle			
<i>Global longitudinal strain</i>			
GLS	≥ -22.0	76	62
<i>Regional longitudinal strain</i>			
basal	≥ -31.5	61	63
mid	≥ -23.5	68	64
Left ventricle			
<i>Global circumferential strain</i>			
GCS	≥ -18.2	79	59
<i>Regional circumferential strain</i>			
anterior	≥ -15.8	63	65
anterolateral	≥ -20.7	63	53
posterolateral	≥ -19.0	63	75
inferior	≥ -17.1	63	63
septal*	≥ -17.3	63	76

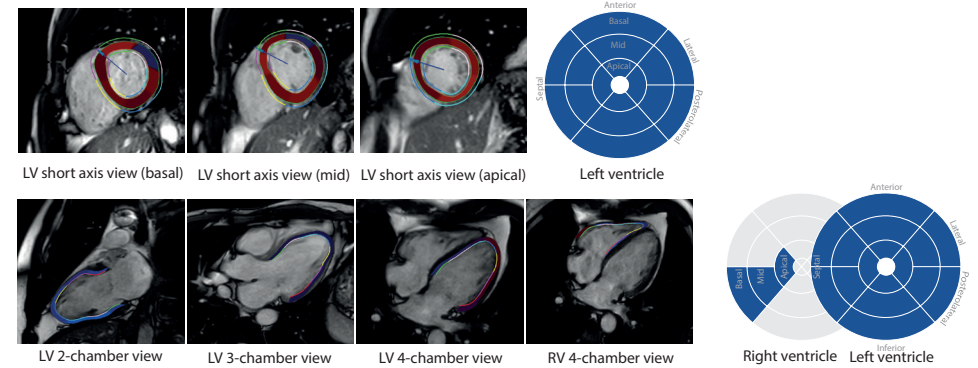
*For septal we combined the anteroseptal and inferoseptal regions.

Abbreviations: GCS= global circumferential strain; GLS= global longitudinal strain; ROC= receiver operating characteristic.

Supplementary Table 2: multivariable Cox proportional hazards model for sustained VA prediction in patients with preserved RVEF and patients with preserved LVEF

	Preserved RVEF ARVC VA risk calculator		Preserved LVEF ARVC VA risk calculator		Preserved LVEF and RVEF ARVC VA risk calculator	
	HR (95% CI)	p-value	HR (95% CI)	p-value	HR (95% CI)	p-value
Right ventricular strain						
GLS	1.06 (0.99-1.13)	0.303	1.05 (0.99-1.13)	0.214	1.07 (0.99-1.15)	0.562
basal region	1.08 (1.01-1.16)	0.303	1.08 (1.01-1.15)	0.170	1.09 (1.01-1.17)	0.290
mid region	1.01 (0.95-1.08)	0.788	1.02 (0.97-1.07)	0.632	0.98 (0.92-1.06)	0.677
apical region	1.04 (0.97-1.12)	0.411	1.00 (0.95-1.05)	0.882	1.03 (0.95-1.12)	0.639
Left ventricular strain						
GCS	1.20 (0.98-1.47)	0.202	1.24 (0.99-1.54)	0.190	1.17 (0.91-1.50)	0.562
anterior region	1.120 (0.93-1.30)	0.411	1.13 (0.97-1.32)	0.214	1.06 (0.89-1.26)	0.639
anterolateral region	1.03 (0.91-1.18)	0.788	1.12 (0.98-1.29)	0.214	1.03 (0.89-1.20)	0.677
posterolateral region	1.10 (0.96-1.25)	0.358	1.09 (0.97-1.22)	0.214	1.07 (0.93-1.23)	0.635
inferior region	0.99 (0.88-1.12)	0.918	1.01 (0.91-1.13)	0.881	0.92 (0.80-1.07)	0.562
septal region	1.19 (0.95-1.51)	0.342	1.21 (1.00-1.46)	0.190	1.17 (0.89-1.52)	0.562

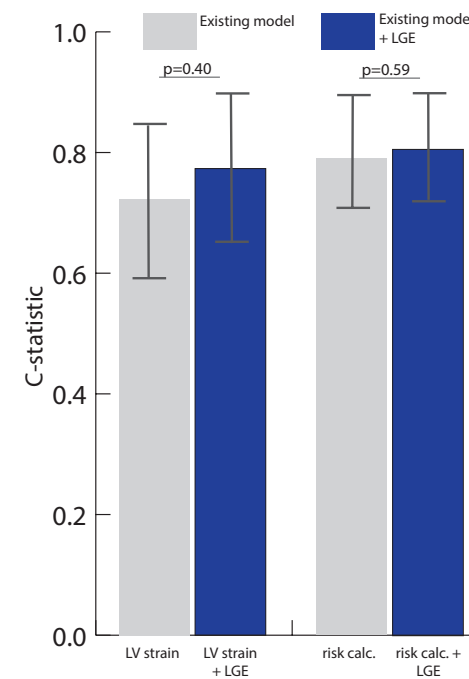
Abbreviations: GCS= global circumferential strain; GLS= global longitudinal strain; LVEF= left ventricular ejection fraction; RVEF= right ventricular ejection fraction. False discovery rate corrected p-values are given in this table.



Supplementary Figure 1: LV and RV FT-CMR segmentation

Example and corresponding segmentation model of LV circumferential (upper panel) and LV and RV longitudinal strain (lower panel). Included segments are highlighted in blue and excluded segments are highlighted in grey in the 16-segments model.

Abbreviations: as in manuscript.



Supplementary Figure 2: Incremental value of LGE over strain the ARVC VA risk calculator

Bar chart with c-statistic per model. Grey bars; model 1 LV strain (LV global and septal strain), model 2 “ARVC VA risk calculator”. Blue bars; addition of LGE (in the LV or RV) to these models. Addition of LGE to the existing models is compared using the DeLong method.(15). Abbreviations as in text.

CHAPTER

7

Diagnostic Value of Native T1 Mapping in Arrhythmogenic Right Ventricular Cardiomyopathy

Mimount Bourfiss MD;
Niek H.J. Prakken MD, PhD;
Jeroen F. van der Heijden, MD, PhD;
Ihab Kamel MD, PhD;
Stefan L. Zimmerman MD;
Folkert W. Asselbergs MD, PhD;
Tim Leiner MD, PhD;
Birgitta K. Velthuis MD, PhD;
Anneline S.J.M. te Riele MD, PhD

Published as a letter to the editor in:
JACC Cardiovasc Imaging. 2019 Aug;12(8 Pt 1):1580-1582.
doi: 10.1016/j.jcmg.2019.01.023.

ABSTRACT

Objectives: We aimed to analyze the diagnostic value of native T1 mapping in Arrhythmogenic Right Ventricular Cardiomyopathy (ARVC).

Background: Early detection of ARVC is pertinent as life-threatening ventricular arrhythmias (VA) can occur. These VAs are associated with myocardial replacement by fibrosis. Native T1 mapping is a promising technique to quantify early changes in cardiac microstructure (including fibrosis) on cardiac magnetic resonance imaging (CMR).

Methods: We analyzed short-axis cine 1.5 Tesla CMR images obtained using a MOLLI sequence in 43 subjects (13 ARVC patients meeting the 2010 diagnostic Task Force Criteria, 17 phenotype negative, genotype positive ARVC relatives, and 13 control subjects with right ventricular outflow tract ventricular tachycardia [RVOT-VT]). Global and regional fibrosis of the left ventricle (LV) were measured using T1 times. Native T1 dispersion, defined as the standard deviation of regional T1 times, was assessed per patient over all analyzed segments.

Results: Mean age was 37±17 years and 51% were female. Mean T1 times increased notably from controls (1038±27ms) to at-risk relatives (1055±38ms) to overt ARVC patients (1067±41ms), reaching significance for the comparison between overt ARVC patients and controls ($p=0.04$). Both overt ARVC patients (93±33ms) and at-risk relatives (79±15ms) had an elevated T1 dispersion compared to controls (67±12ms, $p \leq 0.03$), indicating a higher heterogeneity of the cardiac microstructure. More specifically, ARVC patients had elevated T1 times in the posterolateral ($p=0.02$), inferior ($p=0.01$) and anterior regions ($p=0.01$), whereas the posterolateral ($p=0.01$) and inferior ($p=0.01$) region were affected in at-risk relatives. Furthermore, 64% of at-risk ARVC relatives with elevated T1 dispersion had no late gadolinium enhancement, suggesting a greater sensitivity of T1 mapping for subtle ventricular changes.

Conclusion: Native T1 mapping differentiates overt ARVC patients and at-risk relatives from control subjects with RVOT-VT. When incorporated into the current diagnostic pathways, T1 mapping may have potential to detect early ARVC.

CONDENSED ABSTRACT

Early detection of Arrhythmogenic Right Ventricular Cardiomyopathy (ARVC) is pertinent as life-threatening ventricular arrhythmias can occur. Arrhythmias are associated by the typical fibrous replacement of the myocardium in ARVC. Early detection of this fibrous replacement may be helpful in the early diagnosis of ARVC. Native T1 mapping is a CMR based technique to quantify subtle and diffuse changes in cardiac microstructure. We show higher mean myocardial T1 times in overt ARVC patients and we show that both overt ARVC patients and at-risk relatives have more dispersion (heterogeneity) of left ventricular native T1 times than controls. This study shows that native T1 mapping has a possible role in differentiating both ARVC patient and at-risk relatives from controls.

Keywords: Arrhythmogenic Right Ventricular Cardiomyopathy, Native T1 mapping, Cardiac magnetic resonance imaging, Inherited cardiomyopathy

INTRODUCTION

Arrhythmogenic right ventricular cardiomyopathy (ARVC) is an inherited cardiomyopathy characterized by progressive replacement of the ventricular myocardium by fibrous and fatty tissue¹. ARVC typically affects the right ventricle (RV), although left ventricular (LV) involvement is common and cases with predominant LV involvement have been described². The ensuing fibro-fatty replacement results in abnormal tissue architecture, which may occur diffusely in both ventricles and gives rise to life-threatening ventricular arrhythmias that may occur early in the disease course³. While this underlines the importance of an accurate determination of the presence and extent of fibro-fatty replacement in ARVC, recent studies including those with biopsy samples⁴⁵ and late gadolinium-enhanced cardiac magnetic resonance (LGE CMR)⁶⁻⁹ yielded controversial results for diagnosing ARVC. CMR-based native T1 mapping may provide a possible solution.

T1 mapping allows for the non-invasive quantitative assessment of myocardial fibrosis using a pixel-wise measurement of absolute T1 relaxation times in milliseconds^{10,11}. These T1 relaxation times vary depending on the cardiac microstructure and the presence of fat or fibrosis⁹⁻¹¹. Compared to the current standard for non-invasive detection of myocardial fibrosis (LGE CMR), T1 mapping is not limited by use of gadolinium and does not require 'nulling' of the background myocardium, which allows detection of diffuse or subtle fibrosis. Indeed, native T1 time has shown to be a promising marker for early diagnosis in hypertrophic (HCM) and dilated cardiomyopathy (DCM)¹². However, no published study has yet evaluated native T1 mapping in ARVC subjects. Using a cohort of well-phenotyped and genotyped ARVC patients, we aimed to analyze the diagnostic value of native T1 mapping in ARVC.

METHODS

Study population

The study population consisted of individuals from the Netherlands ACM registry (www.acmregistry.nl) who were evaluated for ARVC between 2014 and 2017, underwent CMR with T1 mapping using a Modified Look-Locker Imaging (MOLLI) sequence and had a clinical evaluation (n=54). To limit heterogeneity of the study subjects, ARVC patients and relatives without a pathogenic ARVC-related mutation were excluded (n=8). In addition, study subjects with a history of radiofrequency ablation that could interfere with fibrosis detection were also excluded (n=3). In total, the study population consisted of 43 study participants. Based on their clinical evaluation, study participants were divided into three groups: 1) patients with a definite diagnosis of ARVC as per 2010 diagnostic Task Force Criteria (TFC) (n=13); 2) at-risk relatives of ARVC patients not fulfilling the 2010 TFC (n=17) and 3) controls who were initially evaluated for ARVC but in whom structural heart disease was

ruled out and RV outflow tract ventricular tachycardia (RVOT-VT) was diagnosed (n=13). The study was conducted in accordance with the Declaration of Helsinki and was approved by the University Medical Center Utrecht Institutional Review Board.

CMR image acquisition

All CMR images were acquired using a 1.5 Tesla scanner (Achieva) equipped with dStream Torso coils (Philips Medical Systems, Best, the Netherlands). Native T1 mapping was acquired in three short-axis image planes (base, mid, apex) using optimized single breath hold 5(3)3 MOLLI sequence. This sequence allows acquisition of images at a standstill of the heart cycle in late diastole, providing high-resolution T1 maps of the myocardium^{13,14}. We used a repetition time/echo time/flip angle of 3.5/0/35 degrees, matrix of 144, field of view of 288mm and a slice thickness of 8mm. The CMR protocol also included an ECG-gated breath hold multiphase steady state-free precession sequence in four-chamber, short-axis, and two-chamber RV and LV, and RVOT views (repetition time/echo time/flip angle 2.9/1.4/60 degrees, matrix 192-256, field of view 320mm, temporal resolution 50msec, slice thickness 8mm) for the assessment of biventricular volume, function and wall motion. For LGE, phase-sensitive inversion recovery images were acquired in four chamber, short axis and two-chamber and RVOT views 15 minutes after administration of a double dose of 0.2ml Gadovist/kg.

Image analysis

Native MOLLI images were processed using cvi42 (Circle Cardiovascular Imaging, Calgary, Alberta, Canada [version 5.6.6]). T1 times were measured by manually drawing endocardial and epicardial contours in the basal, mid, and apical short axis views on the native images. Since T1 measurements are not validated for the thin-walled RV, we only measured T1 times of the LV including the ventricular septum. Global T1 values were calculated as the mean T1 time (ms) of the LV. For regional analysis, T1 times were assessed according to the American Heart Association 16-segment LV model (see **Figure 1**). To assess dispersion of regional T1 times within a given patient, the standard deviation of all analyzed LV segments was calculated.

Intra-observer variability was evaluated by re-measuring native T1 times in 15 randomly selected subjects by the first observer. For inter-observer variability, the same 15 subjects were measured by a second observer, independent from the first observer. Observers were blinded for clinical and demographic data at the time of CMR measurements.

Ventricular function and dimensions were measured using QMass (Medis, Leiden, The Netherlands [version 7.6]). LGE and wall motion abnormalities were qualitatively assessed as part of the clinical assessment. Clinical data was retrieved from electronic health records.

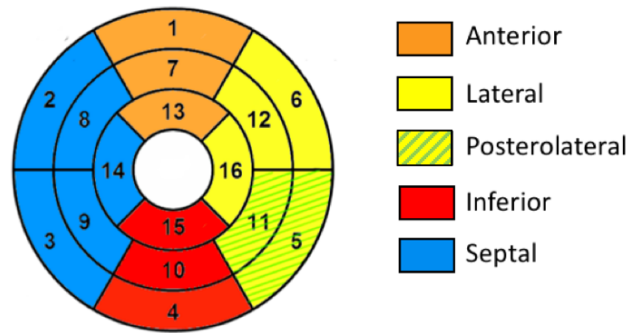


Figure 1: Example of LV segmentation according to the AHA 16-segments model.

Anterior, lateral, posterolateral, inferior and septal region are segmented according to the legend. In addition, basal region includes segments 1-6; mid region includes segments 7-12; apical region includes segments 13-16.

Statistical analysis

Statistical analyses were performed using SPSS version 25 (IBM, Chicago, Illinois). Continuous variables were expressed as mean (\pm standard deviation) or as median (interquartile range, IQR) as appropriate. For continuous comparisons of two groups, a two-tailed Student's t-test or Mann Whitney U-test was used, as appropriate. For continuous comparisons of three or more groups, one-way ANOVA or Kruskal Wallis was used. Categorical data were compared using the chi-square test or Fisher exact test. Post-hoc Bonferroni correction was used for multiple comparisons. Correlation was assessed by the Intraclass Correlation Coefficient (ICC). For ICC, a value ≥ 0.90 was considered excellent, < 0.90 to ≥ 0.75 good, < 0.75 to ≥ 0.50 moderate, and < 0.50 poor¹⁵. Diagnostic accuracy was evaluated using the area under the Receiver Operating Characteristic (ROC) curve. For the area under the curve (AUC), a value of 0.90–1.0 was considered excellent, 0.80–0.90 good, 0.70–0.80 fair, 0.60–0.70 poor and 0.50–0.60 fail¹⁶.

RESULTS

Patient population

We evaluated CMR images of 43 subjects (13 overt ARVC patients [mutation+, phenotype+], 17 at-risk relatives [mutation+, phenotype-] and 13 control subjects). Baseline characteristics of the study population are shown in **Table 1**. Mean age of study subjects was 37 ± 17 years and 51% were female. There were no significant differences in age ($p=0.10$) and sex ($p=0.53$) between the three groups. By study design, all overt ARVC patients and at-risk relatives carried an ARVC-associated pathogenic mutation, the most common being Plakophilin-2 (*PKP2*, 70%), followed by Phospholamban (*PLN*, 27%) and Desmoplakin (*DSP*, 3%). Overt

ARVC patients had a median of 5 [IQR 4-7] TFC points, while at-risk relatives had a median of 2 [IQR 2-3] TFC points.

Table 1: Baseline characteristics

	Cases		Controls
	Overt patients (n=13)	At risk relatives (n=17)	RVOT-VT patients (n=13)
Age	40.3 \pm 18.6	30.8 \pm 14.7	43.2 \pm 15.7
Male gender	5 (38)	10 (59)	6 (46)
Genotype			
<i>PKP2</i>	10 (77)	11 (65)	n/a
<i>PLN</i>	3 (23)	5 (29)	
<i>DSP</i>	0 (0)	1 (6)	
Clinical Phenotype			
Median Number of TFC	5 [4-7]	2 [2-3]	n/a
TWI V1-3	3 (23)	0 (0)	
TWI V1-2	5 (38)	0 (0)	
TWI V1-4 RBBB	0 (0)	0 (0)	
TWI V4-6	3 (23)	0 (0)	
Epsilon wave	0 (0)	0 (0)	
Prolonged TAD	6 (46)	0 (0)	
Late potentials	1 (8)	1 (6)	
LBBB VT superior axis	0 (0)	0 (0)	
LBBB VT inferior/unknown axis	2 (15)	0 (0)	
>500 PVCs/24h	9 (69)	3 (18)	
Structural major	7 (54)	0 (0)	
Structural minor	2 (15)	1 (6)	

Abbreviations: DSP= desmoplakin; LBBB= left bundle branch block; PKP2= plakophilin-2; PLN= phospholamban; PVC= premature ventricular contraction; RBBB= right bundle branch block; RVOT-VT= right ventricular outflow tract ventricular tachycardia; TAD= terminal activation duration; TFC= Task Force Criteria; VT= ventricular tachycardia

Conventional CMR

Overt ARVC patients showed a trend towards reduced global RV function ($p=0.08$) with more regional RV wall motion abnormalities ($p<0.01$) compared to control subjects (**Table 2**). LV volume and function were similar between overt ARVC patients and controls ($p>0.51$). In addition, at-risk relatives were similar to control subjects for all metrics of biventricular volume and function ($p>0.24$).

LV LGE was observed in 69% ($n=9$) of overt ARVC patients, compared to 41% ($n=7$) of at-risk relatives, and none of the control subjects ($p=0.002$). LGE was predominantly observed at the insertion point of the RV (33% [$n=3/9$] of overt ARVC patients and 86% [$n=6/7$] of at-risk relatives) and in the posterolateral LV (55% [$n=5/9$] of overt ARVC patients).

Table 2: Conventional CMR parameters

	Cases		Controls	p-value*
	Overt patients (n=13)	At-risk relatives (n=17)	RVOT-VT patients (n=13)	
Ventricular Function				
RV wall motion abnormality	10 (77) [†]	2 (12)	0 (0)	<0.001
RV EF (%)	50 ± 6	54 ± 5	55 ± 4	0.152
LV wall motion abnormality	0	1 (6)	0 (0)	0.372
LV EF (%)	57 ± 6	57 ± 6	58 ± 4	0.838
Ventricular Volume				
RV EDV/BSA (mL/m ²)	102 ± 27	95 ± 13	101 ± 14	0.549
RV ESV/BSA (mL/m ²)	51 ± 19	44 ± 10	46 ± 8	0.370
LV EDV/BSA (mL/m ²)	92 ± 17	92 ± 13	97 ± 16	0.707
LV ESV/BSA (mL/m ²)	40 ± 10	40 ± 9	41 ± 9	0.975
Focal Fibrosis by Contrast-enhanced CMR				
RV LGE	2 (15)	0 (0)	0 (0)	0.089
LV LGE	9 (69) [†]	7 (41) [†]	0 (0)	0.002

* Comparison between three groups

[†] Significant difference compared to controls <0.01

Abbreviations: BSA= body surface area; CMR= cardiac magnetic resonance; EDV= end diastolic volume; EF= ejection fraction; ESV= end systolic volume; LGE= late gadolinium enhancement; LV= left ventricle; RV= right ventricle; RVOT-VT= right ventricular outflow tract ventricular tachycardia.

Table 3: Global and regional native T1 times of the left ventricle

	Cases		Controls	p-value*
	Overt patients (n=13)	At risk relatives (n=17)	RVOT-VT patients (n=13)	
Global				
Native T1 mean	1067 ± 41 [†]	1055 ± 38	1038 ± 27	0.128
Native T1 dispersion	93 ± 33 [†]	79 ± 15 [†]	67 ± 12	0.015
Regional				
Native T1 LV basal	1060 ± 52 [†]	1044 ± 35 [†]	1020 ± 26	0.050
Native T1 LV mid	1064 ± 35 [†]	1051 ± 37 [†]	1027 ± 22	0.024
Native T1 LV apical	1084 ± 58	1083 ± 58	1057 ± 38	0.354
Native T1 anterior	1085 ± 62 [†]	1049 ± 45	1028 ± 24	0.014
Native T1 LV septal	1070 ± 36	1067 ± 45	1050 ± 31	0.392
Native T1 LV inferior	1065 ± 40 [†]	1066 ± 43 [†]	1027 ± 30	0.020
Native T1 LV posterolateral	1050 ± 61 [†]	1032 ± 32 [†]	1001 ± 28	0.020
Native T1 LV lateral	1056 ± 60 [†]	1042 ± 34 [†]	1019 ± 26	0.096

*Comparison between three groups

[†]Significant difference (p<0.05) compared to controls[‡]Significant trend (p<0.10) compared to controls

Abbreviations: LV= left ventricle; RV= right ventricle; RVOT-VT= right ventricular outflow tract ventricular tachycardia.

Native T1 mapping of the left ventricle

Global T1 times

As shown in **Table 3**, mean T1 times increased from controls (1038±27 ms) to at-risk relatives (1055±38 ms) to overt ARVC patients (1067±41 ms). While this trend was not significant in a three-group comparison (p=0.13), statistical significance was reached for the comparison between overt ARVC patients and controls (p=0.04).

Regional T1 times

T1 dispersion, as determined by the standard deviation of T1 time in all LV regions within a given patient, was significantly larger in overt ARVC patients compared to control subjects (93±33ms vs. 67±12ms, p=0.02). As shown in **Table 3** and **Figure 2**, this was due to elevated native T1 in the LV posterolateral (p=0.02), inferior (p=0.01) and anterior (p=0.01) regions. Interestingly, T1 dispersion was also significantly greater in at-risk relatives compared to controls (79±15ms vs. 67±12ms, p=0.03). As shown in **Table 3** and **Figure 2**, this was driven by elevated native T1 in the LV posterolateral (p=0.01) and inferior (p=0.01) regions.

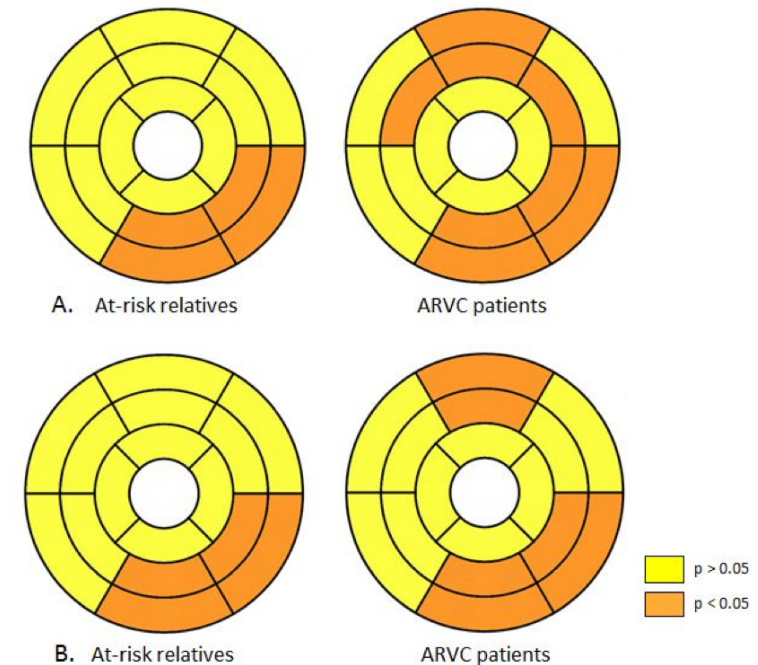


Figure 2: Bullseyes of native T1 times of ARVC patients vs. controls and at-risk subject vs. controls without (A) and with (B) Bonferroni correction. Yellow indicates no significant difference compared to RVOT-VT control subjects and orange indicates a significant difference compared to RVOT-VT control subjects.

Clinical implications

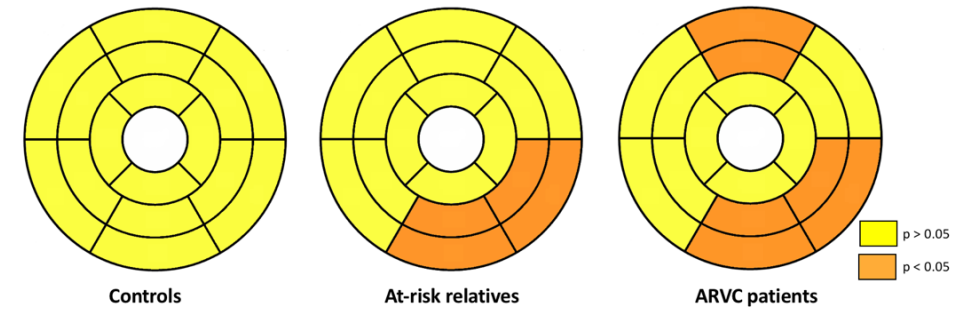
We subsequently sought to determine the clinical correlates of increased native T1 times in ARVC. We focused these efforts on native T1 dispersion, since this parameter showed the greatest discriminative potential between overt ARVC patients and controls. Native T1 dispersion correlated significantly with RVEF ($r=-0.36$, $p=0.02$), LVEF ($r=-0.33$, $p=0.03$), and LV LGE ($r=0.35$, $p=0.02$). No correlation was found for T1 dispersion with RV EDV/BSA ($r=0.04$, $p=0.78$), LV EDV/BSA ($r=-0.04$, $p=0.79$), and RV wall motion abnormalities ($r=0.26$, $p=0.09$). ROC curve analysis was used to identify the optimal threshold for abnormal T1 dispersion with the highest sensitivity and specificity. Using a cutoff of smaller than 73ms as normal T1 dispersion, ARVC patients were separated from controls with 73% sensitivity and 77% specificity (AUC=0.80).

We next evaluated the incremental value of T1 dispersion over the imaging criteria in the diagnostic TFC. Given our limited sample size, we divided our cases in those with ($n=10$, 33%) vs. without ($n=20$, 67%) major or minor imaging criteria for ARVC. Among 20 cases without imaging criteria for ARVC ($n=4/13$ ARVC patients, $n=16/17$ at-risk relatives, see **Table 1**), we observed an elevated T1 dispersion in the 4 patients with a definite ARVC diagnosis (97.0 ± 56.3 vs. 78.8 ± 15.7 ms). Although this was not statistically significant in our population ($p=0.78$), these results suggest there is potential for T1 dispersion to unmask disease expression prior to fulfillment of imaging TFC.

To further evaluate the value of T1 mapping in early diagnosis of ARVC, we specifically focused on at-risk relatives. Among 17 relatives, 11 (65%) subjects had abnormal T1 dispersion. Interestingly, 64% ($n=7/11$) of at-risk relatives with abnormal T1 dispersion had no LGE. As shown in **Supplementary Table 1**, no other signs of structural or electrical disease were seen.

Reproducibility

In a subset of 15 subjects, intra-observer correlation was excellent for both global and regional native T1 times ($ICC \geq 0.94$). Also, the inter-observer correlation for the same subset of subjects was excellent for both the global and regional native T1 times ($ICC \geq 0.94$) (**Table 4**).



Central Illustration: Pattern of elevated native T1 times in ARVC patients and at-risk relatives compared to control subjects

Table 4: Intra- and inter-observer reproducibility of native T1 times per region

	Intra-observer ICC	Inter-observer ICC
Global		
Mean	0.984 (0.954-0.995)	0.978 (0.934-0.993)
Dispersion	0.942 (0.828-0.981)	0.935 (0.807-0.978)
Regional		
Basal	0.984 (0.949-0.995)	0.977 (0.928-0.993)
Mid	0.977 (0.924-0.993)	0.964 (0.888-0.989)
Apical	0.978 (0.929-0.993)	0.989 (0.965-0.996)
Anterior region	0.979 (0.930-0.993)	0.979 (0.936-0.993)
Lateral region	0.990 (0.967-0.997)	0.989 (0.967-0.997)
Posterolateral region	0.990 (0.967-0.997)	0.966 (0.893-0.989)
Inferior region	0.948 (0.829-0.984)	0.951 (0.846-0.984)
Septal region	0.964 (0.883-0.989)	0.969 (0.904-0.990)

DISCUSSION

This study is the first to compare T1 times between ARVC patients and control subjects. Several interesting insights were obtained. First, we showed that global mean native T1 time differentiates overt ARVC patients from control subjects with RVOT-VT. Second, both overt ARVC patients and at-risk relatives have a greater dispersion of native T1 times compared to controls. More specifically, ARVC patients have elevated T1 times in the posterolateral, inferior and anterior regions, whereas the posterolateral and inferior region are affected in at-risk relatives. Finally, we determined the clinical correlates and diagnostic value of native T1 in ARVC. Overall, our results indicate a potential role for native T1 mapping in early ARVC diagnosis.

Left ventricular fibrosis in ARVC

Previous studies have shown that fibro-fatty myocardial replacement in ARVC occurs diffusely in both ventricles with LV involvement in up to 76% of affected patients^{17–21}. This was corroborated in the present study where 77% of our ARVC patient population had abnormal T1 times in the LV (based on a 73ms threshold for abnormal T1 dispersion). The high dispersion of native T1 times in both ARVC patients and at-risk relatives indicates a higher heterogeneity of cardiac microstructures in ARVC patients and relatives which could be caused by the presence of a mixture of both increased fibrous (increases native T1 times) and fatty tissue (decreases native T1 times)¹¹. Interestingly, on average, ARVC patients had higher native T1 times compared to controls which suggests that the cardiac microstructural changes are dominated by fibrosis rather than fatty replacement. While our study was cross-sectional in design, and was not designed to investigate disease progression, our results suggest that fibrous infiltration in ARVC starts in the posterolateral/inferior region and disseminates when the disease progresses, thereby also affecting global native T1 times in more advanced stages. This is in alignment with previous studies, which show that regional LV changes in ARVC typically affect the posterolateral wall^{17,21}. Of note, these results were shown to be specific to both ARVC patients with a desmosomal mutation as well as to *PLN* mutation carriers²¹. Our results confirm and extend these prior studies, by revealing that these changes can already be observed in asymptomatic mutation carriers prior to the development of an overt clinical phenotype. LV enhancement was seen in 16 out of 30 cases, however most enhancement (n=9/16) was present in the insertion point of the RV, which is a nonspecific finding. Using T1 mapping, elevated T1 times were also seen in regions without LGE. This indicates that T1 mapping shows a more diffuse process.

Our study was limited in the evaluation of fibrosis in the RV since the thin RV wall renders native T1 mapping susceptible to partial volume effects²². While the presence of diffuse (i.e. also LV) fibrosis in ARVC suggests a possible diagnostic role for abnormal LV tissue architecture in ARVC, further validation of this technique requires a comparison with histopathological data. Also, we were unable to use extracellular volume (ECV) as a measure for diffuse fibrosis since reliable hematocrit data was unavailable. Follow-up studies should also look at this measure in the diagnostic evaluation of ARVC using T1 mapping.

Clinical application of T1 mapping for ARVC evaluation

Recent studies have shown that native T1 times are elevated in affected patients with HCM and DCM compared to controls^{12,23}. Accordingly, elevated T1 times in our study were able to differentiate ARVC patients from control subjects. Comparable to the results in other cardiomyopathies, we determined that 64% of at-risk ARVC relatives with elevated T1 dispersion had no LGE²⁴, suggesting a greater sensitivity of T1 mapping for subtle ventricular changes. While these results are promising, a larger population of ARVC patients and at-risk relatives need to be prospectively studied to define the incremental diagnostic value of T1

mapping over other established diagnostic tests for ARVC.

Recently, Puntmann *et al.* evaluated the prognostic value of T1 mapping in patients with non-ischemic DCM. They showed an association of T1 mapping with all-cause mortality that was independent of conventional CMR parameters (EF<35% and LGE)²⁵. While our study design limits our ability to draw inference on prognostic value of T1 mapping, this suggests that T1 mapping is a promising biomarker in the prediction of disease outcome.

Feasibility of T1 mapping

Native T1 times in our study showed excellent reproducibility. Of note, this was achieved through a standardized data collection method, in which we only included subjects scanned with the same field strength, sequence, and CMR vendor. While this influenced the population size and generalizability of our study, we believe it strengthened the homogeneity of study results and thereby the true evaluation of native T1 mapping in ARVC. Although the results of our study are promising, predefined reference ranges for native T1 times will be essential before this technique can be routinely applied in clinically applied.

CONCLUSION

Native T1 mapping can help to differentiate overt ARVC patients and at-risk relatives from patients with RVOT-VT and correlates with ventricular function. Interestingly, nearly two-thirds of at-risk relatives with elevated T1 times did not show enhancement on LGE, indicating the potential of native T1 mapping to detect early disease in this subgroup.

Perspectives

Competency in medical knowledge

Native T1 mapping has a possible role in differentiating overt ARVC patients and at-risk relatives from controls, and is significantly correlated with ventricular function. Therefore, T1 mapping may be a promising tool in the early recognition of ARVC when combined with current diagnostic tests for ARVC.

Translational Outlook

Future studies (using a larger population of ARVC patients and at-risk relatives) are required to determine the incremental diagnostic value of T1 mapping over other diagnostic tests for ARVC.

Acknowledgements

The authors are grateful to the ARVC patients and families who have made this work possible.

Abbreviations

ARVC = Arrhythmogenic right ventricular cardiomyopathy

CMR = Cardiac magnetic resonance imaging

DCM = Dilated cardiomyopathy

DSP = Desmoplakin

ECG = Electrocardiogram

HCM = Hypertrophic cardiomyopathy

LV = Left ventricle

LGE = Late gadolinium enhancement

MOLLI = Modified look-locker inversion recovery

PLN = Phospholamban

PKP2 = Plakophilin-2

RV = Right ventricle

RVOT-VT = Right ventricular outflow tract ventricular tachycardia

TFC = Task Force Criteria

VA = Ventricular arrhythmias

REFERENCES

- Marcus FI, Fontaine GH, Guiraudon G, et al. Right ventricular dysplasia: a report of 24 adult cases. *Circulation*. 1982;65(2):384-398.
- Saguner AM, Brunckhorst C, Duru F. Arrhythmogenic ventricular cardiomyopathy: A paradigm shift from right to biventricular disease. *World J Cardiol*. 2014;6(4):154-174. doi:10.4330/wjcv.v6.i4.154
- Wu KC, Weiss RG, Thiemann DR, et al. Late gadolinium enhancement by cardiovascular magnetic resonance heralds an adverse prognosis in nonischemic cardiomyopathy. *J Am Coll Cardiol*. 2008;51(25):2414-2421. doi:10.1016/j.jacc.2008.03.018
- Basso C, Corrado D, Thiene G. Arrhythmogenic right ventricular cardiomyopathy in athletes: diagnosis, management, and recommendations for sport activity. *Cardiol Clin*. 2007;25(3):415-422. vi. doi:10.1016/j.ccl.2007.08.009
- Angelini A, Basso C, Nava A, Thiene G. Endomyocardial biopsy in arrhythmogenic right ventricular cardiomyopathy. *Am Heart J*. 1996;132(1 Pt 1):203-206.
- Rastegar N, Burt JR, Corona-Villalobos CP, et al. Cardiac MR findings and potential diagnostic pitfalls in patients evaluated for arrhythmogenic right ventricular cardiomyopathy. *Radiographics*. 2014;34(6):1553-1570. doi:10.1148/rg.346140194
- Tandri H, Calkins H, Nasir K, et al. Magnetic resonance imaging findings in patients meeting task force criteria for arrhythmogenic right ventricular dysplasia. *J Cardiovasc Electrophysiol*. 2003;14(5):476-482.
- Te Riele ASJM, Tandri H, Sanborn DM, Bluemke DA. Noninvasive multimodality imaging in ARVD/C. *JACC Cardiovasc Imaging*. 2015;8(5):597-611. doi:10.1016/j.jcmg.2015.02.007
- Schelbert EB, Messroghli DR. State of the Art: Clinical Applications of Cardiac T1 Mapping. *Radiology*. 2016;278(3):658-676. doi:10.1148/radiol.2016141802
- Moon JC, Messroghli DR, Kellman P, et al. Myocardial T1 mapping and extracellular volume quantification: a Society for Cardiovascular Magnetic Resonance (SCMR) and CMR Working Group of the European Society of Cardiology consensus statement. *J Cardiovasc Magn Reson*. 2013;15:92. doi:10.1186/1532-429X-15-92
- Haaf P, Garg P, Messroghli DR, Broadbent DA, Greenwood JP, Plein S. Cardiac T1 Mapping and Extracellular Volume (ECV) in clinical practice: a comprehensive review. *J Cardiovasc Magn Reson*. 2016;18(1):89. doi:10.1186/s12968-016-0308-4
- Puntmann VO, Voigt T, Chen Z, et al. Native T1 mapping in differentiation of normal myocardium from diffuse disease in hypertrophic and dilated cardiomyopathy. *JACC Cardiovasc Imaging*. 2013;6(4):475-484. doi:10.1016/j.jcmg.2012.08.019
- Messroghli DR, Radjenovic A, Kozerke S, Higgins DM, Sivananthan MU, Ridgway JP. Modified Look-Locker inversion recovery (MOLLI) for high-resolution T1 mapping of the heart. *Magn Reson Med*. 2004;52(1):141-146. doi:10.1002/mrm.20110
- Rogers T, Dabir D, Mahmoud I, et al. Standardization of T1 measurements with MOLLI in differentiation between health and disease--the ConSept study. *J Cardiovasc Magn Reson*. 2013;15:78. doi:10.1186/1532-429X-15-78
- Koo TK, Li MY. A Guideline of Selecting and Reporting Intraclass Correlation Coefficients for Reliability Research. *J Chiropr Med*. 2016;15(2):155-163. doi:10.1016/j.jcm.2016.02.012
- Hosmer DW LS. *Applied Logistic Regression*. 2nd ed. New York: John Wiley & Sons; 2000.
- Corrado D, Basso C, Thiene G, et al. Spectrum of clinicopathologic manifestations of arrhythmogenic right ventricular cardiomyopathy/dysplasia: a multicenter study. *J Am Coll Cardiol*. 1997;30(6):1512-1520.
- Norman M, Simpson M, Mogensen J, et al. Novel mutation in desmoplakin causes arrhythmogenic left ventricular cardiomyopathy. *Circulation*. 2005;112(5):636-642. doi:10.1161/CIRCULATIONAHA.104.532234
- Sen-Chowdhry S, Syrris P, Prasad SK, et al. Left-dominant arrhythmogenic cardiomyopathy: an under-recognized clinical entity. *J Am Coll Cardiol*. 2008;52(25):2175-2187. doi:10.1016/j.jacc.2008.09.019
- Sen-Chowdhry S, Syrris P, Ward D, Asimaki A, Sevdalis E, McKenna WJ. Clinical and genetic characterization of families with arrhythmogenic right ventricular dysplasia/cardiomyopathy provides novel insights into patterns of disease expression. *Circulation*. 2007;115(13):1710-1720. doi:10.1161/CIRCULATIONAHA.106.660241
- Sepehrkhoy S, Gho JMIH, van Es R, et al. Distinct fibrosis pattern in desmosomal and phospholamban mutation carriers in hereditary cardiomyopathies. *Heart Rhythm*. 2017;14(7):1024-1032. doi:10.1016/j.hrthm.2017.03.034
- Swoboda PP, McDiarmid AK, Page SP, Greenwood JP, Plein S. Role of T1 Mapping in Inherited Cardiomyopathies. *Eur Cardiol*. 2016;11(2):96-101. doi:10.15420/ecr/2016;28:2
- Dass S, Suttie JJ, Piechnik SK, et al. Myocardial tissue characterization using magnetic resonance noncontrast t1 mapping in hypertrophic and dilated cardiomyopathy. *Circ Cardiovasc Imaging*. 2012;5(6):726-733. doi:10.1161/CIRCIMAGING.112.976738
- Kato S, Nakamori S, Bellm S, et al. Myocardial Native T1 Time in Patients With Hypertrophic Cardiomyopathy. *Am J Cardiol*. 2016;118(7):1057-1062. doi:10.1016/j.amjcard.2016.07.010
- Puntmann VO, Carr-White G, Jabbour A, et al. T1-Mapping and Outcome in Nonischemic Cardiomyopathy: All-Cause Mortality and Heart Failure. *JACC Cardiovasc Imaging*. 2016;9(1):40-50. doi:10.1016/j.jcmg.2015.12.001

SUPPLEMENTARY INFORMATION

Supplementary Table 1: Clinical characteristics of at-risk relatives with abnormal T1 dispersion without enhancement on LGE.

	Sex	Age at CMR	Number of TFC points	NSVT (yes/no)	RV EF (%)	LV EF (%)	WMA (yes/no)
Case 1	Male	13	2	No	54	61	no
Case 2	Female	23	2	No	49	51	no
Case 3	Male	25	2	No	62	63	no
Case 4	Male	27	2	No	55	50	no
Case 5	Male	30	2	No	39	46	yes
Case 6	Female	31	2	No	52	55	no
Case 7	Male	68	2	No	59	66	no

Abbreviations: CMR= cardiac magnetic resonance; EF= ejection fraction; LV= left ventricle; NSVT= non-sustained ventricular tachycardia; RV= right ventricle; RVOT-VT= right ventricular outflow tract ventricular tachycardia; TFC=Task Force Criteria; WMA= wall motion abnormalities.

CHAPTER

8

Towards automatic classification
of cardiovascular magnetic
resonance task force criteria for
diagnosis of arrhythmogenic right
ventricular cardiomyopathy

Mimount Bourfiss, MD*;
Jörg Sander MSc*;
Bob D. de Vos PhD;
Anneline S.J.M. te Riele MD, PhD;
Folkert W. Asselbergs MD, PhD;
Ivana Išgum PhD;
Birgitta K. Velthuis MD, PhD

*Shared first authorship

Clinical Research in Cardiology. 2022 Sep 6.

doi: 10.1007/s00392-022-02088-x.

Epub ahead of print. PMID: 36066609

ABSTRACT

Background. Arrhythmogenic cardiomyopathy (ACM) is diagnosed according to the Task Force Criteria (TFC) in which cardiovascular magnetic resonance (CMR) imaging plays an important role. Our study aims to apply an automatic deep learning-based segmentation for right and left ventricular CMR assessment and evaluate this approach for classification of the CMR TFC.

Methods. We included 227 subjects suspected of ACM who underwent CMR. Subjects were classified into 1) ACM patients fulfilling TFC; 2) at-risk family members; and 3) controls. To perform automatic segmentation, a Bayesian Dilated Residual Neural Network was trained and tested. Performance of automatic versus manual segmentation was assessed using Dice-coefficient and Hausdorff distance. Since automatic segmentation is most challenging in basal slices, manual correction of the automatic segmentation in the most basal slice was simulated (automatic^{-basal}). CMR TFC calculated using manual and automatic^{-basal} segmentations were compared using Cohen's Kappa (κ).

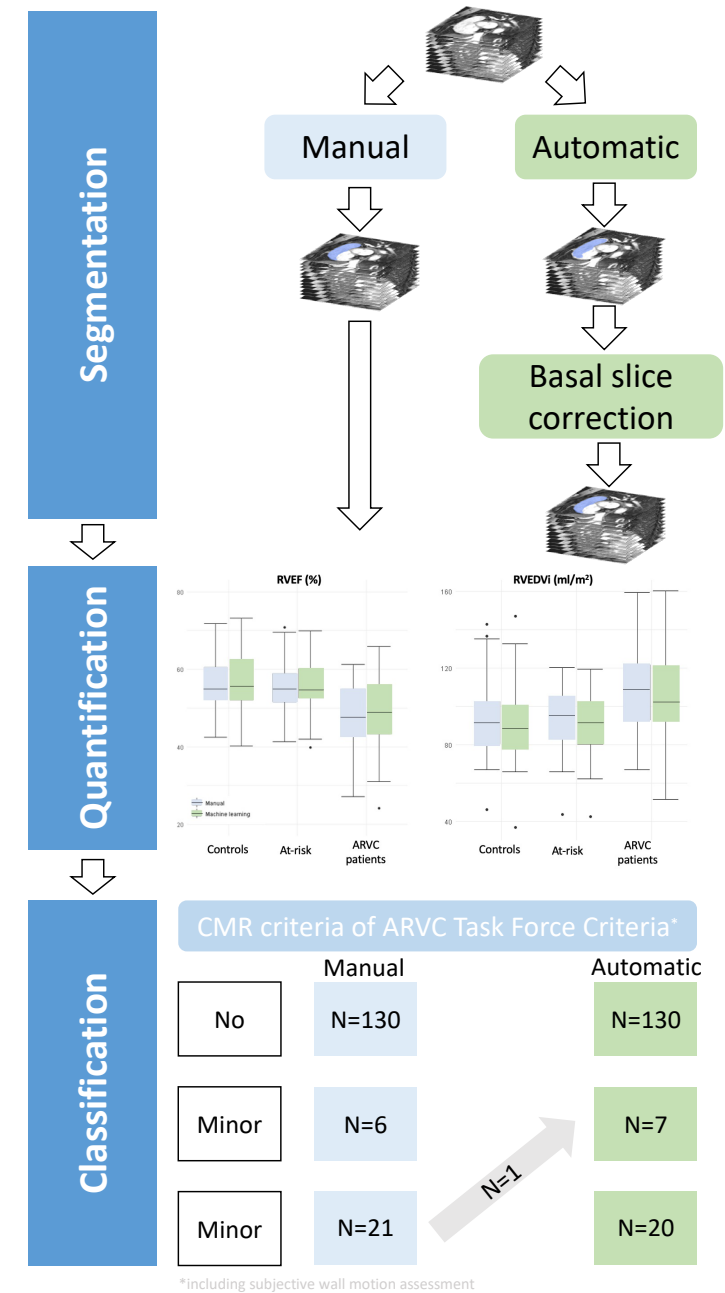
Results. Automatic segmentation was trained on CMRs of 70 subjects (39.6±18.1 years, 47% female) and tested on 157 subjects (36.9±17.6 years, 59% female). Dice-coefficient and Hausdorff distance showed good agreement between manual and automatic segmentations (≥ 0.89 and ≤ 10.6 mm, respectively) which further improved after simulated correction of the most basal slice (≥ 0.92 and ≤ 9.2 mm, $p < 0.001$). Pearson correlation of volumetric and functional CMR measurements was good to excellent (automatic ($r = 0.78-0.99$, $p < 0.001$) and automatic^{-basal} ($r = 0.88-0.99$, $p < 0.001$) measurements). CMR TFC classification using automatic^{-basal} segmentations was comparable to manual segmentations ($\kappa = 0.98 \pm 0.02$) with comparable diagnostic performance.

Conclusions. Combining automatic segmentation of CMRs with correction of the most basal slice results in accurate CMR TFC classification of subjects suspected of ACM.

Keywords: Arrhythmogenic Cardiomyopathy; Cardiac Magnetic Resonance Imaging; Deep learning; Automatic segmentation

GRAPHICAL ABSTRACT

Towards automatic classification of the ARVC CMR Task Force Criteria



BACKGROUND

Arrhythmogenic right ventricular cardiomyopathy (ARVC) is an inherited heart disease that is characterized by ventricular dysfunction, predominantly affecting the right ventricle (RV), and potentially life-threatening ventricular arrhythmias. Accurate recognition of this disease is vital since the implantation of an implantable cardioverter defibrillator can be life-saving. ARVC is diagnosed according to the revised 2010 Task Force Criteria (TFC)¹. Apart from electrical and family history criteria, an important role is given to the assessment of ventricular dysfunction and structural alterations. Cardiac magnetic resonance (CMR) imaging is the modality of choice for the assessment of cardiac function and dimensions in ARVC² since the asymmetric geometry and the position of the RV in the chest hampers visualization of the entire RV by 2-D echocardiography³.

The CMR TFC are based on RV regional wall motion abnormalities combined with cut-off values for RV ejection fraction (EF) or sex-specific cut-off values for RV indexed end-diastolic volume (EDVI)¹. CMR can deliver one minor or two major points of the necessary four TFC points for an ARVC diagnosis. Therefore, accurate RV assessment is essential. Segmenting CMRs to measure functional and structural parameters is a laborious task, taking about 25 minutes to segment both ventricles in end-diastole (ED) and end-systole (ES)^{4,5}. Notably, RV segmentation takes two-thirds of this segmentation time and is prone to intra- and inter-observer variability⁶. RV segmentation difficulties can arise from the trabeculated and complex RV geometry^{7,8}. In ARVC, RV and left ventricular (LV) anatomy can be further complicated by pathological wall thinning and aneurysms due to fibrofatty replacement of the myocardial wall². As a consequence, CMR misinterpretations are a key cause of over-diagnosis in ARVC². The use of automatic methods for the segmentation of the ventricles may overcome these challenges. Over the last few years many state-of-the-art deep learning segmentation approaches for short-axis CMR have been developed^{4,9-11}. For automatic LV segmentation such methods can achieve performance level of human experts^{12,13}. However, previous studies also demonstrated that in manual and automatic segmentation of short-axis CMR, the largest disagreements and errors occur in the most basal and apical slices^{8,12-15}. Moreover, previous methods have often been evaluated on CMR datasets with limited pathology especially related to the RV. In contrast, this study included a large hospital population being evaluated for ARVC, including subjects with structurally normal hearts and those with complex structural abnormalities. In this work we apply a previously validated state-of-the-art segmentation approach¹⁶ on a large heterogeneous hospital population of patients suspected of ARVC. The purpose of this study was to (i) evaluate our previously developed deep learning segmentation approach for RV and LV CMR assessment in patients suspected of ARVC and (ii) evaluate the clinical implication of this approach for classification of the CMR TFC in subjects suspected of ARVC.

METHODS

Study population

We included a consecutive cohort of subjects suspected of ARVC who underwent CMR as part of their clinical evaluation between 2014 and 2019 at the University Medical Center (UMC) Utrecht. This yielded 241 subjects, of whom 14 were excluded because of an equivocal diagnosis (ARVC neither confirmed nor rejected) (n=12), prior chemotherapy (n=1) and imaging artefacts due to irregular heart rhythm (n=1). This led to a study population of 227 subjects who were classified into three groups: 1) ARVC patients diagnosed according to the 2010 TFC (n=53); 2) family members at-risk of developing ARVC (n=96); and 3) control subjects initially suspected of ARVC but in whom ARVC was excluded after full clinical assessment (n=78). Diagnosis in the control patients included RV outflow tract tachycardia (n=45), premature ventricular contractions/non-sustained ventricular tachycardia (n=19), mutation-negative family members of mutation-positive ARVC patients (n= 3), healthy athletes (n=3), syncope without a cardiac cause (n=3) repolarization abnormalities with a structurally normal heart (n=3) and pectus excavatum (n=2). This study was reviewed by the UMC Utrecht Institutional Review Board and was granted a waiver of informed consent.

ARVC diagnosis

ARVC diagnosis was based on the revised 2010 diagnostic TFC¹. In short, these consensus-based criteria rely on major and minor criteria for six different categories: 1) global and regional dysfunction and structural alterations; 2) tissue characterization; 3) repolarization abnormalities; 4) depolarization/conduction abnormalities; 5) arrhythmias; and 6) family history/genetics. In each of these six categories subjects can score a minor criterium (one point), a major criterium (two points) or no criteria (0 points). A definite ARVC diagnosis was made if a subject has at least four points. The first category can be assessed by CMR, with minor criteria for regional RV wall motion abnormalities plus RVEF >40 to ≤45% or RVEDVI ≥100 to <110 ml/m² (males) or ≥90 to <100 mL/m² (females) and major criteria for RV regional wall motion abnormalities plus RVEF ≤40% or RVEDVI ≥110ml/m² (males) or ≥100 ml/m² (females)¹.

CMR dataset

All subjects underwent CMR using either 1.5 or 3 Tesla Ingenia or Achieva Philips scanners (Best, the Netherlands). The CMR dataset consisted of conventional steady-state free precession sequence short-axis and longitudinal-axis (4-chamber, 2-chamber and 3-chamber of both ventricles) cine CMR images acquired during breath holds. For this work, we only included the short-axis CMR volumes consisting of 12-18 contiguous slices covering both ventricles. The short-axis imaging parameters were as follows: each slice containing 25 to 40 phases covering one cardiac cycle with repetition time 2.6-3.4 ms and echo time 1.3-1.7 ms, flip angle 45-60 degrees. The CMR images have an in-plane resolution ranging

from 1.11 to 1.45 with a slice thickness varying from 7 to 10 mm. Furthermore, reconstruction matrix of images ranges from 240x240 to 288x288 voxels. Expert radiology technicians made manual reference segmentations of the RV and LV endocardium for all CMR slices at ED and ES time frames. Both time points were manually chosen by the same experts. The CMR segmentation protocol was published previously¹⁷ and adheres to the guidelines of the Society of Cardiovascular Magnetic Resonance (SCMR)¹⁸. Furthermore, the presence of RV and/or LV wall motion abnormalities was visually evaluated by an experienced cardiovascular radiologist on all available cine images and used for the calculation of the CMR TFC.

Automatic segmentation of CMR

Prior to segmentation, voxel intensities in CMR scans were normalized by rescaling the values between [0,1] based on their 1st and 99th percentiles per scan. Furthermore, voxels intensities below or above the 1st and 99th percentiles were clamped to 0 and 1, respectively. To perform automatic segmentation of RV and LV in the 2D short-axis CMR images, we trained a Bayesian Dilated Residual Neural Network (DRN)¹⁹ that was previously developed and evaluated by Sander *et al.*¹⁶. The Bayesian DRN was based on the original DRN from Yu *et al.*¹⁹ for image segmentation. To convert the original DRN¹⁹ into a Bayesian DRN, we implemented *Monte Carlo* dropout (MC dropout) introduced by Gal & Ghahramani²⁰. Using a Bayesian i.e. MC dropout approach is advantageous because multiple predictions for the same voxel can be averaged to obtain an improved final prediction per voxel¹⁶. Furthermore, architecture and parameters of the Bayesian DRN were identical to the model described in¹⁶. The network used a 2D CMR image as input and had three output channels, each providing probability for the LV, RV or background. Softmax probabilities were calculated over the three tissue classes. To train the model a combination of soft-Dice²¹ and cross-entropy was used as loss function. For completeness, we provide the equations for both loss functions:

$$\text{soft-Dice}_c = \frac{\sum_{i=1}^N R_c(i) A_c(i)}{\sum_{i=1}^N R_c(i) + \sum_{i=1}^N A_c(i)},$$

where N denotes the number of voxels in an image, R_c is the binary reference image for class c and A_c is the probability map for class c .

$$\text{Cross-Entropy}_c = - \sum_{i=1}^N t_{ic} \log p(y_i = c | x_i),$$

where p denotes the probability for a specific voxel x_i with corresponding reference label y_i for class c ; and $t_{ic} = 1$ if $y_i = c$; and 0 otherwise. Hyper-parameters of the network were determined in our previous work¹⁶ using CMR images from the MICCAI 2017 Automated Cardiac Diagnosis Challenge (ACDC)¹². Therefore, no validation set was required in the current work.

To train the model, patches of 160x160 voxels were randomly chosen from the training set. Training data was augmented by 90 degree rotations, elastic deformations and gamma transformations of the images. The model was trained for 160,000 iterations using mini-batch stochastic gradient descent with batch-size 16 and Adam as optimizer²². Learning rate was set to 0.001 and decayed with a factor of 0.1 after every 40,000 steps. To increase generalization performance weight decay was used and set to 0.0005. Furthermore, dropout percentage was set to 0.1. Enabling MC dropout during testing, tissue class per voxel was determined using the mean softmax probabilities over 15 samples. Voxel wise segmentation may result in isolated (small clusters of) voxels. To address this, only the largest 3D connected component for each class was retained in the automatic segmentations.

Simulation of the correction of automatic segmentation

Previous research demonstrated that most segmentation inaccuracies occur in the most basal slice on the CMR^{8,12-15}. To evaluate whether these inaccuracies of our method impact TFC classification, correction of the automatic segmentation in the most basal slice of each CMR volume was simulated. This was achieved by replacing the automatic segmentation of the most basal slice with the corresponding manual reference defined by specially trained radiology technicians as a part of a regular clinical workup. We refer to this scenario as *automatic^{-basal}* hereafter.

Automatic ED/ES phase selection

Accurate identification of ED and ES phase in the cardiac cycle is a prerequisite to automatically compute RVEDV and RVESV. To show the potential of the method to automatically determine the ED and ES phase we automatically segmented all CMR volumes of the patients in the test set, and derived the RV and LV volumes for all time points of the cardiac cycle. For each patient ED was identified as the phase in which the fully automatically segmented volume was maximal and ES as the phase in which the volume was minimal. Automatically identified phases were compared with the manually selected phases using Bland-Altman analysis. In these plots (e.g. Figure 2a) the distance between automatically and manually selected phases is expressed as percentage of a complete cardiac cycle. Evaluation was performed for RV and LV separately, and for automatic and automatic^{-basal} segmentations separately.

Evaluation of automatic segmentation

To evaluate performance of the automatic segmentation method 3D Dice-coefficient and 3D Hausdorff distance between manual and automatic segmentations were computed. For this, the 2D automatic segmentation masks were stacked into a 3D volume per patient and cardiac phase. The Dice-coefficient quantifies overlap between manual and automatic segmentation and its value ranges between 0 and 1. A higher Dice-coefficient indicates better agreement between manual and automatic segmentations. The Hausdorff distance

evaluates segmentation along the boundary of the target structure by measuring the maximum distance between manual and automatic segmentation. Qualitative performance of the automatic segmentation method was visually assessed. To investigate whether segmentation errors accumulate at specific slice locations in the CMR volume the distribution of segmentation errors over slice location was computed. For this, four slice locations in a volume were distinguished: (i) most apical slice; (ii) most basal slice; (iii) mid-ventricular slices and (vi) slices located below the apex or above the base of the heart. Furthermore, to evaluate the clinical implications of our automatic CMR segmentation approach for the classification of the CMR TFC in subjects suspected of ARVC, the following CMR measurements were computed for manual, automatic and *automatic-basal* segmentations: LV end-diastolic volume (EDV); LV end-systolic volume (ESV); LV stroke volume (SV); LVEF; RVEDV; RVESV; RVSV and RVEF.

Statistical analysis

Statistical analysis was performed using RStudio Version 1.3.1093 (Boston, MA, USA) and IBM SPSS Statistics (version 25, USA). Continuous values were presented as mean \pm standard deviation or median [interquartile range]. Categorical data was displayed as absolute frequency (n) and percentages (%). For continuous comparisons of two groups, two-tailed Student's t-test was used. For continuous comparisons of three or more groups, one-way ANOVA was used. Categorical data were compared using the chi-square χ^2 test. A p-value of <0.05 was considered significant. Comparison of automatic and manual absolute CMR measurements were assessed using Bland-Altman analysis and the Pearson correlation coefficient (*r*). CMR TFC was first classified using visual assessment of wall motion abnormalities and manually derived RVEDVI and RVEF, and next using visual assessment of wall motion abnormalities and automatically derived RVEDVI and RVEF.

CMR TFC classification agreement between manually vs. automatically derived CMR measurements was assessed using Cohen's kappa (κ). Furthermore, sensitivity and specificity of CMR TFC by manual and automatic approach was determined and compared using the McNemar test.

RESULTS

Study population

We included 70 subjects in the training set (mean age 39.6 ± 18.1 years, 47% female) and 157 subjects in the test set (mean age 36.9 ± 17.6 years, 59% female). Patient characteristics are shown in **Table 1**. The test set included 37 ARVC patients, 66 at-risk family members and 54 controls subjects. The distribution of subjects across the three patient categories was the same for training and test sets (34% controls, 42% at risk, 24% ARVC patients). No

statistically significant difference in sex existed between the three subgroups ($p=0.37$), but at-risk family members were younger than ARVC patients ($p=0.021$) and controls ($p<0.001$). ARVC patients had a median of 5 [4-6] diagnostic TFC points, while at-risk family members had a median of 2 [1-3] points ($p<0.001$). In total, 84% of ARVC patients and 3% of at-risk family members had minor or major CMR TFC (RV wall motion abnormalities combined with abnormal RVEF or RVEDVI cut-off values). Among 103 ARVC patients and at-risk family members, 90 (87%) carried a pathogenic variant, mostly in plakophilin-2 ($n=57$, 63%) followed by phospholamban ($n=26$, 29%) and desmoplakin ($n=5$, 6%).

Table 1: Baseline characteristics

	ACM patients (n=37)	At-risk ACM group (n=66)	Control group (n=54)	p-value
Demographics				
Age at CMR (years)	39.1 \pm 19.0	30.7 \pm 16.2 ^{††}	42.9 \pm 15.9	<0.001
Female (%)	20 (54)	43 (65)	29 (54)	0.37
Proband (%)	10 (27)	0 (0) [‡]	na	<0.001
Genetic status				
Pathogenic variant	36 (97)	56 (85)	na	0.06
PKP2 (%)	24 (71)	33 (59)		
PLN (%)	4 (12)	22 (39)		
DSP (%)	4 (12)	1 (2)		
Other (%)	4 (12)	0		
Clinical phenotype				
Total TFC score	5 [4-6]	2 [1-3]	0	<0.001
<i>Repolarization criteria</i>				
Minor	10 (27)	0 (0)		
Major	8 (22)	3 (5)		
<i>Depolarization criteria</i>				
Minor	23 (62)	9 (14)		
Major	0 (0)	0 (0)		
<i>Arrhythmia criteria</i>				
Minor	25 (68)	6 (9)		
Major	2 (5)	0 (0)		
<i>Structural criteria</i>				
Minor	6 (16)	1 (3)		
Major	25 (68)	0 (0)		

* Significant difference between control and ACM patients

† Significant difference between control and at-risk subjects

‡ Significant difference between ACM patients and at-risk subjects

Abbreviations: ACM= arrhythmogenic cardiomyopathy; CMR= cardiac magnetic resonance imaging; DSP= desmoplakin; PKP2= plakophilin-2; PLN= phospholamban; TFC=Task Force Criteria

Assessment of segmentation performance

Table 2 lists quantitative results of the automatic segmentation. The automatic method achieved mean Dice-coefficient for ED and ES 0.96 ± 0.01 and 0.93 ± 0.03 , respectively for the LV and 0.93 ± 0.04 and 0.89 ± 0.04 , respectively for the RV. Visual assessment of automatic segmentation results depicted in **Figure 1** reveal that performance was higher for mid-ventricular slices (second and third rows Figure 1) compared with apical and basal slices (first and fourth row Figure 1), while an under-segmentation of trabeculated areas occurred in the apical slices (first row Figure 1). Furthermore, as depicted in **Supplementary Figure 1**, visual assessment of the manual reference segmentation revealed a high variability of the RV shape in the basal slices in both ED and ES time points. Furthermore, as listed in **Table 3**, comparison of automatic with manual reference segmentations disclosed that on average 24.5% of the segmentation errors i.e. misclassified voxels were located in the most basal slice (30.7 and 18.3% for RV and LV, respectively). In contrast, on average only 6.5% of the errors were located in an apical slice (5.4 and 7.6% for RV and LV, respectively).

Table 2 lists segmentation results after the simulated correction of the automatic RV and LV segmentation in the most basal slice. The results show an increased segmentation performance: mean Dice-coefficient for the ED and ES are 0.97 ± 0.01 and 0.95 ± 0.03 (vs. 0.96 ± 0.01 and 0.93 ± 0.03 uncorrected) respectively for the LV and 0.95 ± 0.02 and 0.92 ± 0.03 (vs. 0.93 ± 0.04 and 0.89 ± 0.04 uncorrected) respectively for the RV ($p < 0.001$ [one side Wilcoxon signed-rank test]).

Table 2: Segmentation performance of deep learning segmentation model

	End-diastole		End-systole	
	LV	RV	LV	RV
Dice-coefficient				
Automatic	0.96 ± 0.01	0.93 ± 0.03	0.93 ± 0.04	0.89 ± 0.04
Automatic+correction	0.97 ± 0.01	0.95 ± 0.02	0.95 ± 0.02	0.92 ± 0.03
Hausdorff-distance				
Automatic	6.42 ± 2.26	10.42 ± 2.99	6.58 ± 2.73	10.60 ± 3.50
Automatic+correction	5.07 ± 2.27	9.19 ± 3.19	5.52 ± 2.47	9.09 ± 3.05

Segmentation performance of deep learning segmentation model in terms of Dice-coefficient (higher is better) and Hausdorff distance (in millimeter, lower is better). *Automatic+correction* refers to the scenario in which the most basal slice of each automatic segmentation volume was replaced with the corresponding manual reference. Depicted values specify mean \pm standard deviation.

Abbreviations: LV= left ventricle; RV= right ventricle.

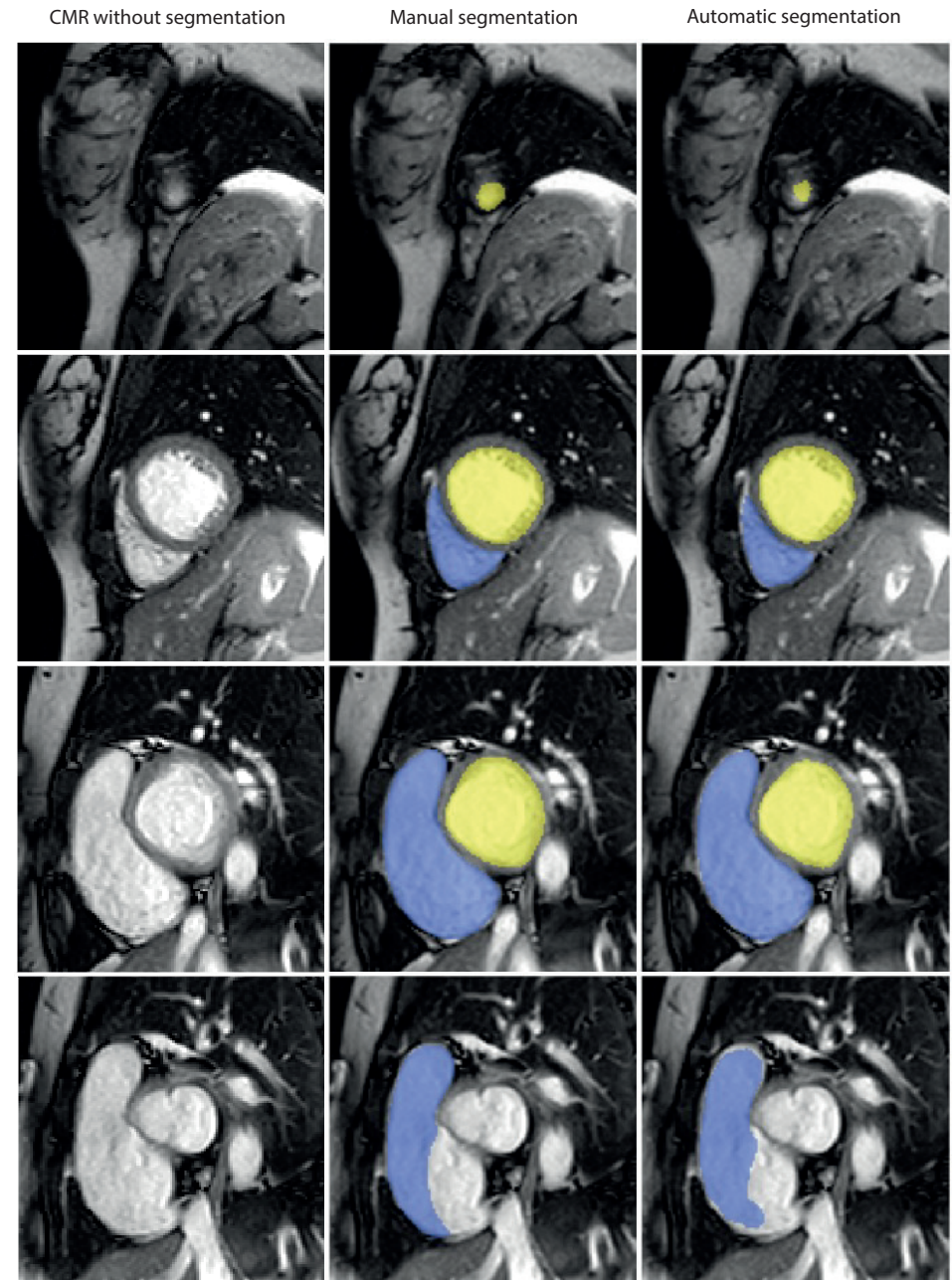


Figure 1: example automatic segmentation vs. manual segmentation

Qualitative segmentation results for left (yellow) and right (blue) ventricles at end-systole for a patient included in the test set. Columns depict raw CMR (first column), CMR with manual reference segmentation (second column) and CMR with automatic segmentation (third column). Rows show apical, mid-ventricular and most basal slices for LV (third row) and RV (fourth row), respectively.

Automatic ED and ES phase selection

The Bland-Altman plots shown in **Figure 2a** demonstrate the comparison between automatically identified cardiac phases using the automatic segmentations with the manually selected ED and ES phases. The bias [limits of agreement] were -0.87 [-6.26, 4.52]% for the ED-LV phase and -1.64 [-10.28, 6.99]% for the ES-LV phase, respectively, and -0.96 [-11.69, 9.76]% for the ED-RV phase and -0.05 [-7.62, 7.53]% for the ES-RV phase, respectively. **Figure 2b** depicts the same comparison using the automatic^{-basal} segmentations to automatically determine the ED and ES phases. For this scenario the bias [limits of agreement] were -0.72 [-5.29, 3.85]% for the ED-LV phase and -3.03 [-10.08, 4.03]% for the ES-LV phase, respectively, and -0.34 [-9.58, 8.89]% for the ED-RV and 0.48 [-7.20, 8.17]% for the ES-RV.

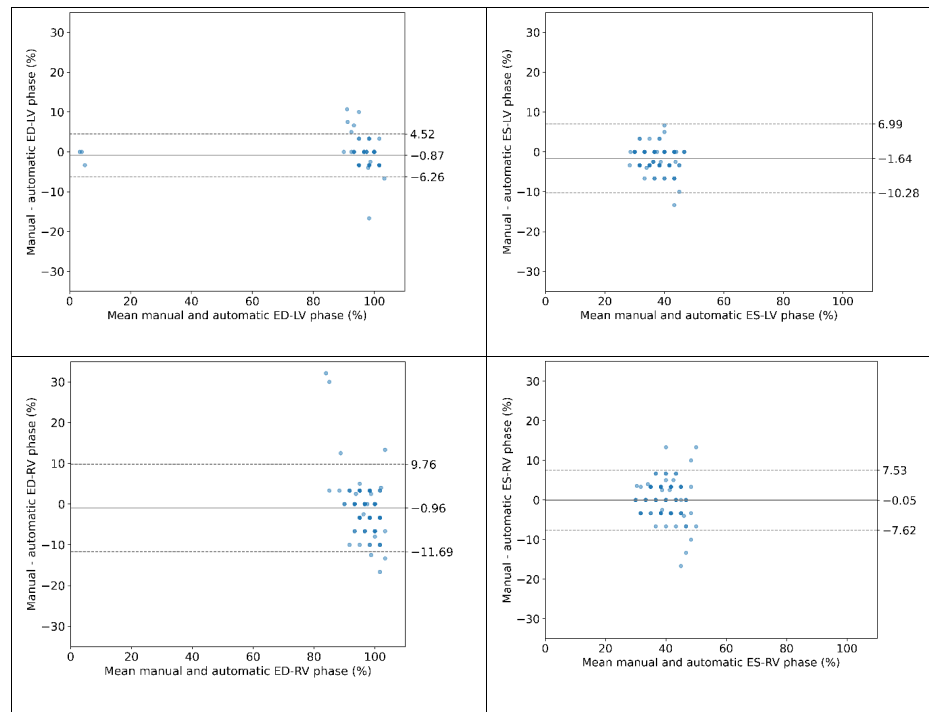


Figure 2a. Bland-Altman plots with the agreement between the manually and automatically selected ED and ES phases for RV and LV, respectively, using automatic segmentations.

Distance between automatically and manually selected phases is expressed as percentage of a complete cardiac cycle. Evaluation was performed for RV (top row) and LV (bottom row) separately. Higher opacity of colors correlates to higher density of data points.

Abbreviations: ED= end-diastolic; ES=end-systolic

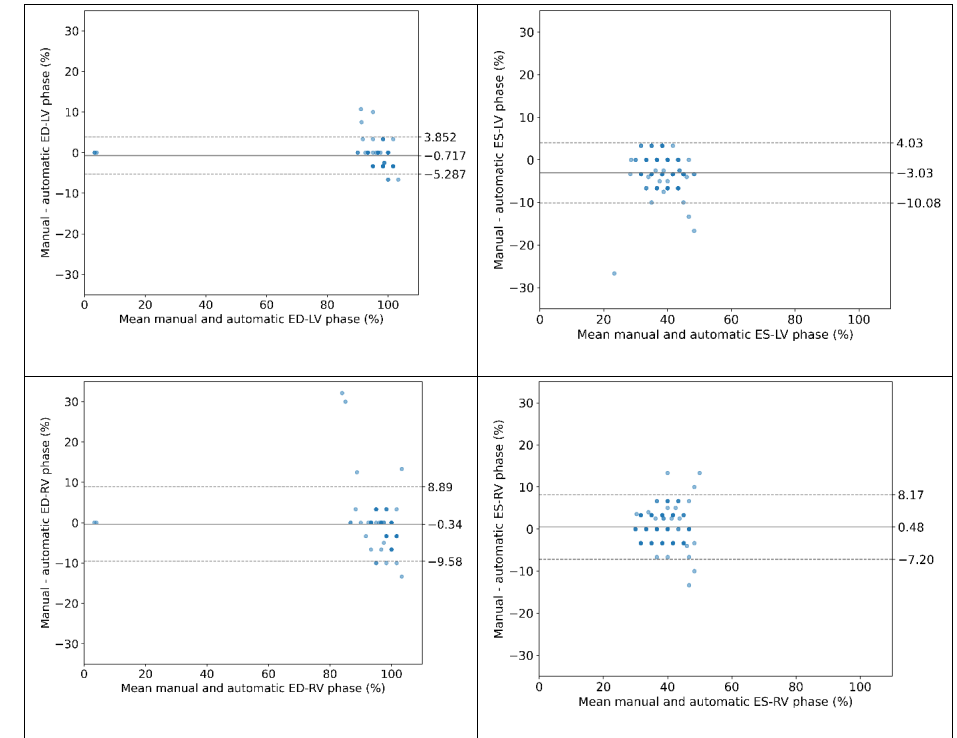


Figure 2b. Bland-Altman plots with the agreement between the manually and automatically selected ED and ES phases for RV and LV, respectively, using automatic^{-basal} segmentations.

Distance between automatically and manually selected phases is expressed as percentage of a complete cardiac cycle. Evaluation was performed for RV (top row) and LV (bottom row) separately. Higher opacity of colors correlates to higher density of data points.

Abbreviations: ED= end-diastolic; ES=end-systolic

Assessment of absolute CMR measurements

Automatically measured volumes (RV and LV EDV and ESV) are slightly underestimated compared to manually measured volumes (**Supplementary Figures 2 and 3**). However, as shown in **Table 4**, the correlations of both RV and LV volumes were excellent (0.95-0.99, $p < 0.001$). For RV and LV EF and SV, automatic measurements seem to be slightly overestimated compared to manual measurements; nonetheless, correlations were excellent 0.82-0.89 for RV and good to excellent (0.78-0.93) for LV. After simulated manual correction of the basal slice, agreement between manual and automated measurements increased, as depicted in the Bland Altman plots (**Supplementary Figures 2 and 3**). This was also reflected in the Pearson correlation coefficient for both the volumetric (EDV, ESV) ($r = 0.97-0.99$, $p < 0.001$) as well as the functional (SV, EF) ($r = 0.88-0.98$, $p < 0.001$) CMR measurements.

Table 3: Distribution of segmentation errors across slices

	Basal	Mid-ventricular	Apical	Slices above/below base/apex
LV	18.3%	70%	7.5%	4.2%
RV	30.7%	61%	5.4%	2.9%

Percentage of segmentation errors per target structure (LV and RV) located in basal, apical, all mid-ventricular or slices above base and below apex. Abbreviations: LV= left ventricle; RV= right ventricle.

Table 4: Correlation between manual and automatic measurements

	Mean absolute difference (vs. manual)	Correlation r (with manual)	Mean absolute difference (vs. manual) Basal corrected	Correlation r (with manual)
<i>Right ventricle</i>				
EF (%)	1.4 ± 4.7	0.82 (0.77-0.87)*	0.9 ± 3.9	0.88 (0.84-0.91)*
SV (ml)	-2.0 ± 10.8	0.89 (0.84-0.91)*	0.7 ± 9.2	0.92 (0.90-0.94)*
EDV (ml)	-9.9 ± 13.9	0.95 (0.94-0.97)*	-5.5 ± 9.6	0.98 (0.97-0.98)*
ESV (ml)	-7.9 ± 11.0	0.95 (0.93-0.96)*	-4.8 ± 8.1	0.97 (0.96-0.98)*
<i>Left ventricle</i>				
EF (%)	2.4 ± 3.6	0.78 (0.71-0.84)*	1.4 ± 2.1	0.92 (0.89-0.94)*
SV (ml)	1.4 ± 7.3	0.93 (0.91-0.95)*	0.04 ± 4.2	0.98 (0.97-0.98)*
EDV (ml)	-4.6 ± 6.1	0.99 (0.98-0.99)*	-4.4 ± 4.1	0.99 (0.99-1.00)*
ESV (ml)	-6.0 ± 6.4	0.95 (0.93-0.96)*	-4.4 ± 4.6	0.97 (0.96-0.98)*

*p-value of correlation <0.001

Abbreviations: EF= ejection fraction; SV= stroke volume; EDV= end-diastolic volume; ESV= end-systolic volume.

Classification of ARVC TFC

Since agreement between manual and automatic measurements was higher in the automatic^{basal}, we used these results for the further analysis. **Supplementary Table 1** depicts the mean and standard deviation of the CMR measurements stratified per subgroup. The trends between the three subgroups (ARVC, at-risk family members and controls) were comparable between manual and automated measurements: ARVC patients had significantly reduced RVEF ($p<0.001$) and LVEF ($p=0.002$), as well as increased RVEDVI ($p<0.001$), RVESVI ($p<0.001$) and LVESVI ($p<0.013$) compared to at-risk family members and controls. These trends between the subgroups were also observed in the boxplots of **Figure 3**.

We next compared CMR TFC classification using manual vs. automatic^{basal} CMR measurements. All but one subject (156/157, 99%) were correctly classified, showing an agreement of κ 0.98 ± 0.02 . As depicted in **Figure 4**, subjects who classified as no ($n=130$) or minor ($n=6$) CMR TFC were correctly classified using the CMR measurements computed using the automatic segmentations obtained from the deep learning segmentation model. For major TFC, all but one subject were correctly classified; with one female subject being misclassified as minor CMR TFC. This classification discrepancy was based on a 5 ml/m² difference in RVEDVI (102 ml/m² using manual measurements and 97ml/m² using automatic

measurements), whereby the cutoff for major CMR TFC is set at >100ml/m² in women. The total TFC in this patient went from 5 to 4, which did not change the ARVC diagnosis. Sensitivity and specificity of minor and major CMR TFC for diagnosis of ARVC were comparable for manual (minor TFC 31% | 99% and major TFC 66% | 100%) and for automatic^{basal} (minor TFC 35% | 100% and major TFC 65% | 100%, $p=0.32$). CMR TFC classification using the uncorrected automatic measurements are depicted in **Supplementary Figure 5**. This resulted in correct classification of 149/157 (95%) subjects.

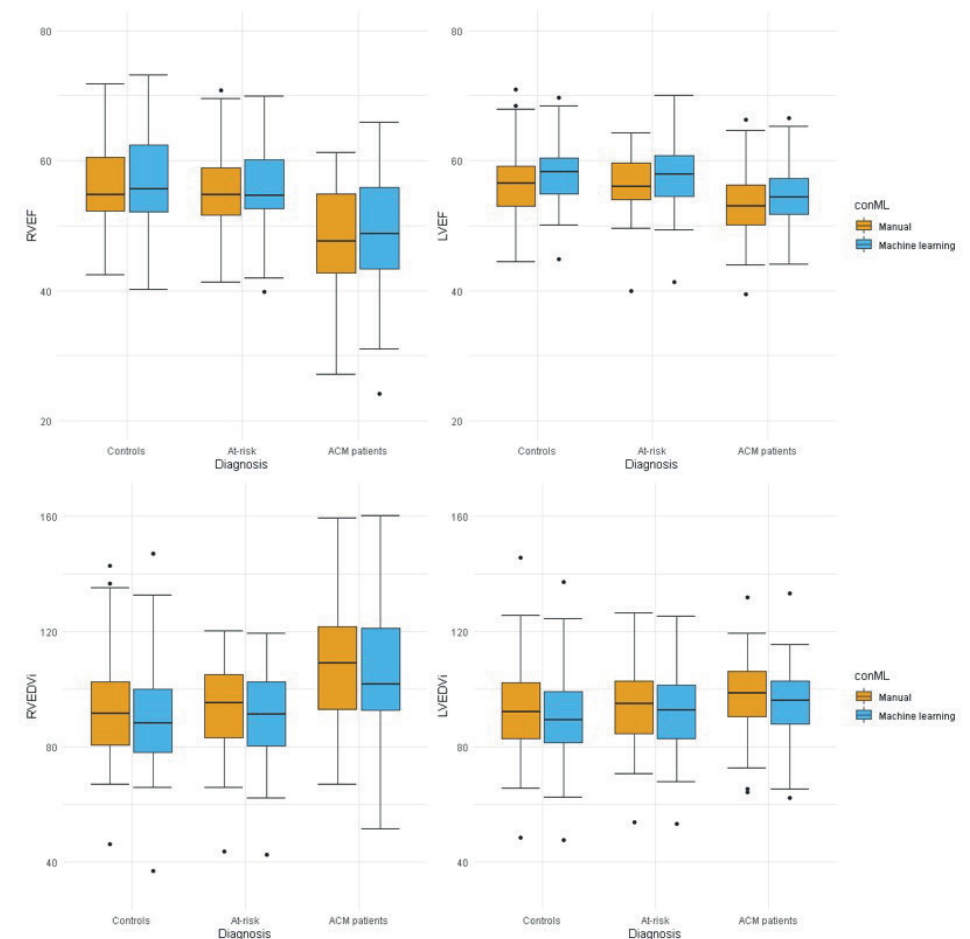


Figure 3: Boxplots depicting RV and LV function and dimension. CMR measurements are given for controls, at-risk family members and ACM patients, stratified per method (manual [orange] vs. automatic [blue]). This data represents the automatic + basal correction data, see **Supplementary Figure 4** for the boxplots of the uncorrected automatic measurements.

Abbreviations: EDVI= end-diastolic volume index; EF= ejection fraction; LV= left ventricle; RV= right ventricle

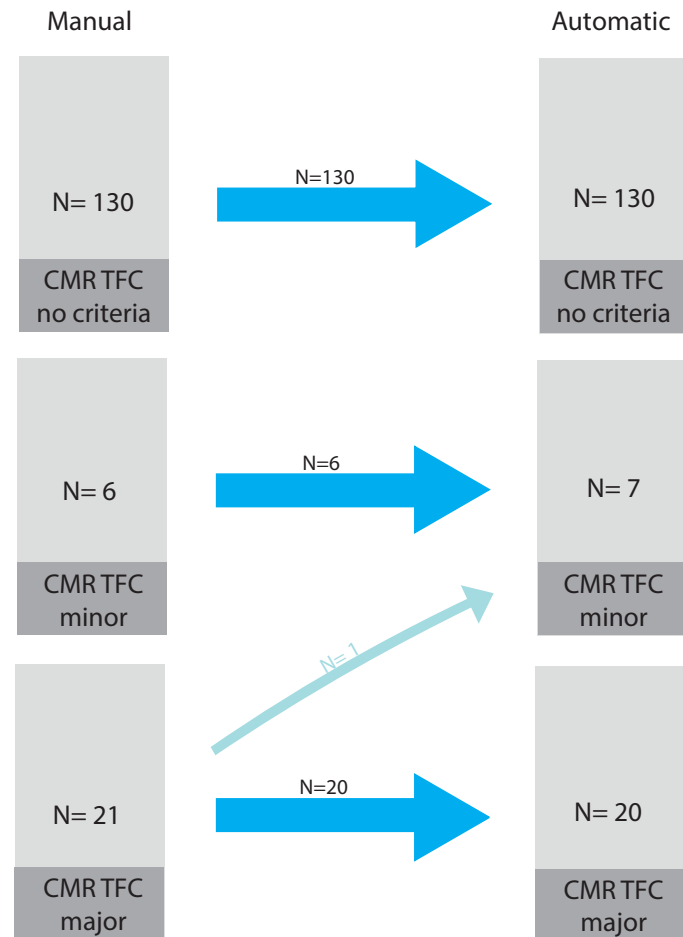


Figure 4: Classification of CMR criteria of TFC (no, minor and major) for manual and automatic + basal correction CMR measurements. The thick blue arrows indicate the matching subjects (between manual and automatic+ basal correction), the thinner blue arrows indicate the number of patients that change CMR classification category when using automated measurements. See **Supplementary Figure 5** for uncorrected automatic measurements. *Abbreviations: CMR= cardiovascular magnetic resonance; N= number of subjects; TFC= task force criteria*

DISCUSSION

In this study, we (i) evaluated our previously developed deep learning segmentation approach for RV and LV ventricular CMR assessment in patients suspected of ARVC and (ii) evaluated the clinical implication of this approach for classification of the CMR TFC in subjects suspected of ARVC. We demonstrated that CMR TFC classification using our automatic segmentation with limited manual correction in the most basal slice was

comparable to classification using manual segmentation performed during clinical work-up. Therefore, CMR TFC classification could potentially be performed using automatically measured CMR parameters with limited expert interaction.

Previous studies

Recently studies^{15,23,24} have shown that deep learning segmentation methods outperform traditional approaches such as those exploiting level set, graph-cuts, deformable models, cardiac atlases and statistical models^{25,26}. Many current state-of-the-art deep learning biventricular segmentation algorithms have been evaluated on publicly available cine CMR data from the MICCAI 2017 ACDC¹². The dataset contains CMR volumes from 150 patients distributed uniformly over normal cardiac function and four disease groups: dilated cardiomyopathy, hypertrophic cardiomyopathy, ischemic cardiomyopathy, and RV abnormality (RVEDVI greater than 110 mL/m² for men, and greater than 100 mL/m² for women, and/or a RVEF below 40%). The ACDC challenge showed that the largest segmentation inaccuracies were located in the most basal and apical slices of the short-axis¹², which is in line with our results presented in Table 3. Comparable results were obtained in the recently held Multi-Centre, Multi-Vendor and Multi-Disease Cardiac Segmentation (M&Ms) challenge¹³. Importantly, in contrast to the ACDC and M&Ms datasets, the clinical annotation protocol used in our study adheres to the guidelines of the SCMR¹⁸. Segmentation of the RV, especially in basal slices, is more challenging when following SCMR guidelines compared with the protocol used for the ACDC and M&Ms datasets. For example, in the SCMR guideline the outflow tract is included as part of the RV blood volume which challenges segmentation of the basal slices due to the unclear ventricular-atrial transition.

Researchers^{27,28} have also trained and evaluated deep learning CMR segmentation algorithms on the large-scale annotated dataset from the UK Biobank²⁹, reaching a performance comparable with human experts. The dataset contains short-axis cine CMR volumes of 5,008 subjects. As the majority of the subjects are healthy, the dataset is considered relatively homogenous²⁹. In the present work, we trained and evaluated a previously developed deep learning segmentation algorithm¹⁶ on a real-life dataset with subjects suspected of ARVC who underwent CMR as part of their clinical evaluation. Compared to the previously mentioned datasets^{12,13,29}, our dataset contains substantially more subjects with RV complexity caused by ARVC due to possible aneurysms and wall thinning and contained CMR images acquired on different field strengths (1.5 and 3 Tesla), pulse sequences and imaging parameters. Hence, the current work demonstrates that by only correcting a single slice per volume, an existing state-of-the-art segmentation method¹⁶ is sufficiently reliable to be applied to a relevant clinical problem. Furthermore, we are the first to compare classification of the CMR TFC of subjects suspected of ARVC using manually and automatically derived CMR measurements and showing that the deep learning segmentation algorithm we use performs well in this diverse clinical environment.

Comparison to manual segmentation

We showed a good to excellent agreement of manual and automated CMR measurements, which significantly increased after simulated correction of the most basal slice of the RV and LV (automatic ($r=0.78-0.99$, $p<0.001$) and automatic^{-basal} ($r=0.88-0.99$, $p<0.001$) measurements). This was also reflected in the significant increase of the Dice coefficients and Hausdorff distance after basal correction ($p<0.001$). This is in agreement with a recent study, showing an improvement of the agreement between automatic and manual segmentation when manually adjusting the most basal slice³⁰.

Large intra- and inter-observer variability is currently the greatest source of error when manually segmenting CMRs^{8,31} with more variability seen for the RV compared to LV due to the RV geometrical complexity¹⁸. Previously published inter-observer variability ranges from 2.6-10.5%^{32,33} for the LV and 6.2-14.1%^{33,34} for the RV. The largest variability between manual readers also appears in the apical and basal slices¹⁴ presumably due to low tissue contrast ratios, hypertrabeculation and unclear ventricular-atrial transition of especially the RV. The variability in contouring of the basal slice is illustrated in **Supplementary Figure 1**. The corresponding manual segmentations convey the difficulty to determine the anatomical boundaries of cardiac structures in these slices. We presumed that such variability also hampers performance of the automatic segmentation method. This limitation can be alleviated by increasing the size training set. To further improve performance of deep learning segmentation approaches, especially of basal and apical short-axis slices, future work could exploit anatomical information extracted from long-axis views (2, 3, 4 chamber views) e.g. valve landmarks and apical point^{35,36}. Furthermore, deep learning based CMR segmentation methods would benefit from short-axis volumes with higher through-plane resolution (e.g. using super-resolution)^{10,37,38}. This would make application of 3D segmentation approaches more feasible and hence, those models could potentially harness any inter-slice dependencies. Finally, using explicit topological prior information³⁹ for model optimization is a promising training approach to prevent automatic models from generating anatomically implausible segmentation.

Clinical implementation of deep learning methods

Depending on the stage of disease, ARVC patients show a wide variety of ventricular changes that can be observed on CMR: ventricular wall motion abnormalities (e.g. aneurysms, akinesia, dyskinesia), wall thinning (due to fibrofatty replacement of the myocardium), increased trabeculations, dilatation and decreased functional measurements, that are especially present in the RV². These challenges make ARVC eminently suitable to study the performance of machine learning algorithms on the RV. Previously published algorithms showed better agreement for LV than RV volumes⁴⁰. Although limits of agreement were smaller for the LV compared to the RV, we showed comparable segmentation performance for RV and LV CMR measurements in this heterogenous study population. Furthermore,

segmentation performance was comparable between structurally normal hearts and hearts affected by ARVC.

Importantly, we showed that calculation of ARVC TFC from automatically computed CMR parameters is feasible when combining automatic segmentation with correction of the most basal slice only. The diagnostic performance of the CMR TFC calculated using automatic segmentations (sensitivity 32-58%, specificity 99-100%) were comparable to manual measurements in this and previously published studies (sensitivity 13-69%, specificity 88-100%)^{41,42}. Although the correlation of manual and automatic measurements is high, the differences in CMR TFC classification without basal correction demonstrates that a fully automatic segmentation approach without human intervention is not yet reliable. However, the conducted experiments reveal that current state-of-the-art deep learning segmentation models can substantially reduce manual effort to semi-automatically segment cardiac structures in a heterogeneous dataset: manual segmentation time would be approximately 2 minutes instead of 25 minutes. Recently, Huellebrand *et al.*⁴³ proposed a human-in-the-loop approach that combines deep learning-based CMR segmentation and cardiac disease classification. The authors show that manual correction of automatic CMR segmentations by a clinical expert results in increased classification performance compared to a fully automatic segmentation approach. To identify volumes that contain segmentation failures the user can explore parallel coordinates plots that visualize CMR measurements along with cardiac shape and texture features. A similar approach was previously presented in Sander *et al.*¹⁶ that combines automatic segmentation and assessment of segmentation uncertainty in CMR to automatically detect image regions containing local segmentation failures. Subsequently, detected regions are manually corrected by a clinical expert. Such a semi-automatic approach could lead to a large reduction in inter-observer variability. This is not only interesting for specialized tertiary ARVC centers, but even more for less experienced centers, since CMR misinterpretations are an important cause of over-diagnosis in ARVC and only 27% of people referred to a tertiary center with a suspected ARVC diagnosis finally meet diagnostic criteria for ARVC⁴⁴. Our work shows that our previously developed deep learning segmentation method is able to fulfill a diagnostic purpose by simplifying accurate calculation of functional and volumetric measurements for the CMR TFC, showing opportunities to facilitate and improve individual patients health.

Limitations

Although we automated the calculation of the dimensional and functional parameters, wall motion abnormalities are also part of the CMR TFC. This was evaluated visually by experienced cardiovascular radiologists in this work, but it is subject to inter-observer variation in less experienced readers. Due to anatomical challenges of the RV a fully automatic RV strain algorithm is not yet available. Future work should focus on automatic computation of RV strain and better automatic segmentation of the basal slice, which could

contribute to full automatization and standardization of the CMR TFC.

Combining automatic segmentation with manual correction of the most basal slice, 99% of the CMR TFC were correctly classified, with misclassification of only one patient from major to minor CMR TFC. Moreover, one could argue that this latter classification falls within measurement error, and it did not change the diagnosis (total TFC score went from 5 to 4). Although the absolute differences in volumetric and functional parameters were small, due to the absolute cutoff values used for the CMR TFC, differences in classification can theoretically exist when the difference is as small as 1 ml/m², and clinical interpretation of automatic measurements remains important. Notably, CMR is no gold standard for the diagnosis of ARVC, but rather part of the diagnostic process.

CONCLUSIONS

Automatic deep learning-based CMR segmentation has the ability to provide a fast, standardized and reproducible method to measure RV and LV volumetric parameters on CMR. We demonstrate that the applied automated segmentations have a good agreement with manual segmentations. Furthermore, combining automatic segmentation with manual correction of the segmentation in the most basal slice results in accurate CMR TFC classification of subjects suspected of ARVC.

List of abbreviations

ARVC= arrhythmogenic right ventricular cardiomyopathy

CMR= cardiovascular magnetic resonance

DRN= Dilated Residual Network

ED= end-diastole

EDV= end-diastolic volume

EDVI= end-diastolic volume index

EF= ejection fraction

ES= end-systolic

ESV= end-systolic volume

ESVI= end-systolic volume index

LV= left ventricle

RV= right ventricle

SV= stroke volume

TFC= task force criteria

Declarations

Ethics approval and consent to participate. This retrospective study was reviewed by the UMC Utrecht Institutional Review Board and was granted a waiver of informed consent.

Consent for publication. Not applicable

Availability of data and material. All data generated or analyzed during this study are included in this published article [and its supplementary/additional information files].

Competing interests. None.

Funding: Dr. Bourfiss is supported by the Alexandre Suerman Stipend of the UMC Utrecht (2017). J. Sander is supported by the Dutch Technology Foundation (DLMedIA program (P15-26)) with participation of Pie Medical Imaging. Dr. te Riele is supported by the Dutch Heart Foundation (grant no. 2015T058), the UMC Utrecht Fellowship Clinical Research Talent, and the CVON PREDICT Young Talent Program. Dr. Asselbergs is supported by UCL Hospitals NIHR Biomedical Research Center. The Netherlands ACM Registry (www.acmregistry.nl) is supported by the Netherlands Heart Institute (project 06901).

Authors' contributions: Mimount Bourfiss and Jörg Sanders were responsible for the conception/design of the study, acquisition/interpretation of data and drafting the manuscript. Birgitta Velthuis and Ivana Išgum were responsible for the conception/design of the study. Bob de Vos made substantial contributions to the method of the algorithm. Birgitta Velthuis, Ivana Išgum, Bob de Vos, Anneline te Riele and Folkert Asselbergs were involved in revising the manuscript critically for important intellectual content.

Acknowledgements: We thank the ARVC patients and families who have made this work possible.

REFERENCES

1. Marcus FI, McKenna WJ, Sherrill D, et al. Diagnosis of arrhythmogenic right ventricular cardiomyopathy/dysplasia: proposed modification of the task force criteria. *Circulation*. 2010;121(13):1533-1541. doi:10.1161/CIRCULATIONAHA.108.840827
2. te Riele ASJM, Tandri H, Bluemke DA. Arrhythmogenic right ventricular cardiomyopathy (ARVC): cardiovascular magnetic resonance update. *J Cardiovasc Magn Reson*. 2014;16:50. doi:10.1186/s12968-014-0050-8
3. von Knobelsdorff-Brenkenhoff F, Pilz G, Schulz-Menger J. Representation of cardiovascular magnetic resonance in the AHA / ACC guidelines. *J Cardiovasc Magn Reson*. 2017;19(1):70. doi:10.1186/s12968-017-0385-z
4. Bai W, Sinclair M, Tarroni G, et al. Automated cardiovascular magnetic resonance image analysis with fully convolutional networks. *J Cardiovasc Magn Reson*. 2018;20(1):65. doi:10.1186/s12968-018-0471-x
5. Corona-Villalobos CP, Kamel IR, Rastegar N, et al. Bidimensional measurements of right ventricular function for prediction of survival in patients with pulmonary hypertension: comparison of reproducibility and time of analysis with volumetric cardiac magnetic resonance imaging analysis. *Pulm Circ*. 2015;5(3):527-537. doi:10.1086/682229
6. Grothues F, Moon JC, Bellenger NG, Smith GS, Klein HU, Pennell DJ. Interstudy reproducibility of right ventricular volumes, function, and mass with cardiovascular magnetic resonance. *Am Heart J*. 2004;147(2):218-223. doi:10.1016/j.ahj.2003.10.005
7. Haddad F, Doyle R, Murphy DJ, Hunt SA. Right ventricular function in cardiovascular disease, part II: pathophysiology, clinical importance, and management of right ventricular failure. *Circulation*. 2008;117(13):1717-1731. doi:10.1161/CIRCULATIONAHA.107.653584
8. Bonnemains L, Mandry D, Marie P-Y, Micard E, Chen B, Vuissoz P-A. Assessment of right ventricle volumes and function by cardiac MRI: quantification of the regional and global interobserver variability. *Magn Reson Med*. 2012;67(6):1740-1746. doi:10.1002/mrm.23143
9. Isensee F, Jaeger P, Full PM, Wolf I, Engelhardt S, Maier-Hein KH. Automatic Cardiac Disease Assessment on cine-MRI via Time-Series Segmentation and Domain Specific Features. *arXiv*. July 2017. doi:10.1007/978-3-319-75541-0
10. Oktay O, Ferrante E, Kamnitsas K, et al. Anatomically Constrained Neural Networks (ACNNs): Application to Cardiac Image Enhancement and Segmentation. *IEEE Trans Med Imaging*. 2018;37(2):384-395. doi:10.1109/TMI.2017.2743464
11. Tao Q, Yan W, Wang Y, et al. Deep Learning-based Method for Fully Automatic Quantification of Left Ventricle Function from Cine MR Images: A Multivendor, Multicenter Study. *Radiology*. 2019;290(1):81-88. doi:10.1148/radiol.2018180513
12. Bernard O, Lalonde A, Zotti C, et al. Deep Learning Techniques for Automatic MRI Cardiac Multi-Structures Segmentation and Diagnosis: Is the Problem Solved? *IEEE Trans Med Imaging*. 2018;37(11):2514-2525. doi:10.1109/TMI.2018.2837502
13. Campello VM, Gkontra P, Izquierdo C, et al. Multi-Centre, Multi-Vendor and Multi-Disease Cardiac Segmentation: The M&Ms Challenge. *IEEE Trans Med Imaging*. 2021;40(12):3543-3554. doi:10.1109/TMI.2021.3090082
14. Suinesiaputra A, Bluemke DA, Cowan BR, et al. Quantification of LV function and mass by cardiovascular magnetic resonance: multi-center variability and consensus contours. *J Cardiovasc Magn Reson Off J Soc Cardiovasc Magn Reson*. 2015;17(1):63. doi:10.1186/s12968-015-0170-9
15. Leiner T, Rueckert D, Suinesiaputra A, et al. Machine learning in cardiovascular magnetic resonance: basic concepts and applications. *J Cardiovasc Magn Reson*. 2019;21(1):61. doi:10.1186/s12968-019-0575-y
16. Sander J, de Vos BD, Išgum I. Automatic segmentation with detection of local segmentation failures in cardiac MRI. *Sci Rep*. 2020;10(1):21769. doi:10.1038/s41598-020-77733-4
17. Prakken NHJ, Velthuis BK, Vonken E, Mali WP, Cramer MJM. Cardiac MRI: Standardized Right and Left Ventricular Quantification by Briefly Coaching Inexperienced Personnel. *Open Magn Reson J*. 2008;1:104-111. doi:10.2174/1874769800801010104
18. Schulz-Menger J, Bluemke DA, Bremerich J, et al. Standardized image interpretation and post-processing in cardiovascular magnetic resonance - 2020 update : Society for Cardiovascular Magnetic Resonance (SCMR): Board of Trustees Task Force on Standardized Post-Processing. *J Cardiovasc Magn Reson Off J Soc Cardiovasc Magn Reson*. 2020;22(1):19. doi:10.1186/s12968-020-00610-6
19. Yu F, Koltun V, Funkhouser T. Dilated Residual Networks. In: *2017 IEEE Conference on Computer Vision and Pattern Recognition (CVPR)*. ; 2017:636-644. doi:10.1109/CVPR.2017.75
20. Gal Y, Ghahramani Z. Dropout as a Bayesian Approximation: Representing Model Uncertainty in Deep Learning. In: Balcan MF, Weinberger KQ, eds. *Proceedings of The 33rd International Conference on Machine Learning*. Vol 48. Proceedings of Machine Learning Research. New York, New York, USA: PMLR; 2016:1050-1059. http://proceedings.mlr.press/v48/gal16.html.
21. Milletari F, Navab N, Ahmadi S-A. V-Net: Fully Convolutional Neural Networks for Volumetric Medical Image Segmentation. June 2016. http://arxiv.org/abs/1606.04797.
22. Kingma DP, Ba J. Adam: A Method for Stochastic Optimization. *arXiv*. 2014;(1412.6980). http://arxiv.org/abs/1412.6980.
23. Litjens G, Kooi T, Bejnordi BE, et al. A survey on deep learning in medical image analysis. *Med Image Anal*. 2017;42:60-88. doi:10.1016/j.media.2017.07.005
24. Chen C, Qin C, Qiu H, et al. Deep Learning for Cardiac Image Segmentation: A Review. *Front Cardiovasc Med*. 2020;7:25. doi:10.3389/fcvm.2020.00025
25. Petitjean C, Dacher J-N. A review of segmentation methods in short axis cardiac MR images. *Med Image Anal*. 2011;15(2):169-184. doi:10.1016/j.media.2010.12.004
26. Peng P, Lekadir K, Gooya A, Shao L, Petersen SE, Frangi AF. A review of heart chamber segmentation for structural and functional analysis using cardiac magnetic resonance imaging. *MAGMA*. 2016;29(2):155-195. doi:10.1007/s10334-015-0521-4
27. Robinson R, Valindria V V, Bai W, et al. Automated quality control in image segmentation: application to the UK Biobank cardiovascular magnetic resonance imaging study. *J Cardiovasc Magn Reson Off J Soc Cardiovasc Magn Reson*. 2019;21(1):18. doi:10.1186/s12968-019-0523-x
28. Attar R, Pereañez M, Gooya A, et al. Quantitative CMR population imaging on 20,000 subjects of the UK Biobank imaging study: LV/RV quantification pipeline and its evaluation. *Med Image Anal*. 2019;56:26-42. doi:10.1016/j.media.2019.05.006
29. Petersen SE, Matthews PM, Francis JM, et al. UK Biobank's cardiovascular magnetic resonance protocol. *J Cardiovasc Magn Reson*. 2016;18:8. doi:10.1186/s12968-016-0227-4
30. G.J.H. S, Poort S, Velthuis BK, et al. Balancing Speed and Accuracy in Cardiac Magnetic Resonance Function Post-Processing: Comparing 2 Levels of Automation in 3 Vendors to Manual Assessment. *Diagnostics (Basel, Switzerland)*. 2021;11:1758. doi:https://doi.org/10.3390/diagnostics11101758
31. Bhuva A, Bai W, Lau C, et al. A Multicenter, Scan-Rescan, Human and Machine Learning CMR Study to Test Generalizability and Precision in Imaging Biomarker Analysis. *Circ Cardiovasc Imaging*. 2019;12(10):e009214. doi:10.1161/CIRCIMAGING.119.009214
32. Moon JCC, Lorenz CH, Francis JM, Smith GC, Pennell DJ. Breath-hold FLASH and FISP cardiovascular MR imaging: left ventricular volume differences and reproducibility. *Radiology*. 2002;223(3):789-797. doi:10.1148/radiol.2233011181
33. Mooij CF, de Wit CJ, Graham DA, Powell AJ, Geva T. Reproducibility of MRI measurements of right ventricular size and function in patients with normal and dilated ventricles. *J Magn Reson Imaging*. 2008;28(1):67-73. doi:10.1002/jmri.21407
34. Grothues F, Smith GC, Moon JCC, et al. Comparison of interstudy reproducibility of cardiovascular magnetic resonance with two-dimensional echocardiography in normal subjects and in patients with heart failure or left ventricular hypertrophy. *Am J Cardiol*. 2002;90(1):29-34. doi:10.1016/s0002-9149(02)02381-0
35. Xue H, Artico J, Fontana M, Moon JC, Davies RH, Kellman P. Landmark Detection in Cardiac MRI Using a Convolutional Neural Network. *Radiol Artif Intell*. July 2021:e200197. doi:10.1148/ryai.2021200197
36. Painchaud N, Skandarani Y, Judge T, Bernard O, Lalonde A, Jodoin P-M. Cardiac Segmentation With Strong Anatomical Guarantees. *IEEE Trans Med Imaging*. 2020;39(11):3703-3713. doi:10.1109/TMI.2020.3003240
37. Bhatia KK, Price AN, Shi W, Hajnal J V, Rueckert D. Super-resolution reconstruction of cardiac MRI using coupled dictionary learning. In: *2014 IEEE 11th International Symposium on Biomedical Imaging (ISBI)*. ; 2014:947-950. doi:10.1109/ISBI.2014.6868028
38. Sander J, de Vos BD, Išgum I. Autoencoding Low-Resolution MRI for Semantically Smooth Interpolation of Anisotropic MRI. *Med Image Anal*. February 2022. doi:10.1016/j.media.2022.102393
39. Clough J, Byrne N, Oksuz I, Zimmer VA, Schnabel JA, King A. A Topological Loss Function for Deep-Learning based Image Segmentation using Persistent Homology. *IEEE Trans Pattern Anal Mach Intell*. 2020;PP. doi:10.1109/TPAMI.2020.3013679
40. Backhaus SJ, Metschies G, Billing M, et al. Cardiovascular magnetic resonance imaging feature tracking: Impact of training on observer performance and reproducibility. *PLoS One*. 2019;14(1):e0210127. doi:10.1371/journal.pone.0210127
41. Bosman LP, Cadrin-Tourigny J, Bourfiss M, et al. Diagnosing arrhythmogenic right ventricular cardiomyopathy by 2010 Task Force Criteria: clinical performance and simplified practical implementation. *Eur Eur pacing, arrhythmias, Card Electrophysiol J Work groups Card pacing, arrhythmias, Card Cell Electrophysiol Eur Soc Cardiol*. 2020;22(5):787-796. doi:10.1093/europace/ea0039
42. Aquaro GD, Barison A, Todiere G, et al. Usefulness of Combined Functional Assessment by Cardiac Magnetic Resonance and Tissue Characterization Versus Task Force Criteria for Diagnosis of Arrhythmogenic Right Ventricular Cardiomyopathy. *Am J Cardiol*. 2016;118(11):1730-1736. doi:10.1016/j.amjcard.2016.08.056
43. Huellebrand M, Ivantsits M, Tautz L, Kelle S, Hennemuth A. A Collaborative Approach for the Development and Application of Machine Learning Solutions for CMR-Based Cardiac Disease Classification. *Front Cardiovasc Med*. 2022;9:829512. doi:10.3389/fcvm.2022.829512
44. Bomma C, Rutberg J, Tandri H, et al. Misdiagnosis of arrhythmogenic right ventricular dysplasia/cardiomyopathy. *J Cardiovasc Electrophysiol*. 2004;15(3):300-306. doi:10.1046/j.1540-8167.2004.03429.x

SUPPLEMENTARY MATERIAL

Supplementary Table 1 CMR measurements stratified per subgroup

Uncorrected automated data

	ACM patients (n=37)	At-risk ACM group (n=66)	Control group (n=54)	p-value
Manual measurements				
<i>Right ventricle</i>				
EF	47.1 ± 9.0**†	55.5 ± 5.9	56.2 ± 6.1	<0.001
SV	99.0 ± 15.9†	92.7 ± 18.3	99.5 ± 23.4	0.116
EDV	218.1 ± 53.2**†	168.6 ± 34.9	178.1 ± 41.3	<0.001
EDVI	111.6 ± 25.4**†	93.7 ± 14.8	92.9 ± 18.5	<0.001
ESV	119.1 ± 45.8**†	76.0 ± 20.8	78.6 ± 22.6	<0.001
ESVI	60.8 ± 22.7**†	42.1 ± 9.9	41.1 ± 11.2	<0.001
<i>Left ventricle</i>				
EF	53.3 ± 5.7**†	56.4 ± 4.4	56.7 ± 5.3	0.003
SV	101.0 ± 18.1	94.6 ± 18.3	101.3 ± 23.1	0.133
EDV	190.5 ± 33.4†	168.6 ± 33.6	179.0 ± 38.3	0.011
EDVI	97.5 ± 14.3	93.6 ± 12.8	93.2 ± 16.0	0.322
ESV	89.6 ± 20.7**†	74.0 ± 18.3	77.7 ± 19.0	0.001
ESVI	45.6 ± 8.7**†	41.0 ± 7.9	40.5 ± 8.9	0.010
Uncorrected automatic measurements				
<i>Right ventricle</i>				
EF	49.2 ± 9.0**†	56.9 ± 5.8	57.4 ± 7.7	<0.001
SV	98.5 ± 21.8	90.2 ± 20.5	97.0 ± 26.6	0.139
EDV	204.7 ± 51.0**†	159.9 ± 35.3	169.2 ± 41.9	<0.001
EDVI	104.6 ± 24.0**†	88.7 ± 15.1	88.0 ± 18.1	<0.001
ESV	106.2 ± 39.5**†	69.7 ± 19.4	72.3 ± 22.7	<0.001
ESVI	54.3 ± 19.5**†	38.6 ± 8.9	37.7 ± 11.1	<0.001
<i>Left ventricle</i>				
EF	55.6 ± 5.7**†	58.7 ± 5.6	59.3 ± 5.3	0.005
SV	102.8 ± 17.9	95.8 ± 17.0	102.6 ± 22.6	0.091
EDV	186.2 ± 32.8†	164.6 ± 32.3	173.5 ± 36.9	0.010
EDVI	95.3 ± 14.3	91.4 ± 12.7	90.4 ± 15.4	0.246
ESV	83.3 ± 20.0**†	68.8 ± 19.2	70.9 ± 18.3	0.001
ESVI	42.5 ± 9.0**†	38.1 ± 8.7	36.9 ± 8.5	0.009

Significant difference 0.01-0.05 (*) or (**<0.01) between control and ACM patients

Significant difference 0.01-0.05 (*) or (†<0.01) between at-risk and ACM patients

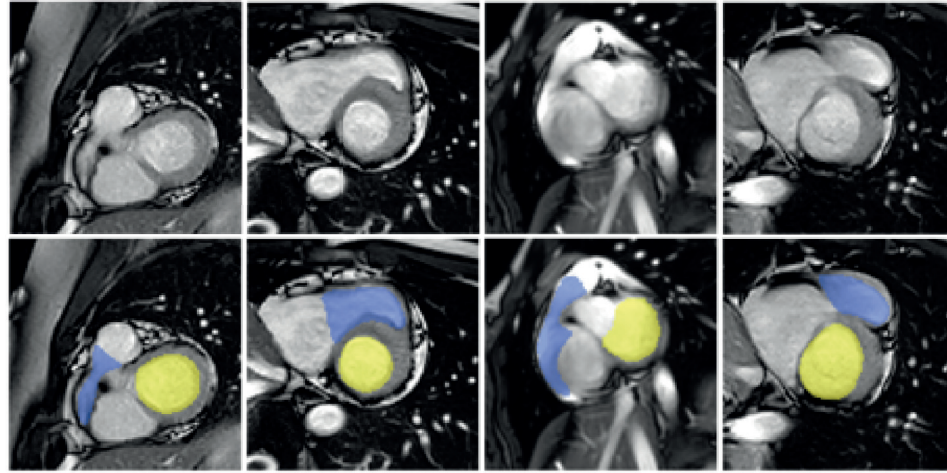
Corrected automated measurements with simulated correction of the most basal slice

	ACM patients (n=37)	At-risk ACM group (n=66)	Control group (n=54)	p-value
Manual measurements				
<i>Right ventricle</i>				
EF	47.1 ± 9.0**†	55.5 ± 5.9	56.2 ± 6.1	<0.001
SV	99.0 ± 15.9†	92.7 ± 18.3	99.5 ± 23.4	0.116
EDV	218.1 ± 53.2**†	168.6 ± 34.9	178.1 ± 41.3	<0.001
EDVI	111.6 ± 25.4**†	93.7 ± 14.8	92.9 ± 18.5	<0.001
ESV	119.1 ± 45.8**†	76.0 ± 20.8	78.6 ± 22.6	<0.001
ESVI	60.8 ± 22.7**†	42.1 ± 9.9	41.1 ± 11.2	<0.001
<i>Left ventricle</i>				
EF	53.3 ± 5.7**†	56.4 ± 4.4	56.7 ± 5.3	0.003
SV	101.0 ± 18.1	94.6 ± 18.3	101.3 ± 23.1	0.133
EDV	190.5 ± 33.4†	168.6 ± 33.6	179.0 ± 38.3	0.011
EDVI	97.5 ± 14.3	93.6 ± 12.8	93.2 ± 16.0	0.322
ESV	89.6 ± 20.7**†	74.0 ± 18.3	77.7 ± 19.0	0.001
ESVI	45.6 ± 8.7**†	41.0 ± 7.9	40.5 ± 8.9	0.010
Corrected automatic measurements				
<i>Right ventricle</i>				
EF	48.3 ± 9.6**†	56.1 ± 6.0	57.2 ± 7.4	<0.001
SV	98.7 ± 20.7	91.6 ± 21.0	99.0 ± 27.3	0.159
EDV	210.1 ± 50.5**†	164.1 ± 35.5	173.2 ± 42.3	<0.001
EDVI	107.4 ± 23.8**†	91.1 ± 14.9	90.1 ± 18.5	<0.001
ESV	111.4 ± 41.8**†	72.5 ± 19.3	74.1 ± 22.2	<0.001
ESVI	56.9 ± 20.7**†	40.2 ± 9.0	38.8 ± 11.1	<0.001
<i>Left ventricle</i>				
EF	54.6 ± 5.2**†	57.8 ± 4.9	58.1 ± 5.2	0.003
SV	100.7 ± 18.0	94.9 ± 18.1	101.3 ± 23.7	0.173
EDV	185.4 ± 33.4†	165.1 ± 33.0	174.2 ± 37.5	0.018
EDVI	94.8 ± 14.4	91.7 ± 12.9	90.7 ± 15.5	0.376
ESV	84.7 ± 19.5**†	70.2 ± 18.2	72.9 ± 17.6	0.001
ESVI	43.2 ± 8.5**†	38.9 ± 8.1	38.0 ± 8.4	0.011

Significant difference 0.01-0.05 (*) or (**<0.01) between control and ACM patients

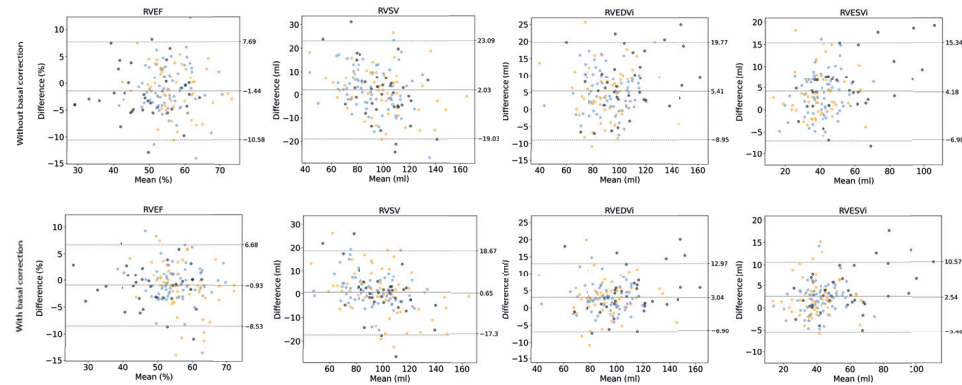
Significant difference 0.01-0.05 (*) or (†<0.01) between at-risk and ACM patients

Abbreviations as in manuscript



Supplementary Figure 1. Examples illustrating RV shape variability in manual reference segmentations for basal slices.

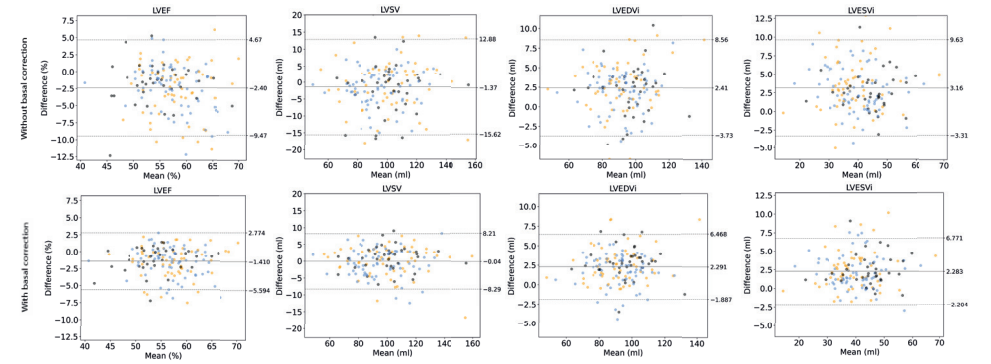
Shown are original CMR without (top row) and with (bottom row) manual reference segmentations of the left (yellow) and right (blue) ventricle.



Supplementary Figure 2. Bland-Altman plots of right ventricular CMR measurements

Absolute agreement between: (top row) manuals vs. uncorrected automatic CMR measurements; and (bottom row) manuals vs. automatic+ basal correction CMR measurements. Data points are stratified by disease classification 1) ACM patients (in black); 2) at-risk family members (in blue) and 3) control subjects (in orange).

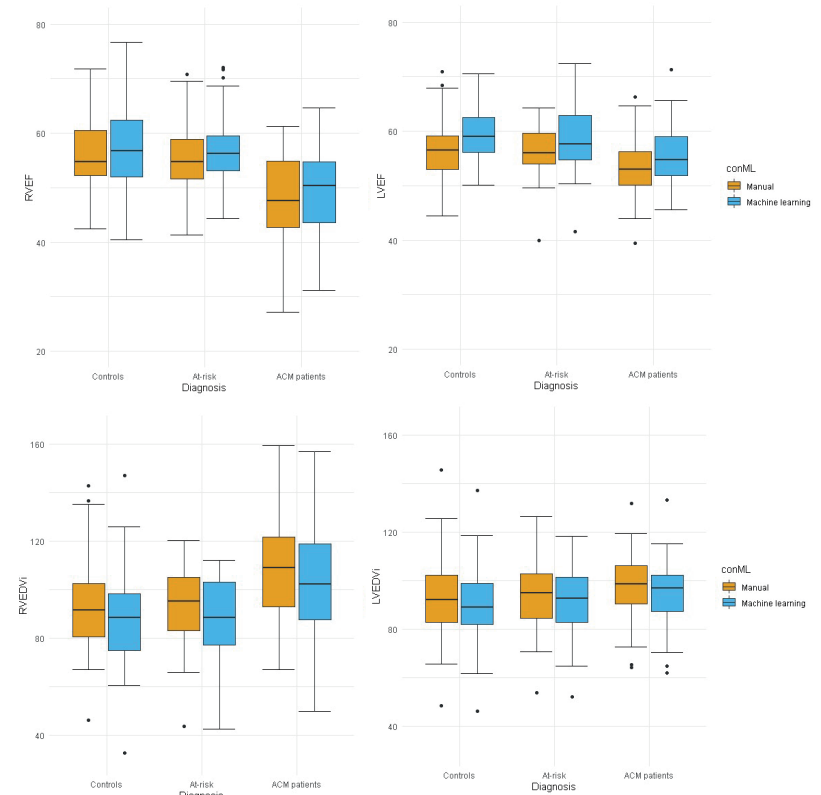
Abbreviations as in manuscript.



Supplementary Figure 3. Bland-Altman plots of left ventricular CMR measurements

Absolute agreement between: (top row) manuals vs. uncorrected automatic CMR measurements; and (bottom row) manuals vs. automatic + basal correction CMR measurements. Data points are stratified by disease classification 1) ACM patients (in black); 2) at-risk family members (in blue) and 3) control subjects (in orange).

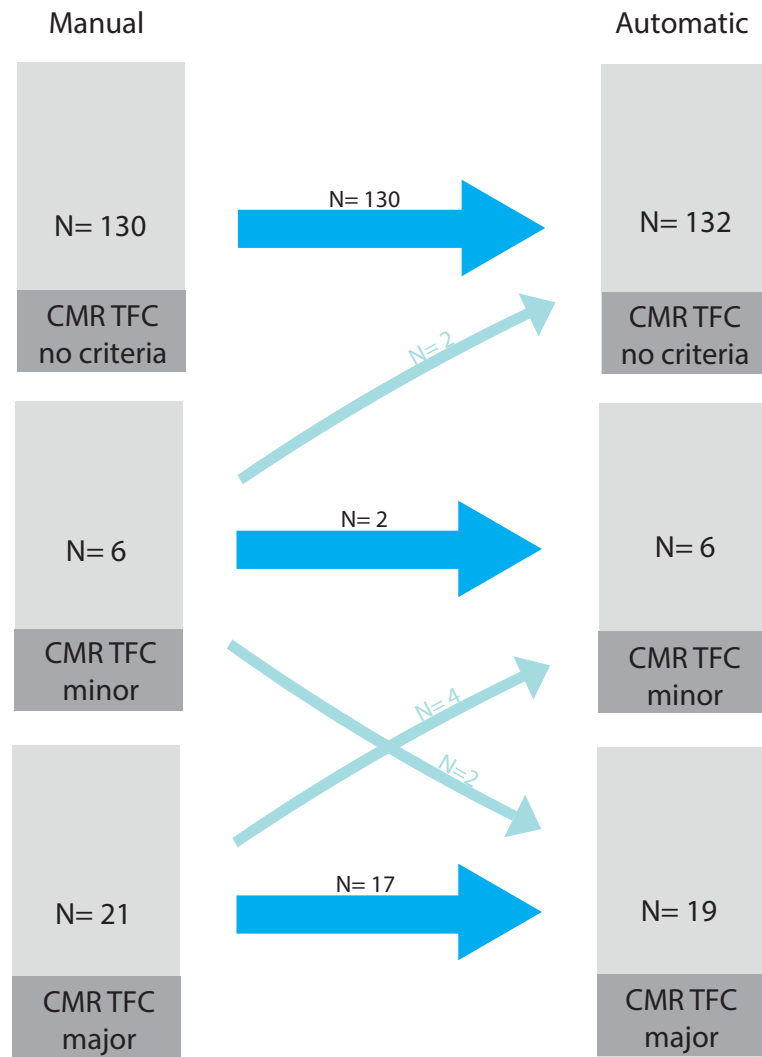
Abbreviations as in manuscript.



Supplementary Figure 4. Boxplots depicting RV and LV function and dimension.

This data represents the basal uncorrected automatic data. CMR measurements are given for controls, at-risk family members and ACM patients, stratified per method (manual [orange] vs. automatic [blue]).

Abbreviations: EDVI= end-diastolic volume index; EF= ejection fraction; LV= left ventricle; RV= right ventricle



Supplementary Figure 5. Classification of CMR criteria of TFC (no, minor and major) for manual and uncorrected automatic CMR measurements. The thick blue arrows indicate the matching subjects (between manual and automatic), the thinner blue arrows indicate the number of patients that change CMR classification category when using automated measurements. Cohen's Kappa between manual and automatic measurements was κ 0.82±0.05. Minor TFC, sensitivity 32% and specificity 100%; major TFC, sensitivity 58% and specificity 99%). *Abbreviations: CMR= cardiovascular magnetic resonance; N= number of subjects; TFC= task force criteria*

PART III

Atrial involvement in ARVC



CHAPTER

9

Influence of Genotype on Structural Atrial Abnormalities and Atrial Fibrillation or Flutter in Arrhythmogenic Right Ventricular Dysplasia/Cardiomyopathy

Mimount Bourfiss, BS;
Anneline S.J.M. te Riele, MD;
Thomas P. Mast, MD;
Maarten J. Cramer, MD, PhD;
Jeroen F. van der Heijden, MD, PhD;
Toon A.B. van Veen, PhD;
Peter Loh, MD, PhD;
Dennis Dooijes, PhD;
Richard N.W. Hauer, MD, PhD;
Birgitta K. Velthuis, MD, PhD

ABSTRACT

Introduction: Arrhythmogenic Right Ventricular Dysplasia/Cardiomyopathy (ARVD/C) is associated with desmosomal mutations. Although desmosomal disruption affects both ventricles and atria, little is known about atrial involvement in ARVD/C.

Objective: To describe the extent and clinical significance of structural atrial involvement and atrial arrhythmias (AA) in ARVD/C stratified by genotype.

Methods: We included 71 patients who met ARVD/C Task Force Criteria and underwent Cardiac Magnetic Resonance (CMR) imaging and molecular genetic analysis. Indexed atrial end-diastolic volume and area-length-ejection-fraction (ALEF) were evaluated on CMR and compared to controls with idiopathic right ventricular outflow tract tachycardia (n=40). The primary outcome was occurrence of AA (atrial fibrillation or atrial flutter) during follow-up, recorded by 12-lead ECG, Holter monitoring or implantable cardioverter defibrillator (ICD) interrogation.

Results: Patients harbored a desmosomal Plakophilin-2 (*PKP2*) (n=37) or non-desmosomal Phospholamban (*PLN*) (n=14) mutation. In 20 subjects, no pathogenic mutation was identified. Compared to controls, right atrial (RA) volumes were reduced in *PKP2* (p=0.002) and comparable in *PLN* (p=0.441) mutation carriers. In patients with no mutation identified, RA (p=0.011) and left atrial (p=0.034) volumes were increased. Bi-atrial ALEF showed no significant difference between the groups. AA were experienced by 27% of patients and occurred equally among *PKP2* (30%) and no mutation identified patients (30%), but less among *PLN* mutation carriers (14%).

Conclusion: Genotype influences atrial volume and occurrence of AA in ARVD/C. While the incidence of AA is similar in *PKP2* mutation carriers and patients with no mutation identified, *PKP2* mutation carriers have significantly smaller atria. This suggests a different arrhythmogenic mechanism.

Keywords: Arrhythmogenic Right Ventricular Dysplasia/ Cardiomyopathy, atria, genotype, Cardiac Magnetic Resonance imaging.

INTRODUCTION

Arrhythmogenic Right Ventricular Dysplasia/Cardiomyopathy (ARVD/C) is an inherited cardiomyopathy characterized by ventricular dysfunction and an increased risk of sudden cardiac death.¹ Starting with the seminal discovery of mutations in Plakoglobin (*JUP*), we now know that ARVD/C is a disease of the cardiac desmosomes in around 60% of cases.² Desmosomes are complex multiprotein structures providing mechanical support to adjacent cardiomyocytes.¹ They are found throughout the heart, including the atria. As such, the tendency of this disease to preferentially involve the ventricles is remarkable, since in animal studies the atria are also affected on a histopathological level.^{3,4}

Only a few small studies focused on atrial involvement in ARVD/C, showing atrial arrhythmias (AA) in a substantial amount of ARVD/C patients.⁵⁻⁸ However, these studies often lacked information on atrial structure and function, which may precede AA. Also no genotype-specific subanalysis was performed. Therefore, it remains unclear whether AA are secondary to ventricular dysfunction or a primary result of atrial alterations.

Over the last years, cardiac magnetic resonance (CMR) imaging has gained popularity as the modality of choice for the evaluation of ARVD/C, allowing for noninvasive morphological and functional evaluation, as well as tissue characterization in a single investigation.⁹⁻¹⁰ CMR is especially useful for evaluation of the atria, which are difficult to visualize using other imaging techniques.¹¹ We hypothesize that structural or functional abnormalities in the atria may be observed by CMR in ARVD/C patients, regardless of the degree of ventricular dysfunction.

Through a cross-sectional study of CMR imaging in a large cohort of ARVD/C patients, we investigated the influence of genotype on structural and functional atrial abnormalities and AA in ARVD/C.

METHODS

Study population

Participants were identified from the University Medical Center ARVD/C registry. This registry was established in 2000 and prospectively enrolls ARVD/C patients and family members with a known or possible history of ARVD/C. We included 71 registry enrollees who fulfilled the 2010 revised diagnostic Task Force Criteria (TFC) for definite ARVD/C¹² and underwent both CMR (with the images available for analysis) and molecular genetic analyses. As a control group, we included 40 consecutive individuals with idiopathic right ventricular outflow tract (RVOT) tachycardia who underwent CMR using the same ARVD/C protocol. The study was approved by the local Institutional Review Board.

Clinical information

Detailed clinical information regarding demographics, presentation, family history and noninvasive and invasive studies was obtained for each ARVD/C patient. All patients underwent 12-lead ECG, which was evaluated for presence of repolarization (T-wave inversions in V1-2 or beyond) or depolarization (epsilon waves or terminal activation duration ≥ 55 ms) criteria for ARVD/C. No individual received medication known to affect ventricular depolarization or repolarization at the time of ECG acquisition. Twenty-four hour Holter monitoring was evaluated for atrial and ventricular arrhythmias, including premature ventricular complex (PVC) count (n=62). The diagnosis of ARVD/C was based on the 2010 revised TFC.¹² ARVD/C was diagnosed when ≥ 4 TFC points from different categories were fulfilled; thus 2 major, 1 major plus 2 minor, or 4 minor criteria sufficed for a definite ARVD/C diagnosis.¹²

CMR acquisition

All 111 participants (71 ARVD/C patients and 40 controls) underwent CMR examination on a 1.5T MRI scanner (Achieva, Philips, Best, The Netherlands) using a standardized protocol, as described in detail previously.¹³ In short, we performed ECG-gated breathhold steady-state-free-precession (SSFP) images (2-chamber right (RV) and left ventricle (LV), left and right ventricular outflow tract, full atrial and ventricular coverage 4-chamber and full ventricle coverage short-axis views), transversal T1-weighted black-blood images, quantitative flow-measurement using phase contrast through plane velocity mapping over the tricuspid and pulmonary valves and phase-sensitive inversion recovery delayed gadolinium enhancement images.

CMR analysis

Atrial and ventricular volume and function were evaluated on a workstation with semi-automated contour tracing software (View Forum cardiac package version R5.1V1L2.SP3, Philips, Best, The Netherlands). Atrial dimensions and function were evaluated on the 4-chamber SSFP images. The end-systolic and end-diastolic images were defined visually as the image with the smallest (at closure of the atrioventricular (AV) valve) and largest (just before opening of the AV valve) atrial cavity size.¹⁴ The area-length-ejection-fraction (ALEF) was used to estimate atrial function, with exclusion of the atrial appendages and pulmonary veins. Atrial length was measured on atrial end-diastolic 4-chamber views. Atrial width was defined as a perpendicular line halfway along the atrial length line, making sure to avoid the inclusion of the atrial appendages or pulmonary veins (**Figure 1**). Ventricular volumes and function were measured on the short-axis cine images.¹⁵ Atrial and ventricular end-diastolic (EDV) and end-systolic volumes (ESV) were corrected for body surface area (BSA) according to the DuBois formula.¹⁶ The tricuspid regurgitation fraction was evaluated for every patient.

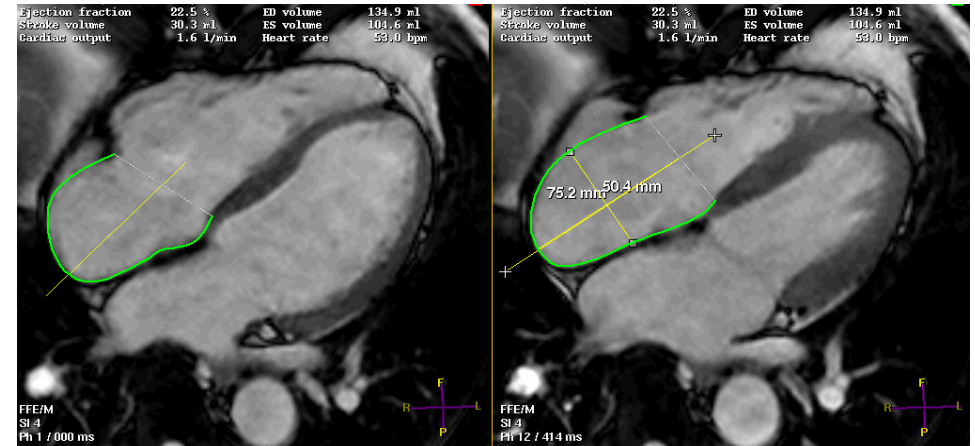


Figure 1: Example of RA measurements

Left picture= atrial end-systolic measurement; Right picture= atrial end-diastolic measurement; 75.2 mm= length; 50.4 mm= width

Molecular genetic analysis:

Comprehensive molecular genetic analysis was performed on desmosomal genes encoding plakophilin-2 (*PKP2*), desmoplakin (*DSP*), plakoglobin (*JUP*), desmoglein-2 (*DSG2*), desmocollin-2 (*DSC2*) and the non-desmosomal genes phospholamban (*PLN*) and transmembrane protein-43 (*TMEM43*) in all probands (first person in a family with confirmed definite ARVD/C diagnosis). In order to maximize genetic homogeneity within mutation groups, exclusively *PKP2* as desmosomal and *PLN* as non-desmosomal mutation carriers were selected for inclusion in the present study based on major mutated gene prevalence in The Netherlands.¹⁷ Family members had comprehensive molecular genetic analysis or were screened for the mutation already identified in the proband.

Outcome measures:

Patients were treated at the discretion of the managing physician. The primary outcome of the study was the occurrence of AA, which were categorized as atrial fibrillation (AF) or atrial flutter (AFL). The included AA had at least one episode lasting ≥ 30 s. This was ascertained through medical record review as recorded by 12-lead ECG, Holter monitoring or implantable cardioverter defibrillator (ICD) interrogation. AA diagnosed exclusively during electrophysiologic study were excluded.

Secondary outcome measures included the development of a life-threatening ventricular arrhythmia (a composite measure of sustained ventricular tachycardia, ventricular fibrillation, or appropriate ICD intervention),¹⁸ stage C heart failure¹⁹ and cardiac death.

Statistical analysis

All continuous data are expressed as mean \pm SD or median (interquartile range [IQR]) and categorical variables as numbers (percentages). Continuous data were compared using the independent Student t-test, Mann-Whitney U test or the Kruskal-Wallis test, and categorical data using chi-square or Fisher exact tests where appropriate. Comparison of more than two groups was done with one-way ANOVA or Kruskal-Wallis for continuous data and chi-square test was used for categorical data. A p-value <0.05 was considered significant. Statistical calculations were performed using SPSS version 19.0 (IBM, Chicago, Illinois).

RESULTS

Study population

We included 71 definite ARVD/C patients and 40 control subjects with idiopathic RVOT tachycardia. Baseline characteristics of ARVD/C patients are shown in **Table 1**. There were no significant differences between ARVD/C subjects and controls in age (46.4 ± 15.8 vs. 45.4 ± 15.2 years, $p=0.748$), gender (58 vs. 68% males, $p=0.311$) and occurrence of secondary diseases (diabetes ($p=0.889$), hypertension ($p=0.075$), obesity ($p=0.853$)). **Table 2** compares global and regional CMR volumes and function between ARVD/C patients and controls. As expected, ARVD/C patients had higher RV EDV/BSA (124.6 ± 39.1 vs. 96.2 ± 21.3 ml/m², $p<0.001$) and lower RV ejection fraction (EF) (39.2 ± 10.4 vs. $54.3 \pm 4.8\%$, $p<0.001$) than control subjects. There were no significant differences in LV volume (96.0 ± 19.4 ARVD/C vs. 96.2 ± 15.7 ml/m² controls, $p=0.822$) and LV EF (54.3 ± 8.7 ARVD/C vs. $57.2 \pm 5.5\%$ controls, $p=0.074$) between the groups.

Structural atrial evaluation by CMR

First we set out to compare atrial volume and function between ARVD/C patients and controls. Since we hypothesized that the presence of a desmosomal mutation would impact atrial morphology and function, we stratified our analyses by mutation burden: ARVD/C patients were classified as mutation-positive desmosomal with a *PKP2* ($n=37$) mutation, mutation-positive non-desmosomal *PLN* ($n=14$) and patients with no mutation identified ($n=20$). Detailed description of the pathogenic mutations identified in the ARVD/C patients are provided in **Supplementary Table 1**. These 3 groups were compared to each other as well as to the controls.

Table 1: Patients characteristics

	ARVD/C (n=71)
Male	41 (58)
Age at CMR	46.4 ± 15.8
<i>Mutation burden</i>	
Mutation-positive desmosomal	
<i>PKP2</i>	37 (52)
Mutation-positive non-desmosomal	
<i>PLN</i> mutation	14 (20)
No mutation identified	20 (28)
<i>Clinical Phenotype</i>	
Repolarization TFC	48 (68)
Major	31 (44)
Minor	17 (24)
Depolarization TFC	53 (75)
Major	7 (10)
Minor	53 (75)
Arrhythmia TFC	65 (92)
Major	28 (39)
Minor	65 (92)
Structural TFC	64 (90)
Major	59 (83)
Minor	5 (7)
Family history TFC	46 (65)
Major	45 (63)
Minor	3 (4)

Mean values \pm standard deviation; number (%)

Abbreviations: CMR= cardiac magnetic resonance; *PKP2*= Plakophilin-2; *PLN*= Phospholamban; TFC= Task Force Criteria.

Results are shown in **Table 2**. Compared to the control population, *PKP2* ARVD/C patients had reduced right atrial (RA) volume (45.9 ± 13.0 vs. 37.9 ± 17.2 ml/m², $p= 0.002$) with preserved function (RA ALEF 44.9 ± 8.7 vs. $44.9 \pm 8.9\%$, $p=0.862$) and comparable left atrial (LA) parameters. In contrast, both RA and LA volume and function were similar between *PLN* mutation carriers and controls. Compared to the controls, patients with no mutation identified had increased RA (RA EDV/BSA 45.9 ± 13.0 vs. 60.4 ± 28.0 ml/m², $p=0.011$) and LA volumes (LA EDV/BSA 45.3 ± 12.0 vs. 52.3 ± 15.7 ml/m², $p=0.034$), with preserved bi-atrial function. Interestingly, RA and LA volumes increased and RA function decreased in patients with no mutation identified and *PLN* mutation carriers when compared to *PKP2* mutation carriers. This trend reached statistical significance for RA length, RA EDV/BSA, and RA ESV/BSA (**Table 2**). Regarding ventricular measurements, LV and RV volumes ($p= 0.425$ and $p=0.286$) and also RV function ($p=0.228$) were comparable between ARVD/C patients with different genotypes (**Table 2**). However, LV function differed significantly among genotypes ($p=0.024$) with the *PLN* mutation carriers having lowest LV function and *PKP2* mutation carriers having highest LV function.

Finally, we also compared the structural parameters of the atria and ventricles in probands and family members (**Supplementary Table 2**). Right ventricular and RA EDV/BSA are significantly larger in probands (136.6 ± 107.6 and 53.3 ± 25.0 ml/m², respectively) than in family members (107.6 ± 33.2 and 36.9 ± 14.9 ml/m², respectively) The left ventricular and LA parameters were similar.

Table 2: Structural evaluation with CMR of ARVD/C patients stratified by mutation status.

	Control (n=40)	Overall ARVD/C (n=71)	PKP2 ARVD/C (n=37)	PLN ARVD/C (n=14)	No mutation identified ARVD/C (n=20)	p-value for trend ⁺
Mean	27 (68)	41 (58)	15 (75)	6 (43)	20 (54)	0.141
R	45.4 ± 15.2	46.4 ± 15.8	44.1 ± 16.4	48.6 ± 10.7	49.2 ± 17.6	0.444
	61.3 ± 10.0	55.8 ± 12.8*	56.0 ± 11.4	55.5 ± 14.0	55.5 ± 15.0	0.980
	56.8 ± 6.9	59.4 ± 9.9	57.7 ± 9.5	58.7 ± 11.9	62.9 ± 8.4*	0.162
	45.6 ± 5.6	44.8 ± 8.9	44.5 ± 8.3	43.1 ± 9.4	46.4 ± 9.8	0.549
SA	45.3 ± 12.0	48.3 ± 14.9	45.7 ± 14.0	48.1 ± 15.4	52.3 ± 15.7*	0.181
SA	18.3 ± 7.9	22.1 ± 14.2	20.4 ± 8.8	22.3 ± 13.0	24.1 ± 12.1*	0.319
	53.9 ± 11.9	51.3 ± 19.5	49.0 ± 18.2	49.3 ± 18.0	56.8 ± 22.6	0.337
	57.2 ± 5.5	54.3 ± 8.7	56.2 ± 9.3	48.9 ± 7.2*	54.6 ± 6.8	0.024
SA	96.2 ± 15.7	96.0 ± 19.4	95.2 ± 15.1	103.1 ± 28.9	94.9 ± 18.7	0.425
SA	41.3 ± 9.2	46.7 ± 20.7	45.5 ± 24.3	55.0 ± 20.8*	42.6 ± 9.5	0.346
	44.9 ± 8.7	41.9 ± 12.7	44.9 ± 8.9	39.9 ± 15.2	37.9 ± 15.8	0.197
	59.6 ± 6.8	58.0 ± 9.3	54.8 ± 7.7*	58.5 ± 8.0	63.7 ± 10.2	0.002
	48.7 ± 7.4	48.0 ± 9.9	45.8 ± 7.4*	50.3 ± 7.7	50.4 ± 14.0	0.152
SA	45.9 ± 13.0	47.2 ± 23.2	37.9 ± 17.2*	51.3 ± 17.6	60.4 ± 28.0*	<0.001
SA	25.0 ± 7.0	29.2 ± 21.1	22.2 ± 13.1*	31.6 ± 15.5	39.5 ± 29.6*	<0.001
	41.7 ± 17.2	36.6 ± 16.0	33.3 ± 11.6*	37.8 ± 16.9	42.0 ± 21.0	0.139
	54.3 ± 4.8	39.2 ± 10.4*	37.8 ± 10.5*	38.5 ± 12.4*	42.7 ± 7.9*	0.228
SA	96.2 ± 21.3	124.6 ± 39.1*	132.8 ± 43.7*	119.0 ± 33.0*	116.4 ± 32.9*	0.286
SA	47.8 ± 22.3	78.4 ± 35.6	86.7 ± 41.2*	73.4 ± 30.7*	66.9 ± 23.1*	0.176

Mean values ± standard deviation; number (%);*Significantly different from control (p<0.05);

⁺Trend between 71 ARVD/C patients stratified by mutation burden.

Abbreviations: ALEF= area length ejection fraction (%); BSA= body surface area (m²); CMR= cardiac magnetic resonance; EDV= end diastolic volume (mL); EF= ejection fraction (%); ESV= end systolic volume (mL); LA= left atrium; PKP2= Plakophilin-2; PLN= Phospholamban; SV= stroke volume (ml).

Atrial arrhythmias

Characteristics of atrial arrhythmias

Among the 71 definite ARVD/C patients, 19 (27%) individuals experienced one or more types of AA during 7.9 ± 6.3 years of follow-up. Mean age at first AA was 54.1 ± 18.2 years, and 15 (79%) were male. The first AA episode was recorded a median of 2.6 (range 0.7-7.8) years after presentation. Two (11%) patients had an AA episode prior to the first sustained ventricular arrhythmia and 3 (16%) patients exclusively had AA without any recorded ventricular arrhythmias. AF was the most common type of arrhythmia (89%), whereas AFL

occurred in 21%, 2 (11%) patients experienced both types of AA. In 10 of the 19 patients with AA the first episode was recorded by 12-lead ECG (after complaints of the patient), in 8 by ICD interrogation (2 discovered after inappropriate ICD intervention) and in 1 with 24 hour Holter monitoring. In 3 patients AFL was seen, which was diagnosed by ECG, 24-hour Holter monitoring and ICD interrogation, respectively. In 12 of the 19 patients with AA at least one other episode of AA was recorded during follow-up.

Table 3 shows a comparison of demographic and clinical characteristics of ARVD/C patients with and without AA. Compared to those without AA, patients with arrhythmias were more likely to be male (79 vs. 50%, p=0.029), and presented with ARVD/C at an older age (48.9 ± 16.9 vs. 40.1 ± 14.8 years, p=0.036). The incidence of secondary diseases that could influence atrial structure (diabetes, hypertension and obesity) did not differ between patients with and without AA.

Patients with and without AA had comparable LA and RA volume and function. The patients with AA had significantly more often left bundle branch block ventricular tachycardia morphology with inferior or unknown axis (p=0.040) and major structural abnormalities on cardiac imaging (p=0.022) than subjects without AA. All other domains of the TFC were similarly divided between the two groups.

An ICD was present in 27/37 (73%) PKP2 mutation carriers, 10/14 (71%) PLN mutation carriers and 10/20 (50%) patients with no mutation identified. This distribution was not significantly different (p=0.194). An ICD was present in all patients who had AA during follow-up, however in 5/19 (26%) patients the first AA event occurred prior to ICD implantation. First AA occurrence did not significantly (p=0.132) differ among patients with or without ICD.

During 7.9 ± 6.3 years of follow-up (similar between the groups), the likelihood of experiencing a life-threatening ventricular arrhythmia (84 vs. 40%, p=0.001) and inappropriate ICD intervention (26 vs 4%, p=0.033) was significantly higher in the AA group. Although it did not reach statistical significance, patients with AA were also more likely to develop heart failure (11 vs 0%, p=0.069) or die during follow-up (11 vs. 2%, p=0.173).

The influence of genotype on atrial arrhythmias

As shown in **Table 3**, AA were recorded in 11/37 (30%) PKP2 mutation carriers, 2/14 (14%) PLN mutation carriers and 6/20 (30%) patients with no mutation identified. While PKP2 mutation carriers had the smallest atria in univariate analyses (RA EDV/BSA 37.9 ± 17.2 and LA EDV/BSA 45.7 ± 14.0 ml/m²), the prevalence of AA was similar to patients with no mutation identified with the largest atria (RA EDV/BSA 60.4 ± 28.0 and LA EDV/BSA 52.3 ± 15.7 ml/m²).

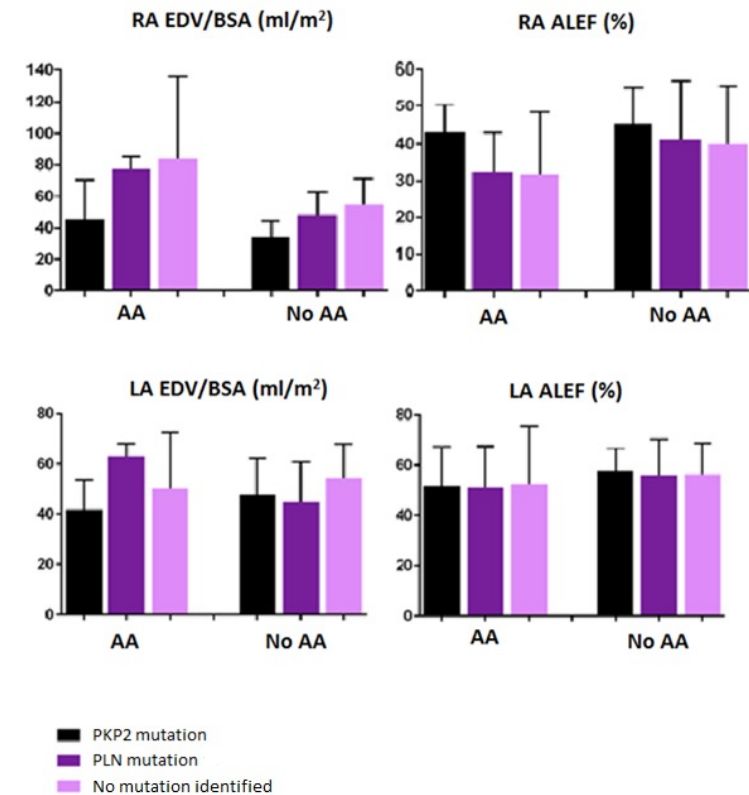
Table 3: ARVD/C Patients Stratified by AA

	Overall (n=71)	AA (n=19)	No AA (n=52)	p-value
Male	41 (58)	15 (79)	26 (50)	0.029
Age at presentation (years)	42.4 ± 15.7	48.9 ± 16.9	40.1 ± 14.8	0.051
Age at first AA (years)	-	54.1 ± 17.7	-	-
Proband	27 (38)	5 (26)	22 (42)	0.075
Diabetes	2 (4)	1 (5)	1 (2)	0.451
Hypertension	4 (6)	2 (10)	2 (4)	0.280
Obesity	7/60 (12)	2/17 (12)	5/43 (12)	0.988
CMR parameters				
LA ALEF	55.8 ± 12.8	52.9 ± 16.5	56.8 ± 11.2	0.612
LA EDV/BSA	48.3 ± 14.9	47.1 ± 15.3	48.8 ± 14.8	0.745
RA ALEF	41.9 ± 12.7	39.4 ± 11.6	42.9 ± 13.1	0.198
RA EDV/BSA	47.2 ± 23.2	60.0 ± 34.9	42.5 ± 14.9	0.058
Genotype				
PKP2 ARVD/C	37 (52)	11 (58)	26 (50)	0.556
PLN ARVD/C	14 (20)	2 (11)	12 (23)	0.239
No mutation identified ARVD/C	20 (28)	6 (32)	14 (27)	0.699
Phenotype				
Repolarization criteria	48 (68)	13 (68)	35 (67)	0.929
TWI V1-3	31 (44)	11 (58)	20 (38)	0.144
TWI V1-2	9 (13)	1 (5)	8 (15)	0.428*
TWI V4-6	7 (10)	0 (0)	7 (13)	0.178*
TWI V1-4 w/ CRBBB	1 (1)	1 (5)	0 (0)	0.268*
Depolarization criteria	53 (75)	17 (89)	36 (69)	0.083
Epsilon wave	7 (10)	3 (16)	4 (8)	0.375*
Prolonged TAD	45 (63)	12 (63)	33 (63)	0.981
Arrhythmia criteria	65 (92)	19 (100)	46 (88)	0.122
LBBB superior axis VT	28 (39)	11 (58)	17 (33)	0.054
LBBB inferior/unkown axis VT	42 (59)	15 (79)	27 (52)	0.040
>500 PVCs / 24 hrs	51/62 (82)	11/14 (79)	40/48 (83)	0.115
Structural criteria	64 (90)	19 (100)	45 (87)	0.092
Major	59 (83)	19 (100)	40 (77)	0.022
Minor	5 (7)	0 (0)	5 (10)	0.315*
Family history criteria	46 (65)	12 (63)	34 (65)	0.862
Major	45 (63)	12 (63)	33 (63)	0.981
Minor	3 (4)	0 (0)	3 (6)	1.000*
Disease course				
Duration of follow-up (years)	7.9 ± 6.3	8.0 ± 5.7	7.9 ± 6.6	0.444
Sustained ventricular arrhythmia	37 (52)	16 (84)	21 (40)	0.001
Inappropriate ICD discharge	6/47 (13)	5/19 (26)	1/28 (4)	0.033*
Heart failure	2 (3)	2 (11)	0 (0)	0.069*
Transplant	0 (0)	0 (0)	0 (0)	-
Death	3 (4)	2 (11)	1 (2)	0.173*

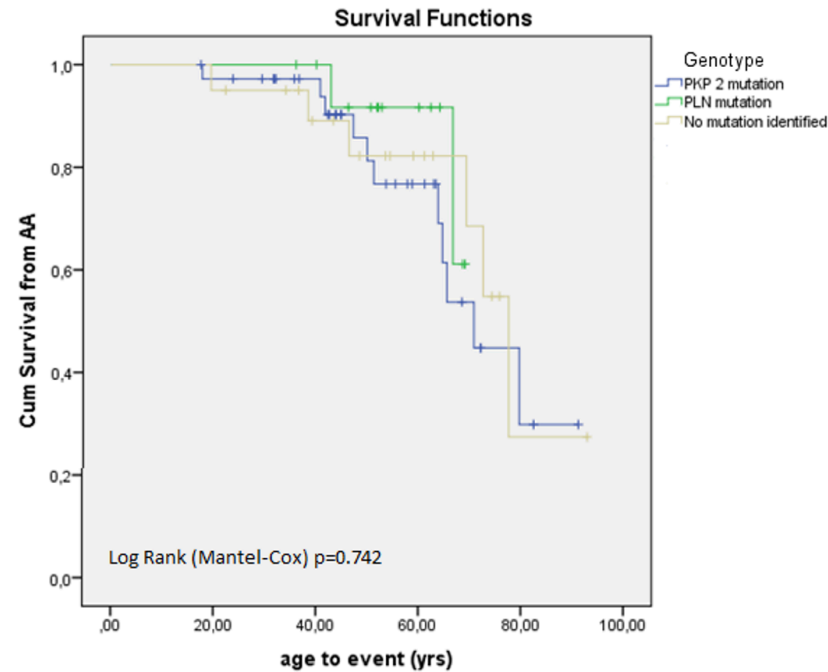
Mean values ± standard deviation; number (%); *Fisher exact test;

Abbreviations: AA= atrial arrhythmias; CRBBB= complete right bundle branch block; ICD= implantable cardioverter defibrillator; LBBB= left bundle branch block; PKP2= Plakophilin-2; PLN= Phospholamban; PVC= premature ventricular complex; TAD= Terminal Activation Duration; TWI= T-Wave Inversion; VT= ventricular tachycardia.

Although all patients with AA experienced their first (recorded) event within 3 months prior to or after CMR, we next set out to exclude the possibility that the structural atrial changes were driven by the occurrence of AA. Therefore, we compared atrial volumes and function between genotypes stratifying for AA (**Figure 2**). Even with stratified analyses, the differences in RA volume and function persisted between the three groups: RA volume increased and RA function decreased in the *PLN* mutation carriers and even more in patients with no mutation identified compared to the *PKP2* mutation carriers. Importantly, only 2 patients with no mutation identified and one *PKP2* ARVD/C patient had > 5% tricuspid regurgitation, with one having >10% regurgitation. Significant differences between the 3 groups still persisted after excluding these 3 patients. Event-free survival did not significantly differ when comparing *PKP2*, *PLN* and no mutation identified patients (log rank= 0.742) as can be seen in **Figure 3**.

**Figure 2:** RA and LA volume and function stratified by AA

Abbreviations: AA= atrial arrhythmias; ALEF= area-length-ejection-fraction; EDV/BSA= end diastolic volume/ body surface area; LA= left atrium; RA= right atrium.



Number at risk						
PKP2	37	35	28	13	2	0
PLN	14	14	12	5	0	0
No mutation	20	19	14	8	19	0

Figure 3 Survival free from AA stratified by genotype. Cumulative survival free from atrial arrhythmias (AA) among patients stratified by genotype (*PKP2*, *PLN* and no mutation identified).

We also analyzed whether increased atrial volumes and reduced function were a primary disease effect of ARVD/C on the atria or whether they were secondary to ventricular dysfunction. Ventricular function was a significant predictor of atrial function for both atria (effect of RV EF on RA ALEF beta=0.35, p=0.035; effect of LVEF on LA ALEF beta=0.57, p=0.002). In addition, ventricular dilatation was a significant predictor of atrial dilatation (effect of RV EDV/BSA on RA EDV/BSA beta =0.20, p=0.005; effect of LV EDV/BSA on LA EDV/BSA beta=0.32, p=0.002). Although this does not indicate etiology, these results suggest that atrial volume and function are significantly associated with ventricular morphology and function. Cause of death of the 2 patients with AA was heart failure and cerebral hemorrhage due to a head trauma after a ventricular tachyarrhythmia.

Finally, we compared the occurrence of atrial arrhythmias between probands and family members and saw no significant difference (Supplementary Table 2).

DISCUSSION

This study aimed to describe the extent and clinical implications of structural atrial involvement in ARVD/C stratified by genotype. This study has three important results. First, our study shows that bi-atrial volume increased in ARVD/C patients with a *PLN* mutation or no mutation identified while the effect was opposite in ARVD/C patients with a *PKP2* mutation. Second, despite having smaller atria, the prevalence of AA is similar in *PKP2* mutation carriers compared to ARVD/C patients with no mutation identified, suggestive of a distinct pathophysiologic mechanism underlying atrial disease. Third, AA in ARVD/C patients increase the likelihood of experiencing inappropriate ICD interventions and are associated with life-threatening ventricular arrhythmias during 8 years of follow-up.

Prior studies

The limited number of previous studies that examined atrial size in ARVD/C do not show uniform results. Two studies compared RA size on echocardiography in ARVD/C patients meeting the 1994 TFC with age and sex matched healthy controls. Yoerger *et al.* found significant RA enlargement in 29 patients,²⁰ while Platonov *et al.* showed no atrial enlargement in 40 ARVD/C patients.⁶ Similar to our study, Tandri *et al.* measured RA dimension using CMR in 12 patients meeting the 1994 TFC, showing non-significant RA enlargement.²¹ They determined atrial size by measuring atrial dimensions. However, LA size is more accurately predicted by LA volume than by dimensions.²² In addition, none of these studies provides information about the patient's genotype. Our study did not find a significant RA enlargement in the overall ARVD/C group. However, when stratified by genotype, significantly larger atria were found in patients with no mutation identified and significantly smaller atria in *PKP2* mutation carriers, compared to our control group with idiopathic RVOT tachycardia. The pathophysiologic significance of this finding is still unclear. Since ARVD/C has genotypic and phenotypic overlap with idiopathic dilated cardiomyopathy (DCM), which is also known to result in atrial dilatation,²³⁻²⁵ it is possible that the structural differences between the different genotypes relate to this overlap area between ARVD/C and DCM. It may be possible that the smaller atria in desmosomal mutation carriers reflect atrial fibrosis that initially leads to a reduction in atrial size with preserved function. No previous study has histopathologically analyzed atrial tissue of human ARVD/C patients. However Basso *et al.* histopathologically examined 23 boxer dogs diagnosed with ARVD/C and observed fibrofatty replacement of the atrial myocardium in 35% of dogs.³ Identification of fibrosis in the thin atrial wall using conventional CMR with gadolinium enhancement is challenging and was not possible in our study. Future studies on humans, including high resolution CMR and histopathological studies are necessary to evaluate the influence of fibrosis on atrial size in ARVD/C.

We are the first to report on bi-atrial function in ARVD/C patients with different genotypes. We found lower LA atrial function in the overall ARVD/C patients compared to controls but no significant difference in bi-atrial function between the different genotypes. No normal reference values for atrial volume and function were available that used the same CMR protocol. We used idiopathic RVOT tachycardia patients as controls, since these individuals underwent the same CMR examination to rule out ARVD/C. The possible influence of RVOT tachycardia on the atria is unknown.

Atrial arrhythmias

An important finding of our study is that patients with a *PKP2* mutation developed AA as often as patients with no mutation identified, despite significantly smaller atria among *PKP2* mutation carriers. This suggests a different pathogenic role for *PKP2* mutations in the development of AA which warrants further investigation. The influence of genotype on the occurrence of ventricular arrhythmias has been described by Bao et al.²⁶ They see more frequent clinical ventricular tachycardia in patients with compared to those without a *PKP2* mutation.

Another important finding of our study is that AA in ARVD/C patients are associated with increased risk of sustained ventricular arrhythmias and inappropriate ICD shocks. Recently, Camm *et al* described that AA occur in 14% of ARVD/C patients, in whom they are associated with male gender, increasing age, and LA enlargement.⁵ Saguner et al found an incidence of 20% in their observational study. They suggest that the presence of AA in ARVD/C patients is associated with an adverse clinical outcome (inappropriate shocks, heart transplantation and cardiac death).²⁷ However, structural data in these studies was based on echocardiographic reports, and did not specifically investigate an association with genotype. In our cohort, AA occurred in 27% of ARVD/C patients, and were associated with male gender and older age, similar to the data observed by Camm *et al*. The high rate (26%) of inappropriate ICD shocks in patients with AA in our cohort is concerning. Beyond doubt, ICD implantation is of great benefit for selected ARVD/C patients in the prevention of sudden cardiac death. However, strategic programming of arrhythmia detection criteria and ICD interventions is necessary to reduce the number of inappropriate interventions.²⁸ While it did not reach statistical significance, there was a trend towards higher incidence of cardiac death in patients with AA in our study. As mentioned by Camm *et al.*, it is unclear whether this can be attributed to the AA or heart failure.⁵

Limitations

ARVD/C studies, particularly involving CMR, are typically small in size. Our results need to be validated in a large prospective study with longitudinal imaging data. As all *PLN* mutation carriers harbored a single founder *PLN* mutation (c.40_42delAGA; p.Arg14del), all desmosomal mutation carried a *PKP2* mutation and some (rare) non-desmosomal mutations were not analyzed (e.g. RYR, CTNNA3), our results may not be applicable to carriers of other mutations.

In our study, ICD was not implanted in each patient. Although no significant difference is seen between AA occurrence in patients with and without ICD, this could influence results since ICD's with continuous rhythm registration increase the chance of registering arrhythmias.

We used single plane ALEF measures to evaluate atrial EF and volumes and no three-dimensional atrial volume measurements. While CMR measures of diastolic function are currently less reliable than echocardiography, future studies will be necessary to further explore the role of diastolic dysfunction in atrial involvement in ARVD/C. To confirm the role of fibrosis in atrial dysfunction in ARVD/C, it would have been interesting to evaluate atrial fibrosis with CMR. However, the resolution of our CMR studies in combination with the thin atrial walls hampered reliable detection of atrial fibrosis. Recent new developments in CMR techniques now make it possible to visualize fibrosis in the thin atrial wall.²⁹

CONCLUSION

Our study shows that genotype influences bi-atrial volume and the occurrence of AA in ARVD/C. Furthermore, AA in ARVD/C patients increases the likelihood of experiencing more inappropriate ICD interventions. These findings provide new insight in the influence of genotype on structural involvement in ARVD/C.

Clinical perspective

Since approximately 60% of Arrhythmogenic Right Ventricular Dysplasia/Cardiomyopathy (ARVD/C) patients harbor a pathogenic desmosomal mutation, ARVD/C is generally considered a disease of the cardiac desmosome. Since desmosomes are also present in the atria, atrial involvement in ARVD/C is to be expected. However, little is known about atrial involvement in ARVD/C and no study has been done to correlate structural atrial changes to genotype.

In the present study we investigated the extent of structural atrial involvement in ARVD/C in comparison with genotype. We show that bi-atrial volume increased in ARVD/C patients without a *PKP2* mutation while the effect is opposite in ARVD/C patients with a *PKP2* mutation. Despite having smaller atria, the prevalence of atrial arrhythmias is similar in *PKP2* mutation carriers compared to ARVD/C patients with no mutation identified, suggestive of a distinct pathophysiologic mechanism underlying atrial disease. These findings give us new insight into the role of genotype on structural changes in ARVD/C. This is important to recognize since atrial arrhythmias in ARVD/C turn out to increase the likelihood of experiencing inappropriate ICD interventions and are associated with life-threatening ventricular arrhythmias.

Investigating the role of genotype in ARVD/C is important since it could add to a more genotype-specific risk stratification. To evaluate the clinical significance of adding structural atrial analysis to ARVD/C diagnostic or risk-stratification models they need to be validated in a large prospective study and correlated to different clinical parameters. Also more research is needed to discover the underlying cause of these genotypic differences.

Abbreviations

AA = atrial arrhythmias

ALEF = area-length-ejection-fraction

ARVD/C = arrhythmogenic right ventricular dysplasia/ cardiomyopathy

AV = atrioventricular

BSA = body surface area

CMR = cardiac magnetic resonance imaging

ECG = electrocardiogram

EDV = end-diastolic volume

ESV = end-systolic volumes

ICD = implantable cardioverter defibrillator

LA = left atrium

LV = left ventricle

PKP2= Plakophilin-2

PLN = Phospholamban

PVC = premature ventricular complex

RA = right atrium

RV = right ventricle

RVOT = right ventricular outflow tract

SAECG = signal-averaged electrocardiogram

SSFP = steady-state free precession

TFC = task force criteria

REFERENCES

1. Sen-Chowdhry S, Morgan RD, Chambers JC, McKenna WJ: Arrhythmogenic cardiomyopathy: etiology, diagnosis, and treatment. *Annu Rev Med* 2010;61:233-53.
2. Cox MGPJ, van der Zwaag PA, van der Werf C, van der Smagt JJ, Noorman M, Bhuiyan ZA, Wiesfeld AC, Volders PG, van Langen IM, Atsma DE, Dooijes D, van den Wijngaard A, Houweling AC, Jongbloed JD, Jordaens L, Cramer MJ, Doevendans PA, de Bakker JM, Wilde AA, van Tintelen JP, Hauer RN: Arrhythmogenic right ventricular dysplasia/cardiomyopathy: pathogenic desmosome mutations in index-patients predict outcome of family screening: Dutch arrhythmogenic right ventricular dysplasia/cardiomyopathy genotype-phenotype follow-up study. *Circulation* 2011;123:2690-700.
3. Basso C, Fox PR, Meurs KM, Towbin JA, Spier AW, Calabrese F, Maron BJ, Thiene G: Arrhythmogenic right ventricular cardiomyopathy causing sudden cardiac death in boxer dogs: a new animal model of human disease. *Circulation* 2004;109:1180-5.
4. Fox PR, Maron BJ, Basso C, Liu SK, Thiene G: Spontaneously occurring arrhythmogenic right ventricular cardiomyopathy in the domestic cat: A new animal model similar to the human disease. *Circulation* 2000;102:1863-70.
5. Camm CF, James CA, Tichnell C, Murray B, Bhonsale A, te Riele ASJM, Judge DP, Tandri H, Calkins H: Prevalence of atrial arrhythmias in arrhythmogenic right ventricular dysplasia/cardiomyopathy. *Heart Rhythm* 2013;10:1661-8.
6. Platonov PG, Christensen AH, Holmqvist F, Carlson J, Haunsø S, Svendsen JH: Abnormal atrial activation is common in patients with arrhythmogenic right ventricular cardiomyopathy. *J Electrocardiol* 2011;44:237-41.
7. Lemola K, Brunckhorst C, Helfenstein U, Oechslin E, Jenni R, Duru F: Predictors of adverse outcome in patients with arrhythmogenic right ventricular dysplasia/cardiomyopathy: long term experience of a tertiary care centre. *Heart* 2005;91:1167-72.
8. Brembilla-Perrot B, Jacquemin L, Houplon P, Houriez P, Beurrier D, Berder V, Terrier de la Chaise A, Louis P: Increased atrial vulnerability in arrhythmogenic right ventricular disease. *Am Heart J* 1998;135:748-54.
9. Sievers B, Addo M, Franken U, Trappe H: Right ventricular wall motion abnormalities found in healthy subjects by cardiovascular magnetic resonance imaging and characterized with a new segmental model. *J Cardiovasc Magn Reson* 2004;6:601-8.
10. Chellamuthu S, Smith AM, Thomas SM, Hill C, Brown PWG, Al-Mohammad A: Is cardiac MRI an effective test for arrhythmogenic right ventricular cardiomyopathy diagnosis? *World J Cardiol* 2014;6:675-81
11. Tops LF, Schalij MJ, Bax JJ: Imaging and atrial fibrillation: the role of multimodality imaging in patient evaluation and management of atrial fibrillation. *Eur Heart J* 2010;31:542-51.
12. Marcus FI, McKenna WJ, Sherrill D, Basso C, Bauce B, Bluemke DA, Calkins H, Corrado D, Cox MG, Daubert JP, Fontaine G, Gear K, Hauer R, Nava A, Picard MH, Protonotarios N, Saffitz JE, Sanborn DM, Steinberg JS, Tandri H, Thiene G, Towbin JA, Tsatsopoulou A, Wichter T, Zareba W: Diagnosis of arrhythmogenic right ventricular cardiomyopathy/dysplasia: proposed modification of the Task Force Criteria. *Eur Heart J* 2010; 31:806-14
13. Prakken NH, Velthuis BK, Bosker AC, Mosterd A, Teske AJ, Mali WP, Cramer MJ: Relationship of ventricular and atrial dilatation to valvular function in endurance athletes. *Br J Sports Med* 2011;45:178-84.
14. Jahnke C, Fischer J, Mirelis JG, Kriatselis C, Gerds-Li J, Gebker R, Manka R, Schnackenburg B, Fleck E, Paetsch I: Cardiovascular magnetic resonance imaging for accurate sizing of the left atrium: predictability of pulmonary vein isolation success in patients with atrial fibrillation. *J Magn Reson Imaging* 2011;33:455-63.
15. Luijckx T, Velthuis BK, Prakken NHJ, Cox, Moniek G P J, Bots ML, Mali, Willem P Th M, Hauer RNW, Cramer MJ: Impact of revised Task Force Criteria: distinguishing the athlete's heart from ARVC/D using cardiac magnetic resonance imaging. *Eur J Prev Cardiol* 2012;19:885-91.
16. Du Bois EF: A formula to estimate the approximate surface area if height and weight be known. *Nutrition* 1989;5:303-11; discussion 312.
17. Groeneweg, JA, Bhonsale A, James CA, Te Riele AS, Dooijes D, Tichnell, C, Murray B, Wiesfeld ACP, Sawant AC, Kassamali B, Atsma DE, Volders PG, de Groot NM, de Boer K, Zimmerman SL, Kamel IR, van der Heijden JF, Russell SD, Cramer MJ, Tedford RJ, Doevendans PA, van Veen TA, Tandri H, Wilde AA, Judge DP, van Tintelen JP, Hauer RN, Calkins H: Clinical presentation, long-term follow-up, and outcomes of 1001 arrhythmogenic right ventricular dysplasia/cardiomyopathy patients and family members. *Circ Cardiovasc Genet* 2015;8:437-446.
18. Corrado D, Calkins H, Link MS, Leoni L, Favale S, Bevilacqua M, Basso C, Ward D, Boriani G, Ricci R, Piccini JP, Dalal D, Santini M, Buja G, Iliceto S, Estes NA 3rd, Wichter T, McKenna WJ, Thiene G, Marcus DP: Prophylactic implantable defibrillator in patients with arrhythmogenic right ventricular cardiomyopathy/dysplasia and no prior ventricular fibrillation or sustained ventricular tachycardia. *Circulation* 2010;122:1144-52.
19. Hunt SA, Abraham WT, Chin MH, Feldman AM, Francis GS, Ganiats TG, Jessup M, Konstam MA, Mancini DM, Michl K, Oates JA, Rahko PS, Silver MA, Stevenson LW, Yancy CW; American College of Cardiology Foundation; American Heart Association: 2009 Focused update incorporated into the ACC/AHA 2005 Guidelines for the Diagnosis and Management of Heart Failure in Adults A Report of the American College of Cardiology Foundation/American Heart Association Task Force on Practice Guidelines Developed in Collaboration With the

- International Society for Heart and Lung Transplantation. *J Am Coll Cardiol* 2009;53:e1-e90.
20. Yoerger DM, Marcus F, Sherrill D, Calkins H, Towbin JA, Zareba W, Picard MH: Echocardiographic findings in patients meeting task force criteria for arrhythmogenic right ventricular dysplasia: new insights from the multidisciplinary study of right ventricular dysplasia. *J Am Coll Cardiol* 2005;45:860-5.
 21. Tandri H, Calkins H, Nasir K, Bomma C, Castillo E, Rutberg J, Tichnell C, Lima JAC, Bluemke DA: Magnetic resonance imaging findings in patients meeting task force criteria for arrhythmogenic right ventricular dysplasia. *J Cardiovasc Electrophysiol* 2003; 14:476-82.
 22. Lester SJ, Ryan EW, Schiller NB, Foster E: Best method in clinical practice and in research studies to determine left atrial size. *Am J Cardiol* 1999;84:829-32
 23. Rossi A, Ciccoira M, Zanolla L, Sandrini R, Golia G, Zardini P, Enriquez-Sarano M: Determinants and prognostic value of left atrial volume in patients with dilated cardiomyopathy. *J Am Coll Cardiol* 2002;40:1425.
 24. Van Rijsingen IAW, van der Zwaag PA, Groeneweg JA, Nannenber EA, Jongbloed JD, Zwinderman AH, Pinto YM, Dit Deprez RH, Post JG, Tan HL, de Boer RA, Hauer RN, Christiaans IJ, van den Berg MP, van Tintelen JP, Wilde AA: Outcome in phospholamban R14del carriers: results of a large multicentre cohort study. *Circ Cardiovasc Genet* 2014;7:455-65
 25. D'Andrea A, Scarafile R, Riegler L, Salerno G, Gravino R, Cocchia R, Castaldo F, Allocca F, Limongelli G, Di Salvo G, Cuomo S, Pacileo G, Caso P, Russo MG, Calabrò R: Right atrial size and deformation in patients with dilated cardiomyopathy undergoing cardiac resynchronization therapy. *Eur J Heart Fail* 2009; 11:1169-77.
 26. Bao J, Wang J, Yao Y, Wang Y, Fan X, Sun K, He DS, Marcus FI, Zhang S, Hui R, Song L: Correlation of ventricular arrhythmias with genotype in arrhythmogenic right ventricular cardiomyopathy. *Circ Cardiovasc Genet* 2013; 6:552-6
 27. Saguner AM, Ganahl S, Kraus A, Baldinger SH, Medeiros-Domingo A, Saguner AR, Mueller-Burri SA, Wolber T, Haegeli LM, Krasniqi N, Tanner FC, Steffel J, Brunckhorst C, Duru F: Clinical role of atrial arrhythmias in patients with arrhythmogenic right ventricular dysplasia. *Circulation Journal*. 2014; 78(12), 2854-61.
 28. Schinkel AFL: Implantable cardioverter defibrillators in arrhythmogenic right ventricular dysplasia/cardiomyopathy: patient outcomes, incidence of appropriate and inappropriate interventions, and complications. *Circ.Arrhythm.Electrophysiol*. 2013;6:562-8.
 29. Marrouche NF, Wilber D, Hindricks G, Jais P, Akoum N, Marchlinski F, Kholmovski E, Burgon N, Hu N, Mont L, Deneke T, Duytschaever M, Neumann T, Mansour M, Mahnkopf C, Herweg B, Daoud E, Wissner E, Bansmann P, Brachmann J: Association of atrial tissue fibrosis identified by delayed enhancement MRI and atrial fibrillation catheter ablation: the DECAAF study. *JAMA* 2014;311:498-506.

SUPPLEMENTARY MATERIAL

Supplementary Table 1: Pathogenic mutations identified in ARVD/C patients

Gene; n (%)	Nucleotide change	Amino Acid change	No. of probands	No. of family members	Total
PKP2; 36 (51)					
	c. 2386T>C	p.Cys796Arg	2	2	4
	c. 2489+4A>C	p.Lys768fs	2	2	4
	c.1848C>A	p.Tyr616*	1	0	1
	c.235C>T	p.Arg79*	2	2	4
	c.1211dup	p.Val406fs	2	3	5
	c.2146-1G>C	p.Met716fs	3	2	5
	c.397C>T	p.Gln133*	1	2	3
	c.1369_1372del	p.Gln457*	1	1	2
	c.2509del	p.Ser837fs	1	0	1
	Deletion exon 1-4		1	1	2
	Deletion exon 1-14		1	3	4
	Deletion exon 10		0	1	1
	Deletion exon 7-14		1	0	1
PLN; 14 (20)					
	c.40_42del	p.Arg14del	9	5	14

Abbreviations: No.= number; PKP2= Plakophilin-2; PLN= Phospholamban.

Supplementary Table 2: ARVD/C patients stratified in proband and family members

	Overall (n=71)	Proband (n=44)	Family member (n=27)	p-value
Male	41 (58)	33/44 (75)	8/27 (30)	<0.001
Age at presentation (years)	42.4 ± 15.7	42.7 ± 15.2	42.0 ± 16.8	0.857
Age at CMR (years)	46.4 ± 15.8	47.3 ± 16.3	45.0 ± 15.2	0.547
ICD present	42 (60)	29 (66)	18 (66)	0.948
Diabetes	2 (4)	(5)	0 (0)	0.261
Hypertension	4 (6)	4 (9)	0 (0)	0.107
Obesity	7/60 (12)	3/36 (8)	4/24 (17)	0.325
CMR parameters				
<i>Ventricular</i>				
LV EF	54.3 ± 8.7	52.9 ± 9.2	56.5 ± 7.6	0.095
LV EDV/BSA	96.0 ± 19.4	98.4 ± 20.7	93.8 ± 17.1	0.351
RV EF	39.2 ± 10.4	35.8 ± 9.9	44.7 ± 8.7	<0.001
RV EDV/BSA	124.6 ± 39.1	136.6 ± 107.6	107.6 ± 33.2	0.003
<i>Atrial</i>				
LA ALEF	55.8 ± 12.8	54.1 ± 14.2	58.5 ± 9.7	0.163
LA EDV/BSA	48.3 ± 14.9	47.8 ± 15.9	49.1 ± 13.2	0.722
RA ALEF	41.9 ± 12.7	39.9 ± 11.0	45.3 ± 11.0	0.084
RA EDV/BSA	47.2 ± 23.2	53.3 ± 25.0	36.9 ± 14.9	0.004
Disease course				
Duration of follow-up (years)	7.9 ± 6.3	8.8 ± 7.2	6.5 ± 4.4	0.139
Sustained ventricular arrhythmia	37 (52)	34 (77)	3 (11)	<0.001
Atrial Arrhythmias	19/71 (27)	15 (34)	4 (15)	0.075
Heart failure	2 (3)	2 (5)	0 (0)	0.261
Transplant	0 (0)	0 (0)	0 (0)	-
Death	3 (4)	3 (7)	0 (0)	0.166*

Mean values ± standard deviation; number (%); *Fisher exact test;

Abbreviations: AA= atrial arrhythmias; ICD= implantable cardioverter defibrillator;

CHAPTER 10

Atrial Dysfunction in Arrhythmogenic Right Ventricular Cardiomyopathy

Mimount Bourfiss, BS*;
Tarek Zghaib, MD*;
Jeroen van der Heijden, MD, PhD;
Peter Loh, MD, PhD;
Richard Hauer, MD, PhD;
Harikrishna Tandri, MD;
Hugh Calkins, MD;
Saman Nazarian, MD, PhD;
Anneline Te Riele, MD, PhD;
Stefan L. Zimmerman, MD§;
Birgitta Velthuis, MD, PhD§

*Shared first authorship

§ Shared last authorship

ABSTRACT

Background: Arrhythmogenic Right Ventricular Cardiomyopathy (ARVC) is associated with mutations in desmosomes. While desmosomes are ubiquitously expressed in all heart chambers, evidence for direct atrial involvement in ARVC remains limited and few studies have characterized atrial arrhythmias (AA) in ARVC.

Objective: We aimed to characterize atrial involvement in ARVC using functional Cardiac Magnetic Resonance (CMR), define the extent of atrial size and function variation attributable to ventricular structural/functional variables, and identify CMR-based predictors of AA in ARVC.

Methods: We analyzed cine-CMR images of 66 definite ARVC patients without a history of AA or severe heart failure (NYHA \geq 3) and 24 healthy control participants. Using tissue-tracking, we evaluated phasic bi-atrial volumes, ejection fractions (EF), peak longitudinal-strain and strain rates (SR). The primary outcome was the occurrence of AA during a median follow-up of 6.8[3.0-10.8] years.

Results: Compared to controls, ARVC patients had higher bi-atrial volumes, lower RA passive-EF, lower peak RA-longitudinal strain, lower systolic and early RA-diastolic SR and lower systolic LA-SR ($p < 0.05$). Although worsening in left and right ventricular size and function was associated with increased bi-atrial volumes and decreased function, variation in atrial parameters was only partially explained by ventricular changes (r^2 ranged from 5-29%). On multivariable analysis, higher atrial volumes (10% increased risk per mL for both RAV_{min} and LAV_{min} , $p < 0.05$), decreased LA reservoir function ($LAEF_{total}$ and LA-PLAS) and decreased RA conduit function ($RAEF_{passive}$ and $RA-SR_{ed}$) were predictors of increased risk of AA during follow-up.

Conclusion: ARVC is characterized by enlarged atria with decreased function as examined on functional CMR, which is only partially explained by ventricular changes. RA and LA parameters predict incident AA after adjusting for clinical and ventricular characteristics, which suggests primary atrial involvement in ARVC.

INTRODUCTION

Arrhythmogenic Right Ventricular Cardiomyopathy (ARVC) is an inheritable heart-muscle disorder that predominantly affects the right ventricle and is one of the leading causes of arrhythmic cardiac arrest in young people and athletes¹. Progressive loss of right ventricular myocardium and its replacement by fibrofatty tissue is the pathological hallmark of the disease². ARVC is predominantly characterized as a disease of the cardiac desmosome, which is a complex of structural proteins providing mechanical support to myocytes³. Despite desmosomes being found throughout the cardiac system, including the atria, evidence for direct atrial involvement with ARVC remains limited. Animal studies showed fibrofatty replacement of atrial myocardium in 17% of cat ARVC models⁴ and in 35% of dog ARVC models⁴; and Platonov *et al.* has demonstrated evidence for altered electrical conduction within the atria of ARVC patients⁵. However, few studies have focused on atrial arrhythmias (AA) such as atrial fibrillation and atrial flutter in patients with ARVC, despite its higher incidence compared to the general population^{6,7}. A recent study by Mazzanti *et al.* brought to light the important prognostic value of AA on incident life-threatening arrhythmias and cardiovascular mortality in this patient population⁸. In a previous study, we identified genotype-specific differences in atrial volumes using cardiac magnetic resonance imaging (CMR) in a large cohort of ARVC patients, suggesting presence of primary atrial involvement in ARVC⁹. This prior work included conventional CMR analyses, which may be less sensitive to subtle atrial functional changes, and did not specifically evaluate atrial involvement in the context of ventricular dysfunction. Recent advances in CMR-based tissue-tracking techniques allow in-depth structural and functional characterization of the atria^{10,11}. The feasibility and reproducibility of CMR-based tissue-tracking to analyze multiple atrial parameters, including atrial dimensions, function and deformation have been shown in several previous studies¹²⁻¹⁴. We hypothesized that structural and functional abnormalities in the atria may be observed using tissue-tracking CMR in ARVC patients free of clinically-manifest AA and heart failure, and that early atrial involvement in ARVC occurs concomitantly with ventricular dysfunction and is not merely its consequence.

In a large prospective cohort of ARVC patients without AA and overt heart failure at baseline, we aim (1) to characterize atrial involvement in ARVC patients compared to controls; (2) to explore the degree to which variation in atrial structural and functional parameters are associated with ventricular involvement; and (3) to detect predictors of AA in ARVC patients using CMR tissue tracking techniques.

METHODS

Study Population

This study is a post-hoc analysis of our recently described patient population⁹. We included 71 participants who fulfilled the 2010 diagnostic Task Force Criteria (TFC) for ARVC¹⁵ and underwent both CMR and molecular genetic analyses. The genetic analysis in all probands included desmosomal (encoding plakophilin-2 (*PKP2*), desmoplakin (*DSP*), plakoglobin (*JUP*), desmoglein-2 (*DSG2*), desmocollin-2 (*DSC2*)), and nondesmosomal genes (phospholamban (*PLN*) and transmembrane protein-43 (*TMEM43*)). ARVC patients who had AA prior to CMR (n=3) and those who had overt congestive heart failure (NYHA functional classification ≥ 3) (n=2) were excluded. As such, the final study population consisted of 66 definite ARVC patients identified from the University Medical Center ARVC registry in Utrecht, the Netherlands. As a control group, we included 24 individuals with no identifiable cardiovascular disease after a comprehensive clinical evaluation at the Center of Excellence for ARVC and Complex Ventricular Arrhythmias of the Johns Hopkins Hospital (Baltimore, USA). The study was approved by the local institutional review boards and all patients provided written consent.

CMR Acquisition

Cine CMR images were acquired on a 1.5T MRI scanner (Achieva, Philips [ARVC patients] and Avanto, Siemens Medical Imaging [control participants]). In short, we performed ECG-gated breathhold steady-state-free-precession (SSFP) cine images (2-chamber right (RV) and left ventricle (LV), left and right ventricular outflow tract and stacks of 4-chamber and short-axis images for complete atrial and ventricular coverage), axial T1-weighted black-blood images, quantitative flow-measurement using phase contrast through plane velocity mapping over the tricuspid and pulmonary valves, and phase-sensitive inversion recovery late gadolinium-enhancement images⁸.

CMR Analysis

Atrial Analysis

We utilized Multimodality Tissue Tracking software (MTT; version 6.0, Toshiba, Japan) to measure phasic left atrial (LA) and right atrial (RA) volumes, strain and strain rate using 4-chamber and 2-chamber cine images. As previously described for LA functional analysis¹⁰, we manually contoured myocardial borders as seen in **Figure 1**. The trabecular region of the RA appendage, which results in poor tracking, was excluded from analysis. In line with the previously reported approach for pulmonary veins and LA appendage⁹. Pixel features were tracked automatically throughout systole, early and late diastole. Manual adjustments were performed when tracking was suboptimal. After confirming accurate tracking, global RA and LA peak longitudinal strain and strain rate curves were generated automatically by averaging strain and strain rate measurements in all segments. Peak longitudinal atrial

strain (PLAS), peak systolic strain rate (SR_s), peak early-diastolic strain rate (SR_{ed}) and peak late-diastolic strain rate (SR_{ld}) were calculated as shown in **Figure 2**. The SR_{ed} and SR_{ld} are negative values by convention and were presented as absolute values in this manuscript. Phasic volume curves were generated to identify maximum, pre-contraction, and minimum atrial volumes as shown in **Figure 2**. RA and LA volumes (RAV and LAV) were indexed for the body surface area (BSA) as calculated by the DuBois formula. Total, passive and active atrial emptying fractions were measured using the following calculations:

- Total atrial emptying fraction: $100 \times (\text{atrial maximum volume} - \text{atrial minimum volume}) / \text{atrial maximum volume}$
- Passive atrial emptying fraction: $100 \times (\text{atrial maximum volume} - \text{atrial pre-contraction volume}) / \text{atrial maximum volume}$
- Active atrial emptying fraction $100 \times (\text{atrial pre-contraction volume} - \text{atrial minimum volume}) / \text{atrial pre-contraction volume}$

The PLAS, SR_s and total emptying fraction represent atrial reservoir function; passive emptying fraction and SR_{ed} represent atrial conduit function, SR_{ld} and active emptying fraction represent atrial pump function.

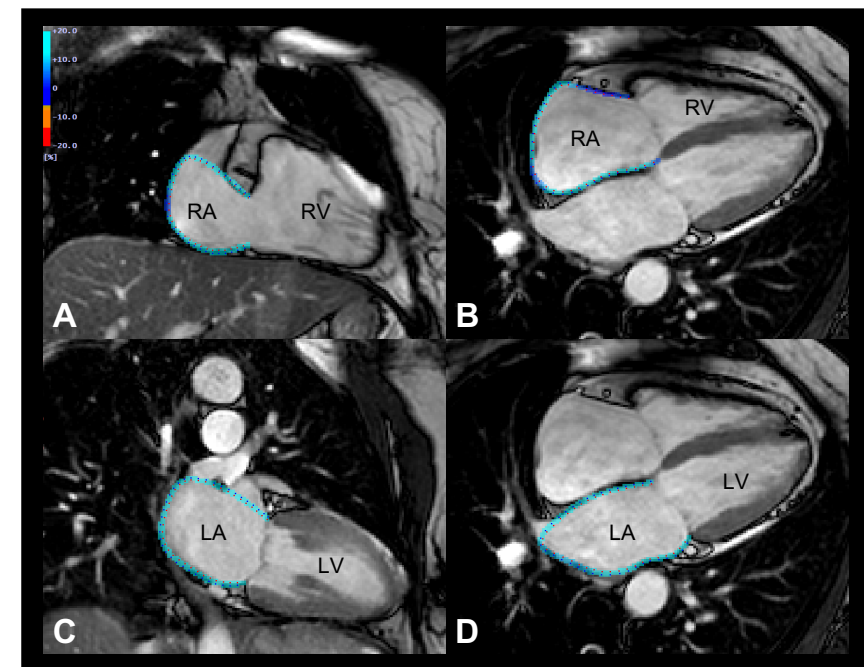


Figure 1: To measure phasic left and right atrial volumes, strain and strain rate, 2-chamber (**A** and **C**) and 4-chamber (**B** and **D**) cine images were used and both endocardial and epicardial contours were manually drawn as displayed. LA= left atrium; RA= right atrium; LV= left ventricle; RV= right ventricle.

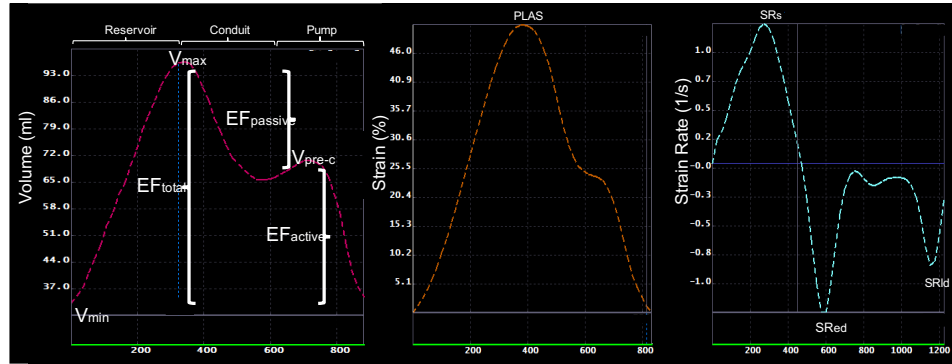


Figure 2: Phasic volume curves were automatically generated, and were utilized to identify maximum (V_{max}), pre-contraction (V_{pre-c}), and minimum (V_{min}) atrial volumes as shown and to calculate total, passive and active atrial ejection fractions (EF) characterizing different phases of the atrial cycle (reservoir, conduit and pump). Peak right and left atrial longitudinal strain and strain rate curves were generated automatically by averaging strain and strain rate measurements in all segments. Peak longitudinal atrial strain (PLAS), peak systolic strain rate (SR_s), peak early diastolic strain rate (SR_{ed}) and peak late diastolic strain rate (SR_{ld}) were calculated as shown.

Global ventricular size and function

Ventricular metrics and ejection fraction (EF) were measured using semi-automated contour tracing software (View Forum cardiac package version R5.1V1L2.SP3, Phillips). Ventricular end-diastolic (EDV) and end-systolic volumes (ESV) were indexed for BSA.

Atrial Arrhythmias

The diagnosis of ARVC was based on the 2010 revised TFC¹⁵. ARVC was diagnosed when ≥ 4 TFC points from different categories were fulfilled; thus 2 major, 1 major plus 2 minor, or 4 minor criteria sufficed for a definite ARVC diagnosis. The primary outcome of this study was the occurrence of at least 1 episode of AA (AF or AFI) lasting ≥ 30 seconds. This was recorded by 12-lead ECG, Holter monitoring or implantable cardioverter defibrillator (ICD) interrogation during clinical follow-up at the discretion of the managing physician.

Statistical Analysis

Continuous and discrete data are presented as mean (\pm SD) and n (%), respectively. Continuous data comparison of two groups were performed using Student's t-test/Rank Sum test. Correlation between atrial and ventricular parameters was analyzed by linear regression. Multivariable Cox proportional-hazards models were used to determine the association with incident atrial arrhythmias during follow-up. To avoid co-linearity, correlations between continuous variables were tested using the Pearson's Correlation Coefficient before fitting any 2 independent variables in the same model. Among the pool of co-linear variables ($r > 0.50$), the parameters with the strongest association with the outcome

were selected for inclusion in the model. A separate Cox Proportional Hazards multivariable model was constructed for each RA/LA functional and structural parameter. To ensure our results are not affected by over-fitting we performed two multivariable analyses as follows: Model 1 was adjusted for age at MRI and number of TFC; while Model 2 was adjusted for age, gender, hypertension, body surface area, number of TFC as well as LV/RV EDV_i and EF. Two-sided p-values less < 0.05 were considered statistically significant. Statistical analysis was performed using STATA software (version 13, StataCorp, College Station, TX, USA).

RESULTS

Study Population Characteristics

We included 66 patients with definite ARVC and 24 control participants with structurally normal hearts. Overall, 58% of ARVC patients and 63% of control participants were male with a mean age of 46.3 ± 15.7 and 38.2 ± 15.8 years, respectively. As seen in **Table 1**, there were no significant differences between ARVC patients and controls in gender ($p=0.887$), age ($p=0.104$), and BSA ($p=0.650$). The distribution of the TFC in the ARVC patients is described in **Table 1**.

CMR Analysis

CMR structural and functional ventricular and atrial measurements of the study participants are summarized in **Table 2**. Comparison between ARVC patients and control participants are also displayed in **Figure 3**. As expected, ARVC patients had higher indexed RV volumes (RV-EDV_i) 123.6 ± 38.2 ml/m² and lower RV function (RV-EF) $39.4 \pm 10.3\%$ compared to controls (RV-EDV_i) 81.1 ± 15.3 ml/m² and RV-EF $53.0 \pm 7.9\%$ respectively ($p < 0.0001$). Compared to controls, ARVC patients had significantly higher atrial volumes at all stages of the cardiac cycle ($p < 0.0001$ for all comparisons). As for functional parameters, ARVC patients had significantly lower RA conduit function (passive-EF [RAEF_{passive}]) and SR_{ed} , RA reservoir function (RA-PLAS and SR_s), and lower LA- SR_s ($p < 0.05$ for all comparisons).

Proportion of Atrial Measurements Attributable to Ventricular Parameters

To determine the extent of atrial anatomical and functional impairment attributable to a primary effect of ARVC as opposed to secondary to ventricular dysfunction, we modeled ventricular and atrial functional and structural parameters as displayed in **Supplemental Table 1**. Increased RV-EDV_i and RV-ESV_i were significantly associated with increased RA volumes and decreased RA and LA function. Similarly, decreased RV-EF was associated with increased RA volumes and decreased RA and LA function. Increased LV volume was associated with increased bi-atrial volumes and decreased bi-atrial strain rates. LV-EF was directly related to left and right atrial strain and strain rates. As seen in **Supplemental Table 1**, the coefficient of determination r^2 for these associations ranged from 5-29%. This

indicates that the proportion of variance in atrial volumes and function that is attributable to variability in ventricular parameters is much lower than that expected if atrial remodeling was a function of ventricular disease.

Table 1: Study Population Characteristics

	ARVC patients (n=66)	Controls (n=24)	P-value
Clinical Characteristics			
Male Gender	38 (58%)	15 (63%)	0.887
Age at CMR	46.2±16.0	38.2±15.8	0.104
BSA	1.9±0.2	1.8±0.2	0.650
Congestive Heart Failure	2 (3%)	0 (0%)	0.391
Hypertension	4 (6%)	0 (0%)	0.220
Diabetes	2 (3%)	0 (0%)	0.391
Genotype			
PKP2 (Desmosomal)	36 (55%)	N/A	
PLN (Non-Desmosomal)	12 (18%)		
No Mutation Identified	18 (27%)		
Clinical Phenotype			
Number of TFC	6.2±1.7	N/A	
Repolarization TFC			
Major	28 (42%)		
Minor	16 (24%)		
Depolarization TFC			
Major	6 (9%)		
Minor	48 (73%)		
Arrhythmia TFC			
Major	26 (39%)		
Minor	60 (91%)		
Structural TFC			
Major	54 (82%)		
Minor	5 (8%)		
Family History TFC			
Major	43 (65%)		
Minor	3 (5%)		
Outcomes (Follow-up of 6.8[IQR 3.0-10.8] years)			
Atrial Arrhythmias	14 (21%)	N/A	
Age at First Atrial Arrhythmias	55.7±17.2		
Heart Transplant	0 (0%)		
Death	3 (5%)		

ARVC= Arrhythmogenic Right Ventricular Cardiomyopathy; CMR= cardiac magnetic resonance; BSA= body surface; PKP2= plakophilin-2; PLN= phospholamben; TFC: task force criteria.

Table 2: Structural and functional left and right atrial measurements in study participants comparing ARVC patients and healthy controls.

Genotype	ARVC (n=66)	Controls (n=24)	p-value
Right atrial parameters			
RAVmax(i)	43.5±13.6	29.5±7.5	<0.0001
RAVpre(i)	34.6±11.5	22.4±6.8	<0.0001
RAVmin(i)	21.3±7.7	13.5±4.5	<0.0001
RAEFpassive	19.4±9.1	24.4±10.0	0.029
RAEFactive	39.3±10.0	39.3±8.9	0.982
RAEFtotal	51.1±10.1	53.8±10.5	0.266
Peak Long Strain	53.5±19.2	63.6±23.4	0.043
SRsys	2.1±0.8	2.9±1.2	0.001
SRearly	1.7±1.0	3.1±1.5	<0.0001
SRLate	2.1±1.1	2.6±0.9	0.11
Left atrial parameters			
LAVmax(i)	42.6±11.6	31.4±6.3	<0.0001
LAVpre(i)	30.5±9.7	22.1±4.8	0.0001
LAVmin(i)	19.2±7.7	13.5±3.2	0.0007
LAEFpassive	29.0±7.7	29.2±8.9	0.934
LAEFactive	37.9±7.5	37.1±8.4	0.743
LAEFtotal	55.7±8.3	56.2±9.3	0.809
Peak Long Strain	35.6±9.9	39.2±12.3	0.165
SRsys	1.4±0.5	1.8±0.5	0.003
SRearly	1.7±0.8	2.0±0.9	0.154
SRLate	1.6±0.6	1.6±0.7	0.102
Ventricular parameters			
LV-EF	54.8±7.9	64.9±5.7	<0.0001
LV-EDV(i)	96.0±19.3	81.4±18.1	0.001
LV-ESV(i)	45.9±20.8	28.4±7.9	<0.0001
RV-EF	39.4±10.3	53.0±7.9	<0.0001
RV-EDV(i)	123.6±38.2	81.1±15.3	<0.0001
RV-ESV(i)	77.6±34.4	37.9±8.5	<0.0001

Mean values ± standard deviation. RA= right atrial, RAVmax(i)= maximum right atrial volume index (mm³/m²); RAVpre(i)= pre-atrial volume (mm³/m²); RAVmin(i)= minimum right atrial volume index (mm³/m²); EF= ejection fraction (%), PLAS= peak longitudinal atrial strain (%), SRsys= systolic strain rate (absolute value), SREd= early diastolic strain rate (absolute value), SRLd= late diastolic strain rate (absolute value), LA= left atrial.

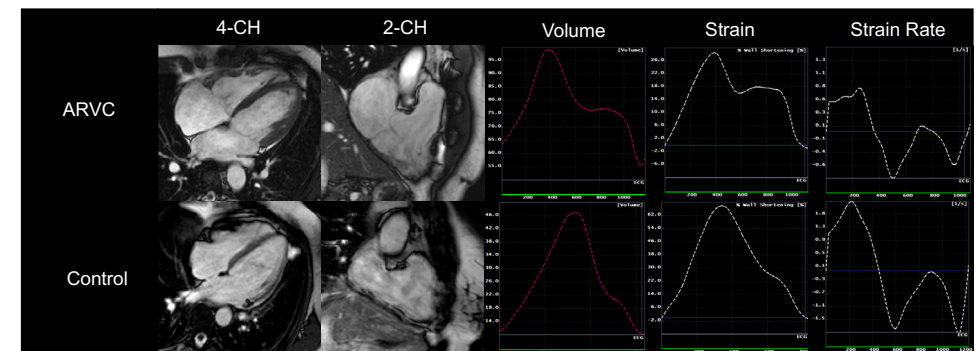


Figure 3: This figure displays differences in right atrial volume, strain and strain-rate curves between a patient with ARVC (top panel), and a healthy control (bottom panel).

Atrial Arrhythmias

Among the 66 ARVC patients, 14 (21%) individuals experienced one or more types of AA during a median follow-up of 6.8[IQR 3.0-10.8] years. In 7/14 patients, the first AA episode was recorded by 12-lead ECG (after complaints of the patient), in 6/14 by ICD interrogation (2 discovered after inappropriate ICD intervention) and in 1 with 24-hour Holter monitoring. Clinical characteristics of arrhythmias in this cohort were previously described by our group⁹. Briefly, atrial fibrillation was the most common type of arrhythmia occurring in 11(79%) patients, atrial flutter occurred in 2(14%), and 1(7%) patient experienced both types of AA. Median age at first AA was 57.3[IQR 42.0-67.4] years. Compared to those without AA, patients with arrhythmias were more likely to be male (81% vs. 50%, $p=0.027$), and present with ARVC at an older age (48.9±16.9 years vs. 40.1±14.8 years, $p=0.036$).

Table 3 compares CMR structural and functional atrial and ventricular measurements in ARVC patients with and without subsequent AA. Patients who developed AA were found to have significantly higher RAVmin(i) at baseline compared to patients who did not develop AA (25.2±5.3 vs. 20.1±7.9ml/m², respectively; $p=0.029$) and comparable RA volumes otherwise ($p>0.05$). Difference in RA function at baseline between the two groups was more striking as patients who developed AA were found to have lower RA-EF in all its components (passive, active and total, $p<0.05$ for all comparisons), lower RA-PLAS (43.7±8.2 vs. 56.3±20.6, $p=0.029$), lower RA-SR_{ed} (1.2±0.5 vs. 1.9±1.1, $p=0.020$) and lower RA-SR_s (1.7±0.7 vs. 2.2±0.9, $p=0.05$). LA volume was not different between the two groups ($p>0.05$ for all comparisons). Passive LA-EF was significantly lower in those who developed AA (25.4±9.2 vs. 30.0±7.0), as was the LA-PLAS (30.2±10.9 vs. 37.1±9.1, $p=0.018$) and LA-SR_s (1.1±0.5 vs. 1.5±0.5, $p=0.038$). There was a trend for lower LA-EF_{total} and LA-SR_{ed} in patients with subsequent AAs. With regards to RV parameters, indexed EDV (140.4±33.5 vs. 119.1±38.5ml/m², $p=0.033$) and ESV (93.9±30.7 vs. 73.3±34.4ml/m², $p=0.025$) were higher in patients with incident AAs compared to those without. Although not significant, a trend of lower RV-EF in the patient group with AA was seen compared to without AA (35.5±8.1 vs. 40.5±10.6%, $p=0.063$). No differences were found in left ventricular volumes and function.

Table 4 summarizes univariable and multivariable Cox regression analyses performed to predict subsequent AAs in our cohort. Co-linear atrial parameters were excluded from the model if Pearson's coefficient >0.50 as described in the methods. Since indexed-RA volumetric parameters were highly co-linear, only RAV_{min} (which had the strongest association with the outcome) was included in the multivariable analysis. Similarly, as all RA-EF parameters (total, active and passive) were co-linear. Only RAEF_{passive} was selected. RA-SR_{ed} was selected for strain measurement, as RA-PLAS, RA-SR_s and RA-SR_{ed} were co-linear. A similar co-linearity screening was performed for LA (LAV_{min}, LAEF_{total} and LA-PLAS were selected). As seen in **Table 4**, all of RAV_{min}, RAEF_{passive}, RA-SR_{ed}, LAV_{min}, LAEF_{total} and LA-PLAS were significant predictors of the outcome in both Model 1 (adjusted for age at MRI and

number of TFC) and Model 2 (adjusted for age, gender, hypertension, body surface area, number of TFC as well as LV/RV EDV_i and EF). In fact, higher atrial volumes (10% increased risk per mL for both RAV_{min} and LAV_{min}, $p<0.05$) were associated with increased risk of AA during follow-up. Moreover, decreased LA reservoir function (LAEF_{total} and LA-PLAS) and RA conduit function (RAEF_{passive} and RA-SR_{ed}) were associated with increased risk of AA during follow-up. **Figure 4** displays Kaplan-Meier survival curves stratified by the median value for RAV_{min}, RAEF_{passive}, RA-SR_{ed}, LAV_{min}, LAEF_{total} and LA-PLAS ($p<0.05$ on log-rank test for all comparisons).

Table 3: Comparison of structural and functional atrial and ventricular measurements in ARVC patients with and without subsequent AA.

	Overall (n=66)	AA (n=14)	No AA (n=52)	p-value
Right atrial parameters				
RAVmax(i)	43.5±13.6	46.4±12.4	42.7±14.0	0.356
RAVpre(i)	34.6±11.5	39.2±10.5	33.2±11.7	0.092
RAVmin(i)	21.3±7.7	25.2±5.3	20.1±7.9	0.029
RAEFpassive	19.4±9.1	15.2±7.0	20.6±9.4	0.047
RAEFactive	39.3±10.0	34.3±10.5	40.7±9.5	0.033
RAEFtotal	51.1±10.1	44.1±11.0	53.1±8.9	0.003
Peak Long Strain	53.5±19.2	43.7±8.2	56.3±20.6	0.029
SRsys	2.1±0.8	1.7±0.7	2.2±0.9	0.05
SRearly	1.7±1.0	1.2±0.5	1.9±1.1	0.02
SRlate	2.1±1.1	2.2±0.7	2.1±1.2	0.912
Left atrial parameters				
LAVmax(i)	42.6±11.6	41.5±12.3	42.9±11.5	0.691
LAVpre(i)	30.5±9.7	31.6±12.4	30.2±9.0	0.63
LAVmin(i)	19.2±7.7	20.9±11.5	18.8±6.3	0.353
LAEFpassive	29.0±7.7	25.4±9.2	30.0±7.0	0.044
LAEFactive	37.9±7.5	36.7±11.0	38.2±6.3	0.513
LAEFtotal	55.7±8.3	52.2±13.1	56.7±6.4	0.071
Peak Long Strain	35.6±9.9	30.2±10.9	37.1±9.1	0.018
SRsys	1.4±0.5	1.1±0.5	1.5±0.5	0.038
SRearly	1.7±0.8	1.3±0.5	1.8±0.9	0.055
SRlate	1.6±0.6	1.5±0.6	1.7±0.6	0.362
Ventricular parameters				
LV-EF	54.8±7.9	57.4±7.2	54.1±8.0	0.162
LV-EDV(i)	96.0±19.3	93.5±12.8	96.7±20.7	0.604
LV-ESV(i)	45.9±20.8	50.2±35.2	44.7±15.3	0.406
RV-EF	39.4±10.3	35.5±8.1	40.5±10.6	0.104
RV-EDV(i)	123.6±38.2	140.4±33.5	119.1±38.5	0.075
RV-ESV(i)	77.6±34.4	93.9±30.7	73.3±34.4	0.055

Mean values ± standard deviation. AA= atrial arrhythmia; RA= right atrial, RAVmax(i)= maximum right atrial volume index (mm³/m²); RAVpre(i)= pre-atrial volume (mm³/m²); RAVmin(i)= minimum right atrial volume index (mm³/m²); EF= ejection fraction (%), PLAS= peak longitudinal atrial strain (%), SR_s= systolic strain rate (absolute value), SR_{ed}= early diastolic strain rate (absolute value), SR_{ld}= late diastolic strain rate (absolute value), LA= left atrial.

Table 4: Univariable and multivariable Cox regression analyses to predict subsequent AA in the study cohort. Each row represents a separate multivariable model for each parameter. Model 1 was adjusted for number of TFC and age at MRI. Model 2 was adjusted for age at MRI, gender, hypertension, body surface area, number of TFC, RV/LV end diastolic volume index and ejection fraction.

	Univariate		Multivariable Model 1			Multivariable Model 2		
	HR	p-value	HR	[95% CI]	p-value	HR	[95% CI]	p-value
RAVmin(i)	1.08	0.013	1.10	[1.02-1.18]	0.019	1.10	[1.01-1.21]	0.026
RAEFpassive	0.89	0.006	0.88	[0.80-0.97]	0.013	0.86	[0.75-0.98]	0.029
RA-SR _{ed}	0.37	0.01	0.31	[0.10-0.92]	0.035	0.19	[0.04-0.84]	0.028
LAVmin(i)	1.09	0.02	1.08	[1.01-1.18]	0.043	1.10	[1.02-1.19]	0.023
LAEFtotal	0.89	0.002	0.92	[0.85-0.99]	0.037	0.91	[0.84-0.99]	0.033
LA-PLAS	0.88	0.004	0.90	[0.82-0.99]	0.033	0.91	[0.83-0.99]	0.046

RAVmin= minimal right atrial volume; EF= ejection fraction; SR_{ed}= early diastolic strain rate; PLAS= peak longitudinal atrial strain; LAEFtotal= total left atrial ejection fraction; RAEFpassive= passive right atrial ejection fraction; LAVmin= minimal left atrial volume.

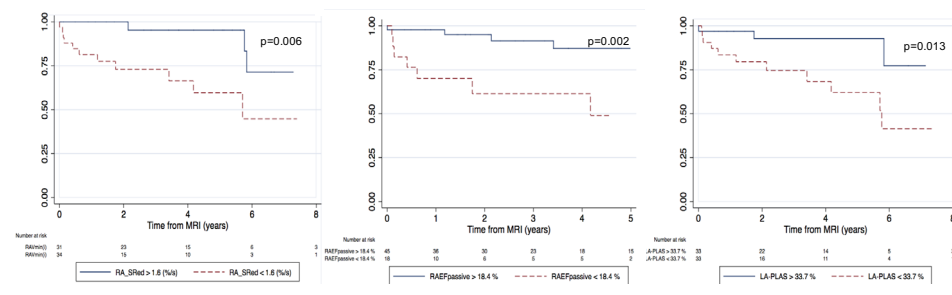


Figure 4: Kaplan-Meier curves displaying atrial arrhythmia-free survival rates stratified by the median values for minimal right atrial volume (RAV_{min}), right atrial passive ejection fraction (RAEF_{passive}), right atrial early diastolic strain rate (RA-SR_{ed}), minimal left atrial volume (LAV_{min}), left atrial total ejection fraction (LAEF_{total}), left atrial peak longitudinal strain (LA-PLAS). Log-rank test was significant for all comparisons (p<0.05).

DISCUSSION

We investigated atrial involvement with ARVC in a large cohort of patients using functional-CMR imaging. This study has three major findings. Firstly, compared to controls, ARVC patients had significantly higher bi-atrial volumes, lower RA passive ejection fraction (conduit function), peak longitudinal RA strain, systolic and early RA diastolic strain rates as well as lower LA systolic strain rate. Secondly, although worsening in RV and LV phenotypes was associated with increased bi-atrial volumes and decreased function, the variation in atrial parameters was only partially explained by ventricular changes suggesting a primary atrial involvement in ARVC. Lastly, patients with subsequent AA during follow-up were found to exhibit lower RA and LA function. On multivariable analysis, higher bi-atrial volumes, as well as decreased LA reservoir function (LAEF_{total} and LA-PLAS) and RA conduit function (RAEF_{passive} and RA-SR_{ed}) were associated with increased risk of AA during follow-up.

Atrial Involvement in ARVC

Previous studies examining atrial structure and function in ARVC are scarce. In concordance with our results, Yoerger *et al* examined echocardiographic structural markers in 29 ARVC patients and found increased RA dimensions compared to age, gender, and body size-matched controls¹⁶. In a cohort of 70 ARVC patients, Saguner *et al*. reported RA and LA enlargement on echocardiography in 26% and 14% of patients, respectively. On adjusted analysis, RA short-axis diameter was an independent predictor of major adverse cardiovascular outcome during follow-up¹⁷. In a cohort of 210 patients, Camm *et al*. showed echocardiographic evidence of right and left atrial enlargement in 32% and 15% respectively⁶. In contrast, Platonov *et al*. showed no atrial enlargement in 40 patients with ARVC by echocardiography⁴. Interpretation of these results is challenging due to the known limitations of atrial dimension measurements on echocardiography. Also, LA enlargement is a known effect of AF¹⁶, which suggests that the structural changes seen in previous studies may be a consequence of AA rather than a causative factor. Interestingly, Bourfiss *et al*. found genotype-specific patterns of volumetric changes in ARVC⁹. Significantly larger atria were found in patients with no mutation identified and significantly smaller atria in *PKP2* mutation carriers, compared to controls with idiopathic RVOT tachycardia. To our knowledge, our study is the first to use the capabilities of tissue-tracking on functional-CMR to characterize atrial size and function in a large cohort of ARVC patients free of overt heart failure and any history of AA at baseline. Our results show that compared to age-, gender-, and body size-matched healthy controls, ARVC patients had remarkably enlarged atria, at all stages of the cardiac cycle. Furthermore, ARVC patients had significantly stiffer and a poorly contractile RA compared to controls (lower RA passive ejection fraction and early diastolic strain rate [atrial conduit function], as well as lower RA peak longitudinal atrial strain and systolic strain rate [atrial reservoir function]). This cross-sectional analysis clearly points to primary atrial involvement in ARVC as our patients were free of overt heart failure as well as any history of AA at the time of the scan.

We aimed at examining whether AA are secondary to ventricular dysfunction or a primary result of atrial involvement in the disease. Camm *et al*. showed no statistically significant difference between the rate of left ventricular enlargement in those with left atrial enlargement (3/12 [25.0%]) and those without (2/21 [9.5%]) (P = .233) in 248 patients with ARVC. In addition, left ventricular ejection fractions were similar between those with left atrial enlargement (54.7%, SD = 8.1%, n = 13) and those without (54.7%, SD = 10.8%, n = 21) (P = .994)⁷. In their study, Camm *et al*. rely solely on echocardiographic reports to detect atrio-ventricular enlargement. Results may thus be influenced by variability in measurements between different echocardiographers. Our results show that, on linear regression analysis, increased RV and LV volumes were associated with increased atrial volumes and decreased atrial function assessed on CMR. Similarly, decreased RV and LV function was associated with increased atrial volumes and decreased atrial function. However, the coefficient of

determination r^2 for these linear associations ranged from 5-29% indicating that the proportion of variance in atrial volumes and function that is predictable from ventricular parameters is much lower than that expected if atrial remodeling was uniquely attributed to ventricular disease.

Atrial Arrhythmias in ARVC

The higher incidence of AA in ARVC was reported early in the characterization of the disease. Incidence rate of AA in previous studies ranges from 14% (without ICD) to 42% (with ICD)^{7,18-20}. The negative prognostic implications of AA on mortality and morbidity in ARVC have also been reported. In 301 consecutive patients with ARVC, history of AF was associated with a 4-fold increase in the occurrence of life-threatening arrhythmic events defined as sudden cardiac death, aborted cardiac arrest, syncopal VT or electrical storm, or cardiovascular mortality⁸. Camm *et al.* reported that 35 (14%) of patients had AA which received a total of 22 inappropriate shocks and 6 (17%) of these AA were initially diagnosed following an inappropriate ICD shock. Patients with AA had increased prevalence of mortality and heart failure compared to patients without AA⁷. Similarly, Saguner *et al.* reported an AA incidence of 20% in 90 patients with ARVC. In their study, they reported higher rates of inappropriate shocks, heart transplants and cardiovascular mortality in those with AA²¹. In our cohort, AA occurred in 24% of ARVC patients during follow up. As previously described by our group, the likelihood of experiencing a life-threatening ventricular arrhythmia and inappropriate ICD intervention was significantly higher in patients with AA as were the rates of heart failure and death during follow-up⁹. The implications of AA underlie the importance of detecting baseline predictors of future AA in patients with early ARVC for an appropriate prevention strategy.

Previous studies had reported male gender, increasing age, right and left atrial enlargement, and moderate or severe tricuspid regurgitation as significant predictors of AA^{7,9,21}. By themselves, these common patient characteristics do not warrant increased and potentially invasive monitoring for AA with implanted devices or prolonged Holter monitoring. In this present study, we aimed at characterizing predictors of future AA in a large ARVC cohort free of overt heart failure or history of AA at baseline. On multivariable analysis, higher atrial volumes as well as decreased LA reservoir function (LAEF_{total} and LA-PLAS) and RA conduit function (RAEF_{passive} and RA-SR_{ed}) were associated with increased risk of AA during follow-up. Therefore, atrial structural and functional parameters are important predictors of AA independent from the overall disease severity as assessed by clinical presentation and ventricular phenotype. This supports the hypothesis that atrial involvement in ARVC occurs independently from ventricular disease and AA are the direct clinical manifestations of such atrial remodeling.

Clinical Implication

Uncovering atrial involvement in ARVC gives important mechanistic insight into the disease and its natural progression. ARVC patients with AF may have higher propensity towards embolic cerebro-vascular accidents by virtue of their fibrillatory atria. Most ARVC patients get early CMR study for diagnosis/classification; therefore, this opportunity to characterize atrial dysfunction in the pre-AF stage may offer an opportunity for stroke prevention (although further studies are needed to show the benefit of such prophylaxis). Increased risk of AAs dictates proper ICD programming and device selection. Indeed, potential overlap of ventricular rates with AAs and VTs requires careful device programming to minimize risk of inappropriate ICD shocks. A lower threshold for atrial lead insertion to increase device diagnostic capabilities and accuracy may be warranted in patients who are found to have early atrial remodeling on functional-CMR.

Limitations

ARVC is a rare disease and as such, our study has a small sample size. Our results need to be validated in a large prospective study with longitudinal imaging data. In this study, most AA were detected on ambulatory ECG, with a minority detected on ICD and Holter-monitoring. Other studies have reported that a large proportion of atrial arrhythmias were diagnosed on implanted devices (both during routine follow-up and as a result of inappropriate shocks) and Holter monitors. This suggests that many atrial arrhythmias in our population may be concealed. As mentioned previously, the link between AA and poor outcomes has been shown in previous studies.

As such, the examination of prognostic value of atrial functional parameters, which predict AA, on VT/VF/mortality would be interesting to explore. However, we did not have the appropriate data to perform such prospective analysis.

CONCLUSION

ARVC is characterized by enlarged atria with decreased function as examined on functional-CMR, which is only partially explained by ventricular changes. RA and LA parameters predict incident AA after adjusting for clinical and ventricular characteristics. This suggests primary atrial involvement in ARVC and points to the potential of CMR-based atrial analysis for prognostication of future AA that could allow implementation of strategies to reduce subsequent morbidity and mortality.

REFERENCES

- Corrado D, Link MS, Calkins H. Arrhythmogenic Right Ventricular Cardiomyopathy. *N. Engl. J. Med.* 2017; 376:61–72.
- Thiene G, Nava A, Corrado D, Rossi L, Pennelli N. Right Ventricular Cardiomyopathy and Sudden Death in Young People. *N. Engl. J. Med.* 1988; 318:129–133.
- Cox MGPJ, van der Zwaag PA, van der Werf C, et al. Arrhythmogenic Right Ventricular Dysplasia/Cardiomyopathy: Pathogenic Desmosome Mutations in Index-Patients Predict Outcome of Family Screening: Dutch Arrhythmogenic Right Ventricular Dysplasia/Cardiomyopathy Genotype-Phenotype Follow-Up Study. *Circulation* 2011; 123:2690–2700.
- Platonov PG, Christensen AH, Holmqvist F et al. Abnormal atrial activation is common in patients with arrhythmogenic right ventricular cardiomyopathy. *J Electrocardiol* 2011; 44:237–241
- Fox PR, Maron BJ, Basso C, Liu S-K, Thiene G. Spontaneously Occurring Arrhythmogenic Right Ventricular Cardiomyopathy in the Domestic Cat. *Circulation* 2000;102.
- Chu AF, Zado E, Marchlinski FE. Atrial Arrhythmias in Patients With Arrhythmogenic Right Ventricular Cardiomyopathy/Dysplasia and Ventricular Tachycardia. *Am. J. Cardiol.* 2010; 106:720–722.
- Camm CF, James CA, Tichnell C, et al. Prevalence of atrial arrhythmias in arrhythmogenic right ventricular dysplasia/cardiomyopathy. *Heart Rhythm* 2013; 10:1661–1668.
- Mazzanti A, Ng K, Faragli A, et al. Arrhythmogenic Right Ventricular Cardiomyopathy: Clinical Course and Predictors of Arrhythmic Risk. *J. Am. Coll. Cardiol.* 2016; 68:2540–2550.
- Bourfiss M, Te Riele ASJM, Mast TP, et al. Influence of Genotype on Structural Atrial Abnormalities and Atrial Fibrillation or Flutter in Arrhythmogenic Right Ventricular Dysplasia/Cardiomyopathy. *J. Cardiovasc. Electrophysiol.* 2016; 27:1420–1428.
- Habibi M, Lima JAC, Khurram IM, et al. Association of Left Atrial Function and Left Atrial Enhancement in Patients With Atrial Fibrillation. *Circ. Cardiovasc. Imaging* 2015;8.
- Dodson JA, Neilan TG, Shah R V., et al. Left Atrial Passive Emptying Function Determined by Cardiac Magnetic Resonance Predicts Atrial Fibrillation Recurrence After Pulmonary Vein Isolation. *Circ. Cardiovasc. Imaging* 2014;7.
- Kowallick JT, Kutty S, Edelman F et al. Quantification of left atrial strain and strain rate using Cardiovascular Magnetic Resonance myocardial feature tracking: a feasibility study. *J Cardiovasc Magn Reson.* 2014;16:60.
- Inoue YY, Alissa A, Khurram IM et al. Quantitative Tissue-Tracking Cardiac Magnetic Resonance (CMR) of Left Atrial Deformation and the Risk of Stroke in Patients With Atrial Fibrillation. *J. Am. Heart Assoc.* 2015; 4(4): e001844
- Zareian M, Ciuffo L, Habibi M et al. Left atrial structure and functional quantitation using cardiovascular magnetic resonance and multimodality tissue tracking: validation and reproducibility assessment. *J Cardiovasc Magn Reson.* 2015; 17(1): 52.
- Marcus FI, McKenna WJ, Sherrill D, et al. Diagnosis of arrhythmogenic right ventricular cardiomyopathy/dysplasia: Proposed Modification of the Task Force Criteria. *Eur. Heart J.* 2010; 31:806–814.
- Yoerger DM, Marcus F, Sherrill D, et al. Multidisciplinary study of Right Ventricular Dysplasia Investigators. Echocardiographic findings in patients meeting task force criteria for arrhythmogenic right ventricular dysplasia: new insights from the multidisciplinary study of right ventricular dysplasia. *J. Am. Coll. Cardiol.* 2005; 45:860–865.
- Saguner AM, Vecchiati A, Baldinger SH, et al. Different prognostic value of functional right ventricular parameters in arrhythmogenic right ventricular cardiomyopathy/dysplasia. *Circ. Cardiovasc. Imaging* 2014; 7:230–239.
- Tonet JL, Castro-Miranda R, Iwa T, Poulain F, Frank R, Fontaine GH. Frequency of supra-ventricular tachyarrhythmias in arrhythmogenic right ventricular dysplasia. *Am. J. Cardiol.* 1991; 67:1153.
- Chu AF, Zado E, Marchlinski FE. Atrial Arrhythmias in Patients With Arrhythmogenic Right Ventricular Cardiomyopathy/Dysplasia and Ventricular Tachycardia. *Am. J. Cardiol.* 2010; 106:720–722.
- Brembilla-Perrot B, Jacquemin L, Houplon P, et al. Increased atrial vulnerability in arrhythmogenic right ventricular disease. *Am. Heart J.* 1998; 135:748–754.
- Saguner AM, Ganahl S, Kraus A, et al. Clinical role of atrial arrhythmias in patients with arrhythmogenic right ventricular dysplasia. *Circ. J.* 2014; 78:2854–61.

SUPPLEMENTAL MATERIAL

Supplemental Table 1: Correlation of left and right ventricular to left and right atrial functional and structural parameters.

Coefficient	RV ESV(i)		RV EDV(i)		RV EF		LV ESV(i)		LV EDV(i)		LV EF	
	r ²	p-value	r ²	p-value	r ²	p-value	r ²	p-value	r ²	p-value	r ²	p-value
RAVmax(i)	14%	0.003	15%	0.002	6%	0.048	6%	0.057	15%	0.002	-	NS
RAVmin(i)	0.25	0.021	0.24	0.018	-0.57	0.091	0.16	NS	0.27	0.024	-	NS
RAEFpassive	8%	0.005	9%	0.006	5%	0.021	-	NS	9%	NS	-	NS
RA-SRed	0.17	<0.0001	12%	<0.0001	-0.42	0.002	-	0.077	0.12	NS	-	0.011
RA-SRed	-0.09	0.001	-0.09	0.001	8%	0.002	6%	0.016	-	NS	10%	<0.0001
LAVmax(i)	29%	NS	22%	NS	0.26	NS	6%	NS	-	0.001	10%	NS
LAVmin(i)	-0.02	NS	-0.01	NS	0.05	NS	-0.01	NS	-	0.089	0.04	NS
LAEFpassive	18%	NS	16%	NS	13%	0.043	9%	NS	-	NS	26%	NS
LAEFactive	-0.01	NS	-0.01	NS	0.04	0.041	-0.02	NS	-	NS	0.07	NS
LA-PLAS	-	0.031	-	0.031	-	0.041	-	NS	-	NS	-	0.056
LA-SRed	7%	0.001	7%	0.001	0.18	0.004	-	NS	-	NS	5%	0.001
	-0.06	0.006	-0.06	0.006	0.2	0.002	6%	0.039	-	NS	0.22	0.008
	-0.12	0.018	-0.11	0.018	11%	0.002	-0.13	0.066	-	NS	15%	0.008
	11%	0.018	9%	0.018	13%	0.002	5%	0.066	-	NS	0.45	0.008
	-0.01	0.018	-0.01	0.018	0.03	0.002	-0.01	0.066	-	NS	10%	0.008
											0.03	

RA= right atrial; RAV= right atrial volume; EF= ejection fraction; PLAS= peak longitudinal atrial strain; SRsys= systolic strain rate; SRed= early diastolic strain rate; SRld= late diastolic strain rate; LA= left atrial; LAV= left atrial volume; LV=left ventricular; EDV(i)= end diastolic volume index; ESV(i)= end systolic volume index; RV= right ventricular.

PART IV

Combining CMR and genetics to unravel genotype phenotype correlations



CHAPTER

11

Prevalence and disease
expression of pathogenic
and likely pathogenic variants
associated with inherited
cardiomyopathies in the
general population

Mimount Bourfiss, MD*;
Marion van Vugt, MSc*;
Abdulrahman I. Alasiri, MSc;
Bram Ruijsink, MD, PhD;
Jessica van Setten, MSc, PhD;
Amand F. Schmidt, MSc, PhD;
Dennis Dooijes, PhD;
Esther Puyol-Antón, PhD;
Birgitta K. Velthuis, MD, PhD;
J. Peter van Tintelen, MD, PhD;
Anneline S.J.M. te Riele, MD, PhD;
Annette F. Baas, MD, PhD;
Folkert W. Asselbergs, MD, PhD.
*Shared first authorship

ABSTRACT

Background. Pathogenic and likely pathogenic variants associated with arrhythmogenic right ventricular cardiomyopathy (ARVC), dilated cardiomyopathy (DCM) and hypertrophic cardiomyopathy (HCM) are recommended to be reported as secondary findings in genome sequencing studies. This provides opportunities for early diagnosis, but also fuels uncertainty in variant carriers (G+), since disease penetrance is incomplete. We assessed the prevalence and disease expression of G+ in the general population.

Methods. We identified pathogenic and likely pathogenic variants associated with ARVC, DCM and/or HCM in 200,643 UK Biobank individuals, who underwent whole exome sequencing. We calculated the prevalence of G+ and analysed the frequency of cardiomyopathy/heart failure diagnosis. In undiagnosed individuals, we analysed early signs of disease expression using available electrocardiography and cardiac magnetic resonance imaging data.

Results. We found a prevalence of 1:578, 1:251 and 1:149 for pathogenic and likely pathogenic variants associated with ARVC, DCM and HCM respectively. Compared to controls, cardiovascular mortality was higher in DCM G+ (OR 1.67 [95% CI 1.04;2.59], $p=0.030$), but similar in ARVC and HCM G+ ($p\geq 0.100$). Cardiomyopathy or heart failure diagnosis were more frequent in DCM G+ (OR 3.66 [95% CI 2.24;5.81], $p=4.9\times 10^{-7}$) and HCM G+ (OR 3.03 [95% CI 1.98;4.56], $p=5.8\times 10^{-7}$), but comparable in ARVC G+ ($p=0.172$). In contrast, ARVC G+ had more ventricular arrhythmias ($p=3.3\times 10^{-4}$). In undiagnosed individuals, left ventricular ejection fraction was reduced in DCM G+ ($p=0.009$).

Conclusions. In the general population, pathogenic and likely pathogenic variants associated with ARVC, DCM or HCM are not uncommon. Although G+ have increased mortality and morbidity, disease penetrance in these carriers from the general population remains low (1.2-3.1%). Follow-up decisions in case of incidental findings should not be based solely on a variant, but on multiple factors, including family history and disease expression.

Key Words: whole exome sequencing, genetics, arrhythmogenic right ventricular cardiomyopathy, dilated cardiomyopathy, hypertrophic cardiomyopathy

BACKGROUND

The major inherited cardiomyopathies arrhythmogenic right ventricular cardiomyopathy (ARVC), dilated cardiomyopathy (DCM) and hypertrophic cardiomyopathy (HCM) are characterized by ventricular dysfunction and ventricular arrhythmias that can lead to progressive heart failure and sudden cardiac death¹. ARVC is mainly caused by pathogenic variants in desmosomal genes, whereas DCM and HCM are mainly caused by sarcomeric gene variants². These cardiomyopathies are typically inherited in an autosomal dominant fashion with incomplete penetrance and variable expressivity. As such, phenotypic expression may vary greatly, even among family members or individuals carrying the same pathogenic variant.

With the implementation of next-generation sequencing (NGS), genetic testing has become an important part of routine clinical care in the diagnosis of inherited cardiomyopathies³. Technical advances and commercial availability of NGS, have led to more affordable and accessible genetic testing. The American College of Medical Genetics and Genomics (ACMG) has developed recommendations for the reporting of incidental or secondary findings unrelated to the test indication⁴. In this framework, variants in genes associated with ARVC, DCM and HCM are recommended to be reported as secondary findings from clinical exome and other genome sequencing tests⁴. Although this offers the potential to prevent morbidity and mortality of heart failure and sudden cardiac death by early treatment, it also fuels uncertainty in carriers of likely pathogenic or pathogenic variants (G+) and their family members, since factors that influence disease penetrance in the general population are largely unknown. More knowledge about disease penetrance of these variants in an unselected population cohort is needed to determine screening protocols in these individuals.

In this study, we aimed to assess the prevalence of pathogenic and likely pathogenic variants in the general population using a set of recently curated genes for ARVC⁵, DCM⁶ and HCM⁷ in two (inter)national databases⁸ (see **Figure 1** and **Table I**). In order to do so, we leveraged data from the UK Biobank (UKB), a population-based cohort with whole exome sequencing (WES) data available of 200,643 individuals⁹. Furthermore, we looked into the UKB-reported phenotypical characteristics of these G+ and assessed the occurrence of early signs of disease in undiagnosed G+ using available electrocardiography and cardiac magnetic resonance (CMR) imaging data.

METHODS

Ethics approval for the UKB study was obtained from the North West Centre for Research Ethics Committee (11/NW/0382) and all participants provided informed consent. All data and materials have been made publicly available on Github and can be accessed at <https://>

github.com/CirculatoryHealth/Inherited-cardiomyopathies. Full methods are available in the **Supplemental Material**. Disease definitions are given in **Table II**.

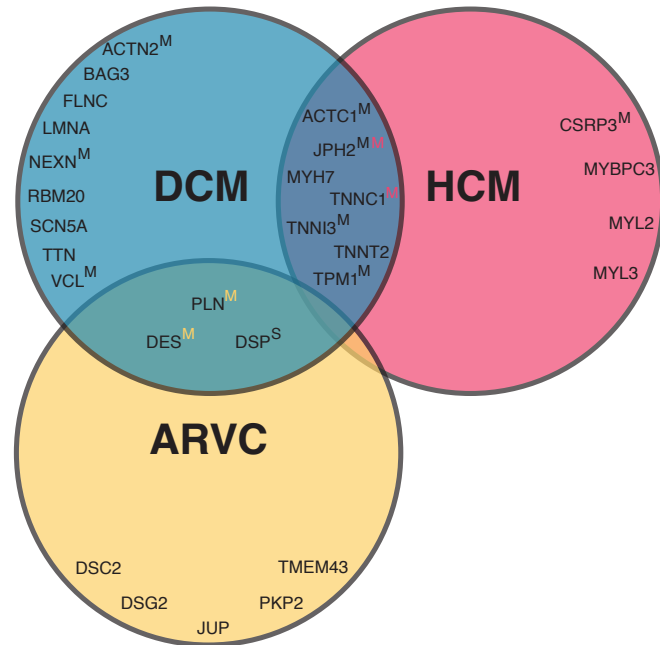


Figure 1: Included curated genes per cardiomyopathy

The Venn diagram of curated genes included in this study shows the overlap in genes per cardiomyopathy. Unless otherwise indicated, pathogenicity of genes are classified as definitive. If a superscript S or M is given, genes are classified as having a strong or moderate pathogenicity respectively. In the overlapping circles, yellow, black and red colors refer to ARVC, DCM, and HCM respectively. **Table I** gives an overview of the included genes and pathogenicity classification per gene and abbreviation per gene.

Abbreviations: ARVC= arrhythmogenic right ventricular cardiomyopathy; DCM= dilated cardiomyopathy; HCM= hypertrophic cardiomyopathy.

RESULTS

Population characteristics

We identified 2,207/200,643 unique G+ individuals from a total of 2,493 included individuals (89%) (see **Figure 2**) classified as 1) ARVC G+ (n=347, 54% female, median age of 57 [50-64] years); 2) DCM G+ (n=800, 56% female, median age of 58 [51-64] years) and; 3) HCM G+ (n=1,346, 54% female, median age of 56 [49-63] years). The matched control group consisted of 9,972 individuals (55% females, median age of 57 [49-63] years). **Table 1** and **Table III** show the baseline characteristics of the included individuals. The majority of G+ were of

white ethnicity (ARVC 90%, DCM 96%, HCM 75%), followed by Asian (ARVC 3%, DCM 1%, HCM 19%) and black ethnicity (ARVC 2%, DCM 2% and HCM 2%). This is comparable to what is observed in the UKB, where the majority is of white ethnicity (94%), followed by Asian (2%) and black ethnicity (2%).

Table 1: Baseline characteristics of variant carriers and controls

	ARVC G+ n=347	DCM G+ n=800	HCM G+ n=1,346	Controls G- n=9,972
<i>Demographics</i>				
Female (%)	187 (54)	450 (56)	720 (54)	5,436 (55)
Age, years	57 [50- 64]	58 [51-64]	56 [49-63]	57 [49- 63]
Ethnicity (%)				
White	311 (90)	760 (96)	1,001 (75)	8,288 (84)
Asian	10 (3)	8 (1)	251 (19)	1,076 (11)
Black	7 (2)	12 (2)	22 (2)	164 (2)
Other	17 (5)	15 (2)	55 (4)	348 (4)
<i>Cardiovascular risk factors</i>				
BMI, kg/m ²	26 [24-30]	27 [24-30]	27 [24-30]	27 [24-30]
Diabetes (%)	35 (10)	62 (8)	154 (11)*	914 (9)
Hypertension (%)	116 (33)	287 (36)	475 (35)	3,420 (34)
Hypercholesterolemia (%)	86 (25)	211 (26)	369 (27)*	2,416 (24)
Ever Smoked (%)	161 (46)	371 (46)*	543 (40)	4,132 (41)
MET minutes per week, ml/kg/min	2,001 [923-3,551]	1,695 [784-3,536]	1,762 [848-3,426]	1,773 [810-3,453]
Family heart disease (%)	179 (52)*	380 (48)	623 (46)	4,458 (45)
<i>Cardiac disease/outcomes</i>				
Cardiomyopathy (%)	3 (0.9)	22 (3)**	27 (2)**	37 (0.4)
DCM (%)	2 (0.6)	9 (1)**	1 (0.1)	14 (0.1)
HCM (%)	1 (0.3)	7 (1)**	20 (2)**	8 (0.1)
Heart failure (%)	9 (3)	36 (5)**	33 (3)	182 (2)
Ventricular arrhythmias (%)	7 (2)**	13 (2)**	8 (1)	33 (0.3)
Atrial arrhythmias (%)	7 (2)	34 (4)**	32 (2)	191 (2)
Chronic ischemic heart disease (%)	35 (10)	73 (9)	93 (7)	725 (7)
Acute myocardial infarction (%)	15 (4)	27 (3)	36 (3)	298 (3)
Cardiac arrest (%)	0 (0)	6 (1)	5 (0.4)	34 (0.3)
Cardiovascular death (%)	11 (3)	24 (3)*	18 (1)	181 (2)
All cause mortality (%)	19 (6)	56 (7)*	62 (5)	513 (5)
<i>Cardiac symptoms</i>				
Cardiac problem	3 (1)	3 (0.4)	5 (0.4)	41 (0.4)
Angina pectoris	16 (5)	30 (4)	56 (4)*	312 (3)

Number (percentages) are given or median [IQR]. * p=0.001-0.05 and ** p <0.001 difference compared to the control group. A more extensive overview of the baseline characteristics are given in **Table III**. Individuals with a variant in *PLN*, *DES* and *DSP* variant were included in both ARVC and DCM. Individuals with a variant in *MYH7*, *ACTC*, *JPH*, *TNNC1*, *TNNI3*, *TNNT2*, *TPM* were included in both DCM and HCM.

Abbreviations: ARVC= arrhythmogenic right ventricular cardiomyopathy; DCM= dilated cardiomyopathy; HCM= hypertrophic cardiomyopathy; BMI= body mass index; MET= metabolic equivalent of task.

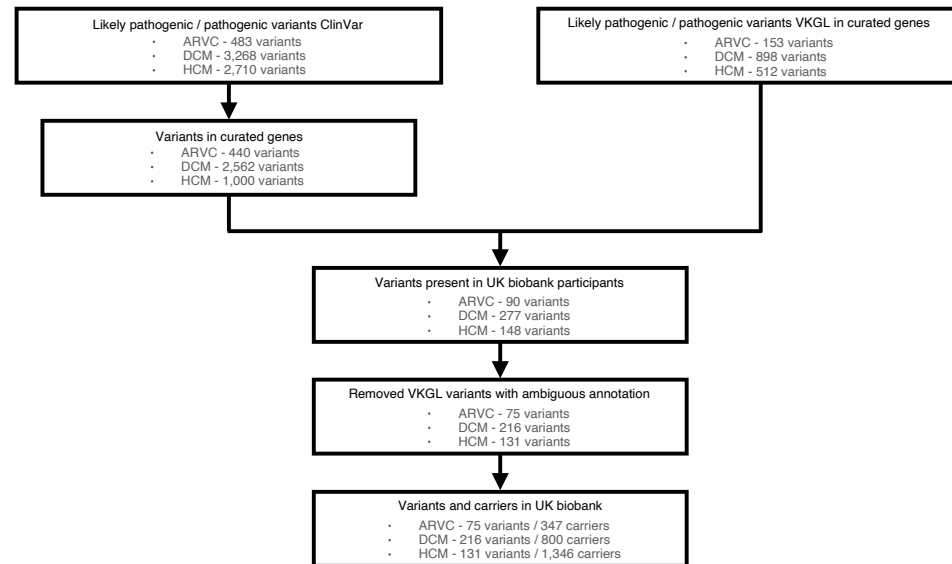


Figure 2: Flowchart inclusion of variants

Flowchart depicting the inclusion of pathogenic and likely pathogenic variants associated with arrhythmogenic cardiomyopathy, dilated cardiomyopathy and hypertrophic cardiomyopathy from the ClinVar[®] and VKGL database.

Abbreviations: ARVC=arrhythmogenic right ventricular cardiomyopathy; DCM=dilated cardiomyopathy; HCM=hypertrophic cardiomyopathy; VKGL=Vereniging Klinische Genetische Laboratoriumdiagnostiek.

Genotypic characteristics of pathogenic and likely pathogenic variant carriers

Prevalence of pathogenic and likely pathogenic variants in the general population

We found a prevalence of 1 ARVC G+ in 578 people in the general population (1:578 [1:521; 1:644]) and identified 75 variants out of the 593 (13%) pathogenic and likely pathogenic variants described in ClinVar and VKGL: 13 missense and 62 loss of function (LoF) (**Table IV**). As shown in **Figure 3**, most ARVC G+ harbored a pathogenic variant in *PKP2* (n=185, 53%), followed by *DSP* (n=49, 14%), *DSC2* (n=42, 12%), *DSG2* (n=31, 9%), *JUP* (n=24, 7%), *DES* (n=15, 4%), and *PLN* (n=1, 0.3%).

We found a prevalence of 1:251 [1:234; 1:269] DCM G+ and identified 216 out of 3,460 (6%) pathogenic and likely pathogenic variants described in ClinVar and VKGL: 80 missense and 136 LoF (**Table IV**). Variants in *TTN* (n=272, 34%) and *MYH7* (n=158, 20%) were most prevalent among DCM G+, followed by *SCN5A* (n=59, 7%), *FLNC* (n=56, 7%), *DSP* (n=49, 6%), *DES* (n=49, 6%), *LMNA* (n=42, 5%), *TNNI3* (n=35, 4%) and *TNNT2* (n=32, 4%). Eight more genes with a frequency of less than 3% were identified: *BAG3*, *PLN*, *TNNC1*, *ACTN2*, *RBM20*, *NEXN*, *TPM1*, and *ACTC1* (**Figure 3**).

We found a prevalence of 1:149 [1:141; 1:157] HCM G+ and identified 131 out of 1,512 (9%) pathogenic and likely pathogenic variants from ClinVar and VKGL: 98 missense and 23 LoF (**Table IV**). Most individuals carried a pathogenic and likely pathogenic variant in *MYBPC3* (n=723, 54%), followed by *TNNT2* (n=274, 20%), *MYH7* (n=232, 17%), and *TNNI3* (n=50, 4%). A frequency of less than 3% was found in *CSRP3*, *MYL2*, *TNNC1*, *JPH2*, *TPM1*, *ACTC1*, and *MYL3* (**Figure 3**). Interestingly, a variant in *TNNT2* (c.862C>T p.Arg288Cys) affected 242 individuals (18%). Four of these carriers were diagnosed with heart failure, of whom one also with HCM. All four heart failure patients also suffered from chronic ischemic heart disease. Furthermore, a variant in *MYBPC3* (c.3628-41_3628-17del) was mainly seen in individuals with an Asian ethnicity (n=237, 18% of the total HCM G+). Four of these individuals were diagnosed with heart failure, of whom two also had coronary artery disease and one was diagnosed with DCM, however none were diagnosed with HCM. When excluding these two variants, we found a HCM G+ prevalence of 1:250 [1:234; 1:269]. *MYBPC3* remained the most prevalent gene (52%), whereas the *TNNT2* frequency decreased to 4%.

The prevalence of G+ per gene for all cardiomyopathies is depicted in **Table V**.

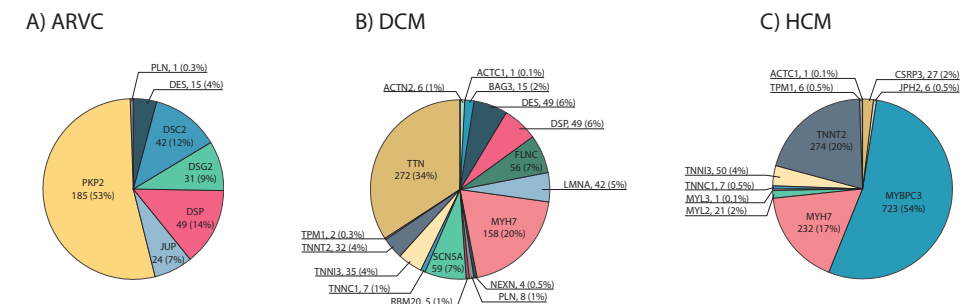


Figure 3: Distribution of genes per cardiomyopathy

Piecharts with the distribution of curated genes for A) arrhythmogenic right ventricular cardiomyopathy (ARVC); B) dilated cardiomyopathy (DCM); C) hypertrophic cardiomyopathy (HCM).

Abbreviations of the different genes are given in **Table III**

Abbreviations: G+= pathogenic variant carrier.

Overlapping variants and individuals

Some pathogenic and likely pathogenic variants were identified in multiple cardiomyopathy subtypes. First, 26 variants were described in both ARVC and DCM, affecting 53 individuals. Most of these variants (n=20/26 variants, 77%) were found in *DSP* (n=37 individuals, 70%), of whom one individual (3%) had heart failure and one (3%) was diagnosed with a cardiomyopathy. Five variants out of 26 (19%) were found in *DES* (n=15 individuals, 28%) of whom two individuals (13%) had heart failure, and one was diagnosed with both DCM and

HCM. One variant out of 26 (4%) was found in *PLN* (c.26G>A; p.Arg9His, NM_002667.5) in one individual (2%) who was not diagnosed with a cardiomyopathy or heart failure.

Second, 52 variants were described in DCM and HCM, affecting 232 individuals. Most of these variants (n=33/52 variants, 63%) were found in *MYH7* (n=158 individuals, 68%), followed by 10 variants (19%) in *TNNT2* (n=29 individuals, 13%), 6 variants (12%) in *TNNI3* (n=35 individuals, 15%), and 1 (2%) variant in *TNNC1*, *ACTC1* as well as *TPM1*. In this group of 232 individuals, 9 (4%) individuals had a cardiomyopathy or heart failure diagnosis, of whom 5 were diagnosed with HCM and none with DCM.

Furthermore, three individuals carried two pathogenic variants. Individual 1 was a 65-year old male, carrying variants in *MYBPC3* (c.3628-41_3628-17del, NM_000256.3) and *TNNT2* (c.460C>T; p.Arg154Trp, NM_001276345.2) and was diagnosed with heart failure, with underlying chronic ischemic heart disease. Individual 2 was a 65-year old male, carrying variants in *FLNC* (c.7450G>A; p.Gly2484Ser, NM_001458.5) and *PKP2* (c.1867G>T; p.Glu623Ter, NM_001005242.3) and was therefore included in both the ARVC as well as the DCM G+ group. Individual 3 was a 64-year old male, carrying variants in *MYBPC3* (c.1504C>T; p.Arg502Trp, NM_000256.3) and *MYH7* (c.5655G>A; p.Ala1885=, NM_000257.4). Individuals 2 and 3 were not diagnosed with a cardiomyopathy or heart failure and none had CMR data available.

Table VI shows the prevalence of the cardiomyopathy variants, with and without the inclusion of overlapping variants.

Phenotypic characteristics of pathogenic and likely pathogenic variant carriers

Cardiovascular risk factors

Hypertension, BMI, and level of activity in metabolic equivalent of task minutes (MET) per week were comparable between G- and G+ for all cardiomyopathies ($p \geq 0.055$; **Table 1** and **Table VII**). Diabetes was more prevalent in G+ HCM (9.2% (G-) vs 11.4% (G+), $p=0.008$), while smoking was more prevalent in DCM G+ (41.4% vs 46.4%, $p=0.007$) (**Table VIII**).

Cardiovascular disease

As seen in **Figure 4** and **Table VIII**, compared to G-, cardiomyopathy/heart failure without previous ischemic heart disease (P+, phenotype positive) was more often diagnosed in DCM G+ (OR 3.66 [95% CI 2.24;5.81], $p=4.9 \times 10^{-7}$) and HCM G+ (OR 3.03 [95% CI 1.98;4.56], $p=5.8 \times 10^{-7}$). Among DCM G+, 25 individuals (3.1%, genes: 8 *MYH7*, 8 *TTN*, 2 *BAG3*, 2 *DSP*, 2 *FLNC*, 1 *DES*, 1 *SCN5A* and 1 *TNNT2*) were P+. Within HCM G+, 32 individuals (4.0%, genes: 20 *MYBPC3*, 10 *MYH7*, 1 *TNNI3* and 1 *TNNT2*) were P+. For ARVC G+, 4 individuals (1.2%, genes: 2 *DSP*, 1 *DES* and 1 *PKP2*) were P+, being comparable to G- controls (87 subjects, 0.8%).

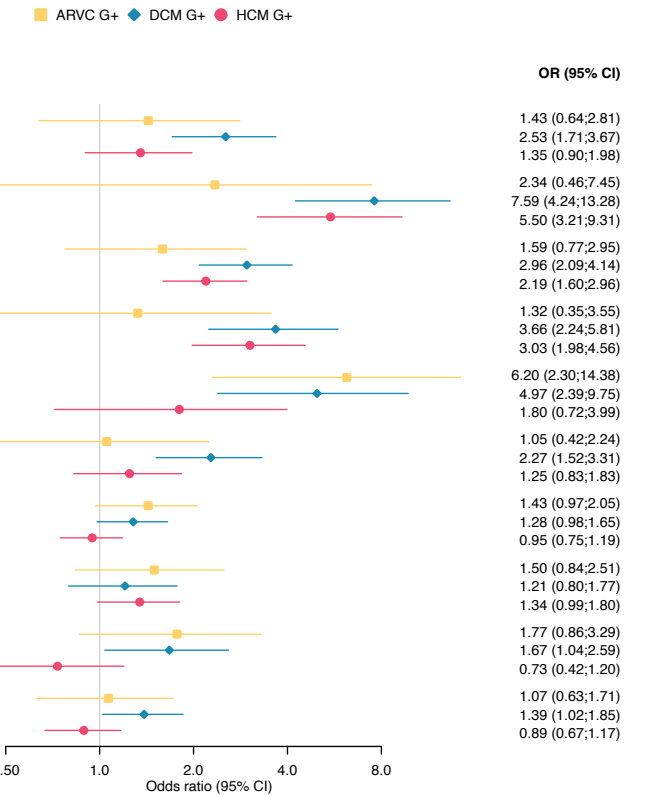


Figure 4: Forest plot cardiac outcomes stratified per inherited cardiomyopathy

Odds ratios and 95% confidence interval are given for the associations between cardiac outcomes and ARVC, DCM, or HCM pathogenic variant carriers.

Abbreviations: ARVC= arrhythmogenic right ventricular cardiomyopathy; DCM= dilated cardiomyopathy; G+= pathogenic variant carrier; HCM= hypertrophic cardiomyopathy.

Ventricular arrhythmias occurred more often in G+ compared to G-, reaching statistical significance for ARVC (OR 6.20 [95% CI 2.30;14.38], $p=3.3 \times 10^{-4}$) and DCM (OR 4.97 [95% CI 2.39;9.75], $p=1.9 \times 10^{-5}$). Atrial arrhythmias were more prevalent among DCM G+ (OR 2.27 [95% CI 1.52;3.31], $p=8.2 \times 10^{-5}$). Finally, all-cause mortality (OR 1.39 [95% CI 1.02;1.85], $p=0.032$) and death due to a cardiovascular cause were more prevalent in DCM G+ (OR 1.67 [95% CI 1.04;2.59], $p=0.030$) but did not reach statistical significance for ARVC G+ and HCM G+ ($p \geq 0.100$). **Figure I** depicts the overlap in cardiomyopathy, heart failure, ventricular arrhythmia and ischemic heart disease diagnosis. **Figure II** depicts the forest plots when excluding the more prevalent *TNNT2* and *MYBPC3* variants in HCM G+ individuals and **Figure III** shows the association between different outcomes stratified by genes for each cardiomyopathy.

Deep phenotyping of undiagnosed pathogenic variant carriers

Next, we set out to study early signs of disease in G+ without a cardiomyopathy/heart failure diagnosis (P-) using registered ICD-10 codes, self-reported cardiac symptoms, and abnormal ECG and CMR values.

Diagnosis and symptoms

Ventricular arrhythmias were more prevalent in ARVC G+P- (OR 5.85 [95% CI 1.98;14.40], $p=0.001$) and DCM G+P- (OR 3.43 [95% CI 1.35;7.68], $p=0.005$) but not in HCM G+P- (OR 1.01 [95% CI 0.26;2.86], $p=1.000$) compared to G-P- controls. Also, atrial arrhythmias (OR 2.12 [95% CI 1.36;3.19], $p=7.9 \times 10^{-4}$) were more frequent in DCM G+P- compared to G-P- controls. Finally, angina pectoris occurred more often in HCM G+P- (OR 1.38 [95% CI 1.01;1.85], $p=0.038$), but not in ARVC G+P- and DCM G+P- ($p \geq 0.117$; **Table VII**).

Electrocardiography

In total, 231 out of 2,207 G+P- and 1,058 out of 9,885 G-P- had various ECG variables available. None of these ECG variables differed significantly between all undiagnosed G+ and control individuals (**Table VIII**).

Cardiac magnetic resonance imaging

CMR data was available in 225 G+P- of the 2,207 unique G+P- individuals: $n=33$ for ARVC G+P-, $n=87$ for DCM G+P- and $n=130$ for HCM G+P- and 986 of the 9,885 G-P- controls. As shown in **Table IX**, G+P- and G-P- individuals with CMR data available were mostly comparable. Only smoking was more prevalent among DCM G+P- compared to G-P- controls (OR 1.59 [95%CI 1.00; 2.53], $p=0.041$). Outliers were observed in G-P- controls: 4 individuals with a median age of 64 [60-67] years had a left ventricular ejection fraction (LVEF) below 40% and 3 of them were diagnosed with hypertension and 2 with acute myocardial infarction in the past. In addition, 2 individuals with an age of 42 and 52 years old had an RVEF below 40%. They did not suffer from hypertension and did not have any cardiac diagnosis.

As shown in **Figure 5** and **Table VIII**, all RV ($p \geq 0.546$) and LV ($p \geq 0.052$) functional and structural parameters in ARVC G+P- were comparable to G-P- controls. Three ARVC G+P- individuals had an RVEDV corrected for body surface area (RVEDVi) between 100-110 mL/m² for males or 90-100 mL/m² for females, meeting the minor CMR task force criteria (TFC) if wall motion abnormalities were present, and two ARVC G+P- individuals had an RVEDVi larger than 110 mL/m² for males or 100 mL/m² for females, meeting the major CMR TFC¹⁰. In addition, ARVC G+P- had reduced inferior and posterolateral wall thickness compared to controls ($p \leq 0.035$).

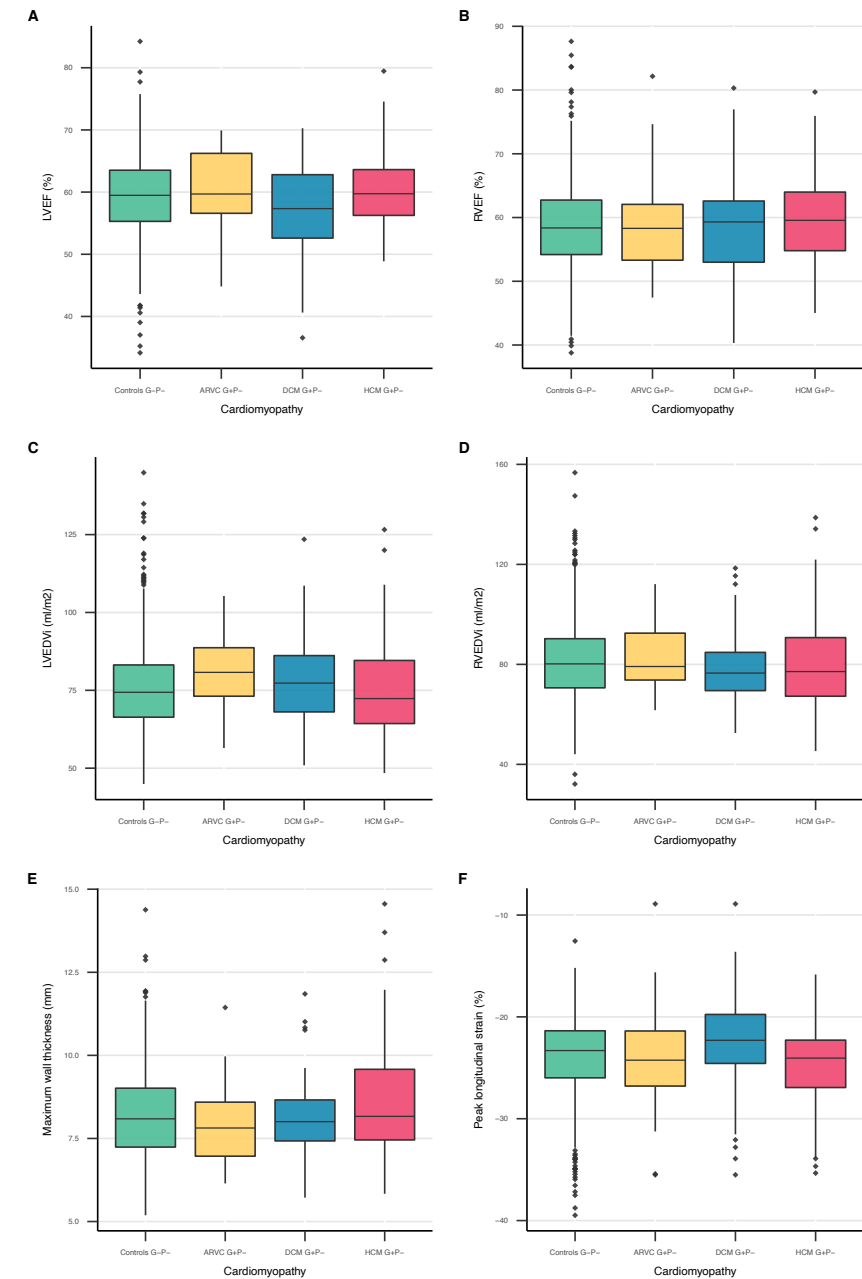


Figure 5: CMR parameters stratified per inherited cardiomyopathy

Boxplots of CMR parameters showing the summary statistics of CMR parameters stratified by controls and individuals with a pathogenic variant associated with ARVC, DCM, or HCM. Displayed summary statistics include the median, first and third quartile (lower and upper box edges), and the whiskers represent values within 1.5 times the interquartile range from the box edges.

Abbreviations: ARVC=arrhythmogenic right ventricular cardiomyopathy; DCM=dilated cardiomyopathy; EDVi= body surface area corrected end-diastolic volume; EF= ejection fraction; G+= pathogenic variant carrier; HCM= hypertrophic cardiomyopathy; LV= left ventricular; RV= right ventricular.

Overall, DCM G+P- and G-P- controls had comparable RV functional and structural measures ($p \geq 0.048$). However, DCM G+P- had lower LVEF (57.3% [52.6, 62.8] vs. 59.5% [55.3, 63.5] vs, $p=0.009$) and less negative LV peak longitudinal strain (-22.3% [-24.6, -19.86] vs. -23.3% [-26.0, -21.4], $p=0.009$). Although LVEDVi was not significantly increased in DCM G+P-, the LVEDV/RVEDV ratio (0.9 [0.9, 1.0] vs 1.0 [0.9, 1.1], $p=8.2 \times 10^{-4}$) and LVESVi (30.0 ml/m² [25.1, 35.7] vs 31.7 ml/m² [26.2, 39.8], $p=0.032$) were increased. Six individuals had an LVEF below 45%, but none of the individuals met the Henry criteria for DCM (LVEF below 45% and LVEDVi two times the normal SD)¹¹.

For HCM G+P-, most RV and LV functional and dimension parameters were comparable to G-P- controls ($p \geq 0.051$). Only RVEF was higher than controls (58.4% [54.2, 62.7] vs 59.6% [54.8, 64.0], $p=0.025$). Importantly, wall thickness was not significantly different between HCM G+P- without a cardiomyopathy/heart failure diagnosis and G-P- ($p \geq 0.160$). None of the G+P- individuals met HCM criteria¹² of ≥ 15 mm wall thickness, but two individuals met the criteria for limited hypertrophy (13-15mm) in the presence of a positive genetic test¹².

Figure IV shows a summary of all the differences tested.

Exclusion of the more prevalent *TNNT2* and *MYBPC3* variants

When excluding the more prevalent *TNNT2* and *MYBPC3* variants in HCM G+P- individuals, the occurrence of ventricular arrhythmias (OR 1.72 [95% CI 0.44;4.89], $p=0.306$) and atrial arrhythmias (OR 1.43 [95% CI 0.84;2.32], $p=0.156$) was comparable to G-P- controls. However, the maximum wall thickness (8.47mm [7.59, 9.94] vs. 8.09mm [7.24, 9.01], $p=0.008$) and basal anterior wall thickness (7.93mm [6.97, 9.11] vs. 7.65mm [6.81, 8.49], $p=0.029$) were significantly increased in HCM G+P- compared to controls (**Table VIII**). Two individuals had a maximum wall thickness between 13-15mm.

DISCUSSION

In this study we leveraged the largest European population database including WES and phenotype data to evaluate the prevalence and penetrance of previously reported pathogenic and likely pathogenic variants associated with ARVC, DCM and HCM. Our study has several interesting findings. First, we found a prevalence of 1:578, 1:251, and 1:149 for variants previously associated with ARVC, DCM and HCM respectively. Second, 1.2% of ARVC G+, 3.1% of DCM G+ and 2.6% of HCM G+ were diagnosed with a cardiomyopathy or heart failure without previous chronic ischemic heart disease. Finally, 3.2% of the undiagnosed ARVC G+, 1.8% of the undiagnosed DCM G+, 0.5% of the undiagnosed HCM G+ reported ventricular arrhythmias or had CMR abnormalities. These results confirm the low disease penetrance in G+ in the general population.

Prevalence of pathogenic and likely pathogenic variant carriers in the general population

Since rare genetic variants are the major cause of inherited cardiomyopathies, a large dataset is needed to accurately identify the population prevalence of these variants. Prevalence of pathogenic variants in populations has been the focus of several previous studies^{4,13-15}, however they were mostly limited by the number of included individuals. At time of analysis, we had access to an unprecedented number of 200,643 individuals.

Previously reported prevalence of ARVC G+ in the general population ranges between 1:143 to 1:1,706¹³⁻¹⁵. This variability is likely to be explained by heterogeneity in study populations and definitions of variant pathogenicity. For example, many previous studies did not include all eight curated genes with strong or moderate disease-gene association but also marked other genes (e.g. *TGFB3*) with only limited evidence as associated with ARVC^{14,15}. In addition, we included both missense and LoF variants whereas prior studies only included LoF variants.

For DCM, little is known about the prevalence of DCM causing variants in the general population. Studies focusing on truncating *TTN* variants in the general population found a prevalence ranging between 1:33 and 1:526^{16,17}. This wide range can partly be explained by the used definition of pathogenicity. Also, disease causing truncating *TTN* variants associated with DCM are known to be highly enriched in the A band. However, recently, truncating variants in the distal I-band region have also been implicated in DCM¹⁸. When solely focussing on *TTN* variants, we found a prevalence of only 1:735. This differs from the previous studies, probably because not all *TTN* variants are reported as pathogenic or likely pathogenic in ClinVar and VKGL. Including all curated DCM-associated genes, we report a prevalence of 1:251.

For HCM, we found a prevalence ranging between 1:250 and 1:149 individuals carrying a pathogenic or likely pathogenic variant, which approaches previous estimates of 1:164¹⁹. In a recent study, including the UKB population, a prevalence of 1:407 was reported²⁰. They included 8 sarcomere-encoding genes described to be associated with HCM (*ACTC1*, *MYBPC3*, *MYH7*, *MYL2*, *MYL3*, *TNNI3*, *TNNT2* and *TPM1*) and variants that were described as pathogenic or likely pathogenic in ClinVar or annotated as pathogenic or likely pathogenic according to ACMG criteria and filtered variants for an allele frequency of 0.00004. We included additional genes (*CSRP3*, *JPH2* and *TNNC1*) and pathogenic and likely pathogenic variants from the VKGL database and filtered for a minor allele frequency of 0.001. Especially the latter is a driving force behind the higher prevalence in this study. When also using a minor allele frequency (MAF) <0.00004, the prevalence of our study would be 1:475, approaching the prevalence reported by de Marvao *et al.*²⁰.

Disease expression of pathogenic and likely pathogenic variants in the general population

Most information on disease penetrance in ARVC, DCM or HCM G+ is based on observations in G+ relatives of cardiomyopathy patients. Previous studies have shown that 37% of ARVC G+ relatives²¹ and up to 50% of HCM G+ relatives with sarcomeric variants²² show disease expression during follow-up. Our findings suggest that disease penetrance in the general population is much lower. We found that 1.2% of ARVC G+, 3.1% of DCM G+ and 2.6% of HCM G+ in the UKB were diagnosed with a cardiomyopathy or heart failure, in the absence of chronic ischemic heart disease. Our additional analysis of ventricular function and ECG in undiagnosed G+ subjects also suggests a low disease penetrance. We found significantly worse LVEF and strain parameters in DCM G+P- compared to controls, however none met the diagnostic Henry criteria (LVEF below 45% and LVEDVi two times the normal SD)¹¹. Although CMR data was only available in a subgroup of undiagnosed G+ patients, these findings make it unlikely that the low penetrance found in our study arises from missed diagnoses or covert disease in the G+ cohort. Furthermore, none of the G+P- individuals met HCM criteria¹² of ≥ 15 mm wall thickness, two individuals did meet the criteria for limited hypertrophy (13-15mm) in the presence of a positive genetic test¹². Interestingly, maximum wall thickness in de Marvao *et al.*²⁰ was higher compared to ours. Although this can partly be explained by the inclusion of P+ by Marvao *et al.*, this may also be explained by differences in wall thickness calculation method. While Marvao *et al.* uses the absolute largest wall thickness value at a single point, we have used the AHA segment with the largest wall thickness (which is an average of all the single points within one AHA segment to reduce random outliers). In ARVC and DCM G+P- we found a low, but significantly higher prevalence of ventricular arrhythmias compared to controls (1.7% vs. 0.3% (OR 5.85 [95% CI 1.98;14.40]) and 1.0% vs. 0.3% (OR 3.43 [95% CI 1.35;7.68]) respectively). In ARVC, electrical abnormalities are known to precede structural abnormalities²³. Therefore, these findings may suggest early disease penetrance in a small subset of undiagnosed G+ individuals. The discrepancy between the high disease penetrance found in G+ family members and the low penetrance in the G+ general population points towards the interaction of possible other (unidentified) genetic and environmental factors leading to this variation. The median age of our study population was 57 [49-63] years, however inherited cardiomyopathies are generally diagnosed at a younger age. For ARVC, Groeneweg *et al.* showed, in a cohort of 439 index-patients, that the mean age of first disease presentation is 36 \pm 14 years. Most of these patients presented with symptoms (95%), of whom 11% with sudden cardiac arrest²¹. Likewise in DCM, the mean age of presentation is mostly between 30-50 years²⁴. Lastly, in HCM a mean age at presentation of 49 \pm 16 years was shown in a cohort of 4893 patients by Lorenzini *et al.*²⁵. Interestingly, although mortality rates were low, young HCM patients showed a worse prognosis compared to their healthy peers, with 80% of mortality being caused by sudden cardiac death²⁵. Therefore, it should be taken into account that younger patients with disease expression are likely underrepresented in our study. This is not only

due to higher mortality and morbidity in especially ARVC and HCM, but also because individuals with a diagnosed cardiomyopathy may be less likely to participate in a large-scale biobank study such as the UKB.

Interestingly, the South Asian *MYBPC3* and the *TNNT2* variant, showed a relatively high prevalence in our cohort. In total, 19% of HCM G+ was Asian and most of these individuals carried the c.3628-41_3628-17del variant in the *MYBPC3* gene. Although this variant is indicated as likely pathogenic in ClinVar, a previous study suggests that this variant may be reclassified as benign²⁶. In our study, none of these variant carriers were diagnosed with HCM. Four were diagnosed with heart failure of whom one was diagnosed with DCM. This suggests that this variant is associated with heart failure in the setting of multiple forms of cardiomyopathy, and not simply HCM²⁶. Secondly, the c.862C>T p.Arg288Cys variant in *TNNT2* was previously found in HCM individuals but is often observed in patients with a mild phenotype or in combination with other variants. These observations suggest that this variant might not be a monogenic cause of severe HCM but acts in concert with other variants²⁷. Interestingly, when excluding these variants from our G+P- population, a significantly higher wall thickness is measured compared to controls. These two examples emphasize that when pathogenic or likely pathogenic variants are identified as a secondary finding, other factors, such as the specific variant and the family history are crucial for follow-up decisions.

We also assessed gene-specific associations with the cardiovascular outcomes. *PKP2* variant carriers showed a stronger association with ventricular arrhythmias (OR 11.90 [95% CI 4.38; 27.86], $p = 6.4 \times 10^{-6}$) compared to heart failure (OR 1.50 [95% CI 0.48; 3.64], $p = 0.395$). This is in concordance with a previous study showing sustained ventricular arrhythmias to be the first clinical presentation in 61% of ARVC patients²¹. During follow-up, sustained arrhythmias occurred in 72% of ARVC patients, highlighting sustained arrhythmias as the most important ARVC disease manifestation. On the contrary, symptomatic heart failure was seen in 13% of ARVC patients²¹. In DCM G+, ventricular arrhythmias were significantly more present compared to G- controls, especially in *TTN* (OR 4.49 [95% CI 1.15; 12.76], $p = 0.016$), *DES* (OR 12.80 [95% CI 1.45; 52.55], $p = 0.013$) and *LMNA* (OR 15.04 [95% CI 1.69; 62.32], $p = 0.009$) variant carriers. A recent meta-analysis assessing predictors for sustained ventricular arrhythmias, showed *PLN* and *LMNA* to be associated with arrhythmogenic outcome²⁸. Although we did not have enough power to study *PLN* G+, *LMNA* G+ did show significantly more ventricular arrhythmias compared to G- controls. Furthermore, *BAG3* variant carriers have been associated with significant risk of progressive heart failure²⁹. In our study, *BAG3* variant carriers were significantly more often diagnosed with a cardiomyopathy (OR 41.18 [95% CI 4.36; 192.17], $p = 0.002$). Even though more heart failure cases were seen compared to G- controls, this did not reach statistical significance (**Table X**).

Interestingly, self-reported health-related quality of life and psychological well-being of 89 asymptomatic HCM G+ were previously evaluated in a Dutch cohort and found to be at least similar to the general population, which suggests that reporting incidental findings will not harm psychological well-being of G+³⁰. However, frequent cardiological examination of G+ and family members turning out to be carriers after cascade screening will put a burden on health care and societal costs³¹. Genetic screening and cardiological examination are necessary in family members of genetic cardiomyopathy patients since disease expression in family members is considerable. Disease expression in the general population on the other hand is low. Therefore, in case of an incidental finding, multiple factors like family history, presence of symptoms, electrical and/or structural abnormalities and gene and variant type should inform follow-up decisions. Further studies on the genotype-phenotype associations and disease penetrance will aid in facilitating these decisions.

Limitations

Several variants are associated with more than one cardiomyopathy. This is mainly due to phenotypic heterogeneity but may also be partly explained by misdiagnosis. Information is submitted to ClinVar by laboratories, not by clinicians. Phenotype description might therefore be less reliable. To avoid selection bias, we included variants associated with multiple cardiomyopathies in both cardiomyopathy categories, possibly leading to increased prevalence estimates. Although the prevalence of cardiomyopathy variants is slightly affected by including or excluding overlapping variants, this did not substantially affect the results and conclusions (**Table XI**). Future studies should focus on reaching consensus on variant-phenotype associations for the variants described in multiple cardiomyopathies to avoid variation in prevalence caused by the use of different definitions. Despite recent efforts to harmonize knowledge on genes associated with inherited cardiomyopathies⁵⁻⁷, and guidelines for variant classification³¹, the adjudication of the clinical significance of single variants can still differ between diagnostic laboratories³¹, which has led to interpretation differences and difficulties to compare results among studies using different criteria. This highlights the importance of a single set of criteria to ascertain clinical significance of a single variant. Furthermore, not all pathogenic or likely pathogenic variants are reported in these databases, especially family-specific variants and pathogenic variants in non-Caucasian populations are underreported.

Lastly, G+P- and G-P- individuals with CMR data available were age, sex and ethnicity matched and comparable in the presence of cardiovascular risk factors and diseases. Interestingly, outliers in CMR values were also present in G-P- controls, which could be partly explained by the presence of past myocardial infarctions. Therefore, differences in cardiac function and structure between G+P+ and G-P- could be underestimated.

CONCLUSION

In a cohort of 200,643 individuals with WES and phenotype data we identified a prevalence of pathogenic variants associated with ARVC, DCM and HCM of 1:578, 1:251 and 1:149 respectively. Among the identified G+ individuals, cardiomyopathy, heart failure and ventricular arrhythmias were more common compared to G-. However, overall disease penetrance was low (1.2-3.1%). Therefore, in case of incidental findings, decisions on application of cascade screening and frequency of cardiological examination should be based on multiple factors besides variant and gene type, such as family history and disease expression.

Acknowledgements

This research has been conducted using the UK Biobank Resource under Application Number 24711.

Funding sources

The work was financially supported by the Netherlands Cardiovascular Research Initiative, an initiative supported by the Dutch Heart Foundation (CardioVasculair Onderzoek Nederland (CVON) projects: DOUBLE-DOSE 2020B005 (AB), PREDICT2 2018-30, eDETECT 2015-12 (PvT, AtR and FA) and PREDICT Young Talent Program (AtR)). In addition, this work was supported by the Dutch Heart Foundation (2015T058 (AtR), 2015T041 (AB) and 2019T045 (MvV and JvS)). Furthermore, MB is supported by the Alexandre Suerman Stipend of the UMC Utrecht (2017), AtR by the UMC Utrecht Fellowship Clinical Research Talent and FA by the UCL Hospitals NIHR Biomedical Research Center.

Disclosures

None

Supplemental Material

Supplemental Methods

Tables I-XI

Figures I-IV

References ³²⁻³⁸

Non-standard Abbreviations and Acronyms

ACMG – American College of Medical Genetics and Genomics

ACTC1 – Actin Alpha Cardiac Muscle 1

ACTN1 – Alpha-actinin 2

AHA – American Heart Association

ARVC – Arrhythmogenic right ventricular cardiomyopathy

BAG3 – BAG Cochaperone 3

BMI – Body mass index
CI – Confidence interval
ClinGen – Clinical Genome Resource
CMR – Cardiac magnetic resonance imaging
CSRP3 – Cysteine And Glycine Rich Protein 3
DCM – Dilated cardiomyopathy
DES – Desmin
DSC2 – Desmocollin 2
DSG2 – Desmoglein 2
DSP – Desmoplakin
ECG – Electrocardiography
EDM – End diastolic mass
EDV – End diastolic volume
EF – Ejection fraction
ESV – End systolic volume
FLNC – Filamin-C
G+ – Genotype positive (variant carriers)
G- – Genotype negative (controls)
i – Indexed, corrected for body surface area
JPH2 – Junctophilin 2
JUP – Junction Plakoglobin
HCM – Hypertrophic cardiomyopathy
LMNA – Lamin A/C
LoF – Loss of function
LV – Left ventricular
MAF – Minor allele frequency
MET – Metabolic equivalent of task minutes
MVR – Mass to EDV ratio
MYBPC3 – Myosin Binding Protein C3
MYH7 – Myosin Heavy Chain 7
MYL2 – Myosin Light Chain 2
MYL3 – Myosin Light Chain 3
NEXN – Nexilin F-Actin Binding Protein
NGS – Next generation sequencing
OR – Odds ratio
P+ – Phenotype positive
P- – Phenotype negative
PKP2 – Plakophilin 2
PLN – Phospholamban
RBM20 – RNA Binding Motif Protein 20

RV – Right ventricular
SCN5A – Sodium Voltage-Gated Channel Alpha Subunit 5
SD – Standard deviation
SV – Stroke volume
TFC – Task force criteria
TMEM43 – Transmembrane Protein 43
TNNC1 – Troponin C1, Slow Skeletal And Cardiac Type
TNNI3 – Troponin I3, Cardiac Type
TNNT2 – Troponin T2, Cardiac Type
TPM1 – Tropomyosin 1
TTN – Titin
UKB – UK Biobank
VKGL – Vereniging Klinische Genetische Laboratoriumdiagnostiek
VCL – Vinculin
WES – Whole exome sequencing

REFERENCES

1. McKenna WJ, Judge DP. Epidemiology of the inherited cardiomyopathies. *Nat Rev Cardiol*. 2021;18:22-36.
2. Hershberger RE, Hedges DJ, Morales A. Dilated cardiomyopathy: the complexity of a diverse genetic architecture. *Nat Rev Cardiol*. 2013;10:531-547.
3. Gersh BJ, Maron BJ, Bonow RO, Dearani JA, Fifer MA, Link MS, Naidu SS, Nishimura RA, Ommen SR, Rakowski H, et al. 2011 ACCF/AHA guideline for the diagnosis and treatment of hypertrophic cardiomyopathy: executive summary: a report of the American College of Cardiology Foundation/American Heart Association Task Force on Practice Guidelines. *Circulation*. 2011;124:2761-2796.
4. Miller DT, Lee K, Chung WK, Gordon AS, Herman GE, Klein TE, Stewart DR, Amendola LM, Adelman K, Bale SJ, et al. ACMG SF v3. 0 list for reporting of secondary findings in clinical exome and genome sequencing: a policy statement of the American College of Medical Genetics and Genomics (ACMG). *Genet Med*. 2021;23:1381-1390.
5. James CA, Jongbloed JD, Hershberger RE, Morales A, Judge DP, Syrris P, Pilichou K, Domingo AM, Murray B, Cadrin-Tourigny J, et al. International evidence based reappraisal of genes associated with arrhythmogenic right ventricular cardiomyopathy using the clinical genome resource framework. *Circ Genom Precis Med*. 2021;14:e003273.
6. Jordan E, Peterson L, Ai T, Asatryan B, Bronicki L, Brown E, Celeghein R, Edwards M, Fan J, Ingles J, et al. Evidence-based assessment of genes in dilated cardiomyopathy. *Circ*. 2021;144:7-19.
7. Ingles J, Goldstein J, Thaxton C, Caleshu C, Corty EW, Crowley SB, Dougherty K, Harrison SM, McGlaughon J, Milko LV, et al. Evaluating the clinical validity of hypertrophic cardiomyopathy genes. *Circ Genom Precis Med*. 2019;12:e002460.
8. Landrum MJ, Lee JM, Benson M, Brown GR, Chao C, Chitipiralla S, Gu B, Hart J, Hoffman D, Jang W, et al. ClinVar: improving access to variant interpretations and supporting evidence. *Nucleic Acids Res*. 2018;46:D1062-D1067.
9. Szustakowski JD, Balasubramanian S, Kvikstad E, Khalid S, Bronson PG, Sasson A, Wong E, Liu D, Wade Davis J, Haefliger C, et al. Advancing human genetics research and drug discovery through exome sequencing of the UK Biobank. *Nat Genet*. 2021;53:942-948.
10. Marcus FI, McKenna WJ, Sherrill D, Basso C, Bauce B, Bluemke DA, Calkins H, Corrado D, Cox MG, Daubert JP, et al. Diagnosis of arrhythmogenic right ventricular cardiomyopathy/dysplasia: proposed modification of the task force criteria. *Circulation*. 2010;121:1533-1541.
11. Henry WL, Gardin J, Ware J. Echocardiographic measurements in normal subjects from infancy to old age. *Circulation*. 1980;62:1054-1061.
12. Ommen SR, Mital S, Burke MA, Day SM, Deswal A, Elliott P, Evanchovich LL, Hung J, Joglar JA, Kantor P, et al. 2020 AHA/ACC guideline for the diagnosis and treatment of patients with hypertrophic cardiomyopathy: executive summary: a report of the American College of Cardiology/American Heart Association Joint Committee on Clinical Practice Guidelines. *J Am Coll Cardiol*. 2020;76:3022-3055.
13. Carruth ED, Young W, Beer D, James CA, Calkins H, Jing L, Raghunath S, Hartzel DN, Leader JB, Kirchner HL, et al. Prevalence and electronic health record-based phenotype of loss-of-function genetic variants in arrhythmogenic right ventricular cardiomyopathy-associated genes. *Circ Genom Precis Med*. 2019;12:e002579.
14. Haggerty CM, James CA, Calkins H, Tichnell C, Leader JB, Hartzel DN, Nevius CD, Pendergrass SA, Person TN, Schwartz M, et al. Electronic health record phenotype in subjects with genetic variants associated with arrhythmogenic right ventricular cardiomyopathy: a study of 30,716 subjects with exome sequencing. *Genet Med*. 2017;19:1245-1252.
15. Hall CL, Sutanto H, Dalageorgou C, McKenna WJ, Syrris P, Futema M. Frequency of genetic variants associated with arrhythmogenic right ventricular cardiomyopathy in the genome aggregation database. *Eur J Hum Genet*. 2018;26:1312-1318.
16. Akinrinade O, Koskenvuo JW, Alastalo T-P. Prevalence of titin truncating variants in general population. *PLoS One*. 2015;10:e0145284.
17. Herman DS, Lam L, Taylor MR, Wang L, Teekakirikul P, Christodoulou D, Conner L, DePalma SR, McDonough B, Sparks E, et al. Truncations of titin causing dilated cardiomyopathy. *N Engl J Med*. 2012;366:619-628.
18. Schafer S, De Marvao A, Adami E, Fiedler LR, Ng B, Khin E, Rackham OJ, Van Heesch S, Pua CJ, Kui M, et al. Titin-truncating variants affect heart function in disease cohorts and the general population. *Nat Genet*. 2017;49:46-53.
19. Bick AG, Flannick J, Ito K, Cheng S, Vasan RS, Parfenov MG, Herman DS, DePalma SR, Gupta N, Gabriel SB, et al. Burden of rare sarcomere gene variants in the Framingham and Jackson Heart Study cohorts. *Am J Hum Genet*. 2012;91:513-519.
20. de Marvao A, McGurk KA, Zheng SL, Thanaj M, Bai W, Duan J, Biffi C, Mazzarotto F, Statton B, Dawes TJ, et al. Phenotypic expression and outcomes in individuals with rare genetic variants of hypertrophic cardiomyopathy. *J Am Coll Cardiol*. 2021;78:1097-1110.
21. Groeneweg JA, Bhonsale A, James CA, Te Riele AS, Dooijes D, Tichnell C, Murray B, Wiesfeld AC, Sawant AC, Kassamali B, et al. Clinical presentation, long-term follow-up, and outcomes of 1001 arrhythmogenic right ventricular dysplasia/cardiomyopathy patients and family members. *Circ Cardiovasc Genet*. 2015;8:437-446.
22. van Velzen HG, Schinkel AF, Baart SJ, Oldenburg RA, Frohn-Mulder IM, van Slegtenhorst MA, Michels M. Outcomes of contemporary family screening in hypertrophic cardiomyopathy. *Circ Genom Precis Med*. 2018;11:e001896.
23. Gomes J, Finlay M, Ahmed AK, Ciaccio EJ, Asimaki A, Saffitz JE, Quarta G, Nobles M, Syrris P, Chaubey S, et al. Electrophysiological abnormalities precede overt structural changes in arrhythmogenic right ventricular cardiomyopathy due to mutations in desmoplakin-A combined murine and human study. *Eur Heart J*. 2012;33:1942-1953.
24. Hershberger RE, Cowan J, Morales A, Siegfried JD. Progress with genetic cardiomyopathies: screening, counseling, and testing in dilated, hypertrophic, and arrhythmogenic right ventricular dysplasia/cardiomyopathy. *Circ Heart Fail*. 2009;2:253-261.
25. Lorenzini M, Anastasiou Z, O'Mahony C, Guttman OP, Gimeno JR, Monserrat L, Anastasakis A, Rapezzi C, Biagini E, Garcia-Pavia P, et al. Mortality among referral patients with hypertrophic cardiomyopathy vs the general European population. *JAMA Cardiol*. 2020;5:73-80.
26. Harper AR, Bowman M, Hayesmoore JB, Sage H, Salatino S, Blair E, Campbell C, Currie B, Goel A, McGuire K, et al. Reevaluation of the South Asian MYBPC3 Δ25bp Intronic Deletion in Hypertrophic Cardiomyopathy. *Circ Genom Precis Med*. 2020;13:e002783.
27. Ripoll-Vera T, Gámez JM, Govea N, Gómez Y, Núñez J, Socías L, Escandell Á, Rosell J. Clinical and prognostic profiles of cardiomyopathies caused by mutations in the troponin T gene. *Rev Esp Cardiol*. 2016;69:149-158.
28. Kayvanpour E, Sedaghat-Hamedani F, Amr A, Lai A, Haas J, Holzer DB, Frese KS, Keller A, Jensen K, Katus HA, et al. Genotype-phenotype associations in dilated cardiomyopathy: meta-analysis on more than 8000 individuals. *Clin Res Cardiol*. 2017;106:127-139.
29. Domínguez F, Cuenca S, Bilińska Z, Toro R, Villard E, Barriales-Villa R, Ochoa JP, Asselbergs F, Sammani A, Franaszczyk M, et al. Dilated cardiomyopathy due to BLC2-associated athanogene 3 (BAG3) mutations. *J Am Coll Cardiol*. 2018;72:2471-2481.
30. Christiaans I, Van Langen IM, Birnie E, Bonsel GJ, Wilde AA, Smets EM. Quality of life and psychological distress in hypertrophic cardiomyopathy mutation carriers: a cross sectional cohort study. *Am J Med Genet*. 2009;149:602-612.
31. Fontes Marx M, Ataguba JE, Vries Jd, Wonkam A. Systematic Review of the Economic Evaluation of Returning Incidental Findings in Genomic Research. *Public Health Front*. 2021;9:873.
32. Strande NT, Riggs ER, Buchanan AH, Ceyhan-Birsoy O, DiStefano M, Dwight SS, Goldstein J, Ghosh R, Seifert BA, Sneddon TP, et al. Evaluating the clinical validity of gene-disease associations: an evidence-based framework developed by the clinical genome resource. *Am J Hum Genet*. 2017;100:895-906.
33. Richards S, Aziz N, Bale S, Bick D, Das S, Gastier-Foster J, Grody WW, Hegde M, Lyon E, Spector E, et al. Standards and guidelines for the interpretation of sequence variants: a joint consensus recommendation of the American College of Medical Genetics and Genomics and the Association for Molecular Pathology. *Genet Med*. 2015;17:405-423.
34. Bamshad MJ, Ng SB, Bigham AW, Tabor HK, Emond MJ, Nickerson DA, Shendure J. Exome sequencing as a tool for Mendelian disease gene discovery. *Nat Rev Genet*. 2011;12:745-755.
35. Petersen SE, Matthews PM, Francis JM, Robson MD, Zemrak F, Boubertakh R, Young AA, Hudson S, Weale P, Garratt S, et al. UK Biobank's cardiovascular magnetic resonance protocol. *J Cardiovasc Magn Reson*. 2015;18:1-7.
36. Ruijsink B, Puyol-Antón E, Oksuz I, Sinclair M, Bai W, Schnabel JA, Razavi R, King AP. Fully automated, quality-controlled cardiac analysis from CMR: validation and large-scale application to characterize cardiac function. *JACC Cardiovasc Imaging*. 2020;13:684-695.
37. Cerqueira MD, Weissman NJ, Dilsizian V, Jacobs AK, Kaul S, Laskey WK, Pennell DJ, Rumberger JA, et al. Standardized myocardial segmentation and nomenclature for tomographic imaging of the heart: a statement for healthcare professionals from the Cardiac Imaging Committee of the Council on Clinical Cardiology of the American Heart Association. *Circulation*. 2002;105:539-542.
38. R Core Team. R: A language and environment for statistical computing: Vienna, Austria: R Foundation for Statistical Computing; 2020.

SUPPLEMENTAL METHODS

Genetic variants in the study population

We identified carriers of a pathogenic or likely pathogenic variant associated with ARVC, DCM or HCM in individuals from the UKB who underwent whole exome sequencing (WES, n=200,643 at time of analysis). For each inherited cardiomyopathy we selected curated genes classified to have definite, strong or moderate evidence of pathogenicity as defined by the standardized evidence-based framework of Clinical Genome Resource (ClinGen)³² and curated by James *et al.*⁵ for ARVC, Jordan *et al.*⁶ for DCM and Ingles *et al.*⁷ for HCM. For ARVC we included *DES*, *DSC2*, *DSG2*, *DSP*, *JUP*, *PKP2*, *PLN* and *TMEM43*; for DCM we included *ACTC1*, *ACTN2*, *BAG3*, *DES*, *DSP*, *FLNC*, *JPH2*, *LMNA*, *MYH7*, *NEXN*, *PLN*, *RBM20*, *SCN5A*, *TNNC1*, *TNNI3*, *TNNT2*, *TPM1*, *TTN* and *VCL*; and for HCM we included *ACTC1*, *CSRP3*, *JPH2*, *MYBPC3*, *MYH7*, *MYL2*, *MYL3*, *TNNC1*, *TNNI3*, *TNNT2* and *TPM1* (Figure 1 and Table I).

Some genetic variants are associated with two cardiomyopathies (Table IV). Individuals carrying these variants were included in the G+ groups of both cardiomyopathies. Next, likely pathogenic and pathogenic variants in these genes were identified using the ClinVar NCBI-NIH database⁸ and the Dutch Society for Clinical Genetic Laboratory Diagnostics (Vereniging Klinische Genetische Laboratoriumdiagnostiek, VKGL) database. Laboratories submitting information to these databases use the criteria for variant classification as defined by the American College of Medical Genetics and Genomics and the Association for Molecular Pathology (ACMG-AMP)³³. An elaborate overview of the ClinVar and VKGL search criteria is given in Figure 2. In short, ClinVar was queried using the disease name(s) and filtered for pathogenic and likely pathogenic variants in the curated genes. For variants mentioned in the VKGL database, which does not specify disease associations, association with one of the cardiomyopathies was confirmed in ClinVar. The minor allele frequency (MAF) cut-off was defined at 0.001, which is the recommended cut-off for including rare variants³⁴ and still include any potentially at-risk variant carriers. Variants were classified as missense or loss of function (LoF), with LoF being defined as frameshift, stop gain, start lost and canonical splice site variants. We matched G+ individuals in a 1:4 ratio to UKB individuals without a pathogenic or likely pathogenic variant associated with one of the cardiomyopathies (G-). Matching of this G-control group was based on age, sex, ethnicity and presence of cardiac magnetic resonance imaging (CMR) measurements. Controls are referred to as G- throughout this study.

Data extraction UKB

Disease definitions

An elaborate overview of the disease definitions used in this study is available in **Table II**. In short, individuals were defined to be phenotype positive (P+) if they had an ICD-10 or self-

reporting code for cardiomyopathy, DCM, HCM or heart failure, without a diagnosis of chronic ischemic heart disease. No ICD-10 or self-reporting code was available for ARVC in the UKB.

CMR and ECG data analysis

We investigated disease expression on cardiac magnetic resonance imaging (CMR, n = 225 unique individuals) and electrocardiography (ECG, n = 231 unique individuals) of G+P- individuals. The full CMR protocol of the UKB has been described in detail³⁵. In short, all CMR examinations were performed on a 1.5 Tesla scanner (Magnetom Aera, Syngo Platform VD13A, Siemens Healthcare, Erlangen, Germany). We used a previously developed and validated deep-learning methodology (AI-CMR³⁶) to extract left (LV) and right ventricular (RV) CMR measurements³⁶. In short, cine images of short-axis and 2- and 4-chamber long-axis views were used to automatically calculate LV and RV functional measures (ejection fraction [EF], stroke volume [SV]) and structural measures (end diastolic volume [EDV], end-systolic volume [ESV], LV end diastolic mass [EDM], LV mass to EDV ratio [LVMVR] and LV maximal and regional [16 segments model according the American Heart Association³⁷] wall thickness). The electrocardiography (ECG) variables P duration, P axis, PQ interval, QRS duration, R axis, QTc interval and T axis were extracted from the UKB for G+P- individuals.

Statistical analysis

Statistical analysis was performed using R version 4.0.2³⁸. Continuous values are presented as median [interquartile range] and for comparisons of two groups, Mann-Whitney-U test was used. Categorical data was displayed as absolute frequency (n) and percentages (%) and Fisher's exact test was used to test for differences. The strength of the association between cardiac outcomes and G+ ARVC, DCM and HCM was calculated by the odds ratio with 95% confidence intervals. The latter was also performed stratifying by genes. A number of included variants are associated with more than one cardiomyopathy. To investigate the effect of the inclusion of individuals in more than one cardiomyopathy, we removed overlapping variants as described in **Table IV** and calculated the odds ratios of the cardiovascular risk factors and diagnoses for these G+ compared to G-. A p-value of less than 0.05 was considered significant.

Supplementary Table I: Included curated genes per cardiomyopathy

Gene*	ARVC	DCM	HCM
<i>ACTC1</i>		Moderate	Definitive
<i>ACTN2</i>		Moderate	
<i>BAG3</i>		Definitive	
<i>CSRP3</i>			Moderate
<i>DES</i>	Moderate	Definitive	
<i>DSC2</i>	Definitive		
<i>DSG2</i>	Definitive		
<i>DSP</i>	Definitive	Strong	
<i>FLNC</i>		Definitive	
<i>JPH2</i>		Moderate	Moderate
<i>JUP</i>	Definitive		
<i>LMNA</i>		Definitive	
<i>MYBPC3</i>			Definitive
<i>MYH7</i>		Definitive	Definitive
<i>MYL2</i>			Definitive
<i>MYL3</i>			Definitive
<i>NEXN</i>		Moderate	
<i>PKP2</i>	Definitive		
<i>PLN</i>	Moderate	Definitive	
<i>RBM20</i>		Definitive	
<i>SCN5A</i>		Definitive	
<i>TMEM43</i>	Definitive		
<i>TNNC1</i>		Definitive	Moderate
<i>TNNI3</i>		Moderate	Definitive
<i>TNNT2</i>		Definitive	Definitive
<i>TPM1</i>		Moderate	Definitive
<i>TTN</i>		Definitive	
<i>VCL</i>		Moderate	

* ARVC genes are curated by ref 5, DCM genes by ref 6 and HCM genes by ref 7. Pathogenicity is classified as moderate, strong and definitive.

Abbreviations:

ACTC1: Actin Alpha Cardiac Muscle 1; *ACTN2*: Alpha-actinin 2;

ARVC: Arrhythmogenic right ventricular cardiomyopathy; *BAG3*: BAG Cochaperone 3; *CSRP3*: Cysteine And Glycine Rich Protein 3; *DCM*: Dilated cardiomyopathy; *DES*: Desmin; *DSC2*: Desmocollin 2; *DSG2*: Desmoglein 2; *DSP*: Desmoplakin; *FLNC*: Filamin-C;

HCM: Hypertrophic cardiomyopathy; *JPH2*: Junctophilin 2; *JUP*: Junction Plakoglobin;

LMNA: Lamin A/C; *MYBPC3*: Myosin Binding Protein C3; *MYH7*: Myosin Heavy Chain 7;

MYL2: Myosin Light Chain 2; *MYL3*: Myosin Light Chain 3; *NEXN*: Nexilin F-Actin Binding Protein;

PKP2: Plakophilin 2; *PLN*: phospholamban; *RBM20*: RNA Binding Motif Protein 20;

SCN5A: Sodium Voltage-Gated Channel Alpha Subunit 5; *TMEM43*: Transmembrane Protein 43; *TNNC1*: Troponin C1, Slow Skeletal And Cardiac Type; *TNNI3*: Troponin I3, Cardiac Type; *TNNT2*: Troponin T2, Cardiac Type; *TPM1*: Tropomyosin 1; *TTN*: Titin; *VCL*: Vinculin.

Supplementary Table II: Disease definitions

Phenotype	Field names	Values (ICD or other coding)
Diabetes	Diagnoses ICD10	
	Underlying (primary) cause of death: ICD10 Contributory (secondary) causes of death: ICD10 External causes ICD10	E10*; E11*; E12*; E13*; E14*
	Diagnoses main ICD10	
	Diagnoses secondary ICD10	
	Non-cancer illness code self-reported	1220; 1222; 1223
	Diabetes diagnosed by doctor	1
	Medication for cholesterol blood pressure or diabetes(, or take exogenous hormones)	3
Hypertension	Diagnoses ICD10	
	Underlying (primary) cause of death: ICD10 Contributory (secondary) causes of death: ICD10 External causes ICD10	I10; I15*
	Diagnoses main ICD10	
	Diagnoses secondary ICD10	
	Non-cancer illness code self-reported	1065; 1072
	Medication for cholesterol blood pressure or diabetes(, or take exogenous hormones)	2
Hypercholesterolaemia	Diagnoses ICD10	
	Underlying (primary) cause of death: ICD10 Contributory (secondary) causes of death: ICD10 External causes ICD10	E780
	Diagnoses main ICD10	
	Diagnoses secondary ICD10	
	Non-cancer illness code self-reported	1473
	Medication for cholesterol blood pressure or diabetes(, or take exogenous hormones)	1
Ever smoked	Smoking status	1; 2
Family heart disease	Illnesses of father	
	Illnesses of mother Illnesses of siblings	1
Cardiac problem	Non-cancer illness code self-reported	1066
Heart failure	Diagnoses ICD10	
	Underlying (primary) cause of death: ICD10 Contributory (secondary) causes of death: ICD10 External causes ICD10	I110; I130; I132; I50*
	Diagnoses main ICD10	
	Diagnoses secondary ICD10	
	Non-cancer illness code self-reported	1076
Cardiomyopathy	Diagnoses ICD10	
	Underlying (primary) cause of death: ICD10 Contributory (secondary) causes of death: ICD10 External causes ICD10	I42*
	Diagnoses main ICD10	
	Diagnoses secondary ICD10	
	Non-cancer illness code self-reported	1079
Dilated cardiomyopathy	Diagnoses ICD10	
	Underlying (primary) cause of death: ICD10 Contributory (secondary) causes of death: ICD10 External causes ICD10	I420
	Diagnoses main ICD10	
	Diagnoses secondary ICD10	
	Non-cancer illness code self-reported	
Hypertrophic cardiomyopathy	Diagnoses ICD10	
	Underlying (primary) cause of death: ICD10 Contributory (secondary) causes of death: ICD10 External causes ICD10	I421; I422
	Diagnoses main ICD10	
	Diagnoses secondary ICD10	
	Non-cancer illness code self-reported	1588

Supplementary Table II: Continued.

Phenotype	Field names	Values (ICD or other coding)
Ventricular arrhythmias	Diagnoses ICD10	
	Underlying (primary) cause of death: ICD10 Contributory (secondary) causes of death: ICD10 External causes ICD10	1470; 1472; 1490; 1493
	Diagnoses main ICD10	
	Diagnoses secondary ICD10	
Atrial arrhythmias	Diagnoses ICD10	
	Underlying (primary) cause of death: ICD10 Contributory (secondary) causes of death: ICD10 External causes ICD10	148*; 1471; 1491
	Diagnoses main ICD10	
	Diagnoses secondary ICD10	
Heart arrhythmia	Non-cancer illness code self-reported	1471; 1483; 1487
	Non-cancer illness code self-reported	1077
Chronic ischemic heart disease	Diagnoses ICD10	
	Underlying (primary) cause of death: ICD10 Contributory (secondary) causes of death: ICD10 External causes ICD10	125*
	Diagnoses main ICD10	
	Diagnoses secondary ICD10	
Acute myocardial infarction	Diagnoses ICD10	
	Underlying (primary) cause of death: ICD10 Contributory (secondary) causes of death: ICD10 External causes ICD10	121*; 122*; 1248; 1249
	Diagnoses main ICD10	
	Diagnoses secondary ICD10	
	Non-cancer illness code self-reported	1075
Cardiac arrest	Diagnoses ICD10	
	Underlying (primary) cause of death: ICD10 Contributory (secondary) causes of death: ICD10 External causes ICD10	146*
	Diagnoses main ICD10	
	Diagnoses secondary ICD10	
Angina pectoris	Non-cancer illness code self-reported	1074
Conduction disorders	Diagnoses ICD10	
	Underlying (primary) cause of death: ICD10 Contributory (secondary) causes of death: ICD10 External causes ICD10	144*; 145*
	Diagnoses main ICD10	
	Diagnoses secondary ICD10	
Valvular disease	Diagnoses ICD10	
	Underlying (primary) cause of death: ICD10 Contributory (secondary) causes of death: ICD10 External causes ICD10	134*; 135*; 136*; 137*; 105*; 106*; 107*; 108*
	Diagnoses main ICD10	
	Diagnoses secondary ICD10	
	Non-cancer illness code self-reported	1078; 1488; 1489; 1490; 1584; 1585; 1586; 1587
Congenital heart disease	Diagnoses ICD10	
	Underlying (primary) cause of death: ICD10 Contributory (secondary) causes of death: ICD10 External causes ICD10	Q20*; Q21*; Q22*; Q23*; Q24*; Q25*; Q26*
	Diagnoses main ICD10	
	Diagnoses secondary ICD10	
Pulmonary obstructive disease	Diagnoses ICD10	
	Underlying (primary) cause of death: ICD10 Contributory (secondary) causes of death: ICD10 External causes ICD10	J44*; J43*; I26*; I27*
	Diagnoses main ICD10	
	Diagnoses secondary ICD10	
All-cause mortality	Non-cancer illness code self-reported	1112; 1113; 1114; 1115; 1121
All-cause mortality	Date of Death	Any non-missing value
Cardiovascular death	Underlying (primary) cause of death: ICD10	I*
	Contributory (secondary) causes of death: ICD10	

* indicates starting with previously indicated code.

Supplementary Table III: extensive baseline tableDue to its size, this table is only available online <https://doi.org/10.1161/CIRCGEN.122.003704>**Supplementary Table IV: detailed information of all included SNPs**Due to its size, this table is only available online <https://doi.org/10.1161/CIRCGEN.122.003704>

Supplementary Table V: Prevalence of all genes per cardiomyopathy

Cardiomyopathy	Gene	N	Proportion	Prevalence
ARVC	<i>DES</i>	15	4.3	7.48E-05
	<i>DSC2</i>	42	12.1	2.09E-04
	<i>DSG2</i>	31	8.9	1.55E-04
	<i>DSP</i>	49	14.1	2.44E-04
	<i>JUP</i>	24	6.9	1.20E-04
	<i>PKP2</i>	185	53.3	9.22E-04
	<i>PLN</i>	1	0.3	4.98E-06
DCM	<i>ACTC1</i>	1	0.1	4.98E-06
	<i>ACTN2</i>	6	0.8	2.99E-05
	<i>BAG3</i>	15	1.9	7.48E-05
	<i>DES</i>	49	6.1	2.44E-04
	<i>DSP</i>	49	6.1	2.44E-04
	<i>FLNC</i>	56	7.0	2.79E-04
	<i>LMNA</i>	42	5.3	2.09E-04
	<i>MYH7</i>	158	19.8	7.87E-04
	<i>NEXN</i>	4	0.5	1.99E-05
	<i>PLN</i>	8	1.0	3.99E-05
	<i>RBM20</i>	5	0.6	2.49E-05
	<i>SCN5A</i>	59	7.4	2.94E-04
	<i>TNNC1</i>	7	0.9	3.49E-05
	<i>TNNI3</i>	35	4.4	1.74E-04
	<i>TNNT2</i>	32	4.0	1.59E-04
	<i>TPM1</i>	2	0.3	9.97E-06
	<i>TTN</i>	272	34.0	1.36E-03
HCM	<i>ACTC1</i>	1	0.1	4.98E-06
	<i>CSRP3</i>	27	2.0	1.35E-04
	<i>JPH2</i>	6	0.4	2.99E-05
	<i>MYBPC3</i>	723	53.6	3.60E-03
	<i>MYH7</i>	232	17.2	1.16E-03
	<i>MYL2</i>	21	1.6	1.05E-04
	<i>MYL3</i>	1	0.1	4.98E-06
	<i>TNNC1</i>	7	0.5	3.49E-05
	<i>TNNI3</i>	50	3.7	2.49E-04
	<i>TNNT2</i>	274	20.3	1.37E-03
<i>TPM1</i>	6	0.4	2.99E-05	

Abbreviations:

ACTC1: Actin Alpha Cardiac Muscle 1; *ACTN2*: Alpha-actinin 2;*ARVC*: Arrhythmogenic right ventricular cardiomyopathy; *BAG3*: BAG Cochaperone 3; *CSRP3*: Cysteine And Glycine Rich Protein 3; *DCM*: Dilated cardiomyopathy; *DES*: Desmin; *DSC2*: Desmocollin 2; *DSG2*: Desmoglein 2; *DSG2*: Desmoglein 2; *DSP*: desmoplakin; *FLNC*: Filamin-C; *HCM*: Hypertrophic cardiomyopathy; *JPH2*: Junctophilin 2;*JUP*: Junction Plakoglobin; *LMNA*: Lamin A/C; *MYBPC3*: Myosin Binding Protein C3; *MYH7*: Myosin Heavy Chain 7; *MYL2*: Myosin Light Chain 2; *MYL3*: Myosin Light Chain 3; *N*: Number of individuals; *NEXN*: Nexilin F-Actin Binding Protein; *PKP2*: Plakophilin 2; *PLN*: phospholamban; *RBM20*: RNA Binding Motif Protein 20;*SCN5A*: Sodium Voltage-Gated Channel Alpha Subunit 5;*TNNC1*: Troponin C1, Slow Skeletal And Cardiac Type; *TNNI3*: Troponin I3, Cardiac Type; *TNNT2*: Troponin T2, Cardiac Type; *TPM1*: Tropomyosin 1; *TTN*: Titin.**Supplementary Table VI: Prevalence of variants associated with the inherited cardiomyopathies**

Cardiomyopathy	Prevalence with overlapping genes	Prevalence without overlapping genes	Previously reported prevalence range
ARVC	1:578	1:712	1:143 - 1:1,706 ¹³⁻¹⁵
DCM	1:251	1:289 (ARVC overlap) / 1:354 (HCM overlap)	1:33 - 1:526 ^{16, 17}
HCM	1:149	1:260	1:164 ¹⁹

Abbreviations:

ARVC: arrhythmogenic right ventricular cardiomyopathy; DCM: dilated cardiomyopathy; HCM: hypertrophic cardiomyopathy.

Supplementary Table VII: Results of Fisher's Exact tests

	ARVC G+ vs G-				DCM G+ vs G-				HCM G+ vs G-			
	OR	95% LCI	95% UCI	p-value	OR	95% LCI	95% UCI	p-value	OR	95% LCI	95% UCI	p-value
CARDIOVASCULAR RISK FACTORS												
Diabetes	1.112	0.755	1.592	0.570	0.833	0.626	1.091	0.200	1.280	1.061	1.537	0.008
Hypertension	0.962	0.760	1.212	0.774	1.072	0.919	1.248	0.374	1.045	0.925	1.179	0.482
Hypercholesterolaemia	1.031	0.795	1.326	0.799	1.120	0.946	1.322	0.185	1.181	1.036	1.345	0.011
Ever Smoked	1.223	0.981	1.525	0.068	1.222	1.055	1.416	0.007	0.956	0.849	1.075	0.461
Family heart disease	1.318	1.058	1.643	0.012	1.119	0.966	1.296	0.130	1.066	0.949	1.197	0.280
CARDIAC DISEASE/OUTCOME												
Cardiac problem	2.112	0.416	6.672	0.183	0.912	0.180	2.868	1.000	0.903	0.278	2.289	1.000
Heart failure*	1.432	0.639	2.812	0.305	2.534	1.708	3.671	5.05E-06	1.352	0.899	1.977	0.135
Cardiomyopathy*	2.341	0.460	7.452	0.150	7.590	4.242	13.283	6.94E-11	5.495	3.206	9.306	8.76E-10
Phenotype positive†	1.325	0.351	3.547	0.550	3.664	2.236	5.813	4.88E-07	3.033	1.979	4.560	5.76E-07
Dilated cardiomyopathy*	4.122	0.453	18.056	0.099	8.090	3.078	20.130	2.08E-05	0.529	0.013	3.481	1.000
Hypertrophic cardiomyopathy*	3.599	0.081	26.974	0.265	10.989	3.383	34.746	4.60E-05	18.775	7.903	49.429	3.41E-13
Ventricular arrhythmias	6.198	2.297	14.376	3.27E-04	4.974	2.392	9.752	1.93E-05	1.801	0.717	3.987	0.143
Atrial arrhythmias	1.054	0.415	2.239	0.841	2.273	1.518	3.314	8.18E-05	1.247	0.826	1.830	0.250
Heart arrhythmia	3.231	1.128	7.573	0.015	2.796	1.356	5.321	0.003	0.547	0.144	1.488	0.310
Chronic ischemic heart disease*	1.431	0.971	2.052	0.059	1.281	0.981	1.652	0.058	0.947	0.748	1.186	0.695
Acute myocardial infarction	1.467	0.801	2.494	0.151	1.134	0.730	1.697	0.519	0.892	0.610	1.270	0.606
Cardiac arrest	0.000	0.000	3.299	0.630	2.209	0.756	5.343	0.118	1.090	0.332	2.808	0.804
Angina pectoris	1.497	0.835	2.506	0.120	1.206	0.795	1.772	0.344	1.344	0.987	1.803	0.049
Conduction disorders	1.535	0.645	3.137	0.260	1.497	0.859	2.464	0.136	1.281	0.807	1.960	0.242
Valvular disease	1.322	0.645	2.439	0.373	1.958	1.335	2.801	4.54E-04	1.269	0.883	1.782	0.163
Congenital heart disease	2.059	0.237	8.219	0.267	1.337	0.260	4.342	0.499	1.059	0.269	3.033	0.788
Pulmonary obstructive disease	1.490	0.940	2.266	0.078	1.198	0.860	1.634	0.240	0.848	0.629	1.125	0.280

Supplementary Table VII: Continued.

	ARVC G+ vs G-				DCM G+ vs G-				HCM G+ vs G-			
	OR	95% LCI	95% UCI	p-value	OR	95% LCI	95% UCI	p-value	OR	95% LCI	95% UCI	p-value
Cardiovascular death	1.771	0.860	3.286	0.100	1.673	1.038	2.588	0.030	0.733	0.423	1.197	0.268
All-cause mortality	1.068	0.629	1.713	0.712	1.388	1.023	1.852	0.032	0.890	0.668	1.169	0.428

* Used to define P+, therefore not included in some tests.

† Defined as diagnosis of cardiomyopathy, DCM, HCM or heart failure, in absence of chronic ischemic heart disease.

Abbreviations:

ARVC: arrhythmogenic right ventricular cardiomyopathy; DCM: dilated cardiomyopathy;

G+: carriers of likely pathogenic and pathogenic variants associated with one of the cardiomyopathies; HCM: hypertrophic cardiomyopathy; LCI: lower limit confidence interval; UCI: upper limit confidence interval.

Supplementary Table VII: Results of Fisher's Exact tests

	strict HCM G+ vs G-			ARVC G+P- vs G-P-			DCM G+P- vs G-P-			
	OR	95% LCI	p-value	OR	95% LCI	p-value	OR	95% LCI	p-value	
CARDIOVASCULAR RISK FACTORS										
Diabetes	0.802	0.601	1.055	1.108	0.749	1.594	0.860	0.645	1.130	0.296
Hypertension	1.093	0.938	1.273	0.954	0.752	1.205	1.032	0.882	1.207	0.694
Hypercholesterolaemia	1.006	0.846	1.193	1.006	0.772	1.298	1.081	0.909	1.281	0.361
Ever Smoked	1.160	1.000	1.344	1.228	0.983	1.533	1.233	1.062	1.432	0.006
Family heart disease	1.168	1.008	1.352	1.286	1.031	1.605	1.134	0.976	1.316	0.099
CARDIAC DISEASE/OUTCOME										
Cardiac problem	1.216	0.315	3.369	2.227	0.438	7.061	0.981	0.194	3.097	1.000
Heart failure*	1.733	1.086	2.661	NA	NA	NA	NA	NA	NA	NA
Cardiomyopathy*	8.647	4.962	14.841	NA	NA	NA	NA	NA	NA	NA
Phenotype positive†	4.727	3.028	7.216	NA	NA	NA	NA	NA	NA	NA
Dilated cardiomyopathy*	0.000	0.000	3.756	NA	NA	NA	NA	NA	NA	NA
Hypertrophic cardiomyopathy*	30.258	12.586	79.971	NA	NA	NA	NA	NA	NA	NA
Ventricular arrhythmias	3.038	1.208	6.738	5.846	1.976	14.398	3.426	1.352	7.682	0.005
Atrial arrhythmias	1.650	1.035	2.530	1.176	0.462	2.504	2.117	1.357	3.194	0.001
Heart arrhythmia	0.690	0.138	2.136	2.797	0.866	7.018	2.471	1.115	4.941	0.013
Chronic ischemic heart disease*	0.885	0.649	1.187	NA	NA	NA	NA	NA	NA	NA
Acute myocardial infarction	0.917	0.562	1.425	1.476	0.806	2.511	1.121	0.715	1.689	0.586
Cardiac arrest	1.467	0.377	4.128	0.000	0.000	3.415	1.938	0.589	5.017	0.195
Angina pectoris	1.288	0.860	1.873	1.511	0.843	2.531	1.244	0.819	1.828	0.244
Conduction disorders	1.241	0.674	2.126	1.650	0.693	3.379	1.364	0.740	2.342	0.274
Valvular disease	1.517	0.987	2.253	1.332	0.624	2.527	1.662	1.072	2.491	0.017
Congenital heart disease	1.335	0.259	4.337	2.313	0.264	9.341	1.020	0.117	4.105	1.000
Pulmonary obstructive disease	0.903	0.620	1.279	1.575	0.993	2.398	1.090	0.762	1.522	0.600
Cardiovascular death	0.684	0.321	1.294	1.916	0.929	3.562	1.454	0.849	2.358	0.153
All-cause mortality	1.097	0.783	1.505	1.134	0.668	1.820	1.277	0.920	1.738	0.123

* Used to define P+, therefore not included in some tests.

† Defined as diagnosis of cardiomyopathy, DCM, HCM or heart failure, in absence of chronic ischemic heart disease.

Abbreviations:

ARVC: arrhythmogenic right ventricular cardiomyopathy; DCM: dilated cardiomyopathy;

G+: carriers of likely pathogenic and pathogenic variants associated with one of the cardiomyopathies; HCM: hypertrophic cardiomyopathy; LCI: lower limit confidence interval; UCI: upper limit confidence interval.

Supplementary Table VII: Results of Fisher's Exact tests

	HCM G+P- vs G-P-			strict HCM G+P- vs G-P-		
	OR	95% LCI	p-value	OR	95% LCI	p-value
CARDIOVASCULAR RISK FACTORS						
Diabetes	1.301	1.075	1.566	0.806	0.599	1.067
Hypertension	1.022	0.903	1.155	1.051	0.897	1.228
Hypercholesterolaemia	1.179	1.032	1.344	0.991	0.830	1.179
Ever Smoked	0.968	0.859	1.090	1.187	1.022	1.380
Family heart disease	1.068	0.949	1.200	1.175	1.012	1.364
CARDIAC DISEASE/OUTCOME						
Cardiac problem	0.967	0.297	2.460	1.320	0.342	3.673
Heart failure*	NA	NA	NA	NA	NA	NA
Cardiomyopathy*	NA	NA	NA	NA	NA	NA
Phenotype positive†	NA	NA	NA	NA	NA	NA
Dilated cardiomyopathy*	NA	NA	NA	NA	NA	NA
Hypertrophic cardiomyopathy*	NA	NA	NA	NA	NA	NA
Ventricular arrhythmias	1.005	0.257	2.859	1.718	0.438	4.892
Atrial arrhythmias	1.143	0.723	1.741	1.431	0.836	2.319
Heart arrhythmia	0.579	0.152	1.577	0.741	0.148	2.296
Chronic ischemic heart disease*	NA	NA	NA	NA	NA	NA
Acute myocardial infarction	0.860	0.581	1.235	0.862	0.516	1.366
Cardiac arrest	1.143	0.348	2.954	1.561	0.401	4.405
Angina pectoris	1.378	1.011	1.849	1.341	0.894	1.950
Conduction disorders	1.071	0.632	1.724	0.910	0.425	1.734
Valvular disease	1.145	0.765	1.665	1.245	0.751	1.966
Congenital heart disease	1.207	0.305	3.503	1.545	0.298	5.079
Pulmonary obstructive disease	0.844	0.619	1.130	0.898	0.606	1.291
Cardiovascular death	0.669	0.365	1.141	0.531	0.210	1.125
All-cause mortality	0.863	0.638	1.148	1.061	0.742	1.481

* Used to define P+, therefore not included in some tests.

† Defined as diagnosis of cardiomyopathy, DCM, HCM or heart failure, in absence of chronic ischemic heart disease.

Abbreviations:

ARVC: arrhythmogenic right ventricular cardiomyopathy; DCM: dilated cardiomyopathy;

G+: carriers of likely pathogenic and pathogenic variants associated with one of the cardiomyopathies; HCM: hypertrophic cardiomyopathy; LCI: lower limit confidence interval; UCI: upper limit confidence interval.

Supplementary Table VIII: P-values of Mann-Whitney U tests

	ARVC G+ vs G-	DCM G+ vs G-	HCM G+ vs G-	strict HCM* G+ vs G-
CARDIOVASCULAR RISK FACTORS				
BMI	0.990	0.812	0.271	0.621
Mean systolic blood pressure	0.774	0.901	0.258	0.508
Mean diastolic blood pressure	0.341	0.734	0.997	0.776
Total cholesterol	0.369	0.844	0.242	0.666
HDL	0.941	0.357	0.076	0.161
LDL	0.214	0.898	0.484	0.778
MET minutes per week for walking	0.545	0.055	0.233	0.017
MET minutes per week for moderate activity	0.950	0.913	0.578	0.155
MET minutes per week for vigorous activity	0.352	0.963	0.350	0.589
Total MET minutes per week	0.278	0.619	0.980	0.052
ECG MEASUREMENTS				
P duration	NA	NA	NA	NA
P axis	NA	NA	NA	NA
PQ interval	NA	NA	NA	NA
QRS duration	NA	NA	NA	NA
R axis	NA	NA	NA	NA
QTC interval	NA	NA	NA	NA
T axis	NA	NA	NA	NA
CMR MEASUREMENTS				
RVEDVi	NA	NA	NA	NA
RVESVi	NA	NA	NA	NA
RVSv	NA	NA	NA	NA
RVSVi	NA	NA	NA	NA
RVEF	NA	NA	NA	NA
RVPER	NA	NA	NA	NA
RVPFR	NA	NA	NA	NA
RVPAFR	NA	NA	NA	NA
LVEDVi	NA	NA	NA	NA
LVESVi	NA	NA	NA	NA
LVSv	NA	NA	NA	NA
LVSVi	NA	NA	NA	NA
LVEF	NA	NA	NA	NA
LVPER	NA	NA	NA	NA
LVPFR	NA	NA	NA	NA
LVPAFR	NA	NA	NA	NA
LVEDMi	NA	NA	NA	NA
LVMVR	NA	NA	NA	NA
LVEDV/RVEDV	NA	NA	NA	NA
LVESV/RVESV	NA	NA	NA	NA
peakEcc	NA	NA	NA	NA
TPKEcc	NA	NA	NA	NA
peakEII2Ch	NA	NA	NA	NA
TPKEII2Ch	NA	NA	NA	NA
peakEII4Ch	NA	NA	NA	NA

Supplementary Table VIII: Continued.

	ARVC G+ vs G-	DCM G+ vs G-	HCM G+ vs G-	strict HCM* G+ vs G-
TPKEII4Ch	NA	NA	NA	NA
Wall thickness segment 1	NA	NA	NA	NA
Wall thickness segment 2	NA	NA	NA	NA
Wall thickness segment 3	NA	NA	NA	NA
Wall thickness segment 4	NA	NA	NA	NA
Wall thickness segment 5	NA	NA	NA	NA
Wall thickness segment 6	NA	NA	NA	NA
Wall thickness segment 7	NA	NA	NA	NA
Wall thickness segment 8	NA	NA	NA	NA
Wall thickness segment 9	NA	NA	NA	NA
Wall thickness segment 10	NA	NA	NA	NA
Wall thickness segment 11	NA	NA	NA	NA
Wall thickness segment 12	NA	NA	NA	NA
Wall thickness segment 13	NA	NA	NA	NA
Wall thickness segment 14	NA	NA	NA	NA
Wall thickness segment 15	NA	NA	NA	NA
Wall thickness segment 16	NA	NA	NA	NA
Global wall thickness	NA	NA	NA	NA
Septal wall thickness	NA	NA	NA	NA
Maximum wall thickness	NA	NA	NA	NA

* strict HCM group: HCM group after excluding carriers of the 3628-41_3628-17del *MYBPC3* and the Arg278Cys 862C>T *TNNI2* variant.

Abbreviations:

ARVC: arrhythmogenic right ventricular cardiomyopathy; BMI: body mass index; CMR: cardiac magnetic resonance imaging; DCM: dilated cardiomyopathy; ECG: Electrocardiography; EDVi: indexed end-diastolic volume; EDMi: indexed end-diastolic mass; EF: ejection fraction; ESVi: indexed end-systolic volume; G+: carriers of likely pathogenic and pathogenic variants associated with one of the cardiomyopathies; HCM: hypertrophic cardiomyopathy; HDL: high-density lipoprotein; LDL: low-density lipoprotein; LV: left ventricular; MET: metabolic equivalent of task; MVR: mass to volume ratio; PAFR: peak atrial filling rate; peakEcc: peak circumferential strain; peakEII2Ch: longitudinal strain analyzed in 2-chamber view; peakEII4Ch: longitudinal strain analyzed in 4-chamber view; PER: peak ejection rate; PFR: peak filling rate; RV: right ventricular; SVi: indexed stroke volume; TPKEcc: global time to peak circumferential strain; TPKEII2Ch: global time to longitudinal strain analyzed in 2-chamber view; TPKEII4Ch: global time to longitudinal strain analyzed in 4-chamber view.

Supplementary Table VIII: P-values of Mann-Whitney U tests

	ARVC G+P- vs G-P-	DCM G+P- vs G-P-	HCM G+P- vs G-P-	strict HCM* G+P- vs G-P-
CARDIOVASCULAR RISK FACTORS				
BMI	0.945	0.800	0.317	0.712
Mean systolic blood pressure	0.917	0.913	0.257	0.608
Mean diastolic blood pressure	0.367	0.760	0.934	0.737
Total cholesterol	0.381	0.780	0.211	0.808
HDL	0.999	0.471	0.070	0.161
LDL	0.223	0.991	0.404	0.991
MET minutes per week for walking	0.500	0.084	0.189	0.010
MET minutes per week for moderate activity	0.989	0.965	0.605	0.137
MET minutes per week for vigorous activity	0.434	0.885	0.379	0.557
Total MET minutes per week	0.290	0.722	0.943	0.038
ECG MEASUREMENTS				
P duration	0.315	0.304	0.997	0.999
P axis	0.477	0.162	0.085	0.179
PQ interval	0.617	0.989	0.527	0.904
QRS duration	0.385	0.043	0.445	0.436
R axis	0.208	0.156	0.868	0.699
QTC interval	0.255	0.422	0.300	0.270
T axis	0.818	0.572	0.074	0.128
CMR MEASUREMENTS				
RVEDVi	0.780	0.058	0.177	0.722
RVESVi	0.707	0.287	0.051	0.118
RVSv	0.713	0.071	0.910	0.140
RVSVi	0.546	0.155	0.872	0.106
RVEF	0.950	0.765	0.025	0.015
RVPER	0.869	0.038	0.711	0.615
RVPFR	0.908	0.120	0.064	0.249
RVPAFR	0.661	0.385	0.192	0.025
LVEDVi	0.060	0.125	0.378	0.444
LVESVi	0.414	0.032	0.276	0.460
LVSv	0.100	0.509	0.889	0.214
LVSVi	0.052	0.430	0.921	0.318
LVEF	0.452	0.009	0.366	0.607
LVPER	0.465	0.023	0.190	0.420
LVPFR	0.114	0.436	0.567	0.485
LVPAFR	0.670	0.412	0.659	0.189
LVEDMi	0.800	0.738	0.928	0.188
LVMVR	0.295	0.061	0.784	0.559
LVEDV/RVEDV	0.360	0.001	0.533	0.747
LVESV/RVESV	0.904	0.000	0.585	0.027
peakEcc	0.319	0.107	0.643	0.812
TPKEcc	0.555	0.155	0.723	0.850
peakEII2Ch	0.751	0.019	0.751	0.179
TPKEII2Ch	0.616	0.701	0.978	0.314
peakEII4Ch	0.483	0.009	0.079	0.286

Supplementary Table VIII: Continued.

	ARVC G+P- vs G-P-	DCM G+P- vs G-P-	HCM G+P- vs G-P-	strict HCM* G+P- vs G-P-
TPKEII4Ch	0.941	0.708	0.227	0.403
Wall thickness segment 1	0.211	0.439	0.740	0.029
Wall thickness segment 2	0.446	0.022	0.160	0.155
Wall thickness segment 3	0.268	0.144	0.450	0.254
Wall thickness segment 4	0.020	0.626	0.460	0.919
Wall thickness segment 5	0.110	0.132	0.189	0.745
Wall thickness segment 6	0.736	0.363	0.978	0.503
Wall thickness segment 7	0.234	0.435	0.539	0.826
Wall thickness segment 8	0.622	0.251	0.348	0.753
Wall thickness segment 9	0.087	0.438	0.850	0.303
Wall thickness segment 10	0.035	0.508	0.789	0.220
Wall thickness segment 11	0.083	0.484	0.482	0.502
Wall thickness segment 12	0.237	0.108	0.361	0.943
Wall thickness segment 13	0.974	0.828	0.987	0.575
Wall thickness segment 14	0.832	0.243	0.479	0.869
Wall thickness segment 15	0.988	0.277	0.571	0.748
Wall thickness segment 16	0.938	0.423	0.836	0.333
Global wall thickness	0.159	0.232	0.961	0.270
Septal wall thickness	0.229	0.071	0.523	0.174
Maximum wall thickness	0.210	0.621	0.166	0.008

* strict HCM group: HCM group after excluding carriers of the 3628-41_3628-17del *MYBPC3* and the Arg278Cys 862C>T *TNN2* variant.

Abbreviations:

ARVC: arrhythmogenic right ventricular cardiomyopathy; BMI: body mass index; CMR: cardiac magnetic resonance imaging; DCM: dilated cardiomyopathy; ECG: Electrocardiography; EDVi: indexed end-diastolic volume; EDMi: indexed end-diastolic mass; EF: ejection fraction; ESVi: indexed end-systolic volume; G+: carriers of likely pathogenic and pathogenic variants associated with one of the cardiomyopathies; HCM: hypertrophic cardiomyopathy; HDL: high-density lipoprotein; LDL: low-density lipoprotein; LV: left ventricular; MET: metabolic equivalent of task; MVR: mass to volume ratio; PAFR: peak atrial filling rate; peakEcc: peak circumferential strain; peakEII2Ch: longitudinal strain analyzed in 2-chamber view; peakEII4Ch: longitudinal strain analyzed in 4-chamber view; PER: peak ejection rate; PFR: peak filling rate; RV: right ventricular; SVi: indexed stroke volume; TPKEcc: global time to peak circumferential strain; TPKEII2Ch: global time to longitudinal strain analyzed in 2-chamber view; TPKEII4Ch: global time to longitudinal strain analyzed in 4-chamber view.

Supplementary Table IX: Extensive baseline table of P- CMR participants

	ARVC G+	DCM G+	HCM G+	Controls G-	Missing
n	33	87	130	986	
Sex = Female (%)	19 (57.6)	46 (52.9)	62 (47.7)	486 (49.3)	0
Age (median [IQR])	54.00 [50.00, 61.00]	55.00 [50.00, 59.50]	54.00 [48.00, 60.00]	55.00 [49.00, 60.00]	0
Ethnicity (%)					
Asian	0 (0.0)	1 (1.1)	18 (13.8)	76 (7.7)	
Black	0 (0.0)	1 (1.1)	2 (1.5)	2 (0.2)	
Chinese	1 (3.0)	1 (1.1)	1 (0.8)	9 (0.9)	
Mixed	0 (0.0)	1 (1.1)	5 (3.8)	15 (1.5)	
Other	0 (0.0)	0 (0.0)	1 (0.8)	5 (0.5)	
White	32 (97.0)	83 (95.4)	103 (79.2)	879 (89.1)	
CARDIOVASCULAR RISK FACTORS					
BMI (median [IQR])	26.10 [24.23, 28.72]	26.27 [23.68, 29.11]	26.07 [23.82, 28.82]	25.84 [23.58, 28.62]	0
Diabetes (%)	2 (6.1)	7 (8.0)	12 (9.2)	78 (7.9)	0
Hypertension (%)	6 (18.2)	27 (31.0)	42 (32.3)	309 (31.3)	0
Mean systolic blood pressure (median [IQR])	131.00 [117.50, 141.00]	134.50 [120.75, 146.75]	133.00 [122.00, 146.50]	133.50 [122.00, 146.00]	0.2
Mean diastolic blood pressure (median [IQR])	79.50 [73.00, 86.50]	80.25 [74.50, 87.38]	81.50 [76.00, 87.50]	81.00 [74.50, 87.00]	0.2
Hypercholesterolaemia (%)	9 (27.3)	26 (29.9)	45 (34.6)	269 (27.3)	0
Total cholesterol (median [IQR])	5.39 [4.92, 6.09]	5.51 [4.76, 6.34]	5.66 [4.85, 6.48]	5.63 [4.94, 6.44]	3.5
HDL (median [IQR])	1.41 [1.12, 1.63]	1.42 [1.19, 1.61]	1.38 [1.14, 1.62]	1.40 [1.18, 1.71]	8.8
LDL (median [IQR])	3.31 [3.00, 4.02]	3.45 [2.87, 4.13]	3.58 [2.89, 4.24]	3.50 [3.00, 4.11]	3.7
Ever Smoked (%)	13 (39.4)	45 (51.7)	53 (40.8)	397 (40.3)	0
MET minutes per week for walking (median [IQR])	693.00 [309.38, 1,386.00]	462.00 [198.00, 1,188.00]	495.00 [247.50, 1,039.50]	594.00 [247.50, 1,188.00]	14.3
MET minutes per week for moderate activity (median [IQR])	360.00 [90.00, 880.00]	570.00 [240.00, 960.00]	360.00 [160.00, 840.00]	360.00 [120.00, 1,080.00]	14.3
[IQR] MET minutes per week for vigorous activity	240.00 [0.00, 1,100.00]	280.00 [0.00, 960.00]	320.00 [0.00, 960.00]	288.00 [0.00, 960.00]	14.3
(median [IQR]) Total MET minutes per week (median [IQR])	1,840.50 [1,113.00, 2,447.25]	1,483.00 [937.50, 3,097.50]	1,436.00 [793.00, 2,559.00]	1,737.00 [736.88, 3,352.50]	14.3
Family heart disease (%)	17 (51.5)	47 (54.0)	82 (61.2)	542 (54.7)	0

Supplementary Table IX: Continued.

	ARVC G+	DCM G+	HCM G+	Controls G-	Missing
CARDIAC DISEASE/OUTCOME					
Cardiac problem (%)	0 (0.0)	1 (1.1)	1 (0.8)6 [0.6]0		
Heart failure (%)	0 (0.0)	0 (0.0)	1 (0.8)5 [0.5]0		
Cardiomyopathy (%)	0 (0.0)	0 (0.0)	0 (0.0)	0 (0.0)	0
Dilated cardiomyopathy (%)	0 (0.0)	0 (0.0)	0 (0.0)	0 (0.0)	0
Hypertrophic cardiomyopathy (%)	0 (0.0)	0 (0.0)	0 (0.0)	0 (0.0)	0
Ventricular arrhythmias (%)	0 (0.0)	0 (0.0)	0 (0.0)	2 (0.2)	0
Atrial arrhythmias (%)	0 (0.0)	5 (5.7)	3 (2.3)	12 (1.2)	0
Heart arrhythmia (%)	1 (3.0)	3 (3.4)	0 (0.0)	5 (0.5)	0
Chronic ischemic heart disease (%)	2 (6.1)	3 (3.4)	3 (2.3)	43 (4.4)	0
(%) Acute myocardial infarction	0 (0.0)	0 (0.0)	1 (0.8)	29 (2.9)	0
(%) Cardiac arrest (%)	0 (0.0)	0 (0.0)	0 (0.0)	1 (0.1)	0
Angina pectoris (%)	1 (3.0)	2 (2.3)	6 (4.6)	18 (1.8)	0
Conduction disorders	0 (0.0)	0 (0.0)	2 (1.5)	10 (1.0)	0
(%) Valvular disease (%)	0 (0.0)	2 (2.3)	0 (0.0)	23 (2.3)	0
Congenital heart disease (%)	0 (0.0)	0 (0.0)	0 (0.0)	0 (0.0)	0
Pulmonary obstructive disease (%)	2 (6.1)	3 (3.4)	4 (3.1)	35 (3.5)	0
Cardiovascular death (%)	0 (0.0)	0 (0.0)	1 (0.8)	3 (0.3)	0
All-cause mortality (%)	0 (0.0)	1 (1.1)	1 (0.8)	12 (1.2)	0
ECG MEASUREMENTS					
n (%)	29 (87.9)	80 (92.0)	110 (84.6)	856 (86.8)	0
P duration (median [IQR])P axis (median [IQR])	100.00 [92.00, 110.00]	98.00 [86.00, 106.00]	100.00 [90.00, 107.00]	100.00 [90.00, 108.00]	16.3
PQ interval (median [IQR])	54.00 [42.25, 61.50]	48.00 [36.00, 61.00]	49.00 [35.00, 62.50]	55.00 [41.00, 67.00]	37.4
QRS duration (median [IQR])	171.00 [147.00, 183.00]	165.00 [144.50, 176.00]	160.00 [146.00, 170.00]	160.00 [144.00, 178.00]	37.5
R axis (median [IQR])	88.00 [80.00, 94.00]	83.00 [78.00, 92.00]	84.00 [80.00, 92.00]	86.00 [80.00, 94.00]	13
QTc interval (median [IQR])	23.50 [-1.75, 50.00]	27.50 [-2.50, 50.00]	40.00 [13.00, 54.00]	35.50 [8.00, 58.00]	35.4
QTc interval (median [IQR])	429.50 [403.25, 440.00]	422.00 [405.50, 435.75]	414.00 [401.00, 429.00]	416.00 [402.00, 432.00]	35.4
T axis (median [IQR])	35.50 [20.25, 54.25]	42.00 [26.25, 57.00]	45.00 [31.00, 61.00]	40.00 [23.00, 55.75]	35.4

Supplementary Table IX: Continued.

	ARVC G+	DCM G+	HCM G+	Controls G-	Missing
CMR MEASUREMENTS					
RVEDVi (median [IQR])	79.14 [73.73, 92.49]	76.54 [69.50, 84.81]	77.12 [67.27, 90.71]	80.19 [70.61, 90.27]	8.4
RVEDV (median [IQR])	35.16 [29.98, 38.71]	32.21 [27.10, 37.43]	31.40 [26.20, 37.28]	32.90 [27.42, 39.70]	8.4
RVSV (median [IQR])	87.13 [71.60, 106.86]	82.22 [69.02, 93.57]	86.09 [69.79, 105.70]	85.85 [72.77, 101.86]	8.4
RVSVi (median [IQR])	48.22 [41.97, 52.24]	44.50 [40.75, 51.29]	45.77 [40.64, 54.04]	46.53 [40.91, 52.81]	8.4
RVEF (median [IQR])	58.30 [53.30, 62.06]	59.31 [52.99, 62.59]	59.56 [54.80, 63.99]	58.37 [54.19, 62.74]	8.7
RVPER (median [IQR])	405.50 [291.70, 489.35]	361.23 [290.08, 443.96]	389.50 [310.20, 475.80]	388.65 [316.52, 465.95]	8.4
RVPAFR (median [IQR])	302.80 [225.65, 375.82]	295.76 [220.44, 343.18]	278.70 [230.80, 334.70]	300.30 [245.10, 363.40]	8.5
RVEDVi (median [IQR])	274.70 [213.70, 343.90]	275.00 [224.92, 344.91]	300.10 [236.43, 366.40]	282.86 [222.52, 360.08]	8.4
RVSVi (median [IQR])	80.77 [73.11, 88.68]	77.32 [68.06, 86.15]	72.34 [64.33, 84.59]	74.37 [66.38, 83.15]	17.8
RVSV (median [IQR])	317.4 [25.91, 39.55]	316.9 [26.19, 39.84]	29.37 [24.09, 34.83]	30.02 [25.13, 35.72]	17.8
LVEF (median [IQR])	91.46 [74.68, 102.10]	80.50 [68.12, 95.54]	82.92 [64.93, 100.22]	81.72 [70.11, 95.72]	17.6
LVPER (median [IQR])	46.82 [43.25, 50.82]	43.18 [37.50, 49.11]	44.07 [38.21, 50.19]	44.06 [39.37, 50.29]	17.6
LVPAFR (median [IQR])	407.30 [307.20, 455.45]	339.21 [259.00, 430.80]	340.46 [264.61, 460.80]	373.80 [302.47, 453.27]	17.6
LVEDMi (median [IQR])	346.20 [290.80, 422.04]	314.20 [258.81, 366.80]	320.25 [248.49, 371.20]	321.50 [259.92, 385.64]	17.6
LVMVR (median [IQR])	208.70 [158.60, 298.40]	253.35 [178.90, 330.36]	241.28 [167.28, 321.50]	233.50 [167.46, 305.10]	17.7
LVEDV/RVEDV (median [IQR])	42.81 [36.04, 48.38]	42.96 [36.56, 46.70]	42.41 [34.90, 49.27]	41.85 [36.55, 48.61]	17.7
LVESV/RVESV (median [IQR])	0.55 [0.49, 0.60]	0.54 [0.49, 0.59]	0.56 [0.50, 0.64]	0.56 [0.50, 0.62]	17.6
peakEcc (median [IQR])	0.94 [0.90, 1.05]	1.00 [0.91, 1.08]	0.94 [0.86, 0.99]	0.93 [0.86, 1.03]	20.3
TPKEcc (median [IQR])	0.91 [0.82, 1.00]	1.02 [0.89, 1.19]	0.90 [0.82, 1.02]	0.91 [0.80, 1.04]	20.3
peakEII2Ch (median [IQR])	-22.87 [-26.91, -21.63]	-22.67 [-24.40, -19.13]	-22.91 [-25.18, -20.88]	-22.72 [-24.98, -20.42]	36.2
TPKEI2Ch (median [IQR])	326.90 [318.44, 363.82]	334.75 [320.35, 360.47]	331.96 [308.18, 353.62]	331.30 [309.75, 354.70]	36.4
peakEII4Ch (median [IQR])	-21.37 [-23.84, -19.31]	-20.29 [-22.24, -17.97]	-21.54 [-23.50, -18.88]	-21.17 [-23.32, -18.93]	37.3
TPKEI4Ch (median [IQR])	346.80 [321.40, 370.50]	353.30 [330.98, 381.65]	353.10 [320.40, 379.60]	349.88 [321.78, 379.08]	37.4
Wall thickness segment 1 (median [IQR])	-24.25 [-26.79, -21.38]	-22.30 [-24.57, -19.76]	-24.05 [-26.94, -22.28]	-23.30 [-25.98, -21.37]	38.3
Wall thickness segment 2 (median [IQR])	354.30 [328.00, 406.60]	354.80 [325.40, 392.55]	349.21 [318.52, 390.17]	357.30 [326.94, 397.80]	38.6
Wall thickness segment 3 (median [IQR])	7.05 [6.25, 8.57]	7.44 [6.78, 8.21]	7.59 [6.72, 8.55]	7.65 [6.81, 8.49]	31.6
Wall thickness segment 4 (median [IQR])	6.81 [5.24, 7.75]	6.03 [5.31, 7.39]	7.06 [5.87, 8.21]	6.75 [5.74, 7.90]	31.6
Wall thickness segment 5 (median [IQR])	5.58 [4.74, 7.16]	6.10 [4.85, 6.66]	6.22 [5.04, 7.39]	6.05 [5.17, 6.95]	31.6
	6.06 [5.49, 6.76]	6.57 [5.89, 6.99]	6.47 [5.85, 6.92]	6.54 [5.81, 7.21]	31.6
	5.96 [5.48, 6.40]	6.08 [5.57, 6.50]	6.03 [5.57, 6.64]	6.20 [5.62, 6.96]	31.6

	ARVC G+	DCM G+	HCM G+	Controls G-	Missing
n	33	87	130	986	
Wall thickness segment 6 (median [IQR])	6.45 [6.15, 6.79]	6.58 [6.05, 7.01]	6.56 [5.93, 7.09]	6.55 [5.97, 7.31]	31.6
Wall thickness segment 7 (median [IQR])	5.52 [5.21, 6.06]	5.56 [5.28, 6.14]	5.75 [5.21, 6.19]	5.73 [5.29, 6.31]	31.7
Wall thickness segment 8 (median [IQR])	6.97 [6.44, 7.28]	6.90 [6.27, 7.47]	6.89 [6.16, 7.49]	7.01 [6.28, 7.75]	31.7
Wall thickness segment 9 (median [IQR])	6.96 [6.18, 7.46]	7.18 [6.64, 7.85]	7.21 [6.38, 8.20]	7.38 [6.48, 8.25]	31.7
Wall thickness segment 10 (median [IQR])	5.88 [5.33, 6.23]	6.28 [5.90, 6.89]	6.18 [5.44, 7.00]	6.24 [5.60, 6.96]	31.7
Wall thickness segment 11 (median [IQR])	5.42 [4.96, 5.81]	5.56 [5.08, 6.08]	5.53 [5.02, 6.37]	5.62 [5.10, 6.32]	31.7
Wall thickness segment 12 (median [IQR])	5.38 [5.17, 6.12]	5.50 [5.14, 6.02]	5.59 [5.08, 6.13]	5.60 [5.22, 6.26]	31.7
Wall thickness segment 13 (median [IQR])	5.38 [5.24, 5.80]	5.44 [5.13, 5.91]	5.49 [5.12, 5.93]	5.48 [5.10, 5.91]	31.7
Wall thickness segment 14 (median [IQR])	5.92 [5.41, 6.60]	5.90 [5.44, 6.28]	5.95 [5.38, 6.58]	6.00 [5.36, 6.66]	31.7
Wall thickness segment 15 (median [IQR])	5.12 [4.78, 5.37]	4.99 [4.56, 5.39]	4.99 [4.44, 5.68]	5.09 [4.48, 5.69]	31.7
Wall thickness segment 16 (median [IQR])	5.32 [4.86, 5.67]	5.13 [4.82, 5.67]	5.23 [4.76, 5.65]	5.26 [4.80, 5.72]	31.7
Global wall thickness (median [IQR])	6.07 [5.57, 6.29]	6.17 [5.90, 6.59]	6.28 [5.70, 6.87]	6.30 [5.72, 6.84]	31.6
Septal wall thickness (median [IQR])	6.43 [5.69, 7.01]	6.37 [6.00, 6.90]	6.62 [6.12, 7.52]	6.67 [5.88, 7.34]	31.7
Maximum wall thickness (median [IQR])	7.81 [6.97, 8.59]	8.01 [7.43, 8.66]	8.16 [7.45, 9.58]	8.09 [7.24, 9.01]	31.7

Abbreviations:

ARVC: arrhythmogenic right ventricular cardiomyopathy; BMI: body mass index; CMR: cardiac magnetic resonance imaging; DCM: dilated cardiomyopathy; ECG: Electrocardiography; EDVi: indexed end-diastolic volume; EDMi: indexed end-diastolic mass; EF: ejection fraction; ESVi: indexed end-systolic volume; G+: carriers of likely pathogenic and pathogenic variants associated with one of the cardiomyopathies; HCM: hypertrophic cardiomyopathy; HDL: high-density lipoprotein; IQR: interquartile range; LDL: low-density lipoprotein; LV: left ventricular; MET: metabolic equivalent of task; MVR: mass to volume ratio; PAFR: peak atrial filling rate; peakEcc: peak circumferential strain; peakEII2Ch: longitudinal strain analyzed in 2-chamber view; peakEII4Ch: longitudinal strain analyzed in 4-chamber view; PER: peak ejection rate; PFR: peak filling rate; RV: right ventricular; SVi: indexed stroke volume; TPKEcc: global time to peak circumferential strain; TPKEI2Ch: global time to longitudinal strain analyzed in 2-chamber view; TPKEI4Ch: global time to peak circumferential strain; TPKEI4Ch: global time to longitudinal strain analyzed in 4-chamber view.

Supplementary Table X: outcome risk stratified by cardiomyopathy and geneDue to its size, this table is only available online <https://doi.org/10.1161/CIRCGEN.122.003704>**Supplementary Table XI: Results of Fisher's Exact tests when excluding overlapping genes**

	ARVC G+ vs G-				DCM G+ vs G- (without ARVC genes)				DCM G+ vs G- (without HCM genes)				HCM G+ vs G-			
	OR	95% LCI	95% UCI	p-value	OR	95% LCI	95% UCI	p-value	OR	95% LCI	95% UCI	p-value	OR	95% LCI	95% UCI	p-value
CARDIOVASCULAR RISK FACTORS																
Diabetes	1.136	0.741	1.684	0.530	0.819	0.602	1.095	0.194	0.835	0.595	1.147	0.293	1.682	1.348	2.083	4.20E-06
Hypertension	0.989	0.762	1.276	0.949	1.092	0.927	1.285	0.283	0.999	0.831	1.198	1.000	1.025	0.875	1.197	0.753
Hypercholesterolaemia	1.033	0.774	1.365	0.833	1.137	0.949	1.356	0.156	1.057	0.864	1.288	0.579	1.192	1.006	1.407	0.041
Ever Smoked	1.158	0.905	1.479	0.244	1.223	1.045	1.432	0.011	1.192	1.002	1.418	0.044	0.869	0.745	1.013	0.069
Family heart disease	1.386	1.086	1.770	0.007	1.134	0.969	1.327	0.114	1.074	0.902	1.277	0.434	1.010	0.869	1.173	0.910
CARDIAC DISEASE/OUTCOME																
Cardiac problem	2.604	0.513	8.240	0.120	1.052	0.208	3.309	0.762	1.291	0.255	4.065	0.511	1.262	0.327	3.497	0.563
Heart failure	1.169	0.420	2.628	0.650	2.600	1.713	3.837	8.40E-06	3.010	1.955	4.497	1.00E-06	1.504	0.903	2.386	0.097
Cardiomyopathy	0.956	0.023	5.708	1.000	7.963	4.354	14.167	1.70E-10	6.807	3.379	12.983	2.90E-07	5.681	2.936	10.526	5.20E-07
Dilated cardiomyopathy	2.531	0.060	16.741	0.342	8.290	3.003	21.263	4.40E-05	11.486	4.365	28.657	1.40E-06	0.923	0.022	6.079	1.000
Hypertrophic cardiomyopathy	0.000	0.000	20.787	1.000	10.856	3.095	35.820	1.40E-04	2.204	0.050	16.486	0.39	17.990	6.569	51.615	1.10E-08
Ventricular arrhythmias	7.664	2.835	17.818	9.50E-05	4.849	2.201	9.888	8.70E-05	5.415	2.368	11.317	7.10E-05	1.963	0.597	5.081	0.192
Atrial arrhythmias	1.113	0.400	2.499	0.663	2.313	1.507	3.444	1.40E-04	2.465	1.556	3.766	1.10E-04	1.015	0.554	1.727	0.892
Heart arrhythmia	2.642	0.690	7.242	0.075	2.685	1.213	5.356	0.008	3.639	1.706	7.089	0.001	0.477	0.056	1.815	0.435
Chronic ischemic heart disease	1.241	0.783	1.889	0.297	1.207	0.901	1.594	0.176	1.318	0.964	1.770	0.069	1.017	0.754	1.349	0.886
Acute myocardial infarction	1.443	0.728	2.600	0.215	1.163	0.728	1.780	0.490	1.005	0.573	1.653	0.900	0.863	0.517	1.368	0.659
Cardiac arrest	0.000	0.000	4.064	1.000	2.549	0.872	6.170	0.043	2.080	0.534	5.863	0.145	1.140	0.224	3.638	0.747
Angina pectoris	1.257	0.613	2.316	0.486	1.157	0.732	1.756	0.500	0.901	0.505	1.500	0.803	1.252	0.824	1.839	0.242
Conduction disorders	1.899	0.797	3.891	0.084	1.633	0.921	2.723	0.080	1.409	0.708	2.554	0.289	1.289	0.700	2.208	0.361
Valvular disease	1.179	0.498	2.394	0.558	2.016	1.345	2.937	0.001	1.866	1.173	2.852	0.006	1.074	0.640	1.708	0.716
Congenital heart disease	2.536	0.291	10.141	0.199	1.542	0.299	5.010	0.452	1.259	0.145	5.016	0.675	1.385	0.269	4.500	0.486
Pulmonary obstructive disease	1.704	1.051	2.643	0.026	1.205	0.845	1.677	0.280	1.112	0.739	1.618	0.551	0.695	0.450	1.033	0.081
Cardiovascular death	1.579	0.665	3.223	0.254	1.605	0.951	2.574	0.058	1.879	1.097	3.049	0.016	0.495	0.196	1.046	0.064
All-cause mortality	1.036	0.567	1.756	0.891	1.432	1.037	1.940	0.022	1.290	0.888	1.826	0.145	0.643	0.413	0.961	0.032

Abbreviations:

ARVC: arrhythmogenic right ventricular cardiomyopathy; DCM: dilated cardiomyopathy; G+: carriers of likely pathogenic and pathogenic variants associated with one of the cardiomyopathies; HCM: hypertrophic cardiomyopathy; LCI: lower limit confidence interval; UCI: upper limit confidence interval.

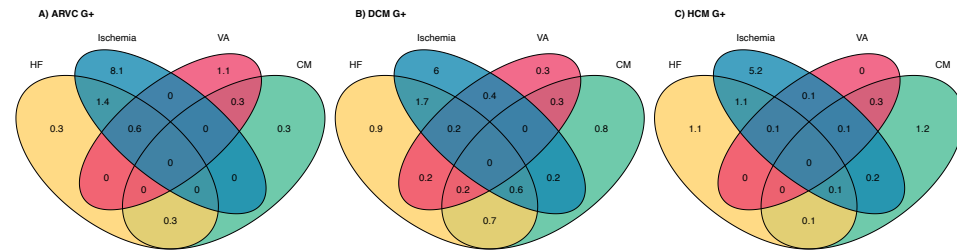


Figure I: Overlap cardiac diagnoses per inherited cardiomyopathy

The Venn diagram of the overlap between cardiomyopathy, heart failure, ventricular arrhythmia and chronic ischemic heart diagnoses in G+ individuals. The numbers in the diagram are the percentages of individuals diagnosed in the G+ of the specified cardiomyopathy.

Abbreviations: ARVC= arrhythmogenic right ventricular cardiomyopathy; CM= cardiomyopathy; DCM= dilated cardiomyopathy; G+= pathogenic variant carrier; HCM= hypertrophic cardiomyopathy; HF= heart failure; VA= ventricular arrhythmias.

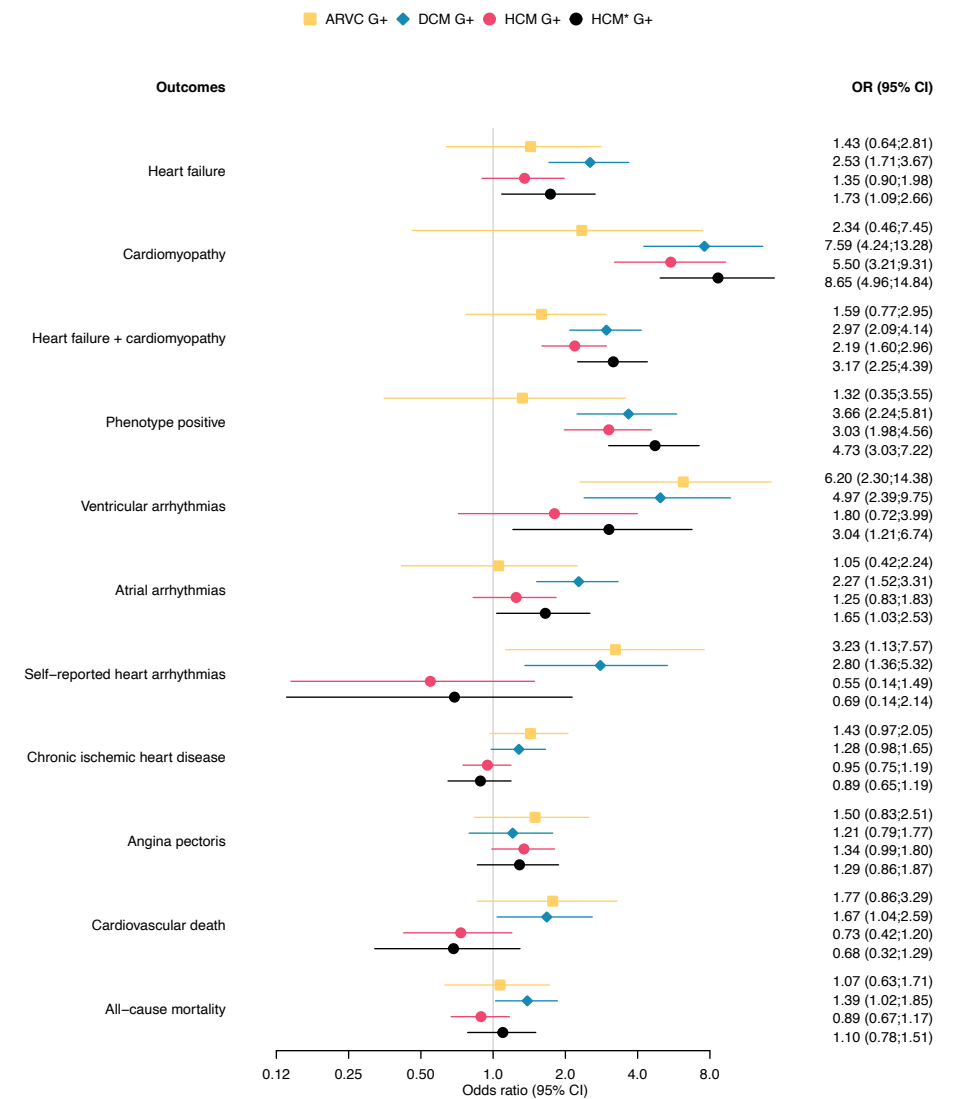


Figure II: Forest plot cardiac outcomes stratified per inherited cardiomyopathy

Odds ratios and 95% confidence intervals are given for the associations between cardiac outcomes and ARVC, DCM, or HCM pathogenic variant carriers.

Abbreviations: ARVC= arrhythmogenic right ventricular cardiomyopathy; DCM= dilated cardiomyopathy; G+= pathogenic variant carrier; HCM= hypertrophic cardiomyopathy.

* strict HCM group: HCM group after excluding carriers of the 3628-41_3628-17del MYBPC3 and the Arg278Cys 862C>T TNNT2 variant.

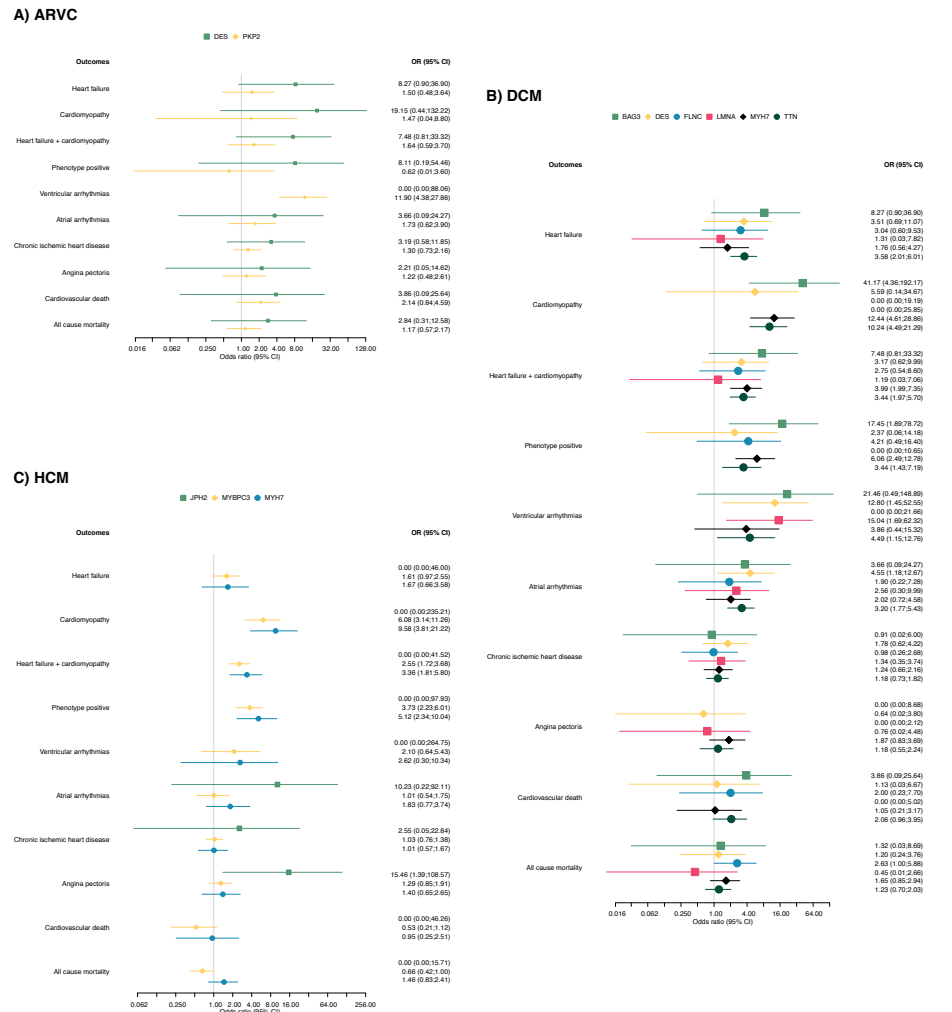


Figure III: Forest plot cardiac outcomes stratified per inherited cardiomyopathy and gene
 Odds ratios and 95% confidence intervals are given for the associations between cardiac outcomes and A) ARVC, B) DCM, or C) HCM pathogenic variant carriers stratified by gene. Results are only visualized for genes with at least one significant result.
 Abbreviations: ARVC= arrhythmogenic right ventricular cardiomyopathy; DCM= dilatedcardiomyopathy; HCM= hypertrophic cardiomyopathy.

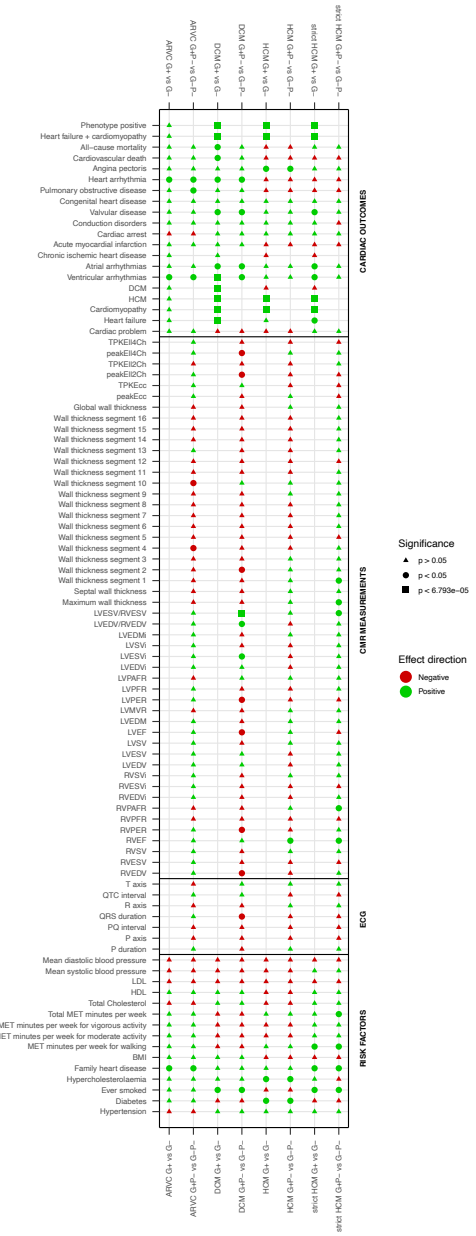


Figure IV: Matrix of all differences tested
 Summary of p-values and effect direction for all performed tests in this study. The p-value is indicated by the shape of the symbol, whereas the effect direction is represented by the color. Red color indicates an odds ratio smaller than one for categorical variables and a lower mean value for the G+ compared to the G- group for continuous variables. No symbol indicates the test was not performed.
 Abbreviations: ARVC= arrhythmogenic right ventricular cardiomyopathy; CMR= cardiac magnetic resonance imaging; DCM= dilated cardiomyopathy; ECG= Electrocardiography; G+= pathogenic variant carrier; HCM= hypertrophic cardiomyopathy; P-= phenotype negative individual; P+= phenotype positive individual.

CHAPTER 12

A drug target analysis prioritizing
circulating plasma proteins
involved with ventricular function
and structure.

Amand F Schmidt, MPH, PhD*;
Mimount Bourfiss, MD*;
Abdulrahim I Alasiri, MSc*;
Esther Puyol-Anton, PhD;
Sandesh Chopade, MSc;
Marion van Vugt, MSc;
Sander W van der Laan, PhD;
Christian Gross, PhD;
Chris Clarkson, PhD;
Albert Henry, MD;
Tom Lumbers, PhD;
Pim van der Harst, MD, PhD;
Nora Franceschini, MD, PhD;
Joshua C Bis, PhD;
Birgitta K Velthuis, MD, PhD;
Anneline S J M te Riele, MD, PhD;
Aroon D Hingorani, MD, PhD;
Bram Ruijsink, MD, PhD;
Folkert W Asselbergs, MD, PhD§;
Jessica van Setten, PhD§;
Chris Finan, PhD §

*Shared first authorship
§ Shared last authorship

Submitted

ABSTRACT

Ventricular impairment can lead to heart failure (HF) and subsequent increased morbidity and mortality. We performed a genome-wide association study (GWAS) of 16 measurements of biventricular function and structure obtained from cardiac magnetic resonance (CMR). Subsequently, we leveraged aggregated data from three independent GWAS on plasma proteome and performed drug target Mendelian randomization (MR) to identify proteins with a likely causal effect on CMR traits. The subset of proteins with a robust CMR effect were prioritized through linkage with mRNA expression from the Human Protein Atlas, protein interaction data from IntAct, drug compound information from the British national formulary and ChEMBL, and by identifying plasma proteins with robust effects on HF, atrial fibrillation, non-ischemic cardiomyopathy, dilated cardiomyopathy, or coronary heart disease. In total, 33 plasma proteins were prioritised, including 24 proteins that were druggable by either an approved or developmental compound. Fifteen proteins could be mapped to compounds with a known cardiovascular indication or side-effect, including repurposing candidates with a causal effect on DCM and/or HF: IL18, IL18R, I17RA, GPC5, LAMC2, PA2GA, CD33, SLAF7. To further inform drug development, we performed a drug-target MR phenome-wide scan of the potential on-target effects of these 33 prioritized proteins on 56 clinically relevant traits. In conclusion, we have identified a prioritized set of plasma proteins involved with CMR and cardiac outcomes, providing indispensable leads to facilitate drug development and drug repurposing.

INTRODUCTION

Impaired ventricular function may indicate the presence, or is a direct cause, of cardiac conditions or disease such as a cardiomyopathy or heart failure¹ (HF). Ventricular dysfunction may be caused by coronary heart disease (CHD), hypertension, myocarditis, protein-altering genetic mutations and/or detrimental life-style choices such as prolonged alcohol abuse.

Despite recent advances offered by drugs such SGLT2 inhibitors for treatment of HF, drug development for cardiac disease is confronted with high failure rates, often occurring during costly late-stage clinical testing²⁻⁴. These late-stage failures are indicative of the poor predictive potential of pre-clinical experiments for cardiac target identification. This is complicated further by the considerable phenotypic heterogeneity that underlies cardiac diagnoses such as HF⁵, resulting in compounds failing for futility that may genuinely benefit a subset of patients.

Cardiac magnetic resonance (CMR) imaging is the gold standard for quantification of biventricular function and morphology that are an expression of underlying cardiac disease; see Supplementary Table 1. Here we utilized CMR images, available from the UK biobank (UKB), and extracted these measures from both left and right ventricle (LV, RV) using a purpose built highly accurate, and competitively fast, deep-learning algorithm⁶.

Proteins constitute the majority of drug targets⁷, which are increasingly analysed through high throughput assays measuring the levels of hundreds of (plasma) proteins⁸. To leverage proteins and CMR measurements for drug target validation, we have developed an analytical framework⁹ to perform drug target analyses using human genetic data. Specifically, through two-sample drug target Mendelian randomization (MR), we can anticipate the on-target effect a drug target protein will have on disease relevant traits such as CMR measurements. Previously, this approach has been extensively validated for cardiovascular drug targets¹⁰⁻¹⁸.

To prioritize circulating plasma proteins on their involvement with LV and RV traits, relevant for cardiac disease, we first performed a genome-wide association study (GWAS) on sixteen CMR traits measured in up to 36,548 UKB subjects. Subsequently, we format-normalized protein quantitative trait loci (pQTLs) data, sourced from three independent GWAS involving cross-platform measurement of plasma protein concentrations using Somalogic⁹, Olink¹⁹ and Luminex²⁰ assays spanning 3000+ plasma proteins. Drug target MR was used to prioritize proteins on their likely causal contribution to CMR traits. Repurposing opportunities were identified by extracting cardiovascular indications and side-effects from ChEMBL²¹ and the British National Formulary (BNF) for drug targets with licensed compounds. Results were further annotated with tissue specific mRNA expression data from the Human Protein Atlas (HPA) database²², and with information from IntAct²³ and Reactome²⁴ to identify druggable protein-protein interaction.

METHODS

Quantification of LV and RV CMR traits

The current study sourced information from 36,548 UKB subjects who had data on both CMR images and genotyping. To minimize influence of pre-existing conditions, we excluded subjects with prevalent diseases (e.g. myocardial infarction, HF, and congenital heart diseases) known to affect the LV or RV traits; see Supplementary Table 2.

The deep-learning methodology (AI-CMR^{9c}) to extract LV and RV CMR measurements has been previously described, and extensively validated⁶. Briefly, the fully automated and quality-controlled cardiac analysis tool calculates LV and RV traits) from cine short axis and 2- and 4-chamber acquisitions, resulting in structural measures on end-diastolic, end-systolic, or stroke volumes (EDV, ESV, SV), end-diastolic mass (EDM), and, LV mass to EDV ratio (LV-MVR), or functional measures such as ejection fraction (EF), peak ejection rate (PER), peak (atrial) filling rates (PAFR, PFR). An example of CMR segmentation is shown in Supplementary Figure 1 and Supplementary Table 1. Automatic quality control steps consisted of pre-analysis check of image-quality (e.g., motion artefacts, erroneous image plane planning) and post-analysis check of accuracy of the image-analysis (e.g., coverage of the segmentations, detected abnormalities in volume and discrepancies between LV and RV parameters) steps; with automatic detection and removal of outlying observations.

GWAS of CMR traits

We used genotyped and imputed data as provided by UKB²⁵ (GRCh37 assembly). In brief, samples were genotyped on the Affymetrix BiLEVE and Axiom arrays, with untyped variants imputed using the Haplotype Reference Consortium, 1000 Genomes and UK10K as reference panels. We excluded samples as recommended by UKB²⁵, and in addition used the following sample exclusion criteria: discordant self-reported and genetically inferred sex, and genotypical missingness rate above 0.01. Variant quality control included removing variants with minor allele frequency (MAF) below 0.1%, imputation quality below 0.3, and those that deviated from the Hardy-Weinberg equilibrium (HWE p -value $< 1 \times 10^{-6}$).

Genetic associations with the 16 CMR traits were estimated using BOLT-LMM²⁶, utilizing a mixed-effects model accounting for any potential bias due to cryptic relatedness and population stratification. The BOLT-LMM models were run using default setting and conditional on age at CMR, sex, body surface area, systolic blood pressure (SBP), genotype measurement batch, 40 principal components (PCs), and assessment centre.

Genetic heritability of CMR variability

BOLT-REML²⁶ (with default settings, excluding variants with a MAF below 0.1%, HWE $P < 1 \times 10^{-6}$ and over 1% missingness) was used to estimate narrow-sense genetic heritability (i.e., the

proportion of phenotypic variance explained by the common genetic variation), as well as the pair-wise genetic correlation between the 16 CMR traits.

Functional and phenotypic annotations, and identification of likely causal loci

Lead variants were identified through LD-clumping (LD: linkage disequilibrium) within a one megabase flanking region, applying a pairwise r -squared threshold of 0.001.

Variants were mapped to likely causal genes through manual curation of purpose built locus-view plots, where AFS, MB, JvS, and CF independently determined the most likely causal genes (Supplementary File 2). Locus-view plots combined variant specific CMR associations around each respective lead variant (\pm 250 kbp flanking region) with information on regional genes and their exon structure. These plots were enhanced with an incidence (i.e., boolean) matrix annotating genes on 23 criteria, including whether the gene was coding, encoded a target for drug compounds with known cardio-metabolic (side-)effects, has a *cis*-MR CMR association, previous associations with cardio-metabolic traits sourced from GWAS catalog²⁷, presence of mRNA expression or splice-sites in cardiac or vascular tissues from GTEx, *trans* protein associations with other CMR loci, protein to protein interactions between CMR associated proteins; please see Supplementary File 2 for a detailed exposition.

Format normalization of cross-platform protein quantitative trait loci

Genetic association with plasma protein concentration were available from the following sources: Somalogic measurements from 3,301 participants of the INTERVAL cohort⁸, Luminex assays from up to 6,861 Framingham participants²⁰, and OLINK assays on 30,931 individuals across 15 cohorts contributing to the SCALLOP consortium¹⁹. Framingham provided pQTLs from a GWAS of common variants as well as an exome GWAS, which were concatenated. For the less than 1% variant overlap between the two Framingham arrays we selected results with the smallest standard error; representing the highest degree of precision.

The GWAS files were normalized using a purpose built normalization pipeline (<https://bit.ly/3pxBKXU>), standardizing file structures, mapping variants against a uniform genome assembly, assigning UniProt identifiers, and providing annotations with Variant Effect Predictor (VEP), Polymorphism Phenotyping v2 (PolyPhen), and Combined Annotation Dependent Depletion (CADD).

Mendelian randomization of plasma protein effects on CMR traits

MR was subsequently employed to ascertain the likely causal consequences of protein concentration on the 16 CMR traits. To prevent potential influence of study specific factors, all drug target MR were conducted per contributing study/consortium, performing separate analyses for SCALLOP, Framingham and INTERVAL. Specifically, drug target MR was

conducted by selecting variants from a 100 kbp windows around the *cis* gene known to encode the protein, clumping variants to an LD of 0.40, where residual LD was modelled using a generalized least square (GLS) model²⁸ and a 5,000 random sample of UKB participants. To reduce the risk of “weak-instrument bias”²⁹, we selected genetic variants with a F-statistic of 15 or higher, furthermore due to the absence of sample overlap between the protein concentration and CMR GWAS any *potential* weak-instrument bias would act towards a null effect and reduce power rather than increase type 1 errors.

MR analyses were conducted using the GLS implementation of the inverse-variance weighted (IVW) estimator, as well as with an Egger correction protecting against horizontal pleiotropy³⁰. To minimize the potential influence of horizontal pleiotropy, we excluded variants with large leverage or outlier statistics and used the Q-statistic to identify possible remaining violations³¹. Finally, a model selection framework was applied to select the most appropriate estimator (IVW or MR-Egger) for each specific protein – CMR relationship^{31,32}.

Protein prioritization

After accounting for multiplicity (see below), we identified drugged proteins with a CMR association, and through linkage with ChEMBL and BNF extracted cardiovascular related indications and side effects (see Supplemental note 1). The BNF draws information from drug medication inserts, scientific literature, regulatory authorities, and professional bodies, and is jointly authored by the British Medical Association and the Royal Pharmaceutical Society. ChEMBL²¹ was extracted for information in clinically used drug targets (from FDA approved drugs) and information on drug targets that are in early phase consideration. ChEMBL was also used to identify proteins that are *potentially* druggable as described by Finan *et al*.⁷

In addition to identifying drugged and druggable proteins with a CMR association, we identified a subset of proteins with a concordant risk increasing or risk decreasing effect. Specifically, results were coded towards the cardiac function or structure improving direction by multiplying estimates for EDV, ESV, EDM, and MVR by -1, and retaining the original effect direction for the remaining traits. Inferentially, this would mean that we can evaluate protein level increases according to potential beneficial cardiac effect rather than simply increase in CMR trait values. A concordant set of prioritized proteins was identified by selecting proteins with at least three CMR associations passing multiple testing correction, that were either all in the beneficial positive direction or the detrimental negative direction (i.e., without directionally discordant results). The above classification of beneficial vs harmful CMR effect direction is of course imperfect and simplifies the more complex relationship observed in observational association studies were relatively low or high CMR measurements such as LV-EF may show a u-shaped association with disease risk. As such these heuristic orientation are used here as a first filtering step, followed by more detailed analyses on clinical cardiac outcomes (see phenome-wide scan below).

These prioritized proteins included drugged and druggable targets, but for the majority included proteins that may not yet be druggable. To determine the potential pharmacological relevance of these proteins we subsequently identified the distance to the nearest (additional) druggable protein based on the in IntAct²³ protein-protein interaction database as modelled in Reactome²⁴ graph database (accessed April 2021). Here distance reflected the number of protein-protein interaction between the “index” protein and the next druggable protein, where a distance of 1 represents a direct link. This set of nearest druggable proteins was annotated with drug compound cardiovascular indications and side-effects (as described above), whether the nearest druggable protein was a direct protein by protein interaction, and whether they were available in the currently used set of plasma pQTLs.

Drug target phenome-wide scan to anticipate effects of prioritized targets

The CMR prioritized set of drugged, druggable, concordant and nearest druggable proteins were further pruned on an association with HF, non-ischemic cardiomyopathy (CM), DCM, AF, and/or CHD using the drug target MR pipeline described above. Next, for CMR prioritized proteins with a cardiac trait association we evaluated their effects on 56 clinically relevant traits, combining drug target MR with a phenome-wide scan to further inform potential on-target protein effects in future drug development programs.

Assessing tissue specificity of prioritized targets

The set of prioritized CMR-associated plasma proteins with cardiac effects was annotated by exploring their tissue specific mRNA expression from the Human Protein Atlas (HPA)²². Sourcing the consensus expression obtained by normalizing TPM (transcripts per million) values from three independent transcriptomics datasets: GTEx³³, Fantom5³⁴, and HPA's own RNAseq experiments²².

The normalized human expression data were used to determine a proteins tissue specificity³⁵, ranging from 0 (ubiquitous expression across all tissues) to 1 (tissue-specific expression). Differentially overexpressed tissues were identified by comparing tissue specific expression against average expression, testing against a standard normal quantile of 1.96 (alpha of 0.025).

Quality control and multiple testing

LD score regression³⁶ was used to explore the possibility of any remaining bias due to population stratification or cryptic relatedness – finding no cause for concern (Supplementary Table 3). Genetic loci were identified using the traditional genome-wide threshold of 5.00×10^{-8} , and a conservative threshold of 7.14×10^{-9} accounting for the correlation between the CMR traits and the seven PCs necessary to explain over 90% of the CMR trait variance (Supplementary Figure 2).

Based on the described instrument selection criteria we had sufficient genetic variants to robustly assess 892 unique proteins. Accounting for the same seven PCs described above and the number of proteins, the MR effect estimates with the CMR traits were evaluated using an alpha of 7.81×10^{-6} . The phenome-wide scan drug target analysis of CMR prioritized plasma proteins were evaluated using a multiplicity corrected alpha of 1.24×10^{-5} . Under the null-hypothesis the p-values of a group of tests follow a uniform distribution between zero and one⁴¹. To additionally explore the potential impact of multiple testing, we performed CMR-trait specific “overall” null-hypothesis tests, comparing the empirical p-value distribution (using Kolmogorov-Smirnov “KS”-tests) against the uniform distribution expected under the null-hypothesis⁴¹.

Unless otherwise specified, any remaining hypothesis tests were evaluated using an alpha of 0.05, and all point estimates (odds ratios [OR] or mean differences) refer to a unit change in the independent variable; typically, one standard deviation in plasma protein concentration for the MR results or an increase in risk allele for the GWAS results. To better illustrate concordance, and only where specified, MR results were orientated towards the cardiac beneficial effect direction by multiplying EDV, ESV, EDM, and MVR MR estimates by -1.

RESULTS

UK biobank participants with LV and RV CMR measurements

CMR measurements were obtained from a sample of 36,548 UKB subjects utilizing an extensively validated deep-learning approach⁶. On average, subjects were 63.9 (standard deviation, SD: 7.6) years old, 18,879 (51.8%) were women. Furthermore, participants had a mean SBP of 138.2 mmHg (SD: 18.4), a mean diastolic blood pressure (DBP) of 78.6 mmHg (SD: 10.0), and a mean heart rate of 62.5 bpm (SD: 10.2); see Supplementary Table 4.

Genomic loci associated CMR traits

We performed GWAS on 16 CMR traits, leveraging genotyped and imputed variants from the Affymetrix BiLEVE and Axiom arrays, and applying BOLT-LMM conditional on age, sex, body surface area, SBP, genotype measurement batch, 40 PCs and assessment centre.

The 91 unique lead variants (**Figure 1-2, Supplementary Tables 5**) were mapped to 53 causal genes based on independent review of annotated local-view plots (**Supplementary file 2**). This resulted in 16 genes for RV-ESV, 15 for LV-EF, 14 for LV-MVR, 14 for LV-ESV, 12 for RV-EF, 10 for RV-EDV, 6 for LV-EDV and LV-EDM, 5 for RV-SV, 4 for LV-SV, 2 for RV-PER, 1 for RV-PAFR, and none for RV-PFR, LV-PFR, LV-PER, and LV-PAFR. We identified five novel locus-trait associations for RV-PAFR (*SCN10A*), RV-PER (*ALDH2* and *HLA-B*), and LV-SV and LV-MVR (both *HLA-B*). Twenty-six genes were associated with multiple CMR traits. For

example variants mapped to *TTN* were associated with 11 traits, *BAG3* with 6 CMR traits, and both *TMEM43* and *ATXN2* with 5 traits. Of these multi-trait genes, 12 were associated with both LV and RV CMR traits: *TTN*, *BAG3*, *TMEM43*, *ATXN2*, *PROB1*, *DMPK*, *ZNF572*, *PLEC*, *HSPB7*, *HLA-B*, *SPON1*, and *OBSCN* (**Figure 1** and **Supplementary Table 4**).

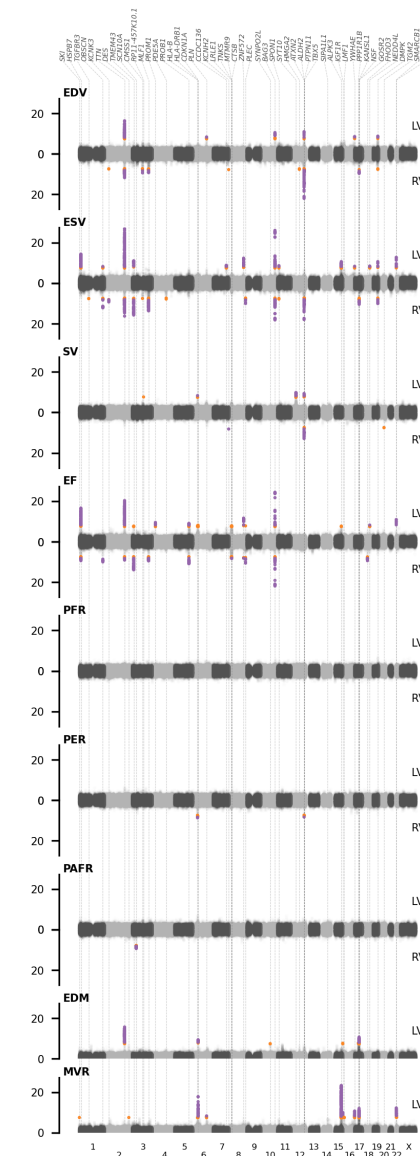


Figure 1 Manhattan plots of genome-wide CMR associations with genomic annotations

N.b. Purple dots indicate associations that pass the conservative significant threshold of 7.14×10^{-9} , with orange dots association between 5.00×10^{-8} and 7.14×10^{-9} , labels indicate the lead gene in the region.

LV, left-ventricle; RV, right-ventricle; EDV, end-diastolic volume; ESV, end-systolic volume; SV, stroke volume; EF, ejection fraction; PER, peak ejection rate; PARF/PFR, peak (atrial) filling rate; EDM, end-diastolic mass; MVR, ratio between end diastolic mass and volume. Results are based on an analysis of 36,548 subjects.

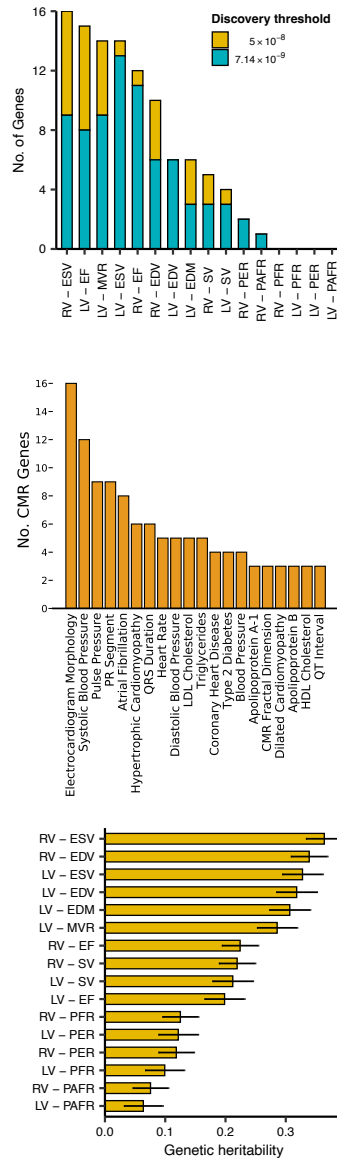


Figure 2 Aggregated GWAS results and genetic heritability estimates

N.b. Top panel depicts the number of significant putative causal genes per CMR trait and significance threshold. The middle panel provides the top 20 most frequent trait associations of the discovered CMR genes, sourced from GWAS catalog. The bottom panel provides the genetic heritability estimates with 95% confidence intervals. Results are based on an analysis of 36,548 subjects, a star indicates significant p-value at an alpha of 0.05.

Genetic heritability of CMR traits and between-trait pairwise genetic correlation

BOLT-REML was used to estimate the amount of phenotypic variation that could be explained by narrow-sense genetic heritability (Figure 2). Heritability estimates ranged between 36% and 31% for both RV and LV measurements of EDV and ESV, as well as LV-EDM. For LV-MVR, EF and SV of both ventricles heritability ranged between 20% and 29%. Despite an absence of GWAS hits for PFR, LV-PER and LV-PAFR, heritability of these traits was between 6% and 12%.

The pairwise genetic correlation (Figure 3) indicated that genetic variants for SV and PER measurements (both LV and RV) were highly correlated (correlation coefficient close to 1.0), which was similarly observed for genetic variants associated with EDV and ESV traits from both ventricles), and strong genetic correlation between variants for LV-PFR and RV-PFR. LV-EDM variants had a moderately strong (correlation around 0.70) association with SV, PER, ESV, EDV of both ventricles. Finally, variants for LV-MVR, RV-EF, and LV-EF showed a positive correlation among themselves (at most 0.68), and negative correlation with EDV, ESV, EDM, and SV traits (as high as -0.86).

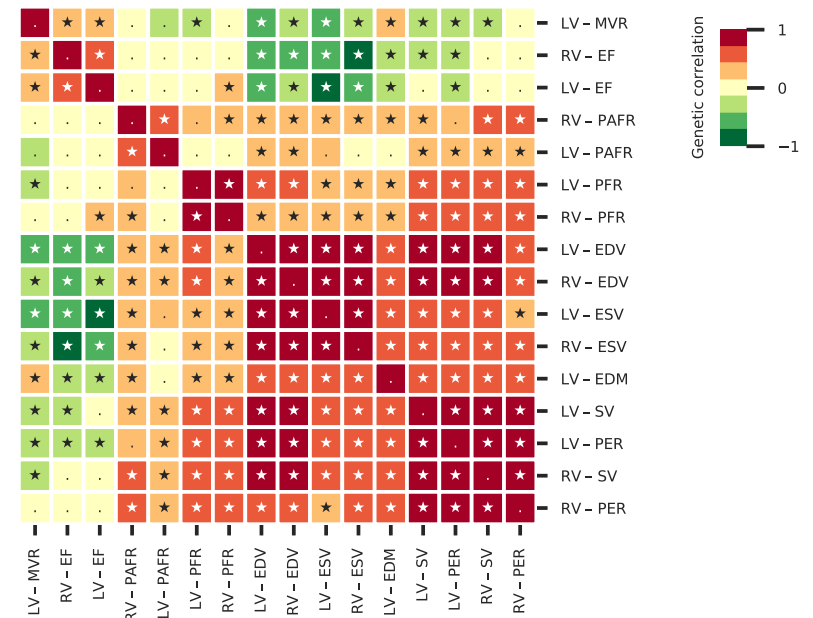


Figure 3 The pairwise genetic correlation between 16 CMR traits

N.b. LV, left-ventricle; RV, right-ventricle; EDV, end-diastolic volume; ESV, end-systolic volume; SV, stroke volume; EF, ejection fraction; PER, peak ejection rate; PARF/PFR, peak (atrial) filling rate; EDM, end-diastolic mass; MVR, ratio between end diastolic mass and volume. Results are based on an analysis of 36,548 subjects. Star-annotated cells indicate significant associations at an alpha of 0.05.

Phenotypic consequences of CMR genes

Comparing these CMR genes to cardio-metabolic traits from GWAS catalog (**Figure 2, Supplementary Figure 3**), we found that our putative CMR genes were frequently associated with electrocardiogram traits (e.g., PR segmentation, QRS duration, QT interval), CMR traits from previous studies (e.g., LV dilatation, LV mass, and fractal dimension), blood pressure and heart rate, as well as plasma concentration of various apolipoproteins and cholesterol-containing lipoproteins. The following CMR genes were previously associated with AF: *SYNPO2L*, *TBX5*, *IGF1R*, *GOSR2*, *TTN*, *SCN10A*, *CDKN1A*, and *KCNH2*. We furthermore found previous associations with hypertrophic CM (HCM) for: *HSPB7*, *SYNPO2L*, *BAG3*, *NSF*, *FHOD3*, *CDKN1A*, as well as for DCM for: *BAG3*, *FHOD3*, *TTN*, and for HF: *SYNPO2L*, *BAG3*. Finally, the following genes were previously associated with CHD: *ATXN2*, *ALDH2*, *PTPN11*, *GOSR2* (**Supplementary Figure 3**).

Druggability of CMR genes

Through linkage to BNF and ChEMBL we identified 18 CMR genes which encoded a druggable protein (**Supplementary Table 4-6**). Out of these, 8 were already drugged by at least one compound: *ALDH2*, *HLA-DRB1*, *IGF1R*, *KCNH2*, *KCNK3*, *PDE5A*, *SCN10A*, *TNKS*. These include genes encoding drug targets for compounds with indications and/or side-effects for AF, HF, CHD, chronic obstructive pulmonary disease (COPD) and diabetes (*IGF1R*, *KCNH2*, *KCNK3*, *PDE5A*, *SCN10A*, **Supplementary Tables 5-6**).

Identifying plasma protein concentration with an effect on CMR traits

We initially linked our putative CMR genes to BNF and ChEMBL and identified 18 genes which encoded a druggable protein (**Supplementary Table 4-6**). These include genes encoding drug targets for compounds with indications and/or side-effects for AF, HF, CHD, chronic obstructive pulmonary disease (COPD) and diabetes (*IGF1R*, *KCNH2*, *KCNK3*, *PDE5A*, *SCN10A*, **Supplementary Tables 5-6**).

We next expanded this analysis to use drug target MR to directly identify casual plasma proteins for CMR traits, which additionally provides effect directions relevant for a potential drug compound effect type (i.e., inhibiting or activating compound effects). Specifically, we leveraged genetic association data on protein concentration from three sources: SCALLOP, Framingham, and INTERVAL (see methods).

We found that 304 proteins were associated with at least one CMR trait (**Supplementary Figure 4**), with the number of associated proteins ranging from 62 for LV-ESV to 33 for LV-PAFR (**Figure 4**) and with Kolmogorov-Smirnov tests providing strong evidence that results were not driven by multiple testing (**Supplementary Figure 5**).

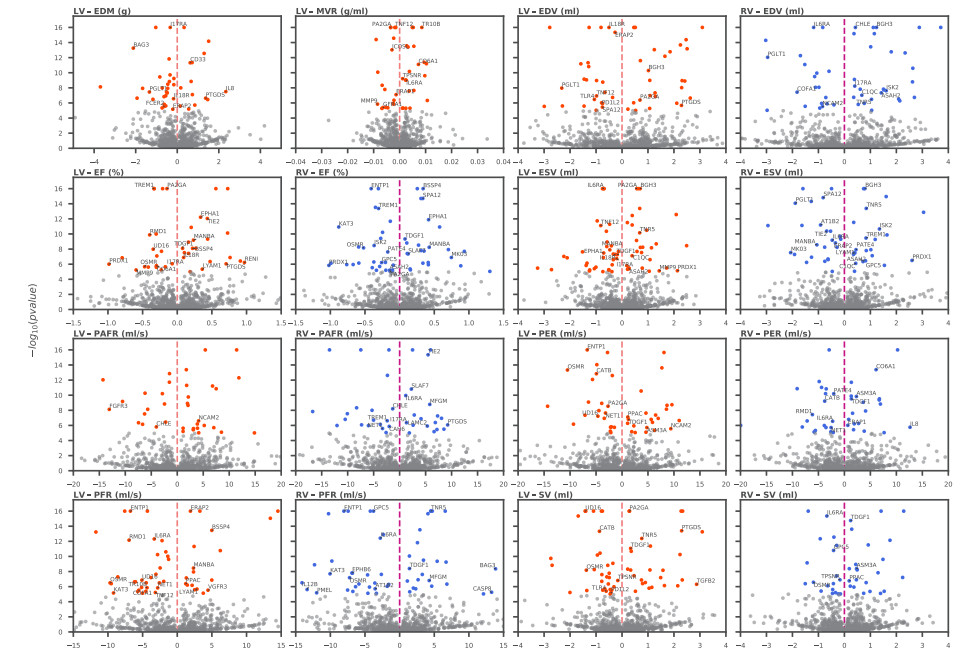


Figure 4 Volcano plots of the plasma protein effect on CMR traits

N.b. Proteins were annotated if they were part of the drugged, druggable, directionally concordant or nearest druggable protein sets. Results were coloured by left and right ventricle if they pass a p-value threshold of 7.81×10^{-6} . The Mendelian randomization effects per unit (in standard deviation) change in the protein are plotted on the x-axis, against the $-\log_{10}(p\text{-value})$ on the y-axis.

Subsequently, the CMR associated proteins were prioritized by 1) leveraging BNF and ChEMBL to identify “drugged” proteins targeted by drug compounds, 2) “druggable” proteins which are amenable to compound perturbation or monoclonal antibody inhibition, 3) a directionally “concordant” set of proteins, which affected three or more CMR traits which either all had beneficial or detrimental effects, and 4) the concordant set of protein was mapped to a “nearest” set of druggable proteins using IntAct data. This set of 72 proteins was further prioritized utilizing drug target MR to pinpoint the subset of 33 proteins (**Table 1**) with an effect on the clinical cardiac outcomes: HF, DCM, non-ischemic CM, AF, and/or CHD.

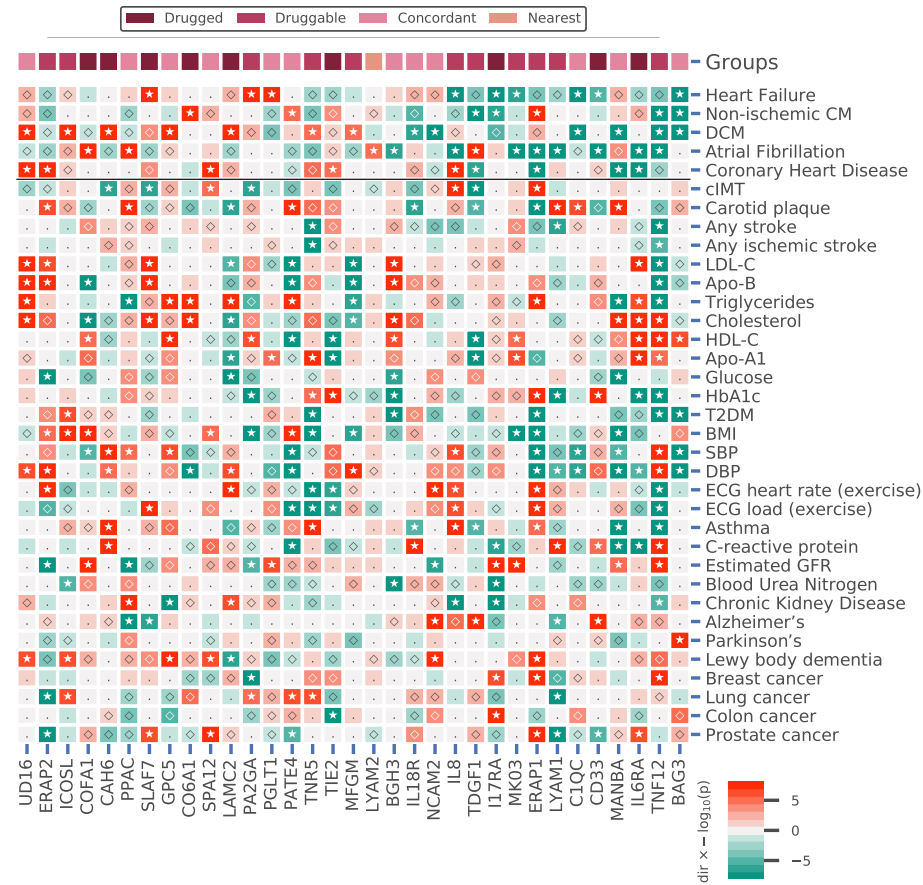


Figure 5 A phenome-wide scan of CMR prioritized proteins associated with one or more cardiac outcome.

N.b. Proteins were curated on having a multiplicity corrected p-value $< 1.29 \times 10^{-5}$ with one or more of the following cardiac traits: heart failure (HF), dilated cardiomyopathy (DCM), non-ischemic CM, atrial fibrillation (AF), or coronary heart disease (CHD). P-values passing the 0.05 threshold are indicated by an open diamond with stars indicating results passing a threshold of 1.29×10^{-5} . Cells were coloured by effect direction times $-\log_{10}(p\text{-value})$; where p-values were truncated at 8 for display purposes. The top column indicates whether the CMR associated proteins were identified as drugged, druggable, directionally concordant, or nearest druggable protein. Y-axis abbreviations: DCM: dilated cardiomyopathy; cIMT: carotid artery intima media thickness; T2DM: type 2 diabetes; BMI: body mass index; DBP/SBP diastolic/systolic blood pressure; estimated GFR: estimated glomerular filtration rate; BUN: blood urea nitrogen; LDL-C: low-density lipoprotein cholesterol; HDL-C: high-density lipoprotein cholesterol; Apo-B: apolipoprotein-B; Apo-A1: apolipoprotein-A1; HbA1c: glycated hemoglobin; ECG: electrocardiography; FVC: forced vital capacity; FEV1 forced expiratory volume during the first second; PEF: peak expiratory flow. Note that all 56 phenome-wide traits are presented in Supplemental Figure 10.

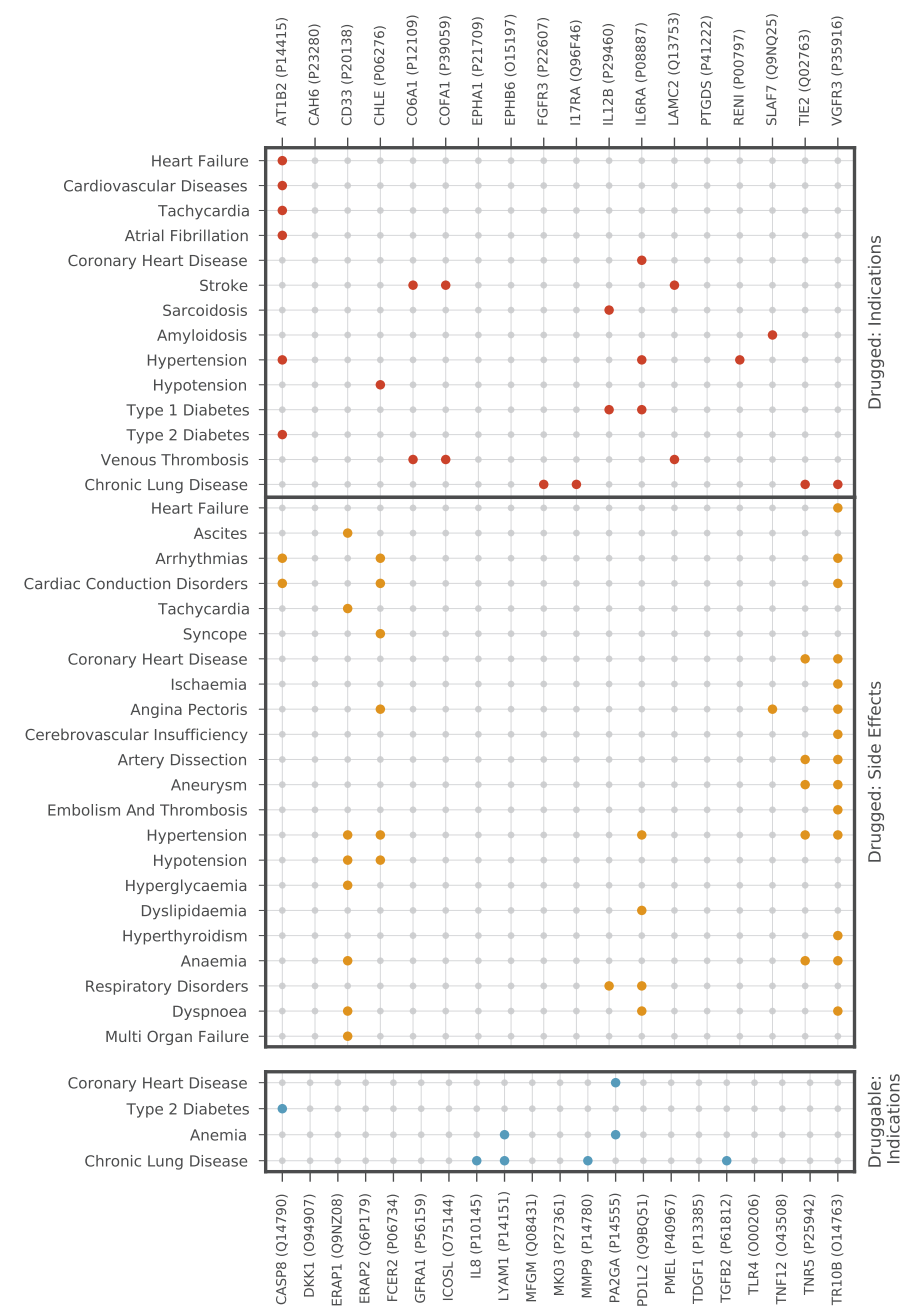


Figure 6 Incidence matrix of cardio-metabolic related indications and side effects of compounds targeting drugged and druggable proteins associated with CMR traits.

N.b. coloured dots represents an established link between the compound and trait; data were extracted from BNF and ChEMBL²¹.

Table 1 Summarizing the prioritized plasma protein information

Protein (uniprot id) (uniprot id)	Nearest druggable protein (uniprot id)	Druggability	Ventricle	CMR effect	Cardiac effect	Clinical development phase	No. compounds	Compound Action types	CVD indication or side effects	Oncological indication or side effects
MANBA (O00462)		Currently not druggable	Both	Beneficial	Beneficial	0	0			
NCAM2 (O15394)		Currently not druggable	Both	Beneficial	Beneficial	0	0			
TNF2 (O43508)		Directly druggable	Left	Mixed	Beneficial	1	2	Inhibitor		✓
ICOSL (O75144)		Directly druggable	Left	Beneficial	Harmful	1	1	Inhibitor		
BAG3 (O95817)	HSP7C (P11142)	Indirectly druggable	Both	Beneficial	Beneficial	3	1	Inhibitor		
C1QC (P02747)		Currently not druggable	Both	Harmful	Beneficial	0	0			✓
IL6RA (P08887)		Directly drugged	Both	Mixed	Beneficial	4	4	Antagonist, Inhibitor		
PATE4 (P0C8F1)		Currently not druggable	Right	Harmful	Harmful	0	0			✓
IL8 (P10145)	IL18 (Q14116)	Directly druggable	Both	Mixed	Mixed	2	2	Inhibitor		✓
CO6A1 (P12109)		Directly drugged	Both	Mixed	Harmful	4	2	Hydrolytic Enzyme		✓
TDF1 (P13385)		Directly druggable	Both	Beneficial	Mixed	1	1	Binding Agent		✓
LYAM1 (P14151)		Directly druggable	Both	Mixed	Beneficial	3	3	Antagonist, Inhibitor		✓
PA2GA (P14555)		Directly druggable	Left	Mixed	Harmful	3	2	Inhibitor		✓
ISK2 (P20155)	LYAM2 (P16581)	Indirectly druggable	None	None	Harmful	3	3	Antagonist, Inhibitor		✓
UDI6 (P19224)		Currently not druggable	Left	Harmful	Harmful	0	0			✓
CD33 (P20138)		Directly drugged	Left	Harmful	Beneficial	4	6	Binding Agent, Other		✓
CAH6 (P23280)		Directly drugged	Right	Harmful	Harmful	4	1	Inhibitor		
PPAC (P24666)	5HT1E (P28566),HDA10 (Q969S8),PDE4D (Q08499),RARA (P10276),VWF (P04275),P2RY4 (P51582),PRS7 (P35998),GBRG1 (Q8N1C3)	Indirectly drugged	Both	Beneficial	Harmful	4	94	Agonist, Allosteric Antagonist, Antagonist, Inhibitor, Inverse Agonist, Modulator, Partial Agonist, Positive Allosteric Modulator, Positive Modulator		✓
TNR5 (P25942)		Directly druggable	Both	Mixed	Harmful	2	5	Agonist, Antagonist, Inhibitor, Partial Agonist		✓

Table 1. Continued

Protein (uniprot id) (uniprot id)	Nearest druggable protein (uniprot id)	Druggability	Ventricle	CMR effect	Cardiac effect	Clinical development phase	No. compounds	Compound Action types	CVD indication or side effects	Oncological indication or side effects
MK03 (P27361)		Directly druggable	Right	Beneficial	Beneficial	2	3	Inhibitor		✓
COFA1 (P39059)		Directly drugged	Both	Mixed	Harmful	4	2	Hydrolytic Enzyme		✓
GPC5 (P78333)	SYUA (P37840),TPH1 (P17752)	Indirectly drugged	Right	Harmful	Harmful	4	4	Inhibitor		✓
TIE2 (Q02763)		Directly drugged	Both	Beneficial	Harmful	4	8	Inhibitor		✓
MFGM (Q08431)		Directly druggable	Right	Beneficial	Harmful	1	1	Binding Agent		
IL18R (Q13478)		Indirectly druggable	Left	Beneficial	Beneficial	2	2	Cross-Linking Agent, Inhibitor		✓
LAMC2 (Q13753)		Directly drugged	Right	Beneficial	Harmful	4	1	Hydrolytic Enzyme		✓
BGH3 (Q15582)		Currently not druggable	Both	Harmful	Beneficial	0	0			
ERAP2 (Q6P179)		Directly druggable	Both	Beneficial	Harmful	2	1	Inhibitor		✓
SPA12 (Q81W75)		Currently not druggable	Both	Beneficial	Harmful	0	0			
PGLT1 (Q8NBL1)		Currently not druggable	Both	Beneficial	Harmful	0	0			
I17RA (Q96F46)		Directly drugged	Both	Mixed	Beneficial	4	1	Antagonist		✓
SLAF7 (Q9NQ25)		Directly drugged	Right	Beneficial	Harmful	4	1	Inhibitor		✓
ERAP1 (Q9NZ08)		Directly druggable	Both	Beneficial	Mixed	2	1	Inhibitor		✓

N.b. indirectly drugged or indirectly druggable proteins were mapped to the nearest druggable protein (Figure 7) potentially resulting in tied proteins at the same distance. Tied proteins were both included in further analyses, for example resulting in 8 nearest druggable proteins for PPAC explaining the large number of mapped compounds. For indirectly drugged/druggable proteins the CMR and cardiac effects represents the indexing protein for which we had plasma pQTL (the first column) and the drug compound data are from the nearest druggable protein(s). The nearest druggable protein of ISK2, LYAM2 was available as pQTL data and here we instead list the LYAM2 effects on CMR and cardiac traits.

Drugged CMR proteins: repurposing opportunity

Eighteen CMR associated proteins (out of 72) were targets of licensed drugs (**Supplementary Figure 6, Tables 9-10**), of which 8 were robustly associated with cardiac traits through *cis*-MR (**Figure 5**): IL6RA, CO6A1, CD33, CAH6, COFA1, TIE2, LAMC2, I17RA, and SLAF7.

CD33, I17RA, SLAF7 affected HF; CO6A1, I17RA affected non-ischemic CM; CAH6, LAMC2 were associated with DCM; IL6RA, CD33, COFA1 with AF, and finally IL6RA and TIE2 affected CHD. Focussing on the proteins affecting multiple cardiac traits,^x we found that increased levels of I17RA (Interleukin-17 receptor A) predominantly improved LV cardiac function (Supplementary Figure 6) and decreased the risk of HF OR 0.97 (95%CI 0.96; 0.98) and non-ischemic CM OR 0.94 (95%CI 0.92; 0.96). I17RA is targeted by the anti-inflammatory monoclonal antibody (mAb) brodalumab (**Figure 6**). IL6RA (Interleukin-6 receptor subunit alpha) had a directionally discordant effect on 9 LV and RV traits (Supplementary Figure 6), with increased levels being associated with decreased risk of AF OR 0.95 (0.94; 0.96) and CHD OR 0.94 (0.93; 0.94). Noting that genetic instruments for IL6R are associated with reduced membrane bound IL6¹⁰, we find directionally concordant effects by IL6R inhibiting compounds such as tocilizumab decreasing cardiovascular risk (**Figure 6**). CD33 (Myeloid cell surface antigen CD33) was found to reduce LV-EDM and is targeted by mAb such as gemtuzumab which are indicated in oncology and have documented cardiovascular side effects (**Figure 6**). Increased levels of CD33 decreased the risk of HF OR 0.96 (95%CI 0.95; 0.98) and AF OR 0.96 (95%CI 0.89; 1.03). Similarly, SLAF7 (SLAM family member 7) and TIE2 (Angiopoietin-1 receptor) are both inhibited by compounds with an oncological indication with known cardio-metabolic side-effects, and non-oncological indications such as amyloidosis (SLAF7) and CHD (TIE2); **Figure 6**. Through MR we found that SLAF7 improved RV-EF and RV-PAFR function, but nevertheless increased the risk of HF OR 1.07 (95%CI 1.05; 1.08), TIE2 beneficially affected CMR traits with an LV-EF effect of 0.43% (95%CI 0.32; 0.55), RV-ESV -0.68 ml (95%CI -0.89; -0.48), and an RV-PAFR effect of 5.47 ml/s (95%CI 4.15; 6.79), while increasing the risk of CHD OR 1.10 (95%CI 1.06; 1.15).

Druggable CMR proteins: de novo developmental targets

We identified 21 *druggable* proteins which affected one or more CMR trait (**Supplementary Figure 7, Supplementary Tables 11-12**), these were pruned down to 11 proteins with an effect on a cardiac outcome (**Figure 5**): TNF12, ICOSL, IL8, TDGF1, LYAM1, PA2GA, TNR5, MK03, MFGM, ERAP2, ERAP1.

PA2GA, MK03 affected HF; TNF12, TDGF1, TNR5, MFGM affected non-ischemic CM; TNF12, ICOSL, TNR5, MFGM, were associated with DCM; TNF12, IL8, TDGF1, LYAM1, MK03, ERAP1 associated with AF, and finally IL8, TDGF1, ERAP2 and ERAP1 with CHD. Focussing on proteins with an effect on multiple cardiac traits, we found that TNF12 (Tumor necrosis factor ligand superfamily member 12) decreased the risk of non-ischemic CM OR 0.82 (95%CI 0.77; 0.88),

AF OR 0.90 (95%CI 0.89; 0.91), and DCM OR 0.80 (95%CI 0.75; 0.85). Higher concentration of TNF12 improved LV dimensions but increased LV-EDM. TNF12 is inhibited by two phase 1 compounds indicated for neoplasm and rheumatoid arthritis. Higher levels of IL8 (Interleukin-8) IL8 increased LV-EDM, while improving RV-PER, and decreased the risk of HF OR 0.74 (95%CI 0.69; 0.81) and AF OR 0.83 (95%CI 0.77; 0.89), while increasing the risk of CHD OR 1.18 (95%CI 1.11; 1.25); **Figure 5, Supplementary Figure 7 & Tables 11-12**. IL8 is the target of mAb in development for treatment of neoplasms and chronic lung disease (**Figure 6, Supplementary Table 8**). TDGF1 (teratocarcinoma-derived growth factor 1), targeted by a developmental immunoconjugate BIIB015 for treatment of tumours, improved LV and RV cardiac traits (EF, SV, PER, RV-PFR), and decreased the risk of CHD, non-ischemic CM OR 0.93 (95%CI 0.92; 0.94), and increased the risk of AF OR 1.01 (95%CI 1.01; 1.01); **Figure 5, Supplementary Figure 7, Tables 11-12**. MK03 (Mitogen-activated protein kinase 3) is inhibited by multiple ERK1/2 kinase compounds for treatment of neoplasms and associated with improved RV-ESV and RV-EF, and decreased the risk of HF OR 0.85 (95%CI 0.80; 0.91) and AF OR 0.86 (95%CI 0.82; 0.91). ERAP1 and ERAP2 (Endoplasmic reticulum aminopeptidase 1 and 2, forming a protein complex³⁷), both improved LV and RV CMR measurements (**Supplementary Figure 6**), and are both inhibited by the same compound tosedostat (currently in development for oncology). Higher ERAP1 was associated with an increased risk of non-ischemic CM OR 1.10 (95%CI 1.07; 1.13), and decreased risk of AF OR 0.99 (95%CI 0.98; 0.99) and HF OR 0.98 (95%CI 0.97; 0.98), while higher levels of ERAP2 in turn increased the risk of CHD OR 1.03 (95%CI 1.02; 1.03); **Figure 5**.

Nearest druggable proteins with directionally concordant CMR effects

Next, proteins with directional concordant effects on three or more CMR traits (i.e., with all beneficial or detrimental effects), were mapped to their (next) nearest druggable gene by counting the number of protein-protein interactions to the nearest druggable genes (**Figure 7, Supplementary Figure 8**). This resulted in drugged and druggable proteins that either directly interacted with an indexing protein or were separate by at most one protein-protein interaction. Ten of these nearest drugged or druggable proteins had pQTL data available (MET, SYUA, EGFR, FA10, IL6RA, IL6RB, PTGDS, PAI1, IL18, LYAM2; **Figure 6**).

Some of these indirectly drugged and druggable proteins had known cardio-metabolic indications and/or side-effects (**Figure 7, Supplementary Figure 9**). For example, PPAC (low molecular weight phosphotyrosine protein phosphatase) beneficially affected LV-PFR, RV-EDV, and RV-ESV, and while not druggable itself, interacted with eight druggable proteins (**Figure 7, Supplementary Figure 7**). Six of these PPAC related proteins (PDE4D, GBRG1, PRS7, VWF, RARA, 5HT1E) were targeted by inhibiting compounds with a recorded cardio-metabolic indication or side effect (**Figure 7, Supplementary Figure 9, Supplementary Tables 13-14**).

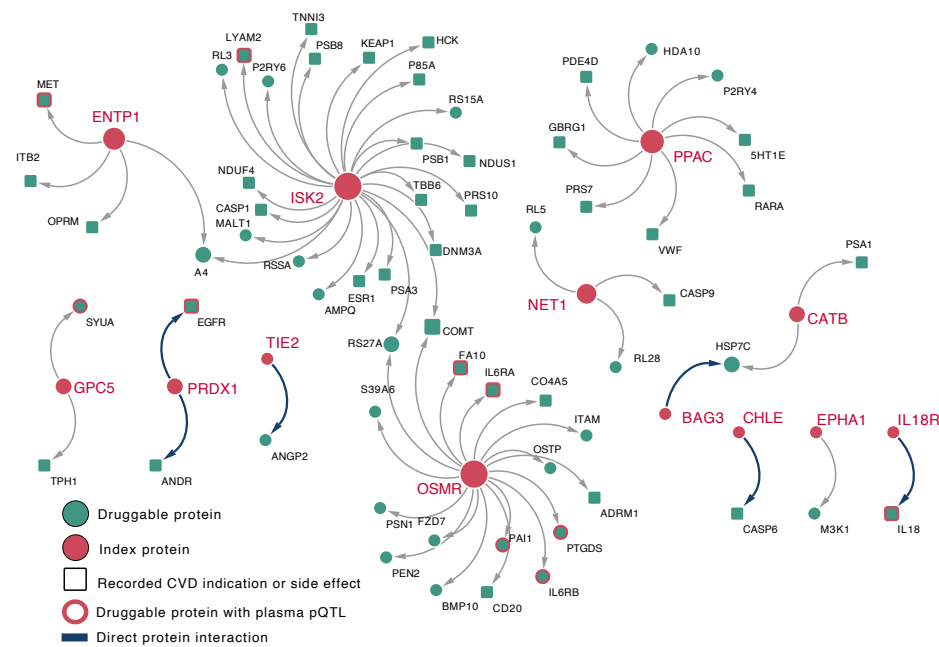


Figure 7 A network of plasma proteins with a directionally concordant CMR effect (index, orange circles) and their nearest druggable protein (green square with record CVD indication or side effect).

N.b. Directly interacting proteins are presented as a thick blue arrow, the remaining druggable proteins were separated by a single intermediate protein. In the presence of ties all druggable proteins with the same distance are presented. Druggable proteins with a CVD indication or side-effect (based on BNF and ChEMBL) are presented as square. Additionally, non-indexing proteins with available plasma pQTL data are represented by an orange outline.

Pruning this combined set of proteins (i.e., the set of directionally concordant proteins and the indirectly drugged or druggable proteins they interacted with) on the presence of cardiac outcome effects (**Figure 5**) resulted in the following prioritized proteins: BAG3, C1QC, PGLT1 affected HF; BAG3, PATE4, affected non-ischemic CM; MANBA, NCAM2, BAG3, C1QC, GPC5, IL18R, were associated with DCM; LYAM2, PPAC, BGH3 associated with AF, and finally MANBA, UD16, SPA12 affected CHD. Focussing on proteins with an effect on multiple cardiac traits, we found that higher concentrations of MANBA improved 5 CMR traits (ESV, EF, LV-PFR), and decreased CHD and DCM risk: OR 0.93 (95%CI 0.91; 0.96) and OR 0.76 (95%CI 0.72; 0.81) respectively. BAG3 (BAG family molecular chaperone regulator 3) improved 6 CMR traits and decreased the risk of HF OR 0.75 (95%CI 0.72; 0.79), non-ischemic CM OR 0.30 (95%CI 0.25; 0.36), and DCM OR 0.14 (95%CI 0.11; 0.17). Higher levels of C1QC (Complement C1q subcomponent subunit C) detrimentally affected 3 CMR traits but nevertheless decreased the risk of HF OR 0.97 (95%CI 0.96; 0.98) and DCM OR 0.86

(95%CI 0.82; 0.90). Higher UD16 (UDP-glucuronosyltransferase 1-6) worsened 4 LV CMR traits, and increased the risk of DCM OR 1.62 (95%CI 1.46; 1.80) and CHD OR 1.06 (95%CI 1.04; 1.08)

Tissue expression and phenome-wide scan of likely on-target clinical effects.

We subsequently explored mRNA expression and performed a phenome-wide scan of the anticipated on-target effects of increased protein concentration (**Figures 5 & 8, Supplementary Figures 10-11**). Tissue specificity did not differ between CMR prioritized proteins and non-prioritized proteins (p -value = 0.20). We did observe a significant difference in tissue-specific expression (p -value 9.01×10^{-3}), with the prioritized plasma protein more frequently higher expressed in spleen, lymph node, liver, granulocytes, kidney, pancreas, and lung tissues (**Supplementary Figure 11**).

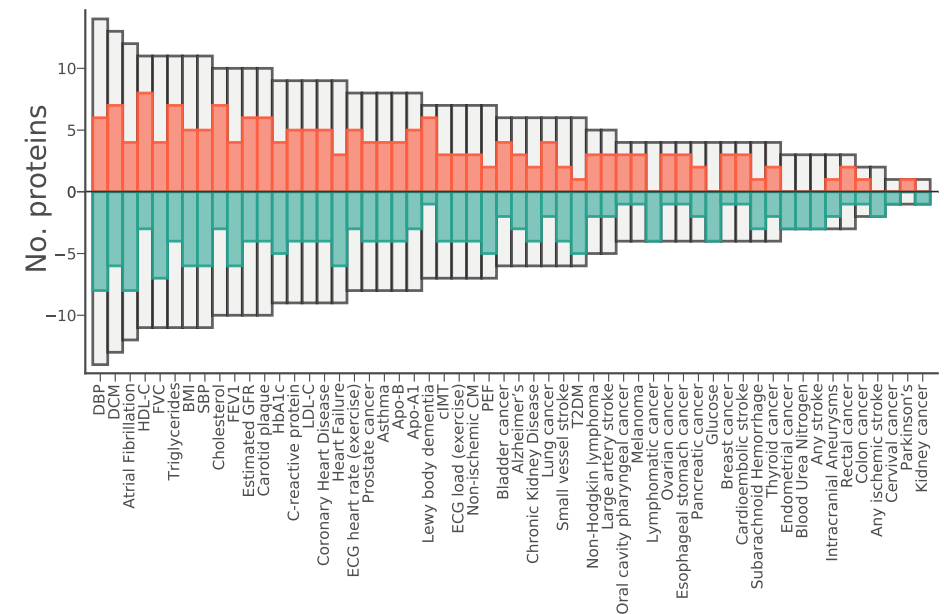


Figure 8 The likely causal consequences of a standard deviation increase of thirty-three CMR and cardiac outcome prioritized plasma proteins.

N.b. Results are presented by the effect direction of the pQTL MR (orange increasing effect, green decreasing effect, and white the total counts irrespective of direction). Counts reflect the number drug target MR estimates that passed a multiplicity corrected p -value threshold of 7.81×10^{-6} . DCM: dilated cardiomyopathy; cIMT: carotid artery intima media thickness; T2DM: type 2 diabetes; BMI: body mass index; DBP/SBP diastolic/systolic blood pressure; estimated GFR: estimated glomerular filtration rate; BUN: blood urea nitrogen; LDL-C: low-density lipoprotein cholesterol; HDL-C: high-density lipoprotein cholesterol; Apo-B: apolipoprotein-B; Apo-A1: apolipoprotein-A1; HbA1c: glycated hemoglobin; ECG: electrocardiography; FVC: forced vital capacity; FEV1 forced expiratory volume during the first second; PEF: peak expiratory flow.

In addition to the cardiac outcomes these proteins were prioritized on, the *cis*-MR phenome-wide scan found that these proteins were frequently associated with DBP, SBP, ECG measurement during exercise, lipid fraction such as (HDL-C, Apo-A1, triglycerides, LDL-C, and Apo-B), estimated glomerular filtration rate (eGFR), body mass index (BMI), glycosylated haemoglobin (HbA1c), c-reactive protein, lung function (FEV1, FVC, PEF), and carotid intima-media thickness (cIMT) (**Figure 8**); protein specific results are presented in **Figure 5**, **Supplementary Figure 10** and **Table 16**.

DISCUSSION

In the current study we derived 16 traits of left and right ventricular structure and function from CMR, and utilized GWAS to identify 87 genetic variants associated with one or more CMR trait. Furthermore, we prioritised 51 genes that likely drive the discovered genetic association, 25 of which affected multiple CMR traits, and with 12 affecting both LV and RV traits. Independently, we leveraged drug target MR to identify 33 CMR associated plasma proteins with robust effects on cardiac outcomes, including HF and DCM. To further inform drug development, we conducted a phenome-wide scan assessing the potential on-target effects of protein perturbation on 56 clinically relevant traits. We found that 15 (60% 95%CI 39; 79) of the 25 drugged or druggable proteins were targeted by compounds with a cardiovascular indication or side effect (**Table 1**).

While the number of discovered genes and genetic heritability differed considerably across CMR traits (16 genes for RV-ESV, compared to zero for RV-PFR, LV-PER, and LV-PAFR), the genetic contribution was balanced across both ventricles, and variants for LV and RV measurements were often highly correlated, suggesting similar genetic burden between LV and RV traits. The relatively high number of multi-CMR loci that affected both LV and RV (12/51 or 24%) additionally supported a shared genetic background. Principal component analyses of the CMR measurement further found that 7 PCs explain more than 90% of the phenotypic variation, where typically LV and RV of a specific trait contributed to the same PC (Supplementary Figure 2). Similar observations were seen in the *cis* MR analyses assessing the causal effects of plasma proteins on CMR traits: 19 proteins out of 33 (58%) affected both ventricles; p -value 5.74×10^{-5} , see **Table 1**.

In the current paper, we used enhanced locus-view plots including extensive annotations (see methods and Supplemental File 2) relevant to prioritize the most likely causal gene. Four raters (AFS, MB, JvS and CF) independently reviewed these data, with discordance resolved through consensus. Compared to previous CMR GWAS^{38,39}, which reported on the nearest gene instead of the likely causal gene, we found 35 novel causal genes of which 19 (58%) were linked with cardiac-metabolic traits sourced from GWAS catalog (**Supplementary**

Figure 3). Additionally, our list of causal genes included 8 drugged proteins with known cardio-metabolic indications or side effects, providing further support for these likely causal genes. Rediscovered CMR genes included variants previously associated with DCM (*TTN*, *BAG3*), HF (*BAG3*), HCM (*BAG3*, *FHOG3*, *CDKN1A*), AF (*IGF1R*, *GOSR2*, *TTN*, *CDKN1A*), and CHD (*ATXN2*, *GOSR2*); **Supplementary Figure 3**. We uniquely determined LV and RV PER, PFR and PAFR, where PFR is especially relevant for HF with preserved EF. Through *cis*-MR of plasma pQTL we identified seven proteins that affected PFR as well as HF or DCM risk: UD16, MANBA, TNFR5, TNF12, MFGM, CPC5, and BAG3, where the last five proteins were drugged or druggable, providing important leads for drug development.

The *cis*-MR analysis leveraged three distinct plasma pQTL resources, distilling a prioritized set of 33 plasma proteins that affect both CMR traits and cardiac outcomes; **Table 1**. While these proteins were prioritized on robust association with CMR traits and cardiac outcome, the association between a proteins' CMR effect direction and cardiac outcome effect direction (both categorized as 'beneficial', 'harmful', or 'mixed', the latter for multiple directionally discordant protein effects) did not reach significance (p -value 0.85). To an extent this likely reflects imperfect understanding of the relation between CMR traits and disease. As mentioned before, some of the considered CMR traits show a u-shaped relationship with cardiac outcomes in clinical settings. Furthermore, given the strong (observational and genetic) correlation between CMR traits, inference might be further improved by considering CMR traits jointly. Despite these caveats, we found that the identified subset of drugged and druggable proteins is enriched for compounds with a known cardiac indication or side effect: 60% (95%CI 39; 79) in our analysis, compared to 15% (172/1151) from a look-up of targets with a level 1 ATC code for cardiovascular system. Additionally it is worth considering that all of the considered CMR related proteins had considerable on-target effects on known cardio-metabolic risk factors which may offer alternative pathways to cardiac disease, which can additionally explain the observed discordance between CMR effect direction and cardiac outcome (**Figure 5, 8**).

Protein effect direction closely relates to whether one wants to develop an agonistic or antagonistic drug compound. This further highlights the importance of our approach to consider multiple clinically relevant traits and outcomes. Importantly, many of the discovered drugged and druggable proteins were targeted by inhibitory compounds, which did not necessarily match the cardiac outcome effect direction (**Table 1**), suggesting beneficial cardiac effects when activating these proteins instead. For example, TNF12, IL18R, I17RA, LYAM1, and MKO3, are all targeted by inhibiting agents, while increased plasma protein concentration was associated with a decreased risk of cardiac outcomes including DCM and HF.

Our analyses have highlighted multiple drug targets that affected the joint risk of multiple cardiac outcomes (**Figure 5** and **Table 1**). Some of these proteins are closely linked. For

example, ERAP1 (Endoplasmic reticulum aminopeptidase 1) affects CHD, AF, and non-ischemic CM, which is closely related to ERAP2 which in turn showed a directionally opposing effect on CHD, likely explained by similar directionally discordant effect on LPA, DBP, and carotid plaque. Both ERAP1 and ERAP2 play a major role in peptides trimming for presentation on major histocompatibility complex (MHC) Class I molecules⁴⁰, which is involved with cardiomyocyte pathogenesis⁴¹. Similarly, TNF12 decreases the risk of non-ischemic CM, DCM, and AF, and promotes IL8 concentration which we linked to a lower risk of AF and HF (and higher risk of CHD). IL8 concentration has been previously associated with HF and AF outcomes, supporting these observations^{42,43}. We found that higher plasma concentrations of BAG3 affected multiple CMR traits as well as HF, DCM, and non-ischemic CM risk. BAG3 is indirectly drugged through a direct protein interaction with HSP7C (heat shock cognate 71 kDa protein), where compounds for HSP7C documented to affect cardiac function and calcium handling⁴⁴.

Through BNF and ChEMBL linkage we found that 13 (52%, 95%CI 0.31; 0.72) of the 25 druggable proteins were targeted by a compound with an oncological indication (**Table 1**). For example, CD33 and SLAF7, together with CD38 (which did not have plasma pQTL data) are targeted by mAbs for multiple myeloma⁴⁵. The high degree of oncological targets suggests that some of the reported cardiotoxicity⁴⁶ (e.g., by tyrosine kinase inhibitors such as TIE2) may likely be due to on-target effects, which are resistant to potential compound improvement. Because oncological compounds are used to prevent cancer progression, compounds activating these proteins may not necessarily cause novel neoplasms. Activator compounds may nevertheless influence the growth of any existing undiagnosed neoplasms, and hence a change in action type should very carefully explored. Aside from the oncological targets we have found many additional repurposing opportunities, for example the PA2GA (Phospholipase A2) inhibitor varespladib previously failed to show a beneficial CHD effect (which we confirmed)⁴⁷, whereas we found convincing effect of PA2GA on CMR traits and HF.

In the current study, we uniquely combined GWAS of UKB derived CMR traits, with cross-platform GWAS of the plasma proteome, with drug target MR of protein effect on CMR and 56 additionally clinically relevant traits, with linkage to GWAS catalog, BNF, ChEMBL, HPA, IntAct and Reactome. By leveraging orthogonal lines of evidence on genetic expression, mRNA expression, protein interactions, and drug compound indications and side effects, we were able to identify a robust set of proteins related with CMR and cardiac outcome traits. The synthesis of these independent evidence sources complimented the already robust analytic techniques used. Genetic analyses were conducted using methods such as BOLT-LMM and BOLT-REML, which appropriately account for any potential population admixture or relatedness²⁶. Drug target MR analyses were guarded against horizontal pleiotropy by removing variants with either high leverage or high heterogeneity statistics (as potential

outliers), and a model selection framework was used to apply the MR-Egger correction (which is unbiased in the presence of 100% pleiotropic variants)³². Furthermore, results were strenuously corrected for multiplicity accounting for the correlation between CMR traits through PCA, where prioritization based on multiple lines of evidence results in an indirect replication that will further reduce the false positive rate. This plausibility of false positives driving these results was further explored through Kolmogorov-Smirnov test, comparing the observed p-value distributions against the p-value distribution expected when all results are false positive, finding considerable difference between both (**Supplementary Figure 5**).

Nevertheless, we feel the following potential limitations deserve consideration. While we did not exclude individuals from non-European ancestry and corrected for any potential population stratification bias through efficient linear-mixed-models²⁶, the majority of participants were of European decent and hence generalizability of our results should be confirmed. The CMR measurements were derived through deep learning, which we have shown to be sufficiently accurate. There are some caveats that suggest that drug target MR analysis may be more useful as a reliable test of effect direction. This is because drugs that inhibit a target usually do so by modifying its function not its concentration, whereas genetic variants used in MR analysis usually affect protein expression and therefore concentration. Furthermore, while trials of drug compounds are closely monitored, and followed for a fixed period, allowing for exploration of induction-times⁴⁸. MR estimates are considered to reflect a life-long exposure, but in the absence of serial assessment, possible changes across age are difficult to explore, as are disease induction-times. For these reasons, we suggest that drug target MR offers a robust indication of effect direction but may not directly anticipate the effect magnitude of pharmacologically interfering with a protein and position our findings as a resource to inform ongoing and future drug trials⁴⁹.

In conclusion, through large scale analyses of the genome and plasma proteome, and linkage to mRNA expression, protein interactions and drug compounds, we have identified a prioritized set of 33 proteins with a robust CMR and cardiac outcome fingerprint and determined anticipated effects of protein perturbation through a highly powered phenome-wide scan. Our analyses provide a detailed overview of potential targets for repurposing or *de novo drug* development for cardiac therapies.

Data availability

Source GWAS CMR data have been deposited XX. We additionally leveraged pQTL data from these sources, which can be accessed from: <https://ega-archive.org/studies/EGAS000001002555> (interval), <https://zenodo.org/record/2615265#.YbNUwr3MLOg> (scallop), ftp://ftp.ncbi.nlm.nih.gov/eqt/original_submissions/FHS_pQTLs/ (Framingham). Genomcis data for the *cis*-MR phewas was sourced for CHD cases from CardiogramplusC4D⁵⁰ (<http://www.cardiogramplusc4d.org/>); non-ischemic CM from (<https://www.ebi.ac.uk/gwas/>

[publications/30586722](https://www.ebi.ac.uk/gwas/publications/30586722)); DCM from (<https://www.ebi.ac.uk/gwas/publications/33677556>) HF from HERMES⁵¹ (<https://www.ebi.ac.uk/gwas/publications/31919418>); AF from AFgen⁵² (<http://csg.sph.umich.edu/willer/public/afib2018/>); stroke (subtypes) from MEGASTROKE⁵³ (<http://www.megastroke.org/index.html>) and intracranial aneurysms and subarachnoid haemorrhage data from (<https://cd.hugeamp.org/>); the presence of carotid plaque and carotid artery intima media thickness were available from a meta-analysis of the Cohorts for Aging Research in Genomic Epidemiology (CHARGE)⁵⁴ and University College London Edinburgh Bristol (UCLEB)⁵⁵ (https://www.ncbi.nlm.nih.gov/projects/gap/cgi-bin/study.cgi?study_id=phs000930.v6.p1); glycemic traits, blood lipid, exercise ECG, and lung function measurement were sourced from (<http://www.nealelab.is/uk-biobank>); type 2 diabetes⁵⁶ from DIAGRAM (<http://diagram-consortium.org/index.html>); BMI from GIANT⁵⁷ (https://portals.broadinstitute.org/collaboration/giant/index.php/GIANT_consortium_data_files); Asthma from (<https://www.ebi.ac.uk/gwas/publications/32296059>); CRP from (<https://www.ebi.ac.uk/gwas/publications/30388399>); the CKDGen consortium provided GWAS associations on blood urea nitrogen (BUN), estimated glomerular filtration rate (eGFR), and chronic kidney disease⁵⁸ (<http://ckdgen.imbi.uni-freiburg.de/>); Alzheimer's disease data was sourced from (https://ctg.cncr.nl/software/summary_statistics); Parkinson's disease data from (<https://www.ebi.ac.uk/gwas/publications/31701892>); Lewy body dementia from (<https://www.ebi.ac.uk/gwas/publications/33589841>); oncological data were sourced from (https://github.com/Wittelab/pancancer_pleiotropy). We additionally leveraged data from the Human Protein Atlas (<https://www.proteinatlas.org/about/download>), IntAct²³ and Reactome²⁴ (<https://reactome.org/download-data>), ChEMBL (<https://chembl.gitbook.io/chembl-interface-documentation/downloads>) and from Finan et al. (<https://www.science.org/doi/10.1126/scitranslmed.aag1166>, Table S1).

Code availability

Analyses were conducted using Python v3.7.4 (for GNU Linux), Pandas v0.25, Numpy v1.15, Matplotlib, Seaborn (for GNU Linux), and ggplot2 (for GNU Linux). Scripts and data necessary to generate the illustrations have been deposited: XX.

Author's contributions

AFS, MB, FWA, JvS, CF, contributed to the idea and design of the study. AFS, MB, AA and CF performed the analyses. AFS, JvS, MB, CF drafted the manuscript. All authors provided critical input on the analyses and the drafted manuscript.

Funding and role of funding sources

AFS is supported by BHF grant PG/18/5033837 and the UCL BHF Research Accelerator AA/18/6/34223. MB is supported by the Alexandre Suerman Stipend of the UMC Utrecht (2017). CF and AFS received additional support from the National Institute for Health Research University College London Hospitals Biomedical Research Centre. ADH is an

NIHR Senior Investigator. This work was supported by grant [R01 LM010098] from the National Institutes of Health (USA) and by EU/EFPIA Innovative Medicines Initiative 2 Joint Undertaking BigData@Heart grant n° 116074. JvS and MvV are supported by Dutch Heart Foundation grant 2019T045. ATR is supported by the CardioVascular Research Initiative of the Netherlands Heart Foundation (CVON 2015-12 eDETECT and 2012-10 PREDICT) and the Dutch Heart Foundation grant number 2015T058. SWvdL is funded through grants from the Netherlands CardioVascular Research Initiative of the Netherlands Heart Foundation (CVON 2011/B019 and CVON 2017-20) and is additionally supported by the ERA-CVD program (grant number: 01KL1802), the EU H2020 TO_AITON (grant number: 848146), and the Leducq Fondation 'PlaQOmics'. AA is supported by King Abdullah International Medical Research Center (KAIMRC).

Conflict of interest statements

AFS and FWA have received Servier funding for unrelated work. SWvdL has received Roche funding for unrelated work.

Guarantor

AFS, CF, AA, performed the presented analyses. AFS had full access to all the data in the study and takes responsibility for the integrity of the data and the accuracy of the data analysis.

Acknowledgement

This research has been conducted using the UK Biobank Resource under Application Number 24711. The authors are grateful to UK Biobank participants. UK Biobank was established by the Wellcome Trust medical charity, Medical Research Council, Department of Health, Scottish Government, and the Northwest Regional Development Agency. It has also had funding from the Welsh Assembly Government and the British Heart Foundation.

Prior postings and presentations

A preprint version of this manuscript has been deposited on biorxiv: <https://doi.org/>.

REFERENCES

1. Ponikowski, P. *et al.* 2016 ESC Guidelines for the diagnosis and treatment of acute and chronic heart failure: The Task Force for the diagnosis and treatment of acute and chronic heart failure of the European Society of Cardiology (ESC) Developed with the special contribution of the Heart Failure Association (HFA) of the ESC. *European Heart Journal* **37**, 2129–2200 (2016).
2. Redfield, M. M. *et al.* Isosorbide Mononitrate in Heart Failure with Preserved Ejection Fraction. *N Engl J Med* **373**, 2314–2324 (2015).
3. Gheorghiadu, M. *et al.* Effect of Vericiguat, a Soluble Guanylate Cyclase Stimulator, on Natriuretic Peptide Levels in Patients With Worsening Chronic Heart Failure and Reduced Ejection Fraction: The SOCRATES-REDUCED Randomized Trial. *JAMA* **314**, 2251–2262 (2015).
4. Fordyce, C. B. *et al.* Cardiovascular drug development: is it dead or just hibernating? *J Am Coll Cardiol* **65**, 1567–1582 (2015).
5. Andersson, C. *et al.* Risk factor-based subphenotyping of heart failure in the community. *PLOS ONE* **14**, e0222886 (2019).
6. Ruijsink, B. *et al.* Fully Automated, Quality-Controlled Cardiac Analysis From CMR: Validation and Large-Scale Application to Characterize Cardiac Function. *JACC: Cardiovascular Imaging* **13**, 684–695 (2020).
7. Finan, C. *et al.* The druggable genome and support for target identification and validation in drug development. *Science Translational Medicine* **9**, (2017).
8. Sun, B. B. *et al.* Genomic atlas of the human plasma proteome. *Nature* (2018) doi:10.1038/s41586-018-0175-2.
9. Schmidt, A. F. *et al.* Genetic drug target validation using Mendelian randomisation. *Nature Communications* **11**, 3255 (2020).
10. Swerdlow, D. I. *et al.* The interleukin-6 receptor as a target for prevention of coronary heart disease: A mendelian randomisation analysis. *The Lancet* **379**, 1214–1224 (2012).
11. Swerdlow, D. I. *et al.* *HMG-coenzyme A reductase inhibition, type 2 diabetes, and bodyweight: Evidence from genetic analysis and randomised trials.* vol. 385 (2015).
12. Schmidt, A. F. *et al.* Phenome-wide association analysis of LDL-cholesterol lowering genetic variants in PCSK9. *BMC Cardiovascular Disorders* **240**, (2019).
13. Schmidt, A. F. *et al.* PCSK9 genetic variants and risk of type 2 diabetes: a mendelian randomisation study. *The Lancet Diabetes & Endocrinology* **5**, 97–105 (2017).
14. Schmidt, A. F. *et al.* Cholesteryl ester transfer protein (CETP) as a drug target for cardiovascular disease. *Nat Commun* **12**, 5640 (2021).
15. Holmes, M. V. *et al.* Secretory phospholipase A2-IIA and cardiovascular disease: A mendelian randomization study. *Journal of the American College of Cardiology* **62**, 1966–1976 (2013).
16. Casas, J. P. *et al.* PLA2G7 Genotype, lipoprotein-associated phospholipase A2 activity, and coronary heart disease risk in 10 494 cases and 15 624 controls of european ancestry. *Circulation* **121**, 2284–2293 (2010).
17. Zheng, J. *et al.* Phenome-wide Mendelian randomization mapping the influence of the plasma proteome on complex diseases. *bioRxiv* 627398 (2019) doi:10.1101/627398.
18. Gordillo-Marañón, M. *et al.* Validation of lipid-related therapeutic targets for coronary heart disease prevention using human genetics. *Nat Commun* **12**, 6120 (2021).
19. Folkersen, L. *et al.* Genomic and drug target evaluation of 90 cardiovascular proteins in 30,931 individuals. *Nat Metab* **2**, 1135–1148 (2020).
20. Yao, C. *et al.* Genome wide mapping of plasma protein QTLs identifies putatively causal genes and pathways for cardiovascular disease. *Nat Commun* **9**, 3268 (2018).
21. Gaulton, A. *et al.* The ChEMBL database in 2017. *Nucleic Acids Res* **45**, D945–D954 (2017).
22. Uhlen, M. *et al.* Towards a knowledge-based Human Protein Atlas. *Nat Biotechnol* **28**, 1248–1250 (2010).
23. Orchard, S. *et al.* The MIntAct project—IntAct as a common curation platform for 11 molecular interaction databases. *Nucleic Acids Res* **42**, D358–363 (2014).
24. Jassal, B. *et al.* The reactome pathway knowledgebase. *Nucleic Acids Res* **48**, D498–D503 (2020).
25. Bycroft, C. *et al.* The UK Biobank resource with deep phenotyping and genomic data. *Nature* **562**, 203–209 (2018).
26. Loh, P.-R. *et al.* Efficient Bayesian mixed-model analysis increases association power in large cohorts. *Nat Genet* **47**, 284–290 (2015).
27. Buniello, A. *et al.* The NHGRI-EBI GWAS Catalog of published genome-wide association studies, targeted arrays and summary statistics 2019. *Nucleic Acids Res* **47**, D1005–D1012 (2019).
28. Burgess, S., Zuber, V., Valdes-Marquez, E., Sun, B. B. & Hopewell, J. C. Mendelian randomization with fine-mapped genetic data: Choosing from large numbers of correlated instrumental variables. *Genetic Epidemiology* **41**, 714–725 (2017).
29. Burgess, S. & Thompson, S. G. Avoiding bias from weak instruments in mendelian randomization studies. *International Journal of Epidemiology* **40**, 755–764 (2011).
30. Bowden, J., Smith, G. D. & Burgess, S. Mendelian randomization with invalid instruments: Effect estimation and bias detection through Egger regression. *International Journal of Epidemiology* **44**, 512–525 (2015).
31. Bowden, J. *et al.* A framework for the investigation of pleiotropy in two-sample summary data Mendelian randomization. *Statistics in medicine* **36**, 1783–1802 (2017).
32. Bowden, J. *et al.* Improving the visualization, interpretation and analysis of two-sample summary data Mendelian randomization via the Radial plot and Radial regression. *Int J Epidemiol* **47**, 1264–1278 (2018).
33. Carithers, L. J. & Moore, H. M. The Genotype-Tissue Expression (GTEx) Project. *Biopreserv Biobank* **13**, 307–308 (2015).
34. Andersson, R. *et al.* An atlas of active enhancers across human cell types and tissues. *Nature* **507**, 455–461 (2014).
35. Kryuchkova-Mostacci, N. & Robinson-Rechavi, M. A benchmark of gene expression tissue-specificity metrics. *Brief Bioinform* **18**, 205–214 (2017).
36. Bulik-Sullivan, B. K. *et al.* LD Score Regression Distinguishes Confounding from Polygenicity in Genome-Wide Association Studies. *Nat Genet* **47**, 291–295 (2015).
37. Saveanu, L. *et al.* Concerted peptide trimming by human ERAP1 and ERAP2 aminopeptidase complexes in the endoplasmic reticulum. *Nat Immunol* **6**, 689–697 (2005).
38. Pirruccello, J. P. *et al.* Analysis of cardiac magnetic resonance imaging in 36,000 individuals yields genetic insights into dilated cardiomyopathy. *Nat Commun* **11**, 2254 (2020).
39. Pirruccello, J. P. *et al.* Genetic Analysis of Right Heart Structure and Function in 40,000 People. *bioRxiv* 2021.02.05.429046 (2021) doi:10.1101/2021.02.05.429046.
40. Agrawal, N. & Brown, M. A. Genetic associations and functional characterization of M1 aminopeptidases and immune-mediated diseases. *Genes Immun* **15**, 521–527 (2014).
41. Gröschel, C. *et al.* T helper cells with specificity for an antigen in cardiomyocytes promote pressure overload-induced progression from hypertrophy to heart failure. *Sci Rep* **7**, 15998 (2017).
42. Nymo, S. H. *et al.* Inflammatory cytokines in chronic heart failure: interleukin-8 is associated with adverse outcome. Results from CORONA. *Eur J Heart Fail* **16**, 68–75 (2014).
43. Guo, Y., Lip, G. Y. H. & Apostolakis, S. Inflammation in atrial fibrillation. *J Am Coll Cardiol* **60**, 2263–2270 (2012).
44. Kim, Y.-K. *et al.* Deletion of the Inducible 70-kDa Heat Shock Protein Genes in Mice Impairs Cardiac Contractile Function and Calcium Handling Associated With Hypertrophy. *Circulation* **113**, 2589–2597 (2006).
45. Petrucci, M. T. & Vozella, F. The Anti-CD38 Antibody Therapy in Multiple Myeloma. *Cells* **8**, E1629 (2019).
46. Han, X., Zhou, Y. & Liu, W. Precision cardio-oncology: understanding the cardiotoxicity of cancer therapy. *NPJ Precis Oncol* **1**, 31 (2017).
47. Nicholls, S. J. *et al.* Varespladib and cardiovascular events in patients with an acute coronary syndrome: the VISTA-16 randomized clinical trial. *JAMA* **311**, 252–262 (2014).
48. The HPS3/TIMI55–REVEAL Collaborative Group. Effects of Anacetrapib in Patients with Atherosclerotic Vascular Disease. *N Engl J Med* **377**, 1217–1227 (2017).
49. Schmidt, A. F., Hingorani, A. D. & Finan, C. Human Genomics and Drug Development. *Cold Spring Harb Perspect Med* a039230 (2021) doi:10.1101/cshperspect.a039230.
50. Nikpay, M. *et al.* A comprehensive 1,000 Genomes-based genome-wide association meta-analysis of coronary artery disease. *Nat Genet* **47**, 1121–1130 (2015).
51. Shah, S. *et al.* Genome-wide association and Mendelian randomisation analysis provide insights into the pathogenesis of heart failure. *Nature Communications* **11**, 1–12 (2020).
52. Nielsen, J. B. *et al.* Biobank-driven genomic discovery yields new insight into atrial fibrillation biology. *Nature Genetics* **50**, 1234–1239 (2018).
53. Multiancestry genome-wide association study of 520,000 subjects identifies 32 loci associated with stroke and stroke subtypes | Nature Genetics. <https://www.nature.com/articles/s41588-018-0058-3>.
54. Psaty, B. M. *et al.* Cohorts for Heart and Aging Research in Genomic Epidemiology (CHARGE) Consortium: Design of prospective meta-analyses of genome-wide association studies from five cohorts. *Circ Cardiovasc Genet* **2**, 73–80 (2009).
55. Shah, T. *et al.* Population genomics of cardiometabolic traits: design of the University College London-London School of Hygiene and Tropical Medicine-Edinburgh-Bristol (UCL-EB) Consortium. *PLoS one* **8**, e71345 (2013).
56. Mahajan, A. *et al.* Refining the accuracy of validated target identification through coding variant fine-mapping in type 2 diabetes. *Nature Genetics* **50**, 559–571 (2018).
57. Pulit, S. L. *et al.* Meta-analysis of genome-wide association studies for body fat distribution in 694 649 individuals of European ancestry. *Hum Mol Genet* **28**, 166–174 (2019).
58. Wuttke, M. *et al.* A catalog of genetic loci associated with kidney function from analyses of a million individuals. *Nat. Genet.* **51**, 957–972 (2019).

SUPPLEMENTARY FILES

Please see <https://www.researchsquare.com/article/rs-1305500/v1> for all supplementary files .

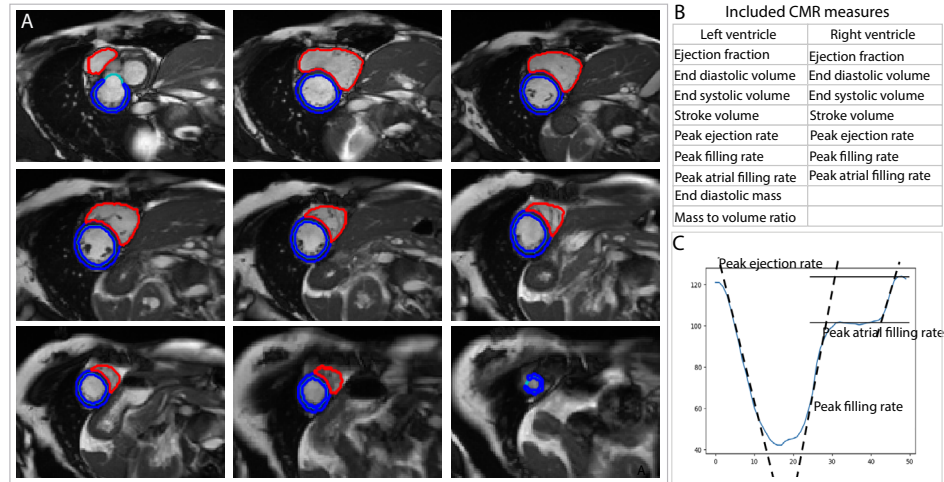


Figure S1: **A)** Examples of automatic segmentation of the left (blue) and right (red) ventricle from basal to apical short axis cine CMR (base to apex). **B)** The included left and right ventricular CMR measures calculated using a deep-learning algorithm. **C)** A graphical explanation of the calculation of the peak ejection rate, peak filling rate and peak atrial filling rate.

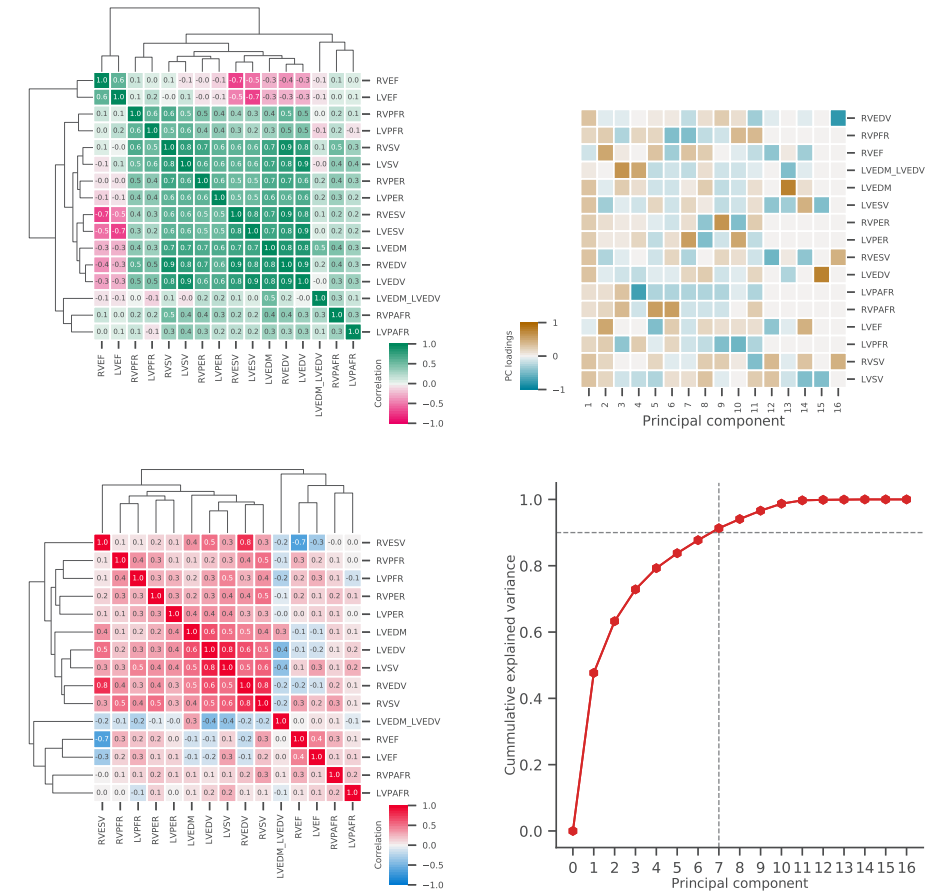


Figure S2: Left column Spearman's pairwise correlation: *top left*, between the phenotypic cardiac MRI measurements (based on a n=36548 UKB sample), and *bottom left*, between the genetic association with these cardiac MRIs. Right column principal components analysis (PCA): *bottom right*, the component loadings, and *top right*, the cumulative explained variance by principal component. The heatmap margins were ordered by hierarchical clustering of the Euclidean distance.

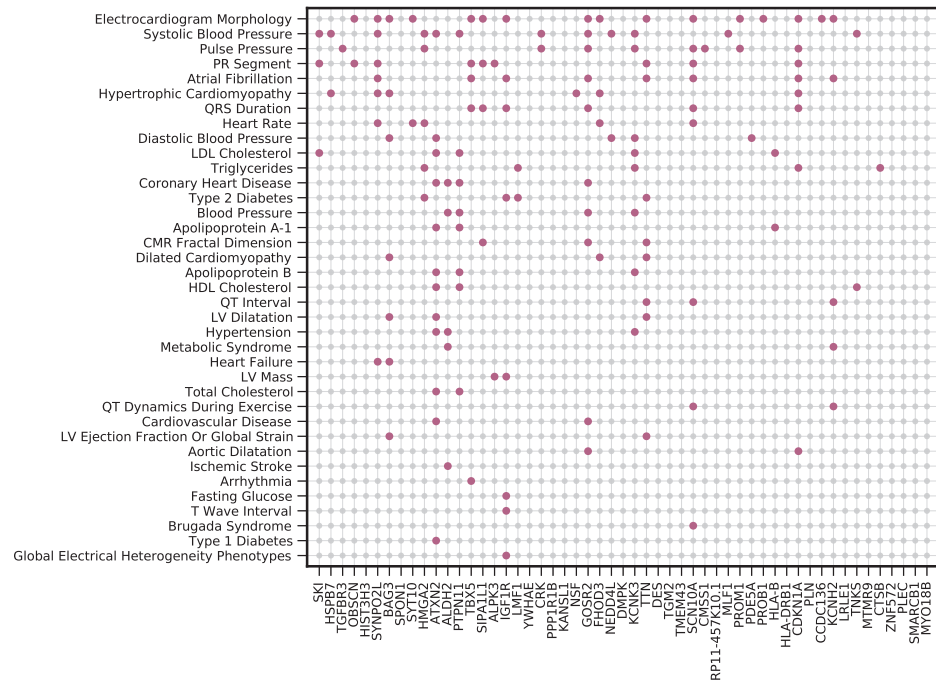


Figure S3: An incidence matrix linking the CMR loci to previous cardio-metabolic GWAS associations from GWAS catalog.

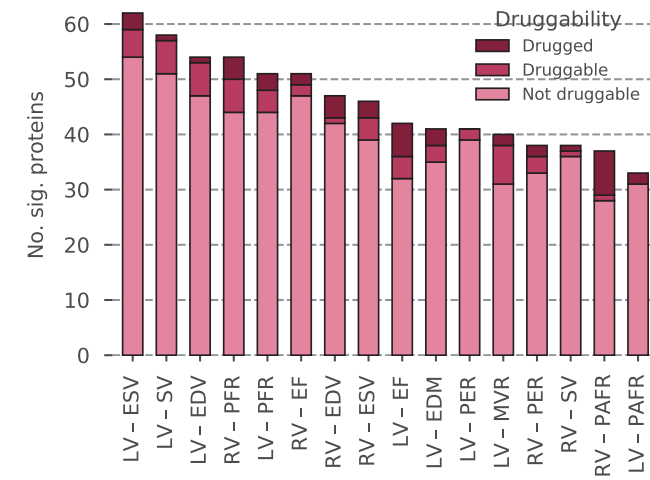


Figure S4: The frequency of plasma protein associations per CMR trait stratified on druggability status. Results are based on *cis* Mendelian randomization analyses and represent estimates that passed a multiplicity corrected p-value threshold of 7.81×10^{-6} . Druggability was based on an update version of Finan *et al*[1]

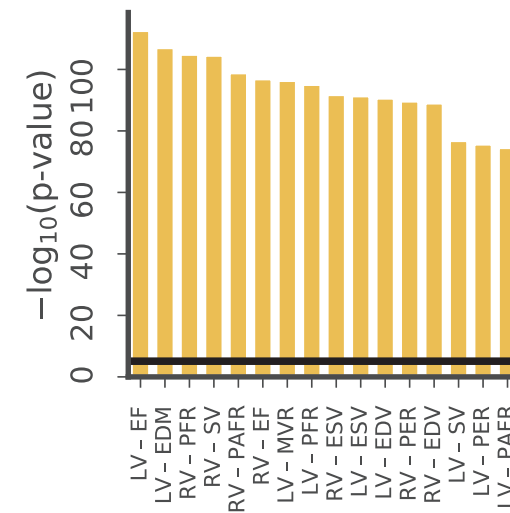


Figure S5: Trait specific Kolmogorov-Smirnoff null-hypothesis tests comparing the empirical p-value distribution to the uniform distribution expected when results are driven by false positive results. The horizontal line indicates the multiplicity corrected alpha of 7.81×10^{-6} .

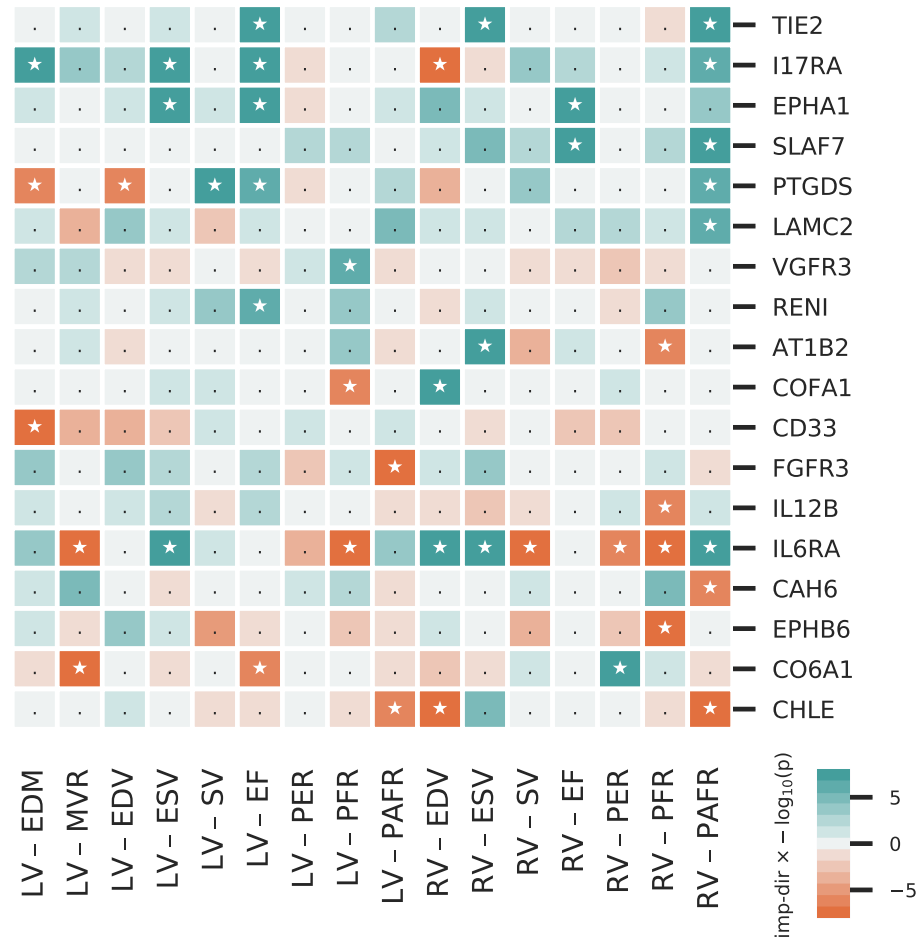


Figure S6: Drug target MR of *drugged* plasma protein concentration (per SD) effects on CMR traits orientated toward the cardiac function improving direction ('imp-dir'). Cells are coloured by truncated p-value (max 8) multiplied by effect direction.

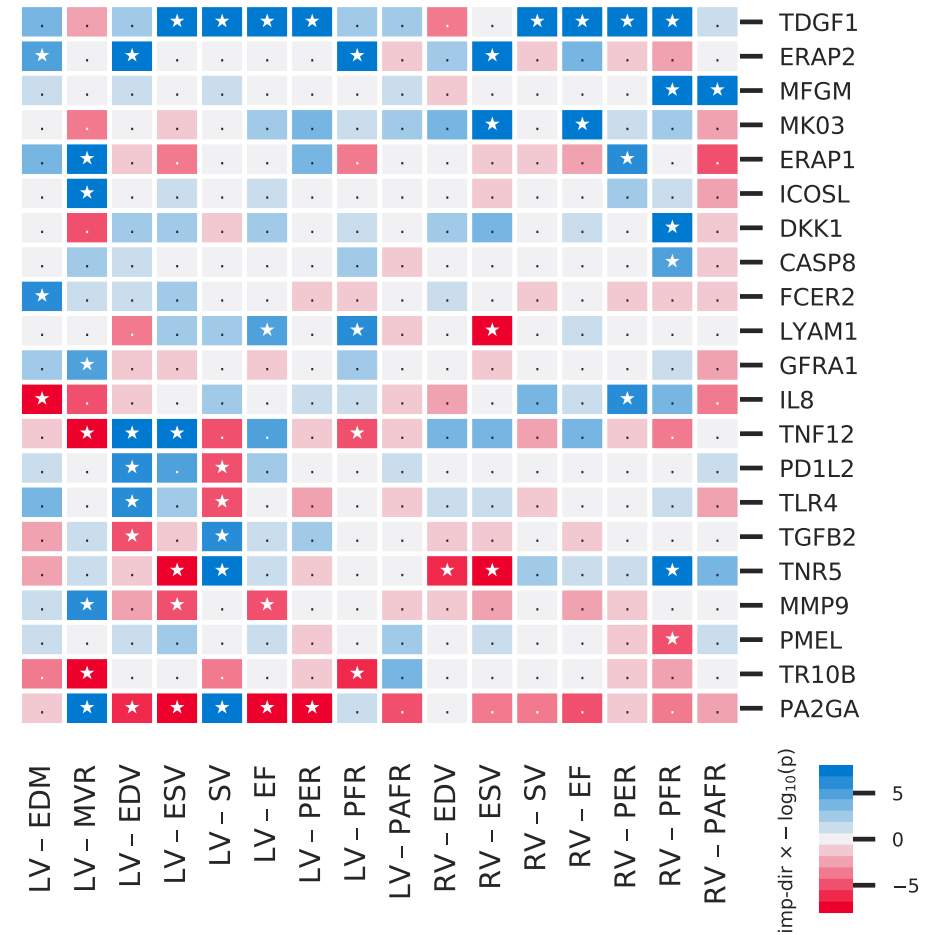


Figure S7: Drug target MR of *druggable* plasma protein concentration (per SD) effects on CMR traits orientated toward the cardiac function improving direction ('imp-dir'). Cells are coloured by truncated p-value (max 8) multiplied by effect direction.

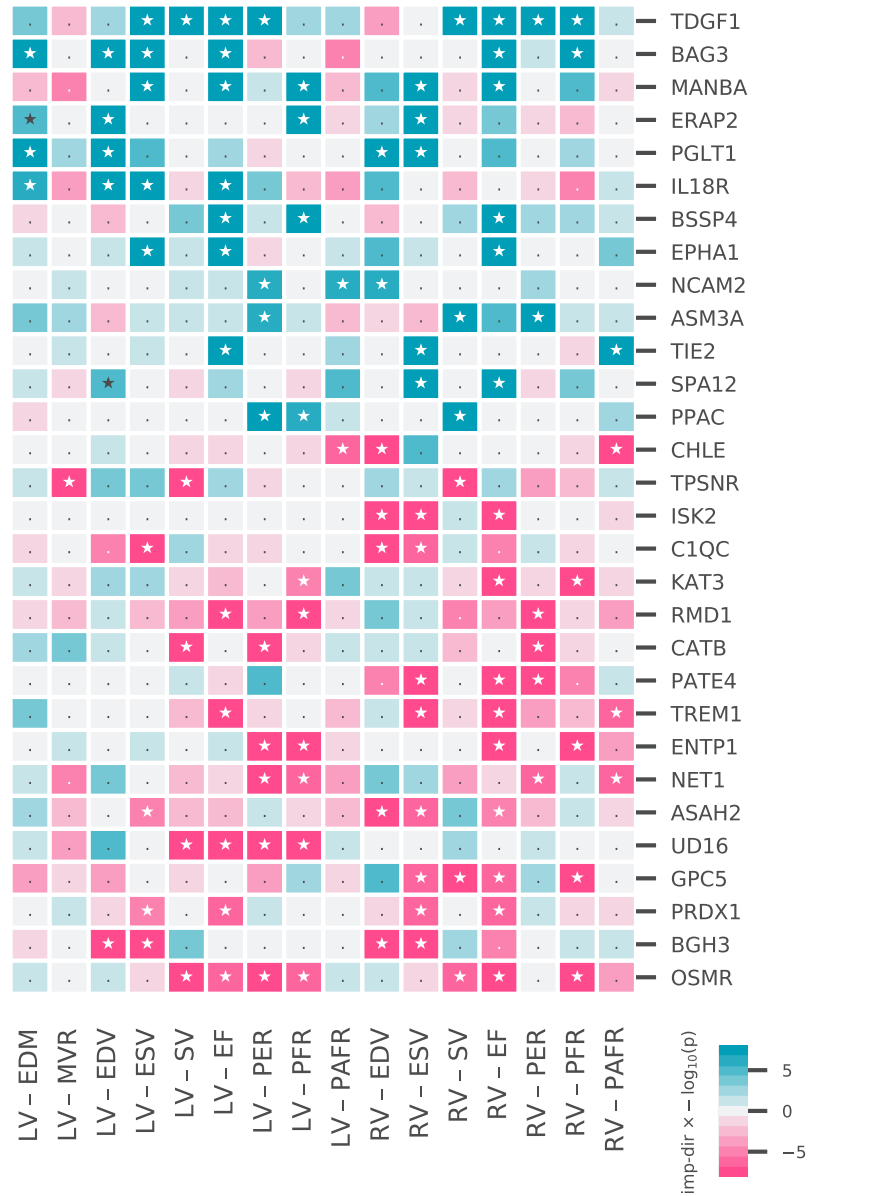


Figure S8: Concordant protein effects on CMR traits orientated toward the cardiac function improving direction (*imp-dir*). Depicting proteins affecting three or more CMR traits, in a concordant risk increasing or decreasing direction. Cells are coloured by truncated p-value (max 8) multiplied by effect direction.

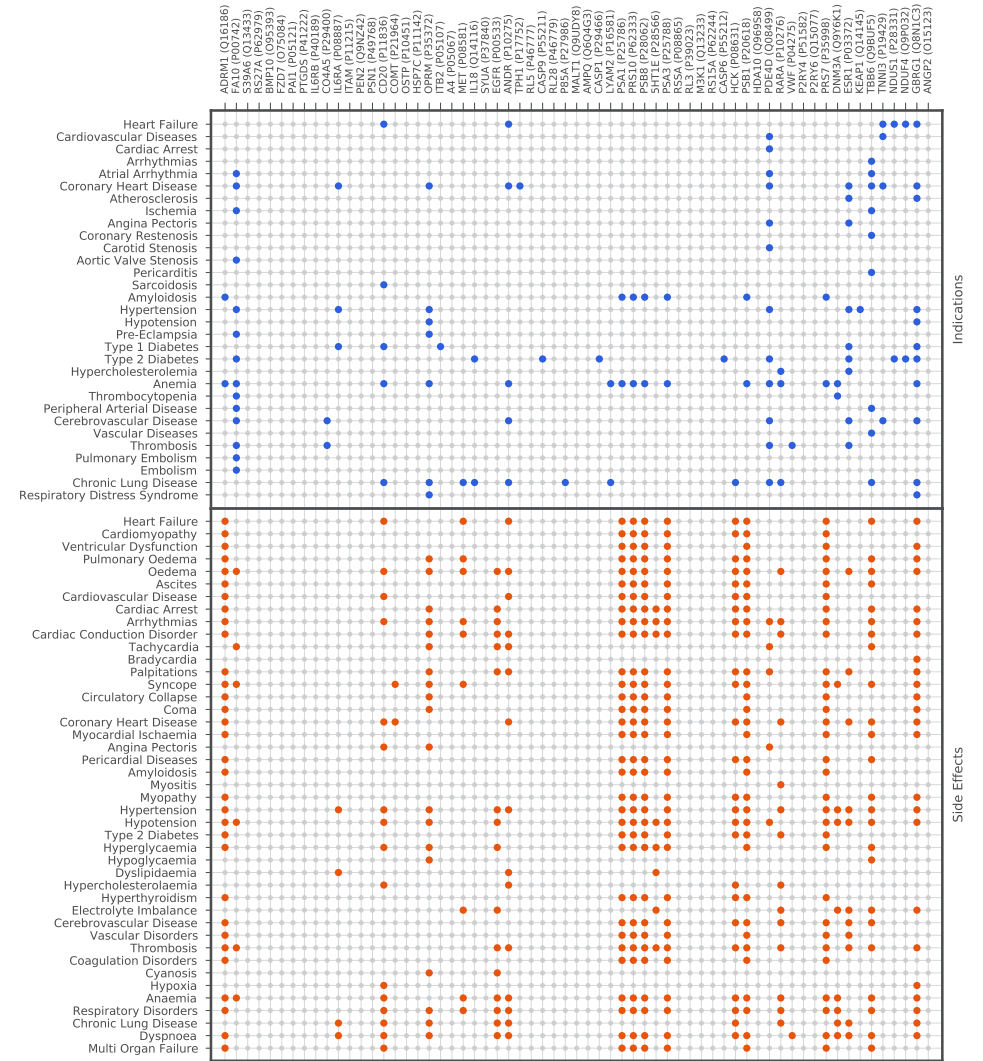


Figure S9: Incidence matrix of cardiovascular related indication and side effect of druggable or druggable protein identified through a Reactome pathway analysis of plasma proteins with concordant CMR effects. Protein name and uniprot id are provided on the top x-axis, with indication or side effect trait on the y-axis. N.b. data were extracted from Reactome, BNF and ChEMBL.

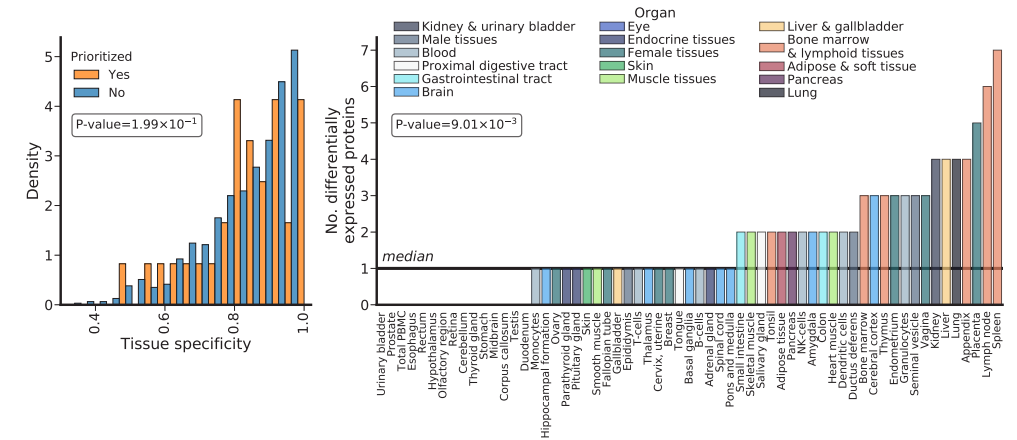
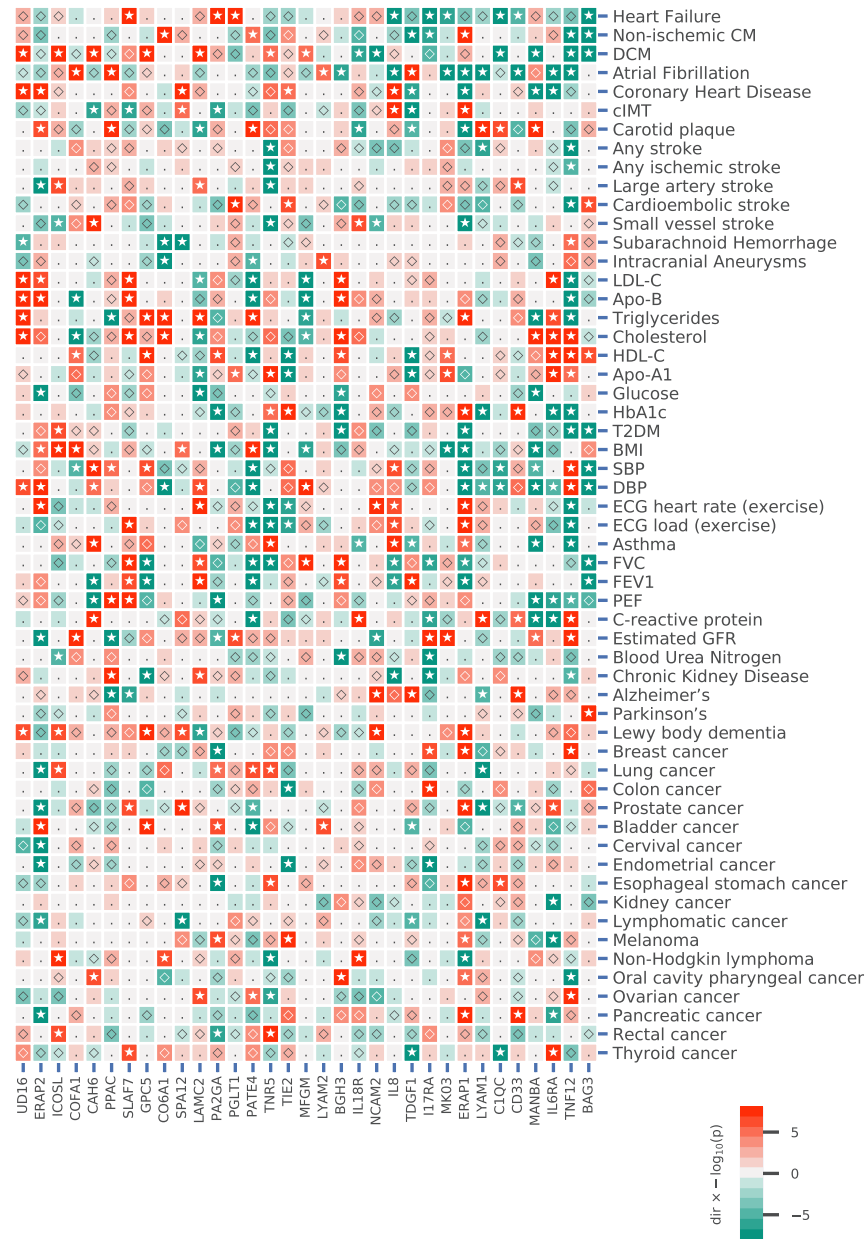


Figure S11: Left: The tissue specificity of plasma proteins prioritized on having an robust CMR and cardiac outcome association; The p-value is based on a Mann-Whitney test. Right: The number of tissues with differentially more mRNA expression of the CMR and cardiac outcome prioritized plasma proteins; with χ^2 -test for equal number differentially expressed proteins per tissue. Data were sourced from the Human Protein Atlas.

Figure S10: A phenome-wide scan of CMR proteins associated with one or more cardiac outcome. N.b. Proteins were curated on having a multiplicity corrected p-value $> 1.29 \times 10^{-5}$ with one or more of the following cardiac traits: Heart Failure (HR), Dilated Cardiac Myopathy (DCM), Non-ischemic CM, Atrial Fibrillation (AF), or Coronary Heart Disease (CHD). P-value passing the 0.05 threshold are indicated by square rotated about 90 degrees, with stars indicating results passing the mentioned multiplicity corrected threshold. Cells were coloured by effect direction times $-\log_{10}(p\text{-value})$; where p-values were truncated to 8.

Table S1: CMR measurements and pathological consequence

Measurement	Abbreviation	Unit	Pathological consequence of higher values
Stroke volume	SV	ml	Beneficial
Peak ejection rate	PER	ml/s	Beneficial
Peak atrial filling rate	PAFR	ml/s	Beneficial
Peak filling rate	PFR	ml/s	Beneficial
End systolic volume	ESV	ml	Harmful
Ejection fraction	EF	%	Beneficial
End diastolic volume	EDV	ml	Harmful
End diastolic mass	EDM	gram	Harmful
Ratio of EDM and EDV	MVR	gram/ml	Harmful

Table S2: UK biobank fields used to exclude participants with possible pre-existing cardiac disease.

Excluded phenotype	UKB field ID/ICD-10 code
Myocardial infarction	42000
Acute transmural myocardial infarction of anterior wall	I21.0
Acute transmural myocardial infarction of inferior wall	I21.1
Acute transmural myocardial infarction of other sites	I21.2
Acute transmural myocardial infarction of unspecified site	I21.3
Acute subendocardial myocardial infarction	I21.4
Acute myocardial infarction	I21.9
Subsequent myocardial infarction of anterior wall	I22.0
Subsequent myocardial infarction of inferior wall	I22.1
Subsequent myocardial infarction of other sites	I22.8
Subsequent myocardial infarction of unspecified site	I22.9
Acute ischaemic heart disease	I24.9
Old myocardial infarction	I25.2
Pulmonary embolism with mention of acute cor pulmonale	I26.0
Primary pulmonary hypertension	I27.0
Kyphoscoliotic heart disease	I27.1
Other secondary pulmonary hypertension	I27.2
Nonrheumatic tricuspid (valve) stenosis	I36.0
Nonrheumatic tricuspid (valve) insufficiency	I36.1
Other nonrheumatic tricuspid valve disorders	I36.8
Nonrheumatic tricuspid valve disorder	I36.9
Pulmonary valve stenosis	I37.0
Pulmonary valve insufficiency	I37.1
Pulmonary valve stenosis with insufficiency	I37.2
Other pulmonary valve disorders	I37.8
Pulmonary valve disorder	I37.9
Congestive heart failure	I50.0
Left ventricular failure	I50.1
Heart failure	I50.9
Hypertensive heart disease with (congestive) heart failure	I11.0
Dilated cardiomyopathy	I42.0
Obstructive hypertrophic cardiomyopathy	I42.1
Other hypertrophic cardiomyopathy	I42.2

Table S2: Continued.

Excluded phenotype	UKB field ID/ICD-10 code
Endocardial fibroelastosis	I42.4
Other restrictive cardiomyopathy	I42.5
Alcoholic cardiomyopathy	I42.6
Cardiomyopathy due to drugs and other external agents	I42.7
Other cardiomyopathies	I42.8
Congenital malformation of cardiac chambers and connexions	Q20.9
Common arterial trunk	Q20.0
Discordant ventriculoarterial connexion	Q20.3
Ventricular septal defect	Q21.0
Atrial septal defect	Q21.1
Atrioventricular septal defect	Q21.2
Tetralogy of Fallot	Q21.3
Aortopulmonary septal defect	Q21.4
Other congenital malformations of cardiac septum	Q21.8
Congenital malformation of cardiac septum	Q21.9
Congenital pulmonary valve stenosis	Q22.1
Congenital pulmonary valve insufficiency	Q22.1
'Ebstein's anomaly'	Q22.5
Other congenital malformations of tricuspid valve	Q22.8
Congenital stenosis of aortic valve	Q23.0
Congenital insufficiency of aortic valve	Q23.1
Congenital mitral insufficiency	Q23.3
Other congenital malformations of aortic and mitral valves	Q23.8
Congenital malformation of aortic and mitral valves	Q23.9
Chronic obstructive pulmonary disease with acute lower respiratory infection	J44.0
Chronic obstructive pulmonary disease with acute exacerbation	J44.1
Other specified chronic obstructive pulmonary disease	J44.8
'MacLeod's syndrome'	J43.0
Panlobular emphysema	J43.1
Centrilobular emphysema	J43.2
Other emphysema	J43.8
Emphysema	J43.9
LVEF <40%	Automated CMR data used

Table S3: Assessing the potential for bias due to cryptic related-ness and population stratification.

CMR trait	LD-Score intercept (SE)
RV - EDV	1.02 (0.01)
RV - EF	1.00 (0.01)
RV - ESV	1.02 (0.01)
RV - PAFR	1.00 (0.01)
RV - PER	0.99 (0.01)
RV - PFR	1.01 (0.01)
RV - SV	1.00 (0.01)
LV - EDM	1.01 (0.01)
LV - MVR	1.01 (0.01)
LV - EDV	1.01 (0.01)
LV - EF	0.99 (0.01)
LV - ESV	1.00 (0.01)
LV - PAFR	1.00 (0.01)
LV - PER	1.01 (0.01)
LV - PFR	1.01 (0.01)
LV - SV	1.00 (0.01)

General: In the absence of bias the intercept is expected to be 1.00. SE: standard error.

Table S4: Characteristics of UK biobank subjects used in the CMRGWAS.

Characteristics	Total (n=36548)	Female (n=18879)	Male (n=17093)	Missing
Age at time of CMR (years)	63.9 (7.6)	63.3 (7.4)	64.5 (7.7)	0
<i>Ethnicity</i>				679
Caucasian	34872 (97.0%)	18336 (97.1%)	16536 (96.8%)	
Black	209 (0.6%)	111 (0.6%)	98 (0.6%)	
Asian	351 (1.0%)	122 (0.6%)	229 (1.3%)	
Other	437 (1.3%)	267 (1.5%)	170 (1.0%)	
Height (cm)	169.2 (89.2)	162.8 (6.2)	176.1 (6.6)	0
Weight (kg)	76.0 (15.1)	69.1 (13.1)	83.7 (13.3)	0
Cardiovascular risk factors				
BMI (kg/m ²)	26.5 (4.4)	26.1 (4.7)	26.9 (3.9)	0
Systolic bloodpressure (mmHg)	138.2 (18.4)	135.1 (19.0)	141.6 (17.1)	3525
Diastolic bloodpressure (mmHg)	78.6 (10.0)	76.8 (9.9)	80.5 (9.7)	2525
Heart rate (bpm)	62.5 (10.2)	63.5 (9.9)	61.5 (10.4)	577
Cholesterol (mmol/l)	5.7 (1.1)	5.9 (1.1)	5.6 (1.1)	2340
Diabetes	1835 (5.1%)	669 (3.5%)	1166 (6.8%)	248
<i>Smoking</i>				248
Past	12227 (33.7%)	5891 (30.9%)	6336 (36.7)	
Current	1254 (3.5%)	541 (2.8%)	713 (4.1%)	
Alcohol intake- daily/almost daily	6104 (16.8%)	2531 (13.3%)	3573 (20.7%)	248
Moderate activity (MET minutes pw)	826.7 (1120.3)	832.7 (1108.8)	820.6 (1133.9)	5191
<i>CMR parameters</i>				
LV-EDV (ml)	143.2 (33.2)	125.1 (22.2)	163.5 (31.7)	4078
LV-ESV (ml)	58.8 (18.5)	48.9 (12.2)	69.8 (18.1)	4082
LV-EDM (g)	80.9 (22.4)	65.9 (12.6)	97.6 (18.9)	4077
LV-MVR (g/ml)	0.6 (0.1)	0.5 (0.1)	0.6 (0.1)	4087
LV-SV (ml)	84.4 (18.9)	76.2 (14.5)	93.7 (19.1)	4079
LV-EF (%)	59.4 (6.2)	61.0 (5.8)	57.5 (5.9)	4075
LV-PFR (ml/s)	321.1 (98.3)	303.4 (86.6)	341.0 (106.5)	4081
LV-PER (ml/s)	377.8 (111.9)	323.5 (84.8)	438.4 (106.5)	4075
LV-PAFR (ml/s)	251.8 (106.5)	225.6 (94.1)	280.9 (111.9)	4076
RV-EDV (ml)	153.7 (38)	131.0 (24.6)	178.7 (34.3)	676
RV-ESV (ml)	64.8 (22.0)	52.2 (14.1)	78.6 (20.9)	689
RV-SV (ml)	88.9 (20.5)	78.8 (15.2)	100.1 (19.8)	685
RV-EF (%)	58.5 (6.8)	60.4 (6.4)	56.3 (6.5)	742
RV-PFR (ml/s)	308.4 (96.3)	282.9 (82.8)	336.6 (102.1)	734
RV-PER (ml/s)	396.3 (111.2)	341.7 (83.1)	456.5 (107.1)	689
RV-PAFR (ml/s)	293.7 (108.6)	260.4 (92.3)	163.9 (31.4)	718

General: Number represents mean/counts with between brackets the standard deviation or percentage. BMI= body mass index; CMR= cardiac magnetic resonance; EDV= end-diastolic volume; EDM= end-diastolic mass; EF= ejection fraction; ESV= end-systolic volume; LV= left ventricle; MET= metabolic equivalent of task; MVR= mass to volume ratio; PAFR= peak atrial filling rate; PER= peak ejection rate; PFR= peak filling rate; RV= right ventricle; SV= stroke volume.

Table S5: Top hits from a cardiac MRI (CMR) GWAS on sixteen leftand right-ventricle (LV,RV) traits.

Marker name	Chr	BP (build 37)	Nearest gene	Causal gene	CMR trait	EF/NEA	MD	p-value	Novel CMR locus
rs2503715	1	2144107	Ctfrf86 (ENSG00000162585)	SKI (ENSG00000157933)	LV – MVR	A/G	-0.005	3.08×10 ⁸	Novel
rs28579893	1	16347534	HSPB7 (ENSG00000173641)	HSPB7 (ENSG00000173641)	LV – EF	A/G	0.410	2.54×10 ¹⁷	Novel
rs28579893	1	16347534	HSPB7 (ENSG00000173641)	HSPB7 (ENSG00000173641)	LV – ES	A/G	-0.924	4.58×10 ¹⁵	Novel
rs945425	1	16348412	HSPB7 (ENSG00000173641)	HSPB7 (ENSG00000173641)	RV – EF	T/C	0.301	3.62×10 ¹⁰	Novel
rs6604061	1	92328613	RN7SL653P (ENSG00000239794)	TGFBR3 (ENSG00000069702)	RV – ES	T/A	0.689	2.18×10 ⁸	Novel
rs3738685	1	228556788	OBSCN (ENSG00000154358)	OBSCN (ENSG00000154358)	LV – ES	C/T	-0.676	6.30×10 ⁹	Rediscovery
rs3738685	1	228556788	OBSCN (ENSG00000154358)	OBSCN (ENSG00000154358)	RV – EF	C/T	0.306	9.29×10 ¹¹	Rediscovery
rs12126782	1	228613648	HIST3H3 (ENSG00000168148)	HIST3H3 (ENSG00000168148)	RV – ES	T/G	-0.910	7.04×10 ¹³	Novel
rs1314982	2	26922062	KCNK3 (ENSG00000171303)	KCNK3 (ENSG00000171303)	RV – EDV	G/A	1.224	3.50×10 ⁸	Rediscovery
rs13394970	2	26929282	KCNK3 (ENSG00000171303)	KCNK3 (ENSG00000171303)	RV – ES	T/G	0.761	5.06×10 ¹⁰	Rediscovery
rs746173377	2	179442292	RP11-1712.5 (ENSG00000271011)	TTN (ENSG00000155657)	RV – ES	T/A/T	-1.090	1.43×10 ⁸	Rediscovery
rs12988307	2	179490478	RP11-1712.4 (ENSG00000271141)	TTN (ENSG00000155657)	LV – ES	T/C	1.522	1.58×10 ²⁷	Rediscovery
rs2562845	2	179514433	RP11-1712.3 (ENSG00000271401)	TTN (ENSG00000155657)	LV – EF	T/C	-0.539	4.98×10 ²¹	Rediscovery
rs2042995	2	179558366	RP11-1712.1 (ENSG00000267784)	TTN (ENSG00000155657)	RV – EDV	T/C	1.620	1.77×10 ¹²	Rediscovery
rs2042995	2	179558366	RP11-1712.1 (ENSG00000267784)	TTN (ENSG00000155657)	RV – EF	T/C	-0.331	7.78×10 ¹⁰	Rediscovery
rs2042995	2	179558366	RP11-1712.1 (ENSG00000267784)	TTN (ENSG00000155657)	RV – ES	T/C	1.190	4.76×10 ¹⁷	Rediscovery
rs11692972	2	179669931	CCDC141 (ENSG00000163492)	TTN (ENSG00000155657)	LV – EDM	C/T	1.809	1.81×10 ¹⁶	Rediscovery
rs11692972	2	179669931	CCDC141 (ENSG00000163492)	TTN (ENSG00000155657)	LV – EDV	C/T	3.371	4.88×10 ¹⁷	Rediscovery
rs6747402	2	179759434	RNU7-104P (ENSG00000238542)	TTN (ENSG00000155657)	RV – EDV	G/A	-1.299	2.29×10 ¹¹	Rediscovery
rs6747402	2	179759434	RNU7-104P (ENSG00000238542)	TTN (ENSG00000155657)	RV – ES	G/A	-0.762	2.05×10 ¹⁰	Rediscovery
rs55844607	2	179770998	RNU7-104P (ENSG00000238542)	TTN (ENSG00000155657)	RV – SV	A/G	1147	4.65×10 ⁸	Rediscovery
rs35009641	2	220432957	INHA (ENSG00000123999)	DES (ENSG00000175084)	LV – MVR	G/A	-0.008	3.36×10 ⁸	Novel
rs200775399	3	14291003	RP11-53816.2 (ENSG00000255021)	TMEM43 (ENSG00000170876)	LV – EF	CTTTT/C	-0.271	2.18×10 ⁸	Novel
rs1170541	3	14291679	RP11-53816.2 (ENSG00000255021)	TMEM43 (ENSG00000170876)	LV – ES	T/C	0.804	9.02×10 ¹²	Novel
rs2170454	3	14294549	RP11-53816.2 (ENSG00000255021)	TMEM43 (ENSG00000170876)	RV – ES	T/C	-0.990	1.49×10 ¹⁶	Novel

Table S5: Top hits from a cardiac MRI (CMR) GWAS on sixteen leftand right-ventricle (LV,RV) traits. (continued)

Marker name	Chr	BP (build 37)	Nearest gene	Causal gene	CMR trait	EF/NEA	MD	p-value	Novel CMR locus
rs10865722	3	14306782	RP11-53816.2 (ENSG00000255021)	TMEM43 (ENSG00000170876)	RV – EF	G/T	-0.375	1.15×10 ¹⁴	Novel
rs34234056	3	14418444	RNA5SP124 (ENSG00000199609)	TMEM43 (ENSG00000170876)	RV – ES	A/G	0.655	4.52×10 ⁸	Novel
rs6795970	3	38766675	SCN10A (ENSG00000185313)	SCN10A (ENSG00000185313)	RV – PAFR	A/G	-4.711	4.44×10 ¹⁰	Novel
rs57848867	3	99779984	FILIP1L (ENSG00000168386)	CMSS1 (ENSG00000184220)	RV – EDV	A/T	-1.223	4.03×10 ¹⁰	Rediscovery
rs57848867	3	99779984	FILIP1L (ENSG00000168386)	CMSS1 (ENSG00000184220)	RV – ES	A/T	-0.674	2.29×10 ⁸	Rediscovery
rs11487301	3	109560677	RP11-457K10.1 (ENSG00000242029)	RP11-457K10.1 (ENSG00000242029)	LV – SV	ATG/A	0.735	2.28×10 ⁸	Novel
rs11710570	3	158056654	RP11-113A111 (ENSG00000241723)	MLF1 (ENSG00000178053)	RV – EDV	T/C	-1.206	4.82×10 ¹⁰	Rediscovery
rs9844502	3	158298615	MLF1 (ENSG00000178053)	MLF1 (ENSG00000178053)	RV – ES	C/T	-0.915	1.97×10 ¹⁴	Rediscovery
rs9864508	3	158298703	MLF1 (ENSG00000178053)	MLF1 (ENSG00000178053)	RV – EF	T/C	0.284	3.44×10 ¹⁰	Rediscovery
rs10939649	4	16034589	RNU6-350P (ENSG00000251758)	PROM1 (ENSG0000007062)	LV – EF	C/T	0.330	3.00×10 ¹⁰	Novel
rs34463475	4	120438654	PDE5A (ENSG00000138735)	PDE5A (ENSG00000138735)	RV – ES	CT/C	-0.764	1.17×10 ⁸	Novel
rs12514667	5	138718825	SLC23A1 (ENSG00000170482)	PROB1 (ENSG00000228672)	RV – ES	C/G	-0.695	4.61×10 ⁸	Novel
rs11242465	5	138762305	DNAJC18 (ENSG00000170464)	PROB1 (ENSG00000228672)	LV – ES	T/G	-0.681	4.92×10 ⁸	Novel
rs4835729	5	138763329	DNAJC18 (ENSG00000170464)	PROB1 (ENSG00000228672)	LV – EF	A/G	0.299	9.11×10 ¹⁰	Novel
rs4835730	5	138763807	DNAJC18 (ENSG00000170464)	PROB1 (ENSG00000228672)	RV – EF	T/C	0.328	1.27×10 ¹¹	Novel
rs34504162	6	31310626	HLA-B (ENSG00000234745)	HLA-B (ENSG00000234745)	LV – MVR	A/G	-0.004	3.09×10 ⁸	Rediscovery
rs9265867	6	31312790	HLA-B (ENSG00000234745)	HLA-B (ENSG00000234745)	RV – PER	A/T	-5.435	1.95×10 ⁹	Rediscovery
rs11721712	6	31315407	HLA-B (ENSG00000234745)	HLA-B (ENSG00000234745)	LV – SV	C/CT	0.702	5.36×10 ⁹	Rediscovery
rs218174821	6	32631426	XXbac-	HLA-DRB1 (ENSG00000196126)	LV – EF	G/A	-0.327	9.09×10 ⁹	Novel
rs7774130	6	36623756	RNU1-88P (ENSG00000238554)	CDKN1A (ENSG00000124762)	LV – EDM	C/T	-0.760	4.24×10 ¹⁰	Rediscovery
rs730506	6	36645968	CDKN1A (ENSG00000124762)	CDKN1A (ENSG00000124762)	LV – MVR	G/C	-0.007	1.51×10 ¹⁸	Rediscovery
rs147436240	6	36648064	CDKN1A (ENSG00000124762)	CDKN1A (ENSG00000124762)	LV – EF	CGCGT/C	-0.339	7.97×10 ⁹	Rediscovery
rs11153730	6	118667522	SLC35F1 (ENSG00000196376)	PLN (ENSG00000198523)	LV – EDV	T/C	-1.114	4.57×10 ⁹	Novel
rs74640693	6	118684824	SLC35F1 (ENSG00000196376)	PLN (ENSG00000198523)	LV – MVR	A/T	-0.008	5.46×10 ⁹	Novel
rs73238147	7	128469917	FLNC (ENSG00000128591)	CCDC136 (ENSG00000128596)	LV – ES	T/C	0.976	1.63×10 ⁹	Novel

Table S5: Top hits from a cardiac MRI (CMR) GWAS on sixteen left and right-ventricle (LV,RV) traits. (continued)

Marker name	Chr	BP (build 37)	Nearest gene	Causal gene	CMR trait	EF/NEA	MD	p-value	Novel CMR locus
rs3918226	7	150690176	NOS3 (ENSG00000164867)	KCNH2 (ENSG00000055118)	RV - EDV	C/T	2.051	1.65×10 ⁸	Novel
rs3918226	7	150690176	NOS3 (ENSG00000164867)	KCNH2 (ENSG00000055118)	RV - SV	C/T	1.272	5.93×10 ⁹	Novel
rs2980441	8	8095129	ALG1L13P (ENSG00000253981)	LRL1 (ENSG00000268955)	RV - EF	G/C	-0.261	9.87×10 ⁹	Novel
rs66645639	8	9591977	MIR597 (ENSG00000207701)	TNKS (ENSG00000173273)	LV - EF	TTACTC/T	0.267	1.56×10 ⁸	Rediscovery
rs7233349	8	10998630	AF131215.4 (ENSG00000254556)	MTMR9 (ENSG00000104643)	RV - EF	G/T	0.266	5.44×10 ⁹	Novel
rs13268810	8	11797430	OR7E16IP (ENSG00000206014)	CTSB (ENSG00000164733)	LV - EF	A/T	-0.265	1.53×10 ⁸	Novel
rs12541595	8	125857359	LINC00964 (ENSG00000249816)	ZNF572 (ENSG00000180938)	LV - EF	G/T	-0.348	2.66×10 ¹²	Novel
rs200712209	8	125858538	LINC00964 (ENSG00000249816)	ZNF572 (ENSG00000180938)	LV - ESV	GA/G	0.879	4.63×10 ¹³	Novel
rs34866937	8	125859850	LINC00964 (ENSG00000249816)	ZNF572 (ENSG00000180938)	RV - EF	G/A	-0.284	6.42×10 ⁹	Novel
rs11784619	8	145013775	MIR661 (ENSG00000207574)	PLEC (ENSG00000178209)	LV - EF	G/A	-0.563	1.61×10 ⁸	Rediscovery
rs11786896	8	145018354	MIR661 (ENSG00000207574)	PLEC (ENSG00000178209)	RV - EF	C/T	-0.702	2.67×10 ¹¹	Rediscovery
rs11786896	8	145018354	MIR661 (ENSG00000207574)	PLEC (ENSG00000178209)	RV - ESV	C/T	1.805	8.29×10 ¹¹	Rediscovery
rs3812629	10	75407290	SYNPO2L (ENSG00000166317)	SYNPO2L (ENSG00000166317)	LV - EDM	G/A	-0.823	3.36×10 ⁸	Novel
rs10886511	10	121307823	RGS10 (ENSG00000148908)	BAG3 (ENSG00000151929)	RV - ESV	G/A	0.793	2.39×10 ⁹	Rediscovery
rs72840788	10	121415685	BAG3 (ENSG00000151929)	BAG3 (ENSG00000151929)	LV - EDV	G/A	1.551	2.83×10 ¹¹	Rediscovery
rs72840788	10	121415685	BAG3 (ENSG00000151929)	BAG3 (ENSG00000151929)	LV - EF	G/A	-0.581	3.98×10 ²⁵	Rediscovery
rs72840788	10	121415685	BAG3 (ENSG00000151929)	BAG3 (ENSG00000151929)	LV - ESV	G/A	1.463	1.12×10 ²⁶	Rediscovery
rs72840788	10	121415685	BAG3 (ENSG00000151929)	BAG3 (ENSG00000151929)	RV - EF	G/A	-0.544	1.21×10 ²²	Rediscovery
rs72840788	10	121415685	BAG3 (ENSG00000151929)	BAG3 (ENSG00000151929)	RV - ESV	G/A	1.303	6.41×10 ¹⁹	Rediscovery
rs1609342	11	14022662	SPONI (ENSG00000152268)	SPONI (ENSG00000152268)	RV - ESV	C/T	-0.684	1.32×10 ⁸	Novel
rs61884835	11	140522348	SPONI (ENSG00000152268)	SPONI (ENSG00000152268)	LV - ESV	T/C	-0.667	2.42×10 ⁹	Novel
rs6488162	12	33593127	SYT10 (ENSG00000110975)	SYT10 (ENSG00000110975)	LV - SV	T/C	-0.782	1.61×10 ¹⁰	Novel
rs1585897	12	66383320	HMG2 (ENSG00000149948)	HMG2 (ENSG00000149948)	RV - EDV	C/A	1.104	1.79×10 ⁸	Rediscovery
rs4766578	12	11904371	ATXN2 (ENSG00000204842)	ATXN2 (ENSG00000204842)	RV - EDV	T/A	-1.913	9.14×10 ²³	Rediscovery
rs4766578	12	11904371	ATXN2 (ENSG00000204842)	ATXN2 (ENSG00000204842)	RV - SV	T/A	-0.869	1.32×10 ¹³	Rediscovery

Table S5: Top hits from a cardiac MRI (CMR) GWAS on sixteen left and right-ventricle (LV,RV) traits. (continued)

Marker name	Chr	BP (build 37)	Nearest gene	Causal gene	CMR trait	EF/NEA	MD	p-value	Novel CMR locus
rs597808	12	11973358	U7 (ENSG00000272215)	ATXN2 (ENSG00000204842)	LV - SV	A/G	-0.750	4.57×10 ¹⁰	Rediscovery
rs653178	12	112007756	U7 (ENSG00000272215)	ATXN2 (ENSG00000204842)	LV - EDV	C/T	-1.295	1.20×10 ¹¹	Rediscovery
rs653178	12	112007756	U7 (ENSG00000272215)	ATXN2 (ENSG00000204842)	RV - ESV	C/T	-1.062	8.93×10 ¹⁹	Rediscovery
rs11513729	12	112273499	MAPKAPK5-AS1 (ENSG00000234608)	ALDH2 (ENSG0000011275)	RV - PER	C/T	3.952	4.85×10 ⁹	Novel
rs11066320	12	112906415	PTPN11 (ENSG00000179295)	PTPN11 (ENSG00000179295)	RV - EDV	A/G	-1.593	9.96×10 ¹⁶	Novel
rs11066320	12	112906415	PTPN11 (ENSG00000179295)	PTPN11 (ENSG00000179295)	RV - SV	A/G	-0.777	8.12×10 ¹¹	Novel
rs1895606	12	114833384	TBX5-AS1 (ENSG00000255399)	TBX5 (ENSG00000089225)	RV - ESV	C/T	-0.680	1.76×10 ⁸	Novel
rs34647020	14	71796137	RPI-261D10.1 (ENSG00000259079)	SIPAL1 (ENSG00000197555)	LV - MVR	G/GT	-0.004	4.86×10 ⁸	Rediscovery
rs56864281	15	85357649	ALPK3 (ENSG00000136383)	ALPK3 (ENSG00000136383)	LV - MVR	C/A	0.007	4.71×10 ²⁴	Rediscovery
rs7164817	15	85379544	SNORA25 (ENSG00000200991)	ALPK3 (ENSG00000136383)	LV - EF	T/C	-0.274	2.08×10 ⁸	Rediscovery
rs12907646	15	85403496	SNORA25 (ENSG00000200991)	ALPK3 (ENSG00000136383)	LV - ESV	G/A	-0.897	2.36×10 ¹¹	Rediscovery
rs6598541	15	99271135	MIR4714 (ENSG00000264480)	IGFIR (ENSG00000140443)	LV - EDM	A/G	-0.611	1.88×10 ⁸	Rediscovery
rs7166287	15	99273075	MIR4714 (ENSG00000264480)	IGFIR (ENSG00000140443)	LV - MVR	C/T	-0.004	1.12×10 ¹⁰	Rediscovery
rs11350493	16	951372	LAI6c-306A4.2 (ENSG00000260316)	LMF1 (ENSG00000103227)	LV - MVR	TG/T	-0.004	2.29×10 ⁸	Novel
rs12452627	17	1302472	YWHAE (ENSG00000108953)	YWHAE (ENSG00000108953)	LV - MVR	G/A	-0.007	2.05×10 ¹¹	Novel
rs2302455	17	1374195	MYOIC (ENSG00000197879)	CRK (ENSG00000167193)	LV - EDV	G/A	1.783	3.09×10 ⁹	Novel
rs2302455	17	1374195	MYOIC (ENSG00000197879)	CRK (ENSG00000167193)	LV - ESV	G/A	1.031	5.52×10 ⁹	Novel
rs11869286	17	37813856	STAR3 (ENSG00000131748)	PPPIR1B (ENSG00000131771)	LV - EDM	G/C	-0.619	1.74×10 ⁸	Novel
rs2696421	17	43667635	DND1P1 (ENSG00000264070)	KANSL1 (ENSG00000120071)	LV - MVR	A/G	-0.005	5.82×10 ¹²	Novel
rs567642046	17	44358811	ARL17B (ENSG00000228696)	KANSL1 (ENSG00000120071)	LV - EDM	G/A	-0.941	1.87×10 ¹¹	Novel
rs17692129	17	44793283	RPS7P11 (ENSG00000213326)	NSF (ENSG00000073969)	LV - MVR	C/T	0.004	2.50×10 ¹⁰	Novel
rs17608766	17	45013271	RPI1-156P1.2 (ENSG00000262633)	GOSR2 (ENSG00000108433)	RV - EDV	T/C	-1.752	2.14×10 ¹⁰	Rediscovery
rs17608766	17	45013271	RPI1-156P1.2 (ENSG00000262633)	GOSR2 (ENSG00000108433)	RV - SV	T/C	-1.129	3.33×10 ¹¹	Rediscovery
rs772756888	18	34219777	SNORD112 (ENSG00000252078)	FHOD3 (ENSG00000134775)	RV - EF	G/GTT	-0.331	4.03×10 ¹⁰	Rediscovery
rs7230600	18	55938204	RPI1-71815.1 (ENSG00000267743)	NEDD4L (ENSG00000049759)	LV - ESV	G/A	-0.693	3.66×10 ⁹	Novel

CHAPTER 13

General discussion and
future perspectives

GENERAL DISCUSSION

This thesis focuses primarily on the improvement of early diagnosis and risk stratification of arrhythmogenic right ventricular cardiomyopathy (ARVC) patients and their relatives using advanced cardiac magnetic resonance (CMR) imaging techniques. In this chapter I summarize and discuss the main findings of each part reported in this thesis.

This thesis addressed the following questions:

Part 1- *What is the reproducibility, variability and applicability of feature tracking (FT)-CMR in the clinical setting?*

Part 2- *What is the clinical value of FT-CMR, T1 mapping and machine learning in ARVC?*

Part 3- *Is atrial involvement present in ARVC?*

Part 4- *What is the contribution of rare and common variants on right and left ventricular function in individuals from the general population?*

Part 1. Feasibility and reproducibility of novel CMR techniques in ARVC

Since the first publication on FT-CMR by Maret *et al.* in 2009¹, this technique has become a rapidly emerging approach for the assessment of regional wall motion. FT-CMR has also gained popularity in ARVC, as several studies already indicated regional abnormalities to occur prior to the onset of global changes in ARVC². However, before entering the clinical arena and contributing as a diagnostic or prognostic marker, variability in FT-CMR strain values due to technical variability has to be understood.

In **chapter 3** we assessed the inter-software agreement of right ventricular (RV) global and regional longitudinal strain using four different FT-CMR software methods (TomTec, Medis, Circle and MTT), in a cohort of well-phenotyped ARVC subjects including affected ARVC patients and at-risk pathogenic variant carriers. We demonstrated significant variability between the FT-CMR software methods. First, differences in RV wall tracking quality were present, with the highest tracking quality in Medis, followed by Circle, TomTec and MTT (with respectively 93%, 89%, 87% and 84% of segments adequately tracked). Second, absolute RV strain values correlated poorly between the software methods. Therefore, strain values obtained in one software method are impossible to translate to another. This is further emphasized by Nagata *et al.* who even showed significant variability of measurements using different versions of the same speckle tracking software³. However, despite software variability, all four FT-CMR software methods were able to identify affected ARVC patients from control subjects using global strain. Furthermore, a moderate to excellent inter- and intra-observer reproducibility of FT-CMR was seen. This suggests robustness of the FT-CMR approach and renders this technique suitable for follow-up of ARVC patients. Based on this study, it is advised to standardize the use of one software method within a clinical center, especially if used for clinical follow-up. In case of ARVC, which is a rare disease in which collaborative

studies are the norm, the ideal solution would be to use the same FT-CMR software method in collaborating centers. Since FT-CMR software methods are generally a black box, developers should give more clarity on the underlying method, to allow for interchangeability of FT-CMR values in and among centers. Besides these algorithm dependent properties, algorithm independent properties were addressed in **chapter 4** and **chapter 5**.

In **chapter 4**, we studied the influence of field strength, resolution and imaging sequence on RV FT-CMR strain values. For global longitudinal RV strain, the inter-field strength (1.5 T and 3 T) and the inter-resolution agreement was good for the bSSFP sequence, whereas this was moderate to poor for regional longitudinal RV strain. This indicates that regional longitudinal RV strain cannot be used interchangeably within different resolutions and CMR field-strengths and field-strength and resolution specific reference values are necessary. This is clinically relevant since various diseases, including ARVC, show affected regional longitudinal strain in a preclinical disease stage making regional strain especially interesting for early diagnosis. In this study, we also used the preclinical ultra-high field strength 7T on MRI. 7T MRI has proven clinical value in brain MRI studies, but the clinical value of 7T MRI is not yet known for CMR. 7T has great potential to detect subtle wall abnormalities due to higher signal- to-noise ratio which enables higher spatial resolutions⁴. Importantly, RV strain values were not comparable between 7T and the conventional field strengths 1.5T and 3T in our study, therefore obtaining 7T-specific normal values should precede clinical implementation.

While CMR is the recommended gold standard for the structural and functional assessment of ARVC, echocardiography remains an important modality for diagnosis and follow-up, due to its easier availability and lower costs. In echocardiography, deformation imaging with speckle tracking is used to quantify myocardial strain⁵. Since both modalities are used in clinical practice, the assessment of interchangeability of RV strain values measured by these different modalities is important. In **chapter 5** we included 34 affected ARVC patients, 30 at-risk pathogenic variant carriers, and 46 healthy control subjects who all underwent CMR and echocardiography. We studied the correlation and agreement between global and regional RV longitudinal strain as measured on speckle tracking echocardiography versus FT-CMR. Furthermore, we compared their clinical performance in ARVC. Both modalities showed reduced strain values in ARVC patients compared to ARVC relatives (speckle tracking global strain: $p < 0.001$; FT-CMR global strain: $p < 0.001$) and reduced strain values in ARVC relatives compared to healthy control subjects (speckle tracking global strain: $p = 0.042$; FT-CMR global strain: $p = 0.084$). However, only a moderate correlation between global RV strain values as measured by speckle tracking echocardiography and FT-CMR existed which deteriorated when regional strain was studied. Unfortunately, no correction factor to correct the bias between the two different modalities could be made. Therefore, these modalities cannot be used interchangeably. The differences between the modalities could be explained by different markers used to quantify myocardial motion in

both techniques; speckle tracking echocardiography uses acoustic backscatters while FT-CMR uses anatomic features. Also, differences in spatial and temporal resolution exist and both modalities use different scanning angles which could potentially cause difficulties in matching myocardial segments between the modalities.

The first part of this thesis taught us that FT-CMR is feasible for clinical implementation. However standardization of software algorithm dependent and independent variables remains necessary. When comparing FT-CMR strain values within a patient or among patients, software method, resolution, field strength and differences in modalities should be taken into account. In an ideal world, software vendors should collaborate to minimize algorithm dependent difference. Until that time, routine use of FT-CMR in ARVC evaluation should take place at an experienced center with experienced CMR readers. Until standardized reference values are available, software method-, scanner- and modality specific references should be used.

Part 2. Clinical value of novel CMR techniques in ARVC

CMR has an important role as a diagnostic tool in ARVC, due to its ability to demonstrate structural and functional abnormalities of the heart. CMR is considered the reference standard for the evaluation of the RV in patients suspected of ARVC⁶. Regional wall motion abnormalities, in combination with RV dysfunction and dilatation, is a prerequisite for fulfilment of CMR criteria in the 2010 diagnostic Task Force Criteria (TFC)⁷. An important part of clinically implemented CMR evaluations is operator-dependent and therefore still “in the eye of the beholder”, which means that misdiagnosis in ARVC is often based on CMR misinterpretations. This is reflected in a high percentage of referrals to CMR centers. Interestingly, only 27% of people referred to a tertiary center with a suspected ARVC diagnosis finally meet diagnostic criteria for ARVC⁸. The operator-dependent factors that hamper inter-observer reproducibility include the subjective assessment of wall motion and fibrosis and the manual segmentations of the RV for the assessment of ejection fraction and dimensions. In this part we studied the clinical value of novel CMR techniques that aim to reduce operator dependency.

Feature tracking CMR

Previous studies have shown the incremental diagnostic value of objective and quantitative wall motion analysis using FT-CMR or speckle tracking echocardiography. Vigneault *et al.* already showed a higher sensitivity and specificity for FT-CMR compared to visual assessment in 110 individuals evaluated for ARVC⁹. However, little was known about the diagnostic and prognostic value of this technique. In **chapter 3**, we hypothesized that FT-CMR may be useful for early disease detection of ARVC by identifying regional myocardial dysfunction prior to overt disease presentation. We showed a reduced global longitudinal RV strain in affected ARVC patients compared to control subjects. These results were reassuring since

global structural abnormalities are thought to occur later in the disease course of ARVC and can therefore be expected to be abnormal in affected ARVC patients. In contrast, global RV strain was comparable in preclinical vs. control subjects. These results suggested that global RV strain is insensitive for early disease detection. Interestingly, preclinical subjects were separated from controls in the subtricuspid region by Medis software ($p = 0.009$). This is also illustrated by a moderate discriminative accuracy of subtricuspid strain to distinguish preclinical from control subjects using Medis (AUC = 0.70). These results are exciting since abnormal subtricuspid strain has previously shown to be an independent predictor for ARVC diagnosis when controlled for sex, RVEF and RVEDV in multivariable analysis⁹. This suggests there is additional value for the assessment of subtricuspid strain beyond RV size and function.

After showing the potential diagnostic role of FT-CMR in the diagnostic value, we set out to study the prognostic value of FT-CMR in ARVC in **chapter 6**. We assessed whether FT-CMR of the RV and left ventricle (LV) is able to predict future sustained ventricular arrhythmias and evaluated the incremental value of FT-CMR over traditional arrhythmic risk factors in a multicenter cohort of 132 ARVC patients without prior sustained ventricular arrhythmias (i.e. primary prevention patients). In our study RV and LV global strain was reduced in ARVC patients who developed sustained ventricular arrhythmias during follow-up. RVEF is a known predictor of sustained ventricular arrhythmias in ARVC¹⁰ and abnormal strain is thought to precede changes in EF. Furthermore, ARVC patients with a reduced RV and LV global and regional strain (basal and mid strain for the RV and posterolateral and septal strain for the LV) more often showed ventricular arrhythmias during follow-up. Importantly, after correcting for RVEF, LVEF, and the ARVC ventricular arrhythmia risk calculator¹⁰ and adjusting for multiple testing, RV and LV strain did not remain a significant predictor of sustained VA. While one may consider it disappointing that strain does not further risk stratify beyond conventional measures, it is important to realize that the majority of patients in this study population were in an advanced disease stage, with structural disease seen in 76% of patients with minor or major structural TFC, and 39% of patients already had a high expected 5-years risk of ventricular arrhythmias as calculated by the ARVC ventricular arrhythmia risk calculator. While there is proven value of adding strain to established CMR parameters for diagnostic purposes, no incremental value is observed for prognostic purposes in ARVC patients. Future studies should focus on the additional prognostic value of strain in unaffected family members who carry a pathogenic variant. Furthermore, FT-CMR could be a marker of disease progression from preclinical to clinical disease, as previously shown using echocardiography deformation imaging¹¹. Future studies should confirm the value of regional strain by FT-CMR as a marker of disease progression.

T1 mapping

In **chapter 7** we performed a proof-of-concept study with the aim to analyze the diagnostic value of native T1 mapping in ARVC. Included subjects ($n = 43$) were divided into 3 groups: 1)

genotype-positive patients with ARVC diagnosed by the 2010 diagnostic TFC (n = 13); 2) at-risk pathogenic variant carriers not fulfilling TFC (n = 17); and 3) control subjects evaluated for ARVC but diagnosed with RV outflow tract ventricular tachycardia (n = 13). We only analyzed LV T1 mapping since the thin RV wall rendered T1 mapping susceptible to partial volume effects. Besides, global native T1, T1 dispersion was calculated as the SD of native T1 times in all segments within a given patient. Mean LV T1 times and T1 dispersion were significantly higher in overt patients compared with control subjects. It is known that fibrosis increases T1 times, while fat decreases T1 times. This suggests that the changes in cardiac microstructure are dominated by fibrosis rather than fatty replacement. Although no statistically significant difference was noted in LV T1 times between relatives and control subjects, T1 dispersion was significantly greater in relatives compared with control subjects. This was driven by elevated T1 times in the LV posterolateral (p ≤ 0.02) and inferior (p = 0.01) regions for both overt patients and relatives. This supports the previously described “displaced” Triangle of dysplasia¹², showing that early disease manifestations often occur in the RV basal inferior wall, RV basal anterior wall and de LV posterolateral wall. We extend these findings by revealing that these changes can already be observed in asymptomatic carriers of a pathogenic variant before the development of an overt clinical phenotype. Moreover, a large proportion of at-risk relatives with elevated T1 dispersion had no LGE, suggesting that T1 mapping has better sensitivity for subtle ventricular changes. To summarize, native T1 mapping helps differentiate patients with overt ARVC and at-risk relatives from control subjects, and it may have the potential to detect early ARVC. However, it remains important to emphasize that these results are obtained in a small group of patients which resulted in a limited statistical power to study the incremental diagnostic value of T1 mapping over 2010 TFC⁷. Future studies should also assess T1 mapping as a prognostic marker and analyze the incremental value over the current ARVC risk calculator.

Machine learning

CMR analysis is a laborious task with large inter-reader variability, not only because of the qualitative analysis of wall motion and LGE, but also due to the manual segmentation of the ventricles to calculate quantitative ejection fraction and volume parameters. Large intra- and inter-observer variability is currently the greatest source of error when manually segmenting the RV on CMRs¹³. The purpose of **chapter 8** was to apply a deep learning segmentation approach for ventricular CMR assessment and evaluate the clinical implication of this approach for classification of the CMR TFC in subjects suspected of ARVC. CMR TFC classification using our automatic segmentation approach was comparable to classification using manual segmentation (226/227 patients had a comparable classification) if the most basal slice in each volume would be manually checked and corrected. Large variability between manual readers appears to happen in the basal slice due to the complex shape of the RV and the unclear ventricular-atrial transition of especially the RV¹⁴. Current state-of-the-art deep learning segmentation models can already reduce manual effort by semi-

automatically segmenting cardiac structures in a complex dataset, reducing segmentation time from 25 minutes to approximately 2 minutes^{15,16}. Such a semi-automatic approach could also reduce the inter-observer variability. This is not only interesting for specialized tertiary ARVC centers, but even more for less experienced centers, since CMR misinterpretations are an important cause of over-diagnosis in ARVC. To further improve the performance of deep learning segmentation approaches, future work should exploit more anatomical information, such as valve landmarks and the apex and allowing for the application of 3D segmentation approaches. Although we automated the calculation of the dimensional and functional parameters, wall motion abnormalities are also part of the CMR TFC. Due to anatomical challenges of the RV, a fully automatic RV strain algorithm is not yet available. Future studies should focus on including automation of biventricular strain as well as providing an accurate automatic assessment of all three structural components (wall motion abnormalities, RVEF, and RV end-diastolic volume) of the CMR criteria of the 2010 TFC.

Part 3. Atrial involvement in ARVC

ARVC is predominantly characterized as a disease of the desmosomes. Despite the fact that desmosomes are also found in the atria, evidence for direct atrial involvement with ARVC remains limited.¹⁷ In a more recent study 5% of ARVC patients with atrial fibrillation had an ischemic stroke.¹⁸ Therefore, systematic screening of atrial fibrillation in ARVC is needed. The ability to characterize and predict atrial dysfunction in the pre-atrial fibrillation stage may offer an opportunity for stroke prevention, especially in this relatively young patient population. In **chapter 9** and **chapter 10** we investigated structural and functional involvement of the atria using CMR in ARVC patients without prior atrial arrhythmias or heart failure. In chapter 9 we learned that genotype influences atrial volume and the occurrence of atrial arrhythmias in ARVC. Interestingly, the occurrence of atrial arrhythmias was comparable in desmosomal pathogenic variant carriers and patients with no pathogenic variant identified, however desmosomal pathogenic variant carriers had significantly smaller atria suggesting another underlying arrhythmogenic mechanism. In chapter 10 we showed that compared with age, sex, and body size-matched healthy controls ARVC patients had enlarged atria at all stages of the cardiac cycle, as well as poorly contractile atria with reduced right atrial conduit function, reduced right and left atrial reservoir function, as well as reduced right atrial and left atrial pump function as measured by FT-CMR. During follow-up 21% of the patients developed atrial arrhythmias. Right atrial and left atrial parameters were able to predict atrial arrhythmias after adjusting for ventricular and clinical characteristics, which suggests there is primary atrial involvement in ARVC. Detecting early atrial remodelling in ARVC may offer an opportunity to prevent atrial arrhythmia-related morbidity and mortality by the timely start of a direct oral anticoagulant (when indicated according to the guidelines for the treatment of atrial fibrillation) and rate or rhythm control to prevent tachycardiomyopathy. ARVC patients with atrial arrhythmias are associated with increased risk of inappropriate ICD shocks (26%). Beyond doubt, ICD implantation is of great benefit for selected ARVC

patients in the prevention of sudden cardiac death. However, strategic programming of arrhythmia detection criteria and ICD interventions is necessary to reduce the number of inappropriate interventions. Atrial arrhythmias in ARVC patients were associated with life threatening ventricular arrhythmias. Therefore, future studies should study atrial parameters as a prognostic marker in ARVC. Although no significant difference was seen between atrial arrhythmias occurrence in patients with and without an ICD, the presence of an ICD could have influenced results since ICDs with continuous rhythm registration increase the chance of registering arrhythmias. The underlying mechanism for atrial arrhythmias in ARVC still remains unclear and is yet to be studied. It could be a direct consequence of the underlying desmosomal dysfunction, leading to a primary atrial myocardial substrate. However, this could also be a secondary consequence of RV or LV dysfunction, leading to atrial overload, increased stress and formation of fibrosis in the atrial walls¹⁹.

Part 4. Combining CMR and genetics to unravel genotype phenotype correlations

In this part we focused on the contribution of rare and common variants on RV and LV function and dimension in individuals from the general population. We leveraged data from the UK Biobank, the largest European population-based cohort.

In **chapter 11** we identified individuals who carried a pathogenic variant associated with one of the inherited cardiomyopathies from the UK Biobank cohort of 200,643 individuals who underwent whole exome sequencing (WES). WES is a genomic technique for the sequencing of the protein-coding regions of the genome (exome). We identified a prevalence of 1:578, 1:251, and 1:149 for pathogenic and likely pathogenic variants associated with ARVC, DCM and HCM respectively. Cardiomyopathy, heart failure and ventricular arrhythmia diagnosis were more common among pathogenic and likely pathogenic variant carriers compared to pathogenic variant negative subjects in the general population. In total, 1.2%, 3.1% and 2.6% of ARVC, DCM and HCM pathogenic variant carriers respectively were diagnosed with a cardiomyopathy or heart failure (without previous chronic ischemic heart disease). Only 3.2%, 1.8% and 0.5% of the undiagnosed ARVC, DCM and HCM pathogenic variant carriers, reported ventricular arrhythmias or had CMR abnormalities. Undiagnosed DCM pathogenic variant carriers had lower LVEF ($p=0.009$) and less negative LV peak longitudinal strain ($p=0.009$). These differences were not present in undiagnosed ARVC or HCM pathogenic variant carriers. Unfortunately, no RV strain data was available. These results confirm the low disease penetrance in pathogenic variant carriers in the general population. Interestingly, disease penetrance in asymptomatic relatives carrying a pathogenic variant is known to be much higher: 37% in ARVC relatives²⁰ and up to 50% in HCM relatives²¹ (these numbers are not available for DCM). This discrepancy between the disease penetrance of pathogenic variant carriers in the general population versus relatives is remarkable. Although the reason behind this discrepancy is unknown, growing evidence suggests that ARVC penetrance may depend upon both (secondary) genetic as well as environmental

factors to reach a threshold for disease expression²². For example, in ARVC, endurance exercise is known to increase disease penetrance²³. The understanding of this discrepancy in disease penetrance and disease expression in the general population has become an even more important topic since The American College of Medical Genetics and Genomics (ACMG) has developed recommendations for the reporting of incidental or secondary findings unrelated to the test indication²⁴. More research on the effect of environmental and secondary genetic factors on disease expression in pathogenic variant carriers could aid in personalizing cascade screening and the frequency of cardiological examinations in these subjects. Furthermore, future studies should include RV strain and T1 mapping data, to understand the RV wall motion and fibrosis pattern in asymptomatic ARVC pathogenic variant carriers from the general population.

To identify genomic variants associated with RV and LV structural and functional measurements as measured on CMR, we performed a genome-wide association study (GWAS) in **chapter 12**. Identification of these genomic variants is a step closer to understanding the variable disease expression and disease penetrance in ARVC patients. In total, 87 genetic variants associated with one or more CMR measurements were identified. We prioritized 51 genes that likely drive the discovered genetic association, 25 of which affected multiple CMR measurements, and with 12 affecting both LV and RV measurements, suggesting similar genetic burden between LV and RV measurements. A next step would be to analyze if ARVC subjects carrying these genomic variants more often show heart failure or ventricular arrhythmias using a polygenic risk score combined with clinical parameters. Furthermore, we aimed to identify potential drug targets for RV and LV dysfunction using our GWAS results together with data from three independent plasma proteome GWAS. Using mendelian randomization, a statistical method that uses genetic variants to assess the presence of a causal relationship between a risk factor and the outcome, we identified proteins with a likely causal effect on biventricular traits. Linkage with drug-discovery databases was performed to assess if identified proteins were druggable. We identified 8 druggable proteins and 11 druggable proteins associated with cardiac outcomes. For example, higher plasma concentrations of BAG3 affected multiple CMR traits, heart failure as well as dilated and non-ischemic cardiomyopathy risk. BAG3 is indirectly druggable through a direct protein interaction with HSP7C (heat shock cognate 71 kDa protein), where compounds for HSP7C have been documented to affect cardiac function and calcium handling²⁵. Although these results are promising findings in the quest to find pharmaceutical therapies to reduce disease progression or improve outcome, they need to be validated and only serve as a resource to inform future drug trials.

FUTURE IMPLICATIONS

The power of the different aspects discussed in this thesis, including advanced CMR (FT-CMR, T1 mapping and machine learning) and genetics (GWAS and WES), lies in the combination of these aspects to enhance personalized medicine in ARVC patients and their relatives. Future studies should focus on the development of a multimodality risk score including advanced genetic data, CMR imaging and other clinical parameters to predict ventricular arrhythmias and heart failure in ARVC patients and family members. This risk score could also be a helpful guide in defining follow-up frequency and disease management. With machine learning being an ever moving field and likely to fundamentally change clinical practice in the future²⁶, new studies should focus on optimizing our machine learning algorithm to automatize all CMR post-processing steps described in this thesis and to automatize the extraction of diagnostic and prognostic information. This will be time saving and lead to less inter-observer and intra-observer variability. For a successful implementation of machine learning and multimodality risk scores, inter- and intra-modality differences should be taken into account. Lastly, by combining CMR and genetic information we have learned about (common and rare) genetic variants influencing cardiac function and structure. This valuable information has the potential to aid in the pursuit to find new treatments for ARVC.

REFERENCES

- Maret E, Todt T, Brudin L, Nylander E, Swahn E, Ohlsson JL, et al. Functional measurements based on feature tracking of cine magnetic resonance images identify left ventricular segments with myocardial scar. *Cardiovasc Ultrasound* 2009;7:53. doi:10.1186/1476-7120-7-53.
- Bomma C, Dalal D, Tandri H, Prakasa K, Nasir K, Roguin A, et al. Regional differences in systolic and diastolic function in arrhythmogenic right ventricular dysplasia/cardiomyopathy using magnetic resonance imaging. *Am J Cardiol* 2005;95:1507–1511. doi:10.1016/j.amjcard.2005.02.026.
- Nagata Y, Takeuchi M, Mizukoshi K, Wu VC-C, Lin F-C, Negishi K, et al. Intervendor variability of two-dimensional strain using vendor-specific and vendor-independent software. *J Am Soc Echocardiogr* 2015;28:630–641. doi:10.1016/j.echo.2015.01.021.
- Steensma BR, Voogt IJ, Leiner T, Lijten PR, Habets J, Klomp DWJ, et al. An 8-channel Tx/Rx dipole array combined with 16 Rx loops for high-resolution functional cardiac imaging at 7 T. *MAGMA* 2018;31:7–18. doi:10.1007/s10334-017-0665-5.
- Amzulescu MS, De Craene M, Langet H, Pasquet A, Vancraeynest D, Pouleur AC, et al. Myocardial strain imaging: review of general principles, validation, and sources of discrepancies. *Eur Hear Journal Cardiovasc Imaging* 2019;20:605–619. doi:10.1093/ehjci/jez041.
- te Riele ASJM, Bhonsale A, James CA, Rastegar N, Murray B, Burt JR, et al. Incremental value of cardiac magnetic resonance imaging in arrhythmic risk stratification of arrhythmogenic right ventricular dysplasia/cardiomyopathy-associated desmosomal mutation carriers. *J Am Coll Cardiol* 2013;62:1761–1769. doi:10.1016/j.jacc.2012.11.087.
- Marcus FI, McKenna WJ, Sherrill D, Basso C, Baucé B, Bluemke DA, et al. Diagnosis of arrhythmogenic right ventricular cardiomyopathy/dysplasia: proposed modification of the task force criteria. *Circulation* 2010;121:1533–1541. doi:10.1161/CIRCULATIONAHA.108.840827.
- Bomma C, Rutberg J, Tandri H, Nasir K, Roguin A, Tichnell C, et al. Misdiagnosis of arrhythmogenic right ventricular dysplasia/cardiomyopathy. *J Cardiovasc Electrophysiol* 2004;15:300–306. doi:10.1046/j.1540-8167.2004.03429.x.
- Vigneault DM, te Riele ASJM, James CA, Zimmerman SL, Selwaness M, Murray B, et al. Right ventricular strain by MR quantitatively identifies regional dysfunction in patients with arrhythmogenic right ventricular cardiomyopathy. *J Magn Reson Imaging* 2016;43:1132–1139. doi:10.1002/jmri.25068.
- Cadrin-Tourigny J, Bosman LP, Nozza A, Wang W, Tadros R, Bhonsale A, et al. A new prediction model for ventricular arrhythmias in arrhythmogenic right ventricular cardiomyopathy. *Eur Heart J* 2019;40. doi:10.1093/eurheartj/ehz103.
- Taha K, Mast TP, Cramer MJ, van der Heijden JF, Asselbergs FW, Doevendans PA, et al. Evaluation of Disease Progression in Arrhythmogenic Cardiomyopathy: The Change of Echocardiographic Deformation Characteristics Over Time. *JACC Cardiovasc Imaging* 2020;13:631–634. doi:10.1016/j.jcmg.2019.08.014.
- Te Riele ASJM, James CA, Philips B, Rastegar N, Bhonsale A, Groeneweg JA, et al. Mutation-positive arrhythmogenic right ventricular dysplasia/cardiomyopathy: the triangle of dysplasia displaced. *J Cardiovasc Electrophysiol* 2013;24:1311–1320. doi:10.1111/jce.12222.
- Bonnemains L, Mandry D, Marie P-Y, Micard E, Chen B, Vuissoz P-A. Assessment of right ventricle volumes and function by cardiac MRI: quantification of the regional and global interobserver variability. *Magn Reson Med* 2012;67:1740–1746. doi:10.1002/mrm.23143.
- Fadil H, Totman JJ, Hausenloy DJ, Ho H-H, Joseph P, Low AF-H, et al. A deep learning pipeline for automatic analysis of multi-scan cardiovascular magnetic resonance. *J Cardiovasc Magn Reson Off J Soc Cardiovasc Magn Reson* 2021;23:47. doi:10.1186/s12968-020-00695-z.
- Bai W, Sinclair M, Tarroni G, Oktay O, Rajchl M, Vaillant G, et al. Automated cardiovascular magnetic resonance image analysis with fully convolutional networks. *J Cardiovasc Magn Reson* 2018;20:65. doi:10.1186/s12968-018-0471-x.
- Corona-Villalobos CP, Kamel IR, Rastegar N, Damico R, Kolb TM, Boyce DM, et al. Bidimensional measurements of right ventricular function for prediction of survival in patients with pulmonary hypertension: comparison of reproducibility and time of analysis with volumetric cardiac magnetic resonance imaging analysis. *Pulm Circ* 2015;5:527–537. doi:10.1086/682229.
- Basso C, Fox PR, Meurs KM, Towbin JA, Spier AW, Calabrese F, et al. Arrhythmogenic right ventricular cardiomyopathy causing sudden cardiac death in boxer dogs: a new animal model of human disease. *Circulation* 2004;109:1180–1185. doi:10.1161/01.CIR.0000118494.07530.65.
- Baturova MA, Haugaa KH, Jensen HK, Svensson A, Gilljam T, Bundgaard H, et al. Atrial fibrillation as a clinical characteristic of arrhythmogenic right ventricular cardiomyopathy: Experience from the Nordic ARVC Registry.

- Int J Cardiol 2020;298:39–43. doi:10.1016/j.ijcard.2019.07.086.
19. Wu L, Guo J, Zheng L, Chen G, Ding L, Qiao Y, et al. Atrial remodeling and atrial tachyarrhythmias in arrhythmogenic right ventricular cardiomyopathy. *Am J Cardiol* 2016;118:750–753. doi:10.1016/j.amjcard.2016.06.003.
 20. Groeneweg JA, Bhonsale A, James CA, te Riele AS, Dooijes D, Tichnell C, et al. Clinical Presentation, Long-Term Follow-Up, and Outcomes of 1001 Arrhythmogenic Right Ventricular Dysplasia/Cardiomyopathy Patients and Family Members. *Circ Cardiovasc Genet* 2015;8:437–446. doi:10.1161/CIRCGENETICS.114.001003.
 21. van Velzen HG, Schinkel AFL, Baart SJ, Oldenburg RA, Frohn-Mulder IME, van Slegtenhorst MA, et al. Outcomes of Contemporary Family Screening in Hypertrophic Cardiomyopathy. *Circ Genomic Precis Med* 2018;11:e001896. doi:10.1161/CIRCGEN.117.001896.
 22. van Lint FHM, Murray B, Tichnell C, Zwart R, Amat N, Lekanne Deprez RH, et al. Arrhythmogenic Right Ventricular Cardiomyopathy-Associated Desmosomal Variants Are Rarely De Novo. *Circ Genomic Precis Med* 2019;12:e002467. doi:10.1161/CIRCGEN.119.002467.
 23. James CA, Bhonsale A, Tichnell C, Murray B, Russell SD, Tandri H, et al. Exercise increases age-related penetrance and arrhythmic risk in arrhythmogenic right ventricular dysplasia/cardiomyopathy-associated desmosomal mutation carriers. *J Am Coll Cardiol* 2013;62:1290–1297. doi:10.1016/j.jacc.2013.06.033.
 24. Miller DT, Lee K, Chung WK, Gordon AS, Herman GE, Klein TE, et al. ACMG SF v3.0 list for reporting of secondary findings in clinical exome and genome sequencing: a policy statement of the American College of Medical Genetics and Genomics (ACMG). *Genet Med* 2021;23:1381–1390. doi:10.1038/s41436-021-01172-3.
 25. Kim Y-K, Suarez J, Hu Y, McDonough PM, Boer C, Dix DJ, et al. Deletion of the inducible 70-kDa heat shock protein genes in mice impairs cardiac contractile function and calcium handling associated with hypertrophy. *Circulation* 2006;113:2589–2597. doi:10.1161/CIRCULATIONAHA.105.598409.
 26. Leiner T, Rueckert D, Suinesiaputra A, Baeßler B, Nezafat R, I'gum I, et al. Machine learning in cardiovascular magnetic resonance: basic concepts and applications. *J Cardiovasc Magn Reson* 2019;21:61. doi:10.1186/s12968-019-0575-y.

APPENDIX

Nederlandstalige samenvatting
List of publications
Acknowledgements/Dankwoord
Curriculum Vitae

NEDERLANDSTALIGE SAMENVATTING

In Nederland overlijden er jaarlijks gemiddeld 16.000 mensen als gevolg van een plotse hartstilstand. Een plotse hartstilstand maakt veel indruk op de samenleving, vooral als het zich voordoet bij voorheen gezonde jonge mensen en atleten. Een plotse hartstilstand door ventriculaire ritmestoornissen zien we vaker in families waarin een erfelijke hartspierziekte voorkomt. Daarom is het achterhalen van een mogelijk genetische onderliggende oorzaak belangrijk. Niet alleen voor de risicostratificatie van de individuele patiënt, maar ook voor vroeg-diagnostiek en risicostratificatie van niet-aangedane familieleden die het risico lopen hetzelfde lot te ondergaan.

Erfelijke hartspierziekten zijn te classificeren in gedilateerde cardiomyopathie (DCM), hypertrofe cardiomyopathie (HCM) en aritmogene cardiomyopathie, ook wel bekend als aritmogene rechter ventrikel cardiomyopathie (ARVC). Vergeleken met andere cardiomyopathieën treden bij ARVC al in een vroege fase van de ziekte ritmestoornissen op, zonder dat er vooraf sprake was van andere symptomen of structurele afwijkingen aan het hart. In 10 tot 50% van de aangedane patiënten kan plotse hartdood het eerste 'symptoom' zijn.

ARVC komt voor bij 1 op de 5.000 mensen en presenteert zich meestal tussen het 20^e en 50^e levensjaar. Kenmerkend zijn de pathologische structurele (fibroadipeuze infiltratie) en elektrische (gap junction remodelering en natriumkanal dysfunctie) veranderingen, welke al in een vroeg stadium aanwezig zijn. Deze kunnen zich klinisch uiten in lethale ventriculaire aritmieën en vermindering van de pompfunctie. Doordat de rechter ventrikel (rechter kamer) dunwandig is, is deze vaak eerder betrokken dan de linker ventrikel in ARVC. In de afgelopen jaren zijn er verschillende ziekte veroorzakende DNA-mutaties ontdekt. Daarom worden familieleden, indien gewenst, genetisch gescreend op dragerschap van deze DNA-mutatie ondanks dat zij nog geen symptomen ervaren. We weten namelijk dat zo'n 30% van de mensen met zo'n ziekte veroorzakende DNA-mutatie uiteindelijk zelf ook ARVC ontwikkeld. Deze wetenschap kan veel onzekerheid met zich meebrengen. Daarom is het belangrijk om al in een vroeg stadium de familieleden met een hoog risico op ziekteontwikkeling op te sporen, zodat er tijdig een behandeling kan plaatsvinden. Na het diagnosticeren van ARVC, is het belangrijkste doel, het voorkomen van plotse hartdood. Dit kan middels een implanteerbare cardioverter-defibrillator (ICD). Tevens wordt ARVC patiënten afgeraden om te sporten, gezien dit de ziekte progressie kan versnellen. Daarnaast is het ook belangrijk om familieleden zonder enige tekenen van ziekte gerust te kunnen stellen. Cardiale magnetische resonantie (CMR) beeldvorming is de gouden standaard voor het bepalen van morfologische, structurele, en functionele veranderingen in ARVC. Echter in de kliniek worden CMR veranderingen voornamelijk kwalitatief (visueel) beoordeeld. Nieuwe en veelbelovende kwantitatieve CMR methoden

kunnen een belangrijke rol spelen bij het ontmaskeren van vroege uitingen van structurele en/of elektrische veranderingen.

De belangrijkste CMR (nabewerkings-) technieken hierbij zijn 1) *Feature Tracking CMR* (FT-CMR) voor het kwantificeren van vroege wandbewegingsstoornissen die het gevolg kunnen zijn van elektrische en structurele veranderingen bij ARVC; 2) *T1-mapping* voor de kwantificatie van fibrosering (verlittekening) die het gevolg zijn van structurele verandering bij ARVC en; 3) *Machine Learning* voor het automatiseren van de segmentaties om de functie en volumina op CMR te kunnen berekenen. Dit wordt momenteel nog manueel uitgevoerd door artsen of laboranten. Om deze CMR technieken van 'bench to bedside' te brengen is het van belang om te onderzoeken hoe we de absolute waarden van deze techniek moeten interpreteren. In welke mate worden bijvoorbeeld de absolute waarden die we uit FT-CMR krijgen (strain waarden) beïnvloed door de software waarmee we meten en de scanner types die we gebruiken. Daarnaast willen we weten wat de diagnostische en prognostische waarde van deze techniek is. Ideale diagnostische en prognostische CMR markers kunnen subtiele ziekte veroorzakende veranderingen al oppikken, zelfs zonder dat deze visueel zichtbaar zijn. Wij onderzoeken dit meestal in patiënten en hun familieleden die een ziekenhuis bezoeken. We weten echter dat mensen in de algemene populatie ook drager kunnen zijn van ziekte veroorzakende DNA mutaties zonder dat zij hiervan op de hoogte zijn. Wij onderzochten hoeveel mensen in de algemene populatie drager zijn van deze DNA mutaties en in welke mate er al structurele of functionele afwijkingen bij hen aanwezig waren. Tevens is het belangrijk om te begrijpen in welke mate genetische variabiliteit in de algemene "gezonde" bevolking invloed heeft op de structuur en functie van het hart. Als we weten welke genetische variaties bijdragen aan de structuur en functie van het hart, kunnen we ook onderzoeken of variaties hierin kunnen bijdragen aan het eerder ontwikkelen van structurele of functionele afwijkingen bij ARVC patiënten.

Het doel van de thesis, zoals beschreven in **hoofdstuk 1**, is het verbeteren van de diagnostiek en risico-stratificatie van patiënten met aritmogene cardiomyopathie en hun niet aangedane familieleden middels nieuwe geavanceerde CMR-technieken. Deze thesis omvat vier delen, die zich focussen op de onderstaande onderzoeksvragen:

1. Wat is de reproduceerbaarheid, variabiliteit en toepasbaarheid van FT-CMR in de kliniek?
2. Wat is de klinische waarde van FT-CMR, T1 mapping en machine learning voor ARVC?
3. Is er sprake van atriale betrokkenheid in ARVC?
4. Wat is de bijdrage van zeldzame en meer voorkomende genetische varianten op rechter en linker ventrikel functie in de algemene populatie?

In dit hoofdstuk zal ik de belangrijkste bevindingen van mijn proefschrift samenvatten voor lezers zonder enige voorkennis van het onderwerp. Voor meer details verwijst ik naar **hoofdstuk 13** van dit proefschrift.

Het proefschrift begint met een Engelstalige inleiding in **hoofdstuk 1**. Een ander inleidend hoofdstuk is **hoofdstuk 2** waarin de huidige uitdagingen in het diagnosticeren van ARVC worden besproken.

Deel 1. Haalbaarheid en reproduceerbaarheid van nieuwe CMR-technieken in ARVC

FT-CMR is een populaire techniek voor het kwantificeren van de regionale myocardiale functie uitgedrukt in *strain*. Wandbewegingsstoornissen zijn een belangrijk diagnostisch criterium bij ARVC. In de huidige praktijk worden deze wandbewegingsstoornissen visueel beoordeeld. Dit gaat gepaard met interpretatieverschillen tussen verschillende beoordelaars. Tevens kunnen subtiele wandbewegingsstoornissen gemist worden. Recent onderzoek laat zien dat deze kwantitatieve strain analyses een hogere sensitiviteit en nauwkeurigheid hebben dan de huidige praktijk waarin visuele kwalitatieve beoordeling van de wandbeweging door CMR experts wordt gedaan. Deze kwantitatieve beoordeling maakt het waarschijnlijk mogelijk om subtiele afwijkingen in de wandbeweging al in een vroeg stadium op te sporen. Echter voordat we deze techniek in de klinische praktijk kunnen toepassen, moet de techniek betrouwbaar genoeg zijn. De haalbaarheid van de techniek moet onderzocht worden. Tevens moet er bekeken worden welke factoren de strain waarden kunnen beïnvloeden. Daarom is er in dit deel van de thesis gefocust op de volgende onderzoeksvraag:

“Wat is de reproduceerbaarheid, variabiliteit en toepasbaarheid van FT-CMR in de klinische setting?”

FT-CMR strain waarden kunnen berekend worden middels verschillende commerciële software methoden. We weten echter weinig over de invloed van verschillende software op de absolute strain waarden. Daarom onderzochten we in **hoofdstuk 3** onder meer in welke mate rechter ventrikel strain waarden overeenkomen tussen de vier meest gebruikte commercieel beschikbare software methoden. Daarnaast onderzochten we de reproduceerbaarheid van de rechter ventrikel strain waarden gemeten met de vier verschillende software methoden. In deze studie laten we zien dat de absolute rechter ventrikel strain waarden slecht correleren tussen de verschillende software methoden. Door deze verschillen kunnen de strain waarden van verschillende software methoden niet door elkaar gebruikt worden gedurende de follow-up van een patiënt. Daarbij bestaat er ook een verschil in kwaliteit van de *tracking* van de endocardiale wand tussen de verschillende methoden waarmee rekening gehouden dient te worden. Interessant genoeg laten alle vier de software methoden wel dezelfde trend zien tussen ziek en niet-ziek, waarbij ARVC

patiënten significant lagere strain waarden vertonen ten opzichte van controles. Dit laat zien dat alhoewel de absolute strain waarden niet vergelijkbaar zijn tussen de verschillende software methodes, de verschillen op groepsniveau wel vergelijkbaar zijn. Verder zien we dat de reproduceerbaarheid van de strain waarden voor alle software methoden tussen gemiddeld en excellent zit wat laat zien dat de FT-CMR methode robuust is.

Binnen en tussen centra wordt er ook gebruik gemaakt van verschillende CMR instellingen. We weten echter weinig over de invloed hiervan op de absolute strain waarden. Voor de interpretatie van strain waarden in de kliniek is dit echter wel belangrijk. Daarom onderzochten we in **hoofdstuk 4** de invloed van verschillende CMR instellingen, zoals veldsterkte, resolutie en sequentie op absolute rechter ventrikel strain waarden. Voor globale rechter ventrikel strain was er een goede overeenkomst tussen de strain waarden bij gebruik van verschillende klinische veldsterkten (1.5T en 3T) en imaging resoluties. Echter voor de regionale rechter ventrikel strain was er een matig tot slechter overeenkomst. Dit laat zien dat in de follow-up van een patiënt regionale strain waarden niet vergeleken kunnen worden indien er gebruik is gemaakt van een andere veldsterkte of resolutie. Daarnaast zullen er voor de verschillende veldsterktes en resoluties aparte normaalwaarden gebruikt moeten worden. Dit is vooral belangrijk in ARVC waar de vroege afwijkingen in de wandbeweging vaak regionaal (met name in de subtricipitale regio, zie deel 2) beginnen. Tevens hebben we in deze studie gebruik gemaakt van de veldsterkte 7T. Alhoewel deze veldsterkte nog niet gebruikt wordt in de klinische praktijk, heeft het de potentie om subtiele afwijkingen in de wandbeweging nog eerder te kunnen detecteren door de hogere spatiale resolutie. In deze studie laten we zien dat strain waarden gemeten op 7T niet vergelijkbaar zijn met de conventionele 1.5T en 3T. Daardoor dienen er ook voor 7T specifieke normaalwaarden onderzocht te worden.

Er is niet alleen weinig bekend over de invloed van intra-modaliteit verschillen op strain waarden, maar ook over de invloed van inter-modaliteit verschillen op strain waarden. In ARVC wordt er voornamelijk voor de follow-up, naast CMR, ook veel gebruik gemaakt van echocardiografie. Doordat deze modaliteit makkelijker beschikbaar is, is het een ideale modaliteit voor de follow-up van ARVC patiënten. Het is nog onduidelijk of de strain waarden gemeten middels CMR en echocardiografie door elkaar gebruikt kunnen worden voor bijvoorbeeld follow-up. Daarom vergeleken we in **hoofdstuk 5** de rechter ventrikel strain waarden zoals gemeten middels FT-CMR en echocardiografie. Deze studie laat zien dat beide modaliteiten een vergelijkbare trend tussen ziek en niet-ziek laten zien. Echter de absolute strain waarden zijn niet vergelijkbaar tussen de beide modaliteiten. Dit is een belangrijk resultaat, want het laat zien dat voor het kwantitatief beoordelen van de wandbeweging deze beide technieken niet afgewisseld mogen worden gedurende de follow-up.

Deel 2. Klinische waarde van nieuwe CMR technieken in ARVC

Een belangrijk deel van de CMR evaluaties wordt visueel gedaan door de radioloog. Deze kwalitatieve manier van evalueren is daardoor onderhevig aan variatie tussen beoordelaars. Tevens kunnen hierdoor subtiele veranderingen die niet met het oog altijd even goed te zien zijn gemist worden. Een belangrijk deel van de foutief gestelde ARVC diagnoses, wordt veroorzaakt door CMR misinterpretaties. In dit deel focussen we ons op de klinische waarde van nieuwe CMR technieken die het mogelijk maken om de subjectieve beoordelingen meer te objectiveren en minder afhankelijk te maken van de beoordelaar. We onderzochten daarbij de volgende onderzoeksvraag:

“Wat is de klinische waarde van FT-CMR, T1 mapping en machine learning voor ARVC?”

Feature Tracking CMR

Nu we na deel 1 meer weten over hoe we absolute strain waarden gemeten middels FT-CMR dienen te interpreteren, bestuderen we in deel 2 de klinische toepasbaarheid van FT-CMR. In **hoofdstuk 2** hebben we naast de software vergelijkingen, ook de diagnostische waarde van FT-CMR onderzocht. Hiervoor includeerden we controles zonder ARVC, ARVC patiënten en mutatie positieve familieleden zonder ziekte-expressie. Vooral deze laatste groep is interessant voor vroegdiagnostiek. Zij hebben (nog) geen ARVC diagnose, echter lopen hierop wel het risico gezien zij drager zijn van een ziekte veroorzakende mutatie. Deze groep wil je tijdig kunnen diagnosticeren voordat er ernstige ritmestoornissen optreden, en wil je gerust kunnen stellen indien er geen enkele tekenen van ziekte expressie aanwezig zijn. In deze studie laten we zien dat de globale strain waarden in gediagnosticeerde ARVC patiënten lager zijn vergeleken met controles. Globale strain waarden waren echter vergelijkbaar tussen niet zieke familieleden en controles. Interessant genoeg, zagen we wel dat de regionale strain, in het bijzonder de strain in de subtricuspidale regio, significant lager was in deze familieleden ten opzichte van de controlegroep. Dit resultaat is hoopgevend, gezien subtricuspidale strain in een eerder studie al heeft laten zien een onafhankelijke predictor voor ARVC diagnose te zijn, wanneer je controleert voor sekse, rechter ventrikel functie en dimensies in multivariabele analyse. Dit suggereert dat subtricuspidale strain een toegevoegde waarde heeft bovenop de bestaande parameter voor systolische functie, de rechter ventrikel ejectie fractie. Nadat we de potentiële diagnostische waarde van FT-CMR in ARVC hebben laten zien, bestudeerden we in **hoofdstuk 6** de prognostische waarde van FT-CMR in ARVC. We onderzochten of rechter- en/of linker ventrikel globale en regionale strain van toegevoegde waarde zijn boven bestaande CMR parameters in het voorspellen van ventriculaire ritmestoornissen in een cohort van gediagnosticeerde ARVC patiënten die niet eerder een ventriculaire ritmestoornis doormaakten. In onze studie laten we inderdaad zien dat de globale en regionale strain verminderd is in patiënten die gedurende follow-up een ventriculaire ritmestoornis zullen ontwikkelen ten opzichte van de patiënten die dit

niet ontwikkelen. Echter lijkt het gebruik maken van strain geen toegevoegde waarde te hebben boven ejectie fractie, een parameter die we momenteel al in de kliniek gebruiken. Alhoewel er dus wel een diagnostische waarde blijkt voor het gebruik van FT-CMR in ARVC patiënten, zien we geen prognostische waarde in gediagnosticeerde ARVC patiënten. Dit zal deels komen doordat de gediagnosticeerde ARVC patiënten vaak al een aangedane rechter ventrikel ejectie fractie hadden. Toekomstige studies zullen moeten kijken naar de prognostische waarde van deze techniek in familieleden zonder ziektepresentatie.

T1 mapping

In **hoofdstuk 7** onderzochten we de diagnostische waarde van T1 mapping in ARVC. T1 mapping is een techniek die het mogelijk maakt om de T1 relaxatietijd op voxel niveau te kwantificeren. De berekende T1 relaxatie geeft informatie over het weefseltype, zo heeft vet een lage T1 relaxatietijd en fibrose een hogere T1 relaxatietijd. Deze manier maakt het mogelijk om fibrose nauwkeurig te kwantificeren. Middels T1 mapping is het technisch alleen mogelijk om de linker ventrikel te beoordelen, gezien de rechter ventrikel hiervoor een te dunne wand heeft. In de huidige praktijk wordt late gadolinium enhancement gebruikt voor fibrose detectie. Hierbij wordt er middels contrastvloeistof gekeken in welke gebieden het contrast minder snel “uitgewassen” wordt. Dit zijn hoogstwaarschijnlijk gebieden met fibrose. Dit wordt meestal visueel beoordeeld en is dus onderhevig aan verschillen tussen beoordelaars. Daarnaast kan late gadolinium enhancement geen diffuse en subtiele fibrose detecteren, terwijl er bij ARVC juist sprake is van diffuse fibrose en er in een vroeg stadium juist sprake is van subtiele fibrose. In hoofdstuk 8 includeerden we ARVC patiënten, familieleden die drager zijn van een ziekte-veroorzakende mutatie, maar nog geen ziekte expressie vertonen en een groep controle patiënten zonder ARVC. We leerden dat T1 tijden en de spreiding van T1 tijden (T1 dispersion) hoger was bij ARVC patiënten vergeleken met controles. Tevens zagen we dat de familieleden een grotere T1 dispersion vertoonden in vergelijking met controles. Deze verhoogde spreiding werd voornamelijk veroorzaakt door hogere T1 tijden in de posterolaterale regio in zowel de ARVC patiënten als de familieleden. Dit resultaat ondersteunt de eerder beschreven hypothese ‘Displaced Triangle of dysplasie’ waarbij gedacht wordt dat de eerste ziektemanifestatie in de linker ventrikel optreedt in de posterolaterale wand. Een volgende stap zou zijn te onderzoeken wat de toegevoegde waarde is om T1 mapping aan de diagnostische criteria voor ARVC toe te voegen. Tevens dient de prognostische waarde van deze techniek nog onderzocht te worden.

Machine learning

Als laatste onderzochten we de klinische waarde van automatische segmentatie (intekening van de ventrikels om zo de functie en volumina te kunnen berekenen) van de linker en rechter ventrikel in ARVC. CMR segmentaties worden in de huidige klinische praktijk manueel uitgevoerd door een arts of een laborant opgeleid voor cardiale beeldbewerking. Dit is een arbeidsintensieve taak waarbij er ook sprake is van grote verschillen tussen

artsen/laboranten onderling, in het bijzonder voor de rechter ventrikel. De rechter ventrikel is gezien de ligging en dunne wand lastiger te segmenteren, voornamelijk bij ARVC waarbij de rechter ventrikel wand nog dunner is, en er ook sprake kan zijn van aneurysmata die de intekening bemoeilijken. In **hoofdstuk 8** pasten we een deep learning segmentatie methode toe in een cohort met patiënten die verdacht waren voor ARVC. Een deel van deze patiënten bleek uiteindelijk ARVC te hebben, een deel waren dragers van een mutatie zonder ziekte uitingen en bij een ander deel was ARVC uitgesloten. Door de automatische segmentatie waren wij in staat om in een enkele seconde segmentaties van een grote groep patiënten uit te voeren en daaruit onder meer de ejectie fractie en de dimensies te berekenen. Ons deep learning algoritme maakte gebruik van manuele segmentaties uitgevoerd door CMR laboranten om te trainen. Hierin zagen wij dat er sprake was van een hoge variabiliteit van het basale segment. Dit wordt voornamelijk veroorzaakt door een onduidelijke overgang van de atria (boezems) naar ventrikels waarmee het deep learning model moeite had. Om de performance van het algoritme te verbeteren hebben wij de manuele segmentaties gebruikt voor de eerste basale slice. Ons model maakte het mogelijk om de segmentatietijd te verlagen van 25 minuten naar 2 minuten. De automatisch berekende ejectie fractie en dimensies werden gebruikt om de CMR criteria van de diagnostische criteria van ARVC te berekenen. De sensitiviteit en specificiteit door de automatisch gemeten methode was hierbij vergelijkbaar met de manueel segmentaties. Alhoewel er we in de toekomst streven naar een volledige automatisatie, waarin niet alleen de ejectie fractie en dimensies automatisch worden gesegmenteerd, maar ook de strain en T1 mapping waarden berekend zullen worden. Het ultieme doel daarbij is automatische berekening van de CMR criteria en een automatische inschatting van de prognose aan de hand van CMR. Echter ons huidige algoritme is al interessant voor klinisch gebruik, gezien het de analysetijd verminderd en tevens een objectieve manier is van segmenteren zonder variatie. Dit is niet alleen interessant voor tertiaire centra, maar juist ook voor de centra die niet gespecialiseerd zijn in ARVC, gezien CMR misinterpretaties een belangrijke oorzaak is voor over-diagnose in ARVC.

Deel 3. Atriale betrokkenheid in ARVC

In deel 3 van dit proefschrift focussen we ons op de betrokkenheid van de atria in ARVC. ARVC wordt voornamelijk gekenmerkt door betrokkenheid van de rechter ventrikel. We weten nu ook dat de linker ventrikel in meer of mindere mate betrokken kan zijn. Echter over de betrokkenheid van de atria in dit ziektebeeld is er nog weinig bekend. Gezien er bij het merendeel van de patiënten sprake is van een mutatie in de desmosomen ("klittenband" tussen de hartspiercellen) en deze ook aanwezig zijn in de atria, is het waarschijnlijk dat de atria ook een bepaalde mate van betrokkenheid vertonen. Daarom onderzochten we in dit deel de volgende vraag:

"Is er sprake van atriale betrokkenheid bij ARVC?"

In **hoofdstuk 9** en **hoofdstuk 10** onderzochten we middels CMR de structurele en functionele (middels FT-CMR) betrokkenheid van de atria in ARVC patiënten zonder hartfalen of atriale aritmieën (atriumfibrilleren of atriumflutter). In vergelijking met een controlegroep hebben ARVC patiënten vergrote atria en een verminderde atriale functie. Tevens ontwikkelde 21% van de ARVC patiënten atriale aritmieën gedurende de follow-up. Atriale functionele parameters zoals gemeten door FT-CMR bleken goede voorspellers te zijn voor het voorspellen van atriale aritmieën in ARVC patiënten, ook nadat we corrigeerden voor ventriculaire functie en andere klinische karakteristieken. Het in een vroeg stadium kunnen detecteren welke patiënten atriale aritmieën zullen ontwikkelen biedt een potentiële rol voor FT-CMR van de atria voor het verbeteren van de prognose van ARVC patiënten. Atriale aritmieën kunnen namelijk leiden tot herseninfarcten indien er niet tijdig met orale antistolling wordt begonnen. Tevens zijn atriale aritmieën geassocieerd met een verhoogd aantal onnodige ICD shocks. Dit biedt mogelijkheden om bij ARVC patiënten die ook ICD-drager zijn en die een verhoogd risico hebben op atriale aritmieën de ICD instellingen hierop aan te passen. Het onderliggende mechanisme voor het ontstaan van atriale aritmieën bij ARVC is nog onbekend. Het zou een secundaire oorzaak kunnen zijn doordat er sprake is van rechter- en linker ventrikel dysfunctie wat tot atriale overbelasting kan leiden, wat door de verhoogde druk voor fibrosering van de atriale wand kan zorgen. Deze fibrosering kan een substraat voor aritmieën worden. De atriale aritmieën kunnen echter ook een primair gevolg zijn van de onderliggende desmosomale mutatie. Toekomstige studies moeten nog uitmaken of atriale parameters van toegevoegde waarde zijn als prognostische marker bij ARVC.

Deel 4. Combinatie van CMR en genetica om genotype-fenotype correlaties te ontrafelen

In de zoektocht naar vroege ziekte markers om ARVC eerder te kunnen diagnosticeren en patiënten met een slechtere prognose eerder te kunnen identificeren hebben we in de vorige delen gebruik gemaakt van patiënten en familieleden die het ziekenhuis bezoeken. In dit deel van de thesis includeerden we juist mensen uit de algemene populatie. Het doel was het onderzoeken of er al tekenen van ziekte aanwezig zijn in asymptomatische dragers met een ziekte veroorzakende mutatie uit de algemene populatie. Daarnaast onderzochten we welke veel voorkomende genetische varianten bijdragen aan linker en rechter ventrikel functie en dimensies. De laatste onderzoeksvraag van deze thesis luidt daarom ook:

"Wat is de bijdrage van zeldzame en meer voorkomende genetische varianten op rechter en linker ventrikel functie in de algemene populatie?"

In **hoofdstuk 11** identificeerden we allereerst de prevalentie van ziekte veroorzakende mutaties geassocieerd met de erfelijke cardiomyopathieën. Hiervoor maakten we gebruik van *Whole Exome Sequencing* (WES). Dit is een genetische test waarbij alle genen in één

keer bekeken kunnen worden doordat het hele DNA wordt afgelezen. Een prevalentie van 1:578, 1:251 en 1:149 werd gevonden voor ARVC, DCM en HCM geassocieerde mutaties respectievelijk. Zoals verwacht, zagen dat deze mutatie dragers vaker gediagnosticeerd werden met een cardiomyopathie, hartfalen en ventriculaire aritmieën. Van de ongediagnosticeerde ARVC, DCM en HCM mutatiedragers, had respectievelijk 3.2%, 1.8% en 0.5% ventriculaire aritmieën of CMR abnormaliteiten. Deze resultaten bevestigen hiermee de lage ziekte penetrantie in dragers van een ziekte veroorzakende mutatie. In **hoofdstuk 12** voerden we een Genome Wide Association Study uit (GWAS), waarbij we verbanden zochten tussen genetische variaties (single nucleotide polymorphisms, SNPs) en CMR parameters voor functie en dimensie van de linker en rechter ventrikel. We vonden 87 genetische varianten die geassocieerd zijn met minimaal één CMR parameter. We zagen een overlap tussen genetische varianten die we vonden voor de linker en rechter ventrikel, wat laat zien dat er een belangrijke overlap is tussen de genetische variantie van de linker en rechter ventrikel. In welke mate een ziekte veroorzakende mutatie in een van deze genetische varianten bijdraagt aan ziekte en ziekteprogressie bij patiënten met ARVC, moet in de toekomst onderzocht worden. Door gebruik te maken van de reeds bekende associatie tussen de gevonden genetische associatie en plasma eiwitten, konden we ook plasma eiwitten identificeren die een belangrijke causale effect hebben op de linker en rechter ventrikel functie of dimensie. Hiervoor maakten we gebruik van de methode Mendeliaanse randomisatie. Deze methode gebruikt de gevonden genetische variatie als surrogaatmarker voor linker en rechter ventrikel functie en dimensies zoals gemeten op CMR. In totaal vonden we 33 plasma eiwitten, waarvan voor 25 van deze plasma eiwitten medicamenten bestaan die goedgekeurd dan wel in ontwikkeling zijn. Dit is een veelbelovend resultaat gezien het een eerste stap is in de toekomstige ontwikkeling van medicamenteuze therapie voor patiënten die vroeg gediagnosticeerd zijn om verdere functionele en structurele ziekteprogressie te voorkomen.

Concluderend

Het overkoepelend doel van deze thesis was het vinden van vroeg diagnostische en prognostische markers voor ARVC. Wij laten zien dat de nieuw ontwikkelde CMR technieken hiervoor hoopvolle resultaten laten zien. Een volgende stap is het onderzoeken van de toegevoegde waarde van deze technieken en de gevonden genetische varianten die bijdragen aan linker en rechter ventrikel functie en dimensie binnen huidige diagnostische en prognostische risicomodellen. Ik verwacht dat in de toekomst machine learning hierin een belangrijke rol gaat spelen, waarbij CMR analyses niet alleen geautomatiseerd zijn en er daarbij rekening gehouden is met technische verschillen tussen de verschillende CMR beelden, maar we door het aanvullen van klinische gegevens ook een indicatie kunnen geven over het risico op ziekteprogressie dan wel gevaarlijke ritmestoornissen.

List of publications

Schmidt A, Finan C, **Bourfiss M**, Velthuis B, Puyol-Antón E, Alasiri A, Ruijsink B, Asselbergs F, Ter Riele A, van Setten J. Cardiac MRI to guide heart failure and atrial fibrillation drug discovery: a Mendelian randomization analysis. *Res Sq [Preprint]*. 2023 Feb 2;rs.3.rs-2449265. doi: 10.21203/rs.3.rs-2449265/v1. PMID: 36778476; PMCID: PMC9915782

Bourfiss M*, van Vugt M*, Alasiri A, Ruijsink B, van Setten J, Amand F, Schmidt AF, Dooijes D, Puyol-Antón E, Velthuis BK, van Tintelen JP, te Riele ASJM, Baas AF, Asselbergs FW. Penetrance and disease expression of (likely) pathogenic variants associated with inherited cardiomyopathies in the general population. *Circ Genom Precis Med*. 2022 Dec;15(6):e003704. doi: 10.1161/CIRCGEN.122.003704

Bourfiss M*, Sander J*, de Vos BD, te Riele ASJM, Asselbergs FW, Išgum I, Velthuis BK. Towards automatic classification of cardiovascular magnetic resonance task force criteria for diagnosis of arrhythmogenic cardiomyopathy. *Clin Res Cardiol*. 2022 Sep 6. doi: 10.1007/s00392-022-02088-x. Epub ahead of print. PMID: 36066609.

Roudijk RW, Verheul L, Bosman LP, **Bourfiss M**, Breur JMPJ, Slieker MG, Blank AC, Dooijes D, van der Heijden JF, van den Heuvel F, Clur SA, Udink Ten Cate FEA, van den Berg MP, Wilde AAM, Asselbergs FW, Peter van Tintelen J, Te Riele ASJM. Clinical Characteristics and Follow-Up of Pediatric-Onset Arrhythmogenic Right Ventricular Cardiomyopathy. *JACC Clin Electrophysiol*. 2022 Mar;8(3):306-318. doi: 10.1016/j.jacep.2021.09.001. Epub 2021 Dec 22. PMID: 35331425.

Bourfiss M, Prakken NHJ, James CA, Planken RN, Boekholdt SM, Ahmetagic D, van den Berg MP, Tichnell C, Van der Heijden JF, Loh P, Murray B, Tandri H, Kamel I, Calkins H, Asselbergs FW, Zimmerman SL, Velthuis BK, Te Riele ASJM. Prognostic value of strain by feature-tracking cardiac magnetic resonance in arrhythmogenic right ventricular cardiomyopathy. *Eur Heart J Cardiovasc Imaging*. 2022 Feb 13;jeac030. doi: 10.1093/ehjci/jeac030. Epub ahead of print. PMID: 35152298.

van der Voorn SM, **Bourfiss M**, Te Riele ASJM, Taha K, Vos MA, de Brouwer R, Verstraelen TE, de Boer RA, Remme CA, van Veen TAB. Exploring the Correlation Between Fibrosis Biomarkers and Clinical Disease Severity in PLN p.Arg14del Patients. *Front Cardiovasc Med*. 2022 Jan 13;8:802998. doi: 10.3389/fcvm.2021.802998. PMID: 35097021; PMCID: PMC8793805.

Driessen HE, van der Voorn SM, **Bourfiss M**, van Lint FHM, Mirzad F, Onsri LE, Vos MA, van Veen TAB. Buccal Mucosa Cells as a Potential Diagnostic Tool to Study Onset and

Progression of Arrhythmogenic Cardiomyopathy. *Int J Mol Sci*. 2021 Dec 21;23(1):57. doi: 10.3390/ijms23010057. PMID: 35008484; PMCID: PMC8744793.

Cerrone M, Marrón-Liñares GM, van Opbergen CJM, Costa S, **Bourfiss M**, Pérez-Hernández M, Schlamp F, Sanchis-Gomar F, Malkani K, Drenkova K, Zhang M, Lin X, Heguy A, Velthuis BK, Prakken NHJ, LaGerche A, Calkins H, James CA, Te Riele ASJM, Delmar M. Role of plakophilin-2 expression on exercise-related progression of arrhythmogenic right ventricular cardiomyopathy: a translational study. *Eur Heart J*. 2022 Mar 21;43(12):1251-1264. doi: 10.1093/eurheartj/ehab772. Erratum in: *Eur Heart J*. 2022 Mar 21;43(12):1250. PMID: 34932122; PMCID: PMC8934688.

Bosman LP, Nielsen Gerlach CL, Cadrin-Tourigny J, Orgeron G, Tichnell C, Murray B, **Bourfiss M**, van der Heijden JF, Yap SC, Zeppenfeld K, van den Berg MP, Wilde AAM, Asselbergs FW, Tandri H, Calkins H, van Tintelen JP, James CA, Te Riele ASJM. Comparing clinical performance of current implantable cardioverter-defibrillator implantation recommendations in arrhythmogenic right ventricular cardiomyopathy. *Europace*. 2022 Feb 2;24(2):296-305. doi: 10.1093/europace/euab162. PMID: 34468736; PMCID: PMC8824519.

Bourfiss M*, Steensma BR*, Te Riele ASJM, Leiner T, Velthuis BK, Raaijmakers AJE. Feature-tracking cardiac magnetic resonance of the right ventricle: Effect of field strength, resolution and imaging sequence. *Eur J Radiol*. 2021 May;138:109671. doi: 10.1016/j.ejrad.2021.109671. Epub 2021 Mar 19. PMID: 33773860.

Roudijk RW, Taha K, **Bourfiss M**, Loh P, van den Heuvel L, Boonstra MJ, van Lint F, van der Voorn SM, Te Riele ASJM, Bosman LP, Christiaans I, van Veen TAB, Remme CA, van den Berg MP, van Tintelen JP, Asselbergs FW. Risk stratification and subclinical phenotyping of dilated and/or arrhythmogenic cardiomyopathy mutation-positive relatives: CVON eDETECT consortium. *Neth Heart J*. 2021 Jun;29(6):301-308. doi: 10.1007/s12471-021-01542-1. Epub 2021 Feb 2. PMID: 33528799; PMCID: PMC8160055.

Cadrin-Tourigny J*, Bosman LP*, Wang W, Tadros R, Bhonsale A, **Bourfiss M**, Lie ØH, Saguner AM, Svensson A, Andorin A, Tichnell C, Murray B, Zeppenfeld K, van den Berg MP, Asselbergs FW, Wilde AAM, Krahn AD, Talajic M, Rivard L, Chelko S, Zimmerman SL, Kamel IR, Crosson JE, Judge DP, Yap SC, Van der Heijden JF, Tandri H, Jongbloed JDH, van Tintelen JP, Platonov PG, Duru F, Haugaa KH, Khairy P, Hauer RNW, Calkins H, Te Riele ASJM, James CA. Sudden Cardiac Death Prediction in Arrhythmogenic Right Ventricular Cardiomyopathy: A Multinational Collaboration. *Circ Arrhythm Electrophysiol*. 2021 Jan;14(1):e008509. doi: 10.1161/CIRCEP.120.008509. Epub 2020 Dec 9. PMID: 33296238; PMCID: PMC7834666.

Bourfiss M*, Taha K*, Te Riele ASJM, Cramer MM, van der Heijden JF, Asselbergs FW, Velthuis BK, Teske AJ. A head-to-head comparison of speckle tracking echocardiography and feature tracking cardiovascular magnetic resonance imaging in right ventricular deformation. *Eur Heart J Cardiovasc Imaging*. 2021 Jul 20;22(8):950-958. doi: 10.1093/ehjci/jeaa088. PMID: 32462176; PMCID: PMC8291671.

Bosman LP*, Cadrin-Tourigny J*, **Bourfiss M**, Aliyari Ghasabeh M, Sharma A, Tichnell C, Roudijk RW, Murray B, Tandri H, Khairy P, Kamel IR, Zimmerman SL, Reitsma JB, Asselbergs FW, van Tintelen JP, van der Heijden JF, Hauer RNW, Calkins H, James CA, Te Riele ASJM. Diagnosing arrhythmogenic right ventricular cardiomyopathy by 2010 Task Force Criteria: clinical performance and simplified practical implementation. *Europace*. 2020 May 1;22(5):787-796. doi: 10.1093/europace/euaa039. PMID: 32294163; PMCID: PMC7203633.

Cadrin-Tourigny J*, Bosman LP*, Nozza A, Wang W, Tadros R, Bhonsale A, **Bourfiss M**, Fortier A, Lie ØH, Saguner AM, Svensson A, Andorin A, Tichnell C, Murray B, Zeppenfeld K, van den Berg MP, Asselbergs FW, Wilde AAM, Krahn AD, Talajic M, Rivard L, Chelko S, Zimmerman SL, Kamel IR, Crosson JE, Judge DP, Yap SC, van der Heijden JF, Tandri H, Jongbloed JDH, Guertin MC, van Tintelen JP, Platonov PG, Duru F, Haugaa KH, Khairy P, Hauer RNW, Calkins H, Te Riele ASJM, James CA. A new prediction model for ventricular arrhythmias in arrhythmogenic right ventricular cardiomyopathy. *Eur Heart J*. 2019 Jun 14;40(23):1850-1858. doi: 10.1093/eurheartj/ehz103. PMID: 30915475; PMCID: PMC6568197.

Bourfiss M, Prakken NHJ, van der Heijden JF, Kamel I, Zimmerman SL, Asselbergs FW, Leiner T, Velthuis BK, Te Riele ASJM. Diagnostic Value of Native T1 Mapping in Arrhythmogenic Right Ventricular Cardiomyopathy. *J Am Coll Cardiol Img*. 2019 Aug;12(8 Pt 1):1580-1582. doi: 10.1016/j.jcmg.2019.01.023. Epub 2019 Mar 13. PMID: 30878423.

Bourfiss M*, Zghaib T*, van der Heijden JF, Loh P, Hauer RN, Tandri H, Calkins H, Nazarian S, Te Riele ASJM, Zimmerman SL, Velthuis BK. Atrial Dysfunction in Arrhythmogenic Right Ventricular Cardiomyopathy. *Circ Cardiovasc Imaging*. 2018 Sep;11(9):e007344. doi: 10.1161/CIRCIMAGING.117.007344. PMID: 30354672.

Bourfiss M, Vigneault DM, Aliyari Ghasebeh M, Murray B, James CA, Tichnell C, Mohamed Hoesein FA, Zimmerman SL, Kamel IR, Calkins H, Tandri H, Velthuis BK, Bluemke DA, Te Riele ASJM. Feature tracking CMR reveals abnormal strain in preclinical arrhythmogenic right ventricular dysplasia/ cardiomyopathy: a multisoftware feasibility and clinical implementation study. *J Cardiovasc Magn Reson*. 2017 Sep 1;19(1):66. doi: 10.1186/s12968-017-0380-4. PMID: 28863780; PMCID: PMC5581480.

Bourfiss M, Te Riele AS, Mast TP, Cramer MJ, van der Heijden JF, van Veen TA, Loh P, Dooijes D, Hauer RN, Velthuis BK. Influence of Genotype on Structural Atrial Abnormalities and Atrial Fibrillation or Flutter in Arrhythmogenic Right Ventricular Dysplasia/Cardiomyopathy. *J Cardiovasc Electrophysiol.* 2016 Dec;27(12):1420-1428. doi: 10.1111/jce.13094. Epub 2016 Oct 6. PMID: 27572111.

Pre-prints

Schmidt AF*, **Bourfiss M***, Alasiri AI*, Chopade S, Puyol-Anton E, van Vugt M, van der Laan S, te Riele AS, Velthuis BK, Franceschini N, Ruijsink B, Hingoranin A, van der Harst P, Gross C, Clarkson C, Henry A, Lumbers R, Bis J, Asselbergs FW, van Setten J, Finan C. Druggable proteins influencing cardiac structure and function: implications for heart failure therapies and cancer related cardiotoxicity, 28 January 2022, PREPRINT (Version 1) available at Research Square [<https://doi.org/10.21203/rs.3.rs-1305500/v1>].

Book chapter

Bourfiss M, Hauer RN. Current challenges in the diagnosis of arrhythmogenic cardiomyopathies.

In C. Brunckhorst, A.M. Saguner, F. Duru, editors. Current concepts in arrhythmogenic cardiomyopathy. Minneapolis: Cardiotext Publishing; 2021. 73-85.

*Shared first authorship

ACKNOWLEDGEMENTS/DANKWOORD

Met mijn dankwoord als een van de laatste onderdelen in dit proefschrift, is mijn promotietraject echt tot een einde gekomen. Ik kijk terug op een bijzondere tijd in mijn leven en dank iedereen die mij hierin heeft gesteund. Bij het doen van een promotietraject komt er meer kijken dan alleen wetenschappelijk onderzoek doen. Het is elkaar motiveren en inspireren, samenwerken en heel veel koffie en thee om aan het eind van de week nog de stip aan de horizon te zien.

Er zijn ontzettend veel mensen direct en indirect betrokken geweest bij de totstandkoming van dit proefschrift. Ik wil daarom iedereen bedanken die een bijdrage heeft geleverd aan dit proefschrift. Allereerst wil ik het **Alexandre Suerman** programma van het UMC Utrecht bedanken voor het toekennen van een persoonlijk stipendium. Dit stipendium is erg waardevol geweest voor mij. Niet alleen heb ik door deze persoonlijke funding veel vrijheden op wetenschappelijk vlak ervaren, maar heb ik mij ook kunnen omgeven door een uitzonderlijke groep wetenschappelijk onderzoekers.

Verder wil ik de onderstaande personen bedanken:

De leden van de **beoordelingscommissie**, prof. dr. P.A.F.M. Doevendans, prof. dr. H.S. Tandri, prof. dr. R. Nijveldt, prof. dr. E. van Rooij en prof. dr. J.P. van Tintelen wil ik bedanken voor de beoordeling van dit proefschrift.

Promotoren

Prof. Dr. B.K. Velthuis, beste **Birgitta** wij kennen elkaar sinds ik als Honoursstudent werkte aan de studie over atriale betrokkenheid bij ARVC. In die tijd viel mij je persoonlijke benadering al op. Er is geen meeting met jou geweest waarbij ik niet volop getraakteerd ben op de lekkerste chocolaatjes, theetjes of lunch. Daarbij nam je altijd uitgebreid de tijd om mij te begeleiden of om gezamenlijk ergens aan te zitten. Wanneer jij betrokken bent bij een project kan ik altijd op je rekenen, dank daarvoor. Ook heb ik warme herinneringen aan onze gezamenlijke diners en struinend door de authentieke straatjes in Venetië toen wij daar waren voor het EuroCMR congres. Je oprechte interesse, kritische blik en betrokkenheid zijn erg waardevol geweest in mijn promotietraject.

Prof. Dr. F.W. Asselbergs, beste **Folkert**, ik vind het inspirerend hoe jij altijd veel ballen hoog weet te houden en toch altijd nauw betrokken bent geweest bij onze gezamenlijke projecten. Dankzij jouw betrokkenheid, oplossingsgericht denken en visie heb ik met veel onderzoekers van verschillende achtergronden kunnen samenwerken. Enkele projecten lagen buiten mijn comfort-zone, en hebben daardoor tot meer verdieping geleid. Dit heb ik uiteindelijk als een van de leerzaamste dingen in mijn promotietraject ervaren. Door

de ruimte die je mij daarin gaf, ben ik gegroeid als onderzoeker. Verder heb ik leuke herinneringen aan de jaarlijkse uitjes waarin jouw alsmaar groeiende onderzoeksgroep bij elkaar kwam. Heel veel succes en veel plezier in het Amsterdam UMC!

Copromotor

Dr. A.S.J.M. te Riele, beste **Anneline** ook wij leerden elkaar kennen tijdens mijn studie, jij was toen bezig met je promotietraject en ik wilde graag onderzoek doen: *the rest is history!* Dankzij jou heb ik stage gelopen aan de NIH in Bethesda. Ik heb hier ontzettend leuke herinneringen aan overgehouden, dank daarvoor. Ik ben erg trots op het eindresultaat waar jij met jouw onuitputtelijke betrokkenheid, enthousiasme en perfectionisme een belangrijke rol in hebt gespeeld. Van jou leerde ik dat een paper zoals een zwangerschap is, 9 maanden van conceptie tot bevallen. Ik vind het bewonderingswaardig hoe jij je jonge groeiende gezin combineert met een succesvolle carrière. Ik verwacht dat wij ook na mijn promoveren nog veel zullen samenwerken, daar kijk ik naar uit!

Onderzoek collega's

Prof. Dr. R.N.W. Hauer, beste **Richard**, onze eerste ontmoeting dateert alweer uit mijn tijd als onderzoeksstudent, toen ik aan mijn eerste paper werkte. Dank voor je onuitputtelijke interesse in mijn studies en in mij als persoon. Ik ben dan ook erg trots dat ons hoofdstuk in het boek "Arrhythmic Cardiomyopathy" mijn proefschrift opent met Chapter 2.

Dr. M.J.M. Cramer, beste **Maarten-Jan** dank voor je enthousiaste betrokkenheid. Erg trots op ons speckle tracking vs. FT-CMR stuk wat we samen met o.a. Karim, Arco en Birgitta schreven.

Dr. A.A.B. van Veen, beste **Toon**, als student liep ik al rond bij de Medische Fysiologie om samen met Elise Kessler te kijken naar de atriale betrokkenheid van ARVC. Hierna wist ik zeker dat ik verder wilde gaan met onderzoek. Dankjewel voor je openheid en continue betrokkenheid.

Dr. N.H.J. Prakken, beste **Niek**, dank voor de fijne samenwerking die mij meerdere keren naar het Noorden deed afreizen. Tevens dank ik **dr. M.P. van den Berg** voor de fijne samenwerking in Groningen.

Beste **dr. Nils Planken** en **dr. Matthijs Boekholdt**, dank voor de fijne samenwerking in het Amsterdam UMC.

Verder dank ik **prof. dr. Peter van Tintelen**, **dr. Annette Baas**, **prof. dr. Tim Leiner**, **prof. dr. Pim van der Harst**, **dr. Peter Loh**, **dr. Jeroen van der Heijden**, **dr. Arco Teske**, en **dr. Magdalena Harakalova** voor de fijne samenwerking. Dank **prof. dr. Roel Goldschmeding**

voor de begeleiding tijdens Honours en de terloopse adviezen nadien. Furthermore, I would also like to thank **prof. dr. David Bluemke** for the amazing time I had at the NIH. Furthermore I would like to thank all the wonderful ARVC colleagues at Johns Hopkins Baltimore for the fruitful collaboration: thank you **dr. Stefan Zimmerman**, **dr. Ihab Kamel**, **prof. dr. Hugh Calkins**, **prof. dr. Hari Tandri**, **dr. Cindy James**, **Brittney Murray**, **Crystal Tichnell**, **dr. Mounes Aliyari Ghasebeh** and **dr. Tarek Zghaib**.

UK Biobank

Dear **Abdul**, I remember how excited we were when we got our first GWAS results after months of hard work. And how disappointed when we got scooped haha. Your inexhaustible positivism, ingenuity and hard work were very inspiring. Happy that our journey led us to collaborating with Floriaan and **Chris**. Beste **Floriaan**, ik denk dat ik niemand ken die zo snel, gestructureerd en doelgericht werkt. Dankzij jou heeft ons UKB project in een snel tempo een nieuwe dimensie gekregen wat heeft geleid tot een prachtig resultaat. Heel veel succes in het Amsterdam UMC! Beste **Jessica**, met jou heb ik de eerste stappen in het werken met de UKB data gezet. Ik herinner me nog dat ik erg onder de indruk was toen ik jou razendsnel een R-code in zag typen, dat wil ik ook dacht ik! Dank voor de fijne samenwerking en dat ik altijd bij jou terecht kon voor vragen! Lieve **Marion**, we *did it!* Supertrots op ons paper waar we samen met Abdul heel wat (nachtelijke) uurtjes aan hebben gezeten. Elke keer wanneer we dachten dat we klaar waren, was er altijd toch weer iets wat we wilden uitzoeken. Hard werken heeft geloond, dank voor de fijne samenwerking! Koffietjes om een paper te vieren houden we er in! Beste **Bram**, zonder jou en **Esther** hadden we dit UKB avontuur niet op korte termijn aan kunnen gaan, dank dat we gebruik konden maken van je processed MRI data! Ik wil **Alicia** en **Sander** van der Laan ook bedanken voor de teamwork!

Machine learning

Beste **Jörg**, jouw harde werken, perfectionisme, expertise en geduld hebben geleid tot de ultieme samenwerking voor ons machine learning project! Wij vulden elkaar goed aan! Ik ben trots op het eindresultaat. Nog zoveel nieuwe ideeën die er uit voort zijn gekomen. Ik wens jou veel succes met het afronden van je PhD. Verder dank ik **dr. Bob de Vos** voor zijn kritische blik en scherpe inhoudelijke feedback wat ons stuk zeker sterker heeft gemaakt. Als laatste veel dank aan **prof. dr. Ivana Isgûm**, voor de fijne samenwerking. Jouw expertise hebben het project naar een hoger niveau getild.

Ik wil het **stafsecretariaat van de cardiologie** bedanken voor alle hulp tijdens mijn promotie. In het bijzonder **Jantine Nieuwkoop**. Lieve Jantine, bijna geen vraag was jou teveel. Dank voor de gezelligheid! Verder veel dank aan Christa, Katinka, Sylvia en Tamara ook voor jullie hulp tijdens mijn ANIOS schap! Tevens wil ik het beeld57000 team van de radiologie bedanken! Geen (software probleem gerelateerde) vraag was jullie te veel (en ik had er

veel haha)! Dank **Merel** en **Hanneke** voor jullie gezellige ondersteuning in het ARVC team.

Paranimfen

Lieve paranimfen, *chicas de papel*, ik ben onwijs dankbaar voor de mooie vriendschap die onze promotietrajecten ons heeft opgeleverd! Lieve **Marijke**, of moet ik zeggen prof. Linschoten. Dank voor je onvoorwaardelijke steun, het aanhoren van urenlang (inmiddels zelfs telefonisch) ventileren. Ik kan altijd bij jou terecht. Door je oplettendheid, olifantengeheugen en kritische blik ben jij mijn favoriete sparringpartner. Ik ben ongelofelijk trots wat jij tot nu toe allemaal bereikt hebt, en weet zeker dat het vanaf hier alleen nog beter wordt! *The sky is the limit* bij jou! Heel veel succes in het Amsterdam UMC! Lieve **Janine**, jij bent een van de meest nuchtere en vrijgevigste personen die ik ken. Ook bezit jij twee uiterste expertises: een iron man kunnen rennen, maar ook een volledig multi-gangen menu kunnen koken en eten. Dank voor je scherpe adviezen, de gezellige etentjes in het verre Oosten (ligt Raalte nou vlak bij Duitsland) en streedfoodclub avondjes samen met Marijke!

Mede promovendi

Lieve Folkerts PhDs of moet ik zeggen Folkert's studieleger. Mede dankzij jullie is mijn promotietraject er ook een geweest waarin veel nieuwe vriendschappen zich vormden. **Arjan**, als chef gezelligheid bracht jij de groep altijd weer bij elkaar. Heel veel succes in de kliniek! **Mark**, jij bent een lopende encyclopedie en een harde werker, heel veel succes in het Erasmus! Lieve **Rob**, jij was naast Marijke en Janine mijn cardiologie PhD roomie! Jij bent een geboren opleider. Ik ken je als de rust zelve, en kon altijd bij je terecht voor advies of om gewoon even mijn hart bij je te luchten. Dank voor de fijne samenwerking en de gezellige momenten. Laten we de Utrecht terugkomdagen er in houden! **Laurens** dank voor jouw harde werken aan het moderniseren van de ARVC database, daar plukken we met zijn allen de vruchten van! Lieve **Machteld**, dank voor je collegialiteit en gezelligheid. Kleine tip: geef je op voor heel Holland bakt! Echo-team Feddo en Karim: **Feddo** met jouw ongekende scherpe humor ben jij onmisbaar in de groep. Dank voor de fijne gesprekken en zie je in de kliniek! **Karim**, we hadden nog zeker 20 echo vs. MRI papers kunnen schrijven. Dank voor de mooie samenwerking, je humor en collegialiteit! Lieve **Lieke**, sinds jij er bent steeg het aantal borrels significant. Ik wens je veel succes met het afronden van je proefschrift! Lieve **Fahima**, jij bent een van de hardst werkende personen die ik ken en ik weet zeker dat jij een mooi proefschrift zult hebben! Kijk er naar uit om jou te zien promoveren! **Steven**, wij losten elkaar af zonder dat we het wisten: jij aan je PhD in de ARVC groep en ik naar de kliniek in het JBZ. Dit is wel dubbel feest want zo kruizen onze paden ook bij beide borrels! Veel succes met je nieuwe eervolle taak in het ARVC team!

Daarnaast wil ik nog mijn mede ARVC promovendi bedanken voor de samenwerking en de gezellige veelal congressmomenten. Dank **Stephanie**, **Chantal** en **Helen** voor de fijne samenwerking en de mooie stukken die hier uit voort zijn gekomen. Lieve **Freyja**, mijn

favoriete congres buddy en roomie: Baltimore, Boston, San Francisco, Parijs. Van jou leerde ik dat een vrouw nooit teveel panty's mee kan nemen. Dank voor de fijne herinneringen en de curly world introductie!

Verder wil ik mijn mede cardiologie promovendi **Anne-Mar**, **Odette**, **Bas**, **Marijn**, **Max**, **Nicole**, **Rosanne**, **Diantha**, **Gideon**, **Philippe**, **Rutger**, **Timion**, **Hugo**, **Mira**, **Lisa**, **Ilse**, **Willeke**, **Evangeline**, **Sanne** (kookclub liefde en mijn eerlijkste klankbord), **Aernoud** (dank voor je adviezen en JBZ gezelligheid), **Thomas**, **Mehran**, **Manon** (want krullen scheppen een band) en **Iris** bedanken voor de gezellige borrels. Vooral het Valencia PhD weekend was een topper!

Ik heb een aan te bevelen dubbelleven geleid op de radiologie en dat was niet alleen voor de luxe broodjes tijdens de woensdagmiddag bespreking. Ook hier had ik een fijn kantoor die ik deelde met **Suzanne**, **Josanne** en later **Gerke** en **Marcia**. Dank voor de motiverende gesprekken en de latte machiatos met chocoladepoeder. Daarnaast dank ik de andere promovendi van de radiologie: **Ahmed** (koffie-expert buddy), **Atia**, **Bianca**, **Caren**, **Esmee**, **Frans**, **Liselore**, **Margot**, **Sander** en **Floor**. De Pannenkoekenparty traditie, zonder pannenkoeken, maar met zelfgekookte diners zijn een mooie herinnering evenals de creatieve radiologie kerstfeesten. Veel succes met het afronden van jullie promotietrajecten! Dank **Bart Steensma** voor de fijne samenwerking aan ons 7T project!

Alexandre Suerman programma

Dank **Wouter**, **Tobias**, **Anneloes**, **Hanneke**, **Floris**, **Maartje**, **Suze**, **Nicola**, **Eelco**, **Jasmijn**, **Arjan**, **Marijke** en alle **oud-Suermanners** voor de inspirerende Masterclasses en de leuke discussies etentjes, fijn dat we die nog wel even voortzetten! Dank **prof. dr. Paul Coffe** voor de begeleiding. Lieve **Lisan** van Os, ik kan altijd bij je terecht om van gedachten te wisselen, dank daarvoor. Jij bezit de gave om de angel uit elk probleem te halen, waardoor ik altijd met een opgelucht gevoel onze gesprekken afsluit. Dank voor de fijne vriendschap. Lieve **Suze**, dank voor de fijne etentjes, je eerlijke en nuchtere blik, veel succes met het afronden van je promotietraject.

Onderzoeks-studenten

Léon en **Dino**, wat was ik blij dat twee supergemotiveerde geneeskundestudenten zich bij mij meldden omdat ze graag onderzoek wilden gaan doen. Dankzij jullie harde werken hebben we een mooie dataset bij elkaar verzameld en liggen er 2 papers bijna publicatieklaar. **Lian**, ook jij klopte aan bij mij omdat je graag onderzoek wilde doen om de covidwachttijd te overbruggen. Daar is een supermooi paper uit gekomen, dankzij jou harde werk. Succes met het afronden van je studie.

Collega's uit de kliniek

Ik wil ook al mijn collega's in de kliniek op de afdeling cardiologie in het UMC Utrecht bedanken voor de fijne ANIOS tijd. In het bijzonder **dr. Gertjan Sieswerda** en **dr. Nick Clappers**.

Vrienden en familie

Vriendinnen van het eerste uur **Jitske** en **Syanah**. Van geodriehoek taferelen naar huisje boompje. Dank voor jullie vriendschap, eerlijkheid en op naar meer spa momentjes. Lieve **Mylene** ook jou ken ik sinds de middelbare school, dank voor de fijne vriendschap.

Lieve koffiebitches, wij bleken de harde kern van een PhD koffieclubje waar het motto vooral ventileren was: als het niet over onze PhD projecten ging, dan wel de staat van de huidige politiek of de laatste achterklap. De mooie vriendschap die hier uit is gekomen is een kado: samen flaneren in München, badderen in de Thermen en de vele sushi en tv-avonden. **Willemijn**, 'twee mensen één gedachte'. Jouw eerlijke mening en behulpzaamheid hebben mij er waar nodig vaak doorheen gesleept. **Carmen**, er is geen opiniestuk of krantenartikel die jij niet gelezen hebt. Dankzij jou bleef ik altijd up-to-date. Erg trots op hoe jij je eigen weg durft te zoeken. **Birgit**, ik ben supertrots op hoe jij je eigen weg hebt gevonden in München waar je nu in opleiding bent tot kinderarts. Dames, op jullie kan ik bouwen: "opdat we nooit vergeten".

Lieve **Timo**, ik ben dankbaar voor je luisterend oor en scherpe adviezen. Lieve **Nora**, dank voor je steun. Op naar meer avonturen samen! Lieve **Sophie** dank voor de fijne vriendschap. Lieve **Eline** wij doen alles bijna tegelijk: honoursprogramma, jarig zijn, in de kliniek werken, en promoveren. Veel succes met je verdediging! Lieve **Nicola**, onze liefde voor eten heeft ons samen met Suze bij elkaar gebracht! Wij raken nooit uitgepraat over PhD en kliniek taferelen. Zin in ons Thailand avontuur! Liefste **Marina**, vriendschap op het eerste gezicht toen wij elkaar leerden kennen in Washington DC! Jij bent mijn leukste cheerleader! Dank voor al je adviezen.

Als laatste wil ik mijn lieve familie bedanken voor hun onvoorwaardelijke steun en relativiseringsvermogen. Thuis groeide ik op samen met mijn drie zus(jes). Lieve **Ouassima**, mijn oudste zus, veel dank voor je interesse in wat ik doe, ik leg het met liefde nog 10 keer uit. Erg trots op jou en je mooie gezin samen met Khalid. Lieve **Hayat**, wij zijn echte virgo's! Ik ben trots op wat je inmiddels al bereikt hebt, en weet zeker dat er nog mooiere dingen op je pad gaan komen. Dank voor je humor. Lieve **Oumaima**, ik ben trots op hoe jij je eigen weg aan het zoeken bent! Ookal ben jij de jongste, vaak kom je met het wijste advies, dank voor je luisterend oor! Lieve mama en papa, jullie zullen letterlijk voor ons door het vuur gaan. Doordat jullie de zaden plantten, konden wij de vruchten plukken. Wij hebben alles aan jullie te danken. Ik ben er trots op om jullie dochter te zijn en kijk er naar uit om

samen het leven te vieren. Lieve **mama**, jij bent de liefste en onbaatzuchtigste vrouw die ik ken. Jij leert mij mijn hart te volgen, kent mij door en door en weet mij altijd op de juiste momenten een spiegel voor te houden. Daarom is jouw advies mij ook het liefst. Lieve **papa**, jij houdt van aanpakken, zo vader zo dochter. Dank voor je onvoorwaardelijke liefde, steun en vertrouwen. Ik kan altijd op jou bouwen, zeker als het er toe doet, dat heb jij mij vaak laten zien.

CURRICULUM VITAE

Mimount Bourfiss was born in Zeist, the Netherlands to Mhamed Bourfiss and Malika El-Faiz. She grew up in Zeist with her parents and three sisters. In 2010, she graduated from the Montessori Lyceum Herman Jordan in Zeist after which she started medical school at Utrecht University.

Already early during her studies, Mimount was involved in research at the department of Cardiology at the University Medical Center in Utrecht. She participated in the Masters Honours program working on the involvement of the atria in arrhythmogenic right ventricular cardiomyopathy (ARVC) using cardiac MRI under the supervision of prof. Birgitta Velthuis and dr. Anneline te Riele. During the last year of her studies Mimount performed her scientific internship at the National Institutes of Health in Bethesda, USA, under the supervision of prof. dr. David Bluemke. There she worked on what has become chapter 3 of her thesis. Mimount also performed an extra-curricular internship at Johns Hopkins Hospital in Baltimore, USA, under the supervision of prof. dr. Hugh Calkins and dr. Stefan Zimmerman.

In 2017 Mimount graduated from medical school and was awarded the Alexandre Suerman stipend, a personal grant for medical students at the UMC Utrecht focusing on recruiting and preserving scientific talents for the UMC Utrecht. This allowed her to continue her research on cardiac MRI in ARVC under the supervision of prof. dr. Birgitta Velthuis, prof. dr. Folkert Asselbergs and dr. Anneline te Riele resulting in this thesis.

From September 2023 onwards, Mimount will start her cardiology training at the University Medical Center Utrecht supervised by dr. Gertjan Sieswerda and dr. Nick Clappers.